UNIVERSITY OF SOUTHAMPTON

FACULTY OF SCIENCE

OCEANOGRAPHY

THE MAGNETOSTRATIGRAPHY OF CONIACIAN-LATE CAMPANIAN CHALK SEQUENCES OF SOUTHERN ENGLAND

by

PAUL MONTGOMERY

Submitted for the Degree of
Doctor of Philosophy

AUGUST 1994

ACKKNOWLEDGEMENTS

I would like to thank Dr. E.A. Hailwood for his continuous supervision and helpful advice during my studies, Professor N. Hamilton for his generous support, Dr. A.S. Gale for his expertise in the field and Dr. J.A. Burnett for her detailed nannofossil biostratigraphy.

Special thanks are extended to my family for putting up with me and financing the many mechanical repairs required during the last four years. I would like to acknowledge the financial support of NERC who funded the project.

Special thanks are also given to Roger Montgomery, Janet Montgomery, Lee Montgomery, Nadine Wickenden, Ruth Watson, Doreen Montgomery, Chris Gatford, Jim Smith, Guy Whittington, George Graham, Jason Ali, Guy Rhodes, Liam Grant, Simon Webster, Justin Dix, Paul Riddy, Kevin Padley, Ting Fung, Portsmouth F.C., Arsenal F.C., Woody Allen, John Major, Gordon Brittas, Arnold Rimmer, Sharon Stone, Michelle Pfieffer and numerous others who have entertained me over the last four years.

UNIVERSITY OF SOUTHAMPTON
ABSTRACT
FACULTY OF SCIENCE
OCEANOGRAPHY
Doctor of Philosophy

THE MAGNETOSTRATIGRAPHY OF CONIACIAN-LATE CAMPANIAN CHALK SEQUENCES OF SOUTHERN ENGLAND

by Paul Montgomery

Results from a detailed palaeomagnetic study of the Late Cretaceous sequences of Culver Cliff and Scratchell's Bay (Isle of Wight) and Seaford Head, East Sussex are presented. The sections range in age from Latest Turonian to early Late Campanian and consist of white chalk with flints. Hand samples and large volume rock cores have been collected. Both thermal and AF demagnetisation have been used to remove magnetic overprints. Measurements have been carried out using a CCL 'discrete sample' and a 2-G 'wholecore' cryogenic magnetometer. Average NRM intensities range between 0.0015 and 1.6008 mA/m. By carrying out repeat measurements on large volume samples, reliable determination of the remanence of such weakly magnetic rock has been possible. A reliability classification scheme is proposed to provide an objective means of assessing the quality of the palaeomagnetic results obtained from thermal and AF demagnetisation.

IRM acquisition experiments suggest the presence of single domain and multi-domain titanomagnetite. Mixtures of hematite and titanomagnetite also occur. Magnetic mineral extractions carried out by Dr. M. Hounslow have revealed the presence of detrital titanomagnetite and hematite preserved as inclusions within silicate grains. Moreover, the finest portion of the magnetic extract (≈10%) have revealed bacterial magnetite preserved as individual grains and chains. Sample horizons which contain the highest proportion of bacterial magnetite appear to have higher NRM intensities.

Geomagnetic polarity zones representing Chrons C33N, C33R and C34N have been located and reliably tied to the macrofossil (Dr. A.S. Gale, *pers. comm.*) and nannofossil (Dr. J.A. Burnett, *pers. comm.*) biostratigraphic zones in the sections studied. A standard magnetic polarity stratigraphy for the Late Cretaceous is proposed.

These studies have thus provided magnetostratigraphic age calibration points of 83.000 and 78.781 Ma (the C34N/C33R and C33R/C33N boundaries of Cande & Kent, 1992) for the English Chalk successions. By constructing a composite magnetostratigraphic section, and by assuming that deposition of the Chalk was relatively constant, a magnetostratigraphic time scale for southern England is proposed and used to calibrate the $^{87}Sr/^{86}Sr$ curve of McArthur *et al.* (1992) and to date Santonian-Campanian chalk-flint cycles.

The characteristic rhythmic bedding of the Upper Cretaceous pelagic carbonate sequences of the UK have been interpreted as the result of orbital variations. Though measurement of chalk-flint cycles within the English Chalk have been previously attempted, difficulties in locating and dating Late Cretaceous stage boundaries has proved a major hindrance in such studies. By determining the mean frequency of the chalk-flint cycles, inaccuracies in section and cycle measurement can be minimised, and an 'idealised' number of cycles for the chalk representing Chron C33R calculated. A histogram of the chalk-flint cycle thickness for strata enclosed within a 170 metre thick, reverse polarity magnetozone representing Chron C33R at Scratchell's Bay reveals a mean cycle thickness of 0.7 metres. A duration of 17, 362 years is inferred for chalk-flint cycles which probably represent the quasi-periodic orbital precession cycle (18kyr).

By employing the best quality palaeomagnetic data, a palaeopole for southern England, during Coniacian-Late Campanian times (78-85 Ma), is proposed (Long.=184°E, Lat.=73.0°N). However, though the Q value (van der Voo, 1988) of this palaeopole is low (Q=5) this pole position helps to confirm the palaeomagnetic pole of Heller & Channell (1979) derived from Late Cretaceous limestone (83 Ma) of the Münster Basin, Germany (Long.=181°E, Lat.=76°N). Thus, during Coniacian-Late Campanian times southern England lay at a palaeolatitude of 34±7°N.

CONTENTS

Chapter 1 Introduction

Chapter 2 Stratigraphy of Late Cretaceous successions in southern England

Chapter 6 Palaeomagnetic results from Coniacian-Late Campanian Chalk, Culver Cliff, the Isle of Wight, southern England

Chapter 8 Palaeomagnetic results from Coniacian-Late Campanian Chalk, Seaford Head, East Sussex, southern England

Chapter 9 Conclusions

LIST OF FIGURES AND TABLES

LIST OF PLATES

LIST OF ABBREVIATIONS

AF	Alternating field
α_{95},Alpha 95	95% confidence limit of Fisher statistics
APW	Apparent polar wander
C-	Carbon isotope
CC16-22B	Nannofossil Zones (Sissingh, 1977)
CC	Prefix to identify samples from Culver Cliff
CC1-CC7	Magnetozones defined at Culver Cliff
ChRM	Characteristic remanent magnetisation
CRM	Chemical remanent magnetisation
D, Dec	Declination of magnetic vector
DRM	Detrital remanent magnetisation
DSDP	Deep Sea Drilling Project
GPTS	Geomagnetic polarity time scale
HPC	Hydraulic piston corer
I, Inc.	Inclination of magnetic vector
IRM	Isothermal remanent magnetisation
IRM_{sat}	Saturation isothermal remanent magnetisation
J	Intensity (mA/m)
k	Precision parameter of Fisher statistics
K-Ar	Potassium-Argon dating
K-N	Cretaceous Normal Superchron
Lat.	Latitude
Long.	Longitude
MAD	Maximum angle of deviation
mA/m	milliampere per metre
MD	Multi domain
MORB	Mid oceanic ridge basalt
MS	Magnetic susceptibility
mT	Millitesla
NRM	Natural remanent magnetisation

O-	Oxygen isotope
opal-CT	Disordered Cristobalite
pDRM	Post detrital remanent magnetisation
Q	Palaeopole quality factor (1-7)
SB	Prefix to identify samples from Scratchell's Bay
SB1- SB7	Magnetozones defined at Scratchell's Bay
SCM	Stable characteristic magnetisation
SD	Single domain
SEM	Scanning electron microscope
SEP	Magnetic vector stable end point
SF	Prefix to identify samples from Seaford Head
SF1-SF3	Magnetozones defined at Seaford Head
Sr-	Strontium isotope
T	Tesla
TEM	Transmission electron microscope
TRM	Thermoremanent magnetisation
VGP	Virtual geomagnetic pole
VRM	Viscous remanent magnetisation
XRD	X-ray diffraction

PREFACE

The term 'chalk' refers to the very fine-grained pure-white limestone found in the Upper Cretaceous deposits of western Europe. However, the term is also used in a stratigraphic sense (with a capital C) as equivalent of the Upper Cretaceous, in western Europe where the strata of this age are dominantly composed of this rock type.

Sample codes consist of a prefix 'CC','SB' and 'SF' followed by a series of numbers and letters. The prefix indicates the sample location (i.e. 'CC'=Culver Cliff) while the first number signifies the sampling level (e.g. CC21). The second number and letter indicate subdivision of the large volume sample collected at a sampling level.

Chapter 1 Introduction

1.1 Magnetostratigraphy: an introduction

Magnetostratigraphy is based on the study of the remanent magnetism of rocks. Provided sedimentary and volcanic rocks, emplaced in the geomagnetic field, possess suitable mineralogy a record of the Earth's magnetic field direction is preserved. Thus, a history of the field's inversions may be recorded in volcanic and sedimentary sequences in which the course of events can be verified by superposition and/or radiometric/isotopic dating. Thus the pattern of geomagnetic reversals can be used to subdivide the geological past.

The geomagnetic field is a global phenomenon and polarity reversals occur simultaneously over the whole earth's surface. Such geomagnetic inversions take between 10^3 and 10^4 years to occur and can be regarded as geologically instantaneous. Furthermore, geomagnetic reversals are more abrupt and synchronous than many extinction intervals and thus provide a basis for identifying true 'time planes' in a geological sequence (Hailwood, 1989).

If a distinctive pattern of polarity reversals is observed in different sections, through a geological formation, then the potential exists to match these sequences and produce a geological correlation. However, magnetostratigraphy is rarely used alone and is normally combined with biostratigraphical information.

Biostratigraphy entails identification of evolutionary changes in fossil organisms and the subdivision of geological time according to those changes. Thus the biostratigraphic record is more definitive than the magnetostratigraphic record since assemblages of fossil organisms are characteristic of restricted intervals of geological time. Biostratigraphy can determine a sedimentary sequence's relative geological age and establish its approximate position against the polarity reversal time scale. Once an initial match has been made a refined correlation of the polarity horizons within the succession with the polarity reversal time scale can be made. Numerical ages can then

be assigned to the correlation points.

1.2 The Earth's magnetic field

The Earth's present day magnetic field approximates to a magnetic dipole located at the centre of the earth. The dipole axis is inclined to the geographical (rotational) axis by an angle of approximately 11.5° (Figure 1.1). This model accounts for approximately 80% of the main field while the remaining 20% has a more intricate non-dipole nature. The orientation of the best-fitting dipole varies with time; however, palaeomagnetic data suggest that, over a few thousand years its position lies close to the geographical axis (Figure 1.2). This model is called the "axial geocentric dipole model". For such a model, the inclination of the magnetic field (I) is related to the latitude of the site (L) by the equation:

$$\tan I = 2\tan L$$

The Earth's core is the main source of the geomagnetic field. Predicted temperatures within the core prevent any possibility of materials within the core carrying permanent magnetism. It has been proposed therefore, that the geomagnetic field is maintained by a process which involves a 'self-exciting dynamo' mechanism. This is thought to arise from the convective motions of hot electrically conductive fluid within the outer core (Hailwood, 1989).

As a result of the dynamic process involved in the generation of the Earth's magnetic field, variations in the field, with time, will occur. It is the record of these variations through geological time, retained in the permanent magnetism of rocks formed on the Earth's surface, that constitutes the foundation of magnetostratigraphy.

1.2.1 Definition of the geomagnetic field

The geomagnetic field vector direction, F, at any point of the earth's surface can be defined by two angles (Figure 1.3), the declination (D) and inclination (I). The

declination is specified relative to geographic north. The inclination is specified relative to the horizontal, and is regarded as positive if the field is downward-directed and negative if upward-directed (Hailwood, 1989).

The intensity of the Earth's field is expressed in tesla (T) and commonly has a value of $50x10^{-6}$T (S.I. units are used throughout this study). The magnetisation of the rock is expressed in terms of declination (D), inclination (I) and intensity (J), where J is measured in milli Amperes per metre (mA/m).

1.3 Variations of the field with time

Fluctuations in both direction and intensity of the Earth's magnetic field occur on a variety of scales, from seconds to millions of years. However, two types of behaviour are of particular interest to palaeomagnetists. These are secular variations and polarity reversals.

1.3.1 Secular variations

Records from magnetic observatories, post-glacial remanent magnetism of lake sediments, archaeological materials and palaeomagnetism of older sedimentary sequences and volcanic lavas show that the declination and inclination of the Earth's field have undergone smooth quasi-cyclical fluctuations with 'periodicities' that range from 10^2 to 10^4 years (Hailwood, 1989). Such variations have been employed to subdivide sequences into stratigraphical units and for correlation purposes on local and regional scales. Cox (1970) proposed a model in which secular variation was caused by "dipole-wobble" combined with non-dipole fluctuations. Brock (1971) used palaeomagnetic data from Tertiary and pre-Tertiary igneous rocks to test this model.

1.3.2. Polarity reversals

The Earth's magnetic field alternates, at irregular intervals, between normal polarity and reverse polarity. Normal polarity describes the geomagnetic field's present state

where the magnetic north pole lies close to the geographic north pole. Reverse polarity describes the opposite state where the magnetic north pole lies close to the geographic south pole. The time spent by the field in either polarity state varies between about 10^4 and 10^7 years (Hailwood, 1989).

Transitions from one state to the other are much shorter in duration, varying between 10^3 and 10^4 years. When considered on a geological time scale, such events can be regarded as instantaneous. Moreover, their globally synchronous nature makes them a particularly effective tool for undertaking geological correlations. Where patterns of reversals can be accurately correlated with the appropriate part of a geochronometrically calibrated polarity time scale it is possible to use magnetostratigraphy to numerically date sedimentary sequences.

1.4 The geomagnetic polarity time scale

A geomagnetic polarity time-scales (GPTS) is based on three separate sources of information (Hailwood, 1989). These are:-

(a) Palaeomagnetic data from isotopically dated igneous rocks, especially basaltic lava sequences.

(b) Palaeomagnetic data from biostratigraphically and/or isotopically dated sedimentary sequences.

(c) Interpretation of oceanic lineated magnetic anomalies.

Heirtzler *et al.* (1968) published the first time scale of the Late Cretaceous-Cenozoic anomalies in the South Atlantic (Vema Track V20). Only one calibration point, the old end of Anomaly 2A, was used and dated using the Cox *et al.* (1965) radiometrically-dated anomaly scale. A constant ocean ridge spreading rate of 1.9 cm/year was assumed and extrapolated back to anomaly 32. Even though only one calibration point was employed, older anomalies were dated with a maximum error of

only 20% when compared with more recent studies (Tarling, 1983).

The Heirtzler *et al.* (1968) time scale represented only about the last 80 million years. It was not until Helsley & Steiner (1969) suggested the existence of a long normal geomagnetic polarity interval in the Cretaceous, prior to anomaly 32 that a more complete picture of Late Cretaceous polarity reversal history was established. Larson & Pitman (1972, Figure 5) improved the resolution further by discovering two intervals of reversed polarity between the base of the Heirtzler *et al.* (1968) time scale and the top of the Cretaceous "Long Normal" interval. As a result, they identified and labelled an anomaly (33) just above the lowest reversed interval of Heirtzler *et al.* (1968). The two new reversed intervals were based on observations in the northwest Pacific, the southwest Atlantic and northern Indian Ocean (Lowrie & Alvarez, 1977a). Anomaly 33 has been added at the top of the Cretaceous Long Normal interval, with anomalies 33 and 34 enclosing the first reversed interval above the Long Normal interval (Figure 4.1). Pitman *et al.* (1974), with the aid of a map of world-wide marine magnetic lineations, has shown the presence of anomaly 33 in the South Atlantic Ocean. However, these 'new' reversed intervals were not universally accepted. For example, Sclater & Fisher (1974) presented polarity intervals which extended back to reversed interval 33R, but ended their time scale without showing the reversed interval between anomalies 33 and 34.

Disagreements over the existence of the reversed interval between anomalies 33 and 34 were increased by the study of palaeomagnetism of the Niobrara Formation in the Western United States by Shive and Frerichs (1974). Related foraminiferal studies (Frerichs & Adams; Adams & Frerichs, 1973) which had been undertaken previously, suggested a Coniacian to Early Maastrichtian age. However, even after numerous samples were collected from four sections, no reversed direction was discovered. The possible explanations considered by Shive & Frerichs (1974) were as follows:

(a) Misdating of marine magnetic anomalies.

(b) Misdating of the Niobrara Formation.

(c) Hiatuses in the sedimentation or sampling gaps in the Niobrara Formation.

(d) Remagnetisation of the Niobrara during a time of normal polarity.

(e) The possibility that some of the Late Cretaceous anomalies might not represent field reversals.

Shive & Frerichs (1974) found reasons to doubt each of these possible explanations. As a result, when Keating *et al.* (1975) compiled a Late Cretaceous reversal sequence based on palaeomagnetic studies of sedimentary sections, the Niobrara data were included and the reversed interval between anomalies 33 and 34 ignored. Moreover, Frerichs & Adams (1973, p.190) stated that the age they had allotted to the Niobrara Formation was significantly younger than that previously thought. Cobban & Reeside (1952) believed the Niobrara Formation to be of Coniacian-Santonian age. This may explain the unbroken normal polarity found throughout Niobrara, since, on the basis of the Gubbio results (Alvarez *et al.*, 1977), the Niobrara would have been deposited entirely during the Cretaceous Long Normal interval (Figure 4.2)(Lowrie & Alvarez, 1977a). Furthermore, the excellent match between the Gubbio profile and the marine magnetic anomalies strongly supports the existence of an interval of reversed polarity between anomalies 33 and 34 (Lowrie & Alvarez, 1977a).

In recent years, several improved versions of the GPTS have been published (e.g. LaBreque *et al.*, 1977; Lowrie & Alvarez, 1981; Berggren *et al.*, 1985a & b; Harland *et al.*, 1990). The time scale used in this study is that published by Cande & Kent (1992) and consists of a composite geomagnetic polarity sequence derived primarily from data from the South Atlantic. Fine scale information, procurred from magnetic profiles on faster spreading ridges in the Pacific and Indian Oceans, was inserted into the South Atlantic sequence. Nine age calibration points were fitted to the composite polarity sequence. More details of this time scale are given in Chapter 4.

1.5 Principal carriers of magnetisation in rocks

One of the principal requirements of a magnetostratigraphic study is to determine whether the magnetisation of the rock was acquired at, or very close to, the original time of formation. The effects of weathering, diagenetic and metamorphic processes can result in the formation of iron oxides which carry components of remanent magnetism which date from the time of alteration. Therefore, an understanding of the composition of any magnetic minerals present, and the processes responsible for their formation is essential.

Almost all rocks display ferromagnetic properties due to the presence of magnetic minerals. The most significant bearers of remanent magnetisation in rocks belong to the titanomagnetite and ilmenohematite solid solution series.

1.5.1 The titanomagnetite series

The titanomagnetites form a solid-solution series with magnetite (Fe_3O_4) and ulvospinel (Fe_2TiO_4) as end members. The magnetic properties are dependant on grain size, composition and crystal lattice impurities (Tarling, 1983). As the magnetite end member is approached the series becomes more strongly magnetic. Low temperature oxidation may result in the formation of maghemite. Maghemite (γFe_3O_4) has a cubic structure and properties similar to magnetite, but the chemical composition of hematite.

1.5.2. The ilmenohematite series

The ilmenohematites form a solid-solution series with hematite (αFe_2O_3) and ilmenite ($FeTiO_3$) as end members. The series has a rhombohedral structure. The magnetic properties are dependant on grain size, composition and crystal lattice impurities. The spontaneous magnetisation of hematite (0.5 Am^2kg^{-1}) is much less than that of magnetite (92 Am^2kg^{-1}). Accordingly, sediments containing hematite rather than magnetite particles have a much weaker remanent magnetism.

Other important magnetic minerals include iron-hydroxides (goethite), iron-sulphide (pyrrhotite) and iron-carbonates (siderite). These minerals are either paramagnetic or only very weakly ferromagnetic. However, the effects of weathering diagenesis and metamorphism could result in the formation of iron-oxides from these minerals.

1.5.3 Magnetisation of marine limestones

Marine limestones deposited in a deep sea environment consist largely of skeletal structures of organisms which extract calcium carbonate ($CaCO_3$) from seawater and secrete it to form their hard parts. Calcium carbonate is diamagnetic and cannot contribute to the remanent magnetism. The remanent magnetism of limestone is therefore determined by the iron-oxides, iron-hydroxides and, in rarer cases iron-sulphide brought into the sediment as terrigenous deposits, formed authigenically from ferrous or ferric irons in interstitial solutions, or precipitated biogenically (Lowrie & Heller, 1982).

Different combinations of minerals most commonly identified in marine limestones are magnetite, goethite, hematite and maghemite (Lowrie & Heller, 1982). Pyrite is also common in certain limestones (van der Voo & Lowrie, 1979). Pyrrhotite has been reported in Swiss Helvetic limestones but is otherwise believed rare (Kligfield & Channell, 1981).

1.5.3.1 Magnetite

Of the various magnetic mineral phases identified in limestones, magnetite is the most commonly observed and magnetically-stable phase. Multi-domain (MD) magnetite extracted from deep-sea sediment cores revealed that grains were either rounded and eroded by water transport or sharply angular indicating wind-transported volcanic dust (Lowrie & Heller, 1982). The shapes and textures of magnetite grains extracted from modern carbonate sediments indicate that one of the most important sources of magnetite in limestone is terrigenous (Lowrie & Heller, 1982). Curie temperature and blocking temperature data from magnetite extracted from limestones indicate low or

negligible titanium (Lowrie & Heller, 1982). This implies that the magnetite present in limestone is derived from source rocks with a high deuteric oxidation state such as continental igneous rocks (Lowrie & Heller, 1982).

However, observations using the scanning electron microscope (SEM) and the optical microscope on magnetic extracts from limestones have successfully identified only the shape and texture of MD magnetite grains due to the limited resolution (>0.5 μm) of the microscopes. Nevertheless, these observations reveal the common occurrence of ultrafine-grained magnetite particles. Many rock magnetic studies have detected the existence of single-domain (SD) magnetite as the primary remanence carrier in a wide range of limestone deposits (Lowrie & Heller, 1982). Chang *et al.* (1987) suggest several possible sources of SD magnetite in limestones. These are:

(a) Weathering of continental igneous rocks (e.g. Morgan & Smith, 1981) and transportation of the magnetite by rivers and ocean currents.

(b) Disseminated crystals in the glassy matrix of mid-oceanic ridge basalt (MORBs) (Smith, 1979) released by submarine weathering.

(c) *In situ* biogenic precipitates by magnetotatic bacteria (Frankel *et al.*, 1979; Towe & Moench, 1981), magnetotatic algae (Torres de Araujo *et al.*, 1986), and/or chitons (Lowenstram, 1962; Kirschvink & Lowenstram, 1979).

(d) Chemical precipitates (Henshaw & Merrill, 1980).

The chemical precipitation origin of magnetite has only been theoretically postulated. As a result, Chang *et al.* (1987) believe that, to assign it as a possible source of SD magnetite in limestone sediments, is highly speculative. MORBs are a potential source of SD magnetite in certain pelagic limestone deposits. However, it seems unlikely that magnetite released from MORBs contributes to the primary remanence of more widespread continental shelf and marginal basin limestones (Chang *et al.*, 1987). Though the deposition of detrital grains is obviously the most important origin

of MD magnetite particles found in marine limestone sediments, a detrital origin for SD magnetite is unlikely to be of great significance. This is due to the small size of SD magnetite crystals and the ease with which transportation and deposition of such fine grained material could be diverted and retarded by various physical and chemical processes operating in the ocean system (Amerigian, 1974; Kirschviink & Chang, 1984).

High population densities of magnetotatic bacteria have been noted in a variety of depositional environments (Moench & Konetzka, 1978; Blakemore, 1982). These bacteria represent the largest source of biogenic magnetite that could be preserved in sediments (Towe & Meonch, 1981). Stolz *et al.* (1986) report that magnetotatic bacteria, and the magnetite they produce, are a major source of stable remanent magnetism is hemipelagic sediments from the Santa Barbara basin. Studies carried out on microbial communities and magnetic phases of carbonate oozes and laminated calcareous sediments have revealed the existence of magnetotatic bacteria and ultrafine-grained single domain magnetite (Chang *et al.*, 1987). These results, combined with the common occurrences of ultrafine-grained magnetite in limestone deposits detected magnetically, suggest that biogenic magnetite may be present and contribute to magnetic remanence of many ancient limestones (Chang *et al.*, 1987).

1.5.3.2 Maghemite

There is little evidence to suggest that maghemite is an abundant magnetic material in limestone. It can form authigenically under oxidising marine conditions (Schwertmann & Thalmann, 1976; Murray, 1979), diagenetically from lepidocrosite or by *in situ* low-temperature oxidation of magnetite (Taylor & Schwertmann, 1974). Maghemite formation occurs after deposition, with the newly formed mineral carrying a chemical remanent magnetisation (CRM). The effects of the CRM upon the primary component of remanence depends on the relative proportion of maghemite formed and the field direction of the time of formation.

1.5.3.3 Goethite

Iron oxyhydroxides are common in many deep-sea sediments (Henshaw & Merrill, 1980). Ferrimagnetic goethite, like lepidocrocite, may form authigenically or by direct or indirect precipitation from seawater (Murray, 1979), and is a polymorph to which the other iron hydroxide phases eventually revert (Henshaw & Merrill, 1980). Goethite can also form diagenetically from pyrite (Turner, 1975). The exact timing of the diagenetic formation of goethite in limestone is hard to estimate since it is determined by the oxidation and weathering processes to which a rock is exposed. However, its formation is more pronounced in limestones with higher porosity (Lowrie & Heller, 1982).

1.5.3.4 Hematite

Hematite is rarely the sole magnetic mineral present in a limestone with detrital hematite of minor importance in limestones generally (Lowrie & Heller, 1982). However, where hematite is present, it is normally formed by diagenetic processes. Goethite is thermodynamically unstable with respect to hematite and under most geological conditions readily inverts to hematite (Berner, 1969). Under more severe oxidizing conditions hematite may form directly from magnetite.

1.6 Processes of magnetisation in carbonates

An understanding of the processes by which a magnetic record is produced in rocks is extremely important in determining the reliability of magnetostratigraphic data. The magnetic properties of individual grains and the mechanisms by which the magnetic moments become aligned within a rock define the nature of the magnetism of that rock.

Different types of naturally occurring remanent magnetisation have been identified according to the mode of magnetic grain alignment. The most relevant types, with regards to pelagic limestones, are reviewed below.

1.6.1 Depositional and post-depositional remanent magnetisation (DRM & pDRM)

Depositional remanent magnetisation (DRM) is acquired by clastic sediments when magnetic mineral grains become physically aligned during deposition. These magnetic grains behave like small magnets and when suspended in the water column rotate freely. In the absence of other aligning forces they will adopt an orientation parallel with the ambient geomagnetic field which may be preserved on deposition. As a result the sediment gains a remanent magnetism which reflects the Earth's magnetic field at the time of deposition.

Due to the fine grain-size of detrital and biogenic magnetite within pelagic marine limestones, settlement through the water column will take a long time. Surface and bottom currents will tend to prolong the time in suspension (Lowrie & Heller, 1982). As a result, orientation of grain magnetic moments by the ambient geomagnetic field ought to result in DRM, with its accompanying inclination and declination errors (see below).

Laboratory experiments have shown that DRM may be subject to possible errors. The gravitational couple acting on the magnetic grains during deposition may result in a shallowing of inclination from that of the ambient geomagnetic field (King, 1955). Magnetic grains deposited on inclined surfaces may show inclination errors (King, 1955; Griffith *et al.*, 1960; Rees, 1966; Tauxe & Kent, 1984) and hydrodynamic couples acting when magnetic grains are deposited in a moving fluid can create rotational errors.

In most natural sediments these errors appear to be less significant and often completely absent. Modern deep-sea sediments appear to faithfully record the axial dipole field direction without inclination error (Keen, 1963; Opdyke, 1972; Opdyke & Henry, 1969). Irving (1957) proposed a post DRM (pDRM) process to explain this phenomena. Magnetic mineral grains within the sediment's water-filled interstitial cavities are free to rotate due to agitation by Brownian motion of water particles. The magnetic grains re-align, correcting any departures from the direction of the ambient

geomagnetic field, prior to compaction or cementation. Irving & Major (1964) demonstrated with synthetic sediments and fine grained magnetite and hematite that acquisition of a pDRM was possible. Kent (1973) concluded that bioturbation assisted this process.

The age of the pDRM will be slightly younger than the sediment's true age. The time-lag between deposition and the acquisition of pDRM is uncertain. Estimates vary between days (Løvlie 1974, 1976; Barton *et al.*, 1980) and hundreds of years (Lowrie & Heller, 1982). If bioturbation occurs, the remanence will be acquired at the base of the bioturbated zone. Biostratigraphic data used for dating the sediment will also be smeared out.

A pDRM may be subject to errors due to compaction. Detailed experiments have shown that volume reduction can result in a shallowing of inclination (e.g. Anson & Kodama, 1987; Deamer & Kodama, 1990). Such inclination shallowing has been noted in several palaeomagnetic investigations of carbonate sediments (e.g. Tauxe *et al.*, 1984; Celaya & Clement, 1988; Tarduno 1990).

1.6.2 Chemical remanent magnetisation (CRM)

Crystallization of new magnetic mineral phases commonly occurs in sedimentary rocks soon after initial formation as the result of lithification, diagenesis or chemical weathering. After nucleation the grains are extremely small, with very short relaxation times (a measure of the response time of the magnetic grains to change in an applied field). As they grow, a particular volume (the blocking volume) is reached, when their magnetisation is fixed in a direction parallel with the ambient geomagnetic field. Thus, the rock acquires a component of magnetisation dating from this time. This is called a chemical remanent magnetisation (CRM). CRM may be particularly important in limestones where it may arise from a variety of processes. For example, the effects of dolomitization on the magnetic properties of limestones, and the extent to which the process could alter the existing magnetic mineralogy, is not fully appreciated (Lowrie & Heller, 1982). Any changes might result in a CRM component

dating from the time of dolomitization. Suitable field tests are essential to establish the time of acquisition of a remanence component.

1.6.3 Thermoremanent magnetisation (TRM)

A thermoremanent magnetisation is acquired by a magnetic mineral as it cools through a particular temperature interval below its blocking temperature. At the blocking temperature the relaxation time rapidly increases and the magnetism of the grain becomes fixed in the direction of the ambient geomagnetic field. On further cooling the relaxation time of the grain increases and may reach 10^9 years or more (Tarling, 1983). Thus, a record of the geomagnetic field at this time is set into the rock for the rest of geological time.

If a sedimentary rock is heated at some stage in its history it will acquire a component of TRM. The direction of this component will be parallel with the geomagnetic field at the time of heating and carried by magnetic grains with blocking temperatures up to the maximum heating temperature. Provided the temperature is less than the Curie point (the temperature above which all substances behave paramagnetically) of the magnetic constituents, a component of the original magnetisation will be preserved in grains whose blocking temperatures lie between the heating temperature and the Curie temperature. This is described as the "principle of superposition of magnetisation" and applies equally to all types of magnetism.

1.6.4 Viscous remanent magnetisation (VRM)

A rock exposed to a weak magnetic field for a long period of time can acquire a viscous component of magnetisation. Since most rocks have been situated in the Earth's magnetic field for long periods, the magnetic moments of grains with short relaxation times gradually align with the ambient field. The development of a magnetic component parallel with the recent field direction results. This type of magnetism can normally be removed by standard demagnetisation procedures.

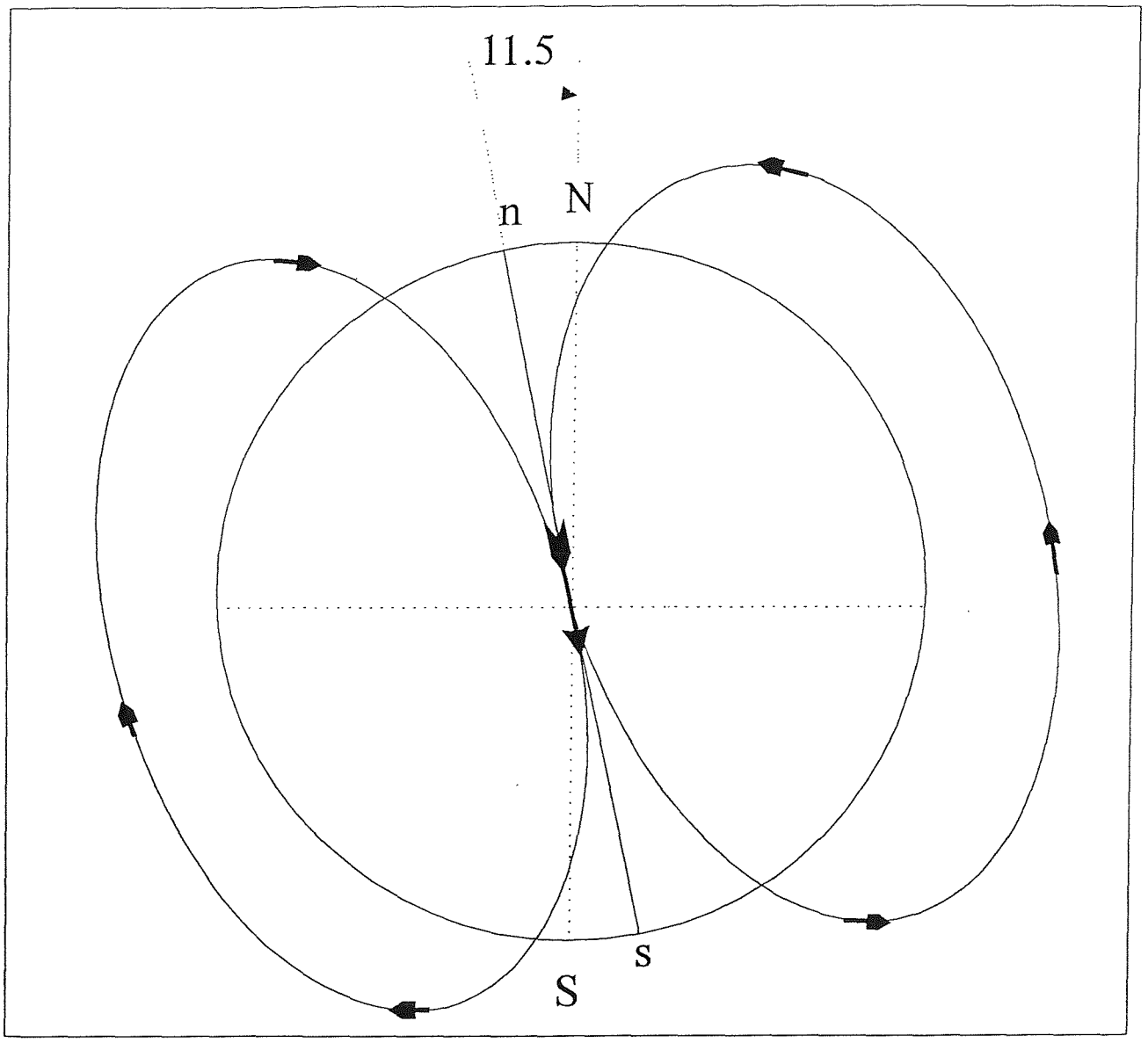

Figure 1.1. Model of the present day geomagnetic field. Best fitting magnetic dipole axis is inclined at 11.5° to the geographical axis. The Earth's geographic poles are indicated by 'N' (north) and 'S' (south) while the geomagnetic poles are indicated by 'n' (north) and 's' (south) (from Hailwood, 1989).

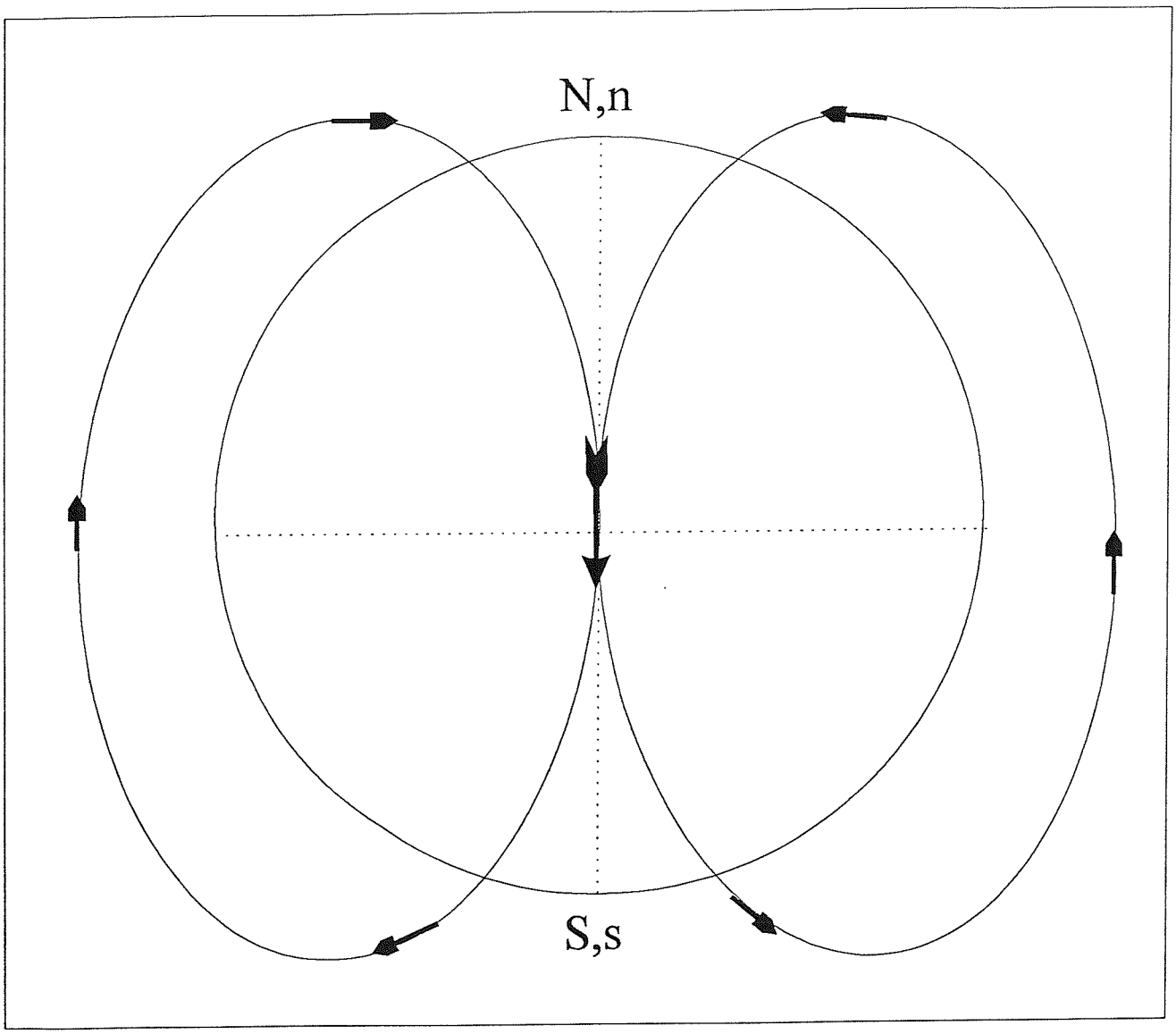

Figure 1.2. Model for time-averaged geomagnetic field (over *c.* 10^4 years). The best fitting dipole axis coincides with the geographical poles; 'n' and 's' are the magnetic poles (from Hailwood, 1989).

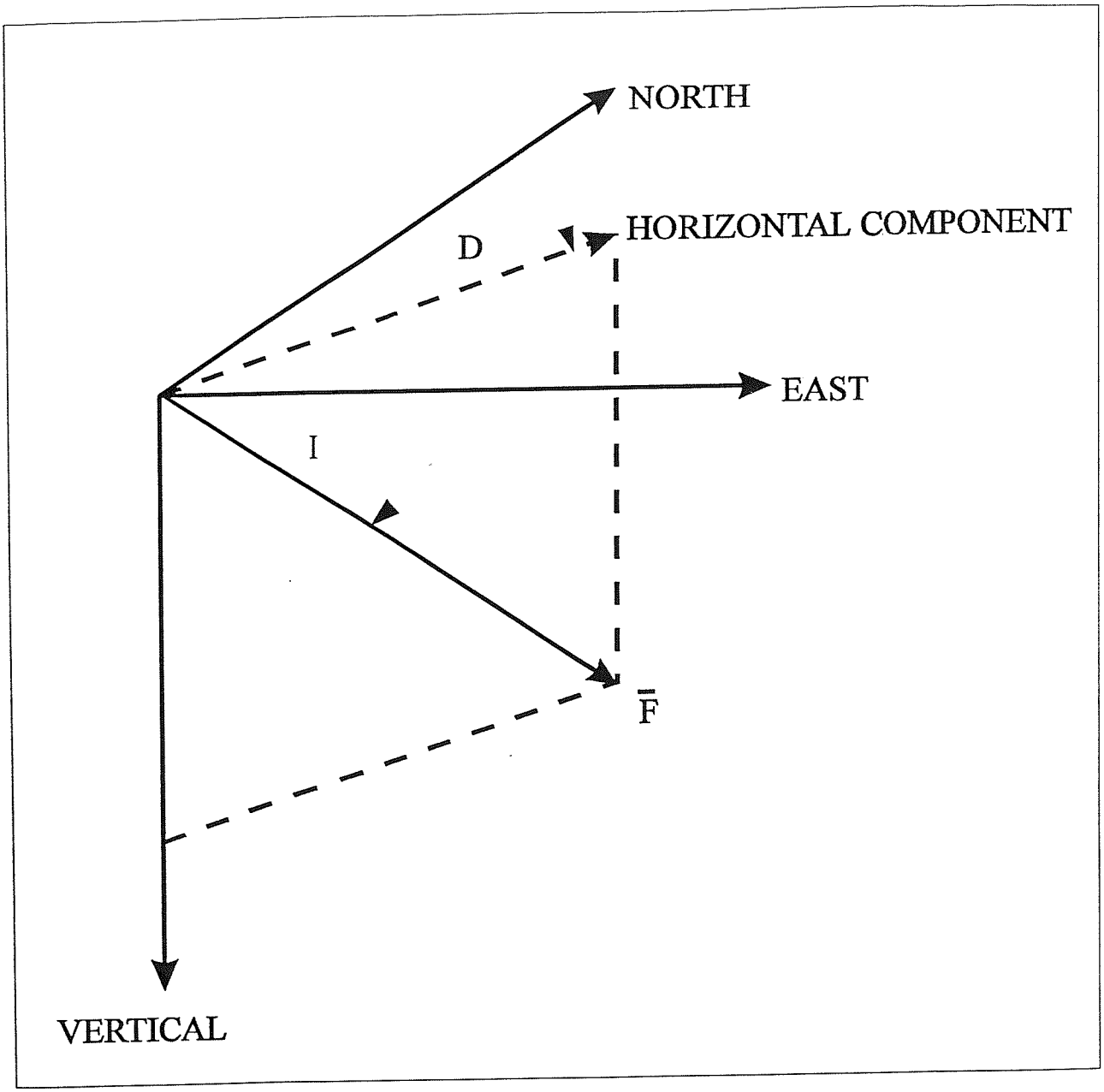

Figure 1.3. Specification of the direction of the geomagnetic field vector, F, in terms of angles of declination (D) and inclination (I) (after Hailwood, 1989).

Chapter 2 Stratigraphy of Late Cretaceous successions in southern England

2.1 Introduction

The Cretaceous Period lasted for approximately 72 million years, from 136 to 64 Ma (Anderton *et al.*, 1979). The name of the "Cretaceous" was adopted by the Belgian d'Halloy in 1822 and introduced into usage in England by Fitton (1847). The period is divided into Lower and Upper intervals at about 100 Ma, with each division further subdivided into six stages. The upper limit is the top of the Maastrichtian stage (Table 2.1).

Lower Cretaceous sediments continued the pattern of Jurassic sedimentation in Britain with the development of lacustrine, deltaic and estuarine facies (Anderton *et al.*, 1979). However, at the beginning of Upper Cretaceous times a widespread marine transgression occurred, which, at its maximum extent, produced the greatest proportion of sea relative to land on the Earth's surface since Palaeozoic times (Jenkyns *et al.*, 1994).

In northern Europe, part of the western United States, south-western Australia and other regions around the world, the Upper Cretaceous is represented by the white pelagic limestone known as chalk. The end of the Cretaceous marks the end of the Mesozoic era.

2.2 Cretaceous stages and zones in Britain

None of the standard Cretaceous stratotype sections are found in the British Isles, and several of the stratotypes belong to a different faunal realm. Problems in interpreting British Cretaceous stages have resulted (Rawson *et al.*, 1978).

The upper Cretaceous is synonymous with chalk over most of the British Isles and the division of the Chalk into Lower, Middle and Upper, based on lithological differences is uncertain in parts of the UK.

The work of Barrois (1876) showed that it was possible to subdivide the Chalk according to the presence of fossil organisms. As the divisions became more refined the relationship between lithology and fauna was nearly overlooked. When standard stage names were applied to the British successions they were fitted into a pre-existing local zonal scheme. This was ill-defined, and zonal limits were more dependant on facies than was realised (Rawson *et al.*, 1978).

The zones used in the UK Cretaceous have been set up empirically, with limited time spent determining which theoretical type of zone they may be. In theory most are *assemblage zones* (Rawson *et al.*, 1978).

In the Turonian to Maastrichtian, problems have arisen due to the scarcity or absence of organisms which originally had aragonitic shells. The rarity of such organisms (e.g. ammonites) may be due to sea-floor dissolution. Most chalk zones are of relatively long duration and the presence or absence of the index species is often of little significance. Other zones are *absolute-range zones* while a few are *lineage zones.*

Some index species may not even be present in the UK Cretaceous sequences. A summary of Upper Cretaceous stages and associated zones, as proposed by Rawson *et al.* (1978) is shown table in Table 2.1. For more details of the UK macrofossil zonation scheme adopted for this study see Section 3.2.

2.3 Late Cretaceous successions in southern England

The coastal exposures in Sussex and the Isle of Wight, constituting the northern part of the Anglo-Paris Basin, provide a composite Late Cretaceous succession which extends into the lower part of the Upper Campanian. Younger Campanian and Maastrichtian successions can only be found offshore in the English Channel (Rawson *et al.*, 1978).

Seaford Head in Sussex (Figure 2.1) provides a continuous, but condensed, sequence from the highest Turonian to the base of the *Gonioteuthis quadrata* Zone in the

Campanian (Dr. A.S. Gale, *per. comm.*). The relatively inaccessible succession of Scratchell's Bay (Figure 2.1) on the western coast of the Isle of Wight extends from the Coniacian *Micraster cortestudinarium* Zone to the early Late Campanian *Belemnitella mucronata* Zone (Dr. A.S. Gale, *pers. comm.*). At Whitecliff Bay, on the southeast coast of the Isle of Wight, the succession also extends from the Coniacian *cortestudinarium* Zone to the Campanian *mucronata* Zone (Dr. A.S. Gale, *pers. comm.*) (Figure 2.1).

Figure 2.2 shows a composite diagram of exposed onshore Late Cretaceous stages and associated zones in southern England, together with the extent of the three sections sampled in this study.

2.4 General Late Cretaceous stratigraphy

During the Late Cretaceous, a rise in sea level resulted in the submergence of large areas of land in the northern Europe area. The encroachment of the sea on to the craton combined with a gradual elimination of sources of terrigenous clastic material eventually resulted in dominance of pelagic deposits during the Late Cretaceous (Anderton *et al.*, 1979).

2.4.1 Late Cretaceous palaeogeography

In NW Europe great thicknesses of chalk were deposited in broad basins many hundreds of kilometres across. Within the Anglo-Paris Basin 400-500 metres of white chalk accumulated (Voight, 1963). Post-Cretaceous erosion has since reduced the thickness of these deposits in the UK to approximately 350 metres (BGS Trunch Borehole, Norfolk).

Such basins often contained troughs in which vast accumulations (as much as 2000 metres) of chalk developed (Voight, 1963). Marginal to these troughs and often over thick Jurassic sediments, elongated oval areas occurred where subsidence during the early Upper Cretaceous ceased and was sometimes reversed. Such uplifted ovals are

referred to as inversion axes.

The depth of the sea in the Cretaceous basin was not only controlled by local rates of subsidence but also by world wide changes in the general sea level. Eustatic changes are revealed from transgressive and regressive clastic sediments banked against the ancient massifs of Europe (Hancock, 1975). Even where chalk deposits extend over buried massifs, deposition was strongly influenced by eustatic changes (Hancock, 1975).

Marginal sediments provide clues to the conditions which prevailed on adjacent land masses. Very little material was eroded from the land. Even close to sizeable land areas the thickness of clastic sediments is small. Furthermore, the scarcity of variegated facies, which are fresh-water in the marginal sediments, suggest very limited erosional activity (Hancock, 1975).

Climatic conditions can be used to explain the lack of detritus. A non-seasonal climate results in limited erosion whether it be glacial, desert or tropical rain forest. No evidence exists to suggest that glacial conditions existed at this time. No terrigenous plant debris has yet been discovered in NW Europe, after the Cenomanian, to infer that tropical rain forests populated the adjacent land areas. However, dolomites and granular phosphates, indicative of an arid non-seasonal climate are present from the Late Turonian to Early Maastrichtian (Hancock, 1975).

In the northwest, evidence of minor late Cretaceous igneous activity (summarized by Hitchen & Ritchie, 1987) has been described. It includes possible Campanian volcanicity on the Anton Dorhn Seamount. Further volcanic activity, associated with the opening of the North Atlantic has been documented from the Biscay margin (White & McKenzie, 1989).

The high eustatic sea level of the Upper Cretaceous allowed pelagic sedimentation, typical of a deep sea environment, to be deposited onto continental shelves. This depositional environment persisted for nearly thirty million years. The effect was

heightened by a non-seasonal climate which suppressed erosion on a small land area. The purity of Chalk is a reflection of this peculiar palaeogeographic combination (Hancock, 1975).

2.4.2 Conditions of deposition

Modern day tropical coccolithophorids live in clear water in depths between 50 and 200 metres (Brasier, 1980). However, their minute skeletons amass between the limits of wave effectiveness and the calcium carbonate compensation depth (approximately 3 km, Brasier, 1980). Little evidence exists to suggest strong scouring and current action on the floor of the Chalk sea, and accumulation in 'deepish' water is suggested (Hancock, 1975). Disagreement between evidence from different fossil groups for the depth of the Chalk sea exists (Anderton *et al.*, 1979). Certain foraminiferas appear to indicate shallow water whereas the occurrence of hexactinelled sponges suggests depths of 80-100 metres (Reid, 1968). Well developed coccoliths in outcropping Chalk suggest that little etching has occurred. Etching of coccoliths in present day depositional environments occurs below about 1 km and provided that the carbonate balance of the Cretaceous seas was not vastly different from that of the present, deposition between 100 metres and 600 metres seems likely (Hancock, 1975). However, the ancient massif areas were probably more shallowly submerged (Hancock, 1975).

Due to the difficulty in assessing the amounts of both compaction and time involved, estimates of Chalk deposition rates vary (Anderton *et al.*, 1979). However, Table 2.2 provides a guide to sediment thickness for each stage in the Isle of Wight. Average figures for the white-chalk facies fall within the range of 20-40 metres per million years (Anderton *et al.*, 1979).

Substrate conditions must have been soft since certain bivalves became specially adapted to soft bottom conditions. For example, certain Inoceramus species had greatly inflated left valves which allowed them to 'float' on the substrate while other

genera developed spines or buoyant cavernous shells (Anderton *et al.*, 1979). Chalk shows signs of intense bioturbation (Kennedy, 1967, 1970; Kennedy & Garrison, 1975) and it is possible that the sea bed was in a thixotropic state, being permanently firm only at depths of a few tens of centimetres (Anderton *et al.*, 1979).

Over the submerged massifs, chalk facies thin and more stratigraphic gaps are present in the sequence. These gaps are frequently associated with hardground development (Hancock, 1975). Encrustation, phosphatisation and glauconisation are all features seen in these chalk hardground horizons. Such chalks have higher magnesium values than normal white-chalk facies which probably reflects early cementation by magnesium-high calcite, remobilised from the shells of the richer benthos associated with the a more stable substrate (Hancock, 1975). However, no evidence exists to indicate exposure, and the early cementation seems to have occurred under wholly submerged marine conditions (Anderton *et al.*, 1979).

The depth of the Chalk sea must have varied with time due to the effects of eustatic sea-level changes. Eustatic fluctuations are interpreted from evidence of synchronous transgressive events that correlate over vast areas (Figure 2.4). No evidence has been found to suggest that polar ice caps existed in the Cretaceous and eustatic fluctuations were probably not the result of expanding and diminishing ice caps. The most likely explanation is that these eustatic fluctuations were controlled by the periodic elevation and collapse of ridge systems during active and inactive phases of central Atlantic sea-floor spreading (Pitman & Talwani, 1972).

2.4.3 Properties of the Chalk

The bulk of this pelagic material is the debris from coccolithophorid planktonic algae. The majority of this occurs in separate micron-sized plates though some have remained in their original rings called coccoliths (Hancock, 1975).

Chalk is dominantly composed of low-magnesian calcite with the bulk of the sediment deposited as low-Mg calcite and not formed via diagenesis from aragonite and/or high

Mg calcite (Hancock, 1975). Small quantities of clay minerals and clay grade detritus, chiefly quartz, are present throughout the chalk. Within the Coniacian, Santonian and Campanian stages in southern England such material makes up less than 1% of the rock. However, centimetre thick beds of very argillaceous material do occur at 2 metre or more intervals (Hancock, 1975). In the higher stages of the English Chalk the clay minerals are chiefly illite and montmorillonite in approximately equal proportions, accompanied by lesser quantities of clay-grade quartz (Young, in Gray, 1965; Perrin, 1957; 1971). Senonian stages in Sussex contain barytes, alkali-feldspar, low-temperature tridymite, euhedral quartz and apatite (Weir & Catt, 1965). A volcanic origin has been suggested for the montmorillonite in the Maastrichtian of north Germany (Valeton, 1960) and for the Aptian fuller's earth of southern England (Hallam & Sellwood, 1968). However, examination of montmorillonite in the Turonian-Campanian white-chalk suggests formation via precipitation within the sediment (Weir & Catt, 1965). There is a progressive loss of detrital clays upwards, and later chalks are normally about 98% $CaCO_3$ (Hancock, 1975).

2.4.4 Flint bands

The chalk is characterised by the presence of irregularly shaped flints which mostly follow, but sometimes cut across, bedding planes. Flint is comprised of micron-sized, randomly arranged, quartz crystals with interstitial water-filled microcavities (Anderton *et al.*, 1979) and is the product of early diagenetic silicification which occurred 5-10 metres below the sediment surface. Silicification proceeded in a sediment of about 75-80% porosity and silica precipitation initiated the dissolution of the host carbonate at this depth (Clayton, 1984).

Clayton (1986) provides a detailed summary of the formation of flint (Figure 2.5). Aerobic bacterial degradation of organic matter in the uppermost layers of sediment caused the gradual depletion of dissolved oxygen in the pore-water. As a result, oxygen content, at depth, became too low to sustain aerobic bacteria. However, oxidation of organic matter continued below this depth using dissolved sulphate, with the sediment becoming sulphate reducing. Under such conditions large amounts of

dissolved sulphide were released into the pore-waters. Combination of sulphide with any iron present resulted in the formation of iron sulphide and the eventual formation of pyrite. However, because of the low clay content and thus low iron content most of the sulphide migrated towards more oxic conditions as hydrogen sulphide (H_2S). The mixing of H_2S with oxic pore-waters, due to the presence of oxidising bacteria, resulted in the liberation of H^+ ions. The host calcite was locally dissolved leading to the precipitation of silica from saturated solution.

Cyclicity in Cretaceous chalk sedimentation has often been proposed (e.g. Kennedy & Garrison, 1975; Felder 1981). The regular repetition of flint bands is believed to reflect the underlying rhymicity of chalk sedimentation (Clayton, 1985). Each hiatus in sedimentation would have created a static redox boundary some metres below the sediment surface and an associated flint band would have formed. On resumption of sedimentation the comparatively rapid rate of chalk accumulation would have prevented the development of a stable redox boundary and flint formation would only have proceeded during the next hiatus (Clayton, 1985). Clayton (1985) concluded that 'well developed laterally continuous flint bands represent basin-wide breaks in sedimentation while impersistent flints may have formed below local washouts or sheltered environments'.

2.4.5. Marl seams

Thin marl seams are a common feature of the Chalk succession. In the Upper Santonian to Middle Campanian chalk of southern England rhythmic variations in the clay content exist. These chalk-marl rhythms are primary and therefore represent true bedding. Many marl bands rest on erosional surfaces (Jefferies, 1963) and indicate a break in calcite deposition accompanied by a supply of clay. Whether it is actually necessary to have a faster supply of clay is doubtful (Hancock, 1975). However, most chalk sequences contain records of small breaks in sedimentation (about 0.5 metres to 2 metres apart) without interventions of marl. Bromley (1975) describes such features as 'omission' surfaces.

Chalk successions also contain streamers of clay or marl. The majority of the streamers run parallel with bedding, but occasionally cut across it at a low angles. Such features have been given a variety of names including wavy bedding (Peak & Hancock, 1961), solution seams (Kennedy, 1969), flaser structures (Kennedy & Garrison, 1975) or simply flasers.

There is no known depositional process capable of forming such bedding. This fact led Hancock (1975) to state that their formation was a product of segregation of clay and carbonate in the sediment after deposition. The main process responsible for this segregation was preferential solution during chalk deposition. Such post-depositional processes have occurred at many horizons in the chalk but, due to an absence of clay, do not readily show up.

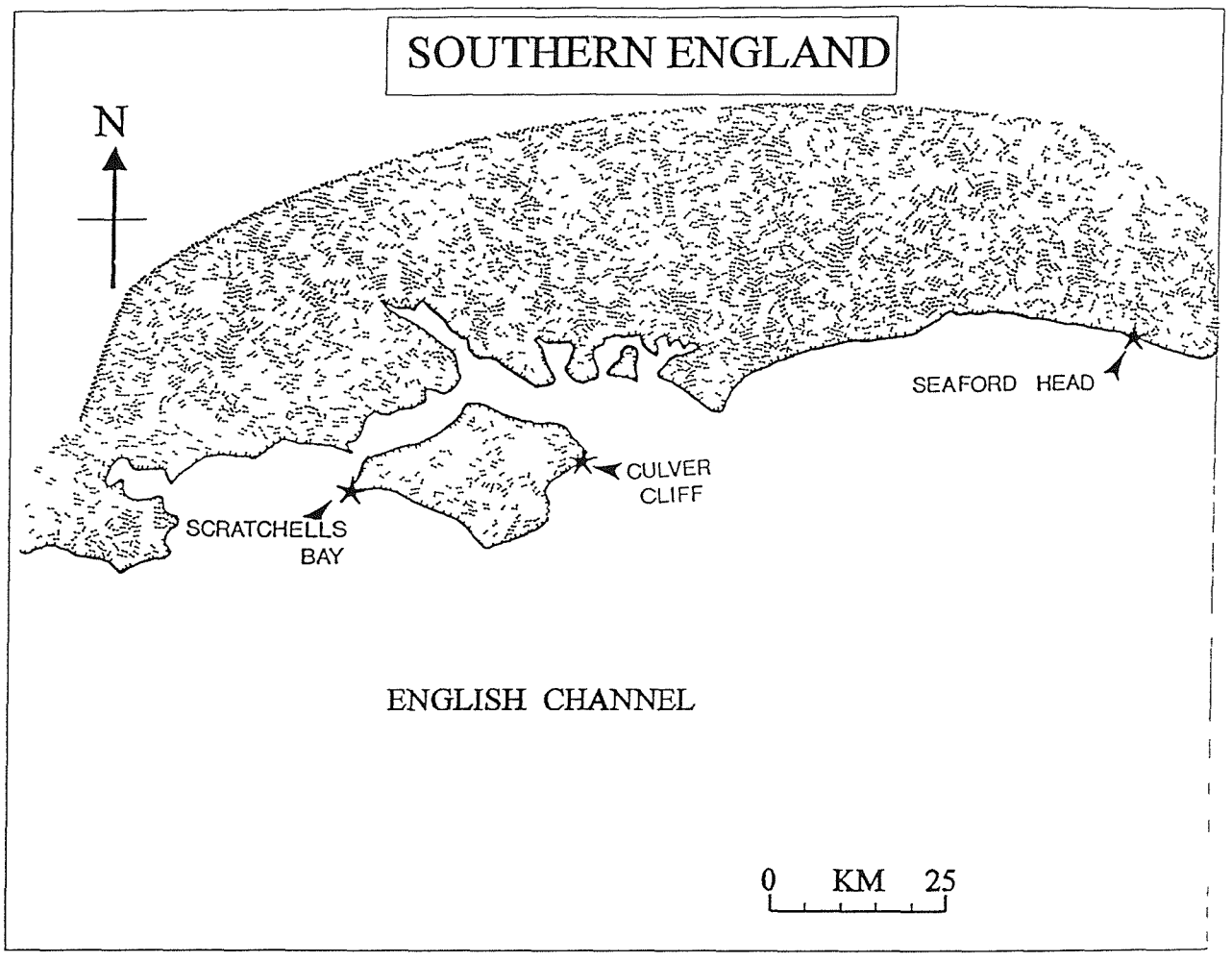

Figure 2 1 A map of southern England showing the locations of the magnetostratigraphic sections investigated during this study

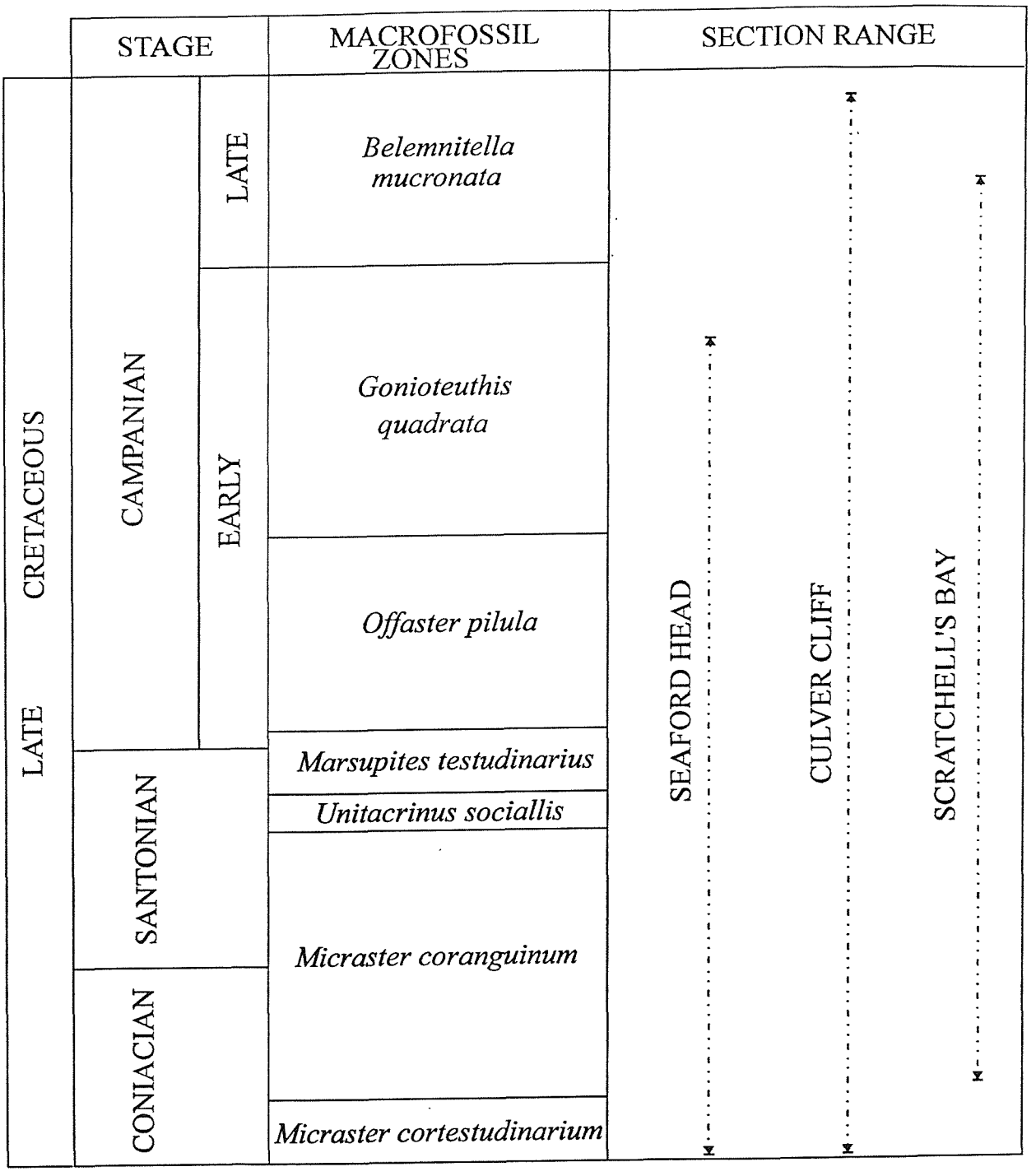

Figure 2.2. Composite diagram of exposed onshore Late Cretaceous stages and associated macrofossil zones of southern England. The extent of each section studied is indicated.

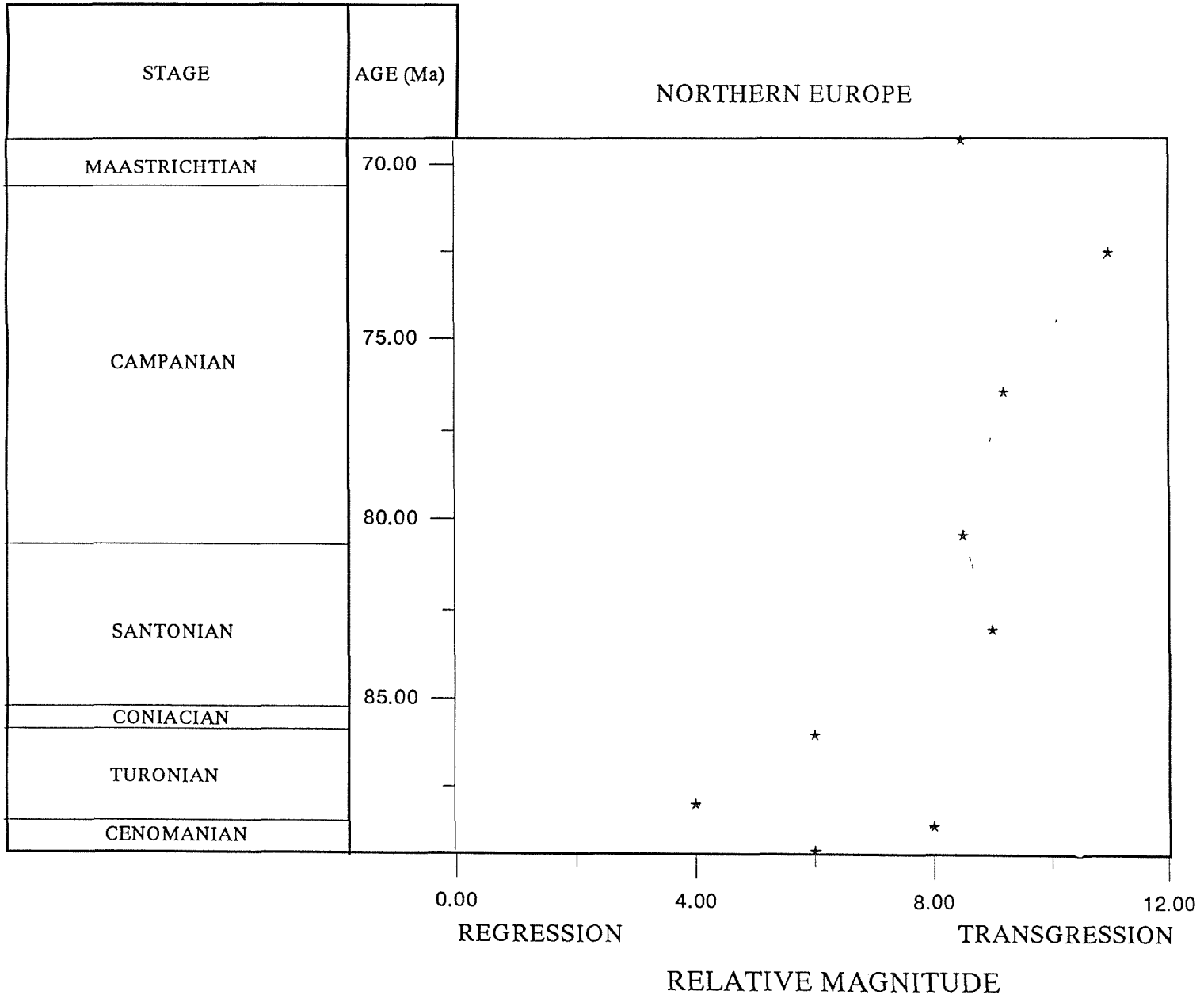

Figure 2.4. Age and relative magnitude of transgressions and regressions in the Northern Europe area (Hancock, 1975)

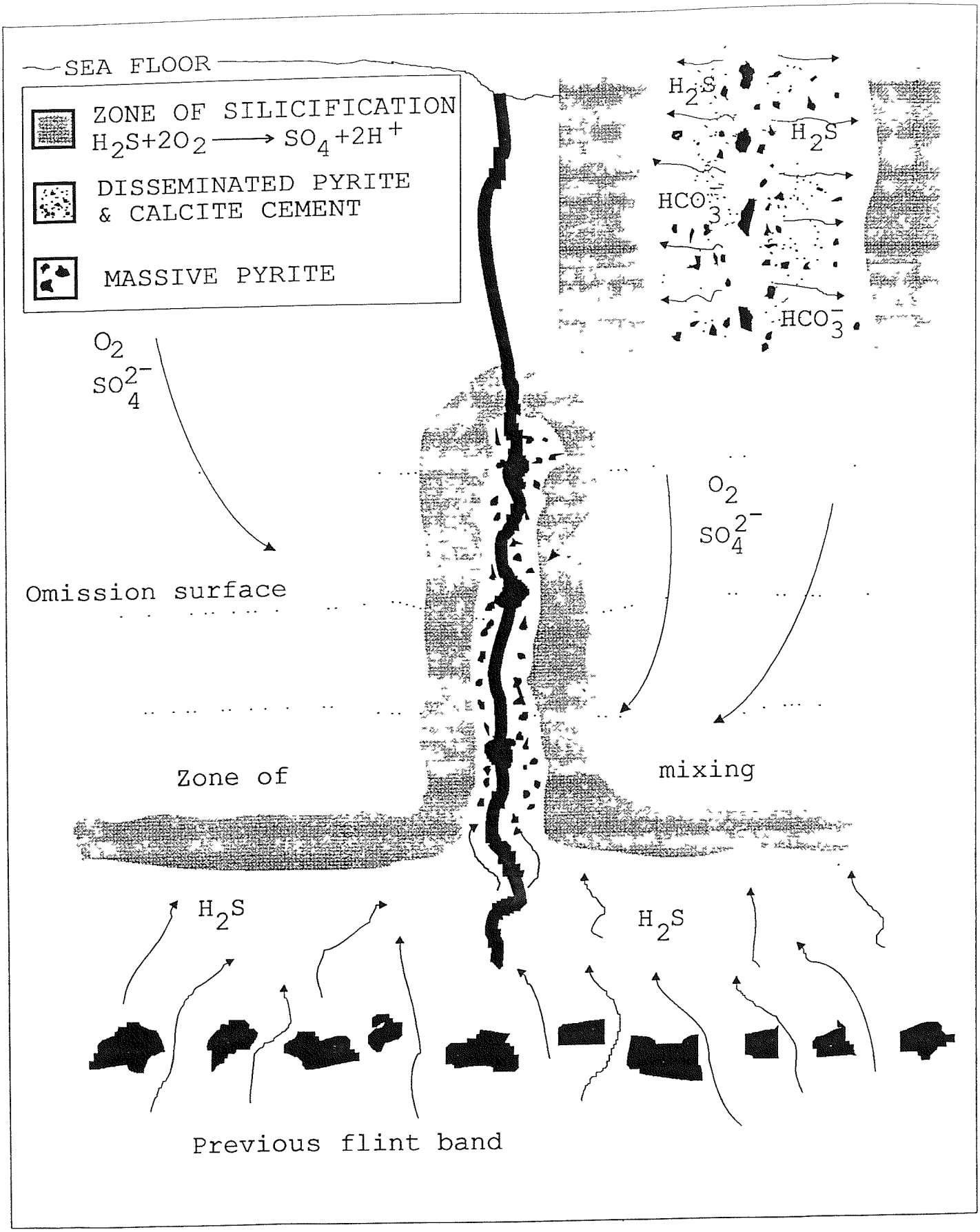

Figure 2.5. Summary model of silicification in Upper Cretaceous chalks. H_2S released by sulphate reduction mixes with dissolved O_2 at the oxic-anoxic boundary. This liberates H^+ ions, dissolving the host calcite, and in turn leading to silica precipitation (from Clayton, 1985).

STAGE		ZONE
UPPER MAASTRICHTIAN		
LOWER MAASTRICHTIAN		*occidentalis*
		lanceolata
SENONIAN	CAMPANIAN	*mucronata*
		quadrata
		pilula
	SANTONIAN	*testudinarius*
		socialis
	CONIACIAN	*coranguinum*
		cortestudinarium
TURONIAN		*planus*
		lata
		labiatus
CENOMANIAN		*gracile*
		naviculare
		rotomagense
		mantelli
ALBIAN (pars)		*dispar*

Table 2 1 Upper Cretaceous stages and biostratigraphic zones proposed by Rawson *et al* (1978) The dotted box highlights the interval of time investigated during this study.

STAGE	DURATION (m.y.)		THICKNESS (m)	APPARENT ACUMULATION RATE (m/m.y.)
CAMPANIAN	UPPER	11.5	144.8	c.50
	LOWER		104.5	18.2
SANTONIAN	4		116.4	29.1
CONIACIAN	1		16.2	6.2

Table 2.2. Thickness in metres and thickness per million years of Late Cretaceous stages in the Isle of Wight (Hancock, 1975).

Chapter 3 Biostratigraphy

3.1 Biostratigraphic zonation schemes

Biostratigraphic zonation schemes have been developed for the Chalk of north-west Europe based on both macro- and microfossil groups. Within each scheme, a series of zones are defined using the first occurrence (F.O.) and last occurrence (L.O.) of a particular species. Each scheme provides an alternative method of subdividing and dating (relative) a geological succession. During the Cretaceous the temperate gradient from pole to equator was less than the present day. Two principal provinces, the Boreal and Tethyan, existed in the North Atlantic area. However, these provinces were separated from each other by a transitional belt created by the action of warm water currents (Douglas & Silter, 1966; Bailey & Hart, 1979). Caron (1985) indicates the boundary between the northern temperate province and the Boreal province lay at a latitude of 40°N. This pattern was mirrored in the southern hemisphere. The northern and southern intermediate zones contain blended fauna due to the mixing of warm and cold waters by oceanic currents.

Palaeogeographic reconstructions of the British Isles area during the Late Cretaceous have indicated that southern England lay just within the northern Temperate province with an approximate palaeolatitude of 40°N. This is reflected in the macro- and microfossil assemblages which are neither Boreal nor Tethyan (Bailey *et al.*, 1983; Rawson *et al.*, 1978), and the associated problems of fitting the fossil assemblages into correlatable biostratigraphic schemes. Biostratigraphic zonation schemes proposed for the Late Cretaceous sequences in southern England are based therefore on blended fauna and are either specific to the area or lack detailed definition.

3.2 Macrofossil Zonation

The classical macrofossil biostratigraphic zonation of the Late Cretaceous is based on ammonites (Table 3.1). However, in France, England and eastward across northern Europe, most of the late Cretaceous is developed as a white-chalk facies with few

ammonites and virtually no rudists (Rawson *et al.*, 1978). This northern region can be divided into faunal subprovinces, which Rawson *et al.* (1978) describe as:

(a) A southern subprovince, which incorporates the Chalk of the Anglo-Paris Basin. Echinoderms are the prevalent type of macrofauna, with bivalves (including Inoceramus) and brachiopods being of less importance. Ammonites, however, are rare, with belemnites moderately common only during the Late Cretaceous. A zonation, largely based on echinoids below the belemnites above, originally proposed by Hebert (1863) in northern France, introduced to England by Barrois (1876) and extended by Jukes-Browne (1904), Rowe (1908), Griffith and Brydone (1914) and Gaster (1941) has achieved acceptance.

(b) A Northern subprovince including Yorkshire, Lincolnshire and parts of north Norfolk extends across the North Sea to Denmark, Germany, Poland and then south-eastward to the northern slopes of the Caucasus in the Soviet Union. Echinoderms are less common, with those that are typical of both subprovinces existing in different proportions. Furthermore, the macrofauna contain more belemnites, inoceramids and porifera, and even a few ammonites. The geographically northern Chalk of Northern Ireland belongs to the southern subprovince.

Different zonal schemes have been proposed for both "Boreal" Yorkshire and the "northern temperate zone" of southern England (see Wright, 1942; Peake & Hancock, 1961; Reid, 1973, 1976; Wood, in Smart & Wood, 1976; Bailey *et al.*, 1983) hindering correlation between the regions.

However, similarities do exist between the zonal schemes of the two subprovinces. A common belemnite zonation is recognisable in both subprovinces for the Campanian and late Santonian stages (Rawson *et al.*, 1978).

With regards to an overall macrofossil biostratigraphic scheme for north-west Europe the Late Cretaceous strata of Britain are of great significance. Within these deposits, fauna characteristic of both the northern and southern subprovinces exist. Though a

distinct faunal divide can be inferred across Britain in northern East Anglia, Rawson *et al.* (1978) proposed a biostratigraphic scheme based solely on macrofossil zones which could be recognised throughout the British Isles. From a stratigraphical point of view, the scheme of Rawson *et al.* (1978) is of great importance, since it provides a basis for correlation between the two subprovinces.

Though subzones, especially in southern England, can be distinguished, a degree of refinement must be sacrificed in order to establish a general zonation adaptable to the region as a whole. A summary table of Late Cretaceous stages and associated zones for the UK, as proposed by Rawson *et al.* (1978), is shown in Table 3.2.

3.3 Foraminifera zonation

Planktic foraminiferal species were almost entirely ignored as stratigraphic markers until the 1940s because the morphological differences between species were not fully appreciated. Numerous workers have since noted and attempted to use foraminifera as stratigraphical markers. However, it was not until Bolli (1966) made an attempt to fit all the available data into a global scale scheme from the Aptian to Maastrichtian that a foraminifera biostratigraphic zonation gained acceptance. Neither the principles of zonation nor the degree of resolution have since been fundamentally modified. Each zone is based on the first and last occurrence of a marker species, some of which represent well established lineages (Caron, 1985). Bolli (1966) originally proposed 19 zones. The present general zonation, which spans an interval of 55 million years from the Hauterivian to Maastrichtian, comprises 28 zones. Table 3.3 indicates the planktic foraminifers zonal scheme of Caron (1985) for the Coniacian to Campanian.

The Cretaceous stratotypes were defined in sediments of an epicontinental sea rich in megafossils, including pelagic forms such as ammonites and belemnites, but poor in planktic foraminifera. It has been necessary to go to other more favourable areas to correlate ammonite assemblages to planktic foraminiferal assemblages. Such correlations are obtained by using previously established ammonite zonal schemes and undertaking simultaneous investigations of macro- and microfossils from well suited

sections rich in faunas.

Close agreement now exists when comparing the several established general zonal schemes, with the assemblage zones of Van Hinte (1976) and Sigal (1977) serving as the basis for most biostratigraphic investigations in recent years. However, due to the inequality in numbers and complexity of taxa between warm and cold provinces, tropical zonal schemes have been preferred when defining general zonal schemes (see details in Robaszynski & Carron, 1979).

Nevertheless, zonal schemes for different geographic or climatic areas have become established. No orbitoid foraminifera are present within the Late Cretaceous white-chalk of northern Europe (Rawson *et al.*, 1978). However, smaller foraminifers are common and published stratigraphical work corresponds to existing macrofaunal zones. Hart *et al.* (1989) defines benthonic and planktic foraminifer zonations from a composite succession based on sections in the Isle of Wight, Kent, Norfolk and offshore boreholes (Table 3.4). Bailey *et al.* (1983) provides a benthic foraminifera biostratigraphy for the Late Cretaceous sequences of southern England and correlates them with Rawson *et al.* (1978) macrofossil zonation (Table 3.5).

3.4 Calcareous nannofossil zonation

Coccoliths are tiny calcite plates produced by unicellular marine algae (coccolithophorids). Fossil coccoliths, together with small calcite bodies called nannoliths constitute calcareous nannofossils. Such fossils have proved to be extremely useful for the biostratigraphy of Cretaceous marine sediments (Perch-Nielsen, 1985). The sequence of F.O.s and L.O.s of many species is quite well known and various authors have used different combinations of these to establish zonal schemes for different geographic or climatic areas (e.g. Perch-Nielsen, 1977; Wise, 1983; Roth, 1983; Doeven, 1983; Roth, 1973; Martini, 1976). While the sequence of calcareous nannofossil events is not exactly the same all over the world (Perch-Nielsen, 1985) and all facies, the zonation of the Upper Cretaceous is well advanced (Perch-Nielsen, 1985). In many cases, the zones are defined by F.O.s and the L.O.s

of a calcareous nannofossil of unknown ancestor and thus there are no problems of species distinction in these cases (Perch-Nielsen, 1985).

The correlation of coccolith zones and classical stages has been studied repeatedly from material collected from the stratotype localities of the stages (e.g. Manivit *et al.*, 1979). However, since coccolith content is sometimes very poorly preserved or coccoliths completely absent, correlations have had to be made via other fossils. As a consequence, boundaries have been shifted higher or lower depending on the authors own preferences, tradition (or wishful thinking!). Perch-Nielsen (1979) provides an overview.

Calcareous nannofossils are abundantly preserved within the Chalk. However, although the Upper Cretaceous chalk is essentially composed of calcareous nannofossils, their preservation is frequently poor due to the effects of pore fluid movement (Hart *el al.*, 1987). The calcareous nannofossil zonation provided for this study by Dr. J.A. Burnett is based on the Tethyan nannofossil zonation scheme (CC zones) of Sissingh (1977), as amended by Perch-Nielsen (1979, 1985) (Table 3.5). However, the nannofloras within the Chalk sequences of southern England appear to belong to neither the Tethyan or the Boreal realms.

	STAGE	AMMONITE ZONATION
LATE CRETACEOUS	CAMPANIAN	*Bostrychoceras polyplocum*
		Hoplitoplacenticeras vari
		Diplacnoceras bidorsatum
	SANTONIAN	*Placenticeras syrtale*
		Texanites texanus
	CONIACIAN	*Parabevahites emscheri*
		Barroischeras haberfellneri

Table 3.1. The "standard" Senonian ammonite zones (Arkell et al., 1957).

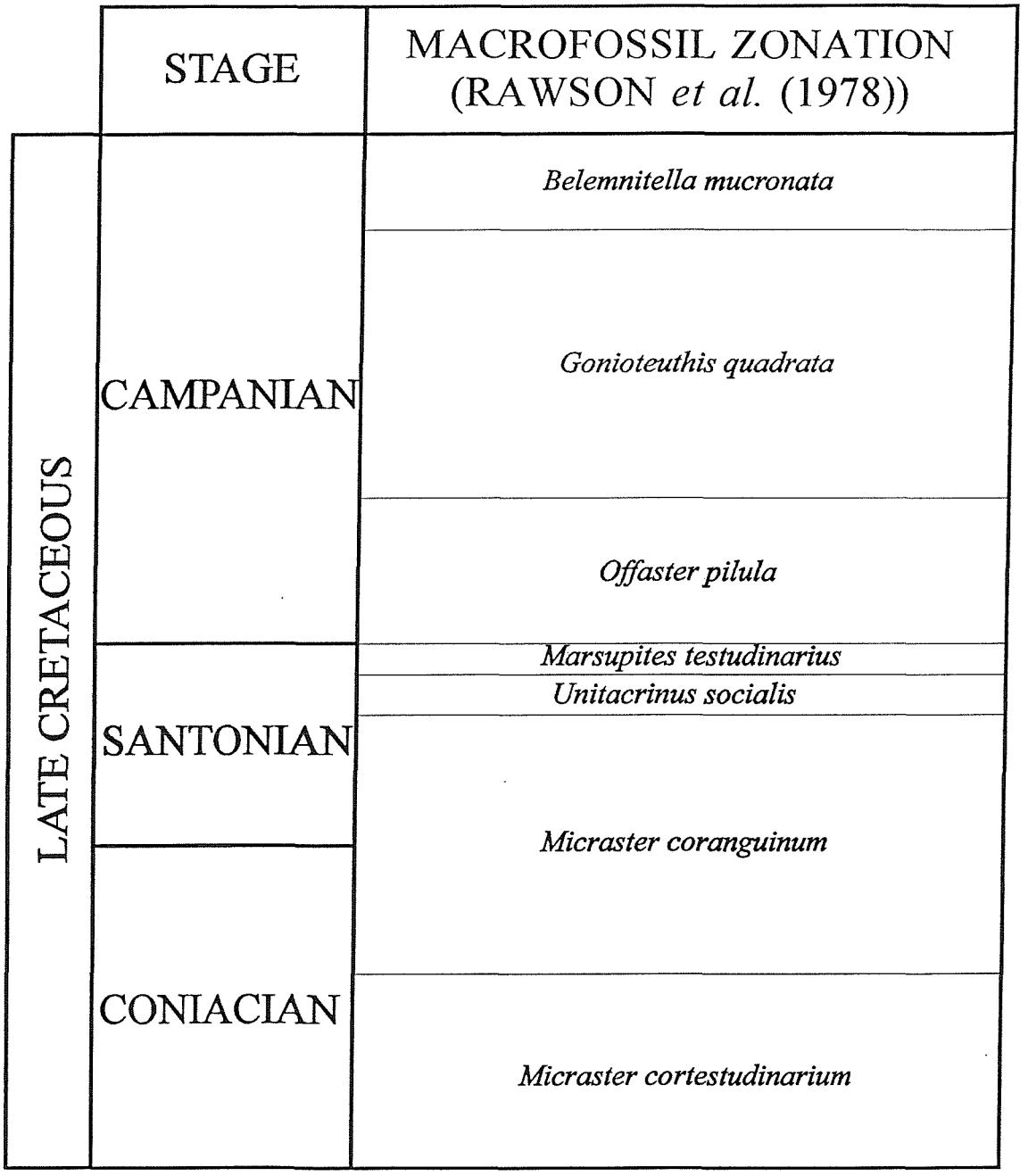

Table 3.2. The traditional biostratigraphy for the British Late Cretaceous based on belemnite and echinoid zonation (Rawson *et al.*, 1978).

	STAGE	PLANTIC FORAMINIFERA ZONATION (CARON, 1985)
LATE CRETACEOUS	CAMPANIAN	*Globotruncanita calcarata*
		Globotruncanita ventricosa
		Globotruncanita elevata
	SANTONIAN	*Dicarinella asymetrica*
	CONIACIAN	*Dicarinella concavata*
		Dicarinella primitiva

Table 3.3. Planktic foraminiferal zonal scheme of Caron (1985) for the Coniacian to Campanian, based on Tethyan fauna.

	STAGE	UK ZONATION: UK BENTHIC FORAMINIFERA (HART *et al.*, 1989)	UK ZONATION: UK PLANKTIC FORAMINIFERA (HART *et al.*, 1989)
LATE CRETACEOUS	CAMPANIAN	UKB.17 *Gavelinella monterelensis/ Gavelinella usakensis*	UKP.13 *Globotruncana rugosa*
		UKB.16 *Bolivinoides culverensis*	UKP.12 *Rugoglobigerina pilula*
		UKB.15 *Bolivinoides strigillatus*	
	SANTONAN	UKB.14 *Stensioeina granulata polonica*	UKP.11 *Globotruncana linneiana*
		UKB.13 *Stensioeina exsculpta exsculpta*	UKP.10 *Dicarinella primitiva*
	CONIACIAN	UKB.12 *Stensioeina granulata granulata*	
		UKB.11 *Ruessella kelleri*	UKP.9 *Whiteinella baltica*

Table 3.4 Benthic and planktic foraminiferal zonations for the British Late Cretaceous (Hart *et al.*, 1989).

	STAGE	FORAMINIFERAL ZONATIONS FOR LATE CRETACEOUS OF SOUTHERN ENGLAND: FORAMINIFERAL BIOZONES	LOCAL FORAMINIFERAL ASSEMBLAGE BIOZONES
LATE CRETACEOUS	CAMPANIAN	*B.decoratus*	
		B.culverensis	*P. quaternaria*
			E. galeata
			G.usakensis
			G.cristata
	SANTONIAN	*B.strigillatus*	*Gavelinella cristata / Globigerinelloides rowei*
		S.g. perfecta	
		S.g.polonica	*Cubiciles ex. gr. beaumontianus*
	CONIACIAN	*S.exsculpta exsculpta*	*L. eleyi*
		S.granulata granulata	*Lingulogavelinella sp. cf. L. vombensis*

Table 3.5. Benthic foraminiferal biostratigraphy for the Late Cretaceous sequences in southern England (from Bailey *et al.*, 1983).

	STAGE	CALCAREOUS NANNOFOSSILS (SISSINGH, 1977)	
LATE CRETACEOUS	CAMPANIAN	CC23	*Tranolithus phacelosus*
		CC22	*Quadrum trifidum*
		CC21	*Quadrum sissinghi*
		CC20	*Ceratolithoides aculeus*
		CC19	*Calculites ovalis*
		CC18	*Aspidolithus parcus*
		CC17	*Calculites obscurus*
	SANTONIAN	CC16	*Lucianorhabdus cayeuxii*
		CC15	*Reinhardtites anthophorus*
		CC14	*Micola decussata*
	CONIACIAN	CC13	*Marthasterites furcatus*
		CC12	*Lucianorhabdus maleformis*

Table 3.6. Calcareous nannofossil zonation of Sissingh (1977) for the Coniacian to Campanian, based on Tethyan fauna.

Chapter 4 Late Cretaceous Magnetostratigraphy

4.1 The marine magnetic anomaly record

The most abundant source of information on the pattern of geomagnetic field reversals from the Late Jurassic onwards, is the marine magnetic anomaly record (Hailwood, 1989). However, these records provide no information on the ages of successive reversals unless they are combined with biostratigraphic or isotopic data.

The term 'magnetic anomaly' describes a local departure of the geomagnetic field intensity from the smooth regional value specified by the International Geomagnetic Reference field. The nature of the magnetic anomaly depends on the composition, concentration and distribution of magnetic mineral grains within the near surface rocks and the direction of magnetisation of those rocks (Hailwood, 1989).

The development of the nuclear precession (proton) magnetometer by Packard & Varian (1954) enabled the absolute determination of the total field intensity and greatly facilitated marine magnetic surveys. Mason (1958) reported the first detailed marine magnetic survey, using a proton magnetometer, off the west coast of the U.S.A. This study revealed an extensive pattern of elongate contours of alternating positive and negative values with a local north-south trend. Further study showed that the lineated anomalies, with typical widths of 10-100 km and lengths in excess of 1000 km, were disposed parallel to the mid-oceanic ridges.

Lineated magnetic anomalies are the result of periodic changes in the direction of remanent magnetisation of sea-floor rocks with distance from the mid-ocean ridges. Vine & Mathews (1963) proposed a model to account for these observations, which combined the known occurrence of geomagnetic reversals at irregular intervals in the geological past with the sea-floor spreading hypothesis of Dietz (1961) and Hess (1962). Hot material rises beneath the mid-ocean ridge axes as a result of Upper Mantle convection. Basaltic magma is generated by near surface partial melting and is emplaced at or beneath the mid-ocean ridge crest, creating new ocean crust. Older

sea-floor is displaced to either side leading to the sea-floor spreading away from the ridge axes.

As the newly formed strip of basaltic crust cools through the Curie temperature of magnetic constituents, acquisition of a strong and stable TRM results. The polarity of the ambient geomagnetic field at this time is thus recorded. The displacement to either side of older rocks, which have acquired their magnetic remanence during a period of different polarity, explains the alternation in the directions of remanent magnetisation of sea-floor rocks and the symmetry of anomaly patterns on either side of mid-ocean ridge axes.

Irregularities in the sea-floor depth and magneto-mineralogical composition of sea-floor rocks creates a certain amount of 'noise' within the marine magnetic anomaly record. However, the correlation between the observed pattern of anomalies and the sequence of geomagnetic polarity changes defined by other methods is remarkable (Hailwood, 1989). Numerous extensive marine magnetic surveys have since revealed symmetrical patterns of lineated magnetic anomalies in all the world's ocean basins.

Pitman *et al.* (1977) proposed a convention, which has achieved popular acceptance, whereby successive conspicuous peaks in magnetic anomaly sequences are numbered in sequence away from the ridge crest. These anomaly numbers, which form the basis of the chron numbering scheme for the Cenozoic to Late Cretaceous (Chrons "C1" to "C34"), refer to normal polarity intervals. Anomalies 29 to 34 represent the Late Cretaceous period.

In many detailed studies of magnetic anomalies from fast spreading ridges, linear and small scale magnetic anomalies ("tiny wiggles"), that are clearly related to palaeomagnetic behaviour, are observed (e.g. Cande & Kent, 1992). However problems exist in interpreting these anomalies.

It is unclear whether "tiny wiggles" are due to short polarity intervals. Larger amplitude features are obviously due to full reversals and can, occasionally, be

correlated with magnetostratographically-identified short polarity intervals. However, most of the smaller amplitude anomalies have not been confirmed in this way and have been modelled as either due to short polarity intervals (Blakely, 1974) or longer period intensity variations of 50 to 200 kyr in duration (Cande & La Breque, 1974). In addition, the record of "tiny wiggles" is not uniform, due to the unevenness of track coverage in different areas of the ocean basins and the fact that the ocean crust has recorded some time intervals with higher resolution than others.

4.1.1. The Late Cretaceous marine magnetic anomaly record

The pattern of marine magnetic anomalies observed in various ocean basins for the Late Cretaceous incorporates anomalies 29 to 34. No regular marine magnetic anomalies are observed on Cretaceous sea-floor older than mid-Cretaceous (older than anomaly 33). As a result of this absence, these regions of sea-floor have been termed the Cretaceous Magnetic Quite Zones. The lack of anomalies indicates that the Earth's magnetic field under went few reversals during the mid-Cretaceous with the geomagnetic field maintaining a dominantly normal polarity. This period has been referred to by Cox (1982) as the *long Cretaceous normal interval* or the *Cretaceous normal polarity superchron*. The occurrence of a long interval of constant normal polarity in the mid-Cretaceous is consistent with observations from mid-Cretaceous rocks exposed on land (Helsley & Steiner, 1969; Channell *et al.*, 1982).

Figure 4.1 shows the reversal pattern recently published as part of Cande & Kent's (1992) 'Geomagnetic Polarity Time Scale for the Late Cretaceous and Cenozoic'. Though some intervals of the anomaly record are well covered, either because of exceptionally detailed surveys or because of good coverage in periods of very fast spreading, an equivalent high resolution record of the geomagnetic field is not, at present, available for anomalies 27 to 34 (Cande & Kent, 1992). As a result Cande & Kent (1992) were unable to model for "tiny wiggles" during this interval.

4.2 Magnetostratigraphy of Late Cretaceous sedimentary sequences exposed on land.

Opdyke (1972) showed that Quaternary and Neogene pelagic deposits in deep sea cores carried reliable records of geomagnetic polarity reversals. The possibility that uplifted sections of indurated Mesozoic and Late Palaeozoic pelagic sediments might carry a similar record lead to an interest in sections exposed in the Umbrian Apennines of northern Italy. Initially, palaeomagnetic investigations of these weakly magnetic formations were inhibited by the limited sensitivity and slow measurement times of laboratory magnetometers (Hailwood, 1989). However, with the development of cryogenic magnetometers, which were capable of more rapid and precise measurements, the systematic investigation of these sections began. Alvarez *et al.* (1977) presented the first comprehensive magneto-biostratigraphical investigation. This provided the first complete biostratigraphical calibration of the sequence of geomagnetic polarity reversals during the Late Cretaceous from one locality.

4.2.1. A Magnetostratigraphic "type section" for the Late Cretaceous

Sedimentological, palaeontological, stratigraphical and palaeomagnetic investigations in a biostratigraphically complete and well-exposed sequence of limestone in the Bottaccione Gorge, near Gubbio, northern Italy have enabled Alvarez *et al.* (1977) to delineate a series of magnetic polarity zones for the Late Cretaceous to early Paleocene.

The pink Scaglia Rossa limestone of Gubbio was deposited under pelagic conditions and consists of foraminifera and coccolith remains (Alvarez *et al.*, 1977). The rate and the type of sedimentation was relatively constant and has formed a well indurated lithology (Alvarez *et al.*, 1977). Foraminifera are abundant within the sequence and have been used to tie the section into the standard planktonic foraminiferal zonations (Alvarez *et al.*, 1977). However, separation of the foraminifera from the limestone matrix proved difficult and as a result identification was carried out in thin section. Nannoplankton were not well preserved while other microfossils and macrofossils were

extremely rare (Alvarez *et al.*, 1977). Stratigraphically, the section is continuous across the Maastrichtian-Paleocene boundary; a significant feature since this important geological boundary is typically marked by an hiatus elsewhere in the world (Luterbacher & Premoli Silva, 1964).

The limestones posses a weak remanent magnetism but after demagnetization of secondary components a stable, well grouped component is revealed (Alvarez *et al.*, 1977).

Though small faults, with displacements less than 1 metre, are present in the sequence, continuity of faunal zones and the close match between reversal sequences confirm the absence of structural disturbance (Alvarez *et al.*, 1977).

Twenty-three physical magnetostratigraphic units of polarity zones have been recognized in the Gubbio section (Figure 4.2). Alvarez *et al.* (1977) designated each with an identification tag. The lowest zone, which appears to represent the long normal episode of the late Cretaceous is referred to as the 'Gubbio Long Normal Zone'. The following zones were designated letters in ascending alphabetical order and allotted the prefix Gubbio. Normal zones are distinguished by '+' and reversed zones '-'. Furthermore, Alvarez *et al.* (1977) recognise some very thin polarity zones and in accordance with the hierarchy of units recommended by the Subcommission on Magnetostratigraphic Nomenclature (1973) refer to these as 'subzones'. For example, the subzones Gubbio D1+, D2- and D3+ make up the Gubbio D+ Zone. The procedure employed in designating the reference labels is analogous to standard practice in lithostratigraphy. Where a section comprises a series of formations and further subdivision is required, the formations may be divided into member units. Each polarity zone recognised in the Gubbio exposures was formed during a period of either normal or reversed geomagnetic polarity. Alvarez *et al.* (1977) refer to these abstract units of time as polarity 'chrons'. By adopting the term 'chron' (*after* Hedberg 1976, p69) instead of 'polarity interval' Alvarez *et al.* (1977) depart from the recommendations of the Subcommission (1973). However, Alvarez *et al.* (1977) believe that a 'chron' refers clearly to time whereas the term 'polarity interval' is

ambiguous. It may, for example, also refer to a lithostratigraphic unit. By identifying such a unit of time with the corresponding zone of the rock record it is possible to refer, for example, to the Gubbio G- Polarity Chron as a unit of time that spans the very latest Cretaceous and the very earliest Paleocene (Alvarez *et al.*, 1977). The magnetic zonal boundaries of Alvarez *et al.* (1977) are shown in Figure 4.2 along with the relative positions of foraminiferal zones of Premoli Silva (1977) (column 7) and various proposed absolute chronologies (columns 8, 9, 10 and 11). The following observations were made by Alvarez *et al.* (1977):-

(i) Although the base of the Gubbio (Cretaceous) Long Normal Zone was not dated by their study, they state that it is at least as old as the Cenomanian.

(ii) The Gubbio Long Normal Zone ends very close to the Santonian-Campanian boundary, at the base of the Gubbio A- Zone.

(iii) The Campanian-Maastrichtian boundary falls near the top of the relatively long Gubbio B+ Zone.

(iv) All Late Cretaceous reversed polarity zones except Gubbio A- are of Maastrichtian age.

(v) In contrast with the Campanian, the Paleocene and Maastrichtian are generally characterized by polarity zones that represent relatively short time intervals.

(vi) The Cretaceous-Tertiary boundary falls near the top of the polarity zone Gubbio G-.

(vii) The section studied does not reach the Paleocene-Eocene boundary, which must occur slightly above the Gubbio N+ zone.

Alvarez *et al.* (1977) also note that 'the calibration of the geomagnetic polarity history

in terms of years remains somewhat uncertain because of inaccuracies in the radiometric age determinations and in correlations between radiometrically dated rocks and those that contain fossils'. Alvarez *et al.* (1977) have, in Figure 4.2 (columns 8 through 11), assigned dates from three contemporary time-scales to the various biostratigraphic boundaries in the section.

In an attempt to corroborate the conclusions drawn from the palaeomagnetic investigation of the Gubbio section, Lowrie & Alvarez (1977b) undertook an investigation of the Moria section, Italy, which lies 16 Km to the north of Gubbio. The polarity sequence was labelled using the zonal scheme devised for the Gubbio section (Alvarez *et al.*, 1977).

Polarity can be determined from either declination or inclination alone. However, it is most safely interpreted on the combination of both these data (Alvarez & Lowrie, 1978). This is conveniently expressed as a single parameter - the computed latitude of the virtual geomagnetic pole (VGP) - and this parameter was employed by Alvarez & Lowrie (1978) in their study at Moria.

A clear difference exists between the lower half of the section at Moira, which is characterized by unbroken polarity, and the upper half, where there are multiple reversals. The lower half corresponds to the Gubbio Long Normal Zone (Alvarez *et al.*, 1977) and to the Cretaceous Quiet Zone of marine magnetic studies. The upper half of the section displays numerous reversals which are well marked, with abrupt changes of hemisphere in the VGP latitude. Only one exception exists and that is the boundary between the Gubbio A- and B+ zones, in which the VGP latitude swings back and forth over a 9 metre transition zone. Alvarez & Lowrie (1978) have identified a minor fault in the section and signs of bedding disturbance in the interval 211-213 metres, which they believe may account for the uneven polarity transition. However, Lowrie and Alvarez (1977b, Figure 9) have noted that there was a similar disturbed zone at the B+/A- boundary in the Gubbio section. Though these disturbances occur at similar levels they may be simply coincidental. However, they occur close to the top of the lower cherty member of the Scaglia Rossa (Alvarez &

Lowrie, 1978), and the presence or absence of chert might cause the limestone to display slightly different mechanical properties resulting in a decoupling at this horizon (Alvarez & Lowrie, 1978). Alternatively, the magnetisation associated with the diagenetic remobilization of silica to form chert may have effected the magnetization of the limestone. Furthermore, the corresponding section of the marine magnetic record (anomaly 33) shows no signs of gradual polarity transition (Alvarez & Lowrie, 1978).

Apart from this single exception, the polarity sequence at Moira is well defined and corresponds to the Gubbio polarity sequence from the Cretaceous Long Normal Zone to the Gubbio I- Zone (Alvarez & Lowrie, 1978). Only the two thinnest polarity subzones (C2+ and F2-) remained undetected but on comparing polarity zone thickness in the two sections an excellent correlation could be established (Alvarez & Lowrie, 1978). Remanent magnetic intensity varied in a cyclic pattern which was virtually identical in both the Gubbio and Moria sections (Alvarez & Lowrie, 1978, figure 9). Alvarez & Lowrie (1978) concluded that 'the result from the Moria section provides strong confirmation of the validity of the magnetic polarity sequence established at Gubbio'.

4.2.2 Correlation of magnetostratigraphic sections in the Umbrian Apennines and southern Alps

The Late Cretaceous pelagic limestones and marls of the Umbrian sequences in the northern peninsular of Italy have yielded excellent records of magnetic polarity and foraminiferal evolution (Lowrie & Alvarez, 1981). In addition, these records can be precisely linked because for each stratigraphical level the magnetic and palaeontological information both come from the same small sample (Lowrie & Alvarez, 1981).

Magnetostratigraphy of the Late Cretaceous has been evaluated in four overlapping sequences of carbonate rocks, three in Umbria and one in the southern Alps. Figure 4.3 shows the Umbrian and southern Alpine sections for which detailed

magnetostratigraphy has been measured. The reversals are confirmed by duplication in separate sections, thus fulfilling a fundamental credibility criteria. The Cretaceous results have been reviewed by Lowrie *et al.*, (1980). Details have been reported in the following papers: Bottaccione; Premoi Silva *et al.* (1974), Lowrie & Alvarez (1975, 1977a, 1977b), Roggenthen and Napoleone (1977), Alvarez *et al.* (1977): Moria; Alvarez & Lowrie (1978), Vandenberg *et al.* (1978); Furlo Upper Road: Alvarez & Lowrie (1980); Cismon, in the southern Alps: Channell *et al.* (1979). A composite magnetic stratigraphy for the Upper Cretaceous has been produced by compiling the confirmed reversals (Figure 4.3).

4.2.3 Correlation between the Gubbio section and the marine magnetic anomaly record

For magnetostratigraphy to reach its full potential and define a geomagnetic polarity time-scale (GPTS) the marine magnetic anomalies and the magnetostratigraphy of vertically accreted sequences of sedimentary and volcanic rocks need to correspond closely with each other, be correlated with the biostratigraphic time-scale, and be graduated in terms of absolute age by correlation with radiometrically or isotopically dated rocks (Alvarez *et al.*, 1977).

Figure 4.4 compares the sequence of polarity intervals deciphered from the section at Gubbio with three marine magnetic anomaly profiles and their interpreted reversal sequences. Within each of these oceanic areas the boundary between the Cretaceous Quiet Zone and the Late Cretaceous-Cenozoic anomaly sequence has been identified. The reversal sequences constructed from the marine magnetic measurements have been uniformly reduced to enable the 'base' of anomaly 29 and the 'top' of the Cretaceous Quiet Zone to be aligned with analogous horizons in the Gubbio column (Lowrie & Alvarez, 1977a).

It is immediately apparent from inspection of Figure 4.4 that a close correlation exists between the Gubbio column and the three marine reversal sequences. Furthermore, Figure 4.4 suggests that the pelagic sediments of the Scaglia Rossa and the oceanic

crust in these areas were recording the same sequence of geomagnetic field inversions (Lowrie & Alvarez, 1977a). Though the pattern of polarity intervals is the same for all the columns, no exact match can be shown to exist between them. However, this can be explained by the independent variations in the sedimentation rate of the Gubbio section and in the spreading rates of the three oceanic areas. On comparing the three oceanic profiles, Lowrie & Alvarez (1977a) concluded that at least two or three changes in the spreading rate in each ocean occurred over an approximate time-span of 20 million years. Figure 4.4 does, however, suggest that there has not been a lasting order-of-magnitude difference in either sedimentation rate at Gubbio or in the spreading rate in the oceanic areas examined (Lowrie & Alvarez, 1977a).

Most of the known Late Cretaceous-Early Tertiary stratigraphic sections in the world do not include the lowest portion of the Palaeocene. However, Luterbacher & Premoli-Silva (1964) have shown that the Gubbio section is more or less continuous across the Cretaceous-Tertiary boundary. Moreover, this boundary can be distinguished by the disappearance of large globotruncanids within the sequence, and falls at a height of 347.6 metres in the measured section of Arthur & Fisher (1977). This is very close to the top of the Gubbio G- reversed polarity zone and corresponds, in the marine magnetic profiles, to the reversed segment preceding anomaly 29 (Lowrie & Alvarez, 1977a). The position of this boundary is further supported by Sclater *et al.*, (1974) who place the Cretaceous-Tertiary boundary between anomalies 29 and 30.

Data from the lower parts of the Gubbio Upper Cretaceous section demonstrate a geomagnetic field with a constant normal polarity. This helps to confirm that the Cretaceous Magnetic Quiet Zone, as seen on marine magnetic anomaly profiles, is due to a lack of polarity inversions and not due to an ineffective magnetic recording mechanism in the oceanic crust (Lowrie & Alvarez, 1977a).

4.2.4 Polarity Chron C33N-C33R

The Late Cretaceous sequence of southern England extends into the early Late

Campanian and on investigation should reveal evidence, in ascending order, of Chron C34N, C33R and C33N. Several recent magnetostratigraphic studies have attempted to locate these magnetzones in a variety of different sedimentary facies. A brief review of the results from these studies is presented below.

Pechersky *et al.* (1983) presented a review of magnetostratigraphical data from the U.S.S.R on the Late Cretaceous Quiet Zone (Chron C34N). Molostovsky *et al.* (1976) had previously subdivided the Mesozoic Era into magnetohyperzones and named them after the place where they were first identified. Chron C34N was first discovered by Shmeleva (1963) in gypsiferous red bed deposits of the Fergana Ridge (U.S.S.R) and was named the normal geomagnetic polarity zone of Jalal. In addition, Shmeleva (1963) found that this magnetohyperzone contained a reverse magnetozone at its top which was subsequently named Kuldja (Chron C33R). The reverse polarity interval has since been traced to several regions of the U.S.S.R and discovered in a variety of different facies. The Kuldja Zone corresponds to magnetozone Gubbio A-. However, where Alvarez *et al.* (1977) and following authors locate the base of this Zone just above the Santonian/Campanian boundary, palaeontological data from the Russian successions suggests that Chron C33R straddles this boundary. Perchersky *et al.* (1983) concluded that the problem lies in the correlation of biostratigraphic zones defined by different groups of fossils. Correlation of planktic and benthic zones with each other and with macrozones lack precision throughout the Late Cretaceous. Zonal boundaries based on different groups of fossil species need not coincide with stage boundaries.

Hambach & Krumsiek (1991) have studied Chron C33 (R,N) for the first time in the Boreal Cretaceous using samples from a marl and limestone core (Metelen 1001) and mine shaft (Radbod 6) in the Munster Cretaceous Basin (NW-Germany). The biostratigraphy of Rescher (1991) was used to assign a Mid-Santonian to early Upper Campanian age to these sediments. However, even though their magnetostratigraphy correlates well with ammonite biostratigraphic zones, it was impossible to fix Chron C33R into a biostratigraphic framework since this magneto-biostratigraphy contradicts the stratigraphy based on benthonic foraminifera. Hambach & Krumsiek (1991)

believe that nannofossils may provide the solution to this problem. Regardless of the biostratigraphic contradictions they concluded that within this interval reversed polarity occurs from the basal Campanian just into the Upper Campanian and includes a mixed polarity zone. This pattern agreed with those published by Keating & Herrero-Bervera (1984) and Fry *et al.*, (1985).

Lerbekmo (1989) undertook a magnetostratigrapahic investigation on middle to lower Campanian strata of the Foremost and Pakowki formations in the Milk River area of southeastern Alberta to determine the position of the Chron C33N-C33R polarity boundary. This magnetozone boundary was located within the *B. asperiformis* ammonite zone of the Western Interior Basin. As with the study of Hambach & Krumseik (1991) ammonite and foraminiferal biostratigraphic zonation schemes contradict each other (Eaton, 1987). According to Bergstresser & Frerichs (1982) study of foraminifera in the Pierre Shale the Campanian/Maastrichtian boundary should be placed at the *B. asperiformis* zone or lower. However, the results of Lerbekmo's (1989) study confine this ammonite zone to low in the Campanian of European foraminiferal sections since the C33N-C33R boundary, as revealed at Gubbio, lies just below the middle of the Campanian *G. elevata* foraminiferal zone.

It is apparent from the preceding studies that even though the pattern of geomagnetic polarity inversions is now relatively well established for this interval of time, problems remain in defining a stratigraphic age. However, these studies have demonstrated the synchroneity of the Santonian/Campanian reverse magnetozone and the negative oceanic magnetic anomaly (C33R) between Nos 33 and 34 (LaBreque *et al.*, 1977). Problems lie, not in the definition of Chron C33R, but in the correlations of biostratigraphic zones defined by different fossil groups.

4.3 Deep Sea Drilling Project Cores

The Deep Sea Drilling Project (DSDP) was initiated in 1968 and as a result, sediment cores recovered from the ocean basins have provided a wealth of new material capable of extending the biostratigraphically-calibrated GPTS further back into the Mesozoic.

Drilling disturbance in cores from early DSDP legs resulted in only isolated sections of core being suitable for magnetostratigraphic investigation. Nevertheless, Henry & Opdyke (1970) reported results from Leg 3 which demonstrated that the Cretaceous-Tertiary boundary occurs within a reverse polarity interval which corresponds with the reverse interval between Chrons C29N and C30N. Magnetostratigraphic studies on Upper Cretaceous sediments (Leg 7) cored in the south-west Pacific indicated that the Earth's magnetic field maintained a predominantly normal polarity throughout the Turonian and Cenomanian ages (Sclater *et al.*, 1974). This event corresponds with the long mid-Cretaceous period of normal polarity which occurred from the Barremian to Santonian. Keating & Helsley (1978a) reported results from a palaeomagnetic study of Cretaceous sediments from Site 369 which indicated that the Late Cretaceous was characterised by a long interval of normal polarity ranging in age from latest Campanian to Aptian. Three intervals of reversed polarity were found in sediments of middle Maastrichtian and late Aptian age. However, further work by Keating & Helsley (1978b), based on 2000 orientated samples, reported results from seven sites drilled in the south Atlantic Ocean (Legs 40, 41, 43 and 44) which represented a reversal sequence for the entire Cretaceous. These results confirmed the marine magnetic anomaly record and the magnetostratigraphic study of Alvarez *et al.*, (1977) from Gubbio.

Due to the potential quality and continuity of the magnetostratigraphic record in the DSDP cores a palaeomagnetic laboratory was installed on the drilling ship Glomar Challenger in 1976. This enabled the rapid acquisition of combined magnetostratigraphic-biostratigraphic data from the drilled core. Furthermore, the development of the Hydraulic Piston Corer (HPC) in 1979 enabled more continuous recovery of sediments than had been possible with the conventional rotary corer. Prior to the advent of the HPC, knowledge of the magnetostratigraphy of deep sea sediments was restricted by the maximum depth of penetration of traditional coring systems to the uppermost 25 to 30 metres of sediment (Tauxe *et al.*, 1980). A dramatic improvement in the quality of data has since resulted.

More recent studies have taken full advantage of the technological advances. Tauxe

et al. (1980) reported results from Leg 70 in which a Lower Palaeocene-Upper Cretaceous magnetostratigraphy was produced revealing Chrons C29 to C31. Chave (1980) carried out a magnetostratigraphic investigation on Lower Palaeocene-Upper Cretaceous sediments from Walvis Ridge in the south Atlantic (Leg 74). This study revealed reverse polarity intervals which correspond to the marine magnetic anomalies 29 to 32. Poore *et al.*, (1983) used overlapping sections in adjacent wells to produce the first direct and semi-continuous correlation of magnetostratigraphic and biostratigraphic time-scales for the Tertiary and Late Cretaceous, based almost exclusively on DSDP cores. Magnetostratigraphic results from Broken Ridge (Leg 121), where a polarity sequence spans middle Eocene to Upper Cretaceous deposits (Chrons C18/C20 to C34), have been reported by Gee *et al.*, (1991). This includes a 500 metre continuous sequence of sediment which extends downwards from the Lower Eocene (C23R) to below the Maastrichtian/Campanian boundary (C32R).

4.4 A geomagnetic polarity time-scale for the Late Cretaceous

Cande & Kent (1992) recently published a new magnetic polarity time-scale for the Late Cretaceous and Cenozoic based on the analysis of marine magnetic profiles from the world's ocean basin. This was the first time-scale since that of Heirtzler *et al.*, (1968) for which the relative widths of the magnetic polarity intervals, for the entire Late Cretaceous and Cenozoic, have been determined from magnetic profiles.

A composite geomagnetic polarity sequence was derived primarily from data from the South Atlantic. Distance to key anomalies were constrained along a synthetic flow line, located at 30°S, in the South Atlantic at intervals of 150 to 300 km and based on 9 finite rotation poles. These rotation pole changes occurred at the younger ends of anomalies 4A, 5C, 7, 13, 20, 24, 30, 33 and 34. The anomaly spacings were further constrained by adopting averages of stacked profiles.

Fine-scale information was derived from magnetic profiles on faster spreading ridges in the Pacific and Indian Oceans and inserted into the South Atlantic sequence. Cande & Kent (1992) have identified additional small scale anomalies' "tiny wiggles" that

represent either very short polarity intervals or intensity fluctuations of the dipole field from several intervals in the Cenozoic. However, during the Late Cretaceous they were unable to model any "tiny wiggles".

By assuming that the spreading rates in the South Atlantic were smoothly varying but not necessarily constant Cande & Kent (1992) produced a time-scale by using a spline function to fit nine age calibration points plus the zero-age ridge axis in the composite polarity sequence. The derived spreading history of the South Atlantic shows regular variation in the spreading rate. During the Late Cretaceous the spreading rate was at its maximum, reaching 70 mm/year at around anomaly 33-34 and decreased to as low as 30 mm/year by anomaly 27, during Palaeocene times.

Two age calibration points, based on K-Ar dates, were used for the Late Cretaceous portion of the Cande & Kent (1992) time scale. These were the Maastrichtian/Campanian boundary and the Campanian/Santonian boundary. In Umbria, the Maastrichtian/Campanian boundary lies in the later part of Chronozone C33N (Alvarez *et al.*, 1977). K-Ar dates obtained from bentonite at a biostratigraphically correlated level in the western interior of North America indicated an age of 74 to 75 Ma (corrected to new decay constants from Obradovich & Cobban (1975). This suggested an age of about 74.5 Ma for the Maastrichtian/Campanian boundary. Evidence which further supports this date was provided by Obradovich *et al.* (1986) who report $^{40}Ar/^{39}Ar$ dates of 73.4 Ma for a bentonite near the top of a normal polarity magnetozone identified as Chron C33N in the San Juan Basin, New Mexico. In addition, Cande & Kent (1992) report a date of 75.2±0.5 Ma which was obtained from a bentonite in southwestern Arkansas. This was located in the lower part of the *Globotruncana calcarata* Zone. From the results obtained at Umbria (Alvarez *et al.*, 1977) the base of the biozone occurs approximately a third of the way down Chron C33N and is thus 0.5 to 1 million years older than the Maastrichtian boundary at the *G. calcarata/G. tricarinata* Zonal boundary.

The Campanian/Santonian boundary was shown by Arthur & Fisher (1977) to be at a level several metres below the top of the Gubbio Long Normal Zone (Chron C34N).

From biostratigraphically-controlled $^{40}Ar/^{39}Ar$ dates on a bentonite in the western interior of North America, Obradovich *et al.* (1986) confirmed an age of about 84 Ma for the Campanian/Santonian boundary. This work was based on dates obtained by Obradovich & Cobban (1975) and corrected for a new decay constant. They estimate an age of 83 Ma for the stratigraphically younger C34N level.

Figure 4.5 shows an expanded section of the Cande & Kent (1992) geomagnetic polarity timescale for the Late Cretaceous, showing the proposed nomenclature of chrons and polarity events.

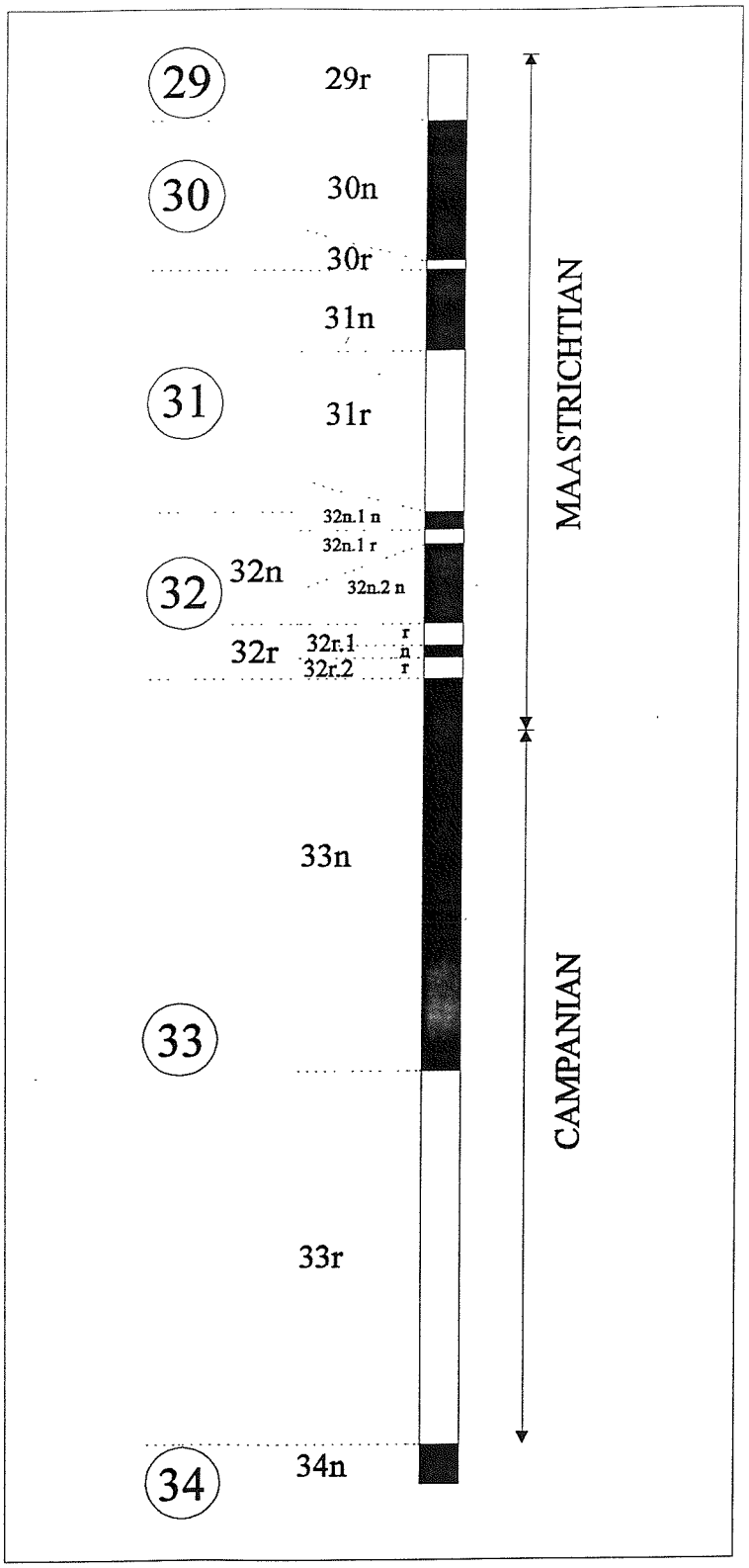

Figure 4.1. Marine magnetic anomaly pattern for the Late Cretaceous showing detailed nomenclature of chrons and polarity events (from Cande & Kent, 1992).

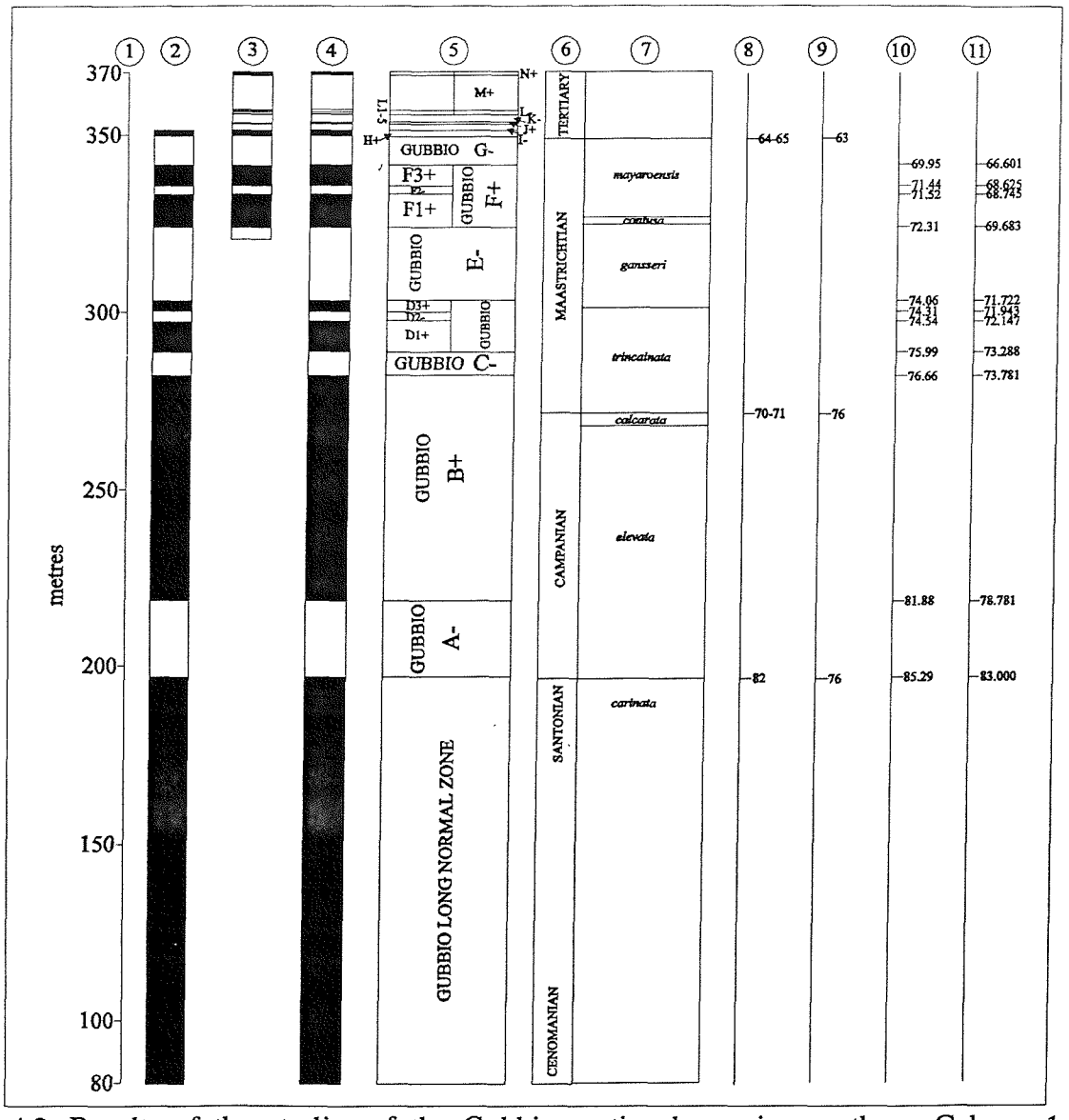

Figure 4.2. Results of the studies of the Gubbio section by various authors. Column 1: measured section in metres (Arthur & Fisher, 1977). Column 2: magnetic results of Lowrie & Alvarez (1977a); black is normal polarity, white is reversed. Column 3: magnetic results of Roggenthen & Napoleone (1977). Column 4: combined magnetic results. Column 5: designation of polarity zones; '+' indicates normal polarity, '-' indicates reverse polarity; zones Gubbio D+, F+, and L+ have been divided into subzones. Column 6: chronostratigraphic units. Column 7: planktic foraminiferal zones of Premoli Silva (1977). Columns 8 through 11: absolute age calibration according to four proposed time scales. 8: Obradovich & Cobban (1975). 9: van Hinte (1972). 10: Harland *et al.* (1989). 11: Cande & Kent (1992). Palaeocene-Eocene boundary age from Berggren (1972) in all cases (Alvarez *et al.*, 1977).

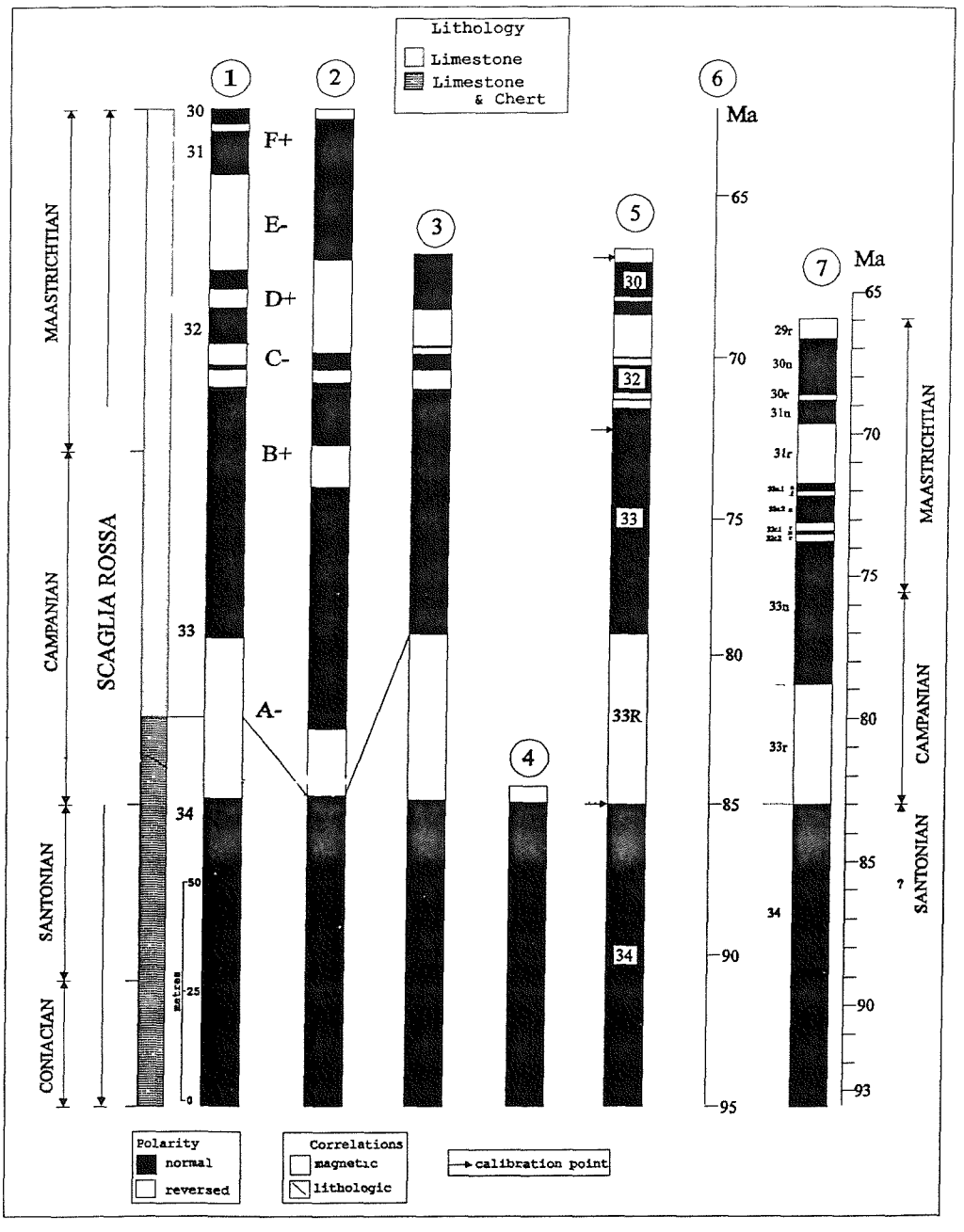

Figure 4.3. Correlation of magnetostratigraphic sections in the Umbrian Apennines and southern Alps with sea-floor magnetic anomalies. Left- hand columns: age (from foraminiferal zonation), formation name and lithology. Columns 1 to 4: detailed magnetostratigraphic sections (references given in text). Column 1: Bottacione. Column 2: Moria. Column 3: Furlo upper road. Column 4: Cismon (S. Alps). Column 5: magnetic-reversal sequence determined from sea-floor magnetic anomalies by LaBreque *et al.* (1977) and redated by interpolation between nine palaeontologically controlled calibration points. Three calibration points, used for the Late Cretaceous, are marked by arrows. Column 6: time-scale (Lowrie & Alvarez, 1981). Column 7: geomagnetic polarity time-scale showing detailed nomenclature of chrons and polarity events (Cande & Kent, 1992).

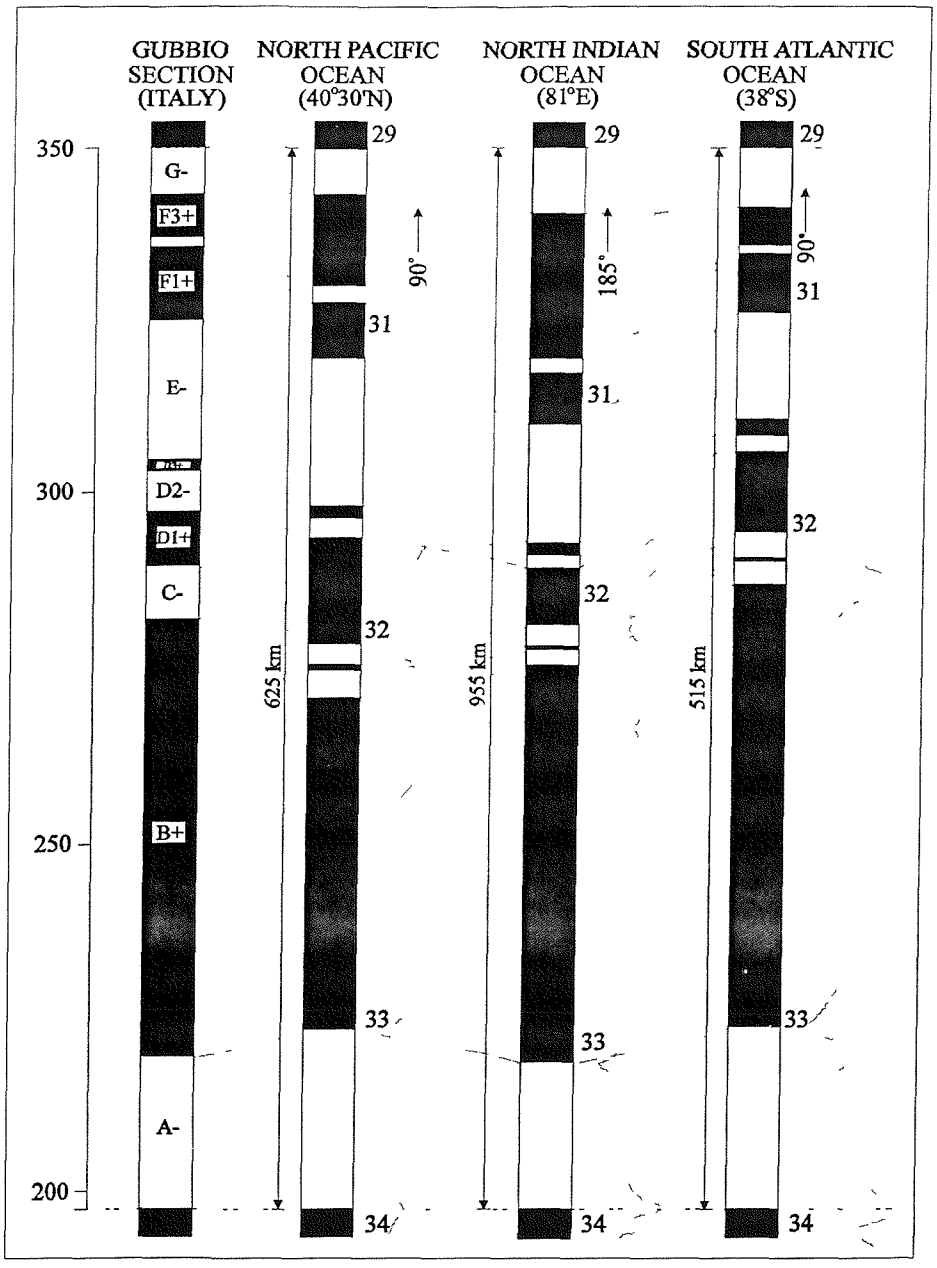

Figure 4.4. Comparison of the Late Cretaceous geomagnetic polarity sequence of the Scaglia Rossa section at Gubbio with the marine magnetic profiles and interpreted geomagnetic polarity sequences from three oceanic areas where the reversed interval between anomalies 33 and 34 can be recognised. The oceanic profiles have been uniformly reduced to bring the reversal boundaries at the beginning and end of the sequence into coincidence with the same horizons in the Gubbio profile. North Pacific: Profile B of Raff (1966); North Indian Ocean: profile V1909 (=V19 of Sclater & Fisher, 1974, Figure 2.); South Atlantic Ocean: profile C1102 (1) of Ladd (1974, p.101), extended to anomaly 34 by Lamont-Doherty profile V3101. Reversal boundaries on all three profiles were picked by R.F. Larson (1975). Note that the oceanic columns tie sideways to their respective anomaly profiles, not diagonally along the correlation lines (Lowrie & Alvarez, 1977a).

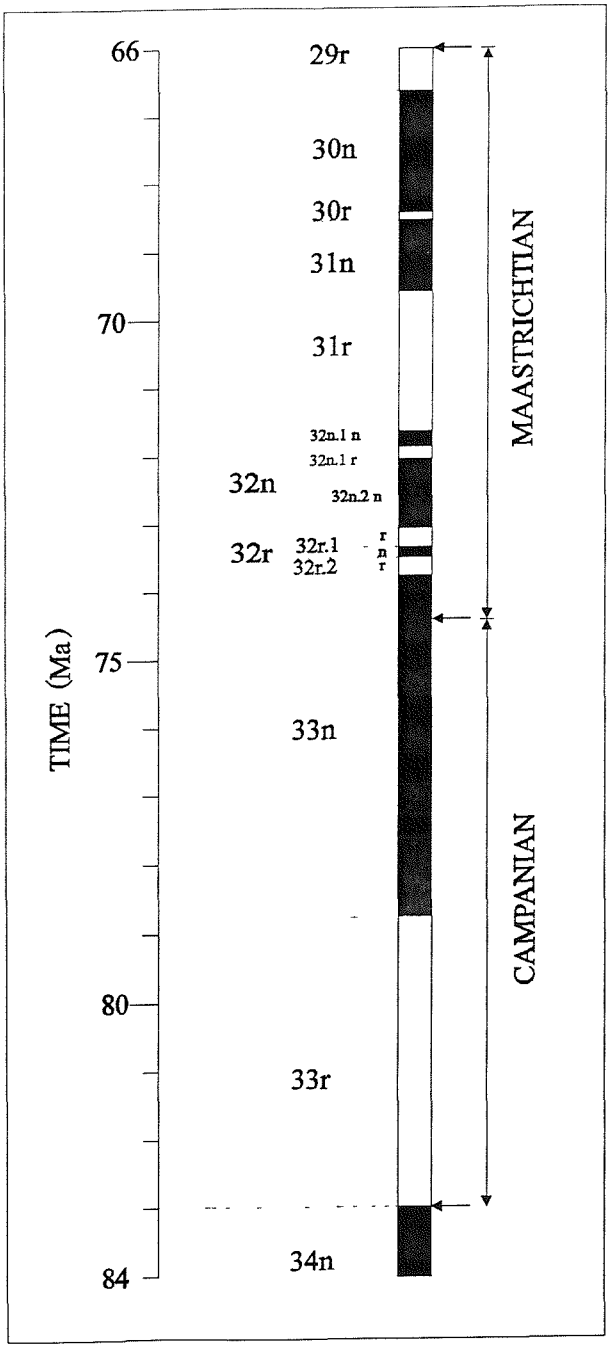

Figure 4.5. Geomagnetic polarity time-scale for the Late Cretaceous showing detailed nomenclature of chrons and polarity events. Calibration points are marked by arrows (Cande & Kent, 1992).

Chapter 5 Field and laboratory techniques

5.1 Sampling

Due to the extremely weak remanent magnetism of the Chalk, large volume samples were collected. Two types of sample were gathered; hand samples and rock drill cores. By dividing these samples into numerous sub-samples it was possible to undertake replicate measurements at each sample level. The methods employed to obtain these samples are described below.

5.1.1. Large volume hand samples

This technique involved forming a smooth, horizontal surface (with an area of approximately 10 cm^2 or more) on an outcrop of chalk. An orientation arrow was then marked onto this surface to indicate North. A roughly cubic sample was cut from the chalk using a hammer and chisel, with the horizontal orientation surface forming the top of the cube.

This technique proved particularly time consuming. However, with the aid of a petrol driven disc cutter (Plates 5.1 to 5.4) the ease and success rate of sample extraction was greatly enhanced. A 12 inch non-magnetic Arrowswift flat cutting wheel (grade C24RBF) was used in a Stihl disc cutter (Plate 5.5). The C24RBF wheel is designed to cut stone and non-ferrous metals and is fully reinforced with fibreglass. The abrasive constituent consists of silicon carbide and is formed by electrically fusing silica sand and carbon in the form of carbon rods. The fused silicon carbide is crushed and magnetically screened to remove magnetic contaminates. The silicon carbide is then bonded to the fibreglass reinforcing using a phenolic resin (bakerlite material)(Arrowswift Ltd., *pers. comm.*). This wheel was found to provide a hardwearing and extremely effective means for taking large volume palaeomagnetic samples. An orientation surface can be rapidly ground and by cutting four perpendicular interlocking slots a block can be formed and easily detached from the outcrop by a single hammer blow. The majority of samples collected during this study

were retrieved in this fashion.

5.1.2 Large volume rock drill cores

A portable coring drill (Plate 5.6) was used to take 35 mm diameter cores, up to 100 mm in length, from which 25 mm long cylindrical specimens were subsequently cut. These cores were orientated with respect to north and the vertical prior to separation from the chalk outcrop, by using a compass/diameter table, placed over the end of the core. A minimum of four separately orientated cores was taken at each stratigraphical level. This technique was used on a very limited basis due to the relatively small size of the samples retrieved.

5.2 Palaeomagnetic measurements

The remanent magnetism of rock specimens is measured by means of laboratory magnetometers. The two most widely used types of instrument are the balanced fluxgate magnetometer and the cryogenic magnetometer (Hailwood, 1989). In magnetostratigraphic investigations of weakly magnetised sediments, the cryogenic magnetometer possesses several advantages over the balanced fluxgate instrument (Hailwood, 1989).

5.2.1 Cryogenic magnetometers

Cryogenic magnetometers are complex systems which are essentially comprised of a superconducting pick up coil and sensor (Tarling, 1983). On introducing a magnetised object into the pick up coil a persistent direct current is induced, the value of which is proportional to the magnetic moment along the pick up coil axis. The current, via a field amplifier, can then be determined by means of a Super Conducting Quantum Interference Device (SQUID) (Goree & Fuller, 1976; Petley, 1980). The SQUID measurements give a measure of the flux change caused by the magnetised sample entering the pick up coil. Since the current is persistent, the field at the SQUID is maintained until either the magnetised object is removed or its magnetisation is

modified in some way (Goree & Fuller, 1976). Measurement of the total intensity of magnetisation can be made by inserting the specimen into the sensing ring in three different mutually perpendicular orientations, or by the use of three mutually perpendicular rings. Superconducting shields are used to eliminate the effects of fluctuations in the geomagnetic field which would otherwise limit the magnetometer's sensitivity. Since the sensor, pick up coils and shield are all superconducting, they are maintained in a cryogenic environment.

A cryogenic magnetometer's sensitivity is controlled by the placement, size and design of the superconducting coils (Weeks *et al.*, in press). By placing the pick up coils closer to a magnetic object, an increase in measurement sensitivity can be achieved. Pick up coil geometry is, therefore, of great importance. The smaller the pick up coil, the closer it can be placed to the magnetised specimen and, therefore, the greater the resolution of the measurement. However, by reducing the pick up coil geometry the sensitivity of the magnetometer is diminished. When measuring very weakly magnetised specimens it is vital to maximise the sample's magnetic moment. This can be readily achieved by increasing sample volume. Large access magnetometers, with large pick up coil geometries, enable very large samples to be measured. However, by increasing the size of the pick up coils a reduction in measurement resolution and an increase in background noise results. The Southampton small access discrete sample cryogenic magnetometer's 3.5 cm diameter sensor has a background noise level of around 2.0×10^{-8} mA/m^2 whereas the 2-G large access magnetometer's 7 cm sensors have a background noise level of approximately 11.0×10^{-8} mA/m^2. By roughly doubling the pick up coil diameter an approximate five fold increase in background noise occurs.

The pick up coils respond to a volume region along the access aperture of the magnetometer. They have a spatial response function where the response is a maximum when the magnetised object is positioned in the centre of the coil and diminished away from the centre (Weeks *et al.*, in press). The response function can be determined by passing a dipole point source through the instrument and measuring the output with distance as the dipole approaches and passes through the sensors.

Figure 5.1 shows the three perpendicular sensor responses for the Southampton 2-G whole-core magnetometer. The form of this curve is a function of the geometry of the measurement system. Usually the half power width of the response curve is taken as a measure of the maximum resolution of the pick up coils (Weeks *et al.*, in press). A large access magnetometer has a broad spatial response whereas a small access magnetometer has a much narrower response curve.

The response of a pick up coil to magnetised object should also be homogeneous, thus avoiding a biased measurement when measuring a sample which possesses a non-homogeneous magnetisation (Weeks *et al.*, in press).

Cryogenic magnetometers are capable of high levels of sensitivity. Hailwood (1989) states that "in principle cryogenic magnetometers are perhaps two orders of magnitude more sensitive than the best balanced fluxgate instrument". However, he adds that "in practice, instrumental noise often limits the effective sensitivity to about 0.01-0.05 mA/m". In addition to their high sensitivity a further advantage of a cryogenic magnetometer is that SQUID electronics operate at radio and high audio frequencies. The measurement response time is very rapid and can be regarded as more-or-less instantaneous (Hailwood, 1989). This means that numerous repeat measurements can be undertaken when measuring very weakly magnetic specimens. This allows for the improved resolution of remanence (Tarling, 1983). More detailed descriptions of cryogenic magnetometers and the principles involved in their operation are presented in Collinson (1983).

Two types of cryogenic magnetometer have been used in this study; they are a CCL discrete sample cryogenic magnetometer and a 2-G whole-core cryogenic magnetometer. Further details on these two systems are presented below.

5.2.1.1 CCL discrete sample cryogenic magnetometer

The CCL discrete sample cryogenic magnetometer system consists of a vertical sample handling device, a shielded "3-axis stationary" AF demagnetiser and a CCL "1-axis"

cryogenic magnetometer (Plate 5.7). This system can be reliably used to measure specimens with intensities as low as 0.003 mA/m.

The sample handling mechanism incorporates a holder (typically made of mylar) and a stepper motor which enables the holder to move up and down in the vertical plane and rotate in the horizontal plane. Sample diameters are restricted to 3.5 cm by the magnetometers aperture and the sample height to 3 cm by the vertical extent of the sensor region. The magnetometer system is comprised of a SQUID sensor and two pick up coils. One coil measures the vertical magnetic component of a specimen while the other measures the horizontal magnetic component. To measure the magnetic components along all three orthogonal axes the specimen is introduced to the sensor region and rotated through 90° increments in the horizontal plane. The direction of the magnetic remanence is measure along the 'X' and 'Y' axes (both positive and negative) and the 'Z' axis (four times) in the positive sense. Each separate orthogonal component can then be determined by solving the simple simultaneous equations (of the form X+Y+Z=N) generated from the four measurements positions. This form of determination is based on the assumption that the specimen is magnetically homogenous. The system does offer an option that allows the sample to be manually inverted so that the 'Z-axis' can be measured in a negative sense. However, this is rarely used since the system was designed to keep specimens in field free space once the measurement/demagnetisation cycle begins. A Hewlett Packard microcomputer is used to control the operation of the magnetometer, the demagnetising system and data acquisition. The remanence direction, specified in terms of declination (D), and inclination (I) is measured relative to the specimen (Figure 5.2) as follows:

$$D=\tan^{-1}(X/Y) \text{ and } I=\tan^{-1}(Z/H)$$

$$(\text{where } H=(X^2+Y^2)^{1/2})$$

The intensity of magnetisation (J) is given by:

where X, Y, and Z, are the components of the magnetisation along the three principal orthogonal axes (Ali, 1989).

The "3-axis stationary" demagnetisation system is mounted above the CCL cryogenic magnetometer and consists of two pairs of demagnetising coils surrounded by a double mu-metal shield, a double Si-Fe shield and a copper RF shield. The demagnetisation procedure is controlled by a Hewlett Packard microcomputer linked to a power amplifier and the sample handling device. The sample is lowered into the upper AF demagnetisation coils and the specimen's "X-axis" is demagnetised. The alternating field is ramped up to the required setting before decaying smoothly back to zero. The sample is then rotated through 90°, about the "Z-axis", and the "Y-axis" is demagnetised as above. The sample is then rotated 270° and lowered into the lower AF demagnetisation coils and the "Z-axis" is demagnetised. The specimen's magnetic remanence is then measured by lowering it into the cryogenic magnetometer.

It is essential that during a measurement the magnetised object is positioned exactly at the centre of the sensor pick up coils and has the correct azimuthal orientation relative to the reference direction (Ting, 1991). Calibration can be carried out manually or by using a computer programme and involves using a synthetic calibration sample with a stable permanent magnetism. A dipole point source is passed through the instrument and the output with distance is measured as the dipole approaches and passes through the sensors. Figure 5.3 shows the typical response function of the CCL instrument in which a minimum value, between two maximum values, represents the optimum measurement position.

5.2.1.2 2-G whole core cryogenic magnetometer

The 2-G Enterprises superconducting horizontal pass-through magnetometer system consists of a 1.5 metre long automatic sample handler, an in-line AF demagnetiser and a "3-axis" cryogenic magnetometer (Plate 5.8). This system can be used to measure large volume samples with magnetic intensities as low as 0.0015 mA/m.

The sample handling system, which consists of a weakly magnetic fibreglass boat, driven by a stepper motor, is capable of passing a 1.5 metre long, 7 cm diameter core through the system. The large access magnetometer contains three "high-resolution" pick up coils and SQUID sensors which enable all three magnetic components to be measured at the same time. The in-line AF demagnetiser consists of 3 coils positioned along the magnetometer access track and arranged to demagnetise in the three perpendicular axes. A sample is demagnetised by passing through the three coils at AF values up to 40 mT. The three coils are closely spaced and as a result interact. Therefore, it is not possible to demagnetise the samples in one pass and separate passes are required for each perpendicular axis. The region of AF decay is well shielded and, as a result, demagnetisation takes place in a negligible magnetic field. The whole integrated system of automatic sample holder, rock magnetometer measuring system and sample demagnetiser system is controlled by a microcomputer which enables a complete sequence of measure and demagnetisation cycles to be completed without removing the sample from the holder.

Hailwood *et al.* (1992) determined empirically the effective resolution of this system without signal deconvolution. Synthetic sediment cores were deposited in controlled laboratory fields and polarity reversals were recorded in successive sediment layers by an applied field direction being changed in increments of 30° between each layer. The layer thicknesses were varied from 2 to 20 cm in successive experiments (Figure 5.4). The results delimit the thinnest discrete magnetostratigraphic unit which can be resolved by this system and define the optimum measurement interval to achieve this resolution. A maximum resolution of 7.5 cm was determined for the sense coils. Although these experiments were undertaken to investigate the measurement procedure for cores, the results can be used to ascertain the optimum length for a single sample. The access aperture of the magnetometer restricts a cylindrical sample diameter to 7 cm or less. The resolution of the sense coils limit sample length to 7.5 cm. Therefore, the maximum sample volume, which can be accommodated by the system, is approximately 290 cm^3. However, samples with volumes ranging between 150-200 cm^3 were used in this study.

A measure of the residual magnetic field inside the 2-G system by Hailwood *et al.* (1992) revealed the position of several peaks on the profile (Figure 5.5). These peaks all coincide with the joins in the magnetic shields surrounding the system. However, the residual magnetic field in the sensor region is particularly low along all three perpendicular axes.

The automatic sample handling system consists of a 1.5 metre weakly magnetic fibreglass boat. This provided an opportunity to measure several samples at a time. However, it was necessary to determine the optimum spacing between each sample. Figure 5.6 shows the effect of three samples, with magnetic intensities of 1.0 mA/m, which have been spaced 10 cm apart (Hailwood *et al.* 1992). Overlapped spectra results. Figure 5.7 shows the result of increasing the sample spacing from 10 cm (as in the previous example) to 20 cm (Hailwood *et al.* 1992). By increasing the sample spacing within the holder, overlap of the sample spectra is largely reduced. Since the vast majority of chalk samples have intensities much lower than 1.0 mA/m a sample spacing of between 15-20 cm was used for this study.

5.3 Measurement procedure

The normal measurement procedure adopted, when using a cryogenic magnetometer proved inadequate, due to the extremely weak nature of the remanent magnetism of the chalk. However, acquisition of remanence data was greatly improved by the adoption of the following steps.

5.3.1 Sample holder

Samples measured in a cryogenic magnetometer are held in a holder which allows the sample to be moved vertically or horizontally into a pick-up coil coupled to a super-conducting ring and thus measured. Ideally, the holder should have a negligible magnetic moment which would allow us to ignore it's presence. However, commonly employed holders often possess a significant magnetic moment which requires subtraction from the measured moment of the combined sample and holder. For this

procedure to work, the sample holder needs to maintain a reasonably constant magnetic moment throughout the measurement.

5.3.1.1 CCL discrete sample cryogenic magnetometer sample holder

This is not the case for the 'standard' holders made from Mylar and used in the CCL system in the past (Plate 5.9). When compared with the background noise level of the magnetometer (typically 2.0 x 10^{-8} mA/m^2 for the discrete sample magnetometer) holders made from Mylar possess a magnetic moment which can be excessive and irregular (Figure 5.8). Such sample holders are thus unsuitable for the measurement of rocks with weak remanent magnetism since their magnetic moments are too strong to ignore and too irregular to be subtracted reliably. However, by using paper, holders can be produced with magnetic moments marginally greater than the background noise level of the magnetometer (Plate 5.10, Figure 5.9). By utilising a sample holder made from paper, the presence of the holder can be disregarded and extremely weakly magnetized samples can be measured quite accurately.

5.3.1.2 2-G whole core magnetometer sample holder

The sample holder employed by the 2-G Enterprises system consists of a weakly magnetic 1.5 metre long fibreglass boat. This is drawn horizontally through the instrument by a cord attached to a stepper motor. The holder possesses a relatively stable magnetic moment (Figure 5.10) which enables a reasonably reliable sample holder correction to be applied. The holder is measured and its magnetic moment is recorded and stored by the computer. Measurement of both the sample and holder is then carried out with the holder magnetic moment subtracted from the combined sample/holder magnetic moment (Figure 5.11). The residual magnetic moment (21.5±7 x 10^{-8} mAm), after the holder correction, is reasonably close to the background noise of the instrument (11.5 x 10^{-8} mAm) and appears to display a random distribution.

5.3.2 Sample volume

By increasing the volume of the sample, a significant improvement in the signal/noise ratio can be produced. Sample volume is controlled by the magnetometer's access aperture and the response function of the magnetometer's pick up coils.

5.3.2.1 CCL discrete sample cryogenic magnetometer and sample volume

Figure 5.12 shows a plot of "signal/noise" ratio against sample volume for three chalk cubes with different NRM intensities measured in the CCL discrete sample magnetometer. Multiple measurements were made on each cube, the volumes of which were successively trimmed from 27.0 cm^3 to 16.4 cm^3 to 5.8 cm^3. Three separate paper holders were made to cater for the different volume cubes measured. The signal/noise ratio was based on the root mean square ratio of magnetometer deflection for sample plus holder to empty holder. The empty holder was rotated through 360° and the magnetometer deflection was recorded at 0°, 90°, 180° and 270°. From the four deflection values obtained the root mean square was calculated. The same procedure was adopted for the measurement of the sample plus holder. The signal/noise ratio was then calculated by dividing the root mean square value of magnetometer deflection for sample plus holder by the root mean square magnetometer deflection value of the empty holder. Multiple measurements were made for each successive sample volume studied. This provided an opportunity to undertake statistical analysis of the experimental data.

The statistical analysis of experimental data requires the use of a distribution function which accurately portrays the configuration of the data set. Before any specific distribution function is employed, a physical basis for utilising the density function is normally given, and/or the observed distribution of experimental data is shown to reproduce the expected distribution within acceptable limits, as defined by the X^2 test (Onstott, 1980). A Fisherian distribution has been assumed for most palaeomagnetic analyses (Hailwood, 1989). The parameter used to specify the mean magnetisation vector in this study is the 95% confidence angle "alpha 95", which represents the

radius of the cone of confidence about the observed mean direction within which there is a 95% probability of the true mean lying (Hailwood, 1980). Further details on the statistical parameters used in this study are given in Section 5.7.

By increasing sample volume from 5.8 cm^3 to 27.0 cm^3 a four fold increase in signal/noise ratio results (Figure 5.12). It can be clearly seen from Figure 5.12 that by increasing sample volume the reliability of measurements obtained from rocks with extremely weak remanent magnetism can be significantly improved. Figures 5.13a, b, c, show plots of alpha 95 values for multiple measurements of magnetic vectors versus intensity for different chalk sample volumes. This further illustrates that an increase in sample volume enables the reliable measurement of rocks with extremely weak remanent magnetism. As sample volume increases, the intensity measurable while maintaining a reasonable alpha 95 value (say <10°), decreases. Figure 5.13a suggests that a sample with a volume of 5.8 cm^3 will return reliable alpha 95 values (about 10°) down to an intensity of approximately 0.03500 mA/m. Figure 5.13b indicates that by increasing the sample volume to 16.4 cm^3 alpha 95 values below 10° can be obtained for intensities of approximately 0.02000 mA/m. By increasing the volume to 27.0 cm^3 (Figure 5.13c) alpha 95 values within this limit can be obtained by chalk sample intensities as low as 0.00500 mA/m.

5.3.2.2 2-G whole core magnetometer and sample volume

The previously described experiment was repeated on the 2-G whole core magnetometer. Figure 5.14 shows a plot of "signal/noise" ratio against sample volume for three large volume chalk cubes with different NRM intensities measured in the 2-G whole core magnetometer. Multiple measurements were made on each cube, the volumes of which were successively trimmed from 216.0 cm^3 to 27.0 cm^3 in 27.0 cm^3 increments. The signal/noise ratio was determined by using the root mean square ratio of the sample magnetic moments along the three principal orthogonal axes (X, Y and Z) for sample plus holder to that of the empty holder. The empty holder was first measured at three equally spaced points along its length. It was then re-measured five times at the same points and the root mean square values for the three positions were

calculated from an average of the "holder-corrected" multiple measurements. An identical procedure was adopted for the sample plus holder.

The non-linear relationship between sample volume and the signal/noise ratio (Figure 5.14) indicates the inhomogeneous nature of the magnetic constituents distribution within the chalk. However, the underlying feature of all the plots is that as sample volume increases the signal/noise ratio increases, leading to an improvement in the reliability of the measurement results.

Figures 5.15 show a plot of alpha 95 values for multiple measurements of magnetic vectors, versus intensity for 200 cm^3 chalk samples. This further illustrates that an increase in sample volume enables the reliable measurement of rocks with extremely weak remanent magnetism. As sample volume increases, the intensity measured, while maintaining an alpha 95 value of less than 10°, decreases. Figures 5.15 suggests that a sample with a volume of 200 cm^3 will return reliable alpha 95 values down to an intensity of approximately 0.00150 mA/m on the 2-G magnetometer.

5.3.3 Replicate measurements

By carrying out repeat measurements on individual samples at each demagnetization step, it is possible to 'average' out background noise, provided the latter is random.

5.3.3.1 Multiple measurements using the CCL discrete sample cryogenic magnetometer

Figure 5.16 shows a plot of alpha 95 versus the number of replicate measurements for (i) the background noise of the magnetometer; (ii) an empty paper holder; and (iii) various 27.0 cm^3 chalk samples (contained in paper holders) with different remanence intensities. The plot illustrates the difference between sample, holder and background noise via the number of repeat measurements required to reduce the alpha-95 value to an acceptable level. Fewer measurements are required to reduce the alpha-95 values for extremely weak samples than for the paper holder or the background noise.

After 25 measurements the alpha 95 value for the "background noise" is still very high, as expected for random noise. To lower the alpha 95 value of the paper holder below about 15° requires at least 20 measurements. However, for weakly magnetic chalk samples, an alpha 95 value of less than 10° can be readily achieved using far fewer measurements. This provides us with a useful criteria for distinguishing between reliable and unreliable results. If after 20 repeat measurements the alpha 95 value exceeds 15°, the data are regarded as completely unreliable. Any demagnetisation vector returned within this limit can be regarded as sufficiently reliable for polarity stratigraphy.

5.3.3.2 Multiple measurements using the 2-G whole core magnetometer

Figure 5.17 shows a plot of alpha 95 versus the number of replicate measurements by the 2-G whole core magnetometer for (i) the background noise of the magnetometer; (ii) the empty holder; (iii) the empty holder after application of a holder correction. This plot illustrates the difference between holder and background noise via the number of repeat measurements required to reduce the alpha 95 value. Curve 1 represents the background noise of the 2-G magnetometer. After 25 measurements the alpha 95 value is still high (*c.* 25°). Curve 2 depicts the residual magnetic moment after a holder correction has been applied. Again, after 25 measurements the alpha alpha 95 value is still high (*c.*30°). The form of both curves intimate random noise. Curve 3 depicts the change in the alpha 95 value with multiple measurements of the sample holder. The alpha 95 value, based on three measurements, is approximately 6°. This signifies a very stable magnetic component. An accurate application of a sample holder correction should therefore be possible.

Figure 5.18 shows a plot of alpha 95 versus replicate measurements for various 150.0 cm^3 chalk samples with extremely weak remanence intensities. This plot illustrates the effect of carrying out repeat measurements on chalk samples with weak magnetic intensities. Even with samples with NRM intensities as low as 0.0038 mA/m multiple repeat measurements can reduce the alpha 95 value to a very low level. As the alpha 95 value is lowered, more confidence can be placed in the reliability of the

palaeomagnetic data.

5.3.4 Replicate sampling and great circle trends

Replicate sampling from the same horizon provided an opportunity to confirm results. Since rocks which possess weak remanent magnetism often only display directional trends (rather than stable end points) during demagnetisation, measurement of multiple samples can provide a measure of consistency. By plotting the behaviour of the remanence from a series of samples on a stereographic projection (Figure 5.19) it is possible to observe 'strung' distributions. Since such distributions fall on great circles (Creer, 1957; Khramov, 1958; Hargraves, 1959) several samples from the same horizon, with different low coercivity components, should generate a point of intersection. However, due to errors present in all palaeomagnetic data the intersecting great circles invariably form a cluster of intersection points instead of one common point (Onstott, 1980). By calculating the Fisher mean for all the intersection points a single mean vector can be determined which is representative of the magnetization vector for that block sample. Moreover, the alpha 95 value calculated for the vector can be used as a measure of reliability. The intersecting great circle technique enables the definition of the direction of a palaeomagnetic component which would not otherwise be identifiable by ordinary laboratory techniques (Onstott, 1980).

5.4 Progressive demagnetisation

Most rocks bear several components of magnetisation which have been accumulated during their past. These components are carried by different populations of magnetic mineral grains within the rock and commonly have different magnetic stabilities. The stability of the grain's magnetism can be specified in terms of blocking temperature or coercivity. The remanent magnetism of the grain can be destroyed by applying a magnetic field in the opposite direction to the magnetism. The coercivity is a measure of this applied field (Hailwood, 1989).

Isolation of separate components of magnetisation in the rock is achieved by

Isolation of separate components of magnetisation in the rock is achieved by progressively demagnetising a rock specimen. Lower stability components are removed during the first stages of demagnetisation and higher stability components during the subsequent stages. Both alternating field and thermal demagnetisation procedures were used in this study.

5.4.1 Alternating field (AF) demagnetisation

The specimen is positioned within a demagnetising coil which is capable of generating an alternating field with an exceptionally clean sinusoidal wave form (Hailwood, 1989) The coil is located inside a magnetic shield which eliminates the effect of external magnetic fields. The applied alternating field is ramped up to a pre-determined value and then smoothly decreased to zero. During each successive half-cycle the magnetism of grains (with coercivities up to the set value) within the rock sample, align in the same direction as the applied field and alternate in direction along the axis of demagnetisation coil (Hailwood, 1989). As a result of the gradual reduction in the alternating field (eventually to zero), equal numbers of grains are left with magnetic moments pointing in opposite directions along this axis. No net magnetism results from these grains since the magnetism of all the grains with coercivities up to the applied demagnetisation field are effectively randomised. This process must be carried our along all three orthogonal axis and repeated at progressively higher applied fields with the magnetisation of the sample measured after each step. From the changes in the resultant magnetisation vector it is possible to identify the different components of magnetisation present in the rocks. This technique is often applied to rocks in which the remanence is carried by titanomagnetites (Hailwood, 1989). AF demagnetisation steps of 2.5 or 5 mT, rising to a maximum value of 35 or 40 mT, were used in this study. During the present investigation, two different AF demagnetisers were employed. Both are maintained within the same shielded environment as the cryogenic magnetometers and the operational procedures adopted are described in sections 5.2.1.1 and 5.2.1.2.

5.4.2. Thermal demagnetisation

A specimen is heated in a non-magnetic oven to a discrete temperature and then cooled back to room temperature in a magnetic field-free space. The thermal fluctuations due to heating randomise the magnetisation of all the grains with blocking temperatures up to the applied temperature (Hailwood, 1989). This procedure is continued until the magnetism of the specimen has been totally destroyed. During this study, temperature increments of 100°C were used up to 300°C after which smaller steps were employed. As the Curie temperature of the magnetic constituents is approached the temperature increments were reduced to 10°C in order to identify the high blocking temperature components. Although the thermal demagnetisation technique often enables the isolation of magnetic components carried by high coercivity grains, which otherwise would not be revealed by using standard AF demagnetisation procedures, it has the drawback that, on heating a rock, undesirable chemical or mineralogical changes (in particular the generation of new magnetic phases) may occur (Hailwood, 1989).

Two different thermal demagnetisers were used in this study; a Schonstedt thermal demagnetiser and a Magnetic Measurements thermal demagnetiser.

The Schonstedt demagnetiser (model TSD1) consists of three parts; a heating compartment, a cooling chamber and the controller. A cylindrical shield, constructed from three layers of Mu-metal surrounds the heating compartment. Two further layers shield the cooling chamber reducing the residual field to less than 5 nT. Heating is supplied by a non-inductively wound furnace and controlled by a thermocouple and proportional temperature controller. A maximum temperature of 700°C can be obtained using this instrument. Samples were contained in a quartz boat. Although a temperature gradient exists within the oven, a 25 cm zone, at the centre of the oven, has a fairly homogeneous temperature distribution (*c.* ±10°C) provided the temperature is maintained below 400°C (Ting, 1991). Samples were demagnetised within this region of the oven.

The Magnetic Measurement model MMTD60 is a programmable thermal demagnetiser which can heat and cool large volume samples fully automatically (Plate 5.11). The oven is surrounded by 4 layers of mu-metal shielding that are automatically degaussed when the unit is switched on and are continuously 'activated' to improve their shielding ability. The residual field inside the oven is normally less than 10nT. The oven heating element is non-inductively wound on a ceramic former and the oven elements are 'open' to the air to allow rapid heating and good temperature control. The temperature is sensed with a Pt/PtRh thermocouple. The oven controller is fully programmable and will allow up to 3 heating or cooling ramps with hold times between. The samples are force cooled (800°C to 35°C in 45 minutes) by automatic operation of a blower unit. The oven has a 7.6 cm internal diameter which enables large volume samples (150 cm^3) to be thermally demagnetised and is 61.0 cm long. At 500°C there is only ±12°C variation over a distance of 30.5 cm within the centre of the oven. The samples were measured within this region. A sample holder made of quartz was used to support the samples.

Samples (27 cm^3) were heated for one hour and then cooled for one hour. However, with an increase in sample volume, longer periods of heating were used to allow sufficient time for the magnetic moments of the grains within the samples to be homogeneously demagnetised. The maximum heating time used was 2.5 hours for samples with volumes of 150 cm^3. A cooling period of similar duration was required.

5.5 Presentation of Palaeomagnetic data

The results of progressive demagnetisation investigations during this study are plotted in two ways.

5.5.1 Stereographic projections

To illustrate the distribution of palaeomagnetic directions the stereographic projection of declination and inclination is used (Phillips, 1971). Individual directions can be plotted on this projection. Declinations are specified clockwise from north, and

inclinations are specified from the equator, which represents horizontal. Conventionally, the projection is of the lower hemisphere. Downward inclinations are plotted as solid symbols, and upward (negative) inclinations are plotted as hollow symbols. The stereographic projection is accompanied by a graph showing the change in intensity of magnetisation.

5.5.2 Vector end point projection

The vector end point (VEP) projection (a Cartesian projection) allows both directional and intensity changes to be plotted on a single diagram. As progressive demagnetization occurs, both the intensities and directions of a vector are displayed. The components chosen are the horizontal component and the vertical component. The horizontal and vertical scales are identical and are chosen as appropriate to the range of intensity of remanence involved. When a single component of magnetisation is removed, the corresponding points lie on a straight line segments in both orthogonal projections of the vector diagram. From the gradients of these lines, the precise direction of the component can be determined (Hailwood, 1989). This projection is not generally suitable for plotting groups of directions. Hailwood (1989) provides a detailed description of VEP plots and explanation of VEP analysis.

5.5.3 Maximum angle of deviation

The multivariate technique of principal component analyses provides a means of detecting and estimating the directions of lines and planes of best least-squares fit along the demagnetisation paths of palaeomagnetic specimens (Kirschvink, 1980). Eigenvalues from the analysis (the variance of the data along each principal axis) can be used as a relative measure of collinearity or coplanarity and define a general palaeomagnetic precision index called the Maximum Angle of Deviation (MAD) (Kirschvink, 1980). The smaller the value of the MAD the greater the degree of collinearity or coplanarity.

Although the MAD is not a strict confidence limit it supplies a foundation for

acceptance or rejection of palaeomagnetic data (Kirschvink, 1980). Errors during measurement and the magnitude of superimposed magnetic components are the only factors which will increase variance and thus lead to larger MAD values. The MAD is purely geometric and has no relationship to the type of demagnetisation treatment used or the intensity of the demagnetisation process between measurements (Kirschvink, 1980). The optimum number of demagnetisation steps for a given specimen depends upon the complexity of its magnetisation. However, three points (including the origin) are the minimum number necessary to specify collinearity while four are required to specify coplanarity (Kirschvink, 1980). The MAD has been used extensively in this study to provide a means of assigning polarity determinations to reliability categories (see section 5.8).

5.6 Field stability tests

Ideally, demagnetisation analyses allow the isolation of different magnetic components within a rock specimen, and also an appraisal of the relative stabilities of the separate components. However, such analysis does not ordinarily provide information on the time of acquisition of these components. The principal objective in the analysis of palaeomagnetic data is to determine whether any of the components of remanent magnetisation identified in the rock, represent primary magnetisation, and also to establish the instances in the rock's past when other magnetic components were acquired. Knowledge concerning the timing of magnetisation processes may sometimes be gained from geological observations made in the field. Such observations are commonly referred to as "field stability tests". The tests used in this study are summarised below.

5.6.1. Fold test

A rock unit, such as a single bed in a sedimentary sequence, magnetised within a short interval of time, should display a uniform direction of magnetisation. If the bed is subsequently deformed by folding and provided the remanent magnetism is stable, the direction of magnetisation will reflect the rotation caused by the folding. The

magnetisation vectors maintain the same angle relative to the bedding plane. However, if tilting is variable, this angle will change from one location to another in the same bed. On application of a bedding correction these vectors are rotated back to the original horizontal attitudes. This should result in the directions of magnetisation of individual samples, from the same unit, moving towards each other. A significant refinement in the grouping of the magnetisation vectors will be produced. Statistical tests are available (McFadden & Jones, 1981) which permit the scatter of the remanence vectors, before and after application of the bedding correction, to be contrasted. Where it can be demonstrated that the application of a bedding correction results in a significant decrease in dispersion it can be concluded that the acquisition of magnetisation pre-dates the time of folding. Conversely, if a significant increase in the dispersion of the magnetisation vectors occurs it can be concluded that magnetisation post-dates folding. Provided the time of folding has been ascertained from other geological sources, an important constraint can be placed on the time of the acquisition of magnetism.

5.6.2 Consistency test

The identification of a corresponding direction of magnetisation in rock units of similar age over a broad area suggests that the magnetisation is stable, and dates from the time of formation of the rock or at least the time of a significant re-magnetisation event (Hailwood, 1989). Where a particular sequence of magnetic polarity reversals can be identified in several different sections of the same formation over a wide area, and these sequences exhibit a good correlation, it is highly probable that the magnetisation is primary (Hailwood, 1989).

5.7 Statistical parameters

The principal usage of statistical parameters in this study is to delineate the reliability of palaeomagnetic data. The most widely used statistical treatment in palaeomagnetic research is that of Fisher (1953). The density function for vector data that was introduced by Fisher (1953) and applied to palaeomagnetic data is given by the

following equation:

$$f(\theta,\Phi)\, dA = \frac{k}{4\pi \sinh k} \exp(K\cos\theta) \sin\theta\, d\theta\, d\Phi$$

where θ and Φ are the polar and azimuthal angles, respectively. The equation generates a density distribution which is circularly symmetric about a mean vector direction; it is similar in shape to a two-dimensional Gausian distribution. The dispersion of the distribution is described by the concentration parameter k; if k=0, the vectors are uniformly distributed in space (Onstott, 1980). However, where k is a large number (*c.* 10^3-10^4) the vectors are grouped closely about the mean (Hailwood, 1989). Since its original conception, a Fisherian distribution has been assumed for most palaeomagnetic analyses (Onstott, 1980).

Other useful parameters used in the specification of mean magnetisation vectors are summarised by Hailwood (1989). These are:

(a) The 95% confidence angle, alpha 95, which represents the radius of the cone of confidence about the observed mean direction within which there is a 95% probability of the true mean lying.

(b) The circular standard deviation, θ_{63}, which is the radius of a circle (on a unit sphere) about the mean direction, containing 63% of the observations.

5.8 Reliability categories

To provide an unbiased appraisal of the quality of the polarity determinations, for each sample, during this investigation, a set of reliability categories have been adopted. This scheme is based on a classification defined by Hailwood (*pers. com*). Each result is placed first in one of two broad divisions:

S- a demagnetisation stable end point (SEP) is reached

or **T-** no demagnetisation end point is reached, but a directional trend, towards either a normal or a reverse polarity vector, occurs.

Within these wide categories, additional reliability divisions were specified as follows:

S1 Highest quality data. The SEP is well-defined by a collection of closely-spaced points on the stereographic plot. On the vector plots, the final linear portions are directed through the origin with MAD values less than 5°. Figure 5.20a & b. shows examples of normal polarity/assigned to this category.

S2 Intermediate quality data. Polarity assignment is regarded as tenable. The SEP is soundly defined by a set of points on the stereographic projection but intensity does not always decrease systematically during demagnetisation (often due to instrument noise effects). Consequently, a final linear segment through the origin is not always present on the vector plot. However, where linear segments through the origin can be approximated, MAD values greater than 5° but less than 10° are used to constrain data to this category. Where linear segments are not observed, alpha 95 values of less than 10° delimit this category. Figure 5.21a & b, show examples of normal and reverse polarity samples assigned to this category. Vector plots are shown to display the non-linear behaviour of the final segments.

S3 Poor quality data. There is some uncertainty about the reliability of the polarity assignment. Palaeomagnetic directions often become erratic as a samples intensity decreases, during demagnetisation, and approaches the background noise of the magnetometer. Examples are shown in Figures 5.22a & b.

T1 Highest quality directional trend data. The trend is relatively long and well defined. There is no doubt about the reliability of polarity assignment. Examples are shown in Figure 5.23.

T2 Intermediate quality directional trend data. Relatively short trend, but sense of directional movement is quite clear. No doubt about polarity assignment. Examples are shown in Figure 5.24.

T3 Poor quality data. Probable trend present, but poorly defined. Some doubt about polarity assignment. Examples are shown in Figure 5.25.

O Overprint. The stable characteristic magnetization (SCM) of the sample possesses, prior to a bedding correction, a similar direction to the recent geomagnetic field. On application of a bedding correction the SCM direction is rotated away from the recent geomagnetic field direction to a spurious direction. Figures 5.26a & b, show examples of such behaviour.

E Erratic behaviour during demagnetisation. The results are completely unreliable and no polarity assignment is possible. The sample's magnetisation is either too unstable or too weak to measure. Examples are shown in Figures 5.27a & b.

5.9 Techniques used to examine magnetic mineralogy

Several non-destructive magnetic procedures are available which are capable of providing information about the magnetic mineralogy of rock samples. Such studies can reveal significant stratigraphic/magnetic relationships. The effects of recent weathering and the development of a CRM can often be identified and thereby enhance the calibre of the measurements used in the magnetostratigraphic data set (Ali, 1989).

5.9.1 NRM Intensity

The NRM intensity can provide a good indication of the relative proportion of ferromagnetic grains in a sample. By plotting a downhole stratigraphic plot of NRM intensity values, such variations may become apparent.

5.9.2 Magnetic susceptibility

Magnetic susceptibility describes the extent to which a substance is attracted to, or repelled by a magnetic field (Robinson, 1992). Low-field volume magnetic susceptibility (k) is defined as the ratio of induced magnetisation intensity (M) per unit volume of a substance, to the strength of the applied magnetic field (H) inducing the magnetisation (Thomspon & Oldfield, 1986):

$$k=M/H$$

In weak magnetic fields (< 1 Oe), it is assumed that M changes with H in a linear fashion. The magnetic moment induced in the substance when subjected to a weak magnetic field reverts to zero when the applied field in removed (Collinson, 1983). It should be noted that this assumption has been challenged by Smith & Banerjee (1987).

Magnetic susceptibility is a measure of the variation in the strength of a magnetic field (positive or negative) when a sample is moved into that field. This variation is controlled by the concentration and composition (mineralogy and grain size/shape) of the magnetisable material contained in the sample (Thompson & Oldfield, 1986).

The volume magnetic susceptibility of a naturally occurring material, such as a marine limestone, is a function of the concentration (per unit volume) of magnetisable material it contains (Robinson, 1992). Magnetisable components of marine sediments consist not only of the ferromagnetic minerals, which are capable of maintaining a remanent magnetisation, but also any compound accommodating Fe^{2+}, Fe^{3+} or Mn^{2+} ions. These paramagnetic substances encompass clay minerals, such as chlorite, smectite and glauconite; ferromagnesian silicates; iron and manganese carbonates; iron sulphides such as pyrite and authigenic, ferric oxyhydroxide mineraloids, collectively referred to as limonite, which customarily arise as colloidal complexes in the pore waters of deep-sea sediments (Burns & Burns, 1981). A review of the remanence-carrying magnetic minerals detected in marine limestones has been

presented by Lowrie and Heller (1982) (see Section 1.5.3). These include strongly magnetic iron-titanium oxides like titanomagnetite and titanomaghemite (MS=2 x 10^{13} to 2 x 10^{15} SI and weakly magnetic (lattice-imperfect antiferomagnetic) iron oxides like titanohematite, and iron oxyhydroxides like goethite (MS=2 x 10^{9} to 2 x 10^{11} SI).

In comparison to strongly magnetisable (ferromagnetic) and moderately magnetisable (paramagnetic) minerals, which occur primarily in the lithogenic portion of deep-sea sediments, biogenic carbonate and silica are not only exceptionally weakly magnetisable, but in reality display diamagnetic behaviour. They are characterised by extremely weak, negative MS values (usually between -1 and -5 x 10^{9} SI) (Robinson, 1992).

Measurements were made using a Bartington Instrument's MD system (Plate 5.12) which is based on a modification of the principle utilized by metal detectors (Robinson, 1992). Robinson (1992) provides a concise description of the fundamental workings of the system. Measurements were made by placing the sample in an 80 mm loop-type sensor and recording the MS. Initially, the response function of the instrument was determined to establish the optimum sample volume the system could measure. Figure 5.28 shows this response function. The response function indicates that the ideal sample length is 4 cm. Samples with diameters approaching 7 cm and therefore volumes of 150 cm^3 were measured. Measurements were taken before and after the sample was placed in the sensor to enable the measurement to be corrected for instrumental drift (assuming a uniform drift). Each sample was measured three times, with the average value and standard deviation calculated. The results are drawn up as a stratigraphic plot with the average value of background noise delineated on the plot. The relationship between cgs units and dimensionless SI units of bulk susceptibility is as follows: 1 cgs unit = $1/4\pi$ SI units. The volume susceptibility value (susceptibility per unit volume) used in this study is obtained by dividing the bulk susceptibility by the effective volume of the sample, specified in m^3.

5.9.3 Isothermal remanence (IRM)

The positive identification of the ferromagnetic minerals in limestones is often a difficult problem to solve (Lowrie & Heller, 1982). A convenient method is that of coercivity spectrum analysis (Dunlop, 1972). The isothermal remanent magnetisation (IRM) of a sample is measured after placing it in a steady magnetic field whose strength is progressively increased in steps, the magnetisation being measured after each stage until saturation is attained. The shape of the IRM acquisition curve and the field at which saturation is reached yield the total coercivity spectrum of the sample by numerical differentiation (Lowrie & Heller, 1982). The magnetic mineral content is deduced by comparison with minerals for which diagnostic coercivities are known (Lowrie & Heller, 1982).

A Molspin pulse magnetiser (Plate 5.13) was used to apply increments of direct magnetic field. The sample was placed in a magnetising coil with its z-axis parallel to the coil axis. A powerful bank of capacitors was then charged, and when charging was complete, discharge occurred. The maximum magnetic field generated by the instrument was 860 mT. The magnetised sample's intensity was then measured after which the next increment of direct field was applied. Sample intensity was plotted against the applied field to produce an IRM acquisition curve.

The saturation magnetization of hematite is less than 1% that of magnetite. The titanomagnetites (and maghemite) saturate in fields of 0.01-0.1 Tesla, while hematite does not saturate in fields of over 1-3 Tesla (Tarling, 1983). Thus, if direct magnetic fields are applied in incremental steps, the magnetic moment of magnetite reaches a maximum constant value before 1 T, but the moment continues to increase at higher applied fields for hematite (Figure 5.29.). Figure 5.30 shows the typical response of a chalk sample to direct magnetic fields applied in incremental steps. By determining the IRM ratio ($IRM_{300\ mT}/IRM_{860\ mT}$, Ali, 1989) an IRM ratio log can be presented. Values range typically between 0.7 and 1.0; specimens with values below 0.9 are probably hematite-rich, whilst those with values above this are more likely to be magnetite-rich (Ali, 1989).

Provided ferromagnetic grains are of similar size, the saturation IRM (IRM_{sat}) of a sample can provide a useful indication of the relative proportion of the magnetic constituents. By plotting a downhole stratigraphic plot of IRM_{sat} intensity values, such variations may become apparent. However, it should be noted that such a plot may also reflect variations in magnetic mineral grain size. Larger grains possess larger magnetic moments which, in turn, will be portrayed in the NRM and IRM_{sat} intensity values.

Information on the presence of single domain (SD) or multi domain (MD) grains can be gained by calculating the ratio of saturated remanent magnetisation to saturated induced magnetisation, NRM/IRM_{sat} (Collinson, 1983). The ratio is higher in SD than MD material. In an assembly of randomly orientated uniaxial SD grains, $NRM/IRM_{sat}=0.5$, which is the maximum expected value for this ratio (Collinson, 1983). In MD material the ratio is usually < 0.1 (Collinson, 1983).

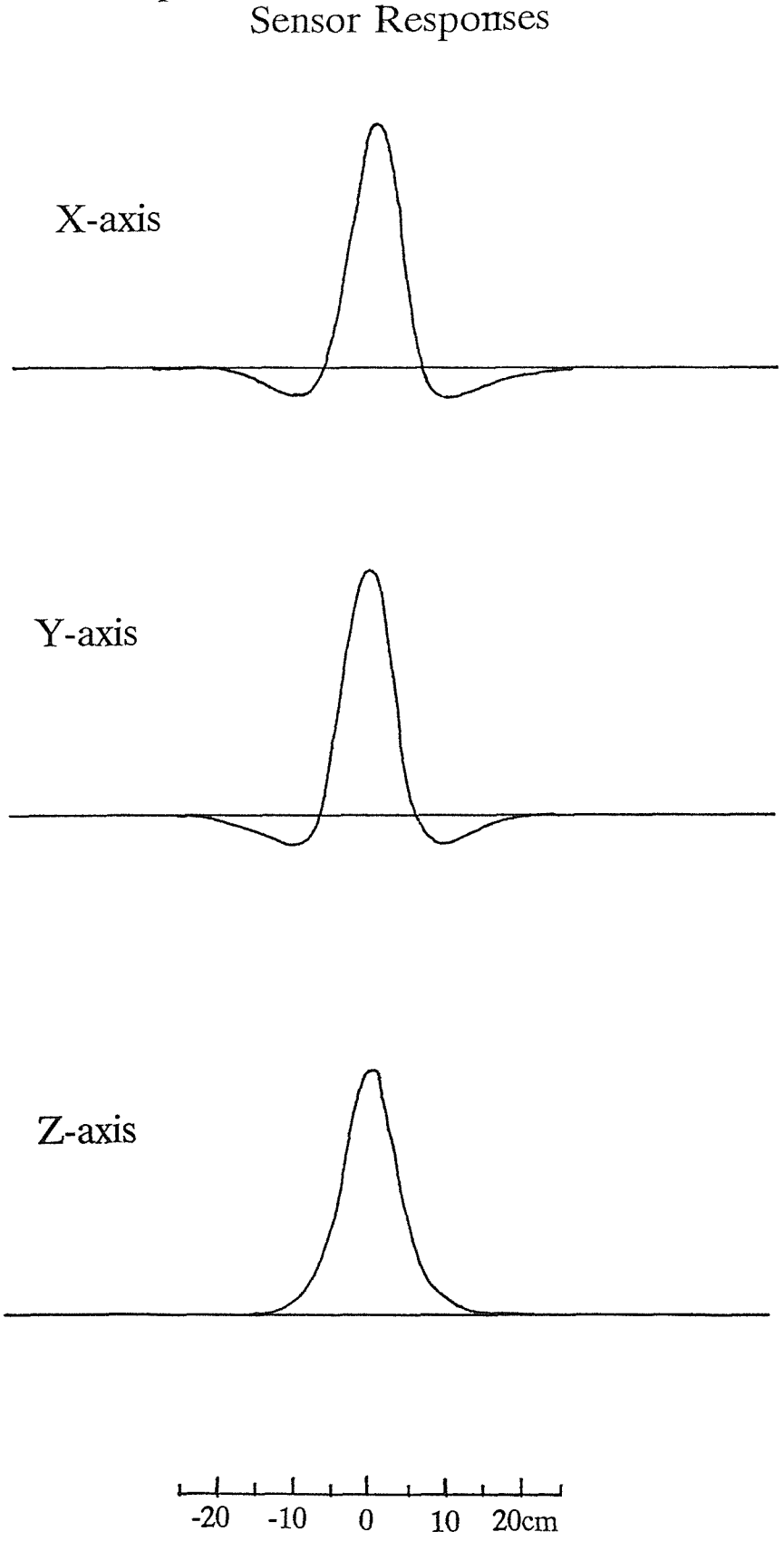

Figure 5.1. The X, Y, and Z-axis sensor responses for the Southampton 2-G wholecore cryogenic magnetometer (Hailwood *et al.* 1992).

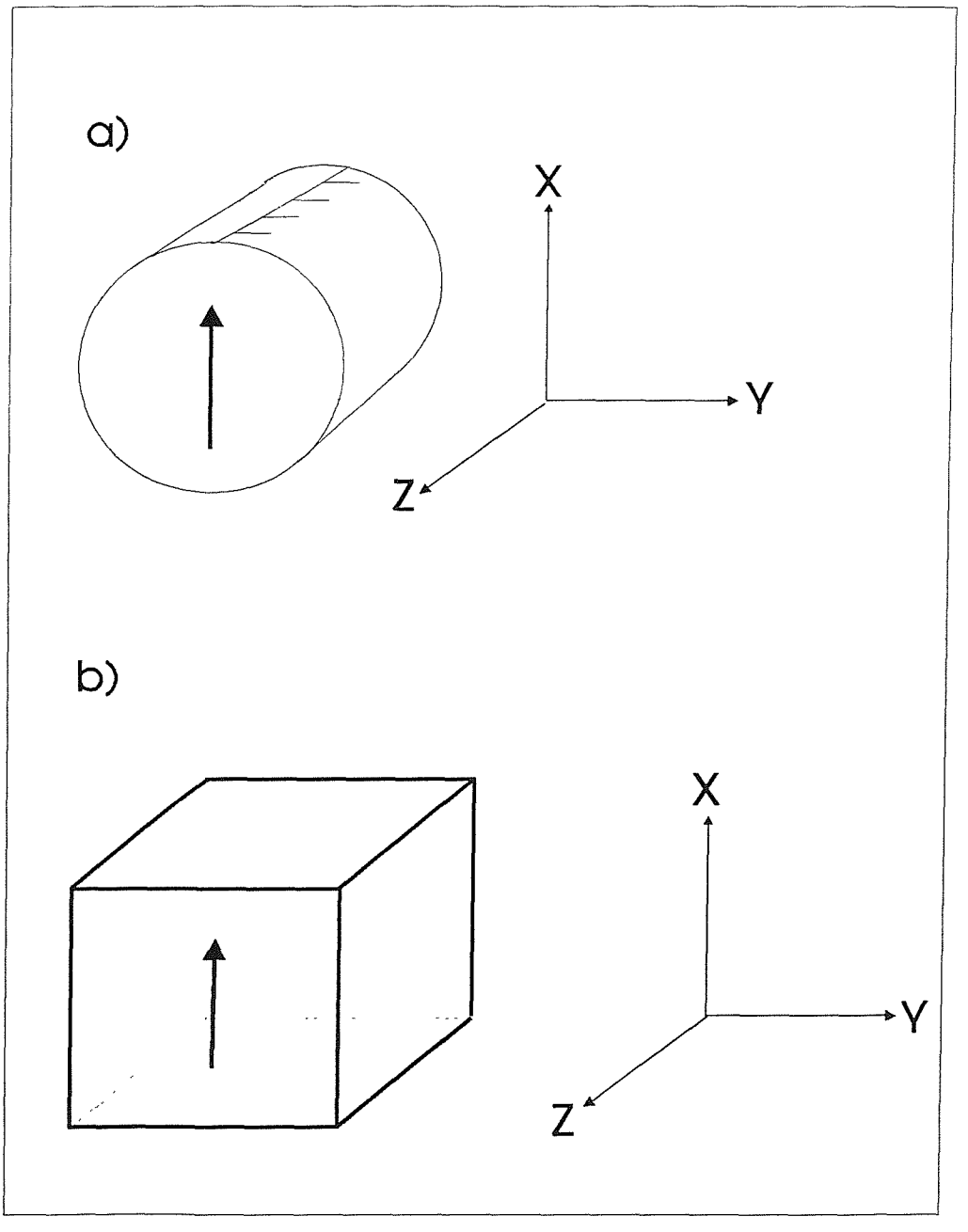

Figure 5.2. The specimen co-ordinate framework for (a) rock cores and (b) rock cubes.

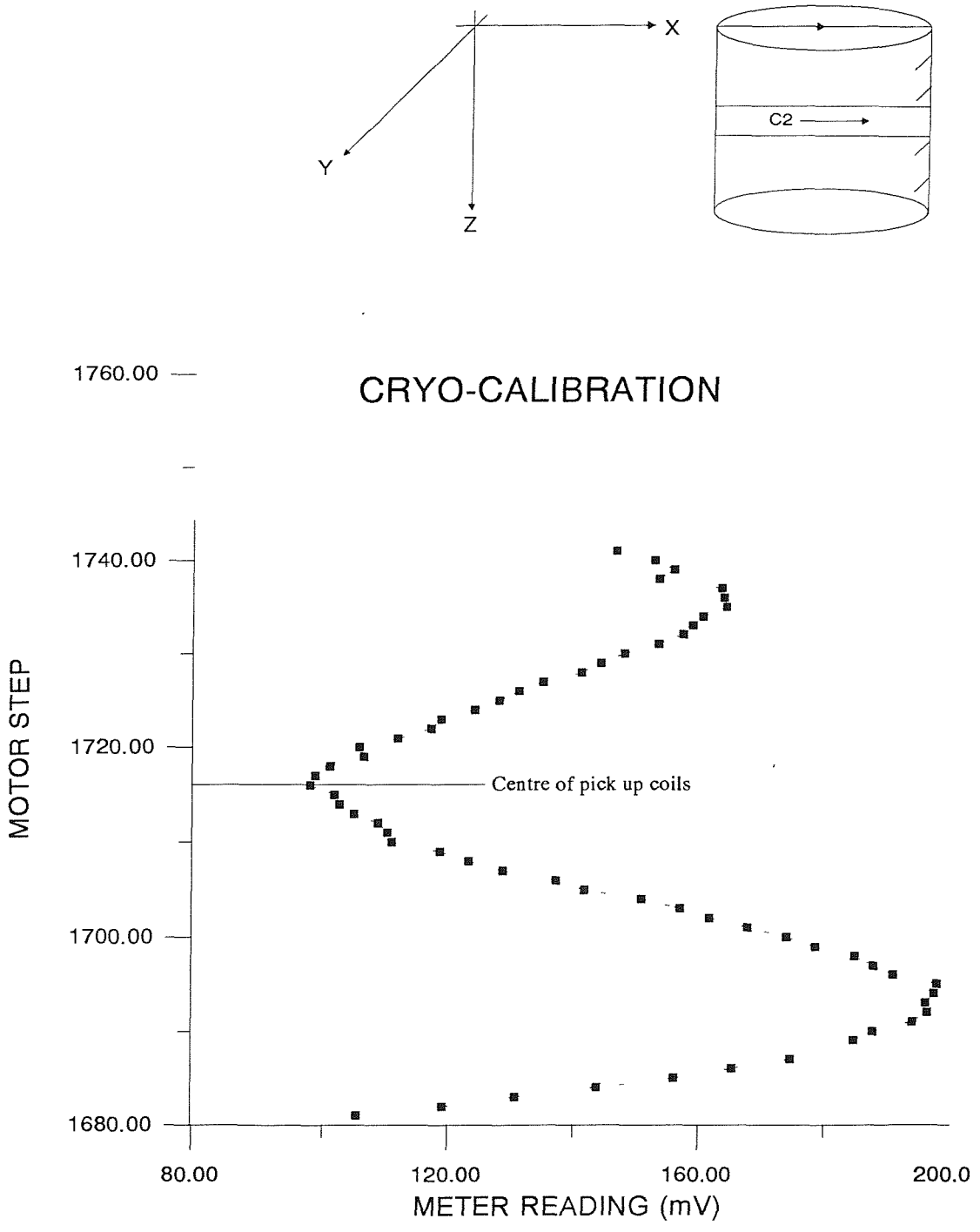

Figure 5.3. A downstepping calibration curve for the CCL cryogenic magnetometer. The minimum meter reading corresponds with the centre of the pick up coil. The insert diagram indicates the orientation of the calibration sample, with its magnetic moment in the horizontal (Ting 1991).

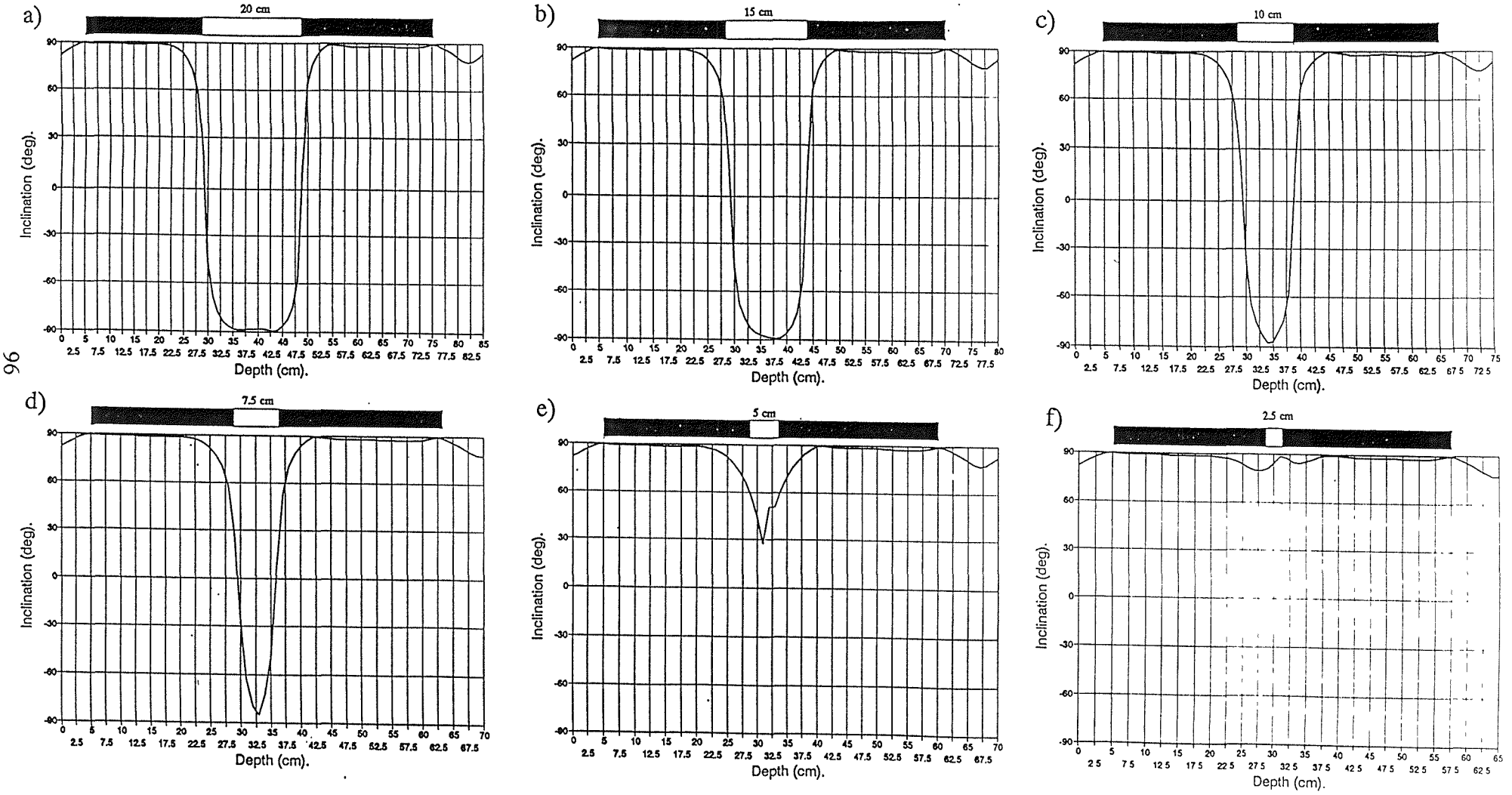

Figure 5.4. Hailwood *et al.* (1992) determined empirically the effective resolution of the 2-G wholecore magnetometer using synthetic layered sediment cores containing polarity reversals. By varying the thickness of the polarity reversals from 20 to 2 cm in successive experiments they determined a maximum resolution of 7.5 cm for the sense coils (d).

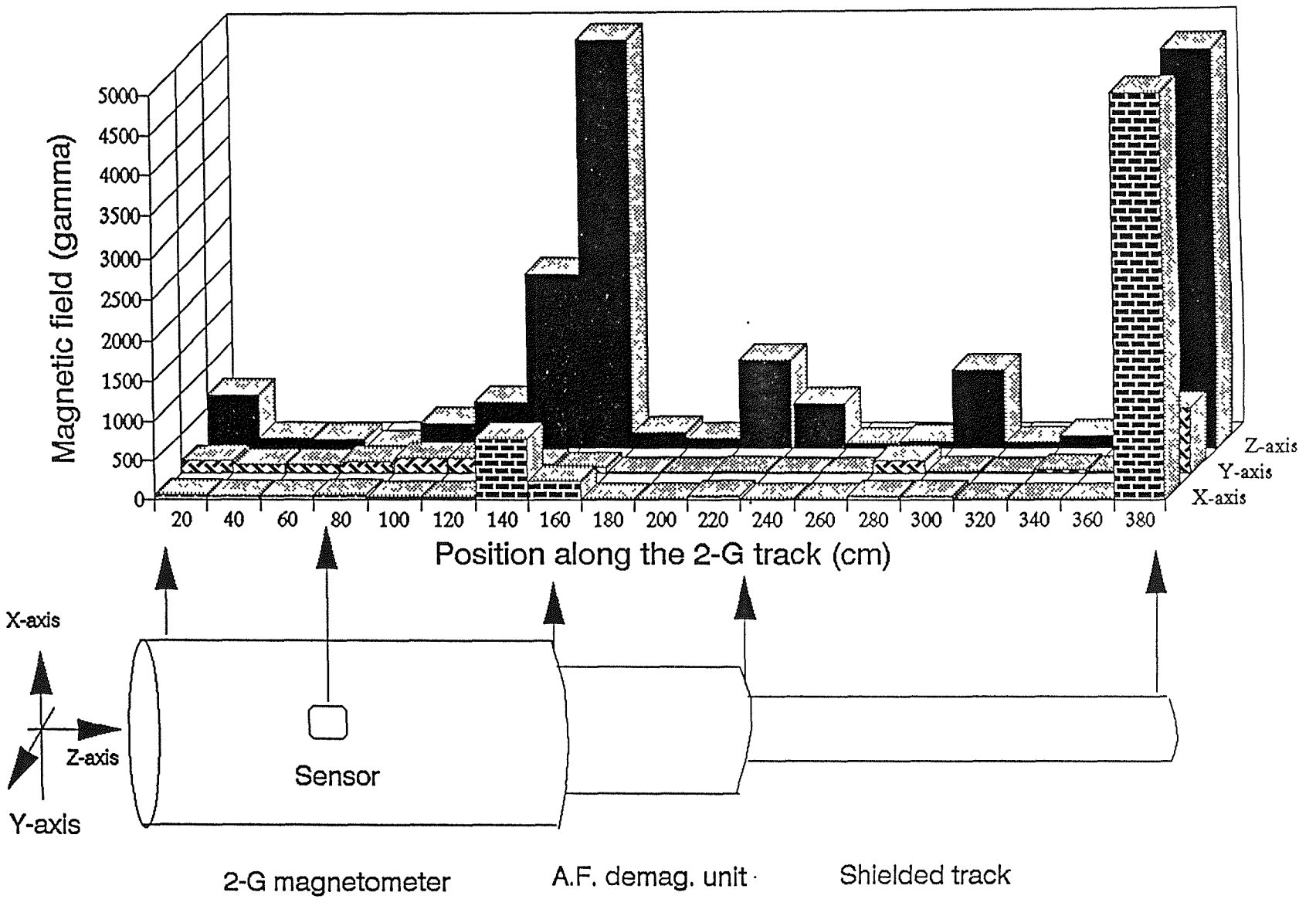

Figure 5.5. A profile of residual magnetic field inside the 2G-system. The relative position are indicated by the up-pointing arrows (Hailwood *et al.* 1992).

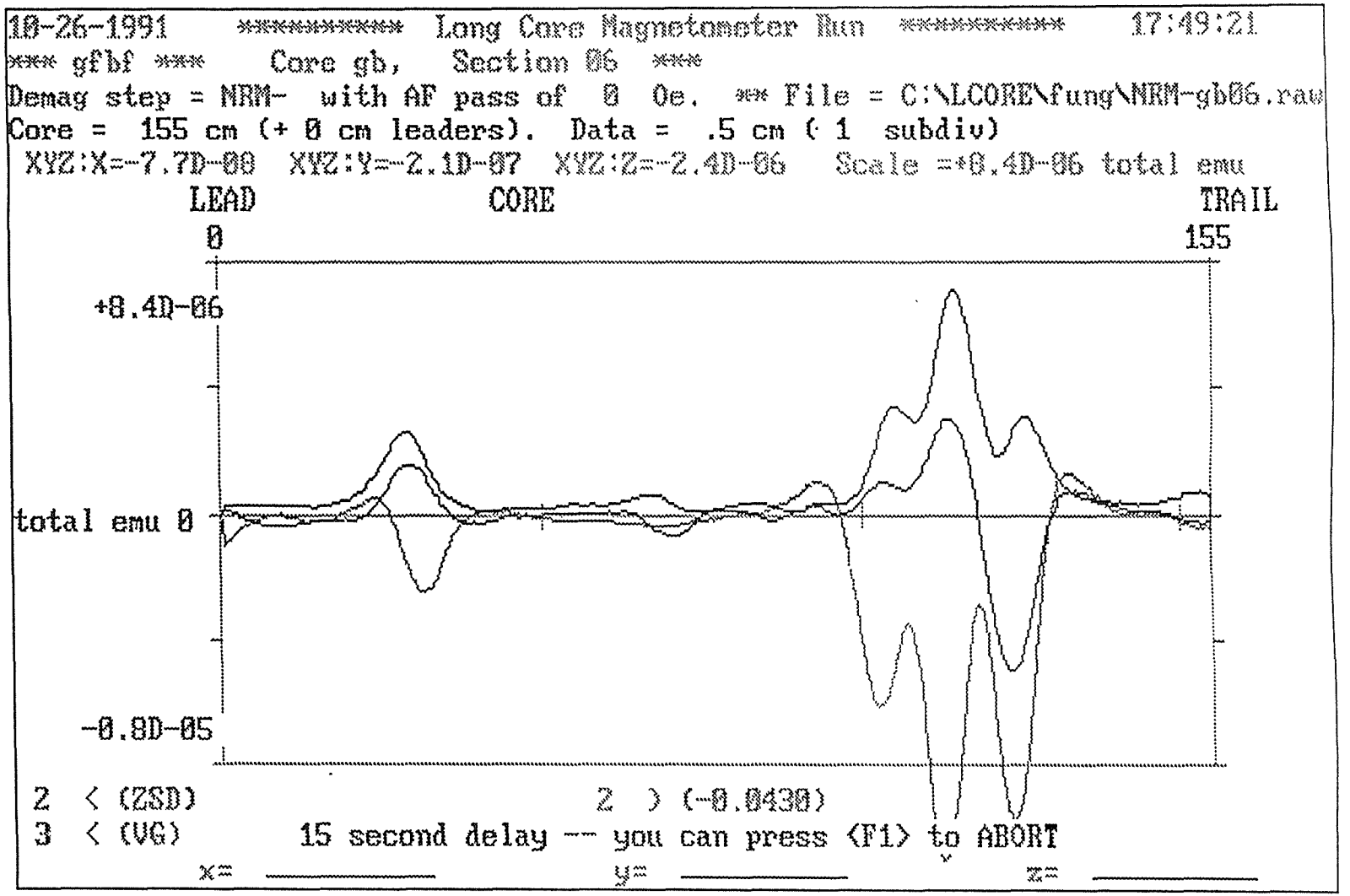

Figure 5.6. An example of serious overlapped spectra of three samples with magnetic intensity values of 1.0 mA/m and a sample spacing of 10 cm (Hailwood *et al.* 1992).

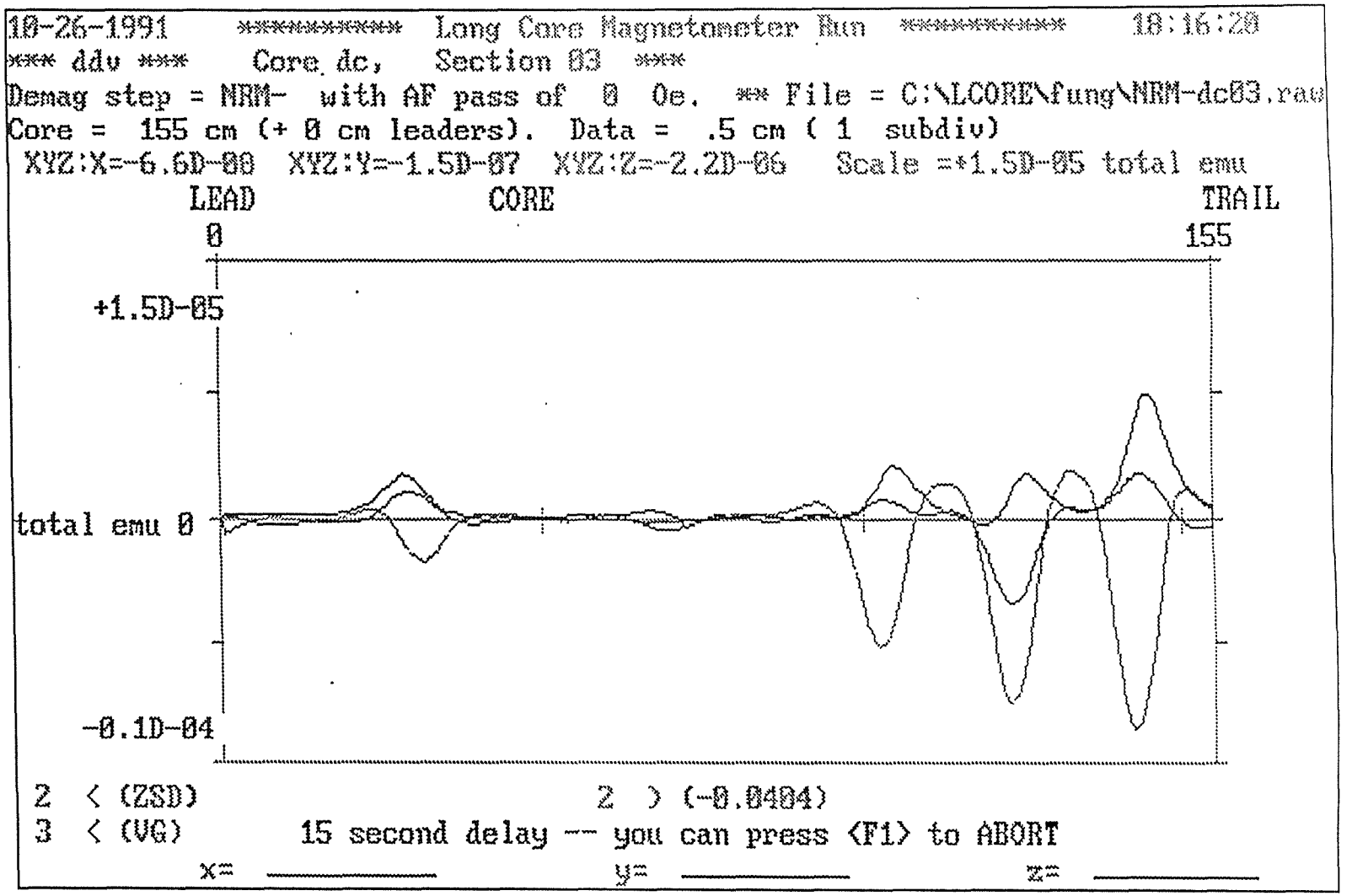

Figure 5.7. The samples as shown in Figure 5.6, but with a sample spacing of 20 cm. There is no significant overlapping of their spectra. The typical width of spectrum for these samples is 20 cm and for sample intensities less than 1.0 mA/m sample spacing might vary fom 15-20 cm (Hailwood *et al.* 1992).

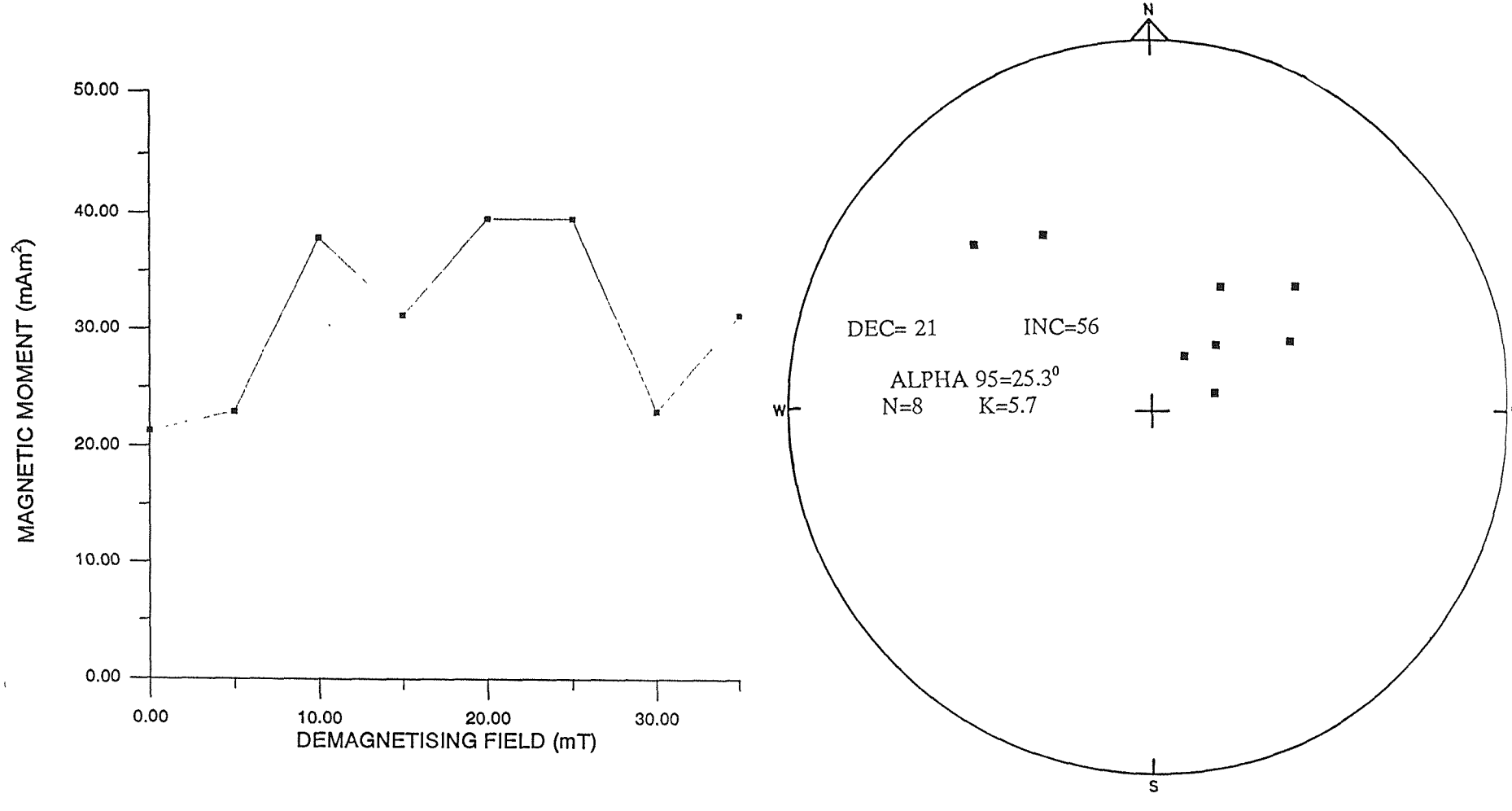

Figure 5.8. Plot of magnetic moment versus demagnetisation field and a stereographic projection for an empty Mylar sample holder. The holder was orientated as if a rock sample was to be measured.

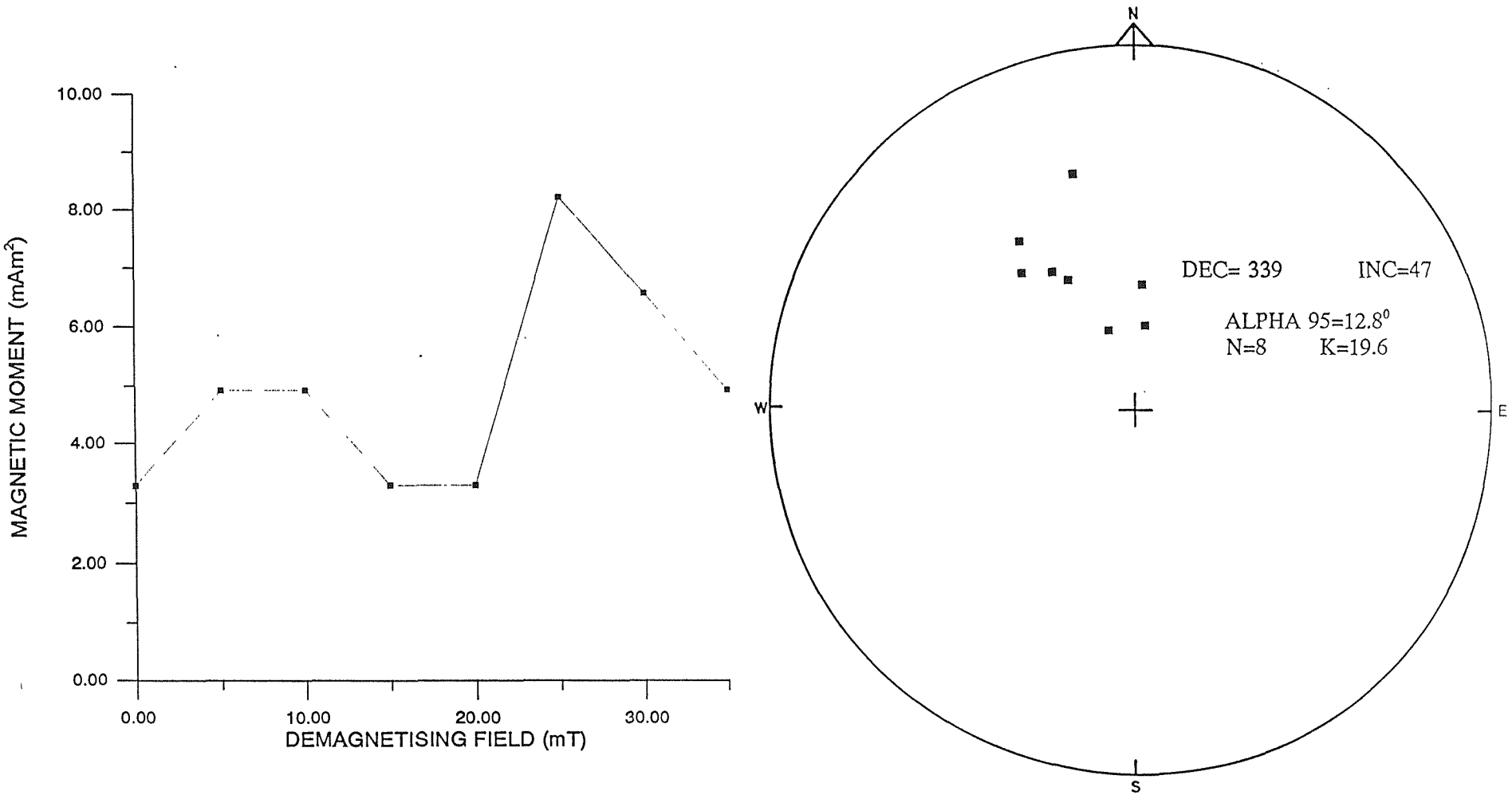

Figure 5.9. Plot of magnetic moment versus demagnetisation field and a stereographic projection for an empty paper sample holder. The holder was orientated as if a rock sample was to be measured.

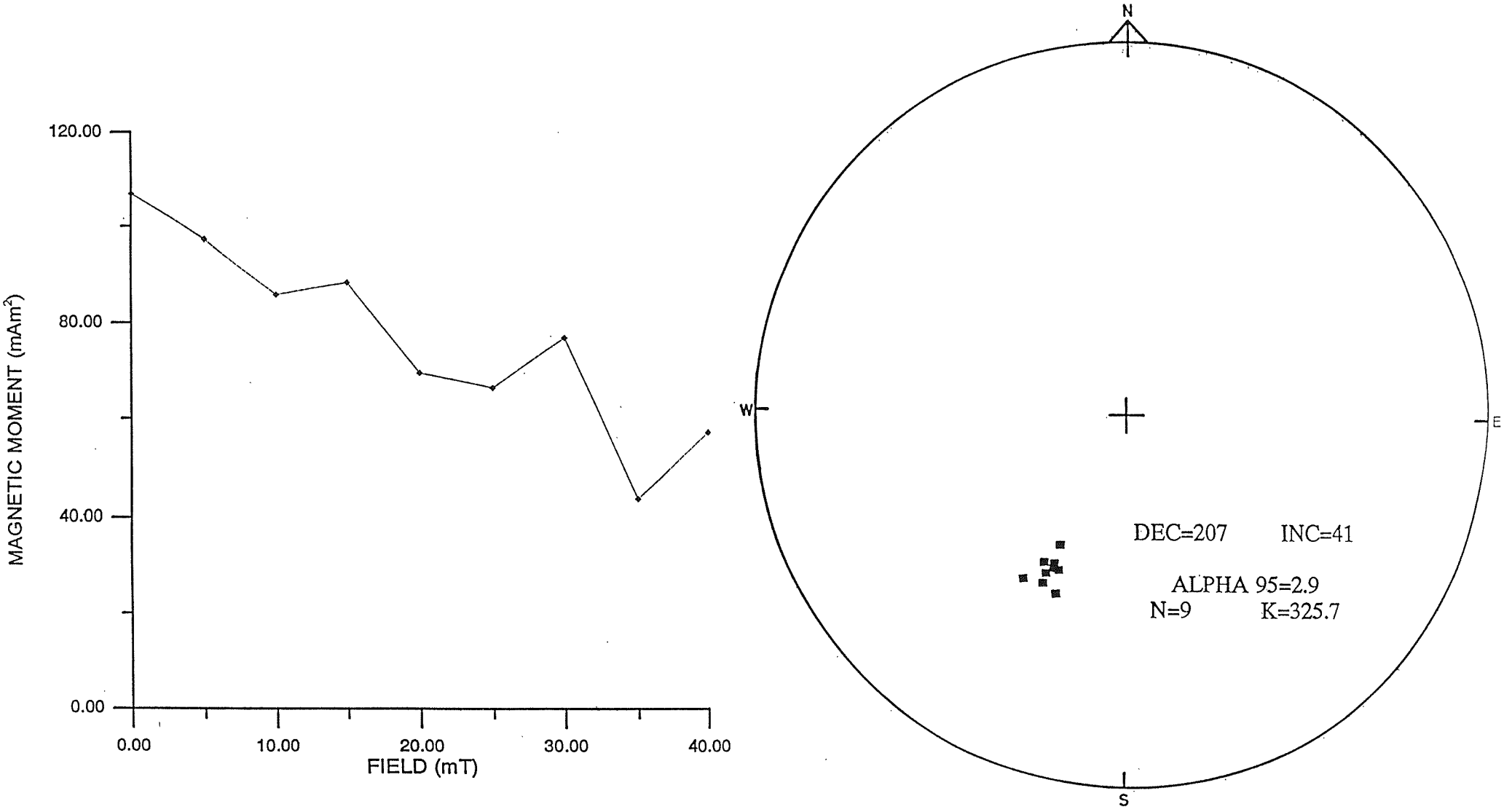

Figure 5.10. Plot of magnetic moment versus demagnetisation field and a stereographic projection for the 2-G Enterprise wholecore sample holder.

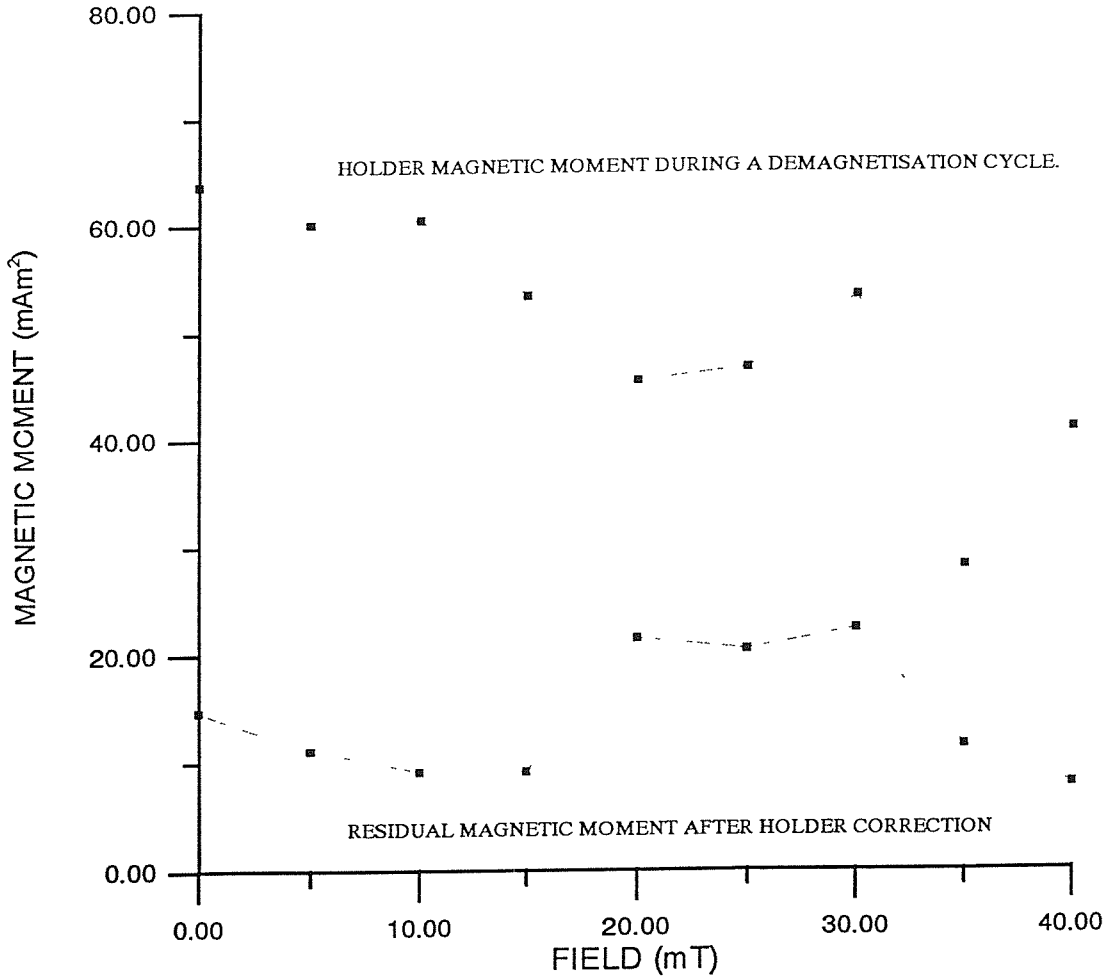

Figure 5.11. Plot of the 2-G wholecore magnetometer's sample holder magnetic moment and the residual magnetic moment after application of holder correction versus demagnetisation field.

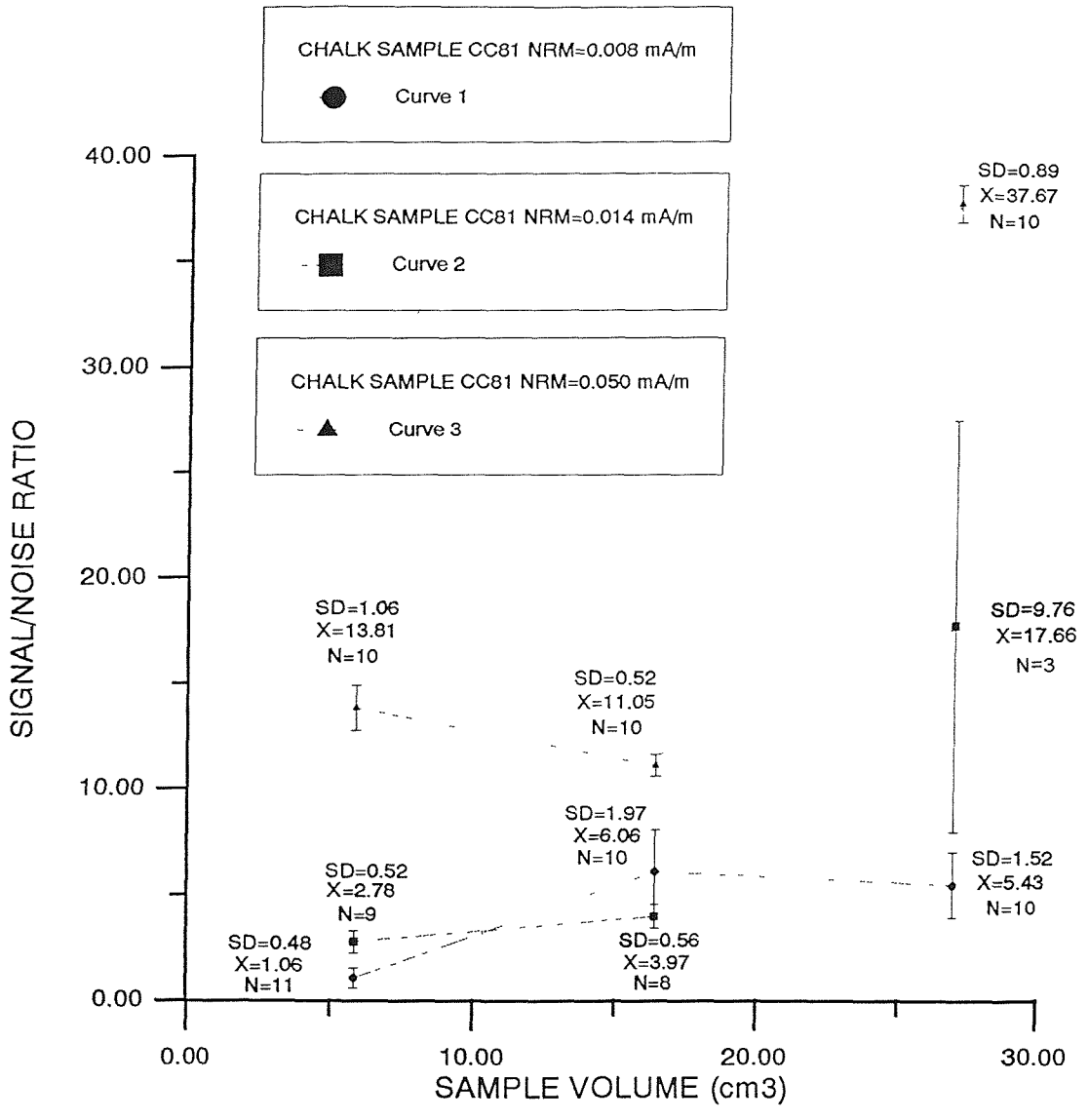

Figure 5.12. A plot of Signal/Noise ratio versus sample volume for three chalk samples taken from the same sampling horizon.

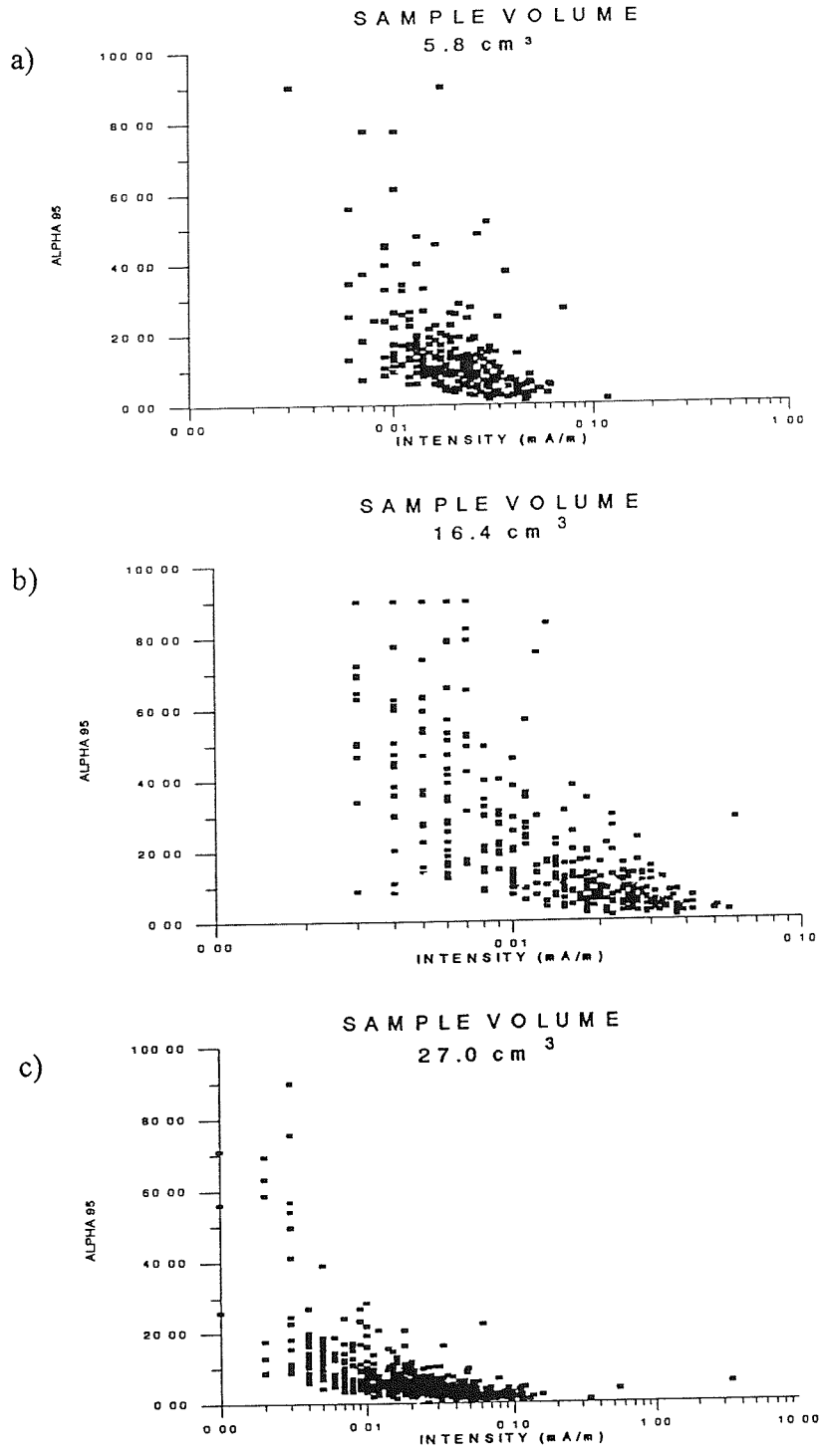

Figure 5.13 a,b & c. Plots of Alpha 95 for multiple measurements versus magnetic intensity (mA/m) for measurements on 5.8 cm^3 (a), 16.4 cm^3 (b) and 27.0 cm^3 (c) volume chalk cubes.

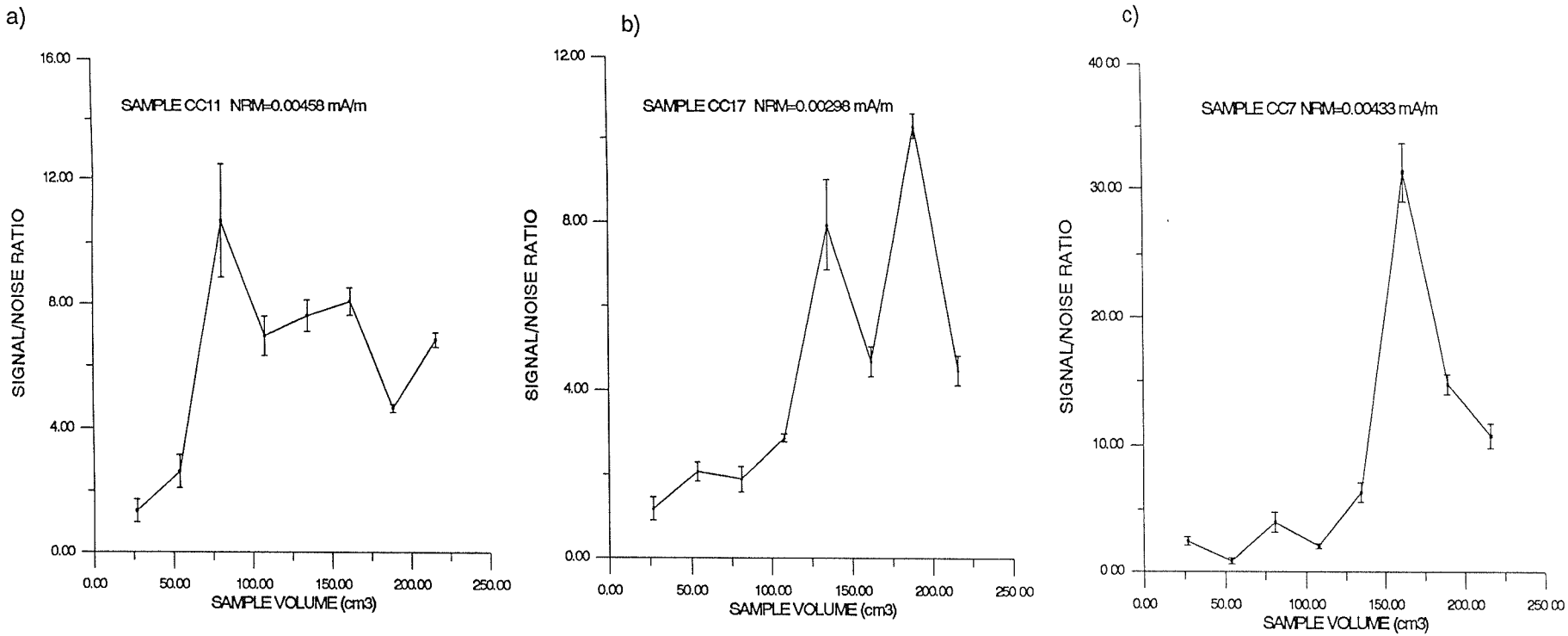

Figure 5.14. Plots of the "signal/noise" ratio against volume for three large volume chalk cubes with weak NRM intensities. The samples were measured in the 2-G wholecore magnetometer. Multiple measurements were made on each cube, the volume of which was successively trimmed from 216.0 cm^3 to 27.0 cm^3 in 27.0 cm^3 increments.

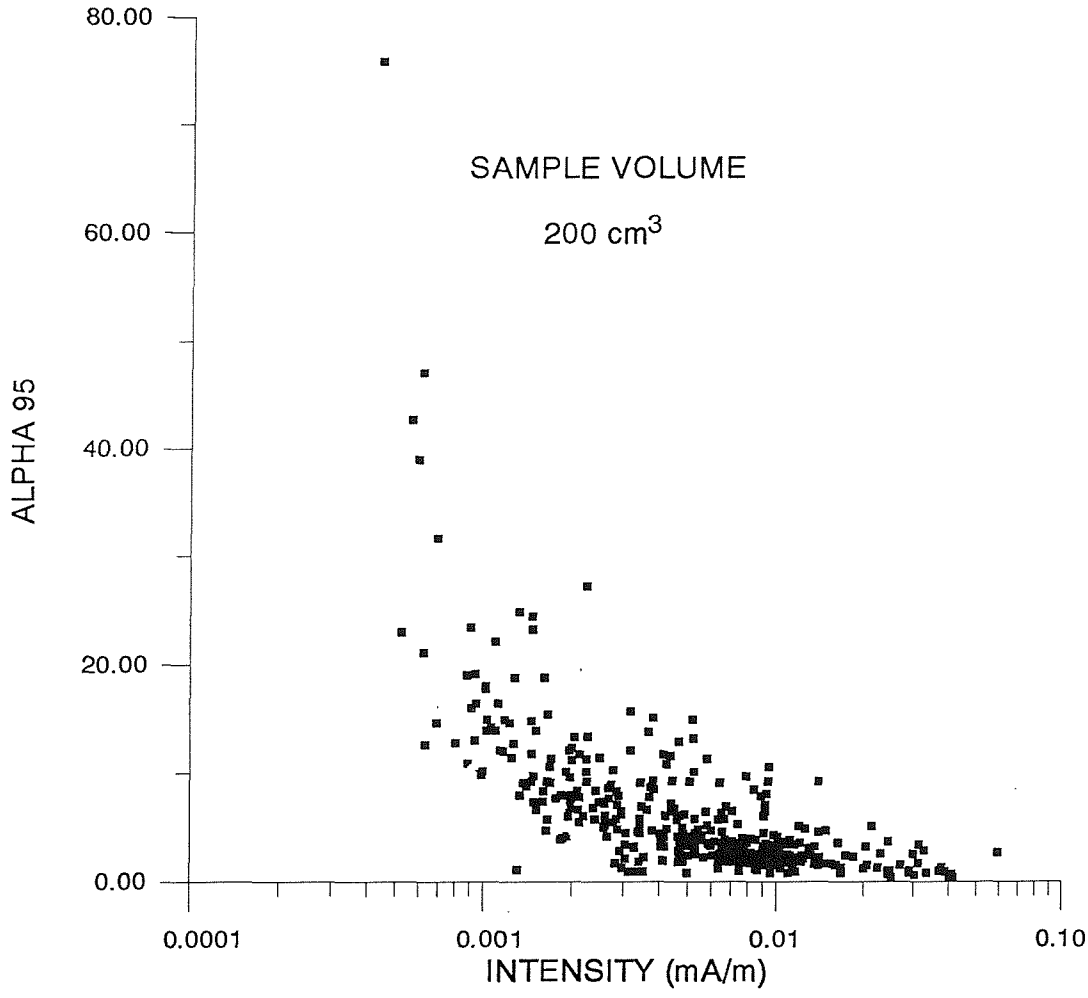

Figure 5.15. A plot of Alpha 95 for multiple measurements versus magnetic intensity (mA/m) for 2-G wholecore magnetometer measurements on chalk samples 200 cm^3 in volume.

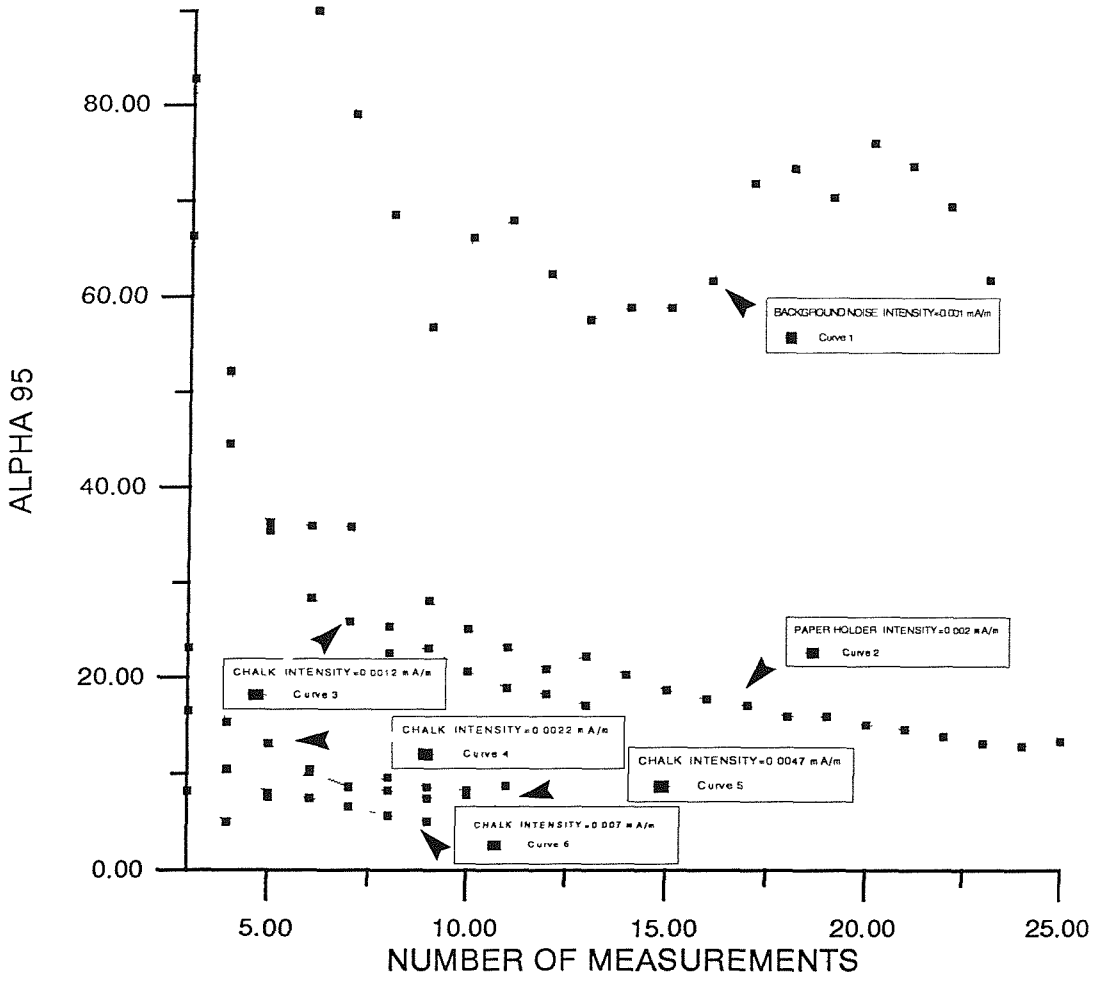

Figure 5.16. A plot of Alpha 95 versus the number of repeat measurements for (i) the CCL discrete sample cryogenic magnetometer's background noise; (ii) an empty paper sample holder and (iii) four 27.0 cm^3 chalk samples with different remanent magnetism intensities.

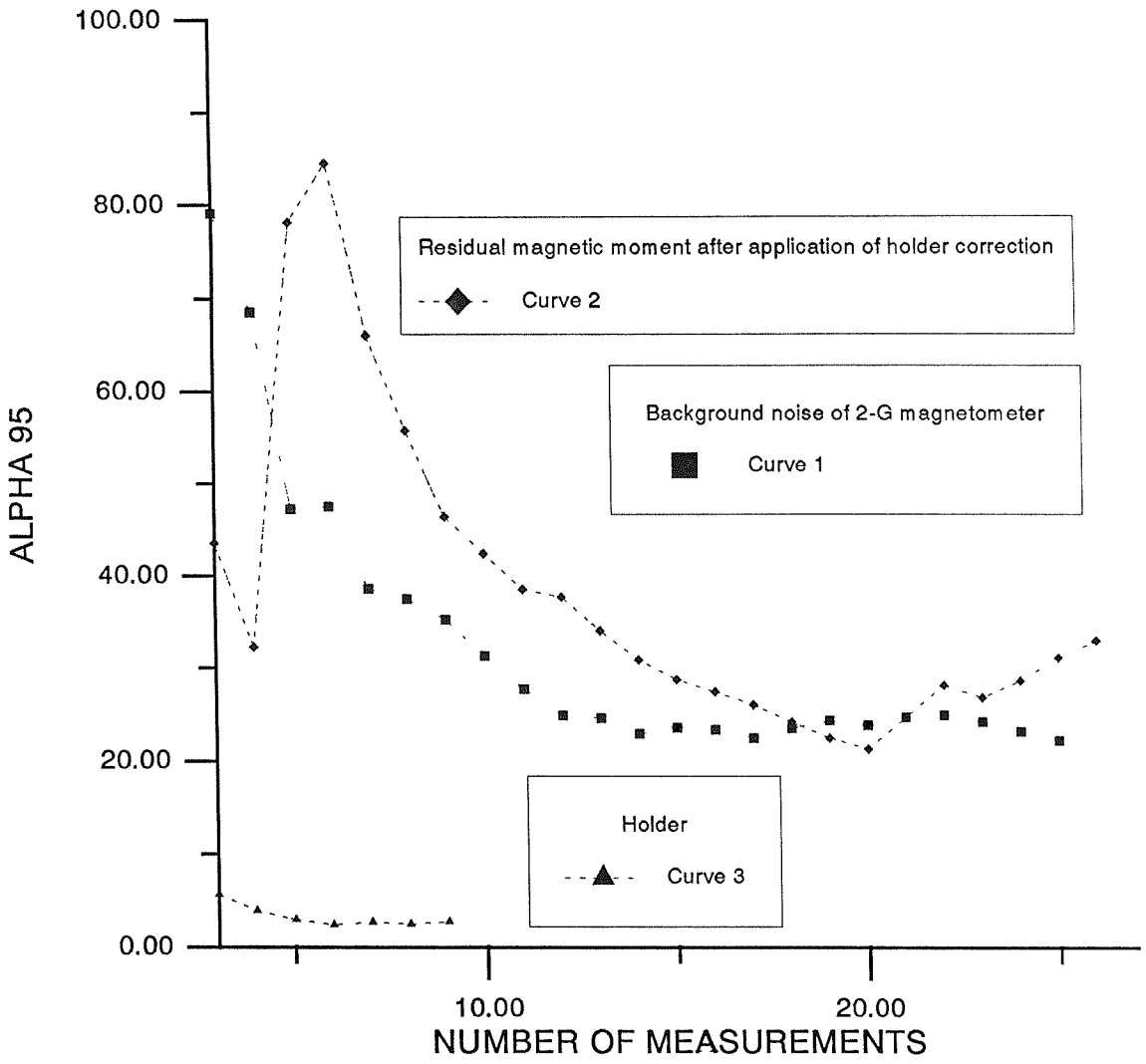

Figure 5.17. Plot of Alpha 95 versus the number of replicate measurements by the 2-G whole core magnetometer for (i) the background noise of the magnetometer (curve 1); (ii) the empty holder (curve 3); (iii) the empty holder after application of a holder correction (curve 2).

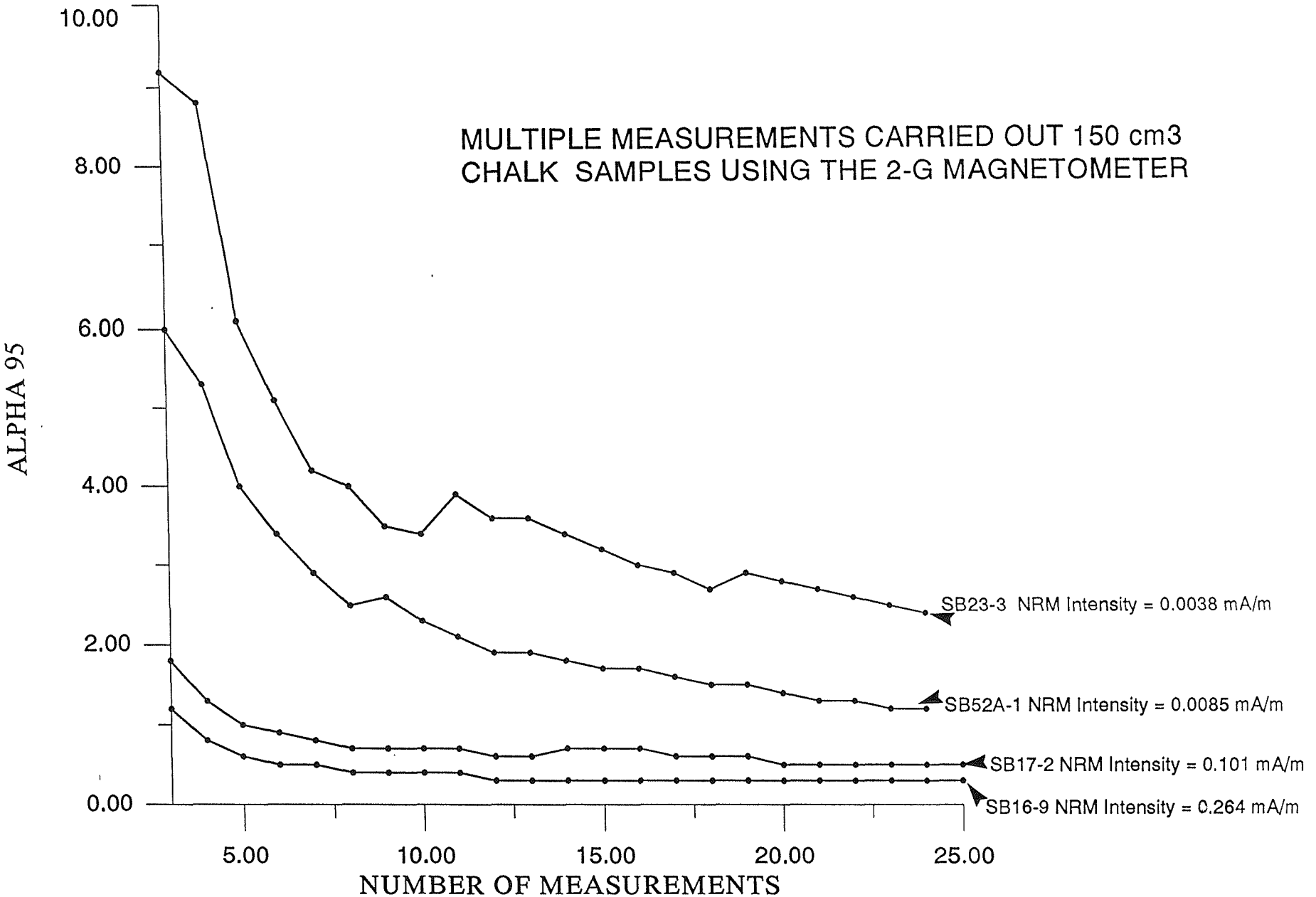

Figure 5.18. A plot of alpha 95 versus replicate measurements of various 150 cm^3 chalk samples. Sample magnetic intensities vary from strong (0.264 mA/m) to extremely weak (0.0038 mA/m).

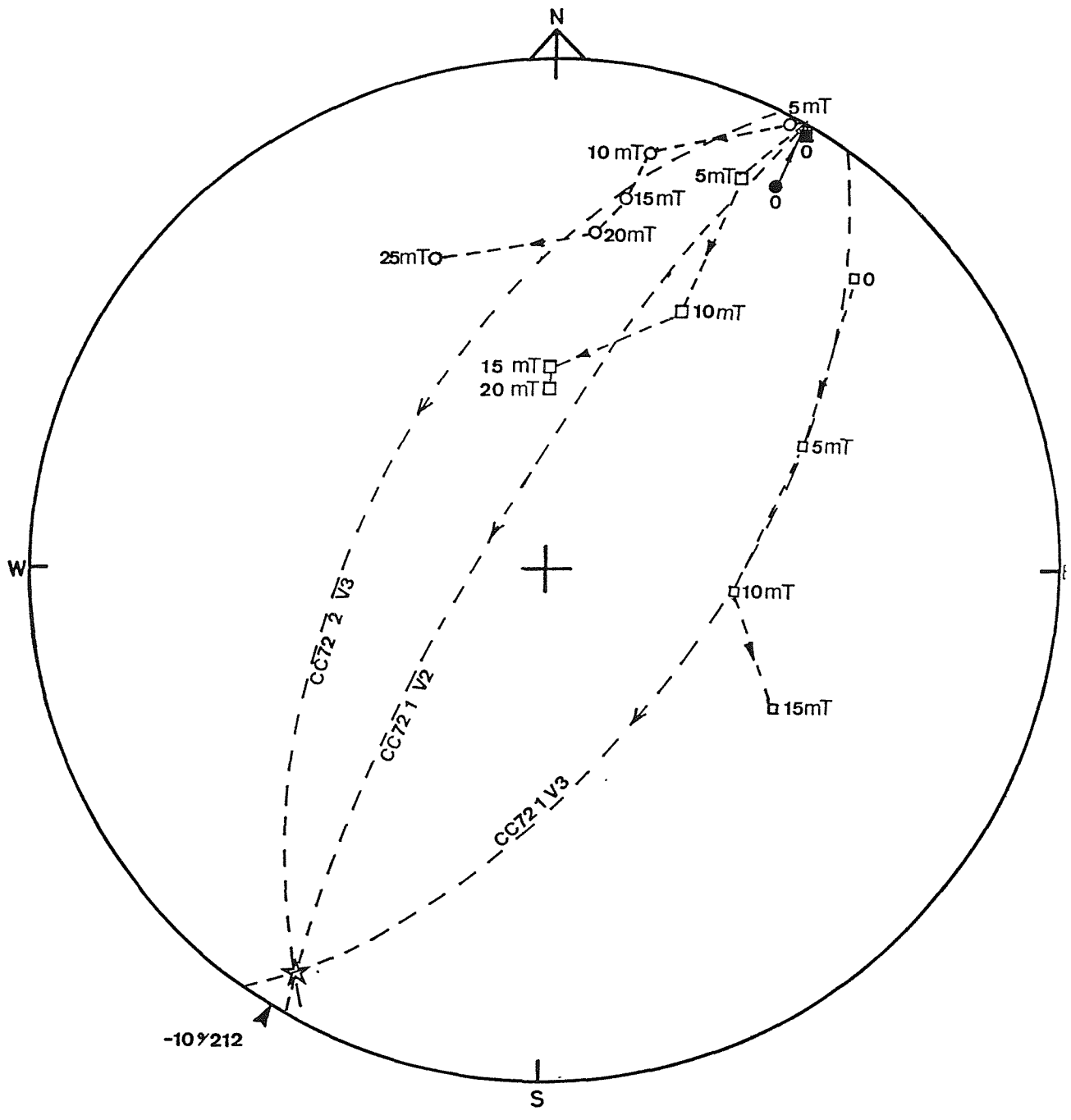

Figure 5.19. A stereographic projection plot of directional trends during alternating field demagnetisation of three 27.0 cm^3 chalk samples from the same sample horizon (after a bedding correction has been applied). The AF demagnetisation fields applied are indicated. Best fit great circles have been plotted to represent the demagnetisation trends observed. These great circles intersect at $-10^0/212^0$.

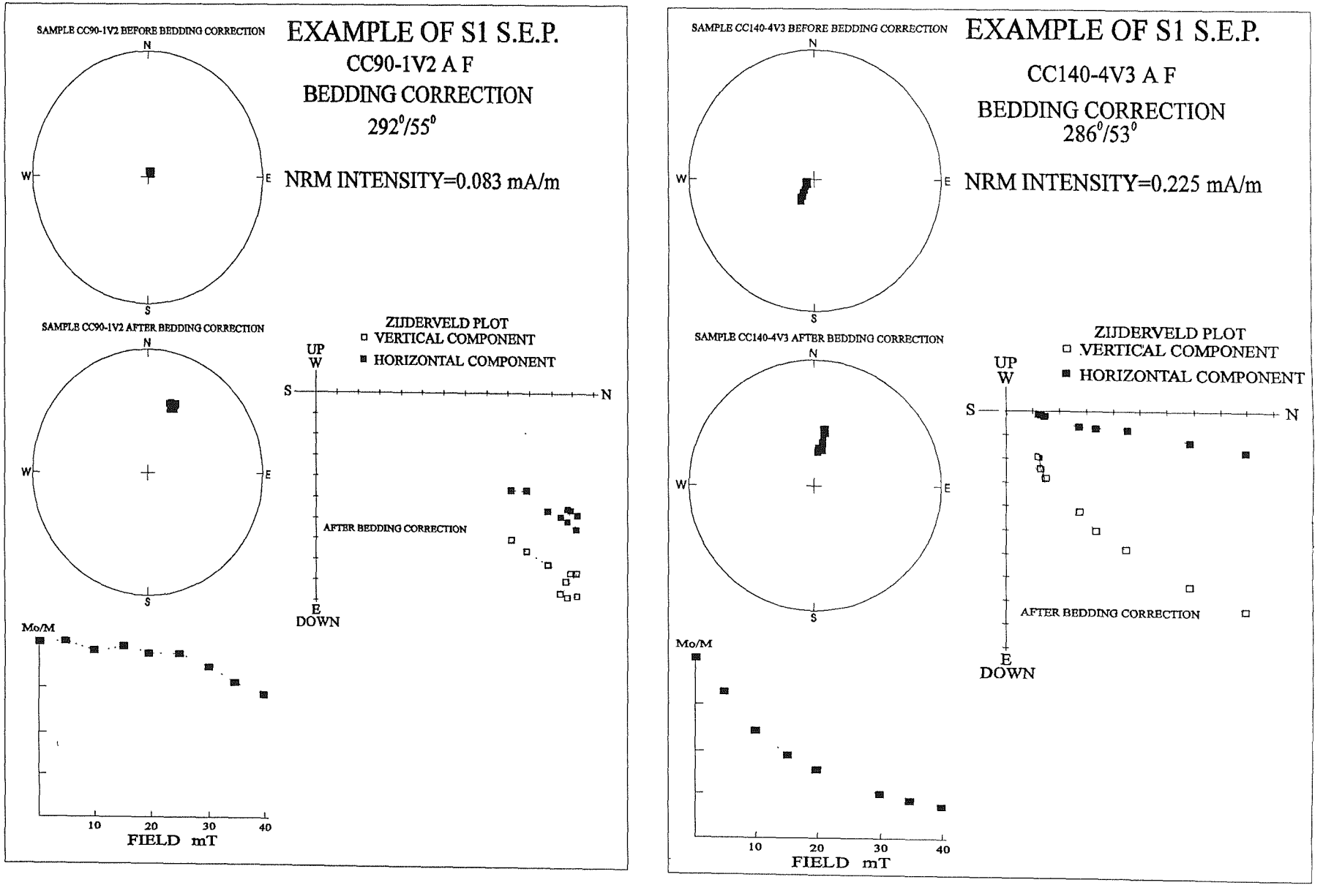

Figure 5.20. Examples of normal polarity assigned to reliability category S1 after subjection to A F demagnetisation.

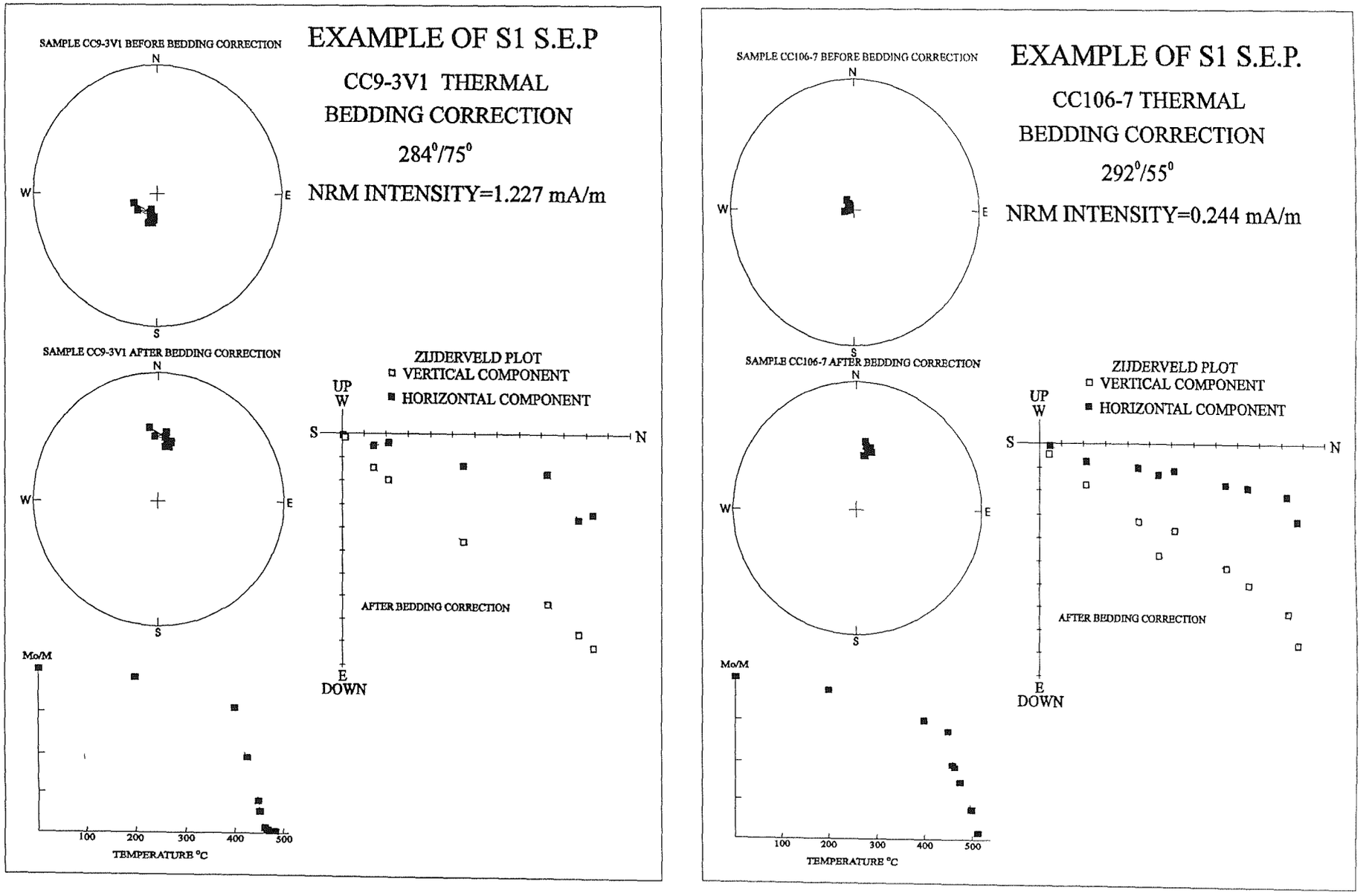

Figure 5.20b. Examples of normal polarity assigned to reliability category S1 after subjection to thermal demagnetisation.

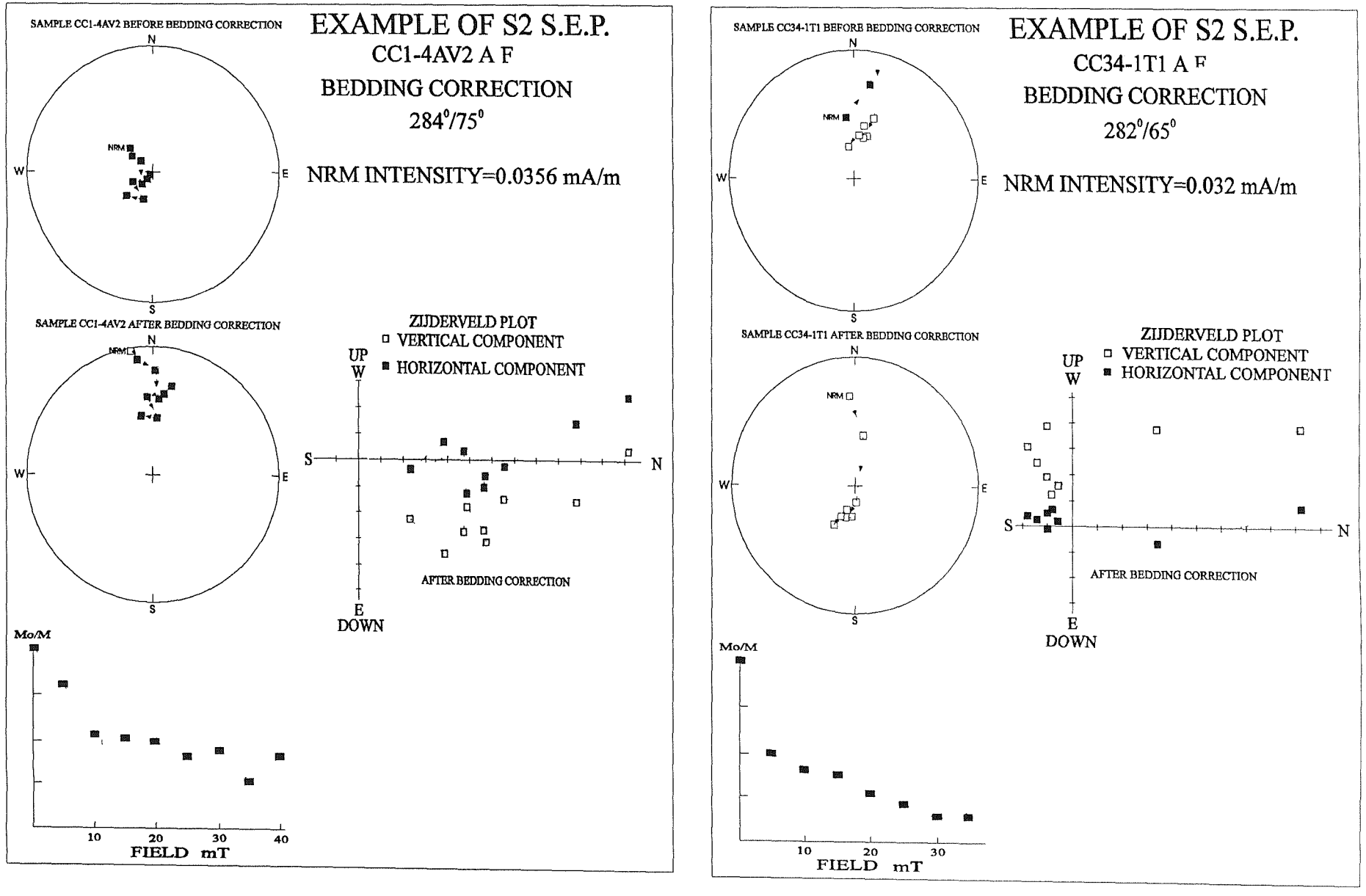

Figure 5.21a. Examples of normal and reverse polarity assigned to reliability category S2 after subjection to A F demagnetisation.

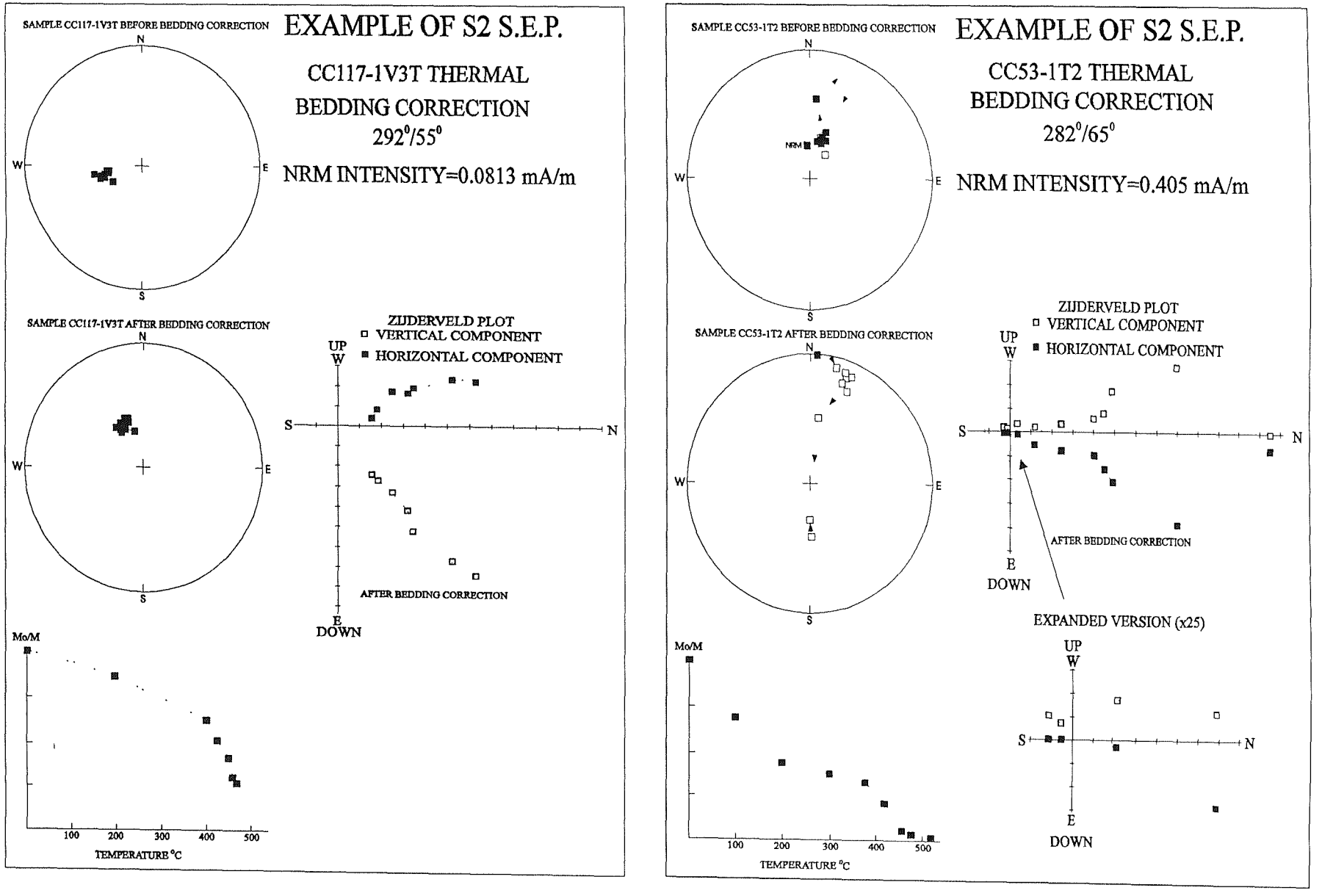

Figure 5.21b. Examples of normal and reverse polarity assigned to reliability category S2 after subjection to thermal demagnetisation.

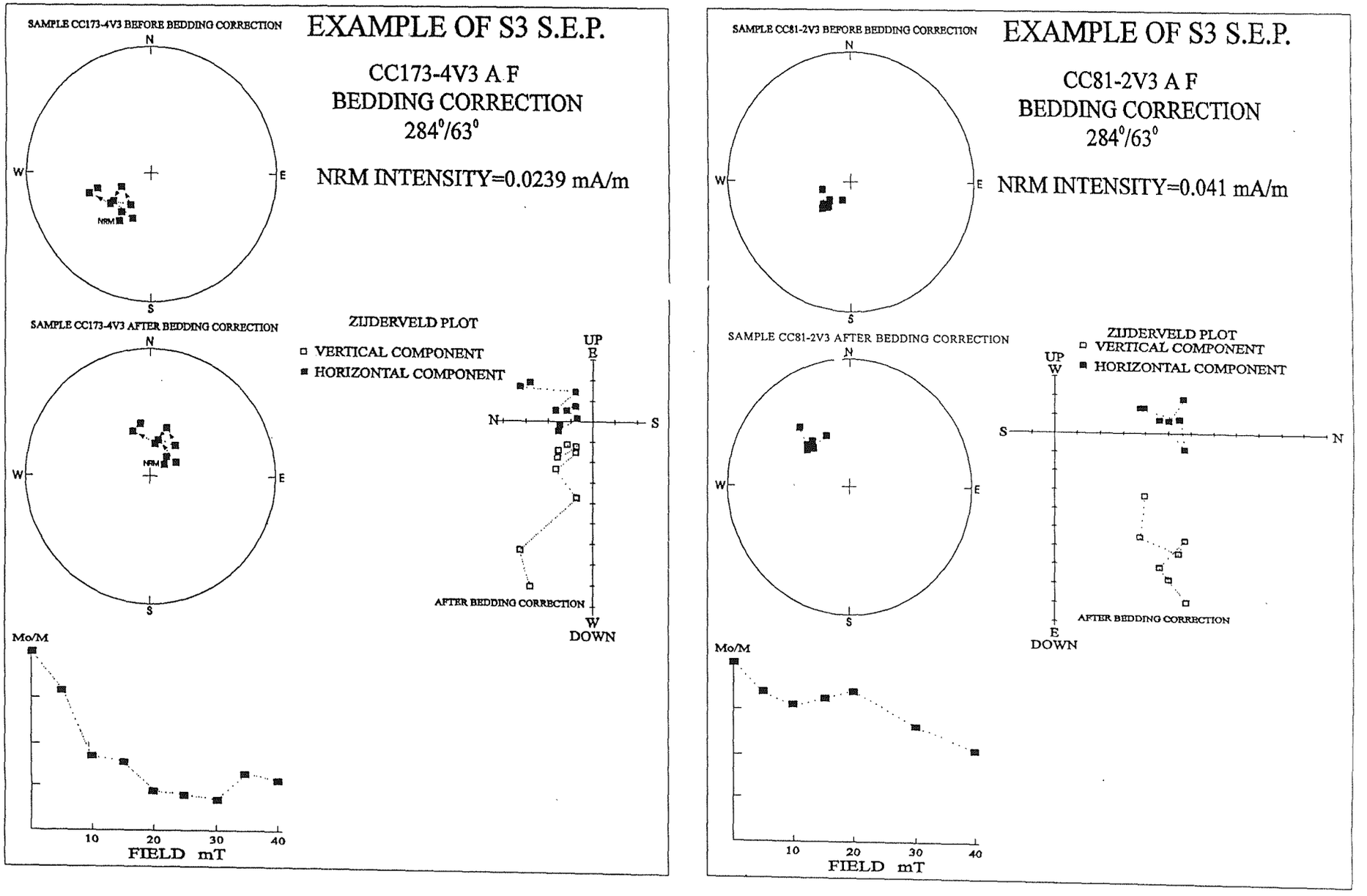

Figure 5.22a. Examples of normal polarity assigned to category S3 after subjection to A F. demagnetisation.

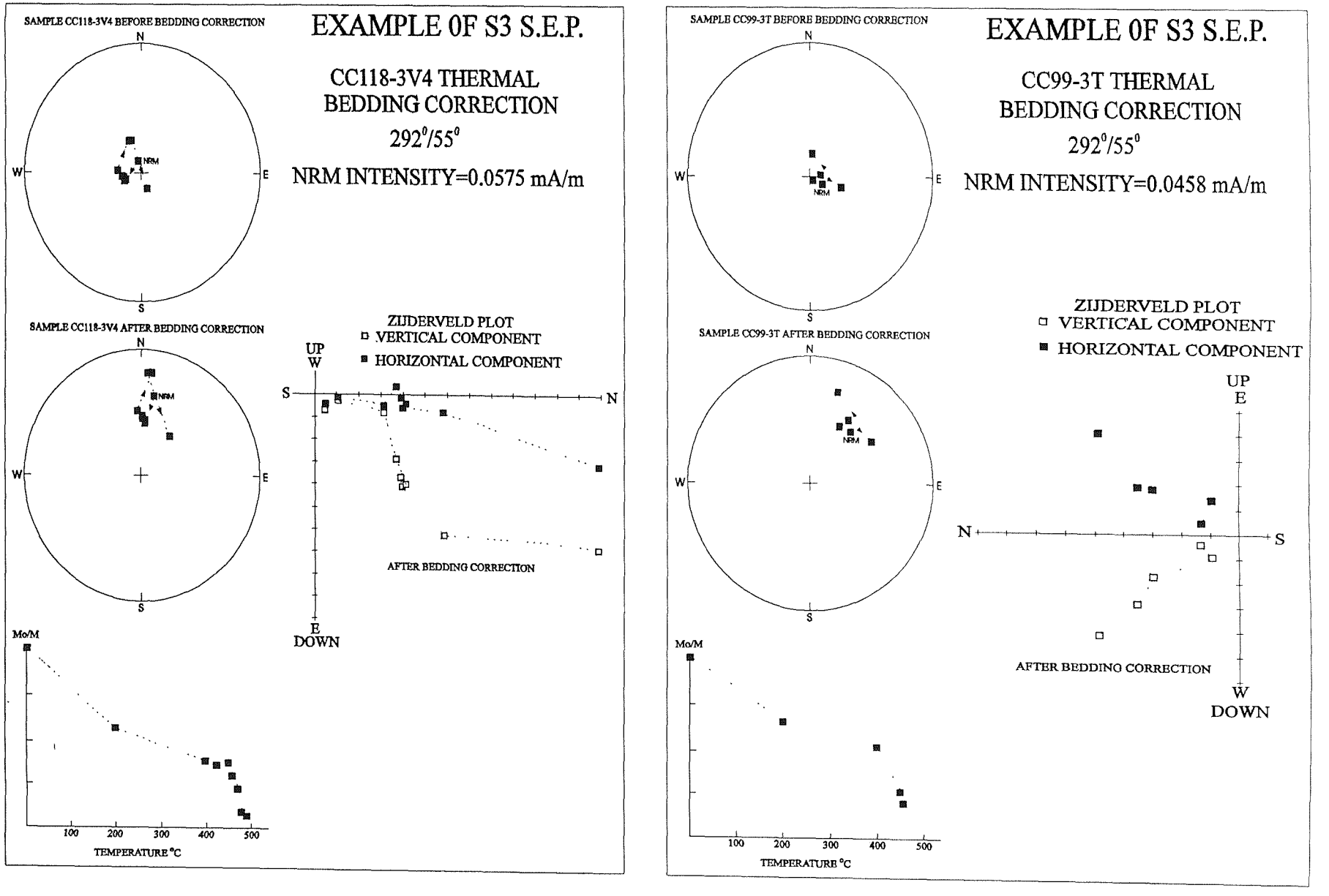

Figure 5.22b. Examples of normal polarity assigned to reliability category S3 after subjection to thermal demagnetisation.

EXAMPLES OF T1 TYPE TRENDS

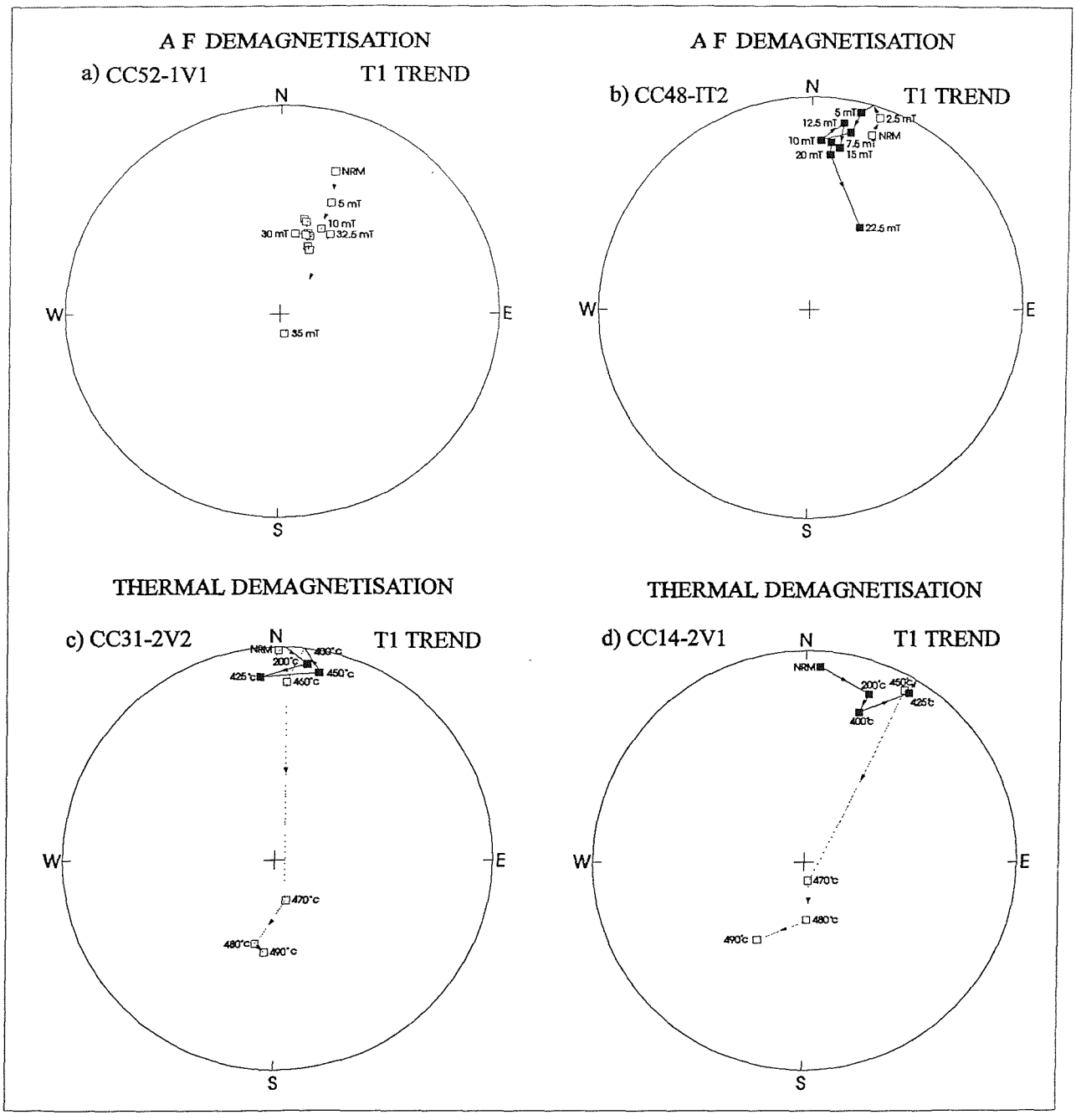

Figure 5.23. Examples of normal and reverse polarity high quality directional trend T1 data after subjection to A F and thermal demagnetisation. Stereograms (a), (c) and (d) indicate trends to reverse polarity while stereogram (b) displays a directional trend to normal polarity.

EXAMPLES OF T2 TYPE TRENDS

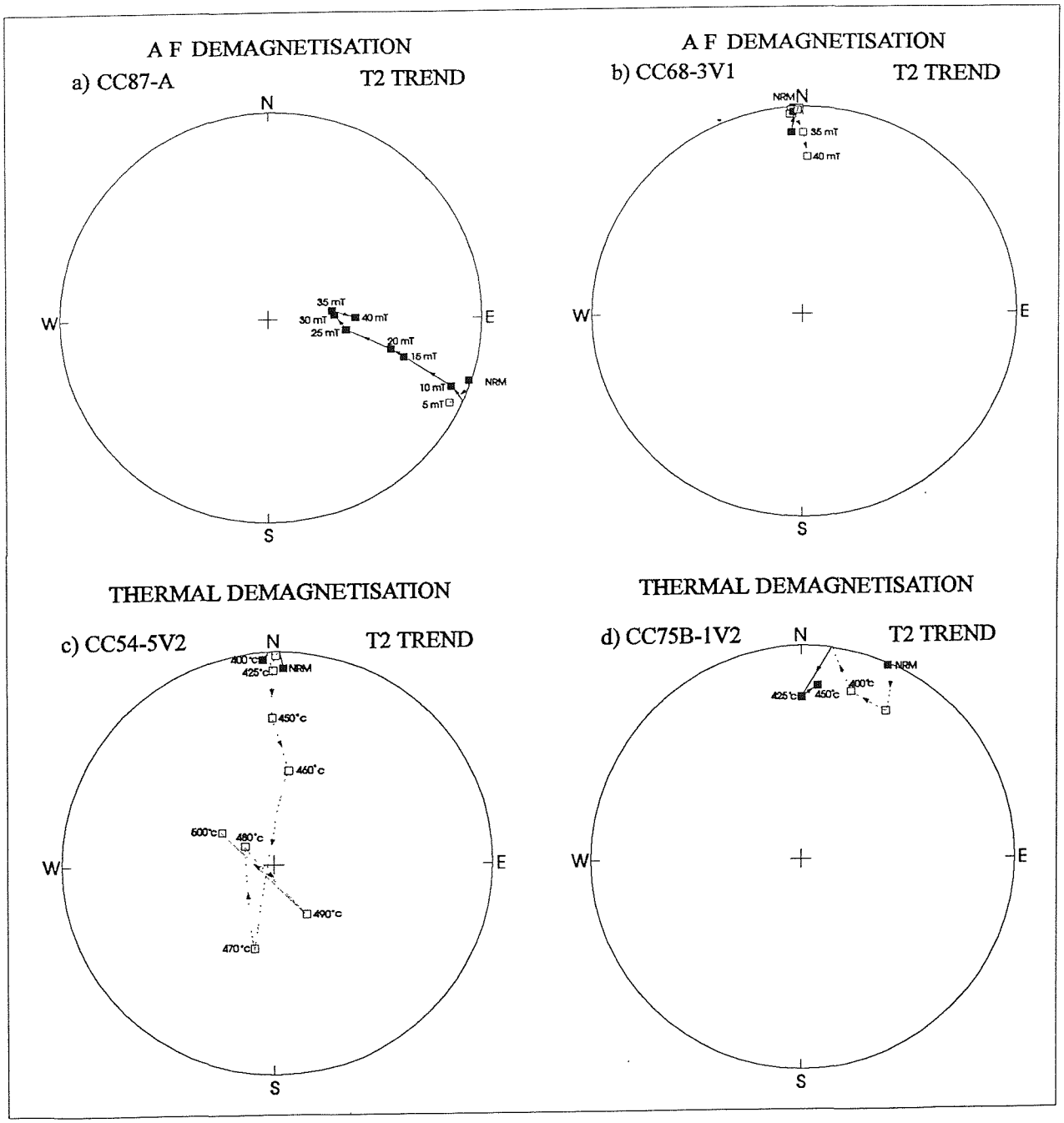

Figure 5.24. Examples of normal and reverse polarity intermediate quality directional trend T2 data after subjection to A F and thermal demagnetisation. Stereograms (b) and (c) indicate trends to reverse polarity while stereograms (a) and (d) display directional trends to normal polarity.

EXAMPLES OF T3 TYPE TRENDS

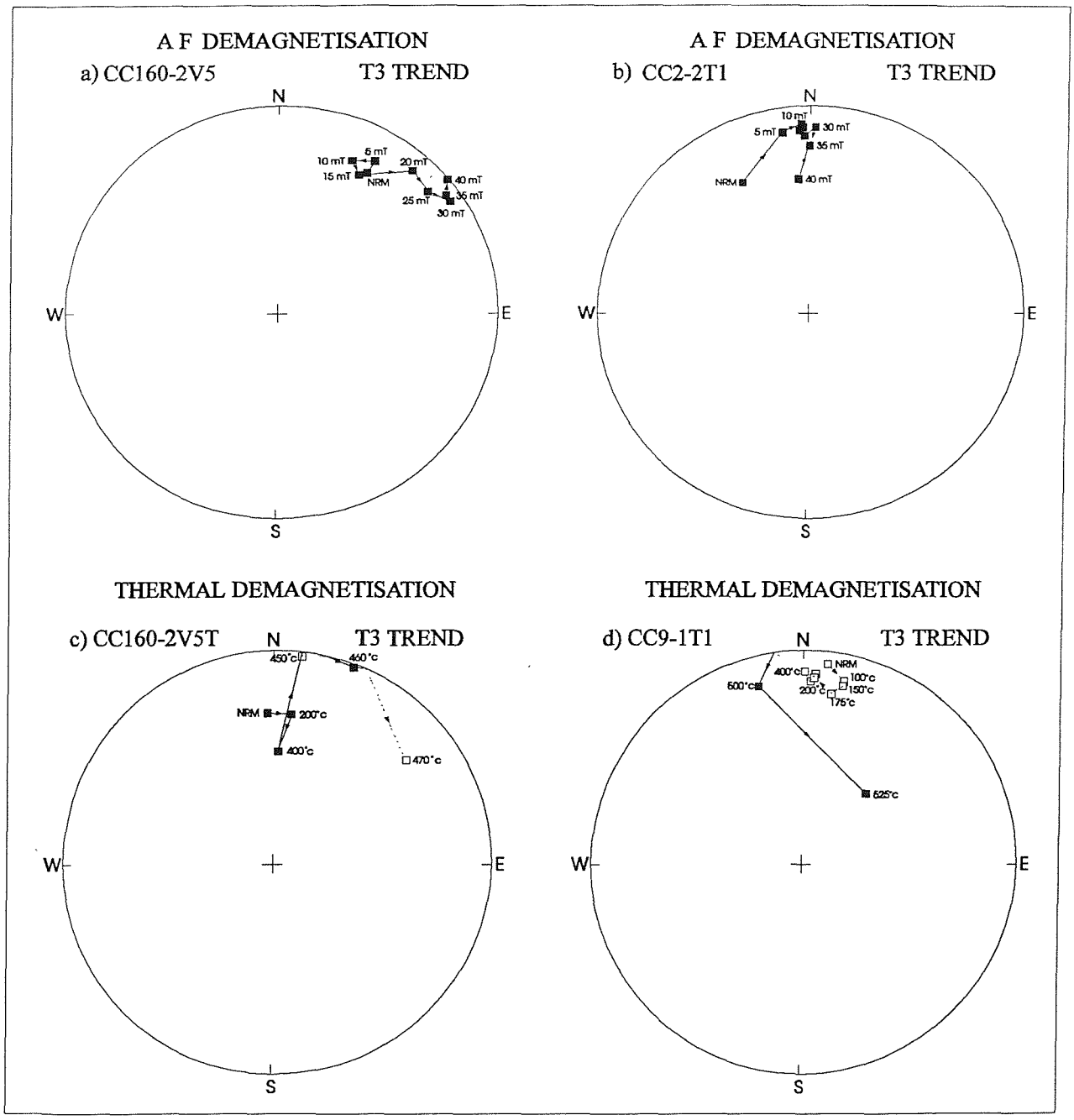

Figure 5.25. Examples of normal and reverse polarity poor quality directional trend T3 data after subjection to A F and thermal demagnetisation. Stereograms (a) and (c) suggest trends to reverse polarity while stereograms (b) and (d) suggest directional trends to normal polarity.

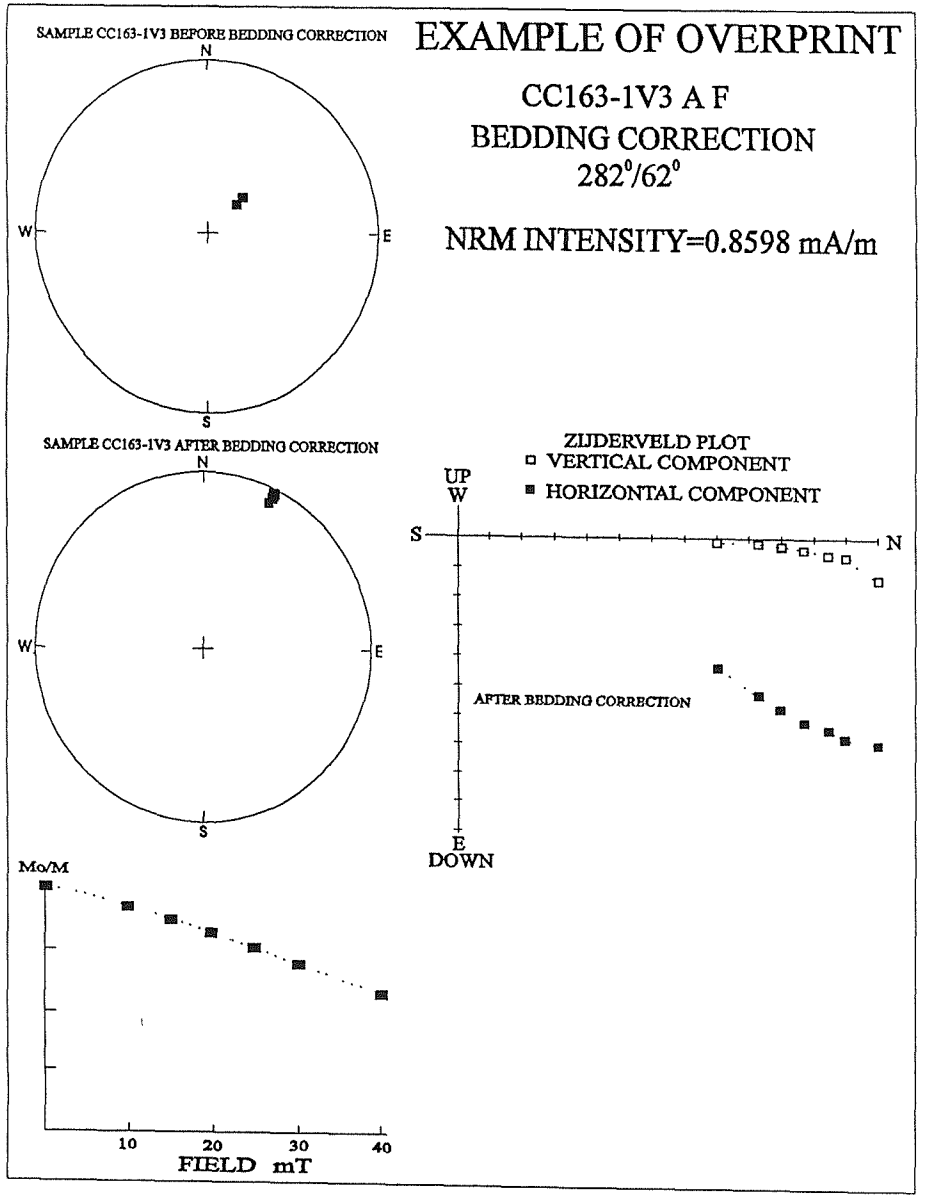

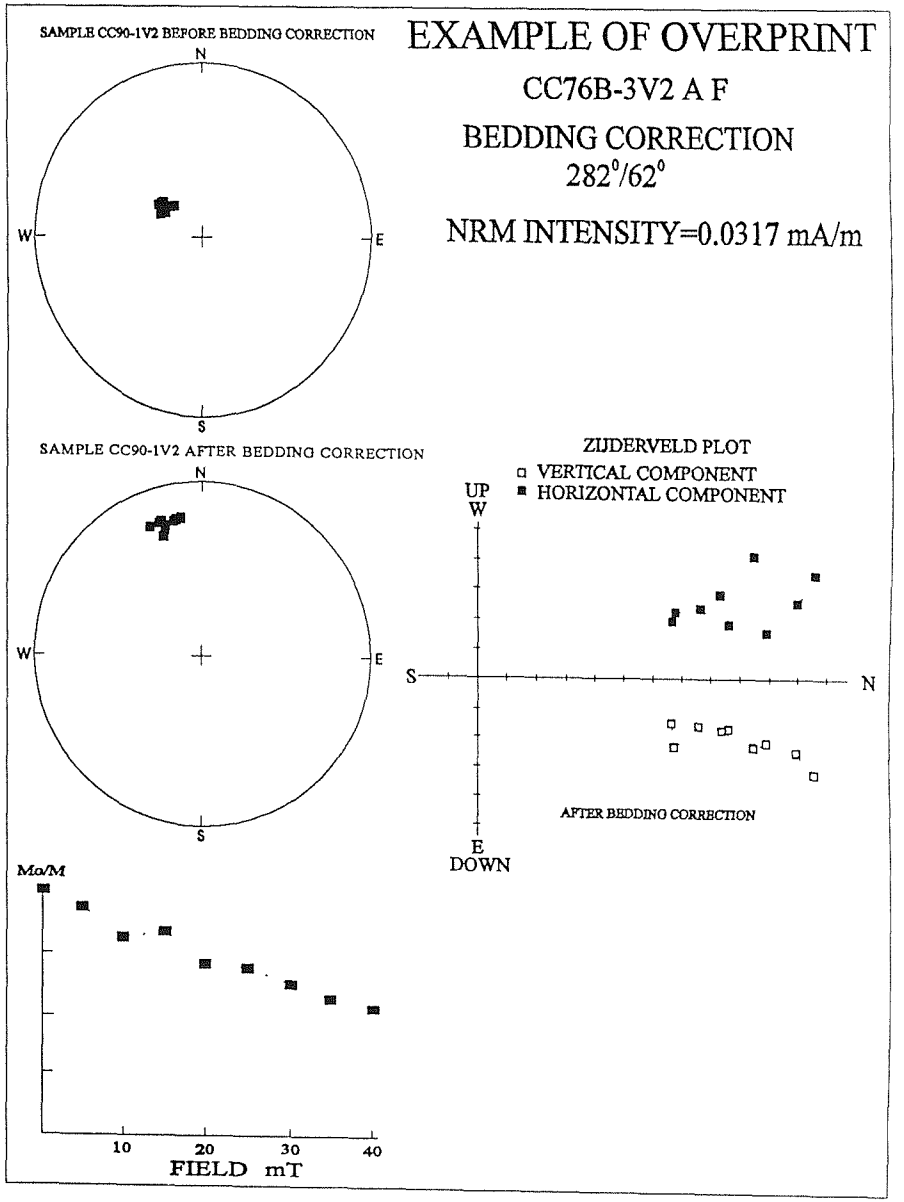

Figure 5.26a. Examples of specimens displaying overprints not removed by A F demagnetisation procedures.

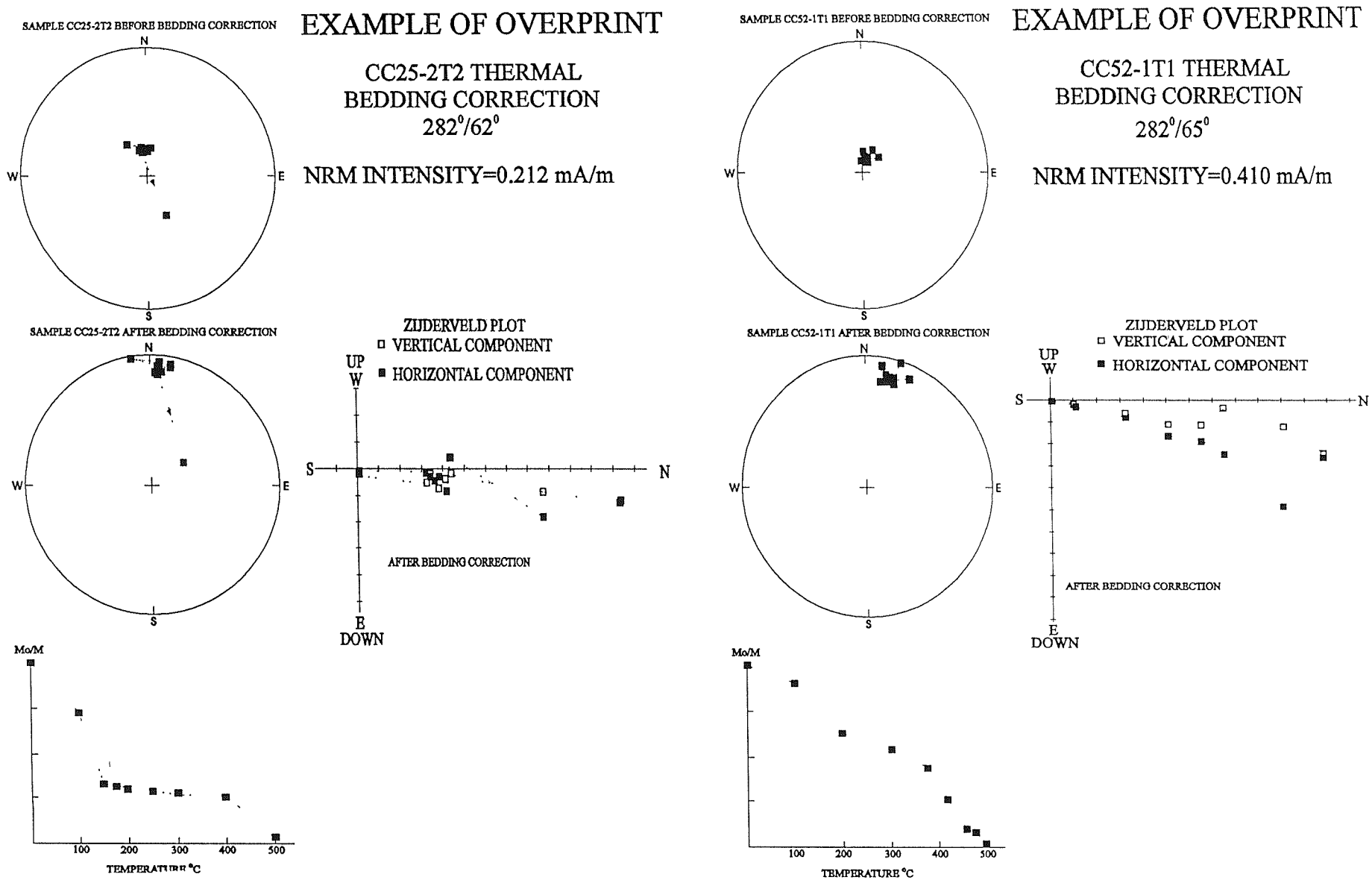

Figure 5.26b. Examples of specimens displaying magnetic overprints not removed by thermal demagnetisation procedures

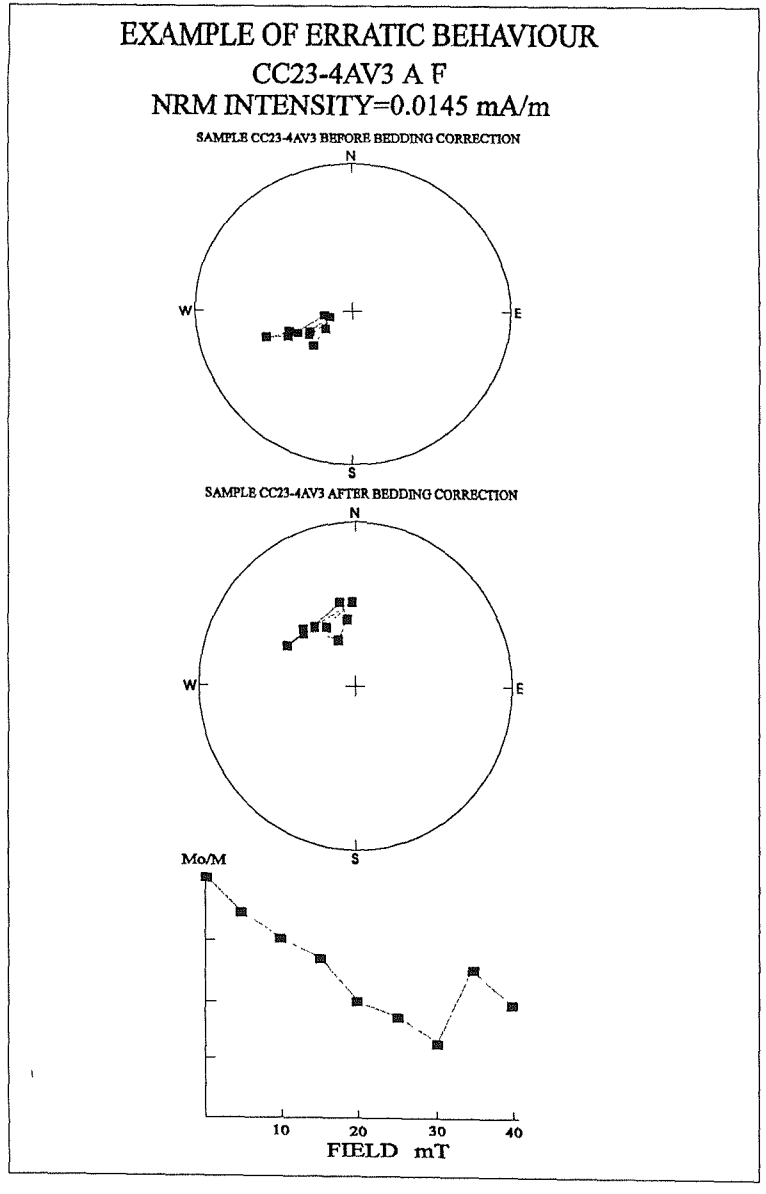

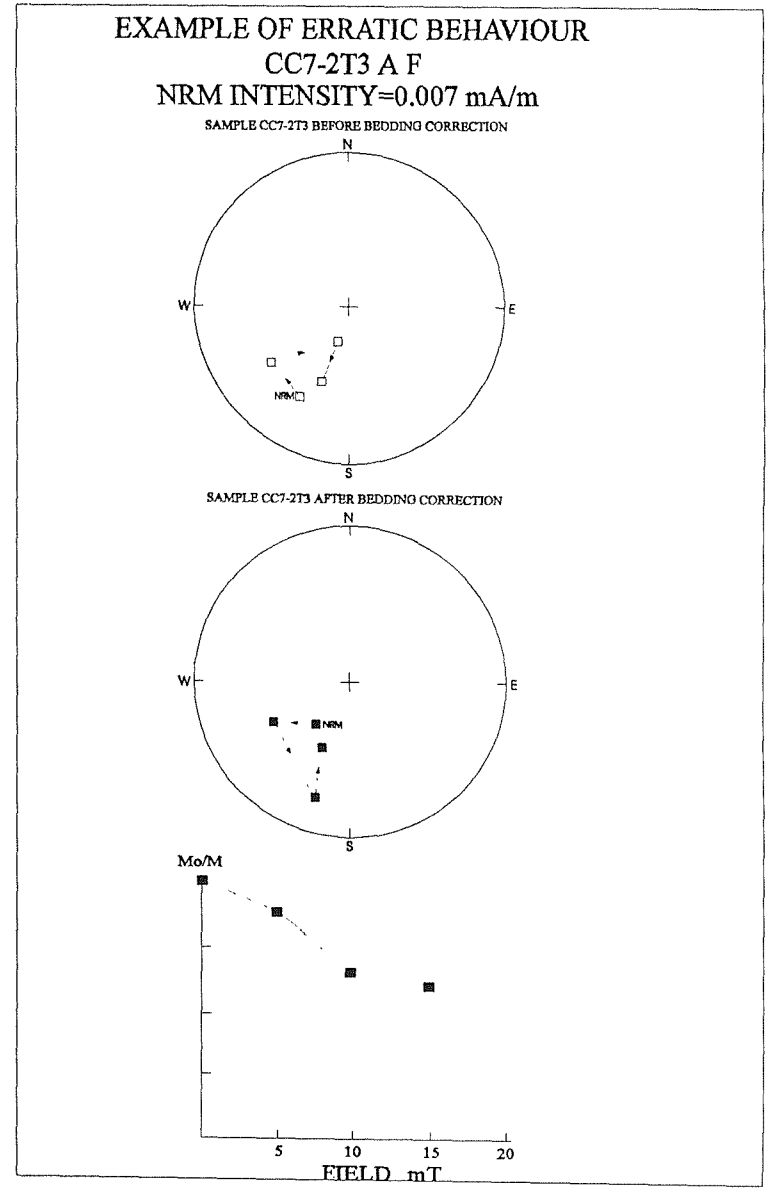

Figure 5.27a. Examples of specimens displaying erratic behaviour during A F demagnetisation procedures.

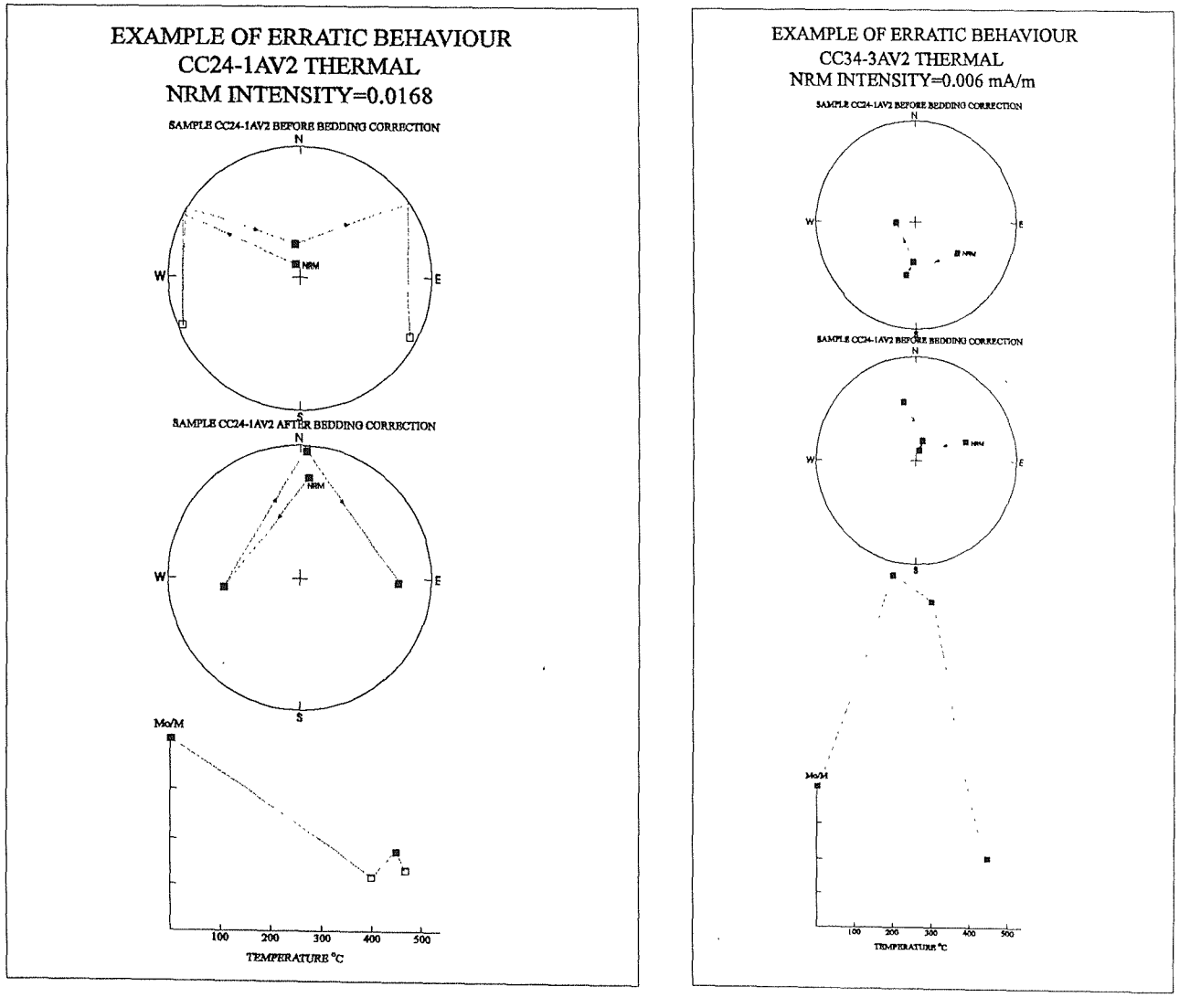

Figure 5.27b. Examples of specimens displaying erratic behaviour during thermal demagnetisation procedures.

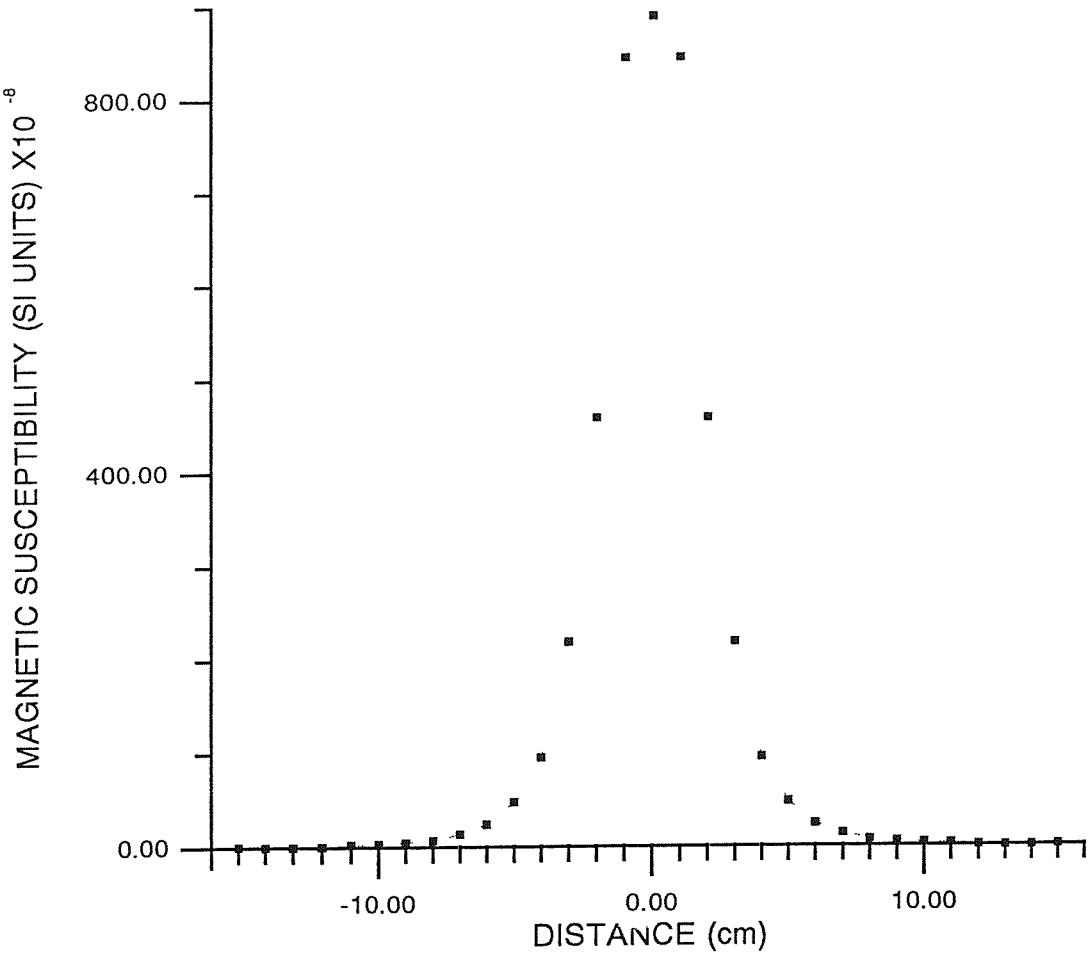

Figure 5.28. The response curve for a 80 mm loop type Bartington susceptibility bridge (model type M.S.1.C).

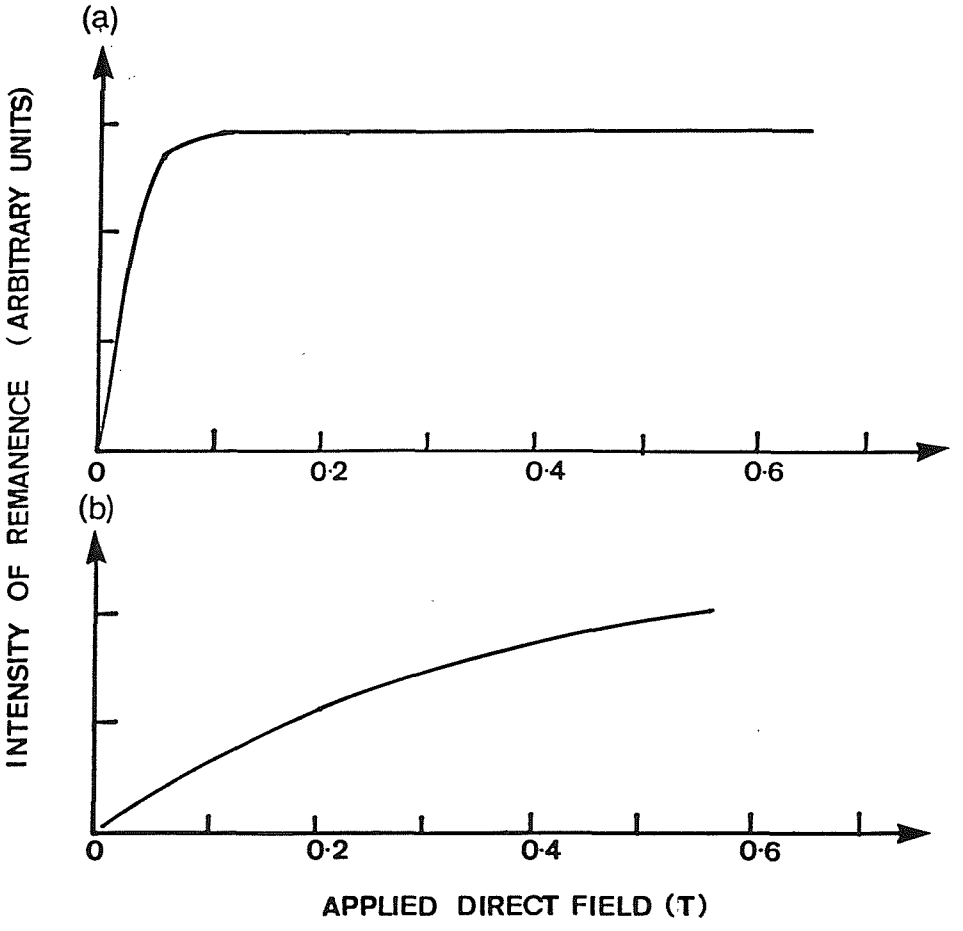

Figure 5.29. Isothermal Remanent Magnetisation (IRM) aquisition curves for magnetite and hematite. (a) Magnetite saturates in weaker magnetic fields than (b) hematite, which is often not saturated in fields available from conventional laboratory apparatus (Tarling 1983).

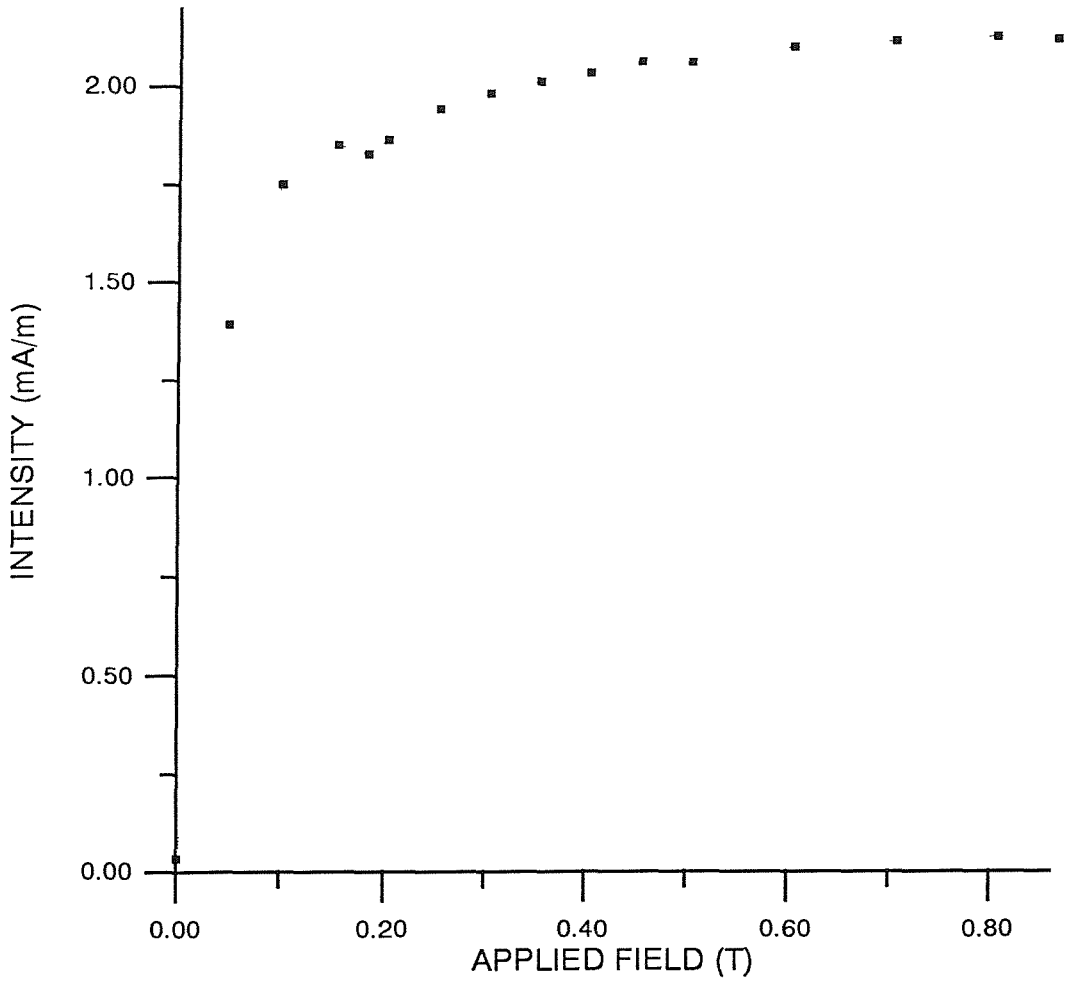

Figure 5.30. Shows the typical response of a chalk sample after being subjected to a series of incremental direct magnetic fields

Plate 5.1 The use of a petrol driven cutter.

Plate 5.2 Formation of a horizontal orientation surface.

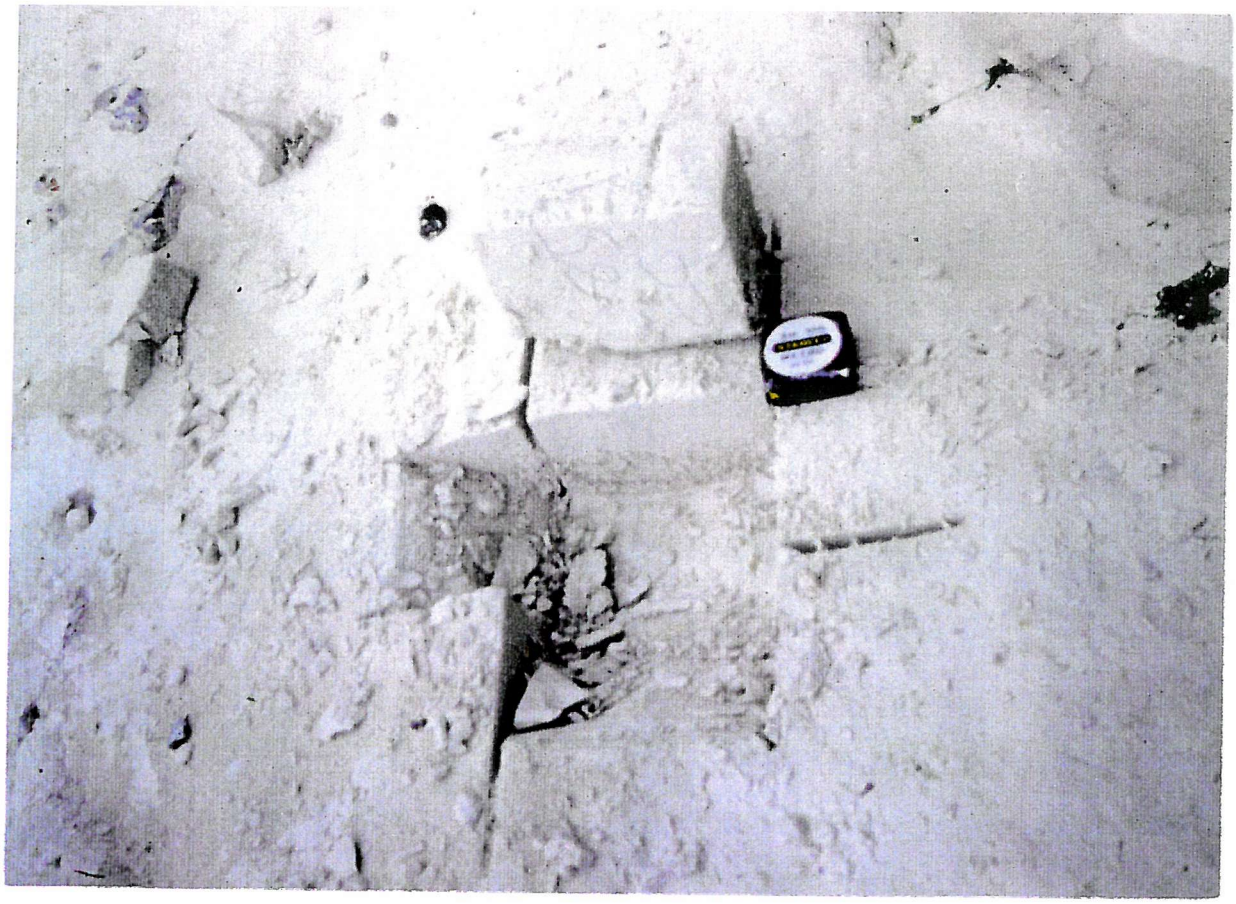

Plate 5.3 Extraction of a roughly cubic hand sample.

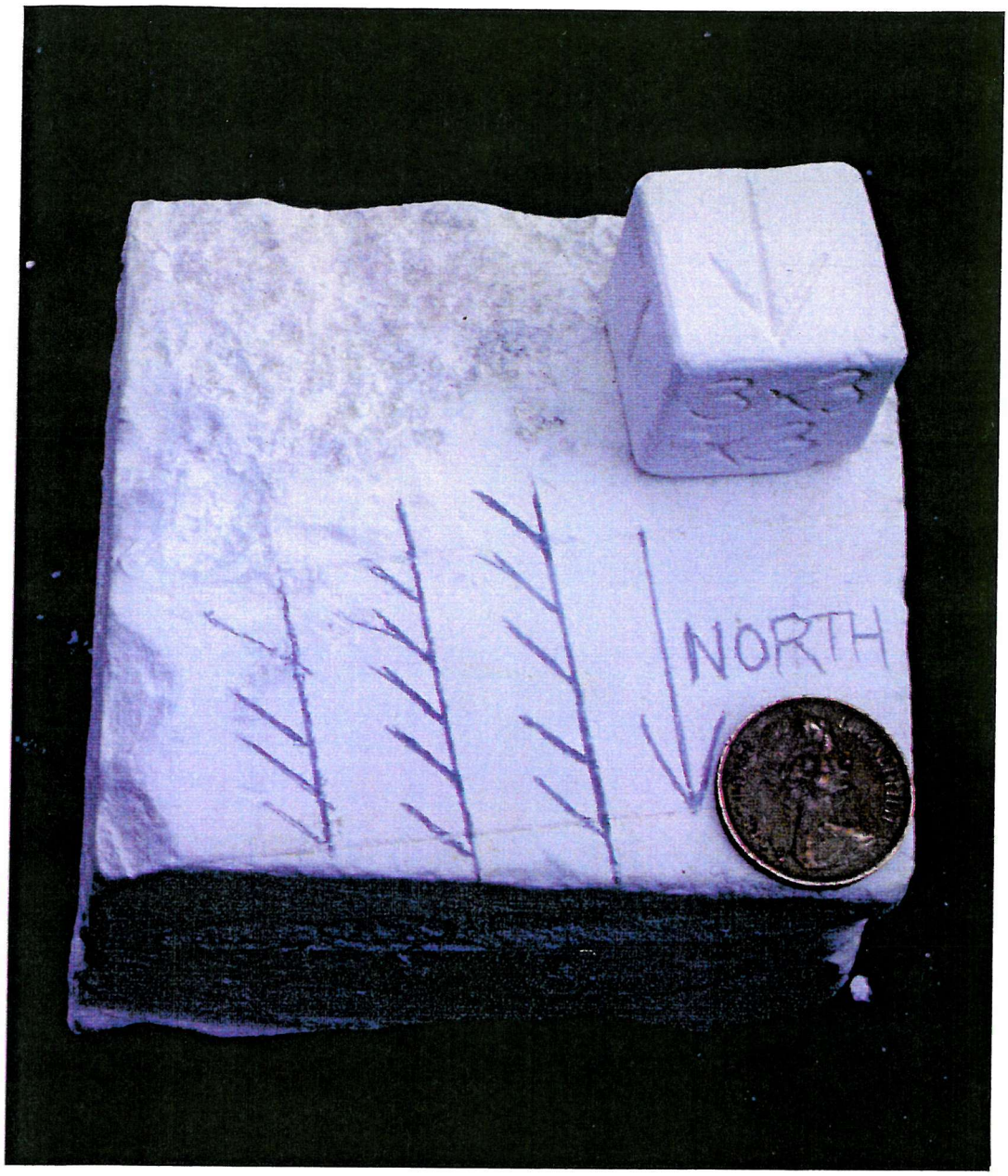

Plate 5.4 Orientated hand sample and 27 cm^3 chalk cube.

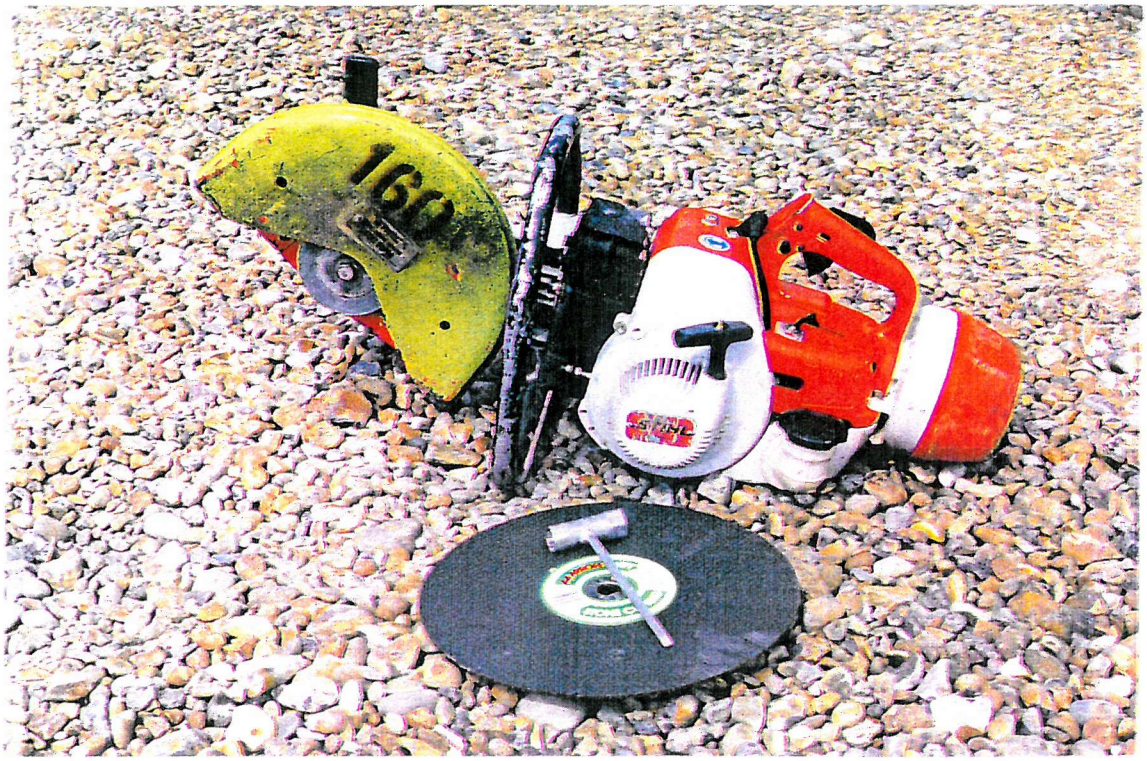

Plate 5.5 Petrol driven disc cutter and 12 inch abrasive non-magnetic wheel.

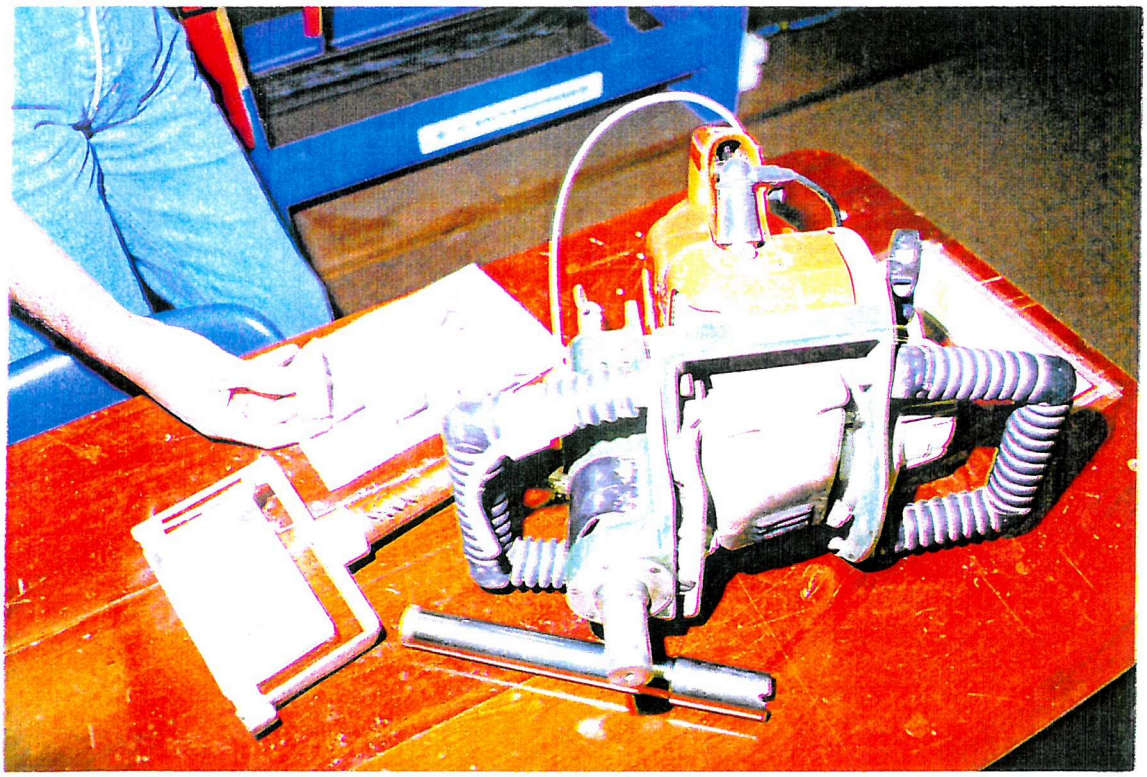

Plate 5.6 Portable rock drill, coring bit, rock cores and orientation table.

Plate 5.7 CCL discrete sample cryogenic magnetometer (a), AF demagnetiser (b) and sample handling device (c).

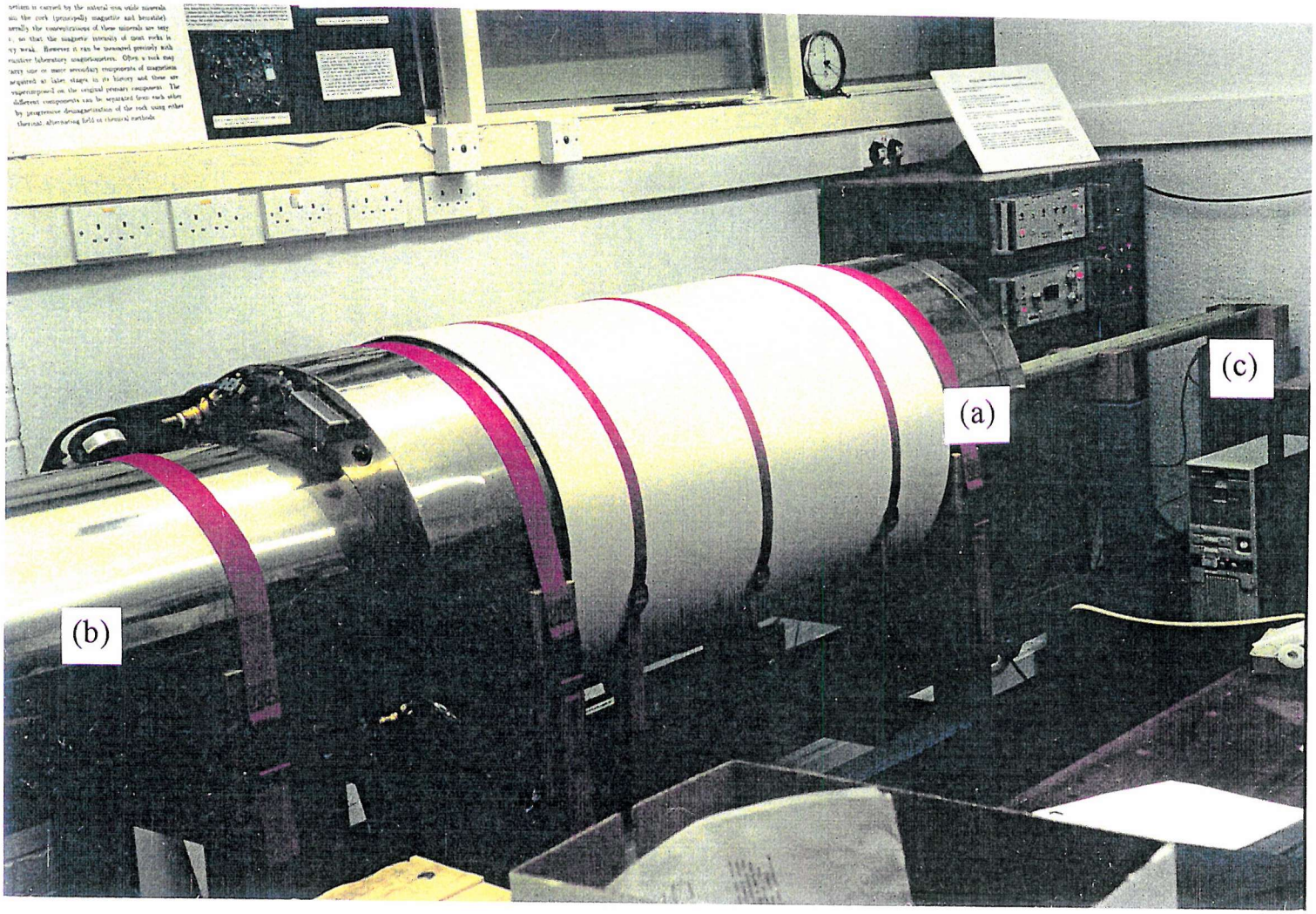

Plate 5.8 2-G wholecore cryogenic magnetometer (a), in-line AF demagnetiser (b) and sample handling device (c).

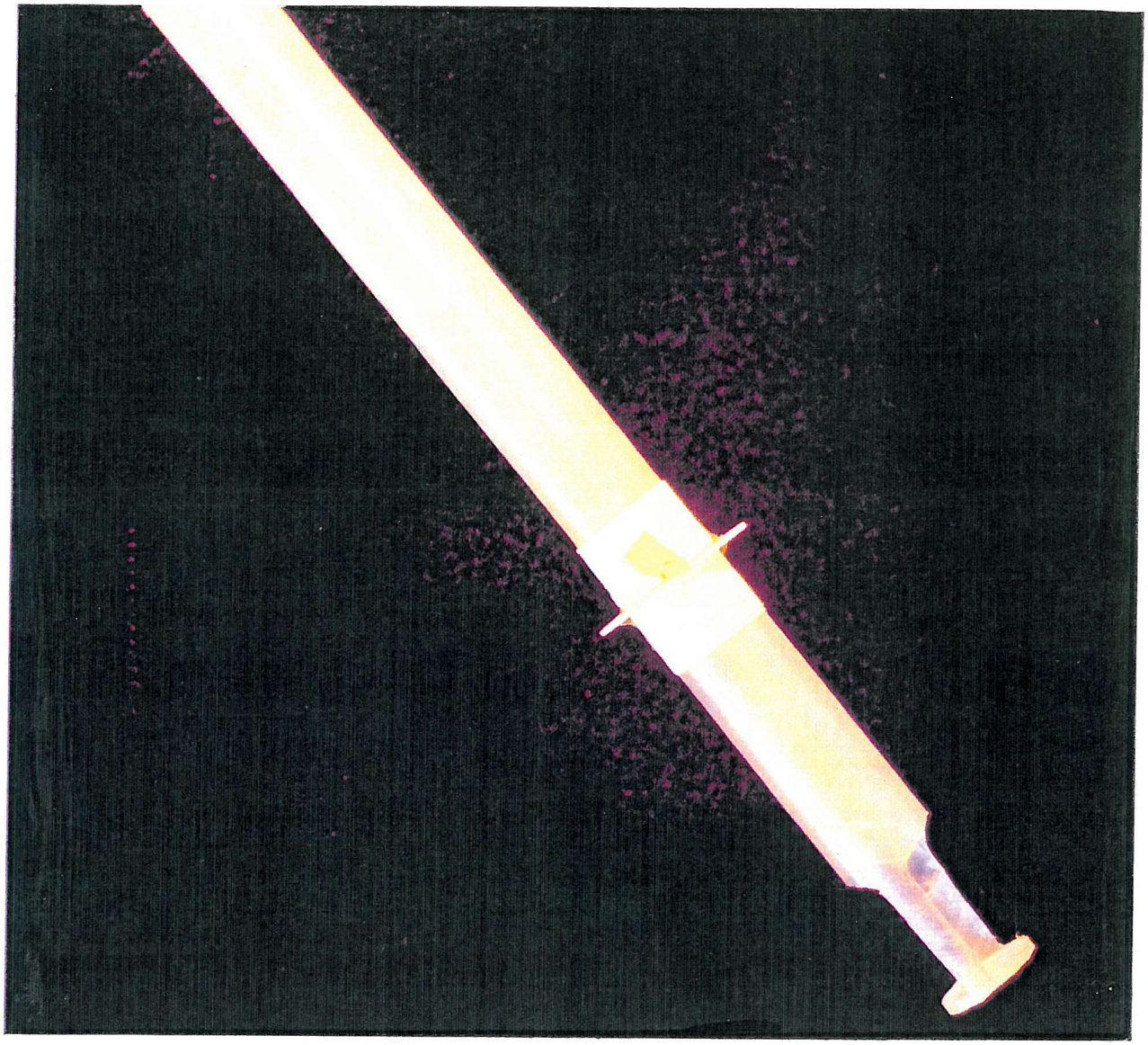

Plate 5.9 Mylar sample holder.

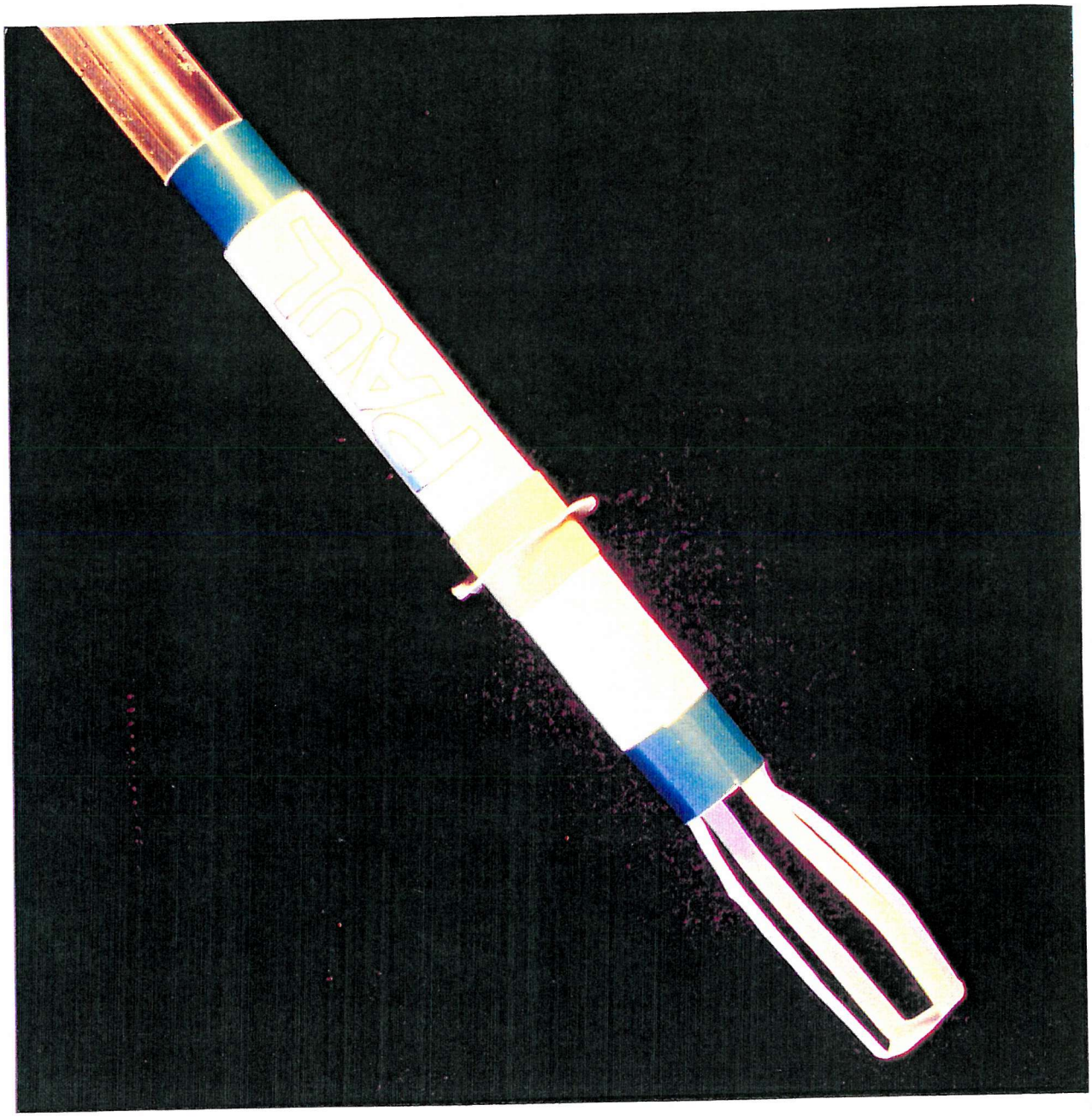

Plate 5.10 Paper sample holder.

Plate 5.11 Magnetic Measurement model MMTD60 programmable thermal demagnetiser.

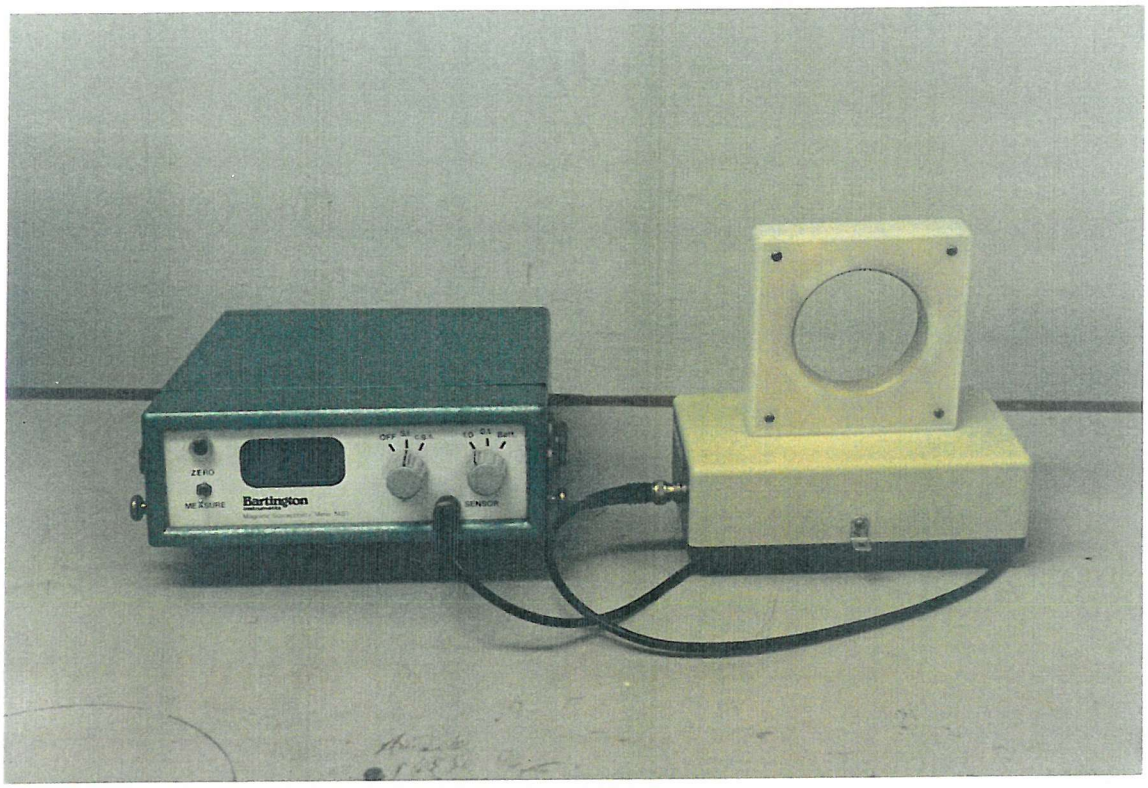

Plate 5.12 Bartington Instrument's MD magnetic susceptibility system.

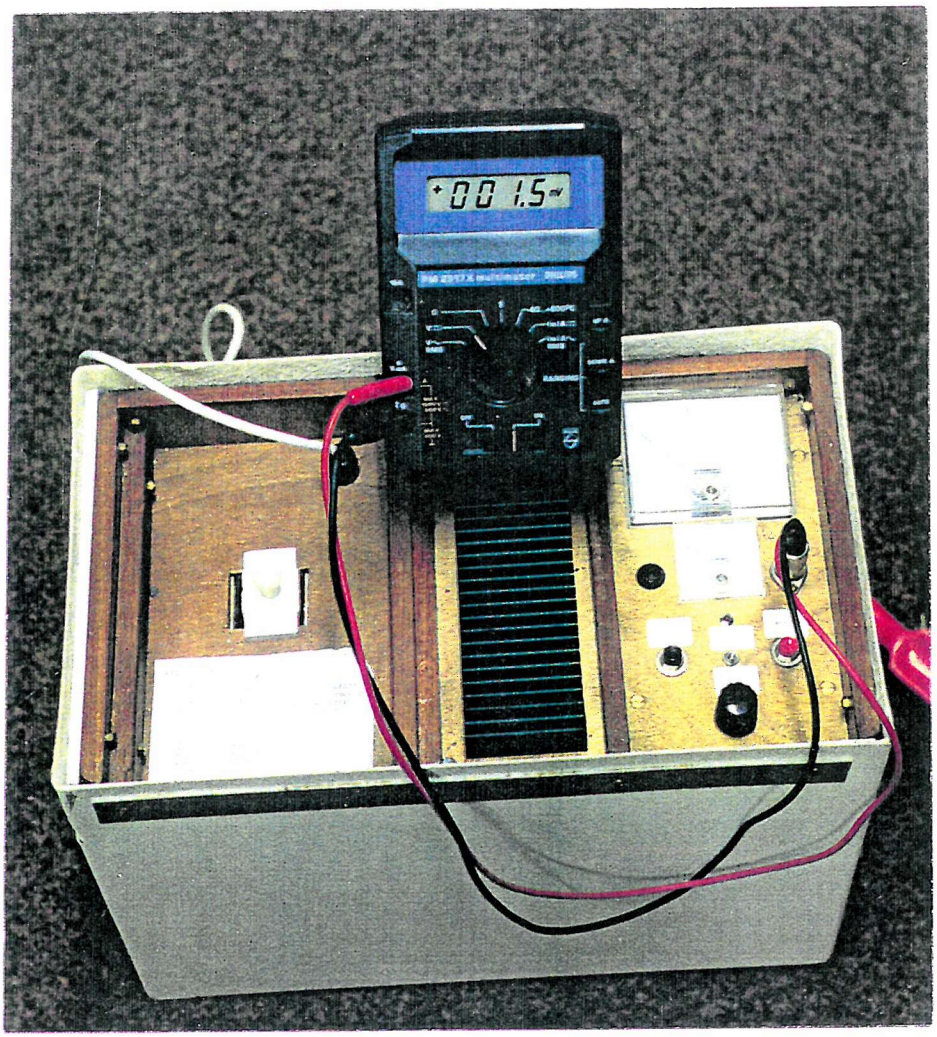

Plate 5.13 A Molspin pulse magnetiser.

Chapter 6 Palaeomagnetic results from Coniacian-Late Campanian Chalk, Culver Cliff, the Isle of Wight, southern England

6.1 Introduction

The main outcrop of Upper Cretaceous deposits in the Isle of Wight runs the length of the Island from the Needles in the west, to Culver Cliff in the East (Figure 6.1). Zonal measurements (Rowe, 1908) have revealed that the thickness of the Upper Chalk at the western end of the Island amounts to about 398 metres, and that at the eastern end to about 307 metres. The decrease in the thickness is believed to be due to post-Cretaceous erosion. As a result the Senonian of the Isle of Wight extends upwards only to the earliest late Campanian (Figure 6.2).

The deposits on the eastern side of the Island (Culver Cliff and Whitecliff Bay) outcrop on the northern limb of the Sandown anticline (Figure 6.3) and consist of a steeply dipping monotonous succession of white chalks with black flints. However, a series of phosphatised and glauconitic hardgrounds are present towards the bottom of the section. The section ranges in age from latest Turonian to earliest Late Campanian (Hart *et al.*, 1987).

The sequence of pelagic sediments provides an opportunity for detailed study of the palaeomagnetic record of the British Late Cretaceous. Apart from the hardgrounds, which may represent stratigraphic gaps (though no evidence for subaerial exposure exists), the sequence can be regarded as continuous. Typical deposition rates of the chalk throughout the Late Cretaceous are relatively high (of the order of 20-40 metres Myr^{-1}) according to Anderton *et al.* (1979) and by sampling closely, a detailed magnetostratigraphic study can be undertaken. The results of an investigation of a 300 metre section at Whitecliff Bay on the Isle of Wight, is presented.

6.2 Biostratigraphy of the Chalk succession at Whitecliff Bay and Culver Cliff

Both macrofossil and nannofossil biostratigraphies were determined, to provide a

detailed stratigraphical framework for this magnetostratigraphic study. The macrofossil biostratigraphy was supplied by Dr. A. Gale (Imperial College London/British Natural History Museum) and based on the Rawson *et al.* (1978) traditional zonation. The nannofossil biostratigraphy was provided by Dr. J. Burnett (University College London) and based on Sissingh's (1977) Tethyan zonation scheme.

6.2.1 Macrofossil biostratigraphy

Macrofossils are rare throughout the sections, and the placing of macrofossil boundaries is exceptionally difficult (Hart *et al.*, 1987). Figure 6.4 indicates the stratigraphic height above the Turonian-Coniacian boundary of various macrofossil zonal boundaries identified within the Culver Cliff section and the location of stage boundaries relative to the zonation. The macro fossil biostratigraphy indicates that the sequence spans Coniacian to early Late Campanian times.

6.2.2 Nannofossil biostratigraphy

Due to the high degree of post-depositional calcium carbonate mobilisation in the English chalk, preservation of the nannofloras was generally poor to moderate. Nannofloral diversity varied from moderate to low (J.A. Burnett, *pers. comm.*).

The nannofloras detected relate to neither the Tethyan nor the Boreal realms, with the Campanian marker species for Sissingh's (1977) Tethyan and Burnett's (1990) Boreal zonation schemes deficient in the late Early and early Late Campanian. As a result (sub-) zones CC19 to CC22A are poorly defined. However, this has not affected the biostratigraphical interpretation of the sequence.

The nannofossil data places the top 225 metres of the sequence wholly within the Campanian (Early to late Late Campanian), standard nannofossil (sub-) zones CC17 to CC22C. The lower 75 metres of chalk lie within the Santonian standard nannofossil zones CC15 to CC16 (*after* Sissingh, 1977 and Perch-Nielsen, 1985).

6.3 Stratigraphy of the Chalk succession at Whitecliff Bay and Culver Cliff

The chalk succession at Whitecliff Bay (Figure 6.5) was first described in detail by Rowe (1908). However, an error in his note book has been subsequently inherited by later workers, notably Barr (1962) and Clarke & Verdier (1967), which has resulted in the need for re-measurement of the sequence (Hart *et al.*, 1987). Figure 6.6 is a diagrammatic summary of the re-measured succession by Hart *et al.* (1987). Macrofossils are extremely rare throughout the section, making the location of macrofaunal boundaries exceptionally difficult (Hart *et al.*, 1987). A short review of each zone's lithological characteristics was published by Osbourne White (1921) and brief summaries are reproduced below. The zones will be reviewed in ascending stratigraphic order.

(a) The zone of *Micraster cortestudinarium* consists of hard, nodular chalk. However, in the upper parts of this sub-division some beds of smoother and softer character occur. The flints are mostly black and solid, and are arranged in close-set irregular courses. Tabular seams are common. At Culver the *cortestudinarium* Zone forms the face of the sheer cliff which ends eastward at the Nostrils, opposite Shag Rock islet.

(b) Except for its base, which contains nodular and lumpy bands, the *Micraster coranguinum* Zone is comprised of smooth and massive chalk. Flint-nodules are present and arranged in numerous regular courses, which are more closely spaced near the base and about the middle than in other parts of the zone. Moreover, the flints are commonly cavernous with a violet tinge and rinds which vary in thickness. Seams of tabular flint and grey marl occur occasionally. At Culver Cliff the zone outcrops between Whitecliff and the Nostrils. Much of the accessible surface, however, is obscured by dust from falls.

(c) No mention of the Zone of *Unitacrinus socialis* is made by Osbourne White (1921). From the re-measured sequence of Hart *et al.* (1987) the

Unitacrinus socialis Zone incorporates approximately 14 metres of the top of Osbourne White's (1921) *Micraster coranguinum* Zone and the bottom 12 metres of the following *Marsupites testudinarius* Zone.

(d) The *Marsupites testudinarius* Zone is comprised of chalk which is pure white, compact, and contains a few marl seams. Flint courses are less closely spaced than in the *coranguinum* Zone, and become rare or absent upwards. For the most part the flints are small, solid and black, with short, hornlike, projections and thick cortices of a faintly pink hue externally. The tabular variety is common in oblique veins and almond-shaped lenticles. Layers of rusty nodules occur in a sequence of hard, marl-seamed, nearly flintless chalk in the little promontory north-east of the White Horse at Culver Cliff. Rowe (1908) draws the upper boundary of the *testudinarius* Zone midway between the lowest distinct green-nodule band and the succeeding layer. The accessible surfaces are hard and worn smooth by waves.

(e) The upper half of the zone of *Offaster pilula* consists of chalk which contains numerous marl seams and courses of nodular flints. However, within the lower 21 metres of the zone flints are absent, apart from a few thin seams of the tabular variety.

(f) The chalk of the zone *Gonioteuthis quadrata* is massive, white and traversed by minute veins of marl. Seams of marl and flint-courses are numerous; the flints being mostly black and solid, and large in size. At Culver Cliff, the ledge that runs out at the extreme eastern point of the cliff is taken as the upper limit of the *quadrata* Zone.

(g) The Zone of *Belemnitella mucronata* is the highest of the Upper Chalk zones found on the Isle of Wight and attains its maximum thickness in Britain (145 metres) at the western end of the Isle of Wight. However, in Whitecliff Bay only 84 metres of this Chalk zone is present. Since there is nothing in the character of the mucronata Chalk which suggests thinning is a product of

sedimentation, this can be attributed to the widespread erosion which preceded the deposition of the oldest Tertiary strata. The chalk of this zone is white and massive, with numerous irregular flint-courses and many thin seams of marl. Some of the flints attain great size and display considerable variation in character but are generally greyish within.

6.4 Structural history

The Late Cretaceous chalk deposits of the Isle of Wight were deposited in a extensional basin, called the Wessex Basin, which persisted from Permian to Cretaceous times. The Wessex Basin can be structurally divided into a set of constituent asymmetrical graben, bounded by major East-West trending zones of *en-echelon* syn-depositional normal faults (Chadwick, 1993). The graben were inverted in Late Cretaceous and Tertiary times by compressive stresses orientated roughly north-south (Chadwick, 1993) Minor inversion movements, coeval with the 'Pyrenean' phase of deformation as Iberia was caught up in the convergence of Africa relative to Europe (Coward & Dietrich, 1989), affected the basin in Late Cretaceous times through to the early Tertiary. However, the major inversion episode did not take place until the Miocene, corresponding with the main Alpine deformation event as continental collision occurred between Africa and Europe (Chadwick, 1993).

The dominant structural features of the Isle of Wight which reflect the Miocene inversion event are two strong, nearly-coincident folds known as the Sandown and Brixton anticlines (Figure 6.3). These features overlap and replace each other west of the River Medina, and are responsible for the up turning of the strata in a belt of country extending the whole length of the Island, from the Needles to Culver Cliff (Osbourne White, 1921).

The deposits at Culver Cliff outcrop on the northern limb of the Sandown Anticline. As a result, they possess dips which range between 53° and 75° and strike approximately East-West.

6.5 Palaeomagnetic results

The palaeomagnetic data for the Culver Cliff section are summarised in Appendix A, Table 1. This table lists every horizon sampled at Culver Cliff and includes palaeomagnetic details of every specimen studied. Sample code, NRM, maximum demagnetisation level, reliability category, magnetic polarity, low coercivity component, high coercivity component, IRM ratio, saturation IRM and volume susceptibility are listed from left to right. The table also includes details of the demagnetisation level or range (either °C or mT) at which the magnetic polarity is best defined. Where a demagnetisation stable end point is identified, the direction of the ChRM vector before and after bedding correction is listed, together with the MAD or 95% confidence angle, which acts as a measure of reliability. Where directional trends where observed, poles to the best fit great circles where recorded, along with the MAD and number of demagnetisation vectors defining it. Great circle poles are indicated by an asterisk and can be found in both the low and high coercivity component columns.

The magnetic polarity stratigraphy of Culver Cliff is summarised in a polarity log (Figure 6.7). From left to right the diagram shows i) stratigraphic depth in metres; ii) Cretaceous Stage; iii) biostratigraphic macrofossil zone (Rawson, *et al.* (1978); i) biostratigraphic nannofossil zone (Sissingh, 1977); v) sampling level; vi) polarity (black=normal, white=reverse, light shading=mixed and dark shading=intermediate); vii) stratigraphic variation of declination of characteristic remanent magnetisation (ChRM); ix) stratigraphic variation of inclination of ChRM; x) stratigraphic variation of the mean Natural Remanent Magnetisation (NRM) intensity; xi) stratigraphic variation of Isothermal Remanent Magnetisation (IRM) ratio. On the right hand side of the diagrams are three columns which define the reliability category of the Stable Characteristic Magnetisation (SCM), the fraction of the samples demagnetised which support the definition of polarity and the demagnetisation procedure employed to define the polarity. Where polarity definition is based solely on directional trends a ChRM vector is generated by great circle intersection. However, where directional trends do not create intersection points a token declination/inclination vector (reverse

polarity=180°/-90°, normal polarity=360°/90°) is employed.

6.5.1 Natural Remanent Magnetisation

The first step in the investigation was to measure the natural remanent magnetization (NRM) of the chalk samples. Figures 6.8 shows the variation of NRM intensities with stratigraphic height above the Turonian-Coniacian stage boundary. The top of the plot coincides with sample horizon CC2, the uppermost sampling horizon of the Culver Cliff section. The top of the sequence lies approximately 5 metres above CC2 and is marked by an unconformity overlain by Eocene sediments (Reading Beds).

Plotted NRM intensities are based on mean values for each sampled stratigraphic horizon. Values lie in the range 0.0053-1.3008 mA/m. The log mean NRM intensity for the section is 0.0654 mA/m. The highest NRM intensity measured for an individual specimen was 3.409 mA/m from sample level CC9. The mean NRM value for this horizon was 1.3008 mA/m which is two orders of magnitude greater than the mean for the section as a whole. Other high NRM values were found at sample sites CC54 (0.7312 mA/m) and CC57A (0.6052 mA/m). The lowest NRM intensity measured for individual specimens was 0.0020 mA/m from sample horizons CC19 and CC21.

Two major NRM intensity peaks were identified between sample horizons CC129 to CC89 (Peak 1) and CC26 to CC8 (Peak 2, Figure 6.8). The mean NRM intensity for Peak 1 is 0.1601 mA/m and Peak 2 is 0.0956 mA/m.

Between the peaks the mean NRM intensity is much lower (0.0243 mA/m). The mean NRM intensity before Peak 1 was 0.0401 mA/m and after Peak 2 was 0.0446 mA/m. Superimposed upon this large scale fluctuation are much smaller extreme variations of magnetic intensity. Since the average NRM intensity of a sample level can be used as a measure of the relative proportion of ferromagnetic grains present at a particular horizon within the Chalk, the observation of large and small scale fluctuations in NRM intensity most likely reflects either changes in terrestrial erosion, resulting in an

increase of deposited clastic ferromagnetic material, or insitu biogenic production of magnetite. Examination of the magnetic mineralogy of the Chalk is required before further conclusions can be drawn on these fluctuations.

6.5.2 Stability of magnetisation

To investigate the stability of the remanent magnetization within the chalk and resolve the separate components in the samples carrying a multi-component remanence, specimens from each stratigraphic level were subjected to incremental demagnetization analysis.

To establish the optimum procedure, samples were subjected to both incremental alternating field (AF) demagnetization and thermal demagnetization.

6.5.2.1 AF demagnetisation

For weakly remanent samples AF demagnetization, at 2.5 mT or 5.0 mT steps, was employed. Sample CC66 1V1, after AF demagnetization treatment, shows a directional trend which can be extrapolated to a reversed polarity (southerly declination, negative inclination) end point (Figure 6.9). However, for the more strongly magnetised samples AF demagnetisation to 40 mT was insufficient to remove secondary magnetic components (Figure 6.10) and thermal demagnetization procedures were adopted.

6.5.2.2 Thermal demagnetisation

Thermal demagnetization steps of 50°C were applied initially until the remanent magnetization became too weak for reliable determinations to be made by the discrete sample cryogenic magnetometer. However, the secondary magnetic component was generally removed between 400°C and 500°C. Steps of 50°C were obviously too small so demagnetization was carried out using the following incremental steps: NRM, 100, 200, 300, 380, 400, 420, 460, 480, 500, 520°C, etc. The response of a representative

sample to this treatment, with bedding correction applied, is shown in Figures 6.11a & b.

Specimen CC27 2T1 (Figure 6.11a.) was initially demagnetized using AF. However, on reaching a demagnetization field of 35 mT the sample's intensity had dropped by only 50% from 0.575 mA/m to 0.286 mA/m. Thermal demagnetization was then applied to the same sample (Figure 6.11b.) and by 520°C the sample's remanent magnetism had become too weak to measure further using the cryogenic magnetometer. In both cases the demagnetization vector maintains an approximately northerly direction and a shallow inclination throughout. Points on the vector end point (VEP) plots define one linear segment. However, whereas the final linear segment for the thermal demagnetization plot is directed towards and passes through the origin, that for the AF demagnetization VEP plot can only be extrapolated to the origin. For example CC27 2T1, thermal demagnetization appears more effective in defining a demagnetisation end point. However, both types of treatment indicate that the stable characteristic magnetization (SCM), at this level, was probably acquired after tilting had occurred. The SCM is aligned in the same sense as the present geomagnetic field (northerly declination, positive, steep inclination) prior to applying the bedding correction of 284°/63° (Figure 6.11c.). The incremental thermal demagnetization steps of 20°C were felt to be still too small, since between 500°C and 520°C sample CC27 2 T1 shows a possible directional trend towards normal polarity (Figure 6.11b.). As a result, thermal demagnetization steps employed for the rest of the study were as follows: NRM, 200, 400, 425, 460, 470, 480, 490, 500°C, etc (Figure 6.12).

6.5.3 Reliability categories

The results of this treatment allow the palaeomagnetic data from each of the sample horizons to be placed in reliability categories. These categories have been previously discussed and illustrated in section 5.7.

Out of 1342 specimens analyzed, demagnetisation stable end points were attained by

39% of the samples. However, only 14% belonged to the S1 category (Figure 6.13), 20% to category S2 (Figure 6.14), and 5% to category S3 (Figure 6.15). Directional trends were recognised in 34% (Figure 6.16a, b and c) of the samples demagnetised while 22% possess recent geomagnetic field over-prints (Figure 6.17 a and b) which could not be removed by A.F. or thermal demagnetisation. Erratic behaviour during demagnetisation was observed in 6% of the samples (Figure 6.18).

6.5.4 Age of remanence

The principal objective in the analysis of palaeomagnetic data is to determine whether any of the components of remanent magnetisation identified in the rock, represent primary magnetisation and, also, to establish the instances in the rock's past when other magnetic components were acquired. Knowledge concerning the timing of magnetisation processes may sometimes be gained from geological observations made in the field. Such observations are commonly referred to as field stability tests.

6.5.4.1 Bedding Corrections

If the sampling site is no longer in the attitude in which it originally acquired its magnetization (i.e. the rocks have been tilted) then orientation corrections are needed for such movements. If the original horizontal can be defined from the bedding planes in the chalk then this plane can be specified in terms of its strike and dip. The magnetic vectors of the samples can then be rotated back to their original, pre-tilt, directions using a simple mathematical rotation.

The deposits at Whitecliff Bay outcrop on the northern limb of the Sandown Anticline. As a result they possess dips which range between 53° and 75° and strike approximately East-West. The bedding corrections for the Culver Cliff section are presented in Table 6.1.

By applying a tectonic correction we can distinguish between magnetic components acquired before and after tilting.

Figures 6.19a and b. show the effect the bedding correction has on the magnetization vectors. In Figure 6.19a, a bedding correction of 282°/62° has been applied for sample CC56 1 T2. The stable characteristic magnetization (SCM) of the sample is rotated away from the recent geomagnetic field direction to a direction with a shallow positive inclination (10°) and an approximately northerly declination. It is apparent that this sample has acquired a recent geomagnetic field overprint after tilting. Figure 6.19b. shows sample CC44 3V2 before and after a tectonic correction of 287°/70°. Prior to correction this sample displays a possible directional trend towards reverse polarity. However, after correction any doubt over the existence of this directional trend is dispelled.

6.5.4.2 Fold test

In an area where rocks of comparable age have been inclined in different directions and sampling has been carried out on bedding planes with different orientations it is possible to undertake a fold test. Magnetisation acquired after tilting will be mutually consistent, whereas components of remanence obtained before tilting will not (Tarling, 1983). If the magnetisation vector follows the geometry of the fold, the test is said to be positive; the magnetisation is primary or at least pre-dates the folding event (positive test). If the magnetisation is identical along the fold-structure the component of remanence can be attributed to a magnetisation event which post-dates the folding (negative test). Analysis of the grouping of direction before and after tectonic correction will display a tighter cluster after tectonic correction if the remanence was acquired before tectonic movements, and a more expansive dispersal if it was acquired after folding (McElhinny, 1964).

Figure 6.20 shows a stereographic equal area plot of the stable characteristic magnetisation for 180 S1 category magnetic vectors from the complete Culver section, before and after bedding corrections have been applied to the individual vectors. Bedding correction inclinations range between 53° and 75° while strikes range between 282° and 292°. Precision parameters 'k' and alpha 95 are reported before and after bedding corrections.

Before application of their respective tectonic corrections the S1 category magnetic vectors express a mean declination of 297° and a mean inclination of 86°, an alpha 95 value of 2.40 and k value of 19.7. After applying the respective corrections a mean declination of 16° and mean inclination of 33°, an alpha 95 value of 2.3° and k value of 22.0. Analysis of the grouping of the directions before and after correction for tectonic tilt show a marginally closer grouping after tectonic correction and though the increase in 'k' is small (19.7 to 22.0), the tectonic corrections applied possess similar directions and therefore a larger increase in 'k' could not be expected.

McFadden & Jones (1980) have shown that the statistical test proposed by McElhinny (1964) is inappropriate and, that more correctly, one should determine whether the mean direction of a group of sites from one limb of a fold may be distinguished statistically from the mean direction of a group of sites from another limb. This test indicates significance under far less folding than does the test suggested by McElhinny. However, application of this test to the data from Culver Cliff is inappropriate since every site was obtained from the northern limb of the Sandown anticline. As a result only the McElhinny fold test has been applied.

Thus this test does not conclusively prove that the remanence is secondary. More importantly, the cluster of the magnetic directions determined at Culver Cliff move from a very unlikely position before correction to a sensible one afterwards. Thus the magnetic stability of the Chalk must be high to withstand such a disturbance and it seems reasonable to assume that it can be related to the time of formation of the Chalk.

6.5.5 Remagnetisation

Twenty-two percent of the samples demagnetised possessed magnetic overprints which could not be removed by using either A.F. or thermal demagnetisation procedures. Of these 399 specimens, 128 possessed stable end points which were well defined by a collection of closely spaced points on the stereographic projection and with the final linear segment (MAD≤5) on the vector plot directed through the origin.

Figure 6.12 shows a stereographic equal area plot of overprint vectors for the Culver section together with an overall mean overprint vector (declination=1°, inclination=69°) similar to the recent geomagnetic field.

6.5.6 Magnetic polarity

The tilt-corrected SCM declination and inclination values defined by the incremental demagnetisation are plotted as a function of stratigraphic height above the Turonian-Coniacian boundary in Figure 6.7.

Polarity definition is based on a combination of demagnetisation stable end points and observations of directional trends during demagnetisation. The succession can be divided into seven polarity intervals (Figure 6.22). These are, in ascending stratigraphic order:

a) **Polarity zone CC1**. A 114 metre thick normal polarity interval containing a short reverse polarity zone and five short mixed polarity zones (*M. cortestudinarium* to *U. socialis* Zone) representing Chron C34N.

b) **Polarity zone CC2.** A 64 metre dominantly reverse polarity interval containing four short intervals of normal polarity, two intervals of intermediate polarity and three intervals of mixed polarity (*U. socialis* to *G quadrata*) representing the early part of Chron C33R.

c) **Polarity zone CC3.** A 32 metre zone of mixed polarity (*G. quadrata* Zone) representing the middle part of Chron C33R.

d) **Polarity zone CC4.** A 40 metre thick reverse polarity zone containing, a short interval of mixed polarity (*G. quadrata* to *B. mucronata* Zones) representing the upper part of Chron C33R.

e) **Polarity zone CC5.** An 11 metre thick normal polarity interval (*B. mucronata*

Zone) representing the lower part of Chron C33N.

f) **Polarity zone CC6.** A 10 metre thick reverse polarity zone (*B. mucronata* Zone) representing the middle part of Chron C33N.

g) **Polarity zone CC7.** A 17 metre thick dominantly normal polarity interval containing two short reverse polarity zones (*B. mucronata* Zone) representing the upper part of Chron C33N.

6.5.7 A Late Cretaceous palaeomagnetic pole for southern England

The magnetic vectors in rocks of any specific age can be used to calculate the position of their corresponding pole on the standard geocentric axial dipole model for the average geomagnetic field (Tarling, 1983). However, it is important to assess the reliability of the palaeomagnetic data used to generate a palaeomagnetic pole. Various schemes have been devised for assessing the reliability of data used for the construction of apparent polar wander (APW) paths. The criteria proposed by Van der Voo (1988) to classify published data has achieved popular acceptance. Van der Voo recognises seven fundamental criteria for palaeomagnetic data. These are:

a) Well-determined rock-magnetic age.

b) Results based on >25 samples with high precision k>10.

c) Demagnetisation/magnetic cleaning results reported in sufficient detail.

d) Positive field (fold-, conglomerate-, contact-) tests, i.e. evidence for a primary magnetisation.

e) Tectonic coherence with continent-structural control.

f) Antipodal reversals identified to assure a good time average of the

geomagnetic field.

g) Lack of similarity with younger poles, i.e. no suspicion that the pole is an overprint if field-tests are inadequate.

In general, palaeomagnetic results as reported will either satisfy or not, each of the seven criteria. A result's 'score' (0 to 7) can be used as a measure of overall reliability. This 'score' is referred to as the 'quality factor' or 'Q' by Van der Voo (1988).

The directions of S1 category vectors are displayed on an equal-area stereographic projection in Figure 6.23, together with the overall mean S1 category vector (declination=16°, inclination=33°, k=22.0, alpha 95=2.3°). From the mean magnetic vector a palaeomagnetic pole of 55.5°N 153.4°E, with quality factor, Q, equal to 6, was calculated for the Coniacian-Late Campanian of southern England. Six of the seven criteria suggested by Van der Voo (1988) are satisfied. A well constrained biostratigraphic/ magnetic age has been determined for the Chalk sequence at Culver Cliff. The palaeomagnetic-pole has been generated from 180 S1 reliability category specimens and has a precision 'k' value greater than 10 and a low 95% confidence level. Both thermal (10%) and AF (90%) demagnetisation techniques have been employed to define the data set. Tectonic coherence and good structural control has been established by previous workers for the Late Cretaceous sequences in southern England (Chadwick, 1993). However, apart from one specimen, displaying reverse polarity, all other S1 category specimens are characterised by normal polarity. As a result, only one antipodal reverse vector was used to assure a good time average of the geomagnetic field. Nevertheless, the magnetostratigraphical interpretation indicates that these vectors span a time interval of several million years, so the time average can be regarded as acceptable. With respect to the McElhinny (1964) fold test (see section 6.5.5.2), a k_2/k_1 ratio value of 1.12 for the data is less than the values tabulated at 95% and 99% significance levels and thus the fold test is failed. Reliability criteria (d) is, thus, failed.

According to numerous authors the Chalk has undergone compaction since its original deposition (Nestler, 1968; Hakansson *et al.*, 1974; Wolfe, 1968; Hancock, 1978). Estimates, based on the compression of burrows, fossil moulds and fossil shapes, vary between 10-33%. As a result a shallowing of magnetic remanence inclination might be expected.

Various researchers have proposed compaction induced inclination shallowing models (King, 1955; Griffiths *et al*, 1960; Blow & Hamilton, 1978; Anion & Kodama, 1987; Arason & Leve, 1990). Arason & Leve (1990) undertook a detailed investigation of the various models of compacting sediment which lead to inclination shallowing of the magnetic remanence. The models were classified as (i) rotation of elongate magnetic grains to more horizontal orientations; (ii) rotation toward the horizontal of flat nonmagnetic fabric grains to which smaller magnetic grains are attached; (iii) randomization of the sediment by grain rotations which lead to decreased intensity of magnetisation and possibly also to inclination shallowing; and (i) they show that the initial within-sample dispersion of the magnetic moments dampens the amount of inclination shallowing of all the models and transforms any form of microscopic mechanism to an equation of standardised form. The physically realistic models give rise to different magnitudes of inclination shallowing, which to the first order obey an equation of the form

$$\tan (I-\Delta I)=(I-a\Delta V)\ \tan I$$

where I is inclination of the ambient field inclination, ΔI the inclination shallowing, ΔV the compaction, and 'a' is constant, chosen to fit inclination shallowing data. By assuming that the Chalk compaction occurs in a similar fashion, to the 'collapsing soft matrix' model of Arason & Leve (1990) and by adopting an extreme estimate of chalk compaction (33%, Nestler, 1968) the maximum inclination error can be determined.

However, Arason & Leve (1990) state that for compaction values lower than 50% the 'collapsing soft matrix' model predicts an inclination shallowing of less than 0.5°. A value which would be very difficult to detect in nature. A compaction induced error

of this form would therefore have no effect on the magnetic remanence inclination. Compaction errors thus seem to have little bearing on the palaeomagnetic directions determined from the Chalk deposits of Culver Cliff.

By using the mean magnetic remanence inclination value of 33±2.4°, determined from 'S1 reliability category' data, a palaeolatitude of 18±2.4°N is inferred for southern England during Coniacian-Late Campanian times. The palaeocontinental reconstructions of Smith *et al.* (1981) indicate that southern England lay at a latitude of approximately 40°N during this interval of time. From the palaeomagnetic-pole of Heller & Channell (1979), derived from limestones exposed in the Munster Basin, Germany, a magnetic field direction of 359.8°/56.24° can be predicted for southern England. This magnetic field direction corresponds to a palaeolatitude for southern England of 36.8±3.1°N. A huge discrepancy of approximately 18° exists between the two figures. Moreover, within the experimental uncertainties (i.e. alpha 95=2.4°) this discrepancy must be regarded as significant.

A possible explanation for the large difference in the predicted palaeolatitude and calculated palaeolatitude for southern England during the Late Cretaceous period is that the Chalk at Culver Cliff possesses an unresolved magnetic component which tends to deflect the inclination of the magnetic remanence to a shallower angle. However, due to the lack of reliable palaeomagnetic-pole data of Cretaceous age for Europe and since no alternative British palaeomagnetic-pole exists, the Culver Cliff data provides a potential alternative for northern Europe during the Late Cretaceous. For a comprehensive review of the palaeomagnetic data available for this period with respect to Eurasia, the reader is referred to Besse & Courtillot (1991).

6.6 Isothermal remanence

The saturation magnetization of hematite is less that 1% of that of magnetite. The titanomagnetites (and maghemite) saturate in fields of 0.01-0.1 Testa, while hematite does not saturate in fields of over 1-3 Tesla (Tarling, 1983). If direct magnetic fields are applied in incremental steps, the magnetic moment of magnetite reaches a

maximum constant value before 1 T, but the moment continues to increase at higher applied fields for haematite.

As the coercivity spectrum of hematite may extend as high as 6.5 T, while the peak coercivities of magnetite are around 0.1 T, the presence of hematite will normally be indicated by the presence of a high coercivity component during alternating field magnetisation (Tarling, 1983). While the presence of such a component can be taken as clear evidence for the presence of hematite, the absence of such high coercivity behaviour does not exclude the presence as only low coercivity grains may be present. In a similar way, magnetite has a high saturation moment and this is often reflected in higher initial intensities of magnetisation that decrease as the coercivity is exceeded. Such behaviour is obviously not a realistic indicator, as similar behaviour could result from the presence of large quantities of lower coercivity minerals of other compositions. Nonetheless, the behaviour of samples during demagnetisation can be indicative of the mineralogy involved.

Isothermal remanent magnetization experiments (IRM) on chalk samples from Whitecliff Bay/Culver Cliff have resulted in the majority of specimens becoming magnetically saturated at applied fields between 0.01 and 0.1 T. Figure 6.24 shows the typical response of a chalk sample to direct magnetic fields applied in incremental steps.

6.6.1 IRM ratio

The IRM ratio (IRM_{300mT}/IRM_{860mT}) is a simple parameter which has been used to distinguish magnetite from hematite (Ali, 1989). By determining the IRM ratio for 131 (of the 163) sample horizons an IRM log of the Whitecliff section is presented (Figure 6.25). The vast majority of samples (93%) studied exhibit IRM ratios of 0.9 or above. The preservation of remanent magnetism of the chalk of Whitecliff Bay can therefore be attributed to either the presence of titanomagnetite, maghemite or, though highly unlikely, large quantities of low coercivity hematite.

6.6.2 Demagnetisation behaviour and IRM curves

Identification of magnetic mineralogy based solely on the use of the IRM ratio is insufficient. By undertaking detailed studies of the curves generated during IRM acquisition it is possible to gain a more complete understanding of a rock's magnetic mineralogy. IRM experiments carried out on AF and thermally demagnetised Chalk specimens suggest the presence not only of titanomagnetite but mixtures of hematite and magnetite (Figure 6.26). Maghemite can be eliminated from the list of magnetic minerals potentially responsible for the Chalk's remanent magnetism since, when heated to temperatures in excess of 350°C, it inverts to hematite, with a very large increase in spontaneous magnetisation (Tarling, 1983). An increase in the specimen's magnetic intensity would occur during thermal demagnetisation while IRM acquisition experiments on thermally demagnetised specimens would identify the presence of hematite. Both AF and thermally demagnetised specimens of chalk possessed the same diagnostic magnetite curve (Figure 6.27).

Magnetite-type IRM curves were observed in 68% of the samples studied (Figure 6.28a & b), while curves indicative of magnetite and hematite mixtures represent 31% (Figure 6.29). Hematite-type IRM curves were found in only 1% of the specimens studied (Figure 6.30).

The IRM acquisition curve generated for sample CC66-2V2 suggests the presence of hematite and titanomagnetite (Figures 6.31a). Figure 6.31b shows the sample behaviour during AF demagnetisation. The samples magnetic moment was reduced to a level close to the background noise of the magnetometer (1.01×10^{-7} mAm^2 at 35 mT). Scanning Electron Microscope (SEM) studies have failed to reveal information concerning the magnetic mineralogy of Chalk because the fine-grained magnetic mineral content lies beyond the resolution capabilities of the SEM. Fine-grained hematite has been reported to have a high coercivity spectrum (Dunlop & Stirling, 1977). Figure 6.31b reveals that on application of alternating fields below 35 mT the sample's magnetic intensity is significantly reduced. This suggests that the magnetic component being demagnetised lies within a titanomagnetite fraction of the magnetic

grain population and not within the hematite fraction.

Figure 6.32 demonstrates the behaviour of two samples (CC16-1T1 and CC30-2V3), which reached magnetic saturation (90%) on application of applied fields of greater than 0.2 Tesla, when subjected to AF and thermal demagnetisation. The IRM acquisition curves of these samples indicate that a mixture of titanomagnetite and hematite is present, with magnetite dominating the curve. Employment of alternating fields as high as 35 mT were insufficient to fully demagnetise such samples (Figure 6.32a). As a result thermal demagnetisation was used. Figure 6.32b shows the behaviour of sample CC30-2V3 when subjected to incremental thermal demagnetisation. On heating the sample to 400°C approximately fifty percent of the Chalk's total remanent magnetism is removed. This corresponds with a lower coercivity magnetic grain fraction which may represent multi-domain titanomagnetite. Between the temperatures of 400°C and 500°C the specimen's magnetic intensity falls to the background noise level of the magnetometer.

The maximum measurable blocking temperature spectra of magnetic grains in Chalk lies around 500°C. The Curie temperature of pure magnetite is 575°C while the Curie temperature of pure hematite is much higher at 675°C (Tarling, 1983). Thus, the measurable high coercivity magnetic grain fraction of Chalk appears to correspond to a highly stable titanomagnetite with a Curie point below 575°C and a single-domain or pseudo single-domain grain size, small enough to resist AF demagnetisation. It can thus be concluded that, on the whole, the primary remanent magnetism of the English Chalk frequents a highly stable single or pseudo-single domain titanomagnetite, while the magnetic component residing within the hematite fraction of the magnetic grain population is beyond the resolution capabilities of modern cryogenic magnetometers.

6.6.3 Saturation IRM

By recording the peak IRM intensity of magnetically saturated chalk (IRM ratio≥0.9), and by assuming that both the magnetic mineralogy and domain state of magnetic grains is consistent throughout the geological section, it is possible to construct a

stratigraphic log which gives an indication of the relative quantity of magnetic minerals contributing to the Chalk's remanent magnetism. Such an assumption would seem justifiable considering the previouly drawn conclusions that the dominant magnetic mineral in Chalk is a titanomagnetite (Section 6.6.1).

Figure 6.33 shows a plot of Saturation IRM (IRM_{sat}) against stratigraphic height above the Turonian-Coniacian boundary at Culver Cliff. Two IRM_{sat} intensity peaks were identified between sample horizons CC129 to CC89 (Peak 1) and CC26 to CC8 (Peak 2) suggesting a large scale cyclicity in the titanomagnetite content of the Chalk at Culver Cliff. Figure 6.34 displays the similarity in shape between the average NRM intensity log and the IRM_{sat} intensity log. This suggests that the NRM intensity of Chalk reflects magnetic mineral content rather than variations in magnetic mineralogy. Superimposed upon the major cyclicity are much finer scale fluctuations in IRM_{sat} which appear to represent large variations in titanomagnetite content from sample horizon to sample horizon. The curve representing IRM_{sat} intensity is 1.5 orders of magnitude greater than the NRM intensity curve suggesting the presence of multi-domain titanomagnetite (NRM/IRM_{sat} ratio$\leq$0.1, Collinson, 1983).

6.7 Volume magnetic susceptibility measurements

Volume magnetic susceptibility measurements were carried out on large Chalk samples (150 cm^3) in a attempt to provide an additional means of correlating between Chalk sequences. Biogenic carbonate is not only very weakly magnetisable, but actually exhibits diamagnetic behaviour (Robinson, 1992) and, due to the extremely low content of strongly magnetisable (ferromagnetic) and moderately magnetisable (paramagnetic) minerals within the English Chalk, magnetic susceptibility measurements proved particularly unsuccessful as a correlation technique. In virtually every instance diamagnetic behaviour was encountered, and in the few instances where it was not large standard deviations calculated for the measurements were excessive. Figure 6.35 shows a log of volume magnetic susceptibility measurements against stratigraphic height above the Turonian-Coniacian boundary. Positive readings were obtained in part of the section which corresponds to Peak 1 as identified in the NRM

log and IRM_{sat} log (approximately 250 metres above the Turonian-Coniacian boundary).

6.8 Conclusions

According to the established magnetostratigraphic type section of Gubbio and the marine magnetic anomaly record the latest Turonian to the earliest Late Campanian strata of Whitecliff Bay should display, in ascending order, evidence of the Chron C34N (Gubbio Long Normal Zone); a reverse polarity interval representing Chron C33R (Gubbio A- zone) and Chron C33N (Gubbio B+ zone) (Figure 4.2, section 4.2.1). Apart from the boundary between Gubbio A- and B+ zones, where an uneven polarity transition occurs over a 9 metre interval, none of these zones appear to contain subzones in the Gubbio section. However, results from Whitecliff Bay suggest that subzones are present with the English Chalk (Figure 6.36).

Sampling level CC35 (Figure 6.7f, 260 metres above the Turonian/ Coniacian boundary and within the *B. mucronata* Zone) would appear to represent the base of Gubbio B+ zone (Chron C33N) (Figure 6.37). The 40 metres of chalk above represent part of the normal polarity zone Gubbio B+ (Chron C33N). Within this normal polarity zone four reverse polarity intervals have been discovered. These subzones may represent the 9 metre, uneven polarity transition between Gubbio A- and B+ magnetozones.

Below Sample Level CC35 (Figure 6.7c to 6.7f) a 145 metre interval of chalk belonging to the *B. mucronata*, *G. quadrata*, *O. pilula*, *M. testudinarius* and *U. socialis* Zones, represents the reverse polarity zone Chron C33R (Gubbio A-). However, this zone is not comprised exclusively of samples displaying reverse polarity, since 13 short normal polarity intervals appear within it. The base of this zone and the top of the Cretaceous Long Normal Zone (Chron C34N) has been located within the *U. socialis* Zone at sample level CC85A. Apart from one short reverse polarity interval at the macrofossil zone boundary *M. cortestudinarium/M. coranguinum* (sample CC144) the rest of the Chalk succession is represented by

normal polarity.

The occurrence of previously undetected reverse and normal polarity subzones within the Culver section might be explained by the differing thicknesses of strata representing the Campanian Stage at Culver and at Gubbio. Approximately 160 metres of Campanian Chalk outcrops in the Culver section, whereas only 75 metres of limestone represents the Campanian stage at Gubbio. Furthermore, the whole of the Campanian is not present at Whitecliff Bay, due to widespread erosion prior to the deposition of the oldest Tertiary strata. As a result, at least twice as much strata represents the Campanian stage at Whitecliff Bay than at the Gubbio section. This would account for the improved magnetostratigraphic resolution at Culver.

Though the geomagnetic polarity sequences recorded in the oceanic crust of different ocean basins are almost in total agreement with the polarity sequence recorded in the Scaglia Rossa limestone, at Gubbio (Lowrie & Alvarez, 1977) evidence of short period geomagnetic events within Chron C33N might be obtained from the study of oceanic magnetic anomaly profiles.

In many detailed studies of magnetic anomalies from fast spreading ridges, linear and small scale magnetic anomalies "tiny wiggles", that are clearly related to palaeomagnetic behaviour, are observed (Cande & Kent, 1992). However, problems exist in interpreting these anomalies. It is unclear whether all "tiny wiggles" are due to short polarity intervals. Larger amplitude features are obviously due to full reversals and can, occasionally, be correlated with magnetostratigraphically identified short polarity intervals. However, most of the smaller amplitude anomalies have not been confirmed in this way and have been modeled as either due to short polarity intervals (Blakely, 1974) or longer period intensity variations of 50 to 200 kyr (Cande & LaBreque, 1974). In addition, the record of "tiny wiggles" is not uniform due to the unevenness of track coverage in different areas of the ocean basins and the fact that the ocean crust has recorded some time intervals with higher resolution than others.

Marine magnetic profiles and interpreted geomagnetic polarity sequences from three oceanic areas, where the reversed interval between anomalies 33 and 34 can be recognised, are shown in Figure 4.4. Of the three profiles in Figure 4.4 only the North Pacific Profile B (Raff 1966) shows evidence of a short period event "tiny wiggle" within Chron C33N. Cande & Kent (1992) included no fine scale anomaly details in their recently published GPTS. They concluded that for this time interval (anomaly 33 to anomaly 34) the distinctive, long wavelength anomalies constrained for the south Atlantic were the best data available. The results of this study indicate that short period geomagnetic polarity reversal events occurred throughout much of this time interval, though the relatively slow ocean ridge spreading rate appear to have precluded their recording in the marine magnetic anomaly profile.

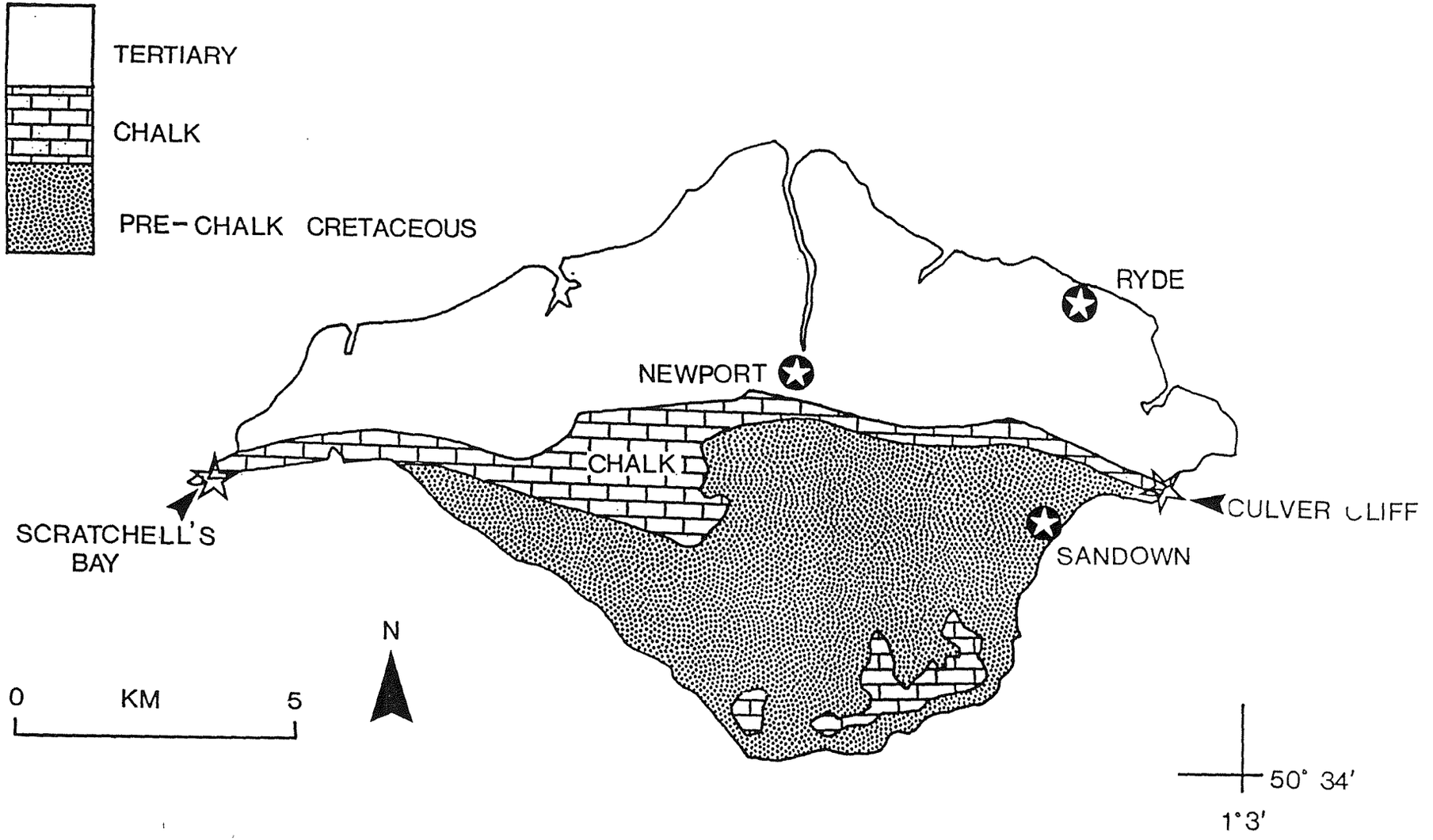

Figure 6.1. Sketch map of the basic geology of the Isle of Wight. The main outcrop of Upper Cretaceous Chalk extends the length of the Island from the Needles in the west, to Culver Cliff in the east (from Hart *et al.*, 1987).

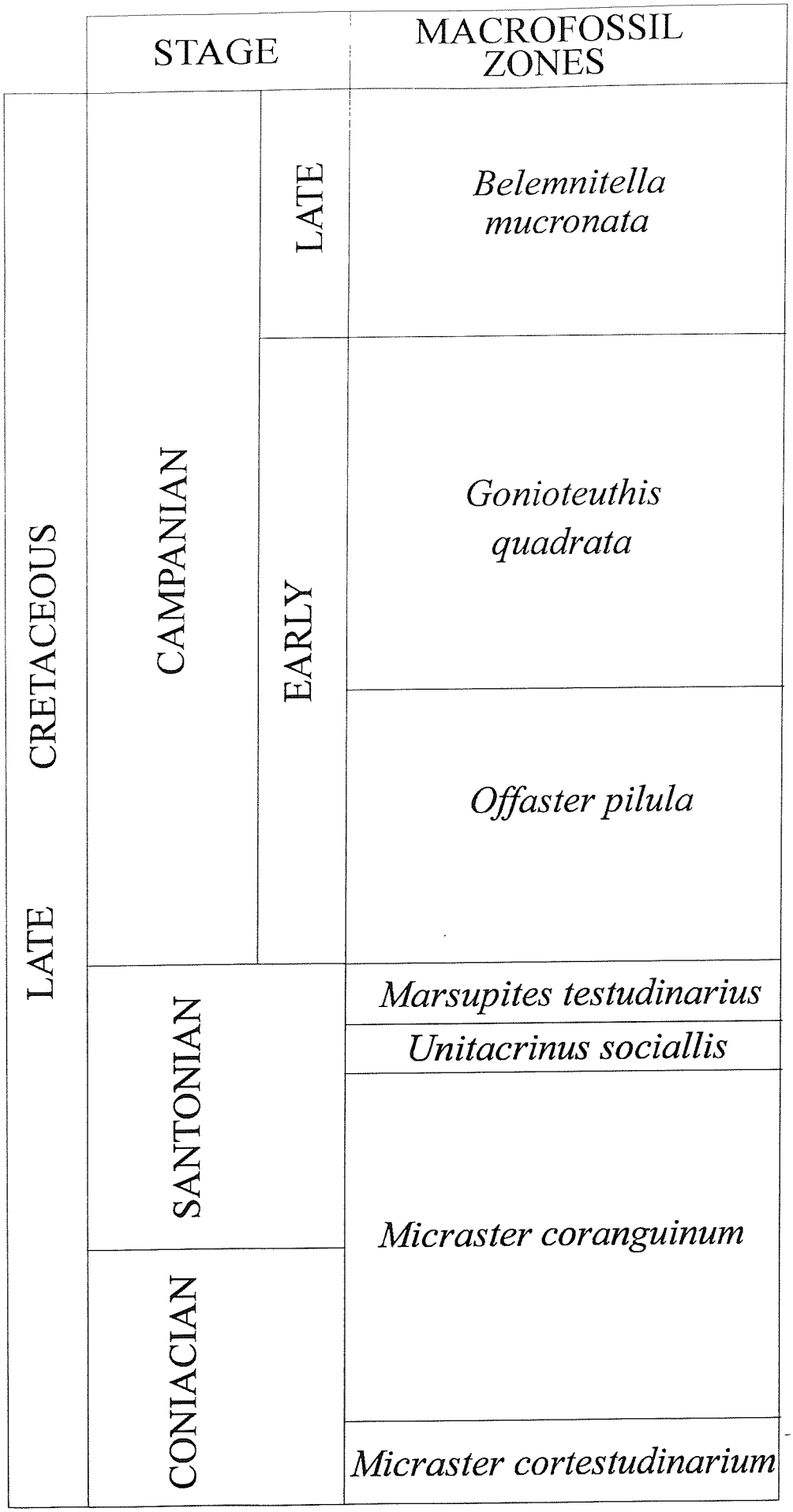

Figure 6.2. Late Cretaceous Stages and macrofossil zones exposed at Culver Cliff, the Isle of Wight.

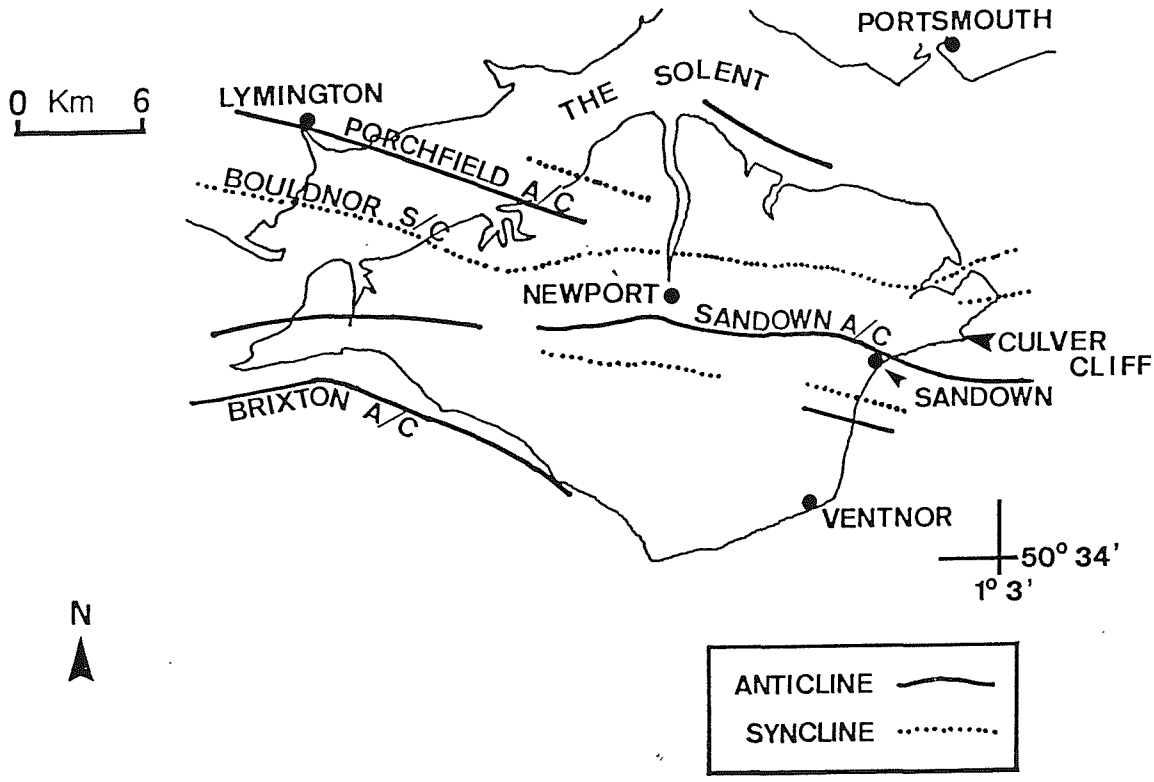

Figure 6.3. Sketch map of the Isle of Wight showing Axes of folding (from Osbourne White, 1921).

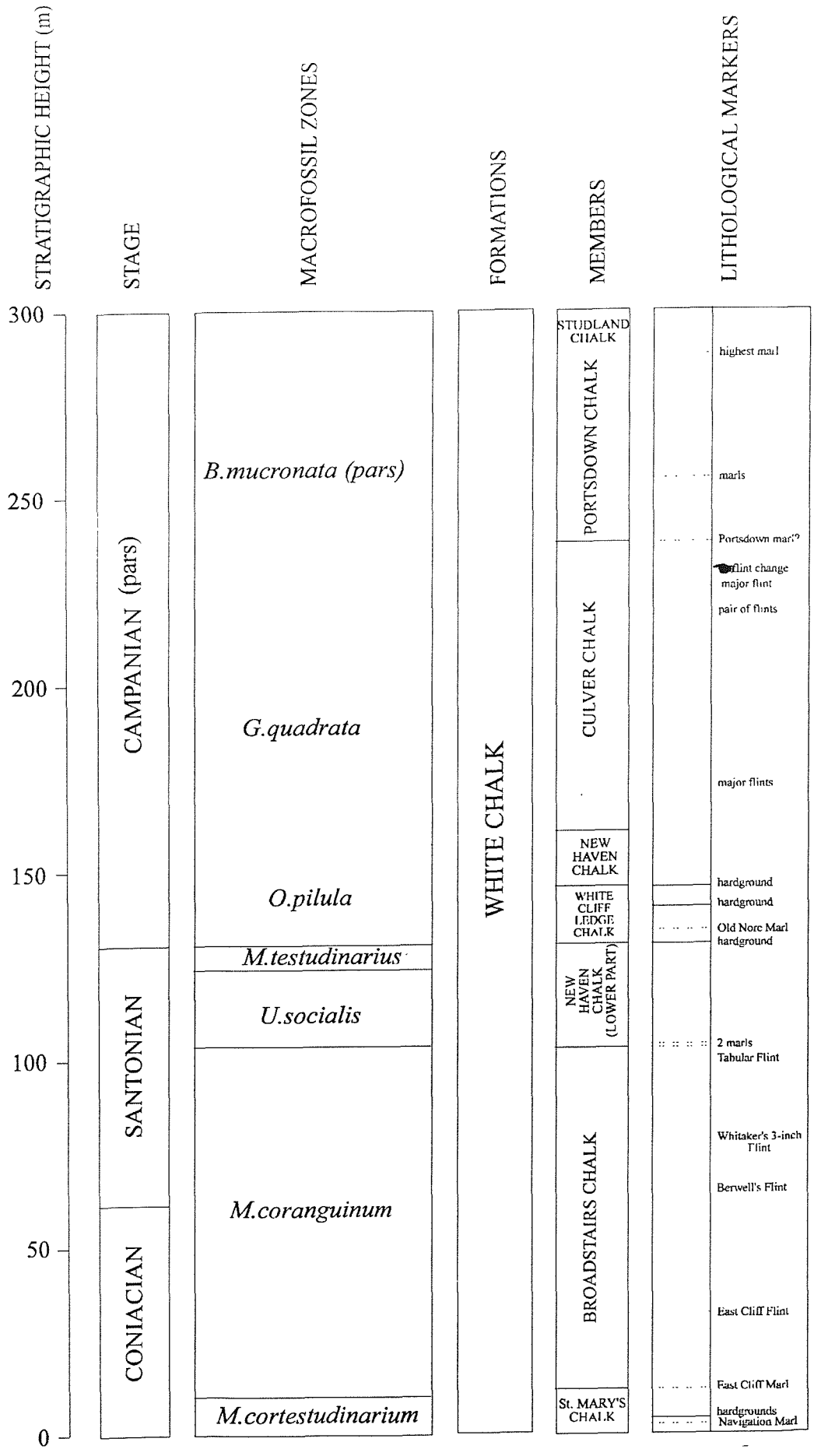

Figure 6.4. Summary diagram showing stratigraphical details of the Late Cretaceous Chalk sequence at Culver Cliff, the Isle of Wight. From left to right the diagram shows stratigraphic height above the Turonian-Coniacian boundary, Late Cretaceous Stages, macrofossil zones (Rawson *et al.*, 1978), formations, members and lithological markers.

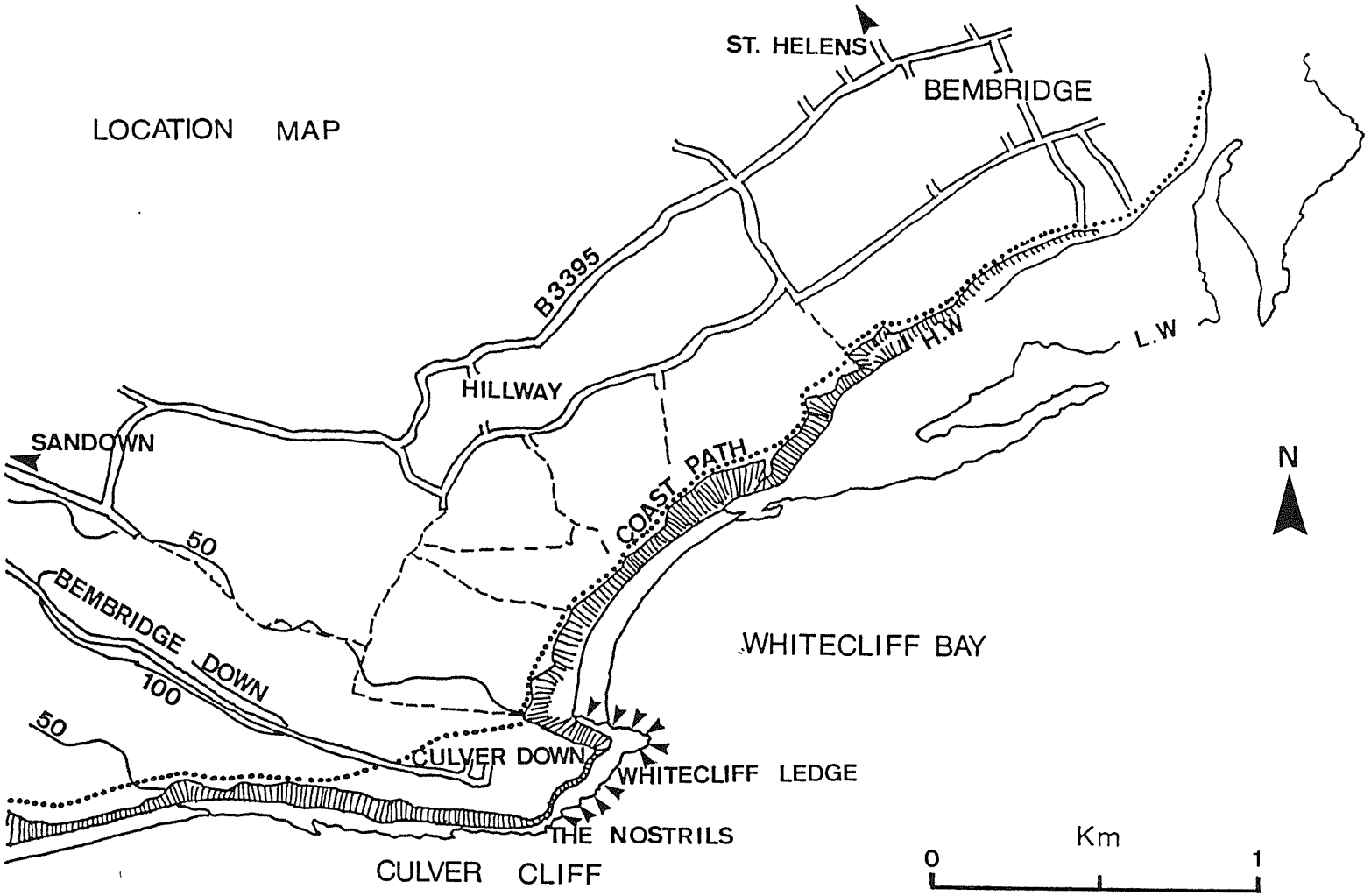

Figure 6.5. Location map of the Whitecliff Bay and Culver Cliff section (Hart *el al.*, 1987). Sampled section indicated by arrow heads.

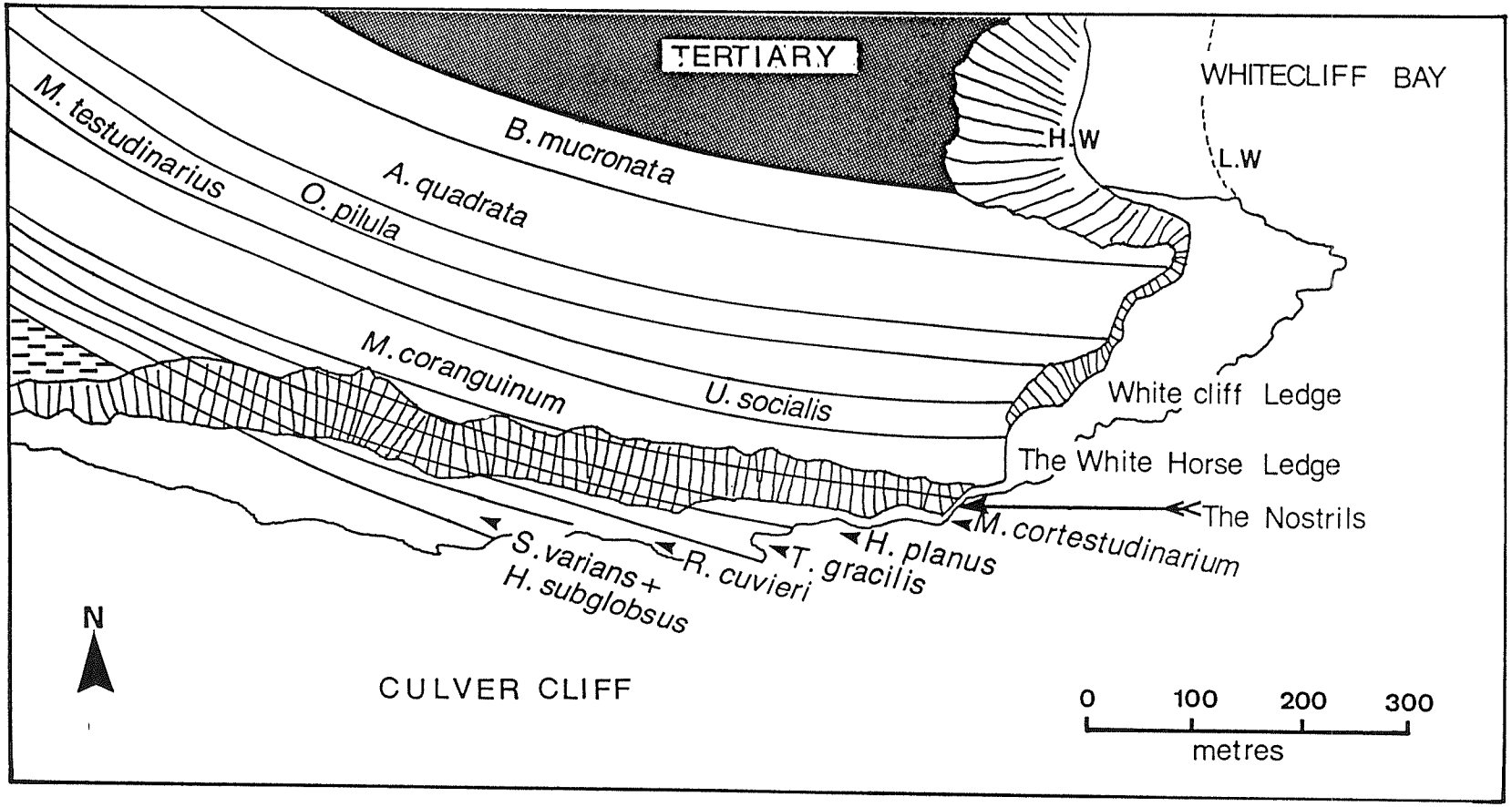

Figure 6.6. The Culver Cliff succession of the Chalk group at the eastern end of the Isle of Wight. Access through to the cortestudinarium Zone is from the Whitecliff Bay end of the section. It is impossible to round the headland by the Nostrils on foot (from Hart *et al.*, 1987).

Figure 6.7a,b,c,d,e, & f. The magnetic polarity stratigraphy of Culver Cliff. From left to right the diagram shows i) stratigraphic depth in metres; ii) Cretaceous Stage; iii) biostratigraphic macrofossil zone (Rawson *et al.*, 1978); iv) biostratigraphic nannofossil zone (Sissingh, 1977); v) sampling horizon; vi) polarity (black=normal, white=reverse, light shading=mixed and dark shading=intermediate), vii) stratigraphic variation of declination of ChRM; ix) stratigraphic variation of inclination of ChRM; x) the mean NRM intensity (solid squares); xi) stratigraphic variation of IRM ratio (solid triangles). On the right hand side of the diagrams are three columns which define the reliability category of the SCM, the fraction of the samples demagnetised which support the definition of polarity and the demagnetisation procedure employed to define the polarity. Where polarity definition is based solely on directional trends a ChRM vector is generated by great circle intersections. However, where directional trends do not create intersection points a token declination/inclination vector of 180°/ - 90° or 360°/90° is employed to represent reverse or normal polarity.

a)

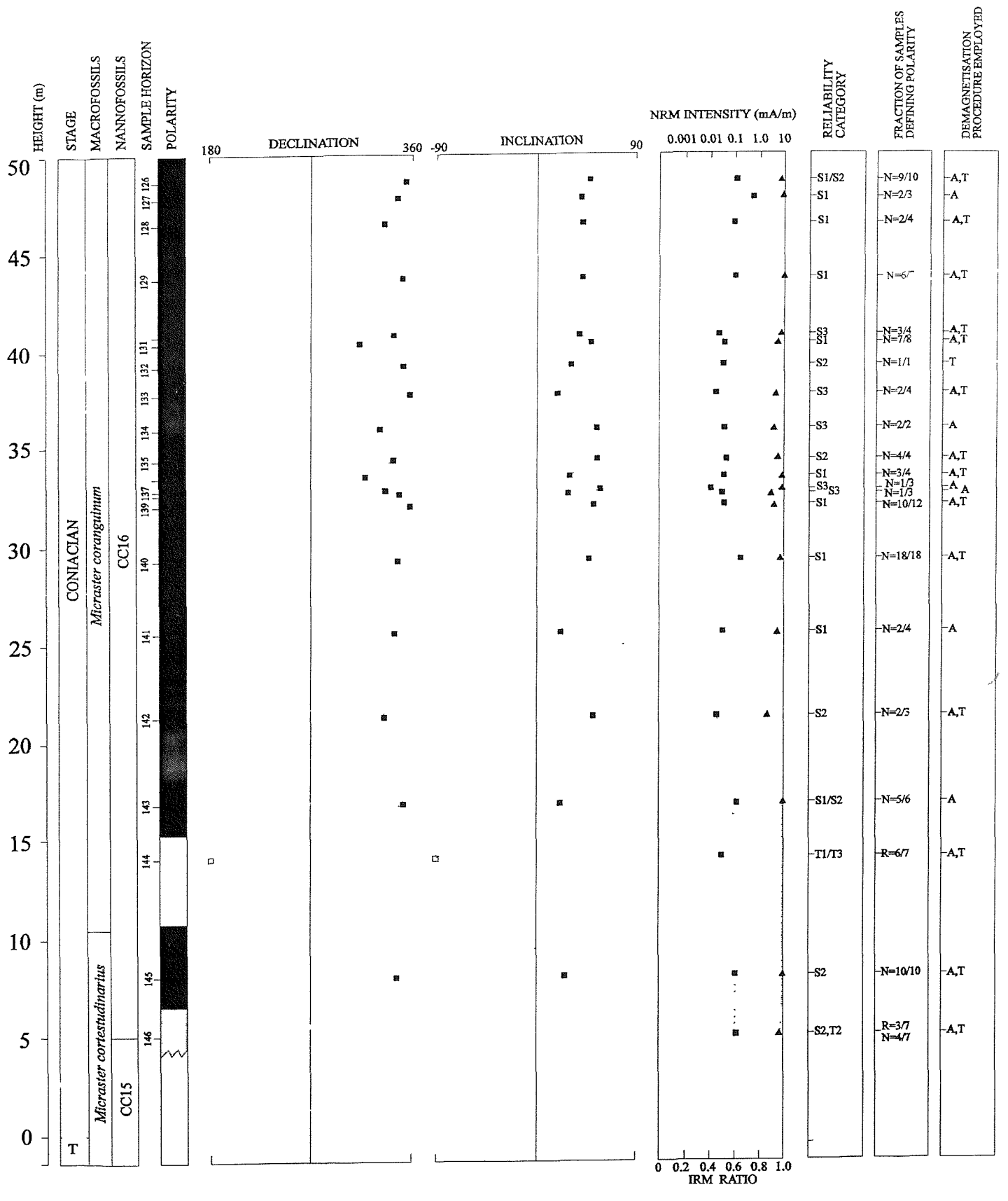
HEIGHT (m)
STAGE
MACROFOSSILS
NANNOFOSSILS
SAMPLE HORIZON
POLARITY
DECLINATION
INCLINATION
NRM INTENSITY (mA/m)
RELIABILITY CATEGORY
FRACTION OF SAMPLES DEFINING POLARITY
DEMAGNETISATION PROCEDURE EMPLOYED
CONIACIAN
Micraster coranguinum
Micraster cortestudinarius
CC16
CC15
T
IRM RATIO

b)

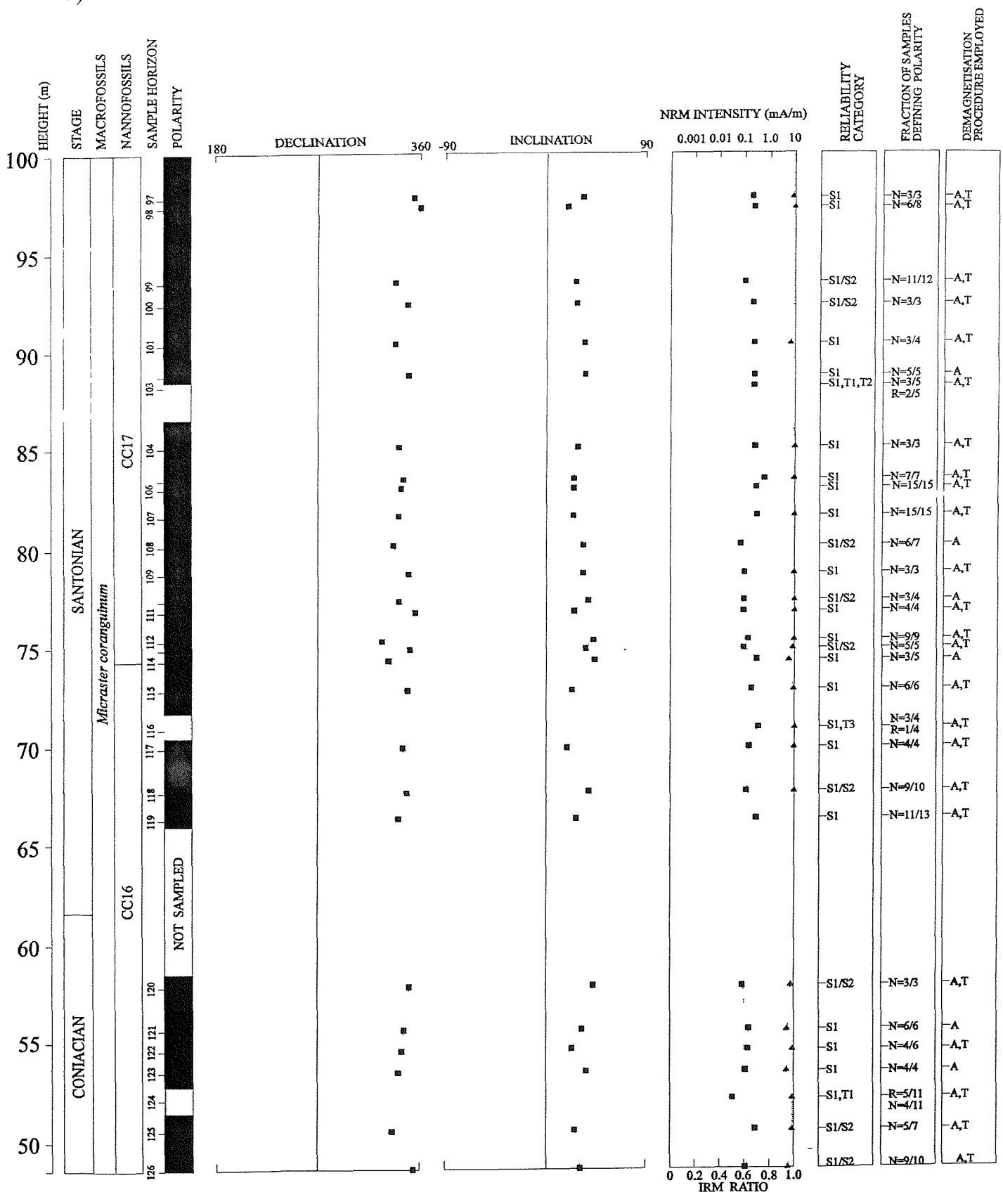
HEIGHT (m)
STAGE
MACROFOSSILS
NANNOFOSSILS
SAMPLE HORIZON
POLARITY
DECLINATION
INCLINATION
NRM INTENSITY (mA/m)
RELIABILITY CATEGORY
FRACTION OF SAMPLES DEFINING POLARITY
DEMAGNETISATION PROCEDURE EMPLOYED
SANTONIAN
CONIACIAN
Micraster coranguinum
CC17
CC16
NOT SAMPLED
IRM RATIO

c)

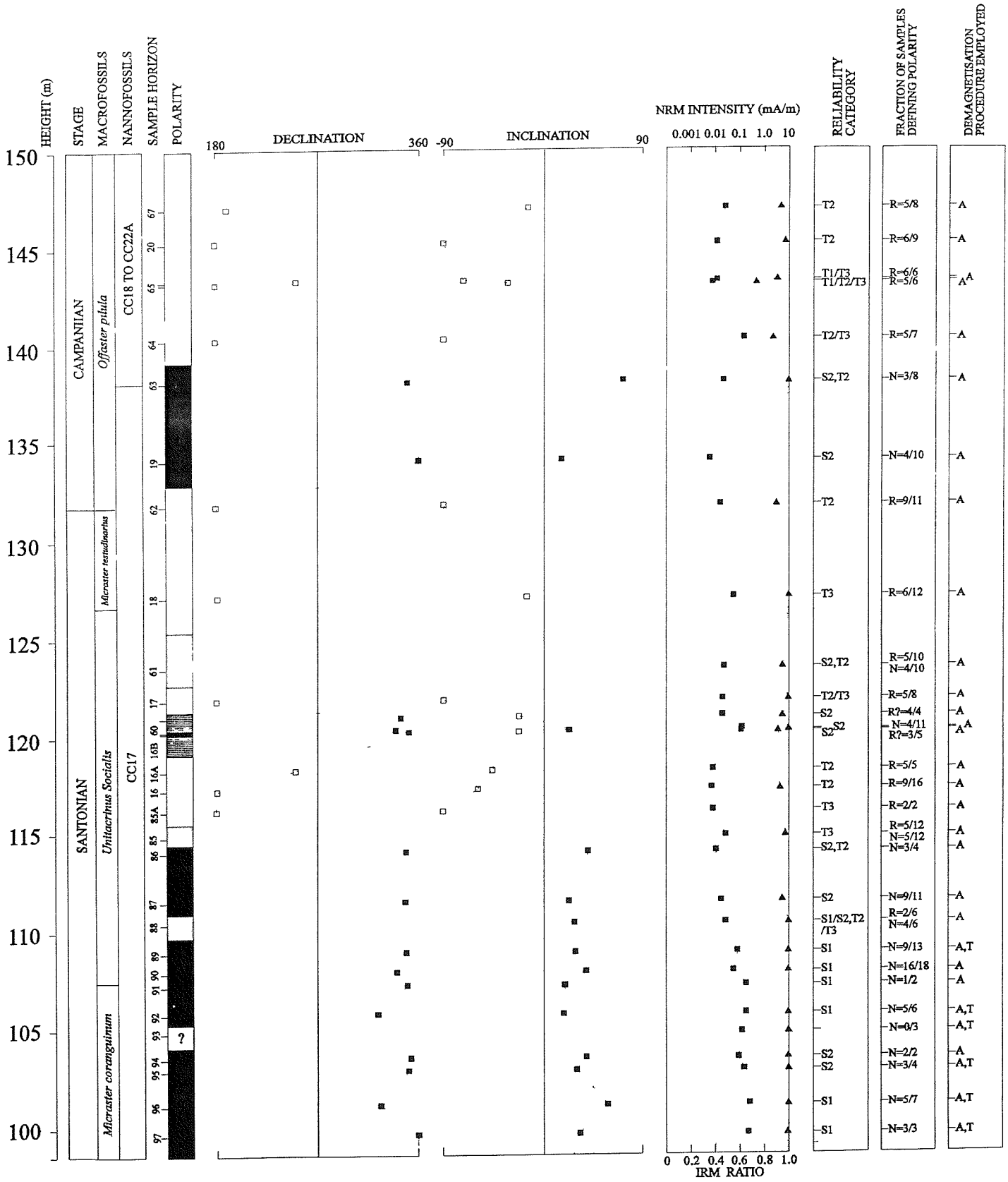
HEIGHT (m)
STAGE
MACROFOSSILS
NANNOFOSSILS
SAMPLE HORIZON
POLARITY
DECLINATION
INCLINATION
NRM INTENSITY (mA/m)
RELIABILITY CATEGORY
FRACTION OF SAMPLES DEFINING POLARITY
DEMAGNETISATION PROCEDURE EMPLOYED
IRM RATIO
CAMPANIAN
SANTONIAN
Offaster pilula
Micraster testudinarius
Uintacrinus Socialis
Micraster coranguinum
CC18 TO CC22A
CC17

d)

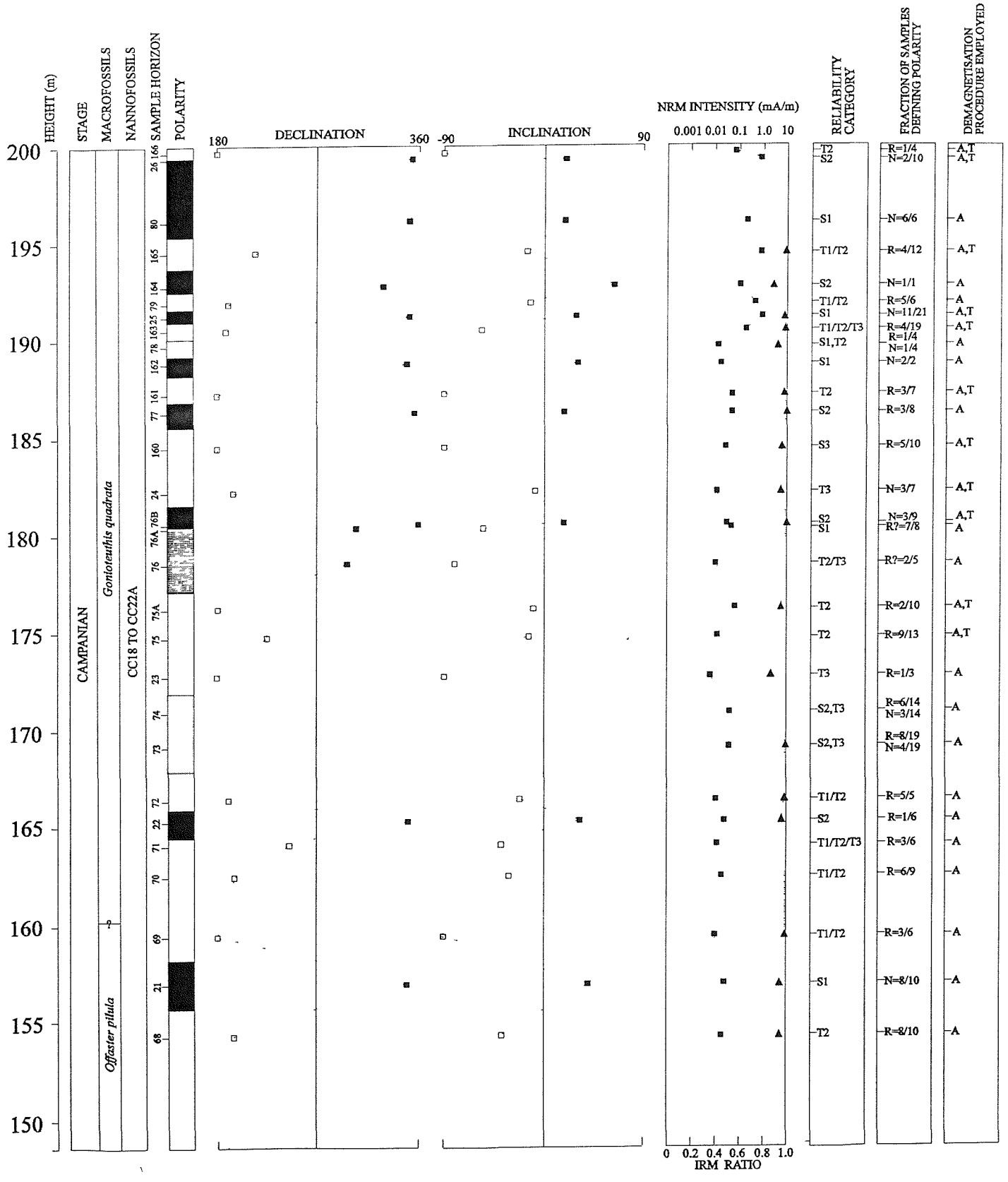
HEIGHT (m)
STAGE
MACROFOSSILS
NANNOFOSSILS
SAMPLE HORIZON
POLARITY
DECLINATION
INCLINATION
NRM INTENSITY (mA/m)
RELIABILITY CATEGORY
FRACTION OF SAMPLES DEFINING POLARITY
DEMAGNETISATION PROCEDURE EMPLOYED
IRM RATIO
CAMPANIAN
Gonioteuthis quadrata
Offaster pilula
CC18 TO CC22A

e)

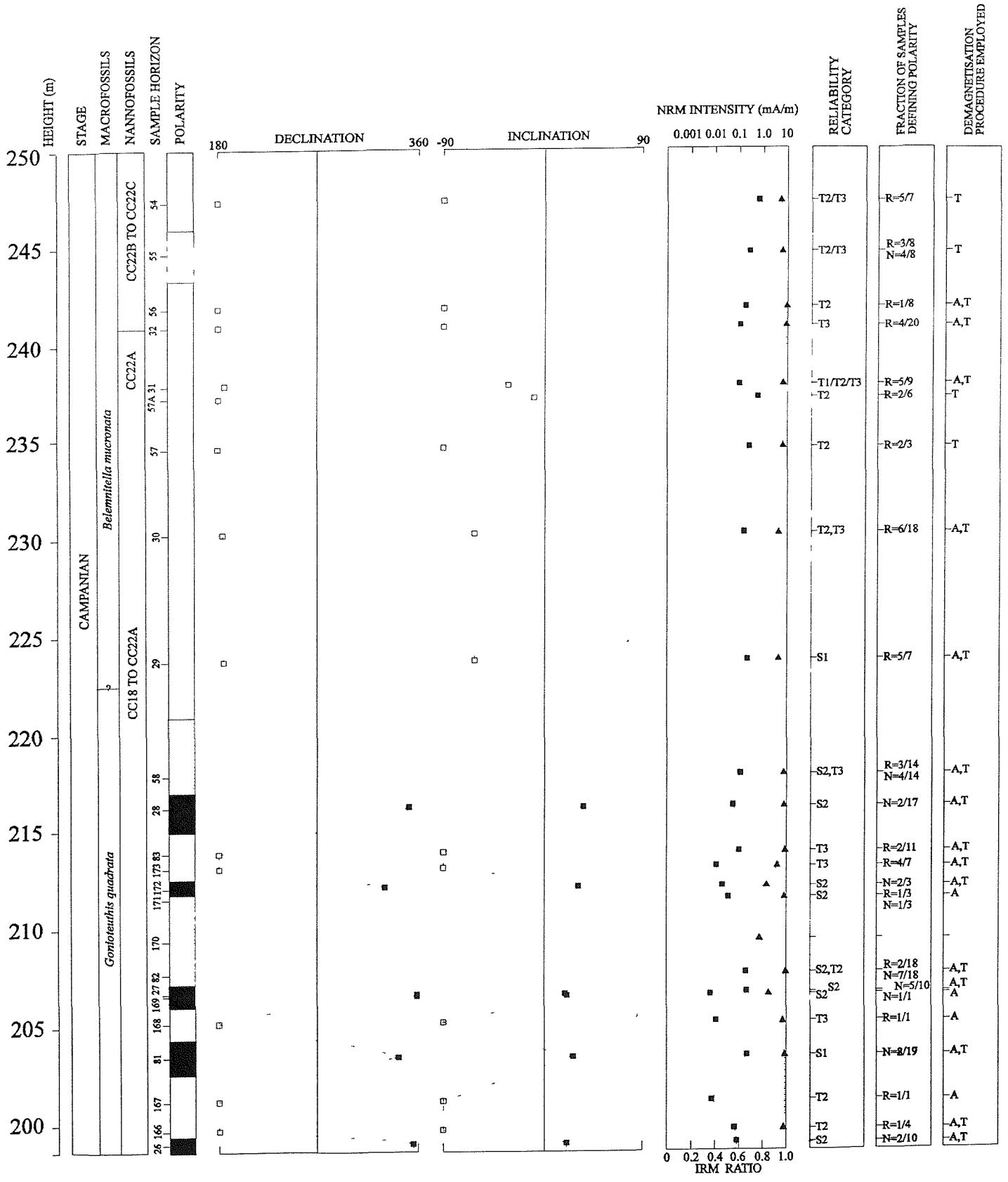
HEIGHT (m)
STAGE
MACROFOSSILS
NANNOFOSSILS
SAMPLE HORIZON
POLARITY
DECLINATION
INCLINATION
NRM INTENSITY (mA/m)
RELIABILITY CATEGORY
FRACTION OF SAMPLES DEFINING POLARITY
DEMAGNETISATION PROCEDURE EMPLOYED
IRM RATIO
CAMPANIAN
Belemnitella mucronata
Gonioteuthis quadrata
CC22B TO CC22C
CC22A
CC18 TO CC22A

f)

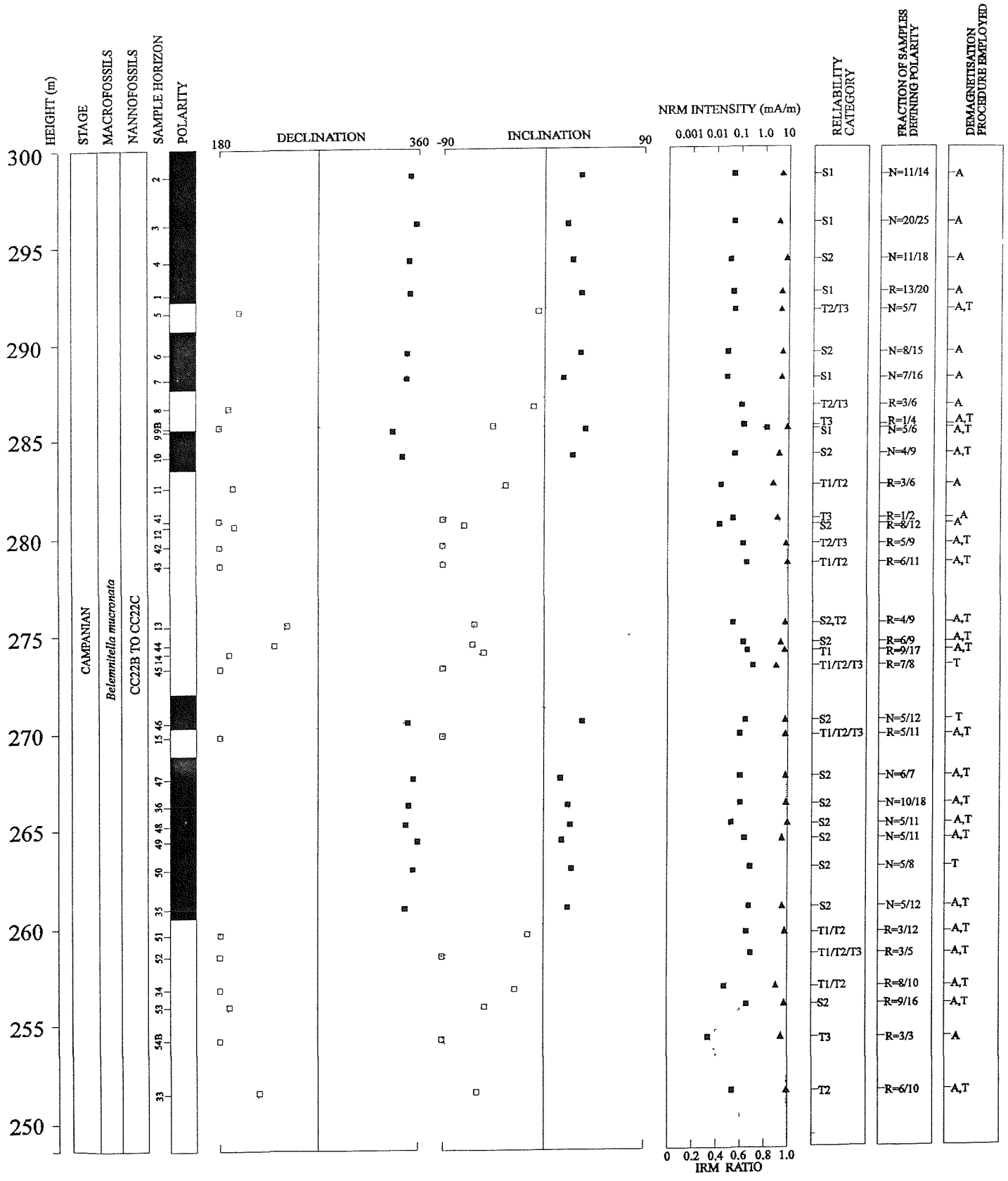
HEIGHT (m)
STAGE
MACROFOSSILS
NANNOFOSSILS
SAMPLE HORIZON
POLARITY
DECLINATION
INCLINATION
NRM INTENSITY (mA/m)
RELIABILITY CATEGORY
FRACTION OF SAMPLES DEFINING POLARITY
DEMAGNETISATION PROCEDURE EMPLOYED
CAMPANIAN
Belemnitella mucronata
CC22B TO CC22C
IRM RATIO

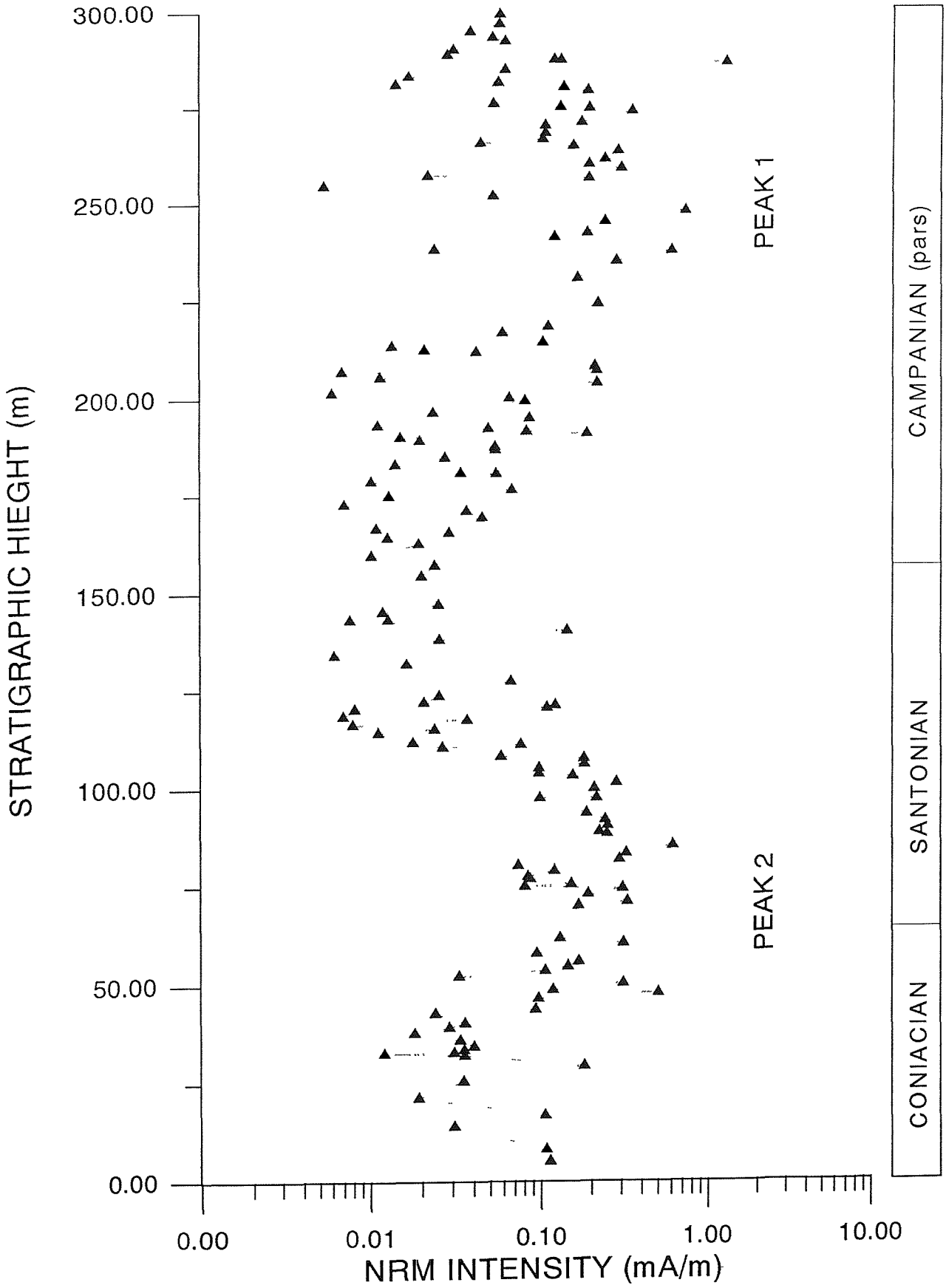

Figure 6.8. Variation of mean NRM intensity with stratigraphic height above the Turonian-Coniacian boundary. The right-hand column indicates the Late Cretaceous Stages represented by the Chalk succession (Rawson et al., 1978).

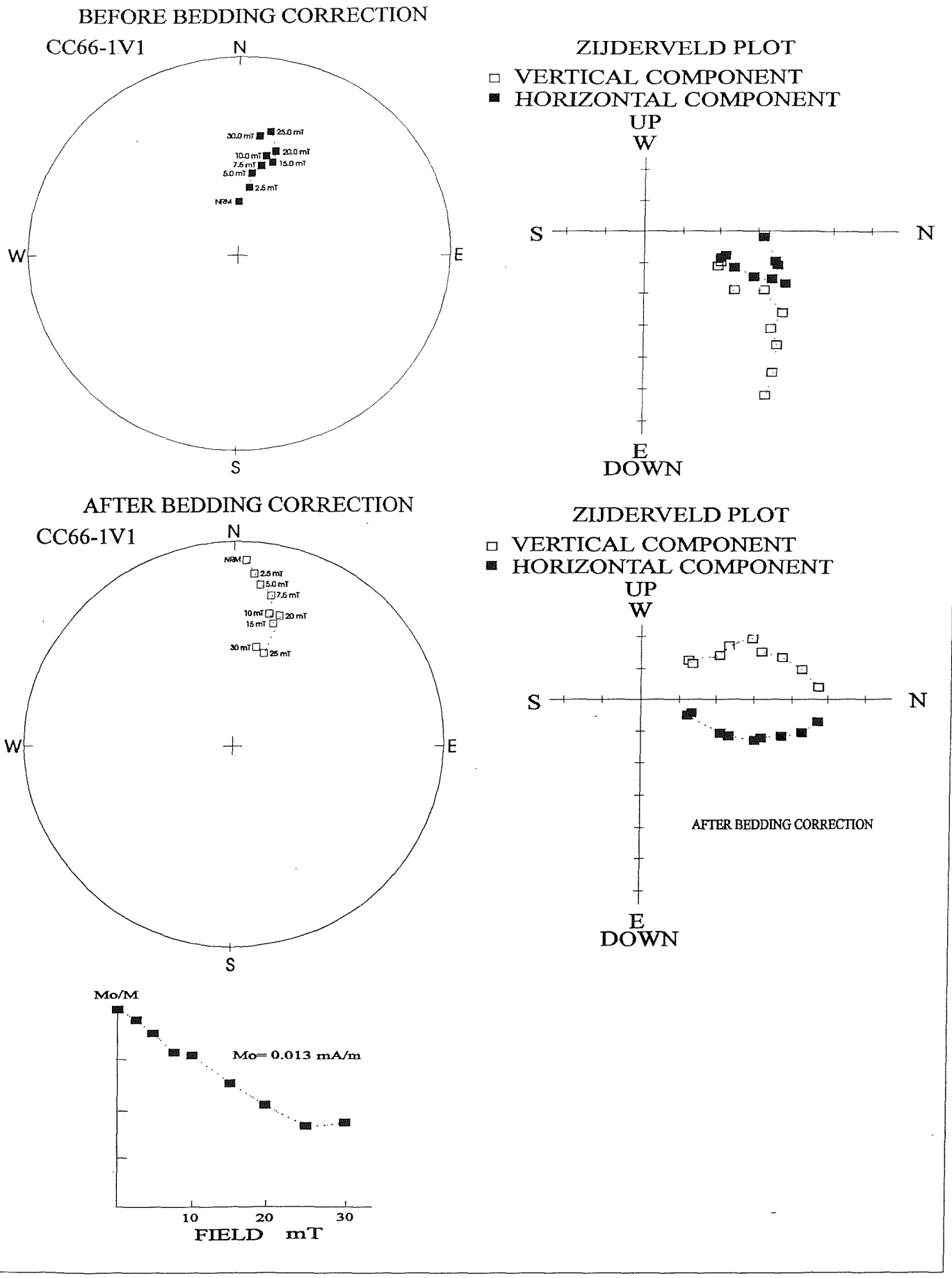

Figure 6.9. Sample CC66-1V1, after demagnetisation treatment, shows a directional trend which can be extrapolated to a reverse polarity (southerly declination, negative inclination) end point. A bedding correction of 282°/62° has been applied.

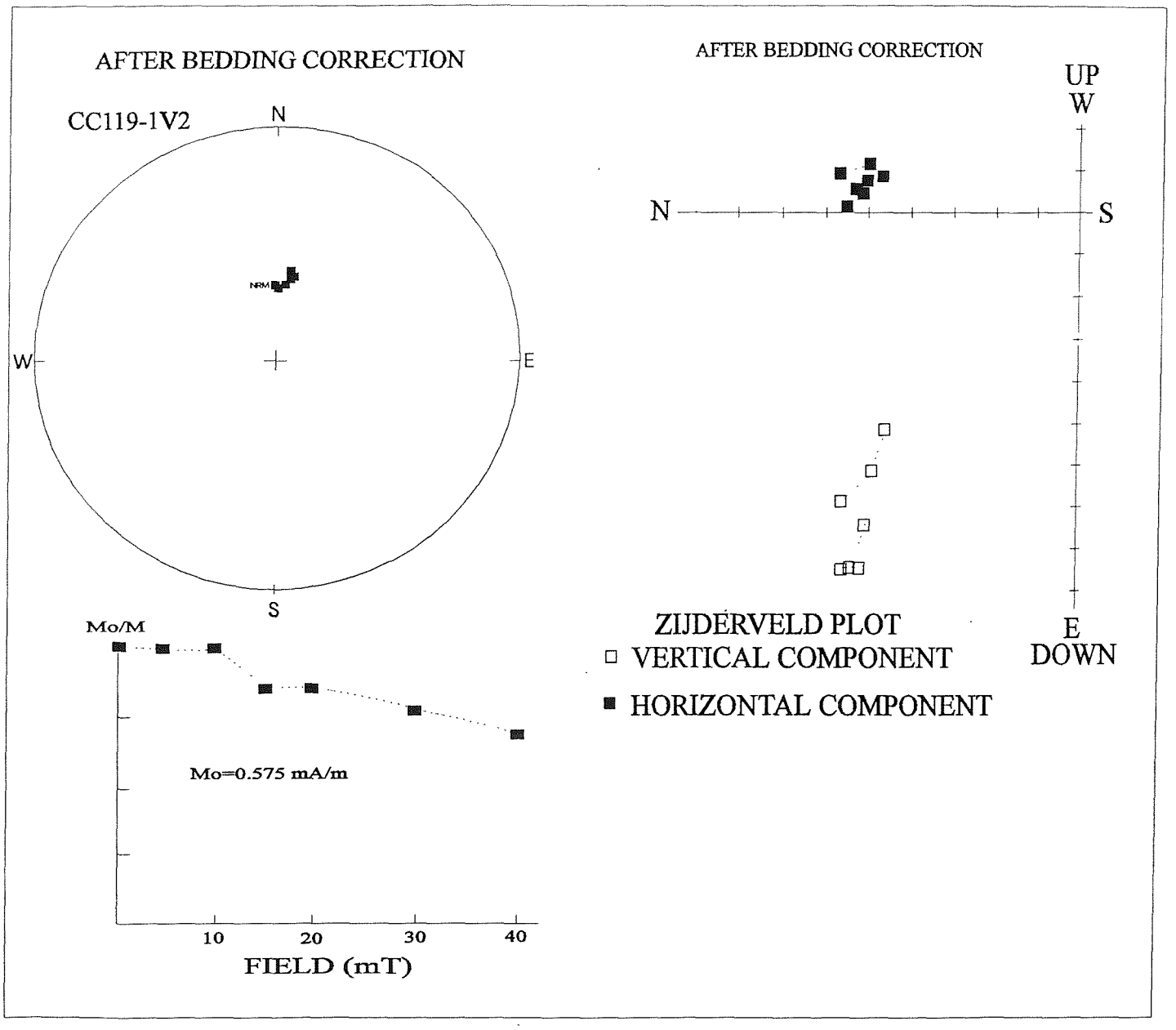

Figure 6.10. AF demagnetisation behaviour of sample CC19-1V2. On reaching a demagnetisation field of 40 mT the NRM intensity has been reduced by approximately 25%.

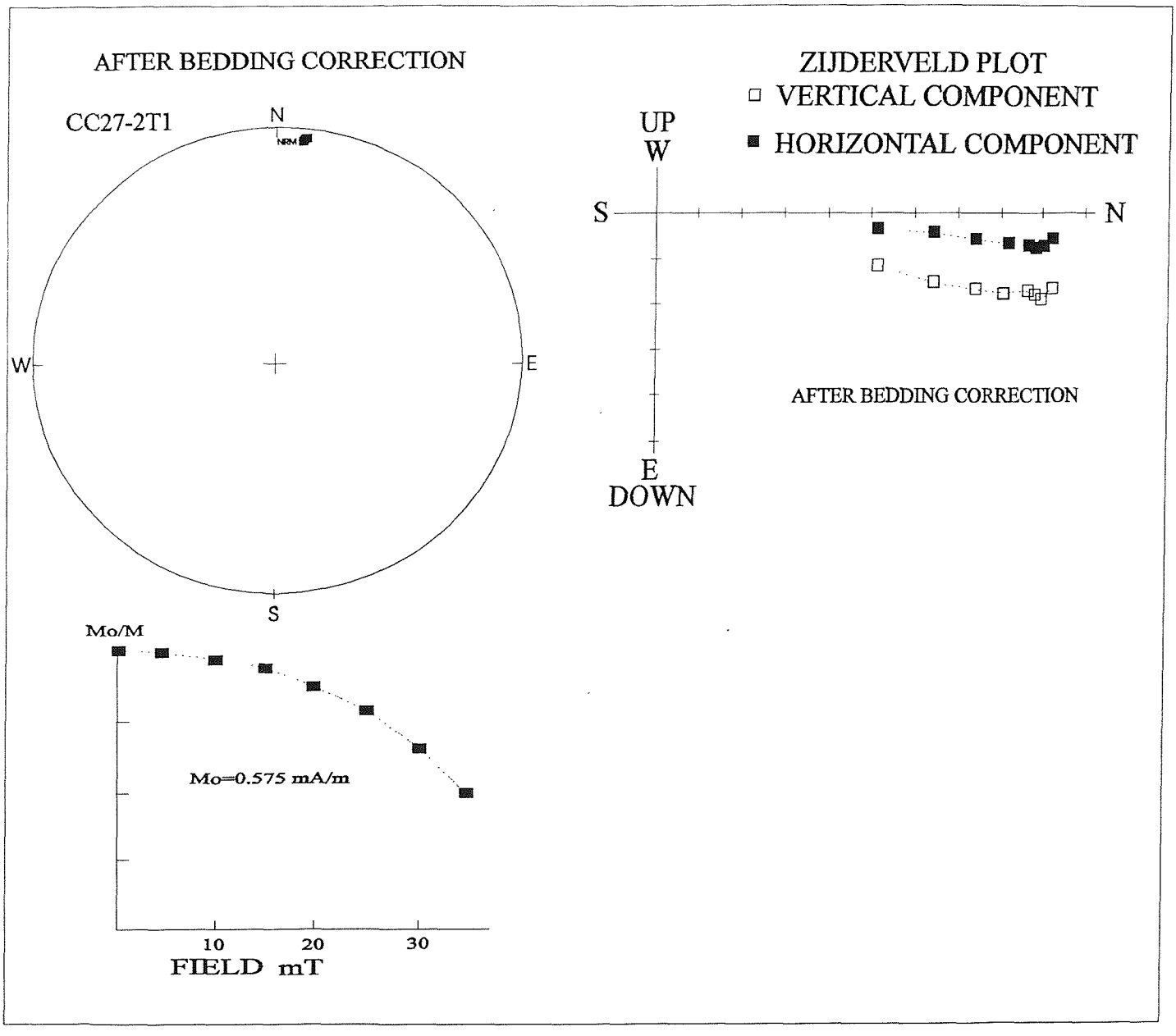

Figure 6.11a. AF demagnetisation was initially used on sample CC27-2T1. On reaching a demagnetisation field of 35 mT the NRM intensity had been reduced by approximately 50% but the direction had remained essentially unchanged.

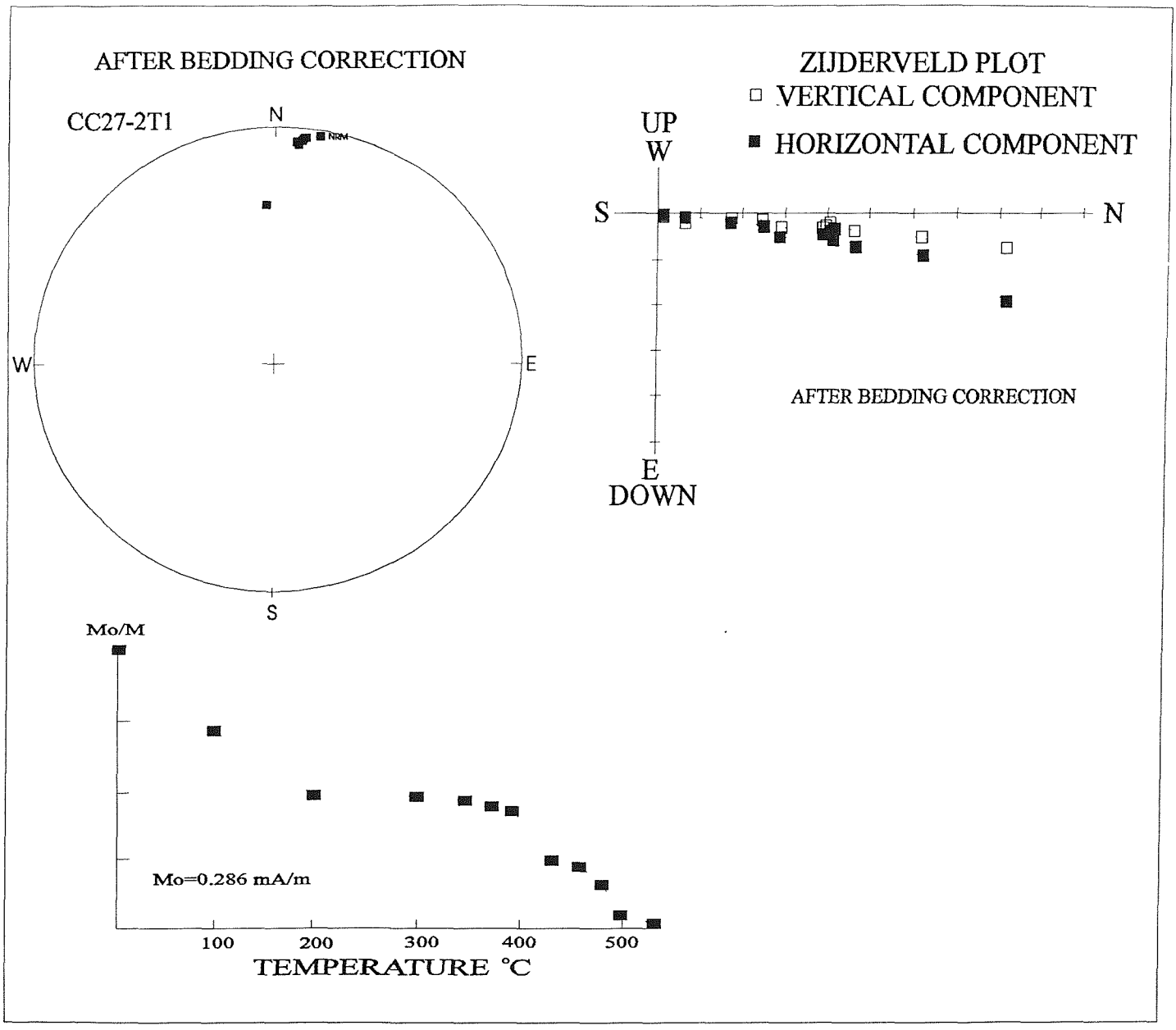

Figure 6.11b. Sample CC27-2T1 was then subjected to thermal demagnetisation. The following incremental steps were employed: NRM, 100, 200, 300, 380, 400, 420, 460, 480, 500, 520°C, etc. The response of the sample to this treatment, with a bedding correction applied is shown.

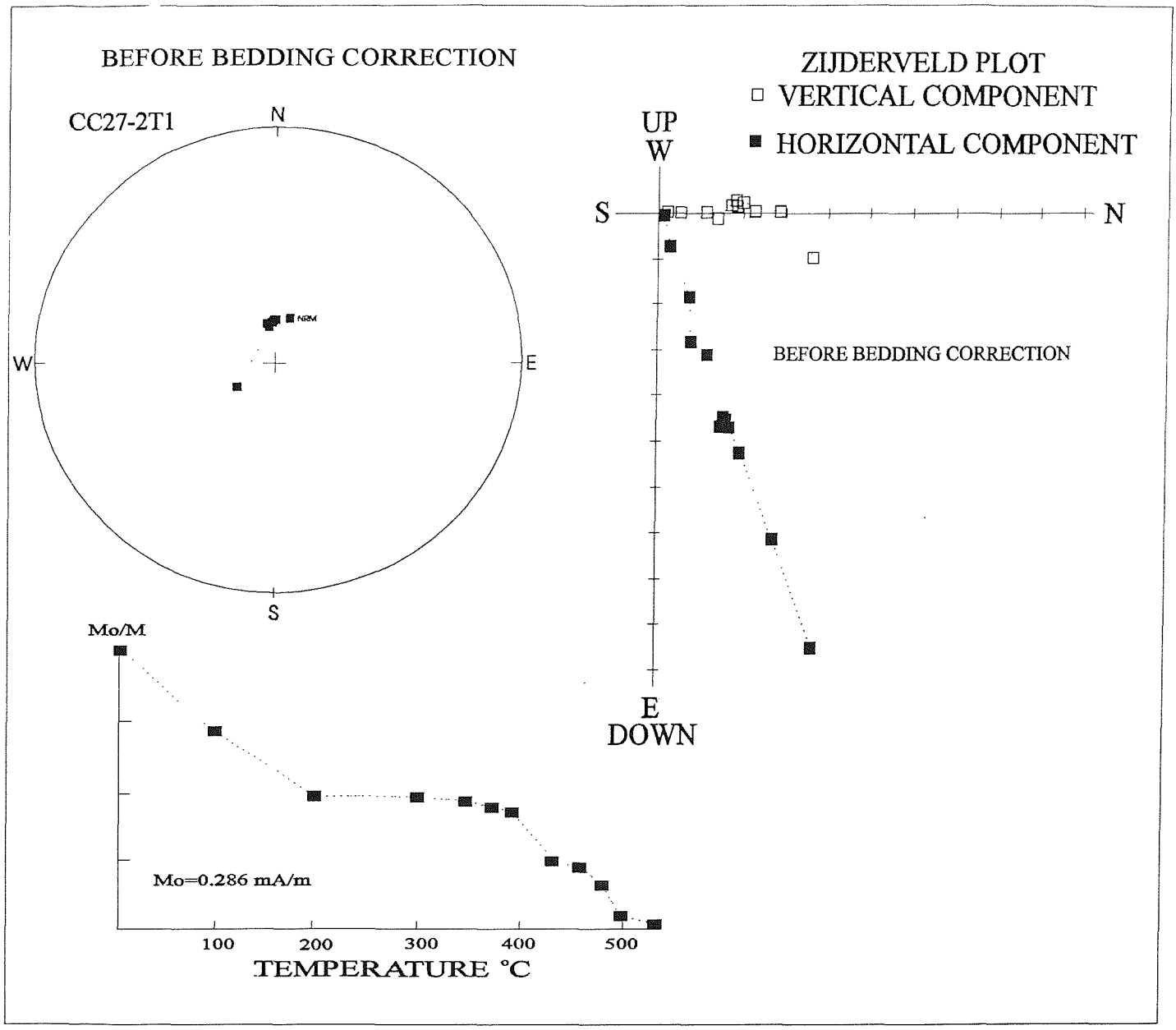

Figure 6.11c. The SCM is aligned in a similar direction to the present geomagnetic field (northerly declination, positive, steep inclination) prior to applying a bedding correction of 284°/63°.

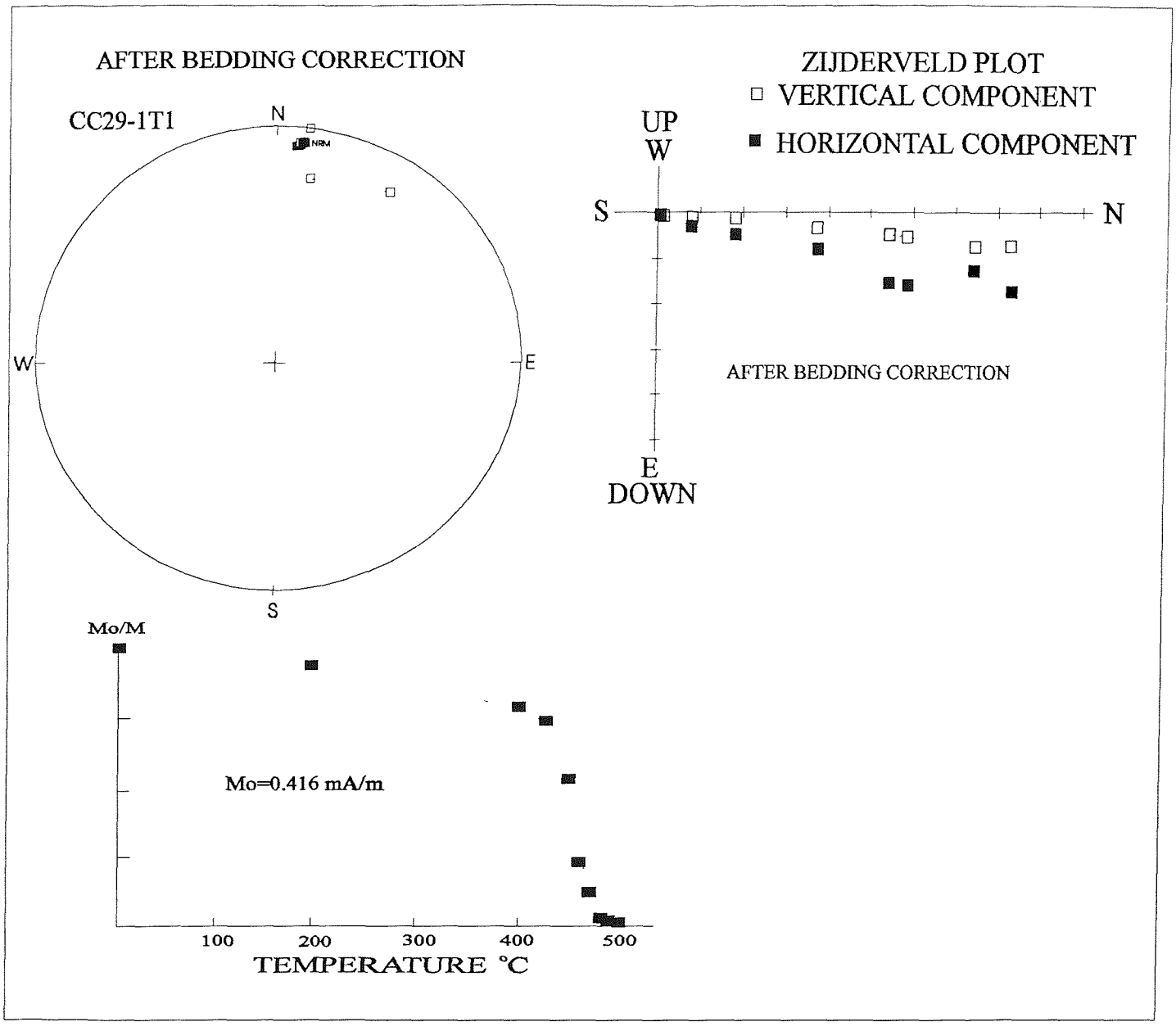

Figure 6.12. Incremental demagnetisation steps of 20°C were too great to reveal possible directional trends. Thermal demagnetisation steps of 0, 200, 400, 425, 450, 460, 470, 480, 490, 500°C, etc were adopted for the rest of the study. Sample CC29-1T1 shows the improved response to this treatment. A clear directional trend towards a negative inclination end point is apparent for the last few treatment steps.

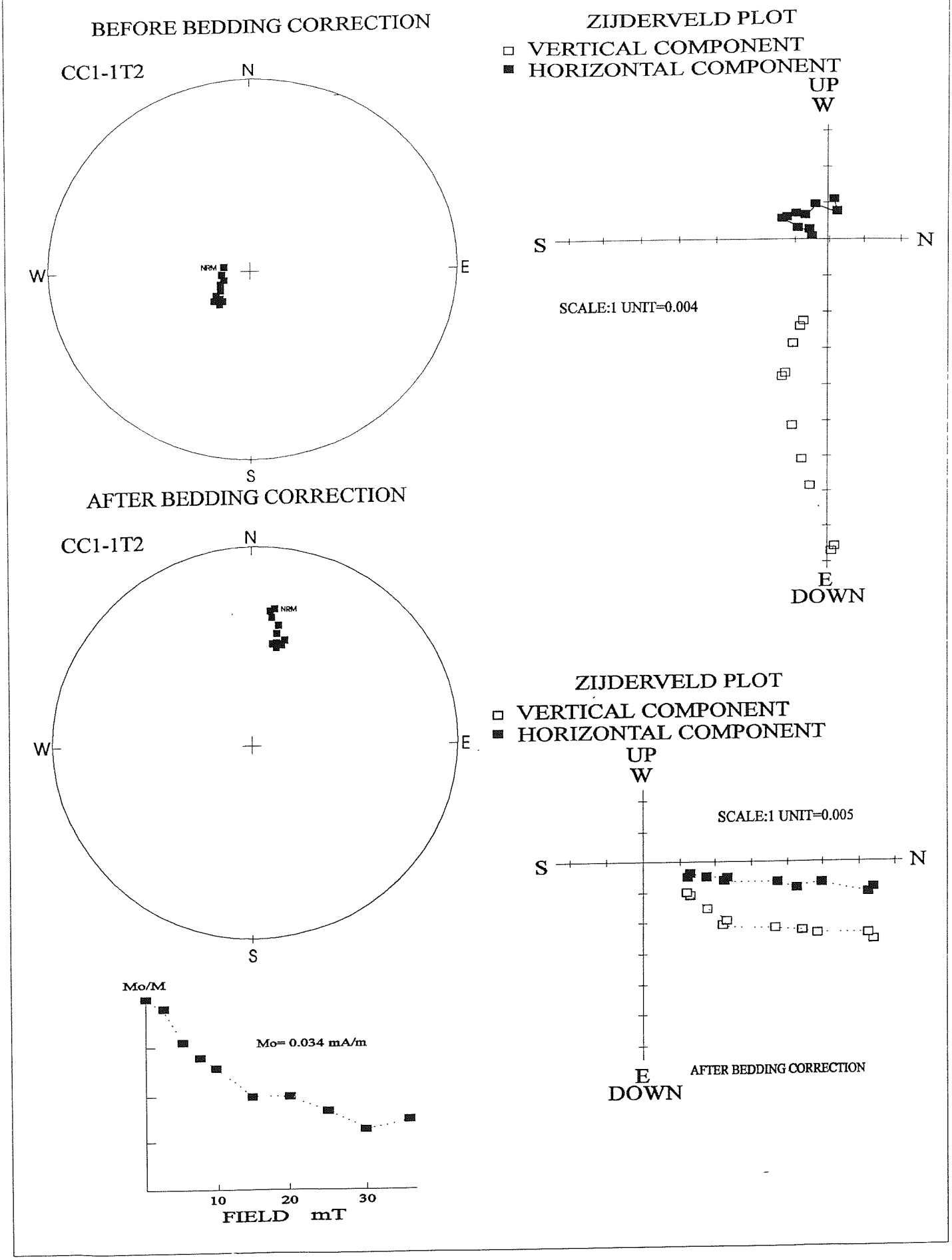

Figure 6.13a. An example of a 'S1 reliability category' AF demagnetised sample (CC1-1T2) before and after bedding correction.

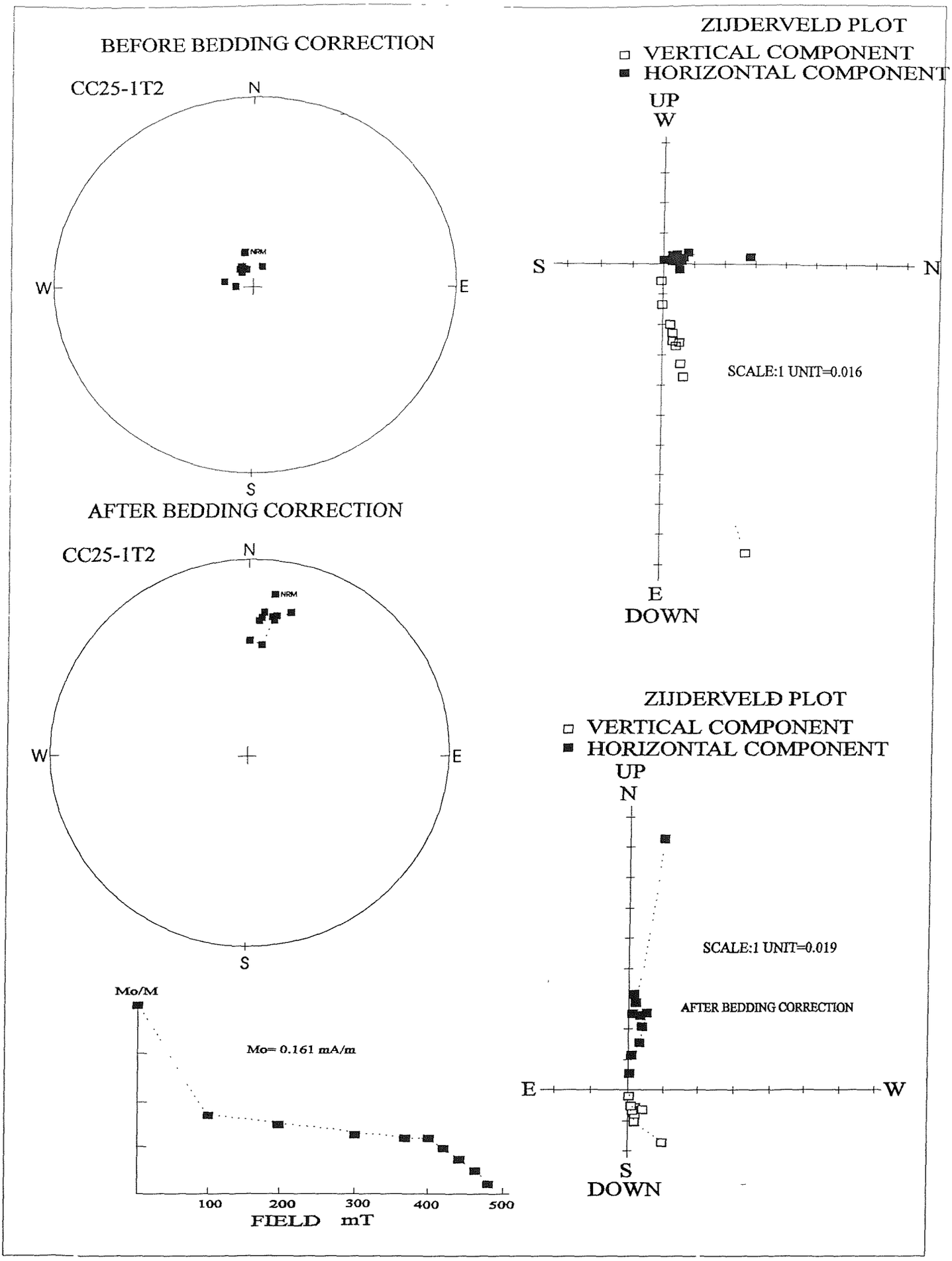

Figure 6.13b. An example of a 'S1 reliability category' thermally demagnetised sample (CC25-1T2) before and after bedding correction.

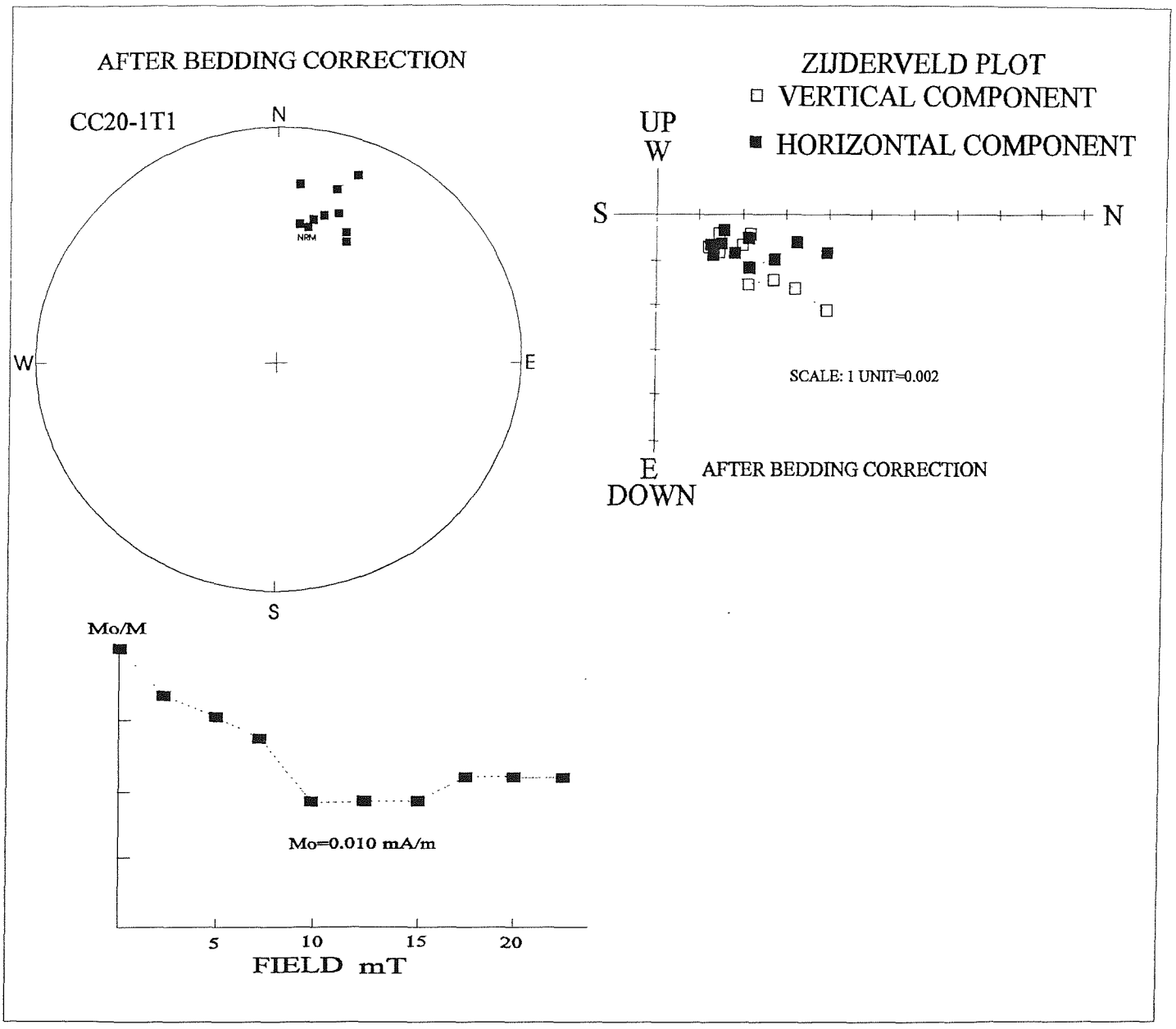

Figure 6.14a. An example of a 'S2 reliability category' A F demagnetised sample (CC20-1T1) after application of a bedding correction of 282°/62°.

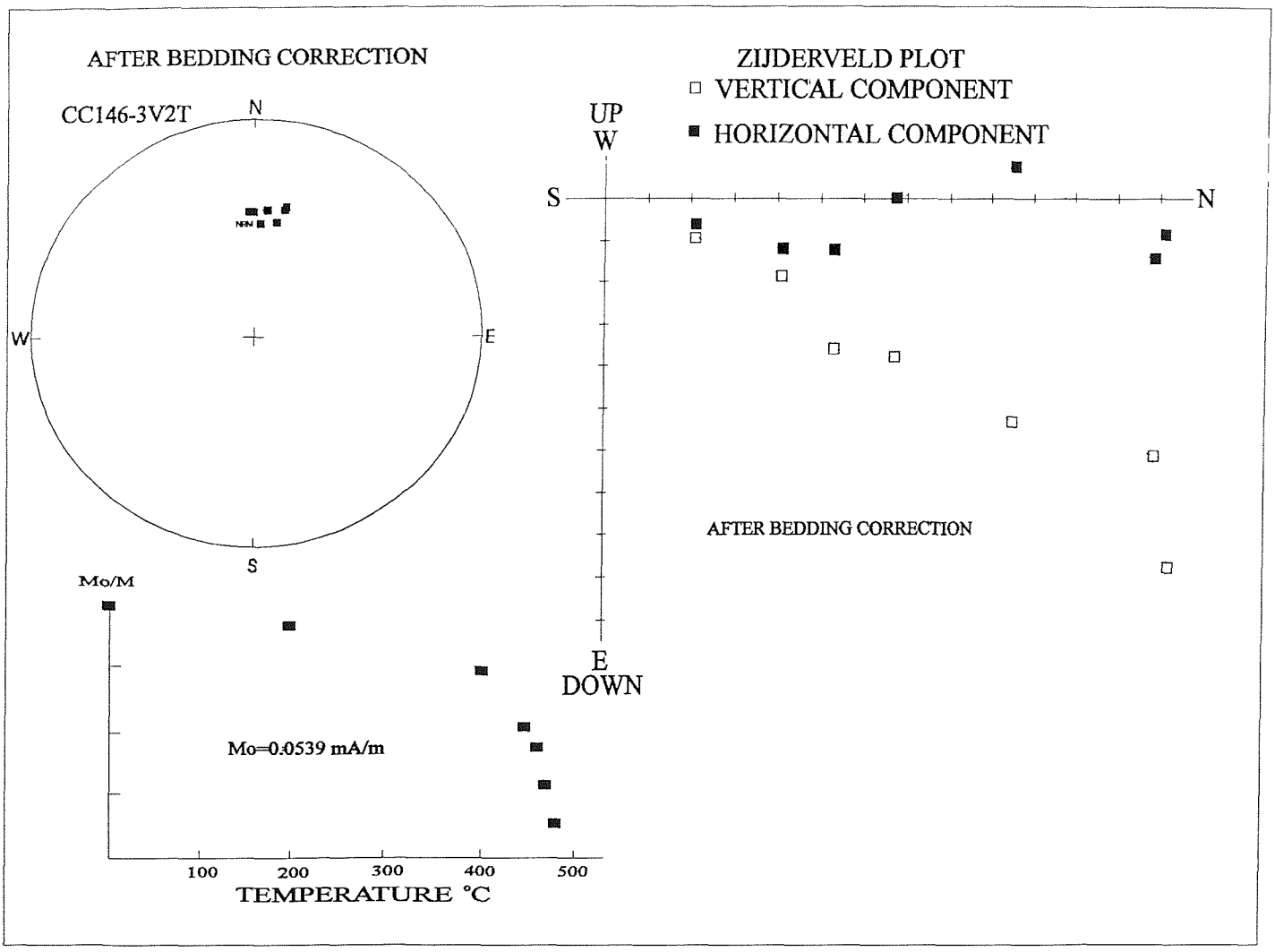

Figure 6.14b. An example of a 'S2 reliability category' thermally demagnetised sample (CC146-3V2T) after application of a bedding correction of 283°/53°.

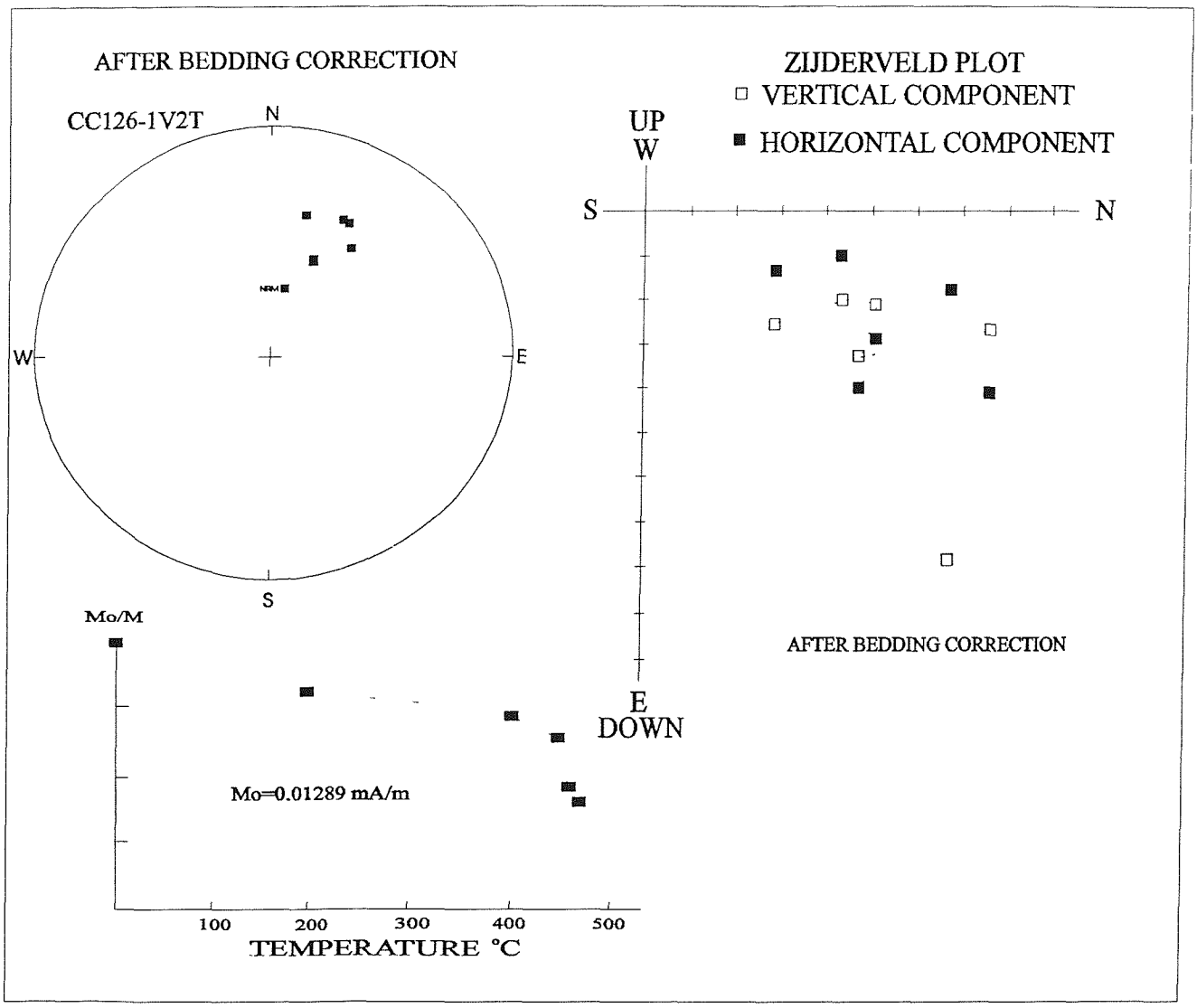

Figure 6.15a. An example of a normal polarity 'S3 reliability category' thermally demagnetised sample (CC126-1V2T) after application of a bedding correction of 292°/55°.

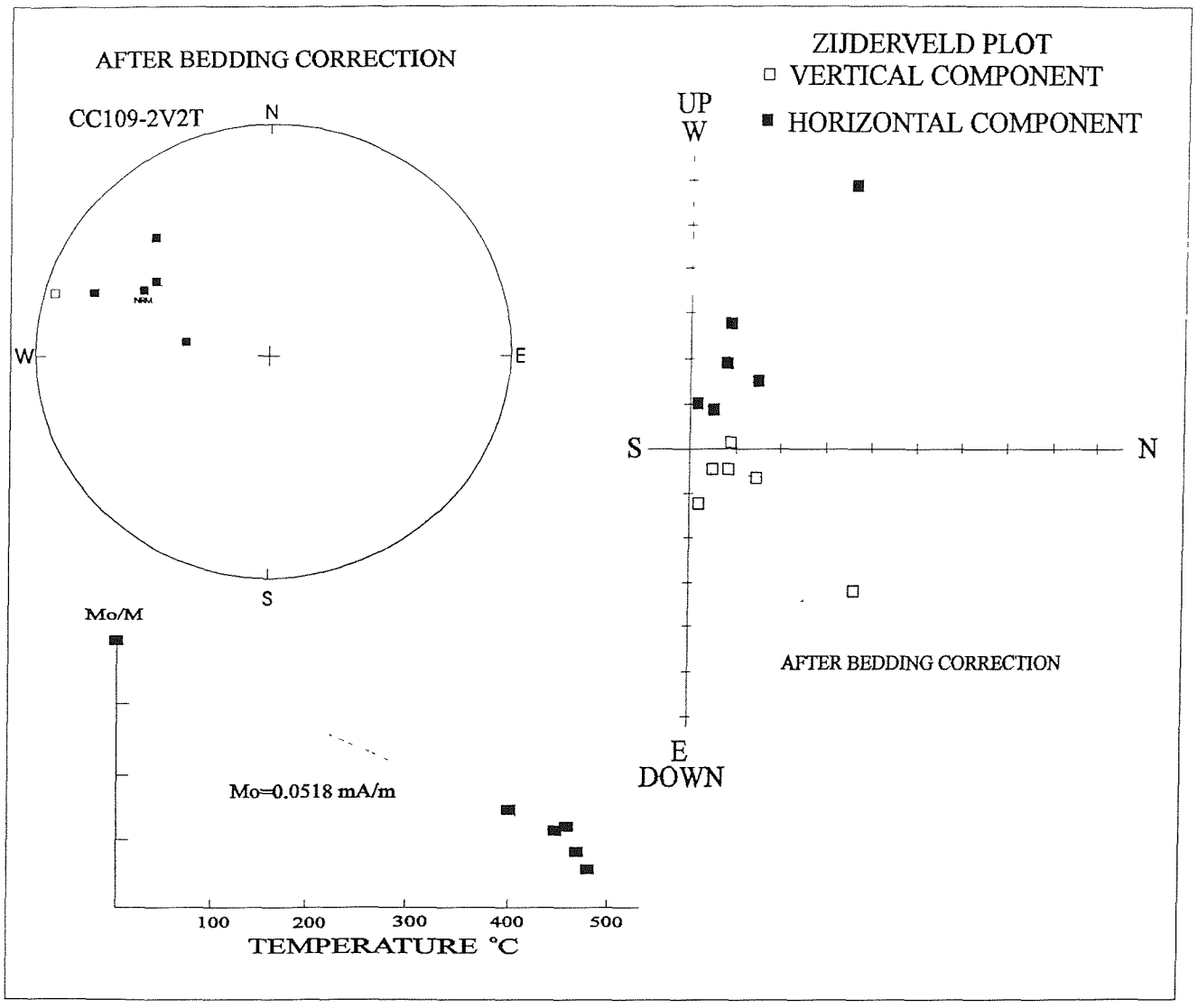

Figure 6.15b. An example of a normal polarity 'S3 reliability category' thermally demagnetised sample (CC109-2V2T) after application of a bedding correction of 292°/55°.

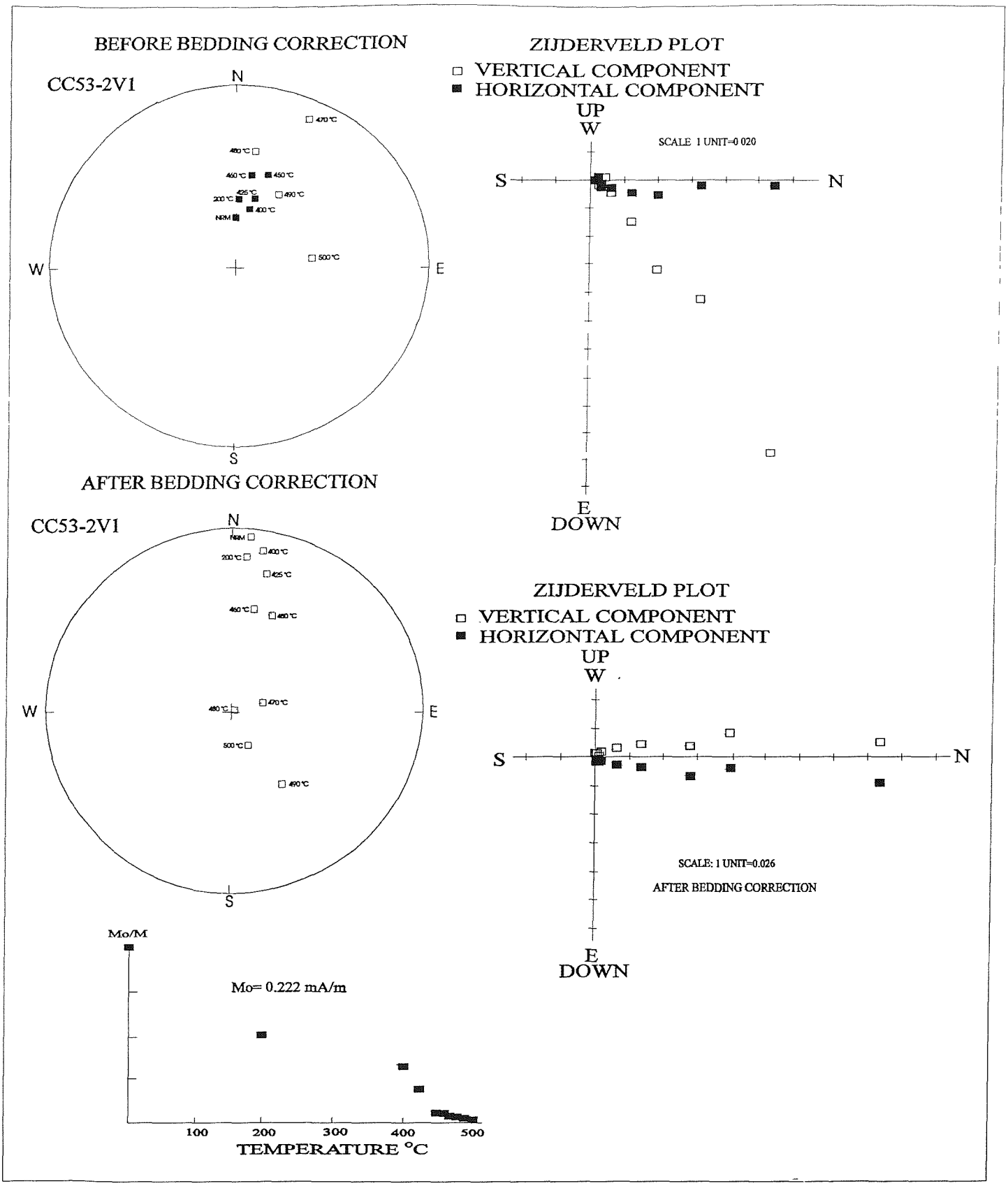

Figure 6.16a (i). An example of a 'T1 reliability category' thermally demagnetised sample (CC44-3V3) before and after application of a bedding correction of 287°/70°.

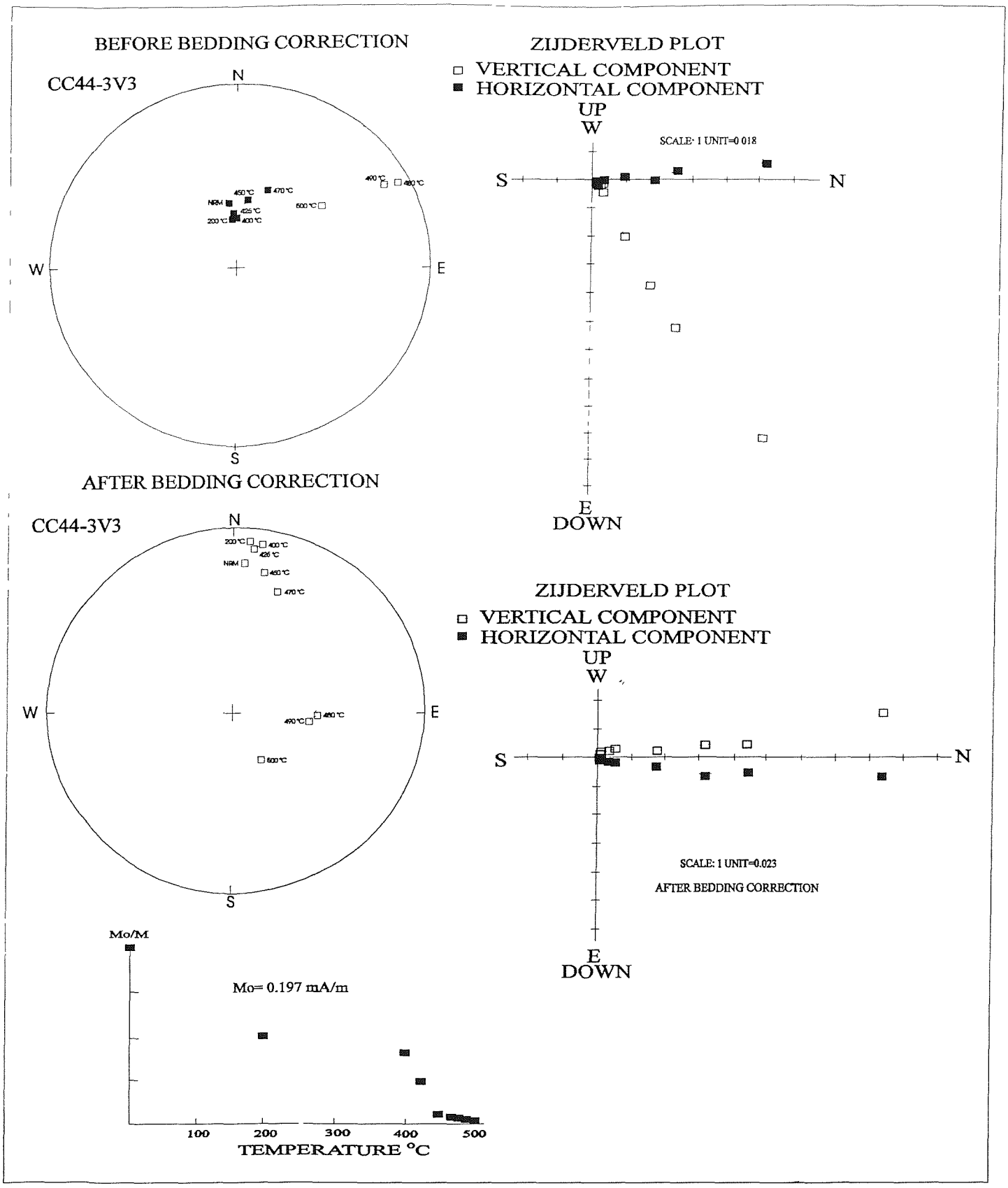

Figure 6.16a (ii). An example of a 'T1 reliability category' thermally demagnetised sample (CC53-2V1) before and after application of a bedding correction of 282°/65°.

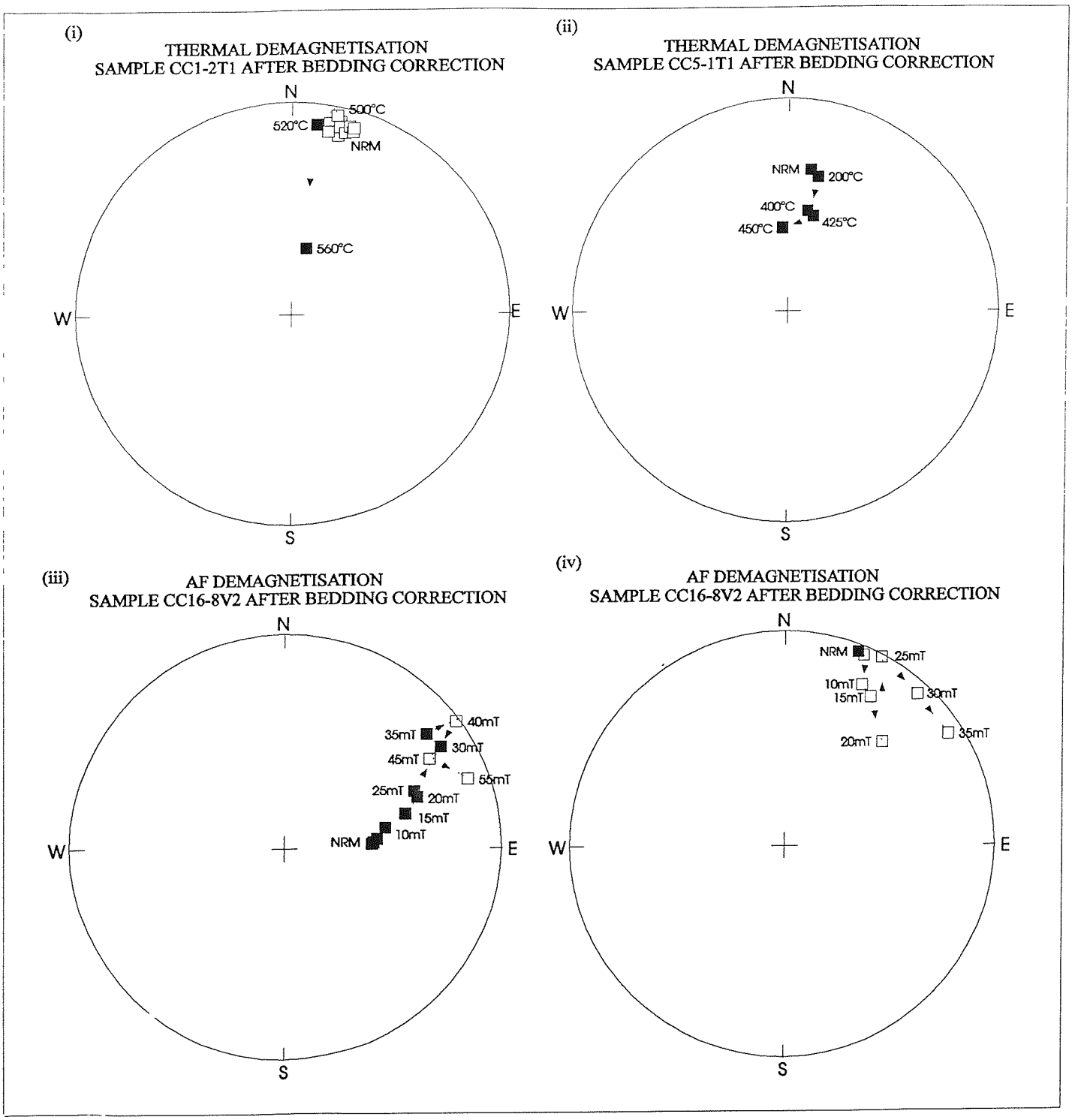

Figure 6.16b. Examples of 'T2 reliability category' thermally (i & ii, trends to normal polarity) and AF (iii & iv, trends to reverse polarity) demagnetised samples (after application of respective bedding corrections).

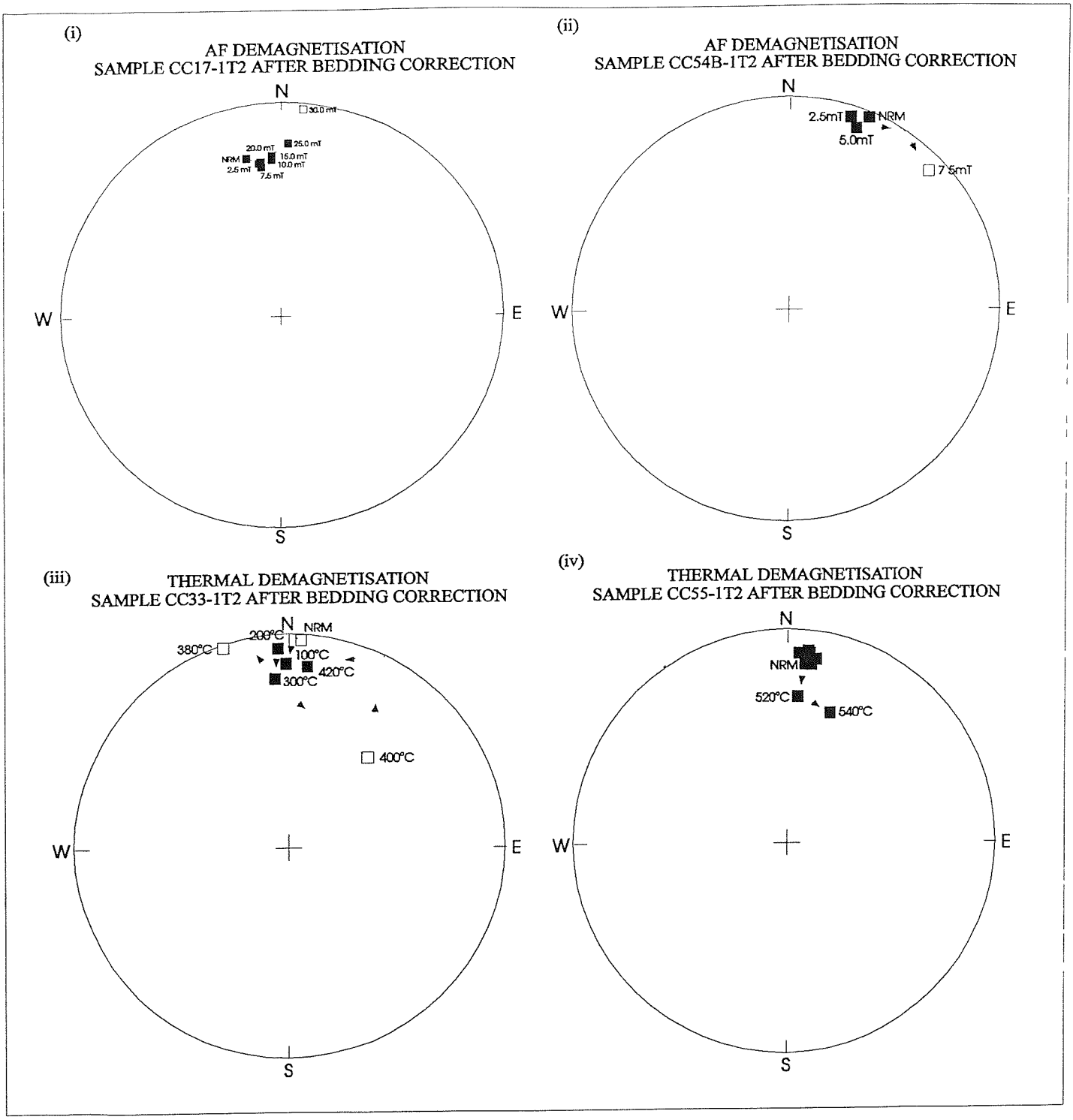

Figure 6.16c. Examples of 'T3 reliability category' AF (i & ii, trends to reverse polarity) and thermally (iii & iv, trends to normal polarity) demagnetised samples (after application of respective bedding corrections).

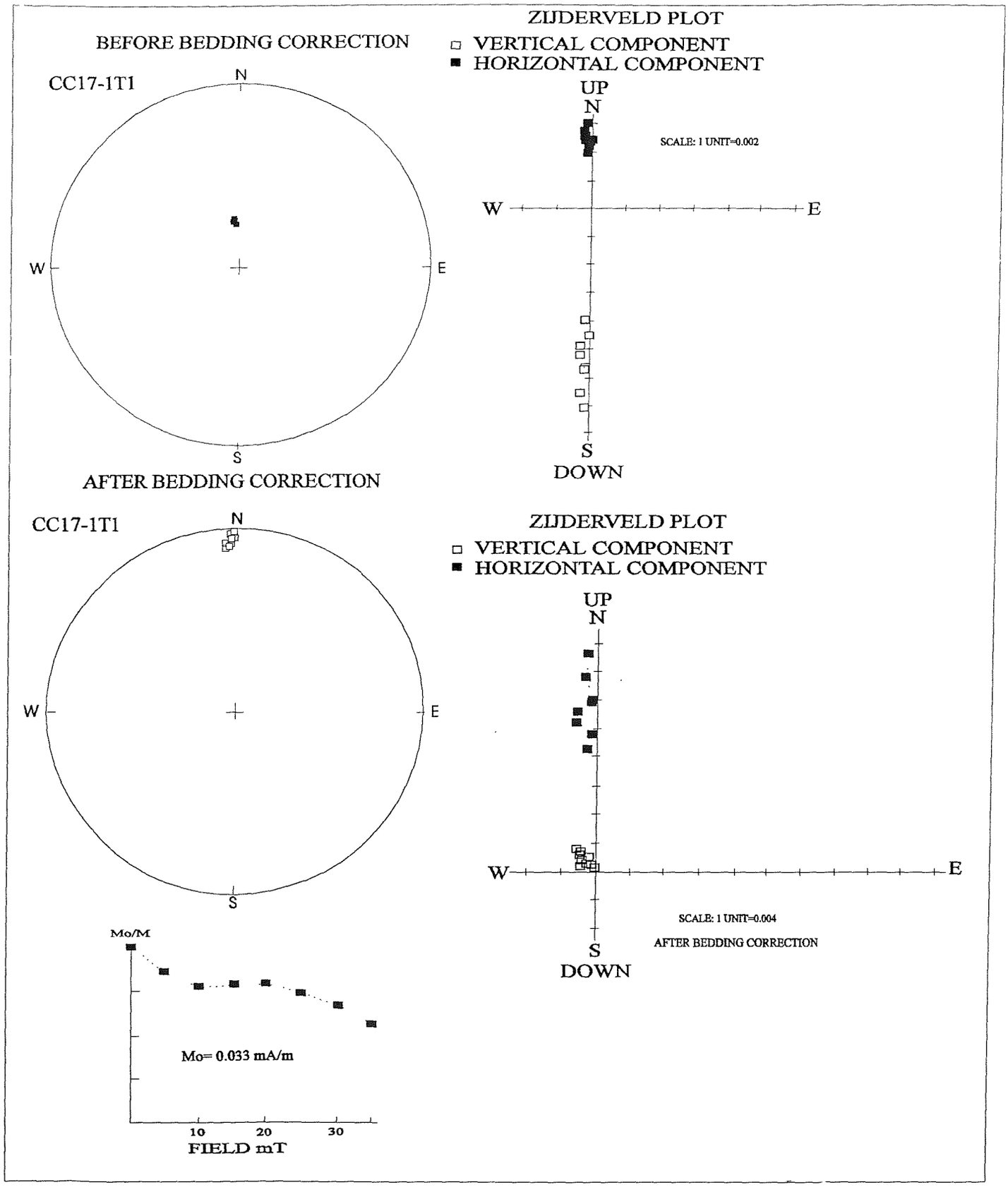

Figure 6.17a. An example of an 'Overprint reliability category' AF demagnetised sample (CC17-1T1) before and after application of a bedding correction of 263°/70°.

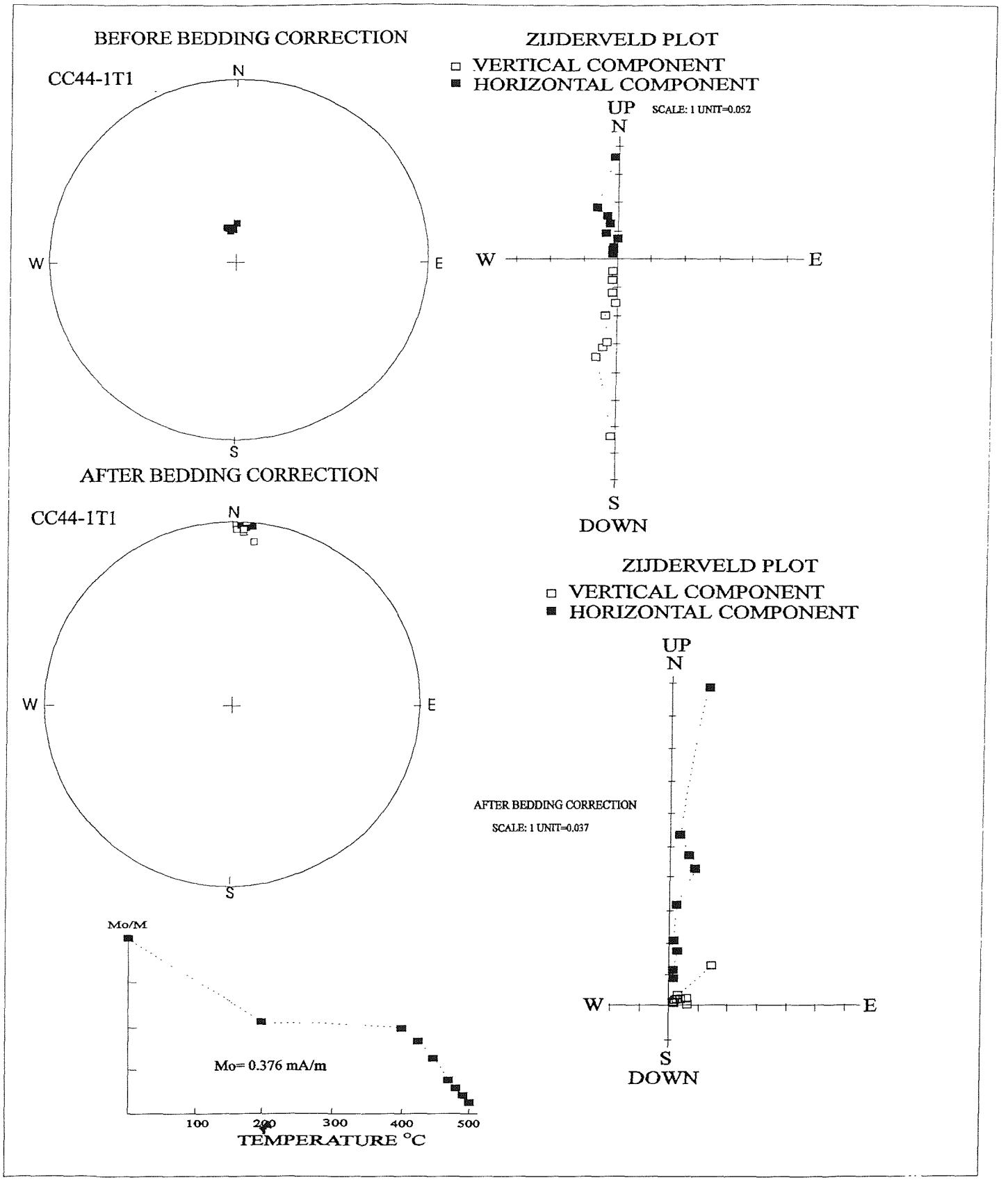

Figure 6.17b. An example of an 'Overprint reliability category' themally demagnetised sample (CC44-1T1) before and after application of a bedding correction of 287°/70°.

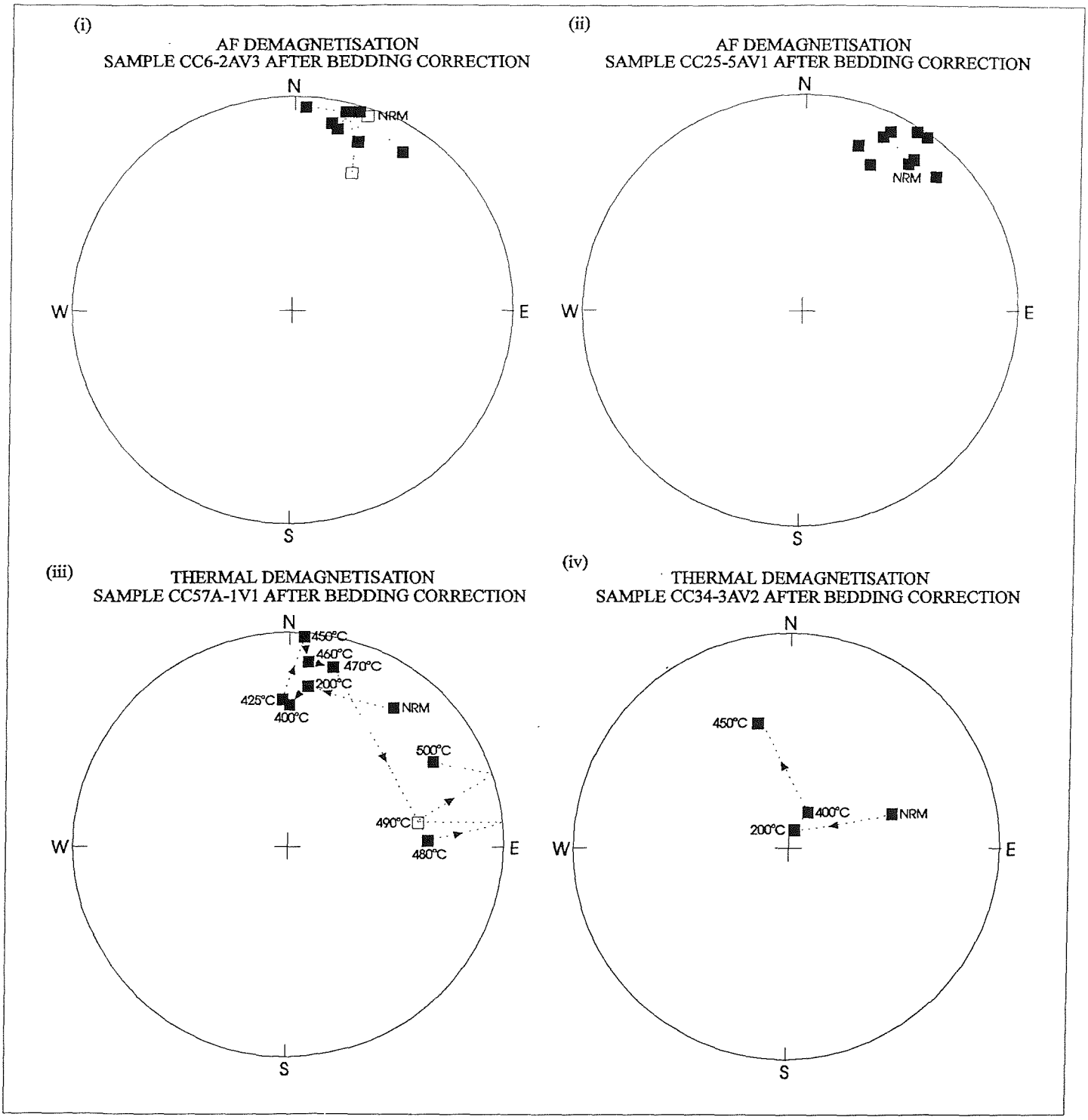

Figure 6.18. Examples of 'Erratic reliability category' AF and thermally demagnetised samples (after application of respective bedding corrections). Polarity definition is impossible.

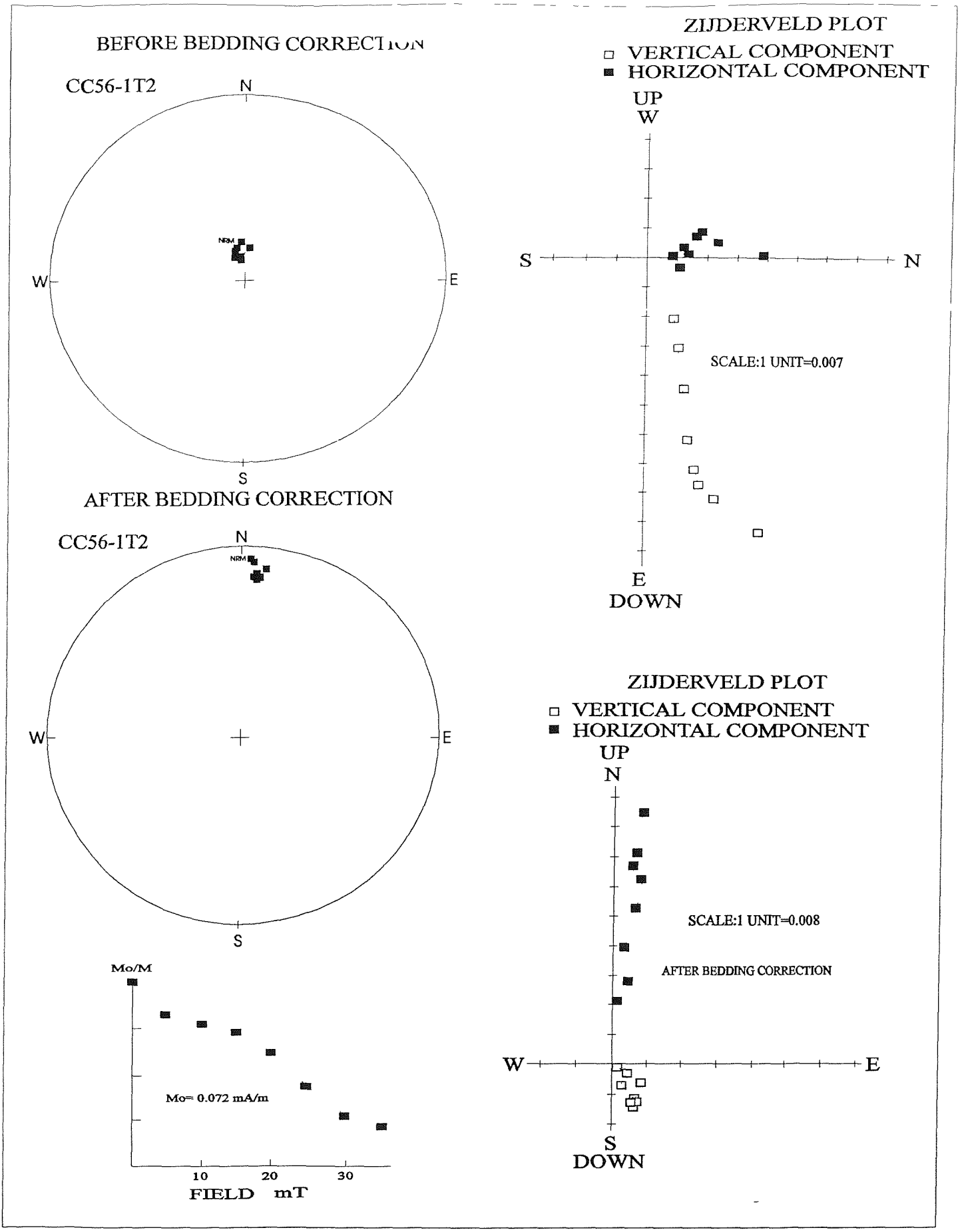

Figure 6.19a. A bedding correction of 282°/62° has been applied for sample CC56-1T2. The Stable Characteristic Magnetisation of the sample is rotated away from the recent geomagnetic field direction (Dec=0°, Inc=68°) to a direction with a shallow positive inclination (10°) and an approximately northerly declination.

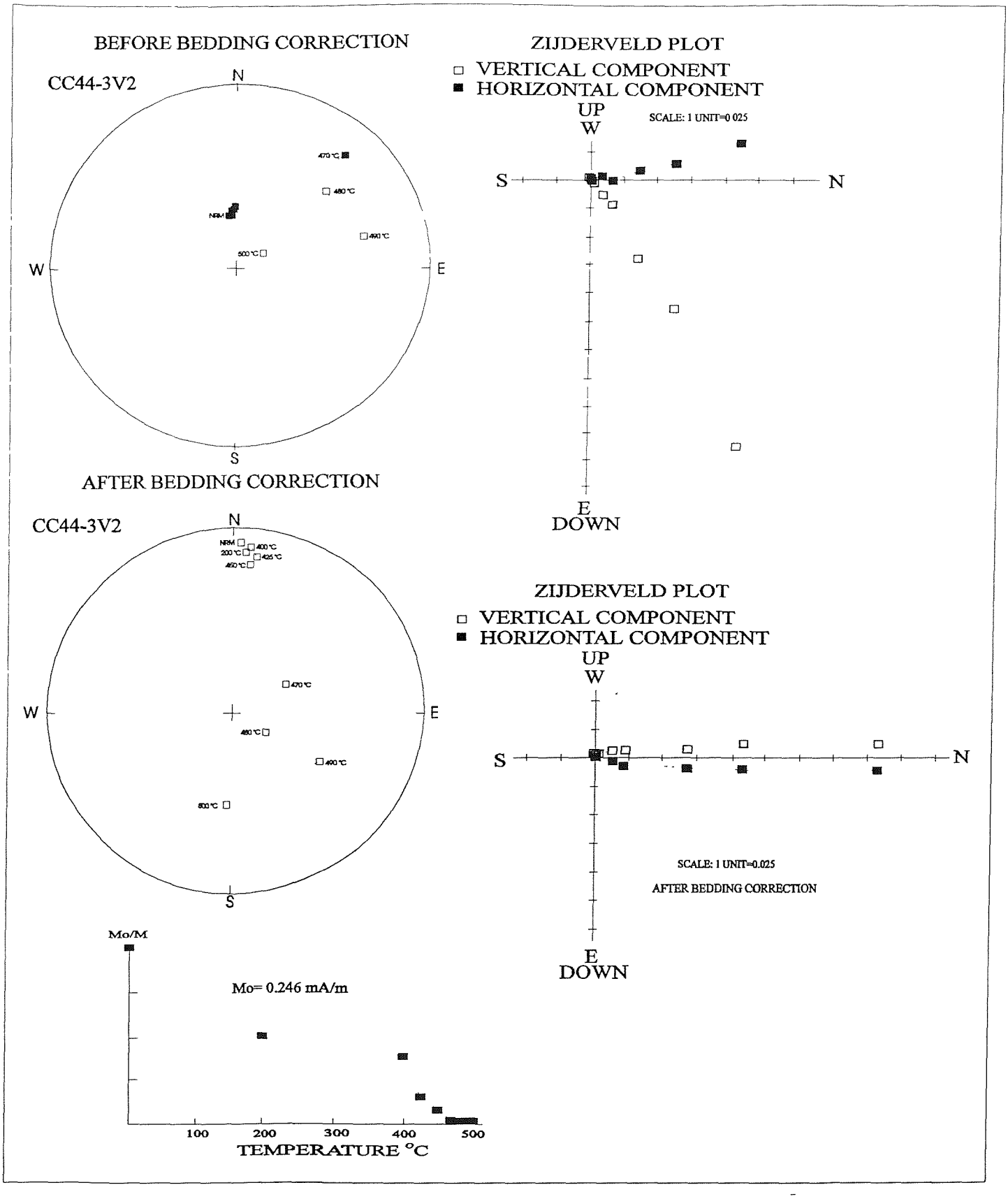

Figure 6.19b. Sample CC44-3V2 before and after a tectonic correction of 287°/70°. Prior to correction, sample CC44-3V2 displays a possible directional trend away from a recent field direction towards reverse polarity. After the tectonic correction is applied to the sample no doubt remains.

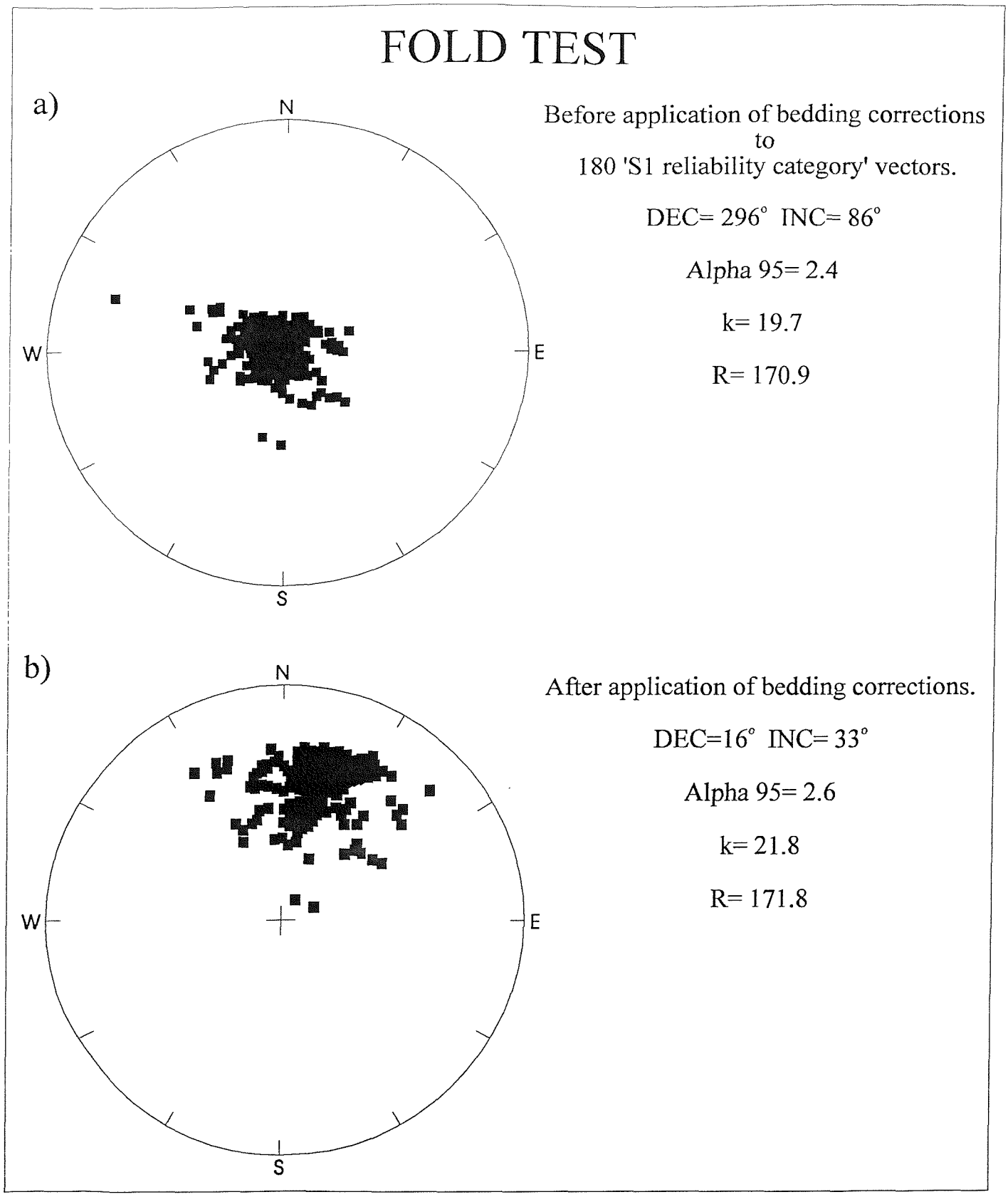

Figure 6.20. A stereographic equal area plot of the stable characteristic magnetisation for 180 'S1 type reliability category' magnetic vectors from the complete Culver section, before (a) and after (b) bedding corrections have been applied to the individual vectors. Bedding correction inclinations range between 53° and 75° while strikes range between 286° and 292°. Precision parameters 'k' and alpha 95 are reported before and after bedding corrections.

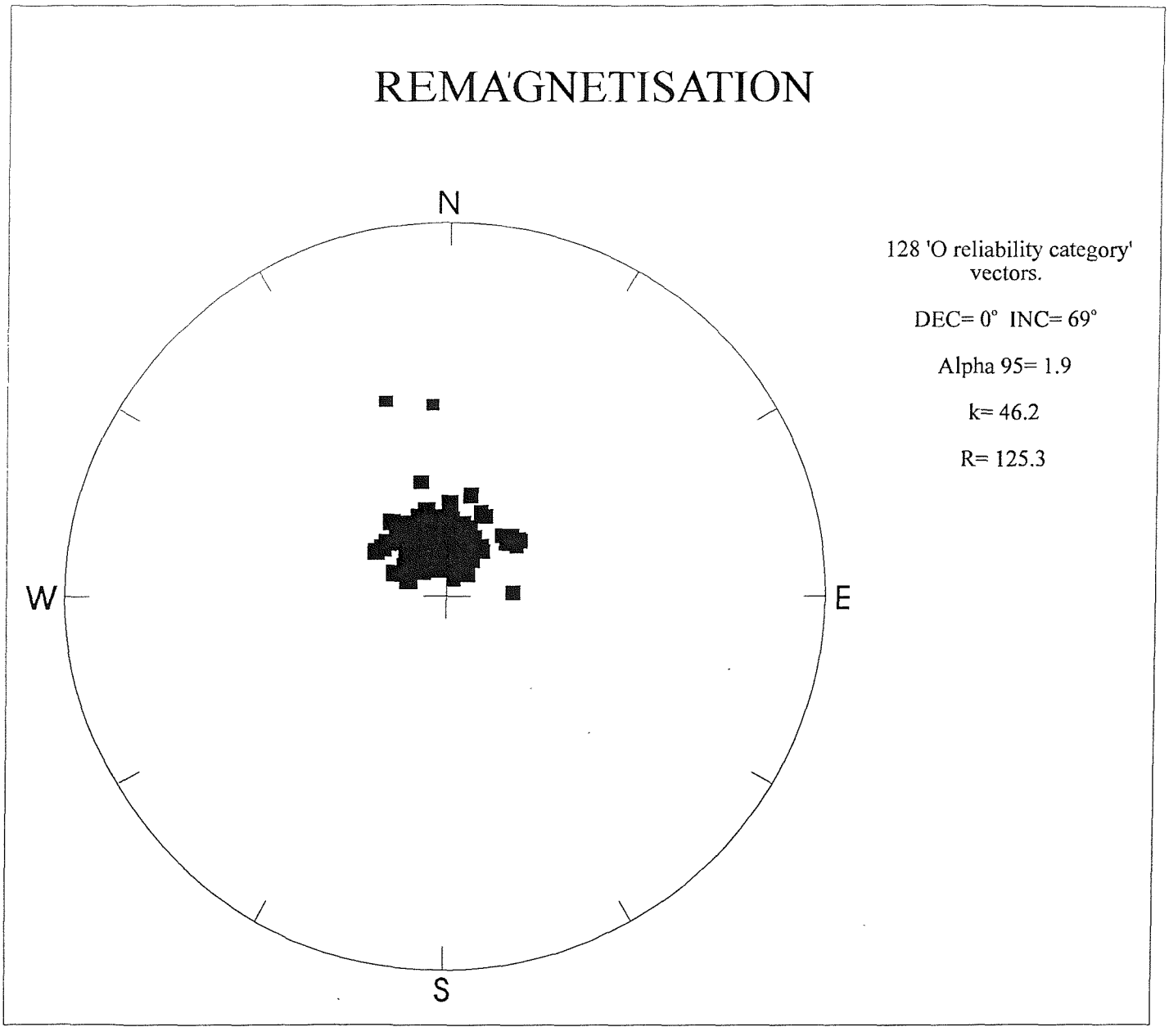

Figure 6.21. A stereographic equal area plot of overprint vectors for the Culver section. Twenty-two percent of the samples demagnetised possessed magnetic overprints which could not be removed by using either A.F. or thermal demagnetisation procedures. Of these 339 specimens 128 possessed stable end points which were well defined by a collection of closely spaced points on the stereographic projection and with the final linear segment (MAD<=5) on the vector plot directed through the origin. An overall mean overprint vector (declination=1°, inclination=69°) similar to the recent geomagnetic field is inferred from this data.

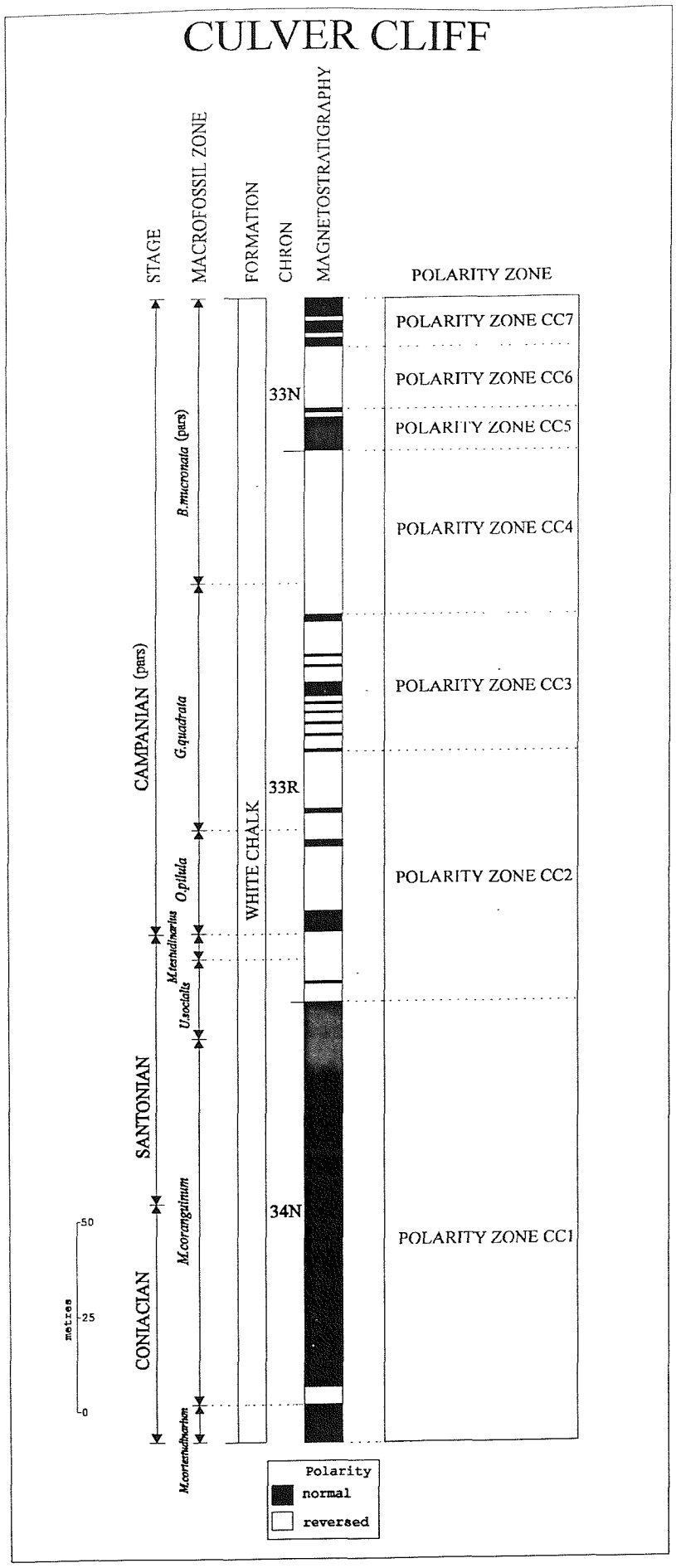

Figure 6.22. The Culver Cliff Chalk succession can be divided into seven polarity intervals. From left to right the diagram shows Late Cretaceous Stages, macrofossil zones (Rawson *et al.* 1978), Formation, geomagnetic polarity Chrons, the magnetostratigraphy of Culver Cliff and the associated polarity zones.

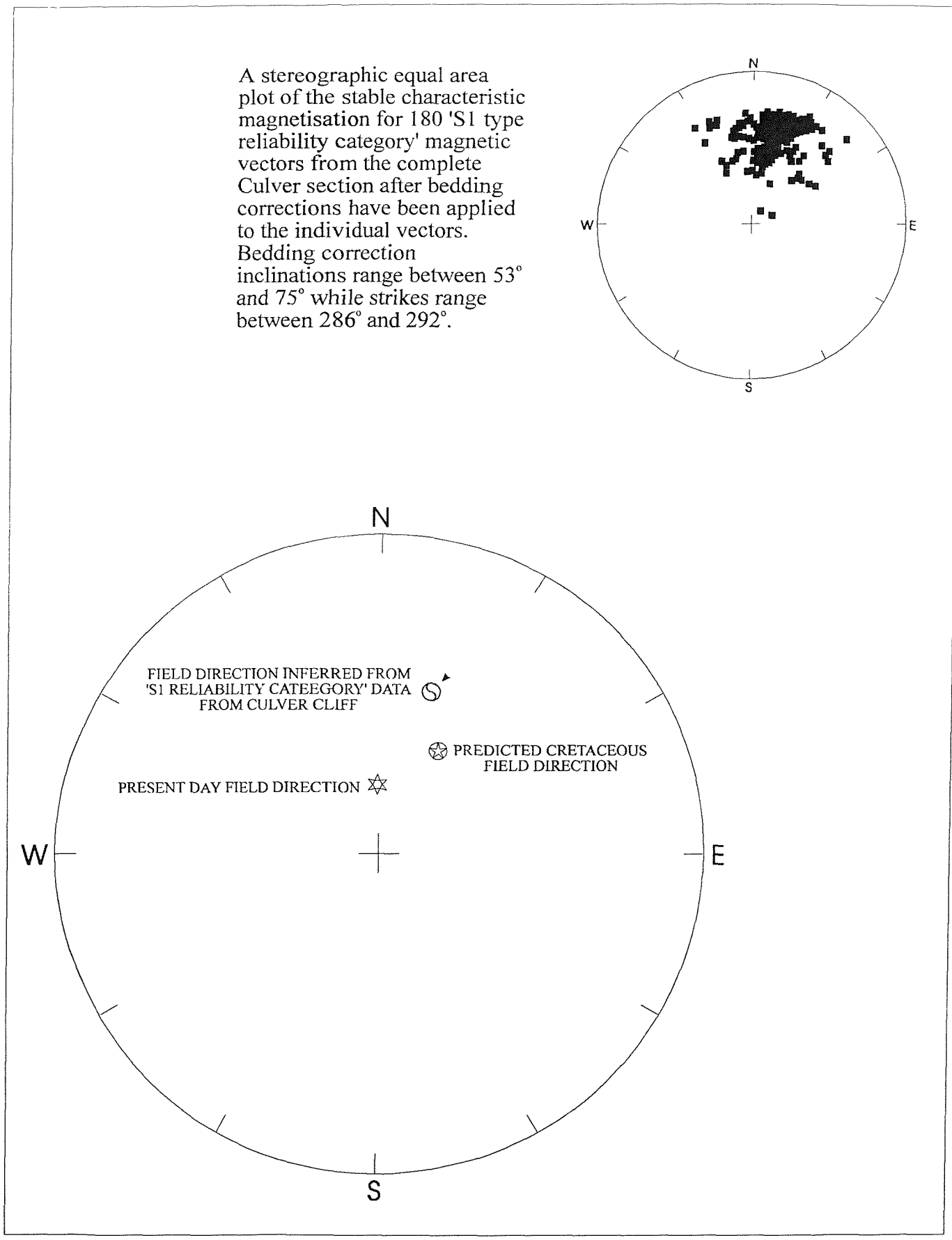

Figure 6.23. A stereographic projection showing the overall mean geomagnetic field direction for southern England (declination= 16°, inclination= 33°, k= 22 and alpha 95= 2.3) based on 'S1 reliability category' palaeomagnetic vectors derived from Late Cretaceous Chalk deposits, the predicted Late Cretaceous geomagnetic field direction for southern England based on the palaeocontinental reconstructions of Smith *et al.* (1981) and the present day geomagnetic field direction. Inset, a stereographic equal area plot of the stable characteristic magnetisation for 180 'S1 reliability category' magnetic vectors from the complete Culver section after bedding corrections have been applied to the individual vectors.

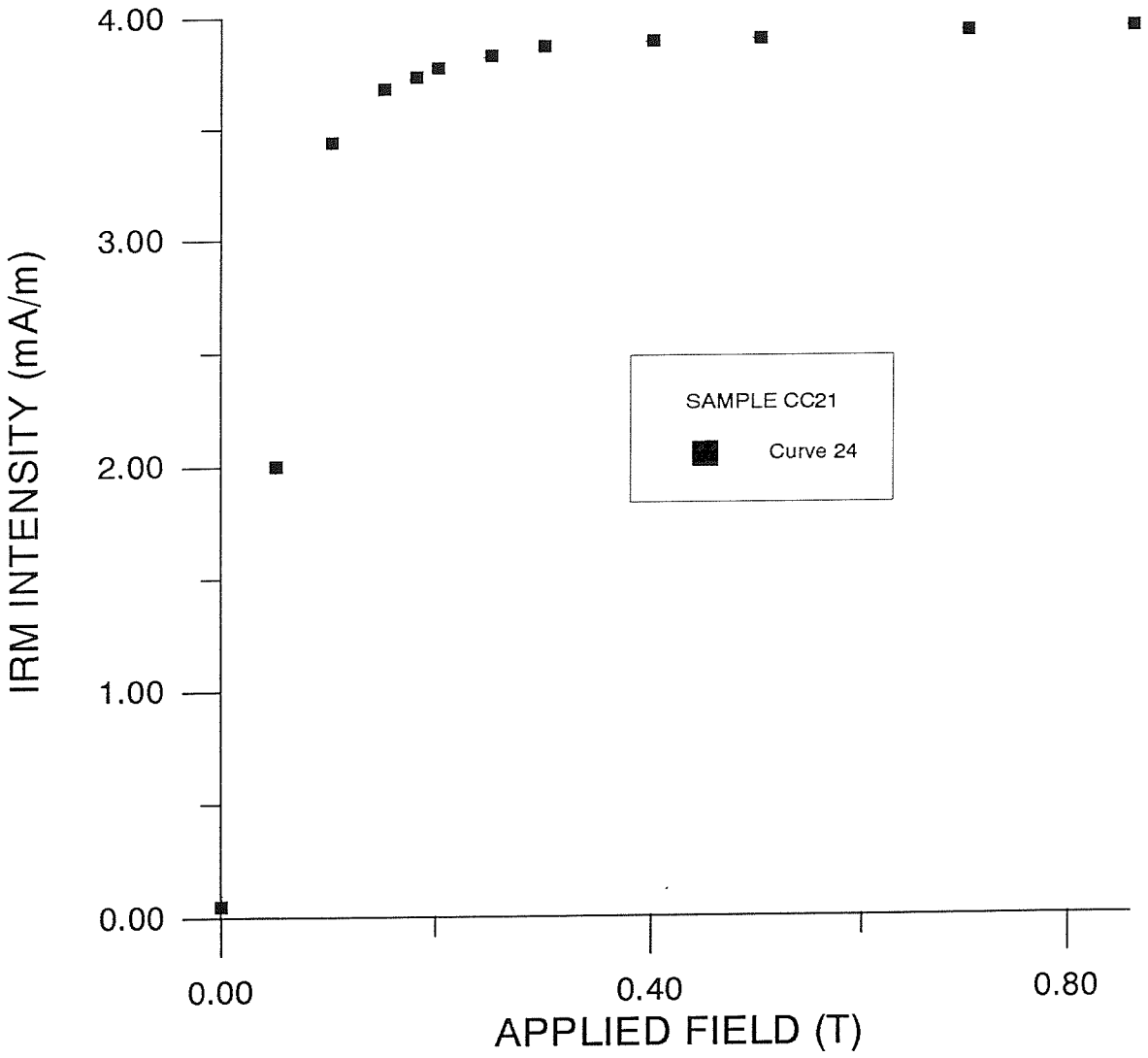

Figure 6.24. Typical response of a chalk sample collected from Culver Cliff after being subjected to a series of incremental direct magnetic fields.

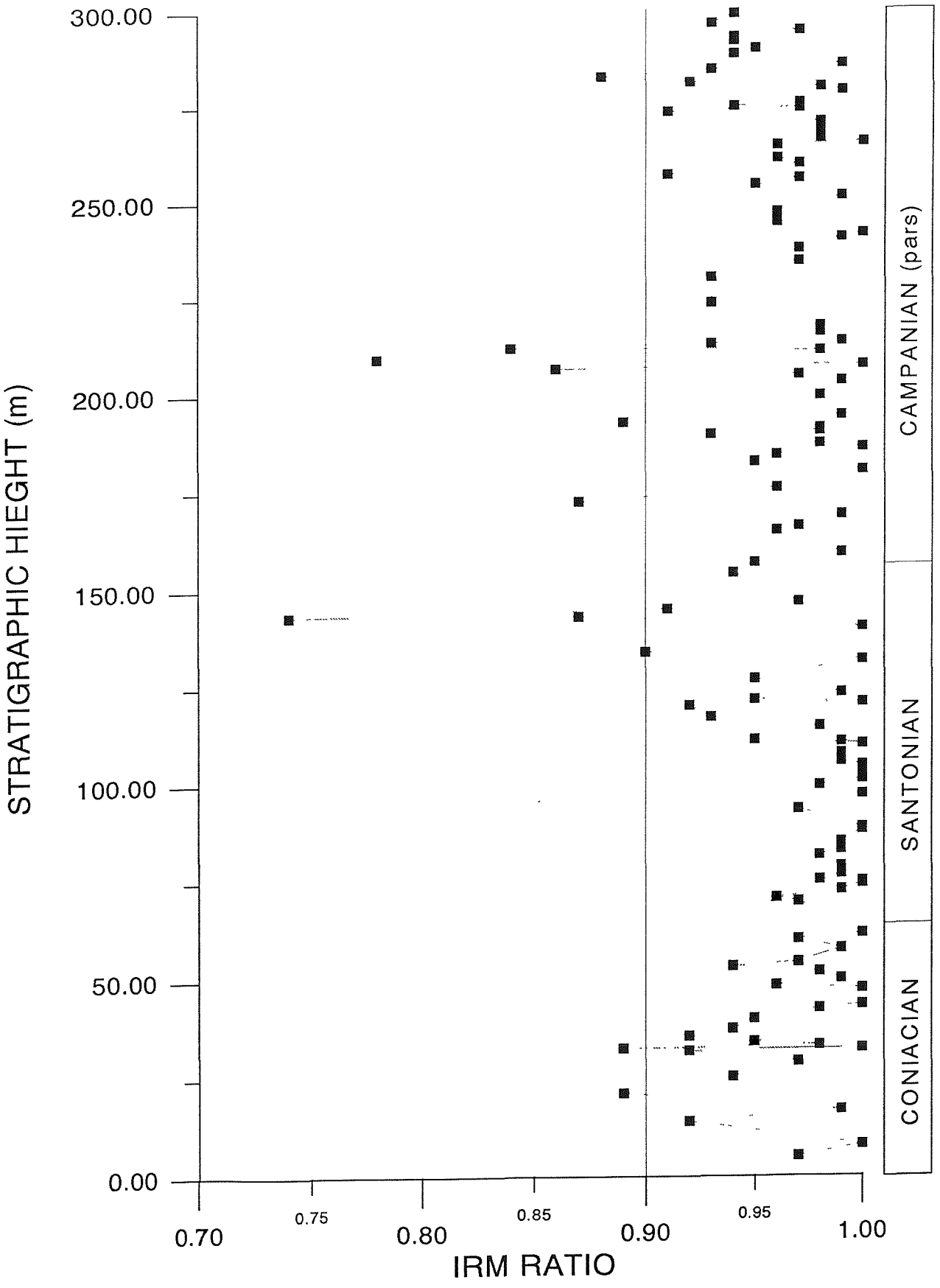

Figure 6.25. Variation in IRM ratio with stratigraphic height above the Turonian-Coniacian boundary. The right hand column indicates the Late Cretaceous stages represented by the Chalk succession at Culver Cliff (Rawson *et al.*, 1978).

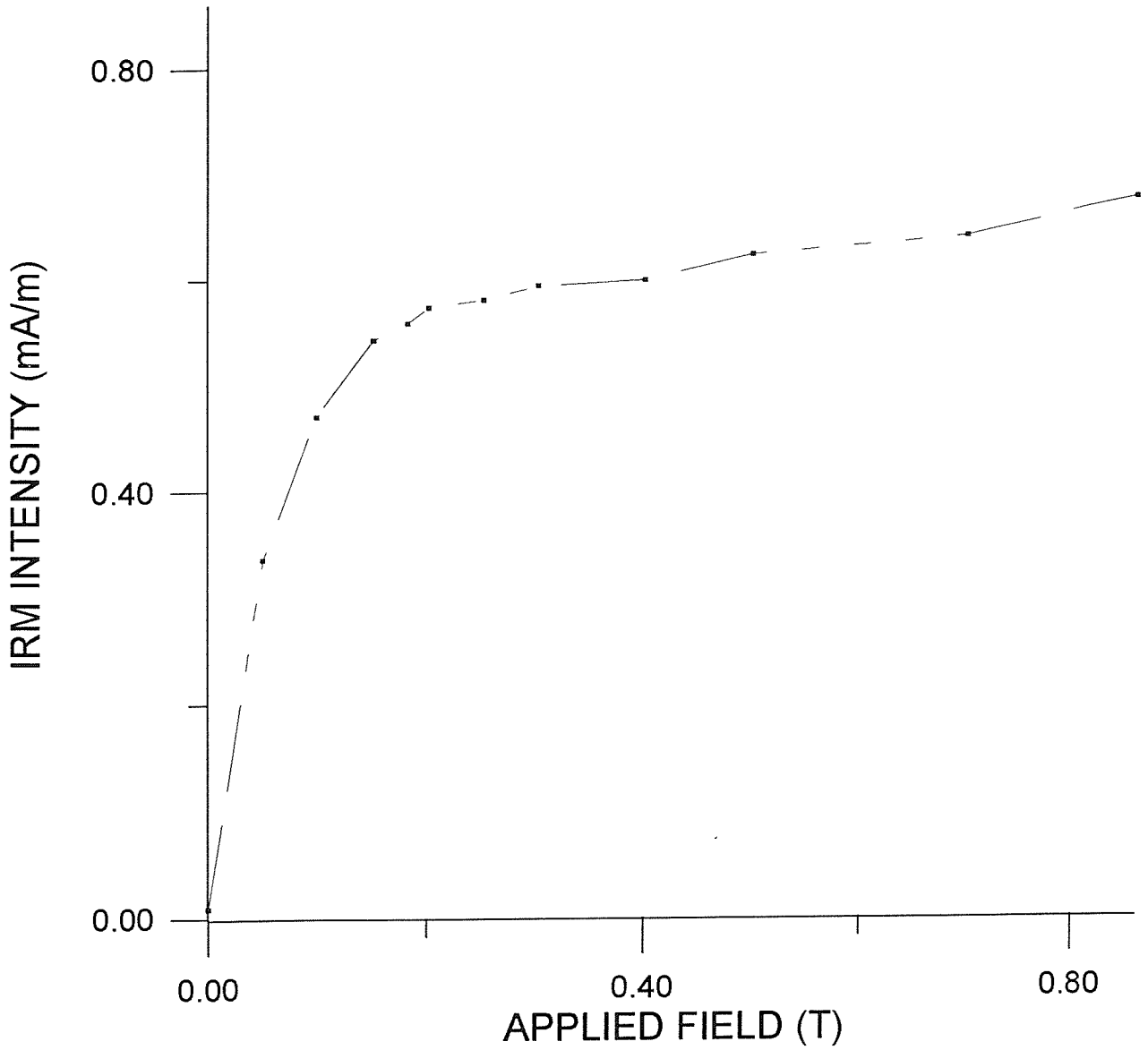

Figure 6.26. IRM acquisition curve for sample CC11-1T2 showing a shape diagnostic of titanomagnetite with addmixtures of hematite.

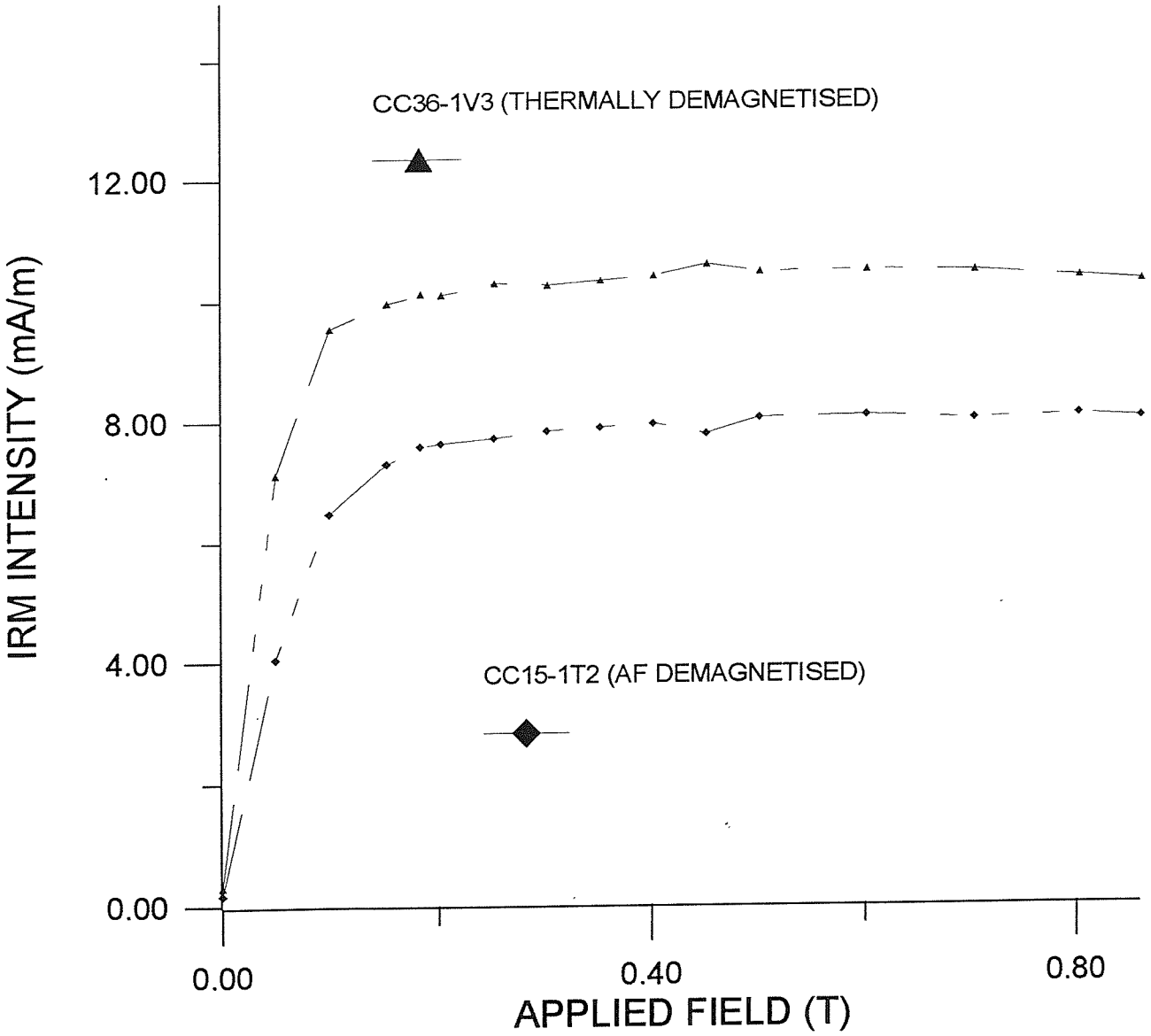

Figure 6.27. IRM acquisition curves for sample CC36-1T2 (thermally demagnetised) and sample CC15-1T2 (AF demagnetised). Both AF and thermally demagnetised specimens possess similar shaped curves (diagnostic of titanomagnetite).

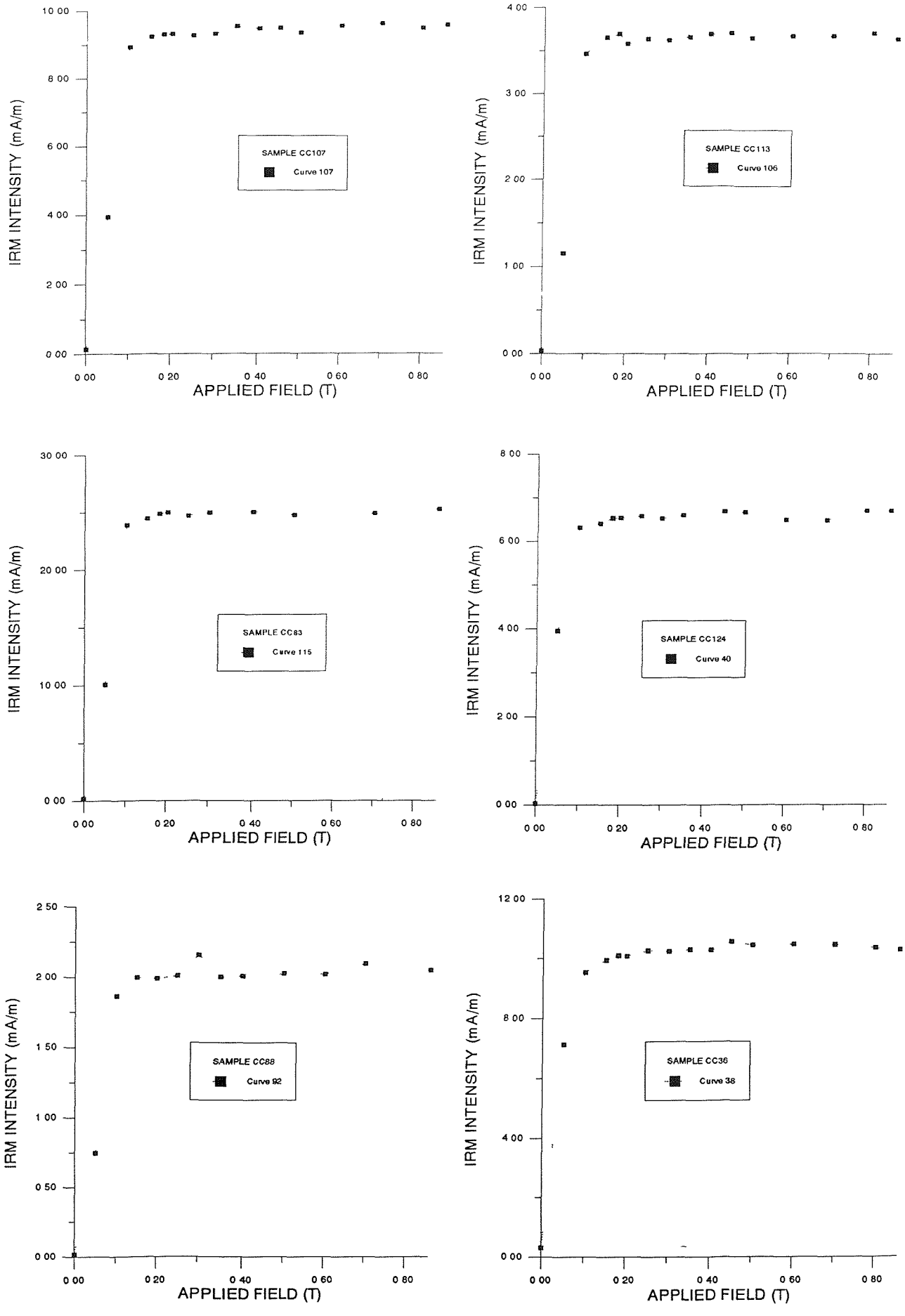

Figure 6.28a. Examples of IRM acquisition curves in which the sample reached magnetic saturation on application of direct magnetic fields greater than 0.05 Tesla. The curves possess shapes diagnostic of titanomagnetite.

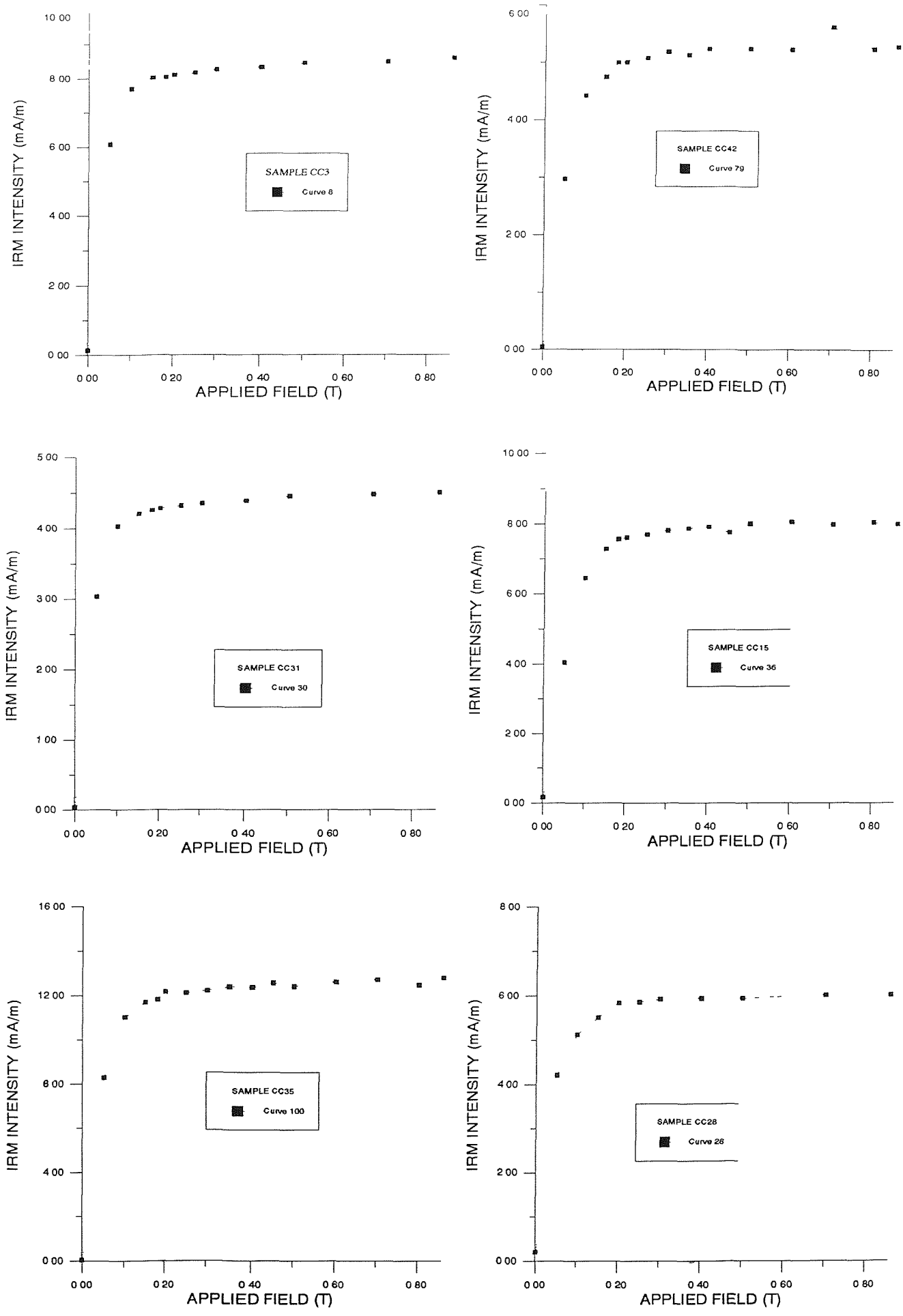

Figure 6.28b. Examples of IRM acquisition curves in which the sample reached magnetic saturation on application of direct magnetic fields greater than 0.1 Tesla. The curves possess shapes diagnostic of titanomagnetite.

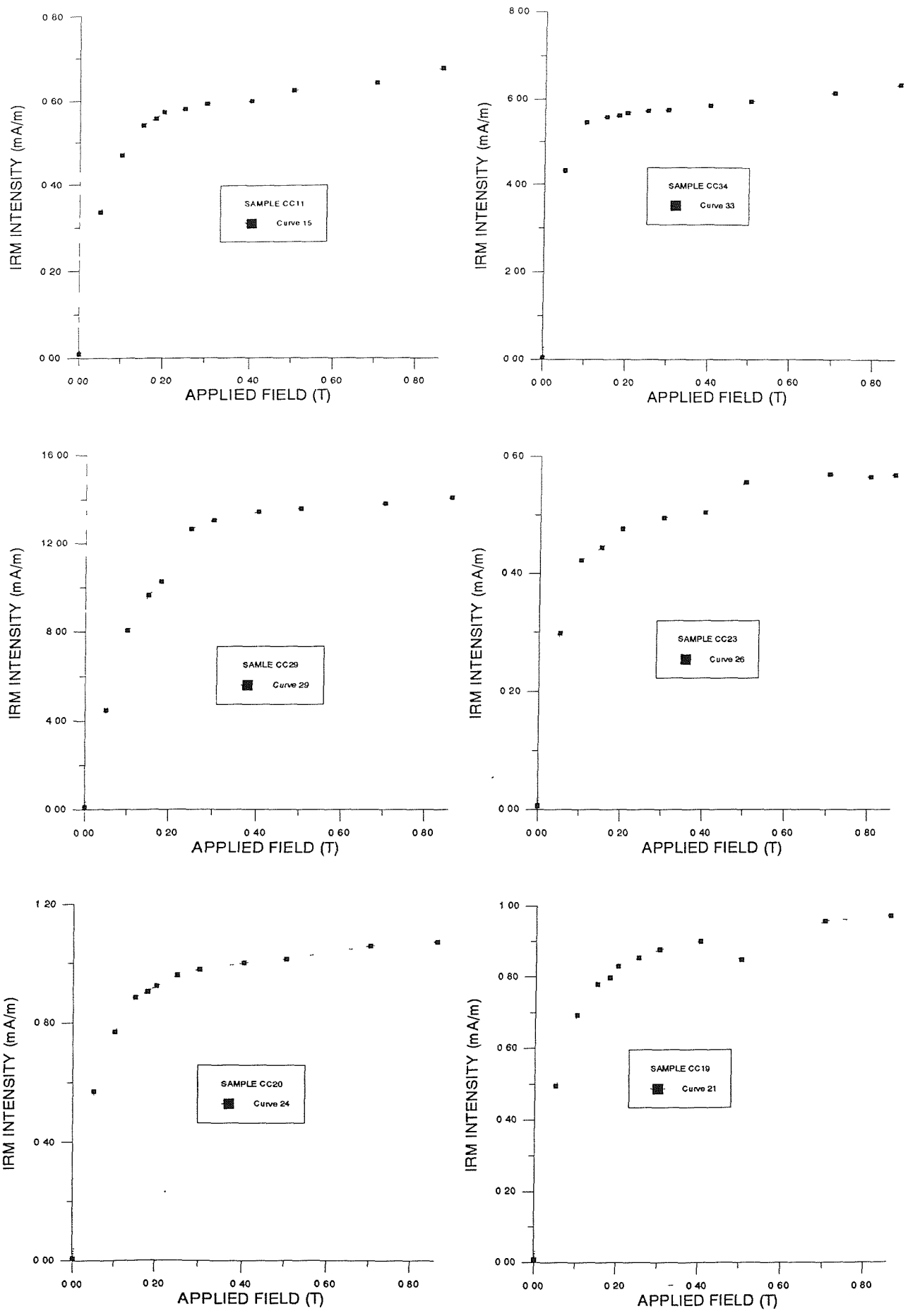

Figure 6.29. Examples of IRM acquisition curves in which the sample approaches magnetic saturation on application of direct magnetic fields greater than 0.2 Tesla. The curves possess shapes diagnostic of mixtures of titanomagnetite and hematite.

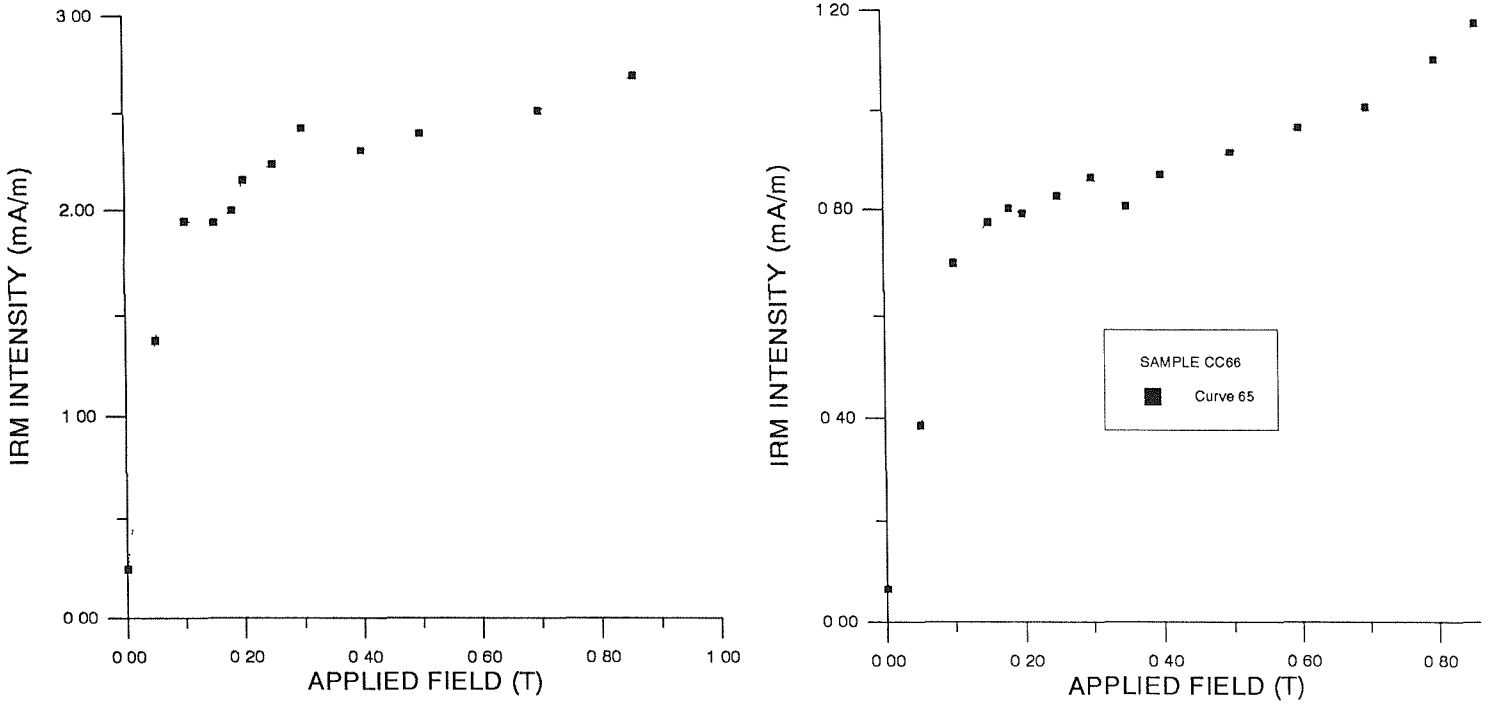

Figure 6.30. Examples of IRM acquisition curves in which the sample does not reach magnetic saturation on application of direct magnetic fields. The curves possess shapes diagnostic of mixtures of hematite and titanomagnetite.

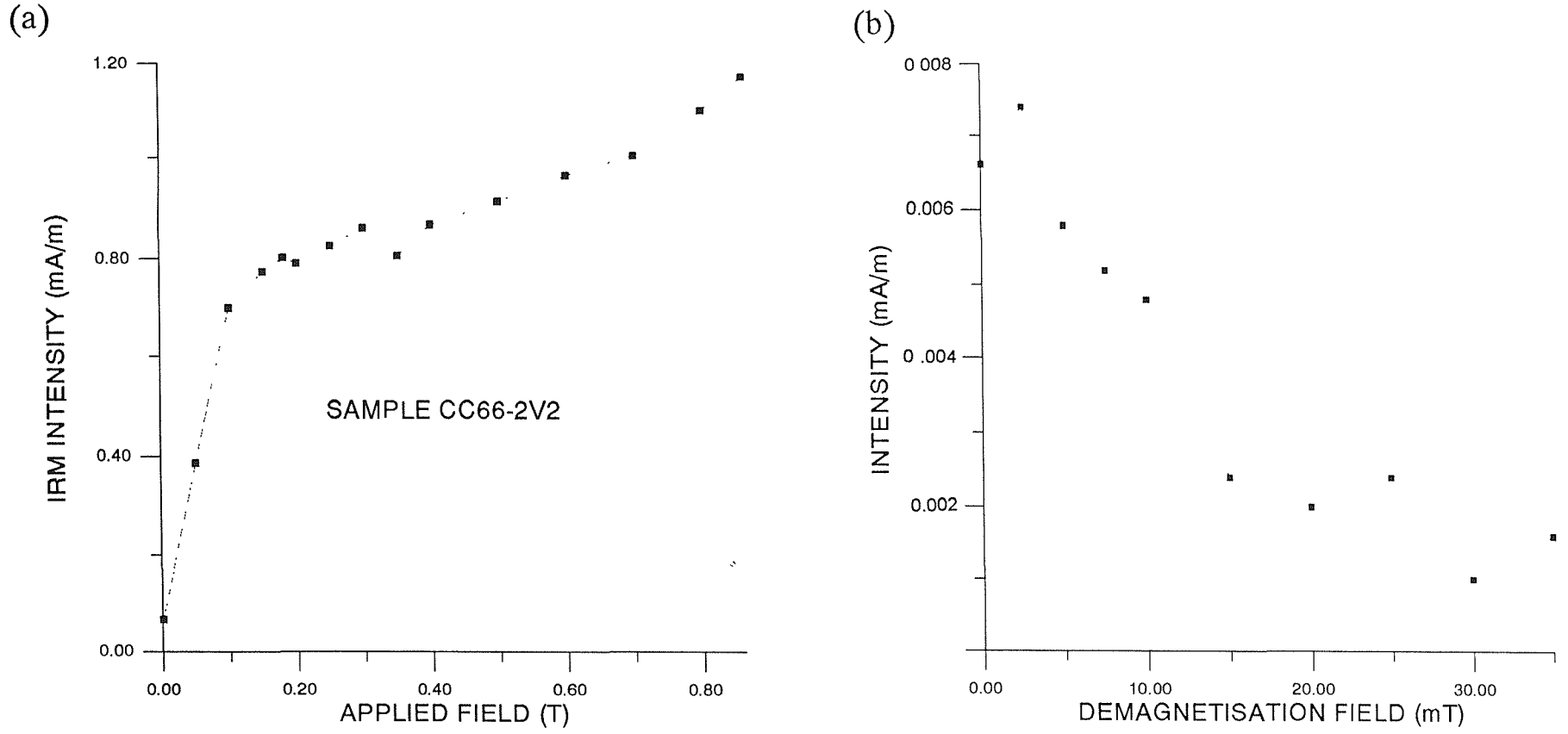

Figure 6.31. (a) IRM acquisition curve and (b) demagnetisation behaviour of sample CC66-2V2 during AF demagnetisation.

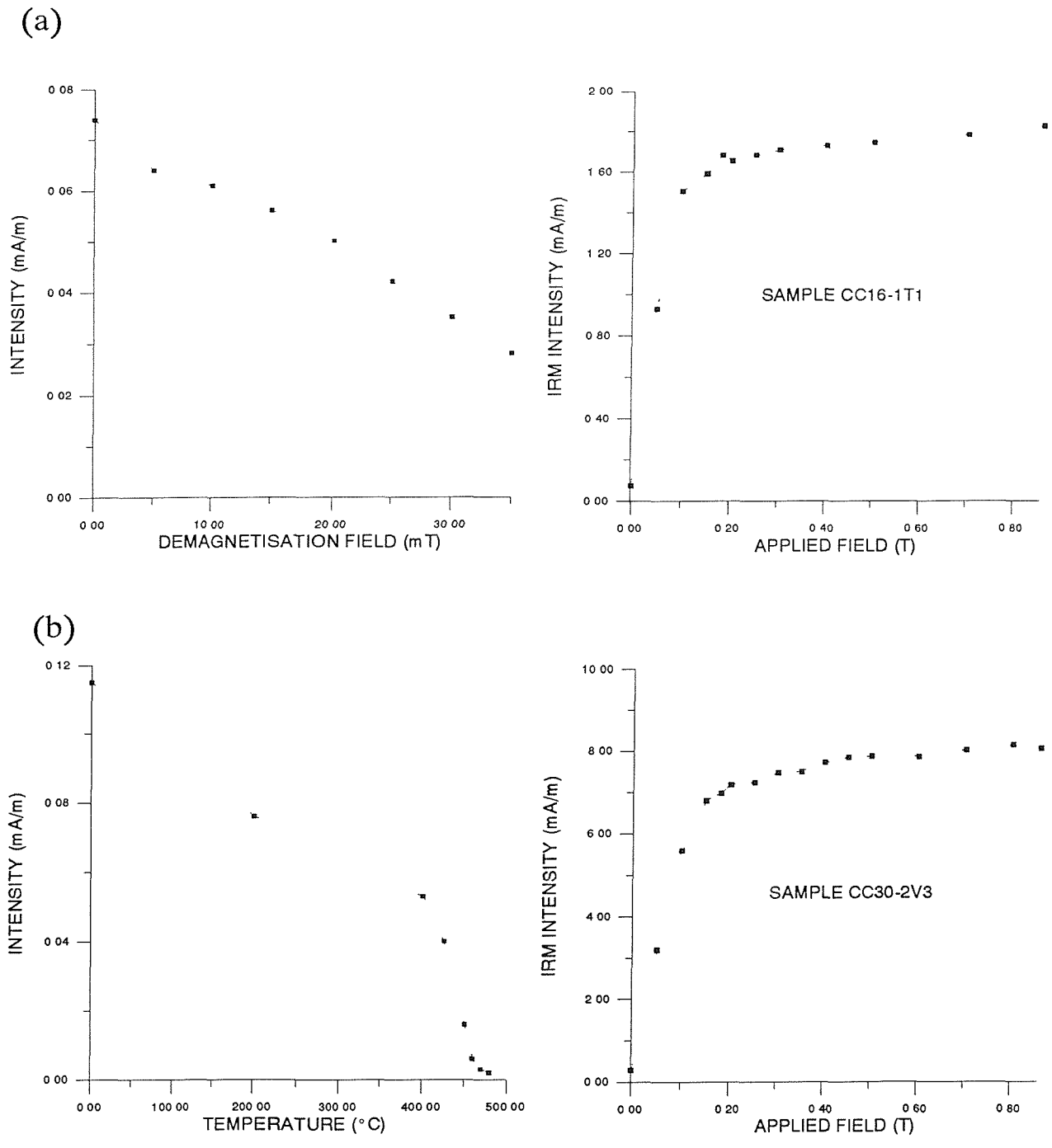

Figure 6.32. (a) IRM acquisition curve and A.F. demagnetisation behaviour of sample CC16-1T1. (b) IRM aquisition curve and thermal demagnetisation of sample CC30-2V3.

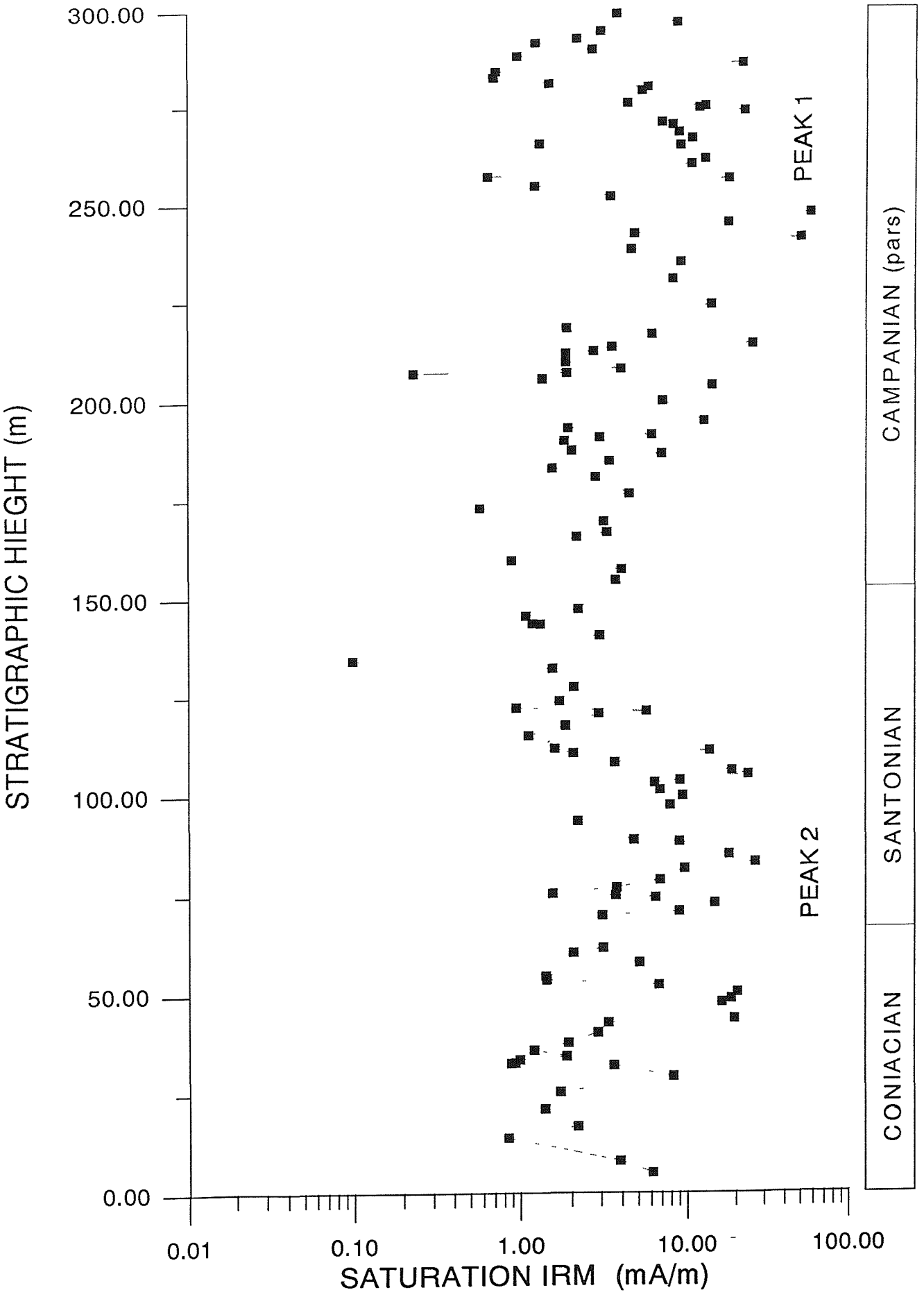

Figure 6.33. Variation of Saturation IRM with stratigraphic height above the Turonian-Coniacian boundary. The right-hand column indicates the Late Cretaceous Stages represented by the Chalk succession at Culver Cliff (Rawson et al. 1978).

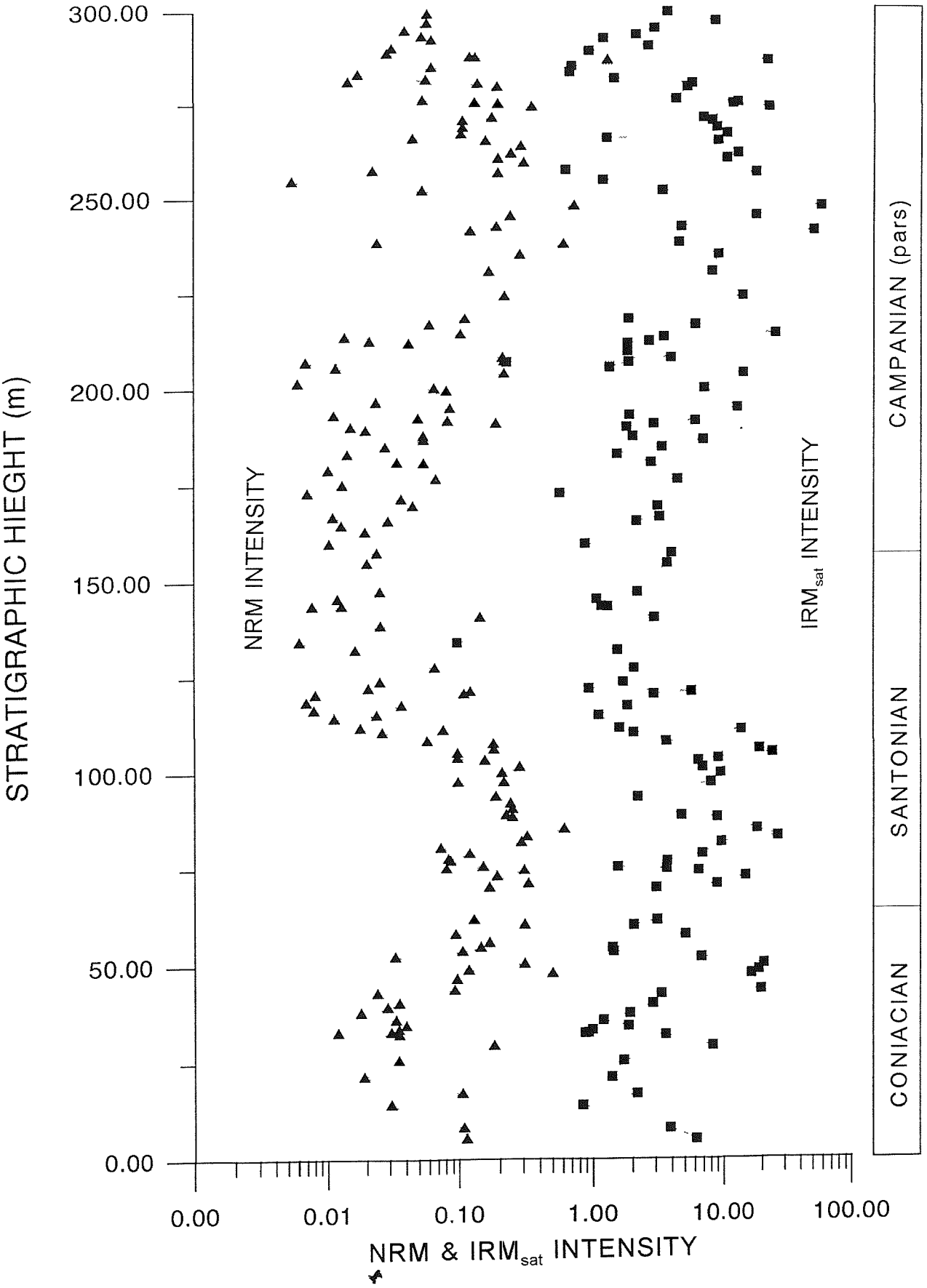

Figure 6.34. Variation of mean NRM intensity and saturation IRM intensity with stratigraphic height above the Turonian-Coniacian boundary. The right-hand column indicates the Late Cretaceous Stages represented by the Chalk succession at Culver Cliff (Rawson *et al.*, 1978).

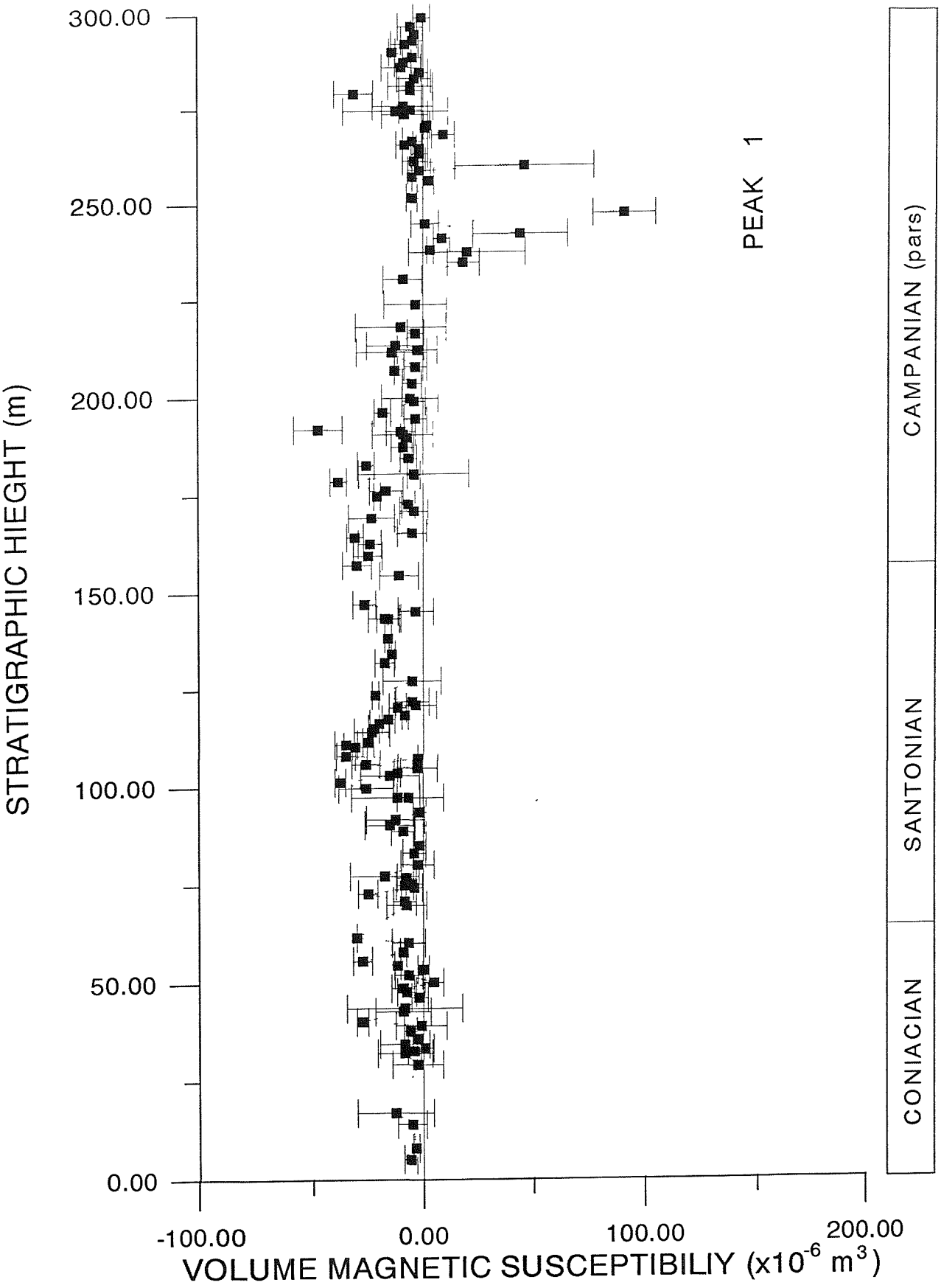

Figure 6.35. Variation of Volume Magnetic Susceptibility with stratigraphic height above the Turonian-Coniacian boundary. The right hand column indicates the Late Cretaceous Stages represented by the Chalk succession at Culver Cliff (Rawson *et al.*, 1978).

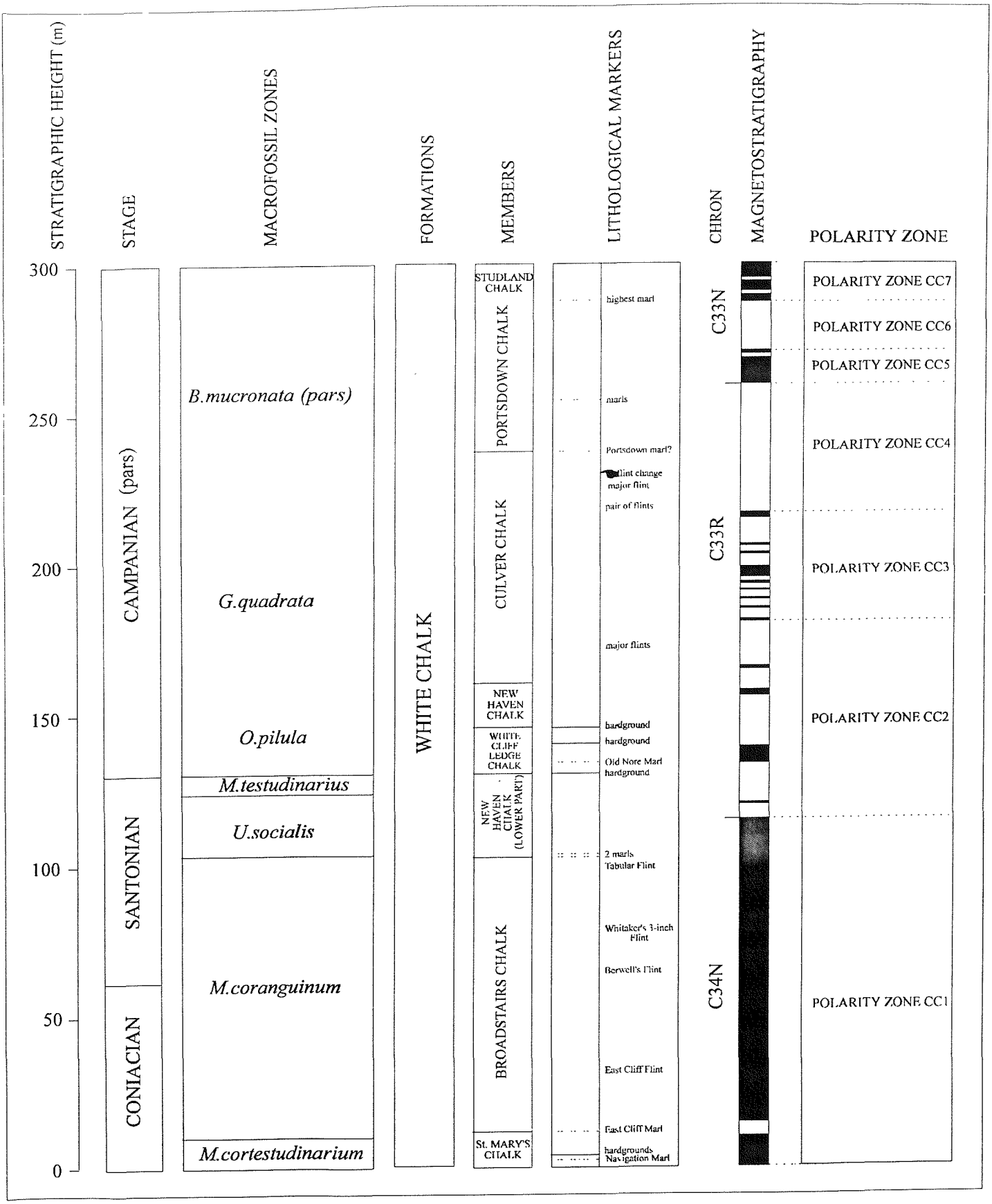

Figure 6.36. Summary diagram showing stratigraphical details of the Late Cretaceous Chalk sequence at Culver Cliff, the Isle of Wight. From left to right the diagram shows stratigraphic height above the Turonian-Coniacian boundary, Late Cretaceous Stages, macrofossil zones (Rawson *et al.*, 1978), formations, members, lithological markers, geomagnetic polarity Chrons, magnetostratigraphy and associated polarity zones.

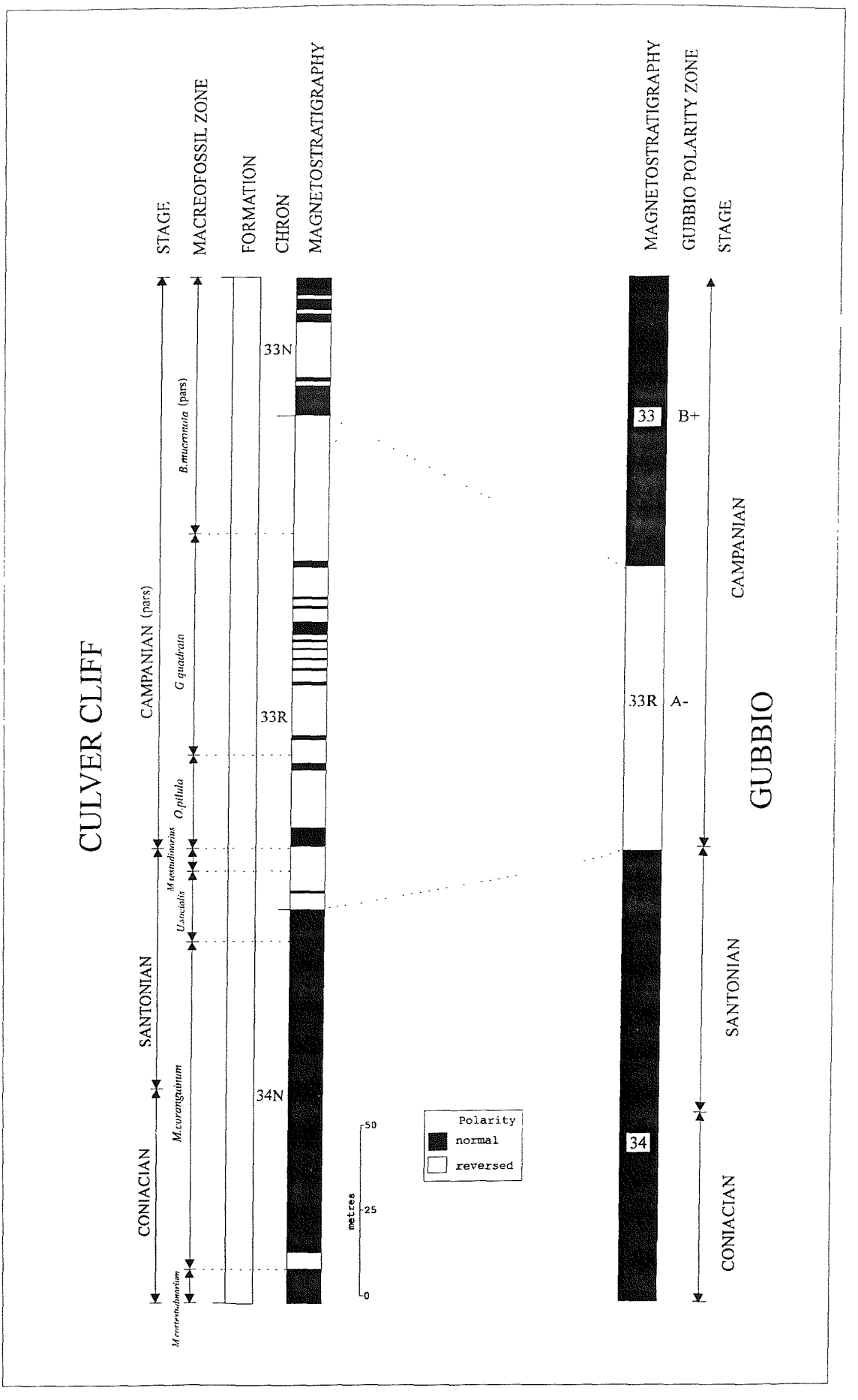

Figure 6.37. Correlation of magnetostratigraphic results from Culver Cliff, the Isle of Wight, with magnetostratigraphic results from Gubbio, northern Italy. The left hand side of the diagram shows Late Cretaceous Stage boundaries, macrofossil zones, geomagnetic polarity Chrons and the magnetostratigraphy determined for the Culver Cliff section. The right hand side of the diagram shows the magnetostratigraphic results of Alvarez *et al.* (1977) determined for the Gubbio section, northern Italy.

	BEDDING CORRECTION	
HEIGHT (m)	STRIKE	DIP
0-32.0	286°	53°
32.0-42.5	290°	52°
42.5-115.0	292°	55°
115.0-129.0	268°	70°
129.0-202.5	282°	62°
202.5-242.0	284°	63°
242.0-269.0	282°	65°
269.0-277.0	287°	70°
277.0-300.0	284°	75°

Table 6.1. Bedding corrections for the Culver Cliff section, the Isle of Wight.

Chapter 7 Palaeomagnetic results from Coniacian-Late Campanian Chalk, Scratchell's Bay, the Isle of Wight, southern England

7.1 Introduction

The Late Cretaceous deposits exposed to Scratchell's Bay, on the western side of the Isle of Wight (latitude=50.65°N, longitude=1.57°W), outcrop on the northern limb of the Brixton anticline (Figure 6.3) and consist of steeply dipping white chalks with black flints. The section ranges in age from early Coniacian to early Late Campanian. Unlike the chalk succession of Culver Cliff, no hardgrounds are present within this chalk sequence. The Scratchell's Bay section thus offers an opportunity to confirm the magnetostratigraphic results obtained from Culver Cliff. A detailed magnetostratigraphic study was undertaken and the results form a 285 metre section of chalk is presented. It should be noted that this section is only accessible by boat.

7.2 Biostratigraphy

Both macrofossil (Rawson, *et al.*, 1978) and nannofossil (Sissingh, 1977) zonations were determined to provide a detailed biostratigraphic framework within which to work. Dr. A. Gale provided the macrofossil biostratigraphy and Dr. J. Burnett the nannofossil biostratigraphy.

7.3 Stratigraphy

Rowe (1908) provided the first detailed description of the chalk succession at Scratchell's Bay. Osbourne White (1921) published lithological details of the biostratigraphic zones exposed and brief summaries are reproduced below. The zones, since modified by Rawson *et al.* (1978), are reviewed in ascending stratigraphical order and shown in graphical form in Figure 7.2.

(a) The zone of *Micraster coranguinum* is exposed in the form of a 'Grand Arch' (Rowe, 1908) at the southern end of the Bay. The condition of exposed chalk surfaces

is generally poor. The chalk of this zone is smooth and massive while flint modules occur in numerous regular courses, which are more closely spaced within the lower and middle parts of the zone.

(b) Osbourne White (1921) does not differentiate the *Unitacrinus socialis* Zone of Rawson *et al.* (1978) from the *Micraster testudinarius* Zone of Rowe (1908). From measurements made during this study the *Unitacrinus socialis* Zone incorporates approximately 17 metres of chalk containing regular courses of flint. The chalk of this zone is pure white in colour, compact and contains only occasional marl seams. Flint bands are more widely spaced than in the *Micraster coranguinum* Zone.

(c) According to the macrofossil zonation scheme of Rawson *et al.* (1978) the zone of *Marsupites testudinarius* consists of approximately 15 metres of chalk at Scratchell's Bay. Lithologically the chalk of this zone is similar to that of the preceding zone but due to the scarcity of fossils, and the inferior conditions of exposed surfaces, the limits of the zone are difficult to ascertain.

(d) The zone of *Offaster pilula* contains approximately 53 metres of chalk which includes numerous marl seams and courses of nodular flints. However, within the lower half of the zone, flint bands occur less frequently.

((e) The chalk of the zone of *Gonioteuthis quadrata* is massive, white and traversed by tiny veins of marl. Marl seams and flint-courses are abundant; the flints are mostly black and solid, and large in size. At Scratchell's Bay, this zone is comprised of approximately 63 metres of chalk.

(f) The zone of *Belemnitella mucronata* is the youngest of the Upper Chalk zones found on the Isle of Wight and reaches its maximum thickness in Britain at the western end of the Isle of Wight (Scratchell's Bay and Alum Bay). However, sampling at Scratchell's Bay was restricted to only 50 metres of this chalk, due to intensive faulting within the chalk of the Needles. Towards the northern horn of the bay the chalk becomes increasingly hard, and attains its maximum induration in the

southern face of the shoreward Needle, where it has been converted into semi-crystalline limestone (Osbourne White, 1921).

7.4 Structural history

The Chalk of Scratchell's Bay lies on the northern limb of the Brixton anticline and dips at angles of between 52° and 68°, with an approximately east-west (260° to 270°) strike.

7.5 Palaeomagnetic results

The Palaeomagnetic data for the Scratchell's bay section are summarised in Appendix B, Table 1.

7.5.1 Natural Remanent Magnetisation

Figures 7.4 shows the variation of NRM intensities with stratigraphic height above a datum approximately 20 metres higher than the Turonian-Coniacian stage boundary and can be located at a ledge at the base of the Grand Arch (Plate 9.2.). The top of the plot coincides with sample horizon SB80, the uppermost sampling horizon of the Scratchell's Bay section.

Plotted NRM intensities are based on average values determined for each sample horizon. Values lie in the range 0.0020-0.1066 mA/m. The log mean NRM intensity for the section is 0.0105 mA/m. The highest NRM intensity measured for an individual specimen was 0.2808 mA/m from sample level SB16. The mean NRM value for this horizon was 0.0640 mA/m which is half an order of magnitude greater than the mean for the whole section. Other high mean NRM values were found at sample sites SB15 (0.0781 mA/m), SB16 (0.0640 mA/m) and SB17 (0.9657 mA/m). The lowest NRM intensity measured for an individual specimen was 0.0013 mA/m from sample horizon SB4.

Five NRM intensity peaks were identified between sample horizons SB13 to SB20 (Peak 1), SB42A to SB46 (Peak 2), SB53 to SB59 (Peak 3), SB62 to SB70 (peak 4) and SB75 to SB77 (Peak 5, Figure 7.4). The mean NRM intensity for Peak 1 is 0.04007 mA/m, Peak 2 is 0.0207 mA/m, Peak 3 is 0.0188 mA/m, Peak 4 is 0.0179 mA/m and Peak 5 is 0.0242 mA/m. Between the peaks the mean NRM intensity is much lower (0.0243 mA/m). The mean NRM intensity before Peak 1 was 0.0401 mA/m and after Peak 2 was 0.0446 mA/m. Superimposed upon this large scale fluctuation are much smaller extreme variations in magnetic intensity.

7.5.2 Stability of magnetisation

To investigate the stability of the remanent magnetisation within the chalk and resolve the separate components in the samples carrying a multi-component remanence, specimens from each stratigraphic level were subjected to incremental demagnetisation analysis.

To establish the optimum procedure, pilot samples were subjected to both incremental alternating field (AF) demagnetisation and thermal demagnetisation.

7.5.2.1 AF demagnetisation

The vast majority of samples studied during the palaeomagnetic investigation of Scratchell's Bay had extremely weak NRM intensities. Forty-eight percent of the samples possessed NRM intensities less than 0.01 mA/m. For such weakly magnetised samples AF demagnetisation, at 2.5 mT or 5.0 mT steps, was employed. Sample SB9-2A, after AF demagnetisation treatment, shows a directional trend which can be extrapolated to a reversed polarity (southerly declination, negative inclination) end point (Figure 7.5). Only 7% of the samples had magnetic intensities of 0.05 mA/m or greater. Due to difficulties in undertaking successful thermal demagnetisation of such weakly magnetised samples AF treatment was used as the main form of demagnetisation treatment. However, thermal demagnetization procedures were adopted for representative samples from 12 of the 100 sample

horizons collected at Scratchell's Bay.

7.5.2.2 Thermal demagnetisation

Thermal demagnetisation steps of NRM, 100, 200, 300, 400, 500, 600°C, etc, were employed for this study (Figure 7.6). Forty-two percent of the thermally demagnetised samples revealed moderate to poor quality SEPs (Figure 7.7) while 42% showed directional trends (Figure 7.8). Erratic behaviour was observed in the remaining 16% (2 samples).

7.5.3 Reliability categories

The results of this treatment allow the palaeomagnetic data from each of the sample horizons to be placed in reliability categories. These categories have been previously discussed and illustrated in Section 5.8.

Out of 547 specimens analyzed for the Scratchell's Bay section, demagnetisation stable end points were attained by 28% of the samples. However, only 5% belonged to the S1 category (Figure 7.9), 20% to category S2 (Figure 7.10), and 2.5% to category S3 (Figure 7.11). Directional trends were recognised in 58% (Figures 7.12, 7.13 & 7.14) of the samples demagnetised while 1.5% possess recent geomagnetic field overprints (Figures 7.15a & b) which could not be removed by A.F. or thermal demagnetisation. 'T1-quality' trends accounted for 11%, 'T2-quality' trend data described 32% of sample behaviour while 'T3-quality' trend data provided magnetic polarity information for 15% of the analyzed samples. Erratic behaviour during demagnetisation was observed in 12% of the samples (Figure 7.16). The main reason for trend data providing the most significant contributions towards palaeomagnetic analysis of chalk from Scratchell's Bay is because of its extremely weak magnetic intensity. Long before a stable end point is reached during demagnetisation the sample's intensity has dropped below the background intensity level of the magnetometers.

7.5.4 Age of remanence

7.5.4.1 Bedding Corrections

The deposits at Scratchell's Bay outcrop on the northern limb of the Brixton Anticline. As a result, they possess dips which range between 52° and 68° and strike approximately East-West. The bedding corrections for the Scratchell's Bay section are presented in Table 7.1.

By applying a tectonic correction we can distinguish between magnetic components acquired before and after tilting.

Figures 7.17a & b, illustrate the effect the bedding correction has on the magnetization vectors. In Figure 7.17a, a bedding correction of 260°/50° has been applied for sample SB47-8. The stable characteristic magnetization (SCM) of the sample prior to application of a bedding correction represents a magnetic field direction of negative inclination and a north-easterly declination. However, after applying the bedding correction the magnetic vector is rotated away from the northern hemisphere towards the southern hemisphere. Prior to correction the sample displays a possible directional trend towards reverse polarity. However, after correction any doubt over the presence of this directional trend is removed. Figure 7.17b shows sample SB46-D before and after a tectonic correction of 260°/52°. Before the bedding correction is applied the magnetic vector indicates normal polarity. However, after correction the normal geomagnetic field vector is rotated to a direction with a shallow positive inclination (<10°) and north-easterly declination (30°). It is apparent that this sample has acquired a normal geomagnetic field overprint at some instance after tilting.

7.5.4.2 Fold test

Figure 7.18 shows stereographic equal area projections of the stable characteristic magnetisation for the 28 SI 'reliability category' magnetic vectors from the complete Scratchell's Bay section before, and after bedding corrections have been applied to the

individual vectors. Bedding correction inclinations range between 52° and 68° while strikes range between 260° and 270°. Precision parameters 'k' and alpha 95 are reported before and after bedding corrections.

Before application of their respective tectonic corrections the S1 category magnetic vectors exhibit a mean declination and inclination of 160° and 73° respectively, an alpha 95 value of 9.0° and 'k' value of 10.3. After correction a mean declination of 8.0°, inclination of 53.0°, an alpha-95 value of 8.4° and 'k' value of 11.4 are revealed. Analysis of the grouping of the directions before and after correction for tectonic tilt fail to show, in accordance with the McElhinny (1964) fold test, a statistically significant closer grouping after tectonic correction (k_2/k_1=1.11). The small increase in 'k', from 10.3 to 11.4 is due to the lack of variation in the strike and dip of the strata at Scratchell's Bay.

The magnetic vectors obtained from chalk samples from Scratchell's Bay do not pass the less rigorous McElhinny fold test. The fold test of McFadden & Jones (1980) was not applied because sampling at Scratchell's Bay was restricted to the one limb (northern) of the Brixton anticline.

Data failing the McElhinny fold test does not conclusively prove that the remanence is secondary. More importantly, the cluster of magnetic directions move from a very unlikely position before correction to a sensible one afterwards. The magnetic stability of the chalk passing this test must be high to withstand such tectonic disturbances and it would seem reasonable to assume that the remanence can be related to the time of formation of the Chalk.

7.5.5 Remagnetisation

One and a half percent of the samples demagnetised possessed magnetic overprints which could not be removed by using either AF, or thermal demagnetisation procedures. No obvious common overprint direction could be identified (Figure 7.19).

7.5.6 Magnetic polarity

The tilt-corrected SCM declination and inclination values defined by the incremental demagnetisation are plotted as a function of stratigraphic height above the datum SB1 in Figure 7.3.

Polarity definition is based on a combination of demagnetisation stable end points and observations of directional trends during demagnetisation. The succession can be divided into seven principal polarity intervals (Figure 7.20). These are, in ascending stratigraphic order:

a) **Polarity zone SB1.** A 35 metre thick normal polarity interval containing a short reverse polarity zone (*M. coranguinum* Zone), representing the lower part of Chron C34N

b) **Polarity zone SB2.** A 20 metre reverse polarity interval (*M. coranguinum* Zone) representing middle part of Chron C34N.

c) **Polarity zone SB3.** A 35 metre zone of normal polarity containing two short intervals of mixed polarity (*M. coranguinum* Zone to *U. socialis* Zone) representing the upper part of Chron C34N.

d) **Polarity zone 4.** A 100 metre thick reverse polarity zone containing five short intervals of mixed polarity and two short intervals of normal polarity (*U. socialis* to *G. quadrata* Zones) representing the lower part of Chron C33R.

e) **Polarity zone SB5.** A 40 metre thick normal polarity interval containing four short normal polarity intervals (*G. quadrata* Zone) representing the middle part of Chron C33R.

f) **Polarity zone SB6.** A 30 metre thick reverse polarity zone containing a mixed polarity interval (*G. quadrata* to *B. mucronata* Zones) representing the upper part of

Chron C33R.

g) **Polarity zone SB7**. A 25 metre thick dominantly normal polarity interval containing three short reverse polarity zones and one mixed polarity zone (*B. mucronata* Zone) representing the lower part of Chron C33N.

7.5.7 A Late Cretaceous palaeomagnetic pole for southern England from the Scratchell's Bay section

The directions of S1 category vectors are displayed on an equal-area stereographic projection in Figure 7.21 together with the overall mean S1 category vector (declination=8°, inclination=53°, k=11.4, alpha 95=8.4°). From the mean magnetic vector a palaeomagnetic pole of 71.9°N 159.6°E, with quality factor, Q, equal to 5, was calculated for the Coniacian-Late Campanian of southern England. Five of the seven criteria suggested by van der Voo (1988) are satisfied. A well constrained biostratigraphic/magnetic age has been determined for the Chalk sequence at Culver Cliff. The palaeomagnetic-pole has been generated from 28 S1 reliability category specimens and has a precision 'k' value greater than 10 and a relatively low 95% confidence level (<10°). A fold test, with respect to the McElhinny (1964), has been applied. However, a k_2/k_1 ratio value of 1.11 for the data at Scratchell's Bay is less than the values tabulated at 95% and 99% significance levels. The fold test is therefore not significant at these levels. Tectonic coherence and good structural control has been established by previous workers for the Late Cretaceous sequences in southern England (e.g. Chadwick, 1993). However, apart from three specimens, displaying reverse polarity, all other S1 category specimens are characterised by normal polarity. As a result, only three antipodal reverse polarity magnetic vectors could be used to assure a good time average of the geomagnetic field. However, the magnetostratigraphical interpretation indicates that these vectors span a time interval of several million years, so the time average should be acceptable. Furthermore, only AF demagnetised samples define the palaeomagnetic-pole data set. Two of the reliability criteria of van der Voo (1988) are thus failed.

By using the mean magnetic remanence inclination value of 53°, determined from 'S1 reliability category' data set, a palaeolatitude of 33.6±8.4°N is inferred for southern England during Coniacian-Late Campanian times. From the palaeomagnetic-pole of Heller & Channell (1979), derived from the Munster Basin, Germany, a magnetic field direction of 359.8°/56.24° can be predicted for southern England which corresponds to a palaeolatitude of 36.8±3.1°N. A discrepancy of 3.2° exists between the two figures. However, within the experimental uncertainties (i.e. alpha 95=8.4°) this discrepancy can be regarded as insignificant.

As previously mentioned, the Late Cretaceous sequences of northern Europe lack reliable palaeomagnetic-pole data. The relatively low quality palaeomagnetic-pole derived for Scratchell's Bay provides a possible alternative for northern Europe during the Late Cretaceous.

7.6 Isothermal remanence

As at Culver Cliff, isothermal remanence experiments were carried out, to gain an insight into the magnetic mineralogy of the remanence carrier in the chalk of Scratchell's Bay.

7.6.1 IRM ratio

By determining the IRM ratio for 82 (of the 100) sample horizons an IRM log of the Scratchell's Bay section was established (Figure 7.22). The vast majority of samples (70%) studied exhibit IRM ratios of 0.9 or above. The preservation of remanent magnetism of the chalk of Scratchell's Bay can therefore be attributed to the presence of titanomagnetite or maghemite and small quantities of hematite.

7.6.2 IRM curves

Magnetite-type IRM curves were observed in 70% of the samples studied (Figure 7.23), while curves indicative of magnetite and hematite mixtures represent 23%

(Figure 7.24). Hematite-type IRM curves were found in only 7% of the specimens studied (Figure 7.25).

7.6.3 Saturation IRM

By recording the peak IRM intensity of magnetically saturated chalk (IRM ratio>0.9), and by assuming that both the magnetic mineralogy and domain state of magnetic grains is consistent throughout the geological section, it is possible to construct a stratigraphic log which gives an indication of the relative quantity of minerals contributing to the Chalk's remanent magnetism. Since 70% of the sample horizons indicate (from IRM analysis) that single domain titanomagnetite is the dominant magnetic mineral present (Section 6.6.1) it can be assummed that mineralogy and domain state of magnetic grains is consistent throughout the section. Thus by plotting a stratigraphic log of IRM_{sat} an indication of the relative quantity of magnetic material contributing to the Chalk's remanent magnetism can be assessed.

Figure 7.26 shows a plot of IRM_{sat} against stratigraphic height above datum SB1. Two major, large scale IRM_{sat} intensity peaks were identified between sample horizons SB7 to SB23 (Peak 1) and SB52A to SB69 (Peak 2). However, in addition to these large scale features numerous smaller scaler IRM_{sat} intensity highs are discernable. These peaks probably present both changes in magnetic mineralogy and magnetic mineral content since, from Figure 7.27, a strong correlation can be seen between low IRM ratio values (hematite dominated sample horizons) and the upper and lower limits of the successive peaks identified from the logs of NRM and IRM_{sat} intensity. (Figures 7.4 & 7.26). In addition there appears to be correlation between the NRM intensity log and the IRM_{sat} intensity log (Figure 7.28). Both curves possess very similar shapes suggesting that the NRM intensity of Chalk reflects magnetic mineral content rather than variations in magnetic mineralogy. Superimposed upon these fluctuations are much finer scale oscillations in NRM and IRM_{sat} intensity which appear to represent large variations in titanomagnetite content from sample horizon to sample horizon. The curve representing IRM_{sat} intensity is approximately 2 orders of magnitude greater than the NRM intensity curve suggesting the presence of multi

domain titanomagnetite (NRM/IRM_{sat} ratio<0.1, Collinson, 1983).

7.7 Volume magnetic susceptibility measurements

Volume magnetic susceptibility measurements were carried out on large volume chalk Samples ($150cm^3$) to provide a further means of correlating between Chalk sequences. In most instances diamagnetic behaviour was observed. Such conduct is easily explained. The extremely low content of strongly magnetizable ferromagnetic and moderately magnetizable paramagnetic minerals would result in a very weak magnetic susceptibility signal. Such a signal might even be too weak to be discernable by the currently available magnetic susceptibility bridges. Moreover, since chalk is composed almost entirely of biogenic calcium carbonate (98% in Late Cretaceous chalks, Hancock, 1975) the few magnetizable minerals present would be swamped by the diamagnetic behaviour of the nannofossil micrites. Nevertheless, six horizons did display ferromagnetic or paramagnetic behaviour, with only two possessing large measurement standard deviations. Figures 7.29 shows a log of volume magnetic susceptibility measurements against stratigraphic height (above datum SB1). The six positive readings (Figure 7.30b) appear to correspond with horizons were the magnetic mineralogy is dominated by hematite and indicated by low IRM ratio values (Figure 7.30a). The relationship between 'hematite-rich' horizons, NRM intensity (Figure 7.30c) and saturation IRM intensity (Figure 7.30d) is less obvious. Nevertheless, an association does exist; lower NRM intensity corresponds to higher concentrations of hematite. A similar correlation between the saturation IRM curve (Figure 7.30d) and the IRM ratio curve (Figure 7.30a) can be inferred.

Biogenic carbonate exhibits diamagnetic behaviour (e.g. Robinson, 1992) and, due to the extremely low content of ferromagnetic and paramagnetic minerals within the English Chalk, magnetic susceptibility measurements proved unsuccessful as a correlation technique (Figure 7.31). No obvious correlations can be drawn between the Scratchell's Bay and Culver Cliff sections using volume magnetic susceptibility measurements.

7.8 Conclusions

Palaeomagnetic results from Scratchell's Bay suggest that several magnetic polarity subzones are present within the English Chalk at Scratchell's Bay which spans magnetochrons C34N, C33R and C33N (Figure 7.32).

Sampling level SB72 (Figure 7.3a, 260 metres above datum SB1 and within the *B. mucronata* Zone) is taken to represent the start of Chron C33N (Gubbio B+ zones, Figure 4.?) with the overlying 25 metres of chalk defining a portion of Chron C33N (normal polarity zone Gubbio B+). Within this normal polarity magnetozone three reverse polarity intervals have been detected. These normal and reverse polarity subzones would seem to represent the 9 metre, uneven polarity transition between Gubbio A- and B+ magnetozones (Alvarez *et al.* 1977).

Below Sample Level SB72 (Figure 7.3f to 7.3b) a 170 metre interval of chalk, belonging to the *B. mucronata*, G. *quadrata*, *O. pilula*, *M. testudinarius* and *U. socialis* Zones, represents the reverse polarity Chron C33R (Gubbio A-). However, this zone is not comprised exclusively of samples exhibiting reverse polarity, since six short normal polarity intervals appear within it. The base of this zone and the top of the Cretaceous Long Normal Zone (Chron C34N) has been located within the *U. socialis* Zone at sample level SB22-2. However, this boundary is not well-defined, since adjacent samples display mixed polarity.

From previous palaeomagnetic investigations of sedimentary sequences of equivalent age to the English Chalk (e.g. Alvarez *et al.*, 1977) and the Late Cretaceous marine magnetic anomaly record (e.g. Cande & Kent, 1992) Chron C34N was considered to be represented exclusively by normal polarity. However, the English chalk of Scratchell's Bay has revealed the presence of two reverse polarity intervals within this period of time which were not detected at Culver Cliff. These are located within the macrofossil zone *M. coranguinum* (sample horizons SB8B to SB11 and sample horizon SB4, Figure 7.3b & a). The rest of the Chalk succession is represented by normal polarity.

The *M. coranguinum* Zone chalk at Culver Cliff has revealed the presence of several mixed polarity sample horizons but no reverse polarity intervals. However, this chalk is extremely resistant to A.F. demagnetisation (even at levels of 40 mT or more). Moreover thermal demagnetisation was not particularly successful in distinguishing higher stability magnetic components when the magnetic intensity of the chalk was reduced to low levels. This appears to be due to the reduction in sample volume which was required to enable the samples to fit within the non-magnetic oven. Furthermore, the bedding inclination of the Chalk shallows (*c.* 50°) within the *M. coranguinum* zone at Culver Cliff. As a result the bedding correction is not ideally suited to distinguishing between primary magnetic components from recent geomagnetic field overprints. Further sampling and thermal demagnetisation of chalk from this zone, using large volume samples, may help to distinguish reverse polarity intervals equivalent to those observed at Scratchell's Bay.

As stated in the previous chapter the occurrence of previously undetected reverse and normal polarity subzones within the Scratchell's Bay section can be explained by the high rate of chalk sedimentation which occurred within the Chalk sea of southern England during the Late Cretaceous and is portrayed by the differing thickness of strata representing the Coniacian-Campanian Stages at Scratchell's Bay when compared with the equivalent Late Cretaceous stages at Gubbio. In excess of 165 metres of Campanian Chalk outcrops in the Scratchell's Bay section, compared with only 75 metres of limestone representing whole of the Campanian stage at Gubbio. Moreover, the whole of the Campanian is not present at Scratchell's Bay, due to the widespread erosion prior to deposition of the oldest Tertiary strata. At Gubbio, approximately 120 metres of sediment represents the Cenomanian to Santonian stages while at Scratchell's Bay 90 metres of chalk represent the late-Early Coniacian to Santonian stages. As a result, more than twice as much strata represents the Coniacian-Late Campanian stages at Scratchell's Bay than at the Gubbio section. This would account for the improved magnetostratigraphic resolution at Scratchell's Bay.

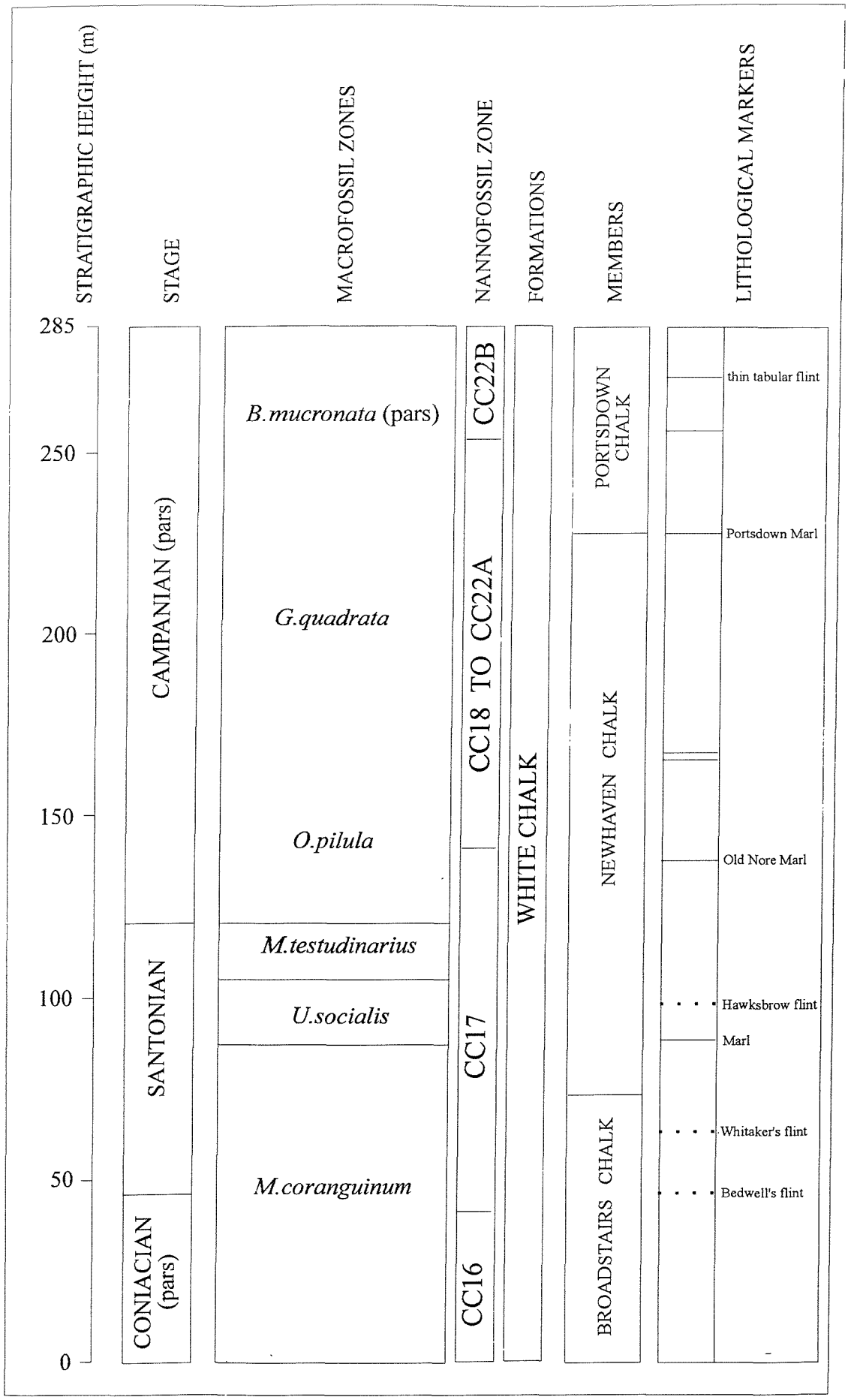

Figure 7.1. Summary diagram showing stratigraphical details of the Late Cretaceous Chalk sequence at Scratchell's Bay, the Isle of Wight. From left to right the diagram shows stratigraphic height above datum SB1 (approximately 20 metres above the Turonian-Coniacian boundary), Late Cretaceous Stages, macrofossil zones (Rawson *et al.*, 1978), nannofossil zones (Sissingh, 1978), formations, members and lithological markers.

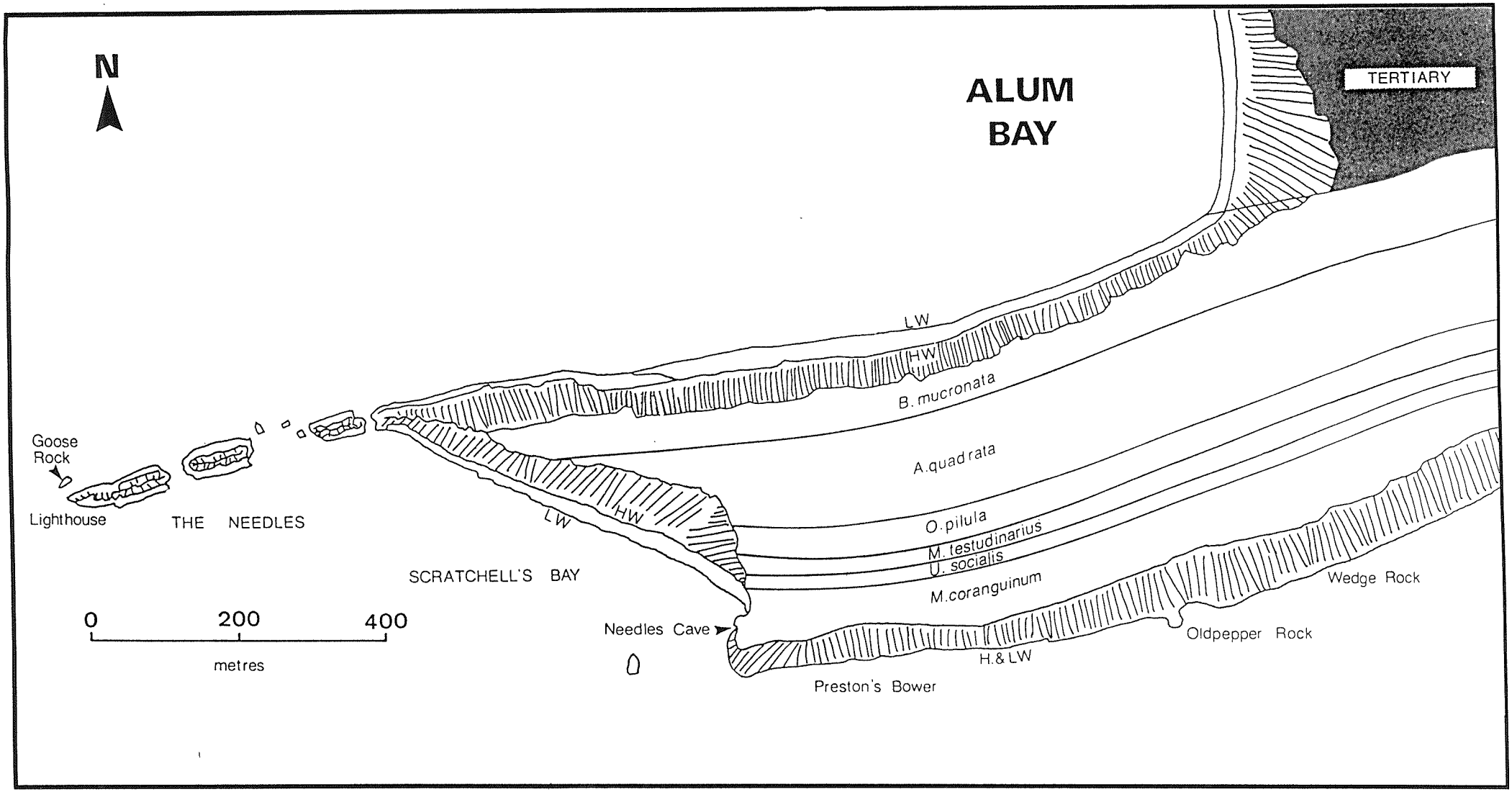

Figure 7.2. The Scratchell's Bay succession of the Chalk group at the western end of the Isle of Wight. The section is only accessible by boat (after Rowe, 1908).

Figure 7.3a, b, c, d, e & f. The magnetic polarity stratigraphy of the Scratchell's Bay section. From left to right the diagram shows, i) stratigraphic height in metres; ii) Late Cretaceous Stages; iii) biostratigraphic macrofossil zones (Rawson *et al.*, 1978); iv) biostratigraphic nannofossil zones (Sissingh, 1977); v) sampling levels; vi) geomagnetic polarity definition (black=normal, white=reverse, light shading=mixed and dark shading=intermediate); vii) the stratigraphic variation of the declination of characteristic remanent magnetisation (ChRM); viii) the stratigraphic variation of the mean natural remanent magnetisation intensity (solid square symbol); ix) the stratigraphic variation of IRM ratio (solid triangle symbol).

On the right hand side of the diagrams are three columns which, from left to right present, i) the reliability category of the SCM; ii) the fraction of the samples demagnetised which support the definition of polarity and; iii) the demagnetisation procedure employed to specify the polarity. Where polarity definition is based solely on directional trends, a ChRM vector is generated by great circle intersection. However, where directional trends do not produce intersection points a token declination/inclination vector (i.e. reverse polarity=180°/-90°; normal polarity=360°/90°) is adopted.

a)

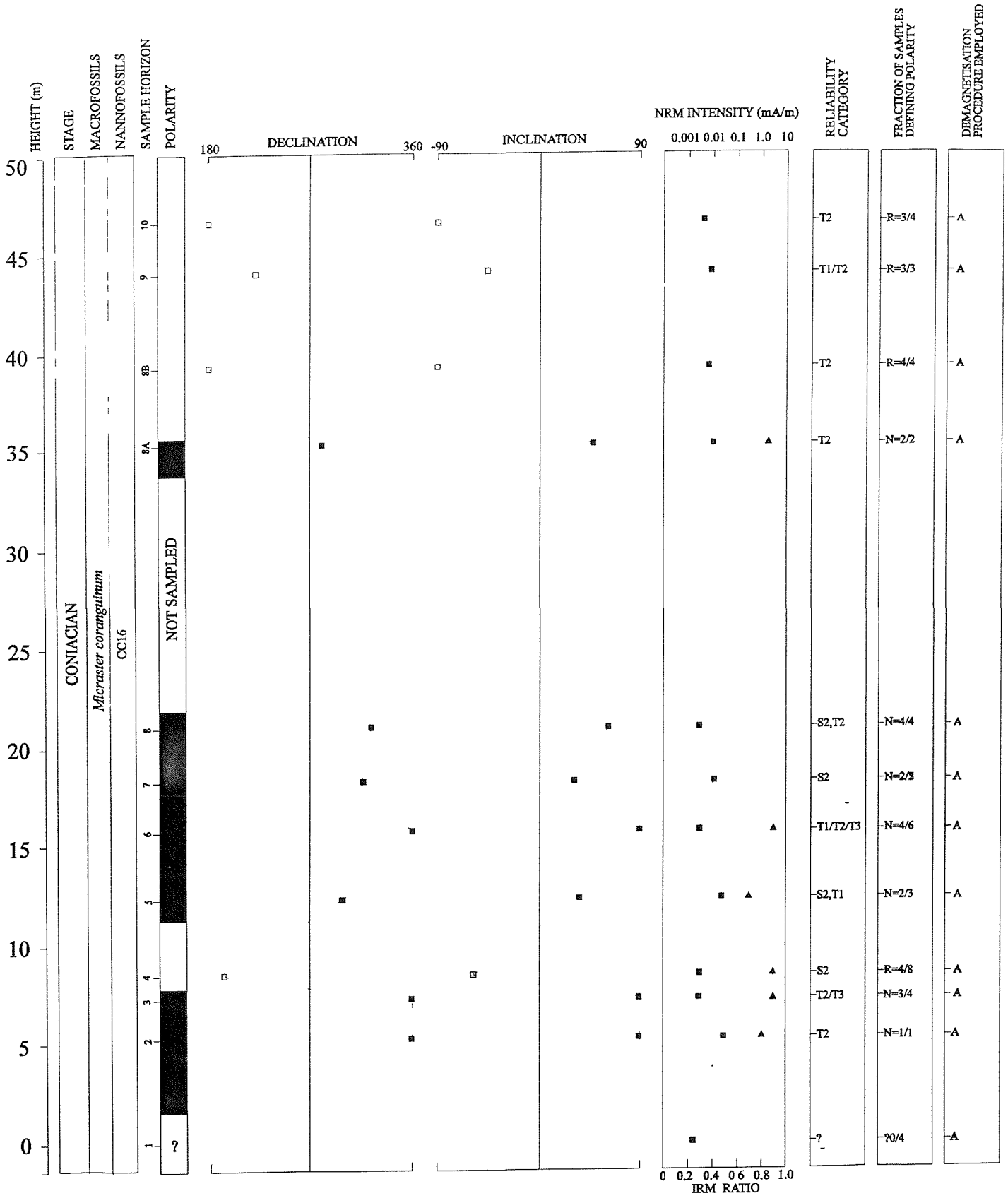
HEIGHT (m)
STAGE
MACROFOSSILS
NANNOFOSSILS
SAMPLE HORIZON
POLARITY
DECLINATION
INCLINATION
NRM INTENSITY (mA/m)
RELIABILITY CATEGORY
FRACTION OF SAMPLES DEFINING POLARITY
DEMAGNETISATION PROCEDURE EMPLOYED
CONIACIAN
Micraster coranguinum
CC16
NOT SAMPLED
IRM RATIO

b)

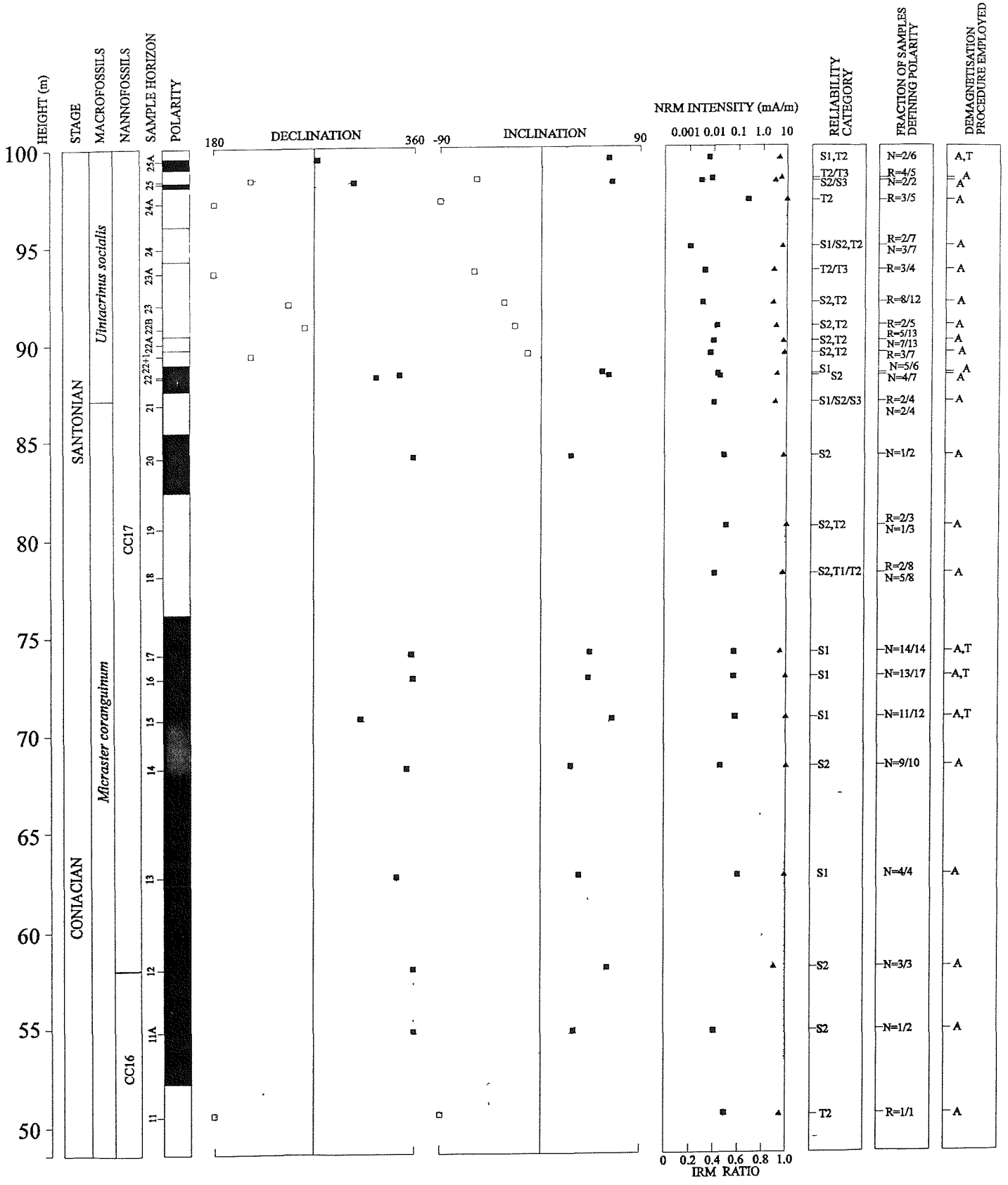
HEIGHT (m)
STAGE
MACROFOSSILS
NANNOFOSSILS
SAMPLE HORIZON
POLARITY
DECLINATION
INCLINATION
NRM INTENSITY (mA/m)
RELIABILITY CATEGORY
FRACTION OF SAMPLES DEFINING POLARITY
DEMAGNETISATION PROCEDURE EMPLOYED
SANTONIAN
CONIACIAN
Uintacrinus socialis
Micraster coranguinum
CC17
CC16
IRM RATIO

c)

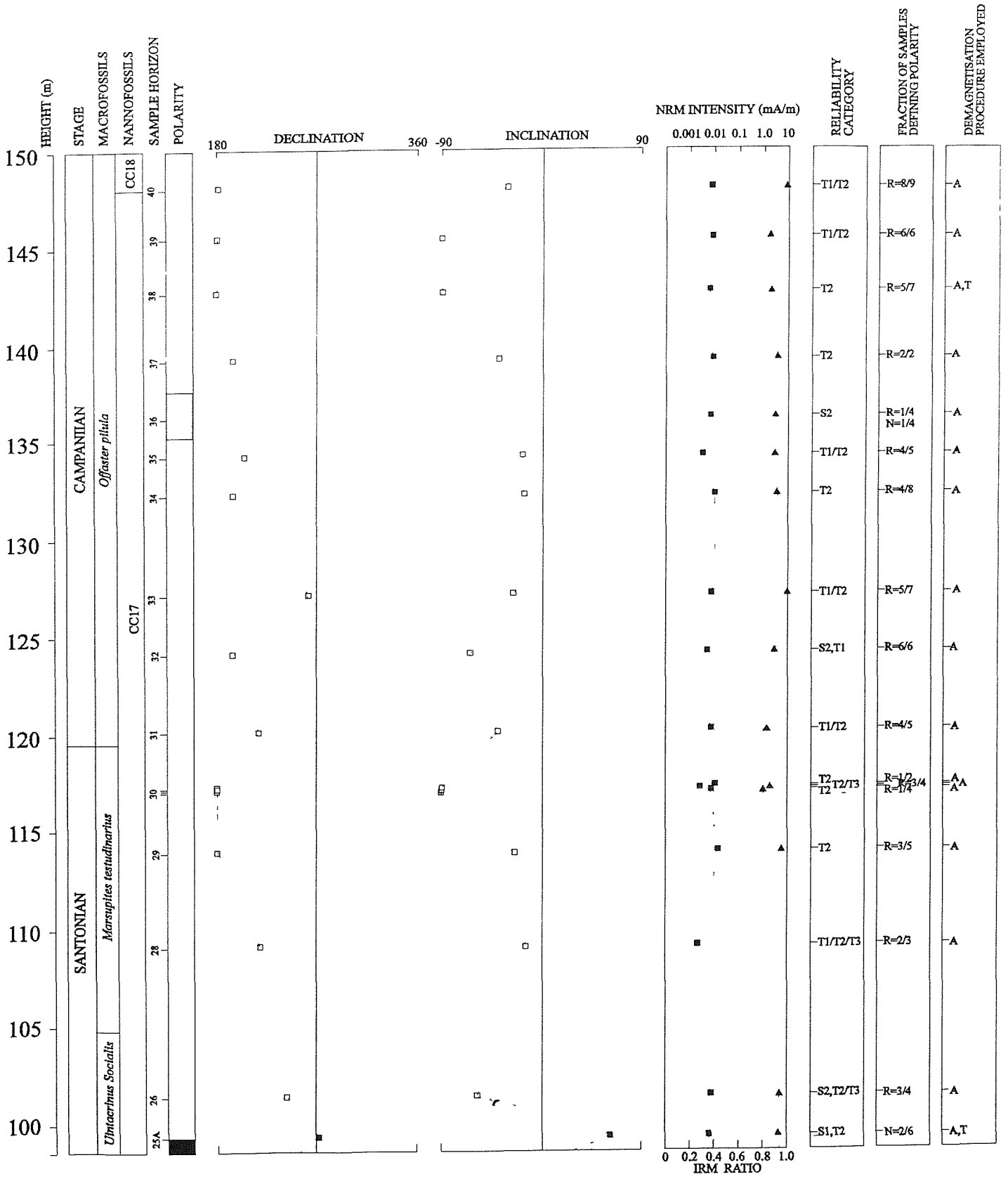
HEIGHT (m)
STAGE
MACROFOSSILS
NANNOFOSSILS
SAMPLE HORIZON
POLARITY
DECLINATION
INCLINATION
NRM INTENSITY (mA/m)
RELIABILITY CATEGORY
FRACTION OF SAMPLES DEFINING POLARITY
DEMAGNETISATION PROCEDURE EMPLOYED
IRM RATIO
CAMPANIAN
SANTONIAN
Offaster pilula
Marsupites testudinarius
Uintacrinus Socialis
CC18
CC17

d)

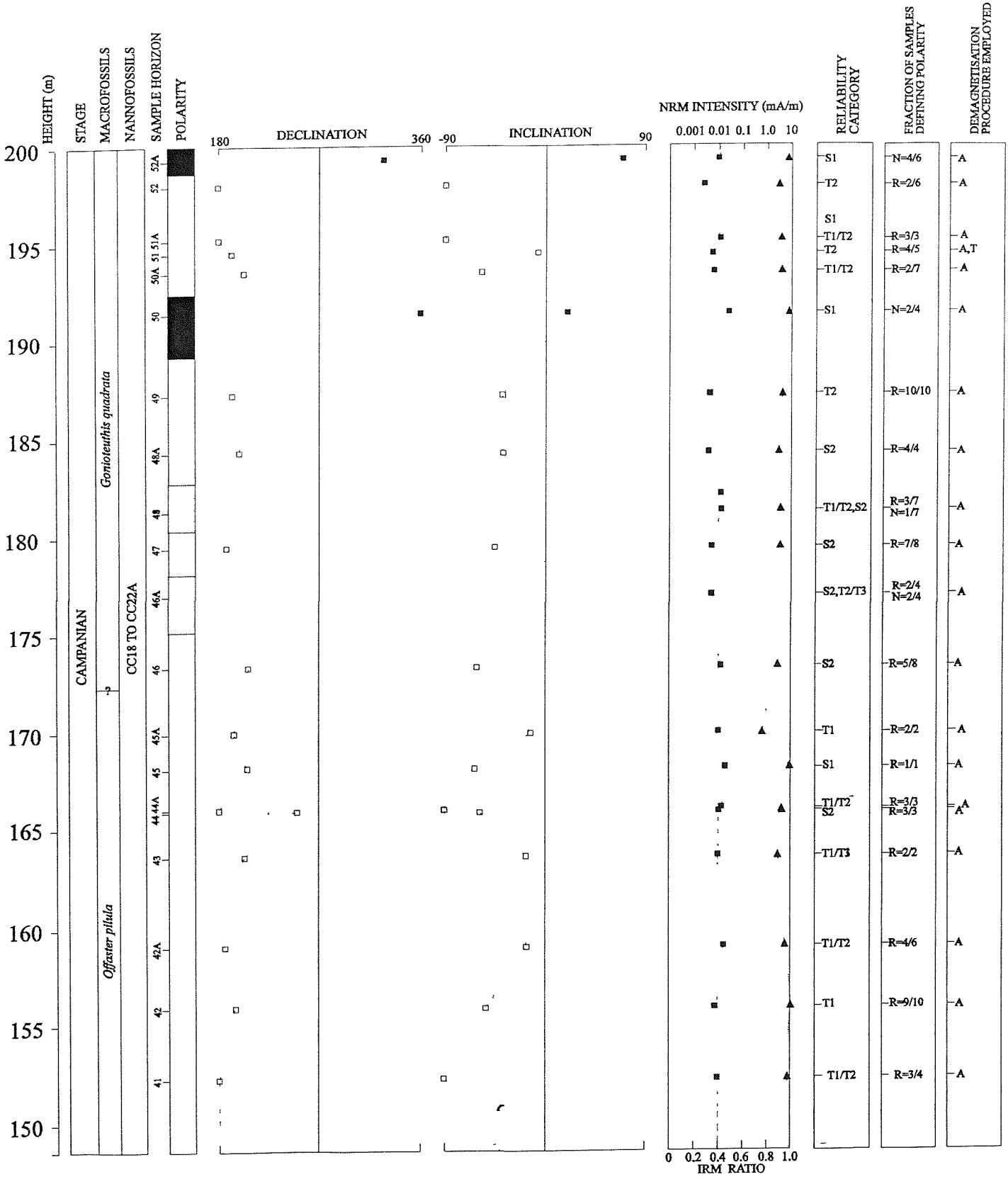
HEIGHT (m)
STAGE
MACROFOSSILS
NANNOFOSSILS
SAMPLE HORIZON
POLARITY
DECLINATION
INCLINATION
NRM INTENSITY (mA/m)
RELIABILITY CATEGORY
FRACTION OF SAMPLES DEFINING POLARITY
DEMAGNETISATION PROCEDURE EMPLOYED
CAMPANIAN
Gonioteuthis quadrata
Offaster pilula
CC18 TO CC22A
IRM RATIO

e)

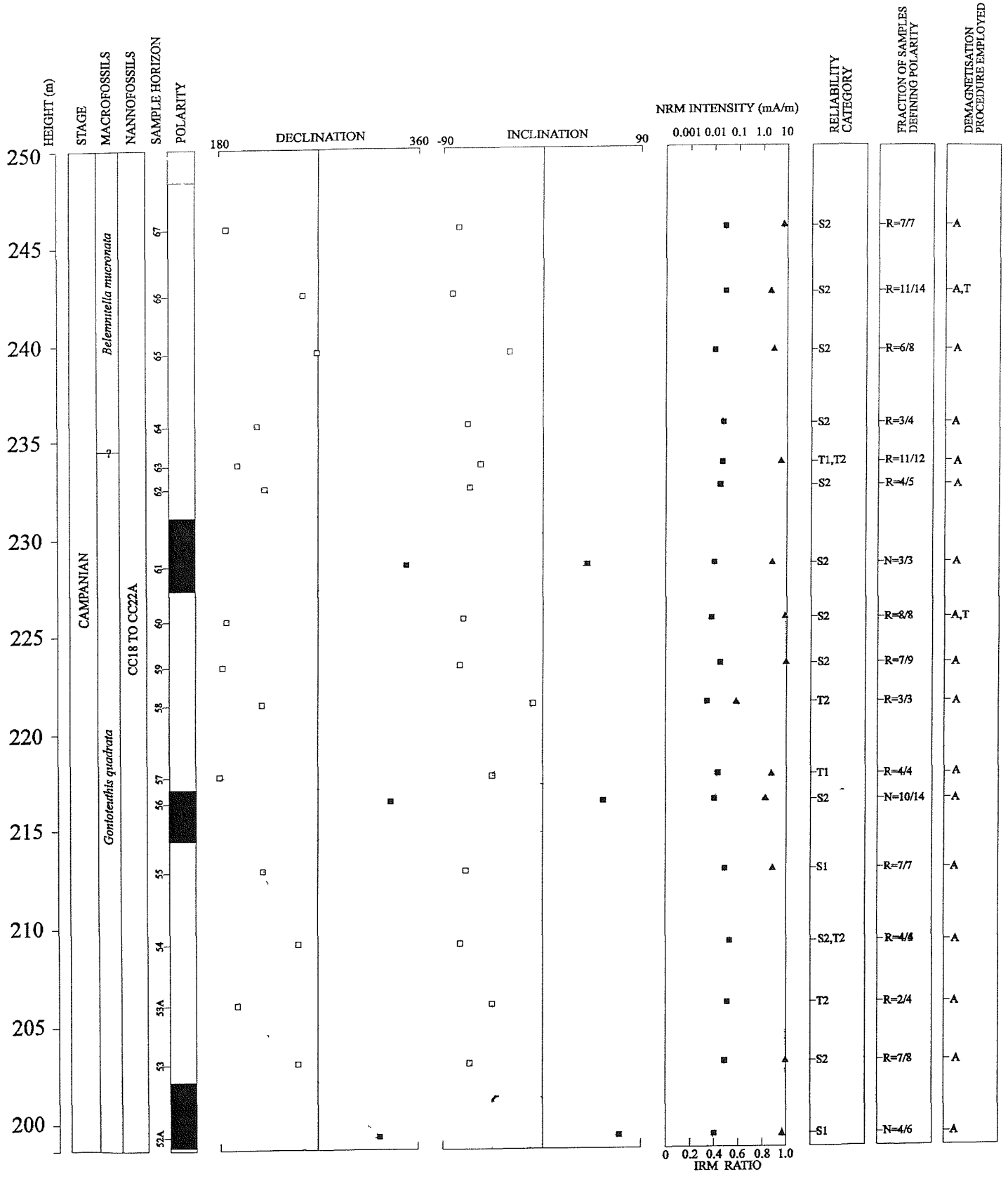
HEIGHT (m)
STAGE
MACROFOSSILS
NANNOFOSSILS
SAMPLE HORIZON
POLARITY
DECLINATION
INCLINATION
NRM INTENSITY (mA/m)
RELIABILITY CATEGORY
FRACTION OF SAMPLES DEFINING POLARITY
DEMAGNETISATION PROCEDURE EMPLOYED
250
245
240
235
230
225
220
215
210
205
200
CAMPANIAN
Belemnitella mucronata
Gonioteuthis quadrata
CC18 TO CC22A
180
360
-90
90
0.001 0.01 0.1 1.0 10
0 0.2 0.4 0.6 0.8 1.0
IRM RATIO
67
66
65
64
63
62
61
60
59
58
57
56
55
54
53A
53
52A
S2
R=7/7
A
S2
R=11/14
A,T
S2
R=6/8
A
S2
R=3/4
A
T1,T2
R=11/12
A
S2
R=4/5
A
S2
N=3/3
A
S2
R=8/8
A,T
S2
R=7/9
A
T2
R=3/3
A
T1
R=4/4
A
S2
N=10/14
A
S1
R=7/7
A
S2,T2
R=4/4
A
T2
R=2/4
A
S2
R=7/8
A
S1
N=4/6
A

f)

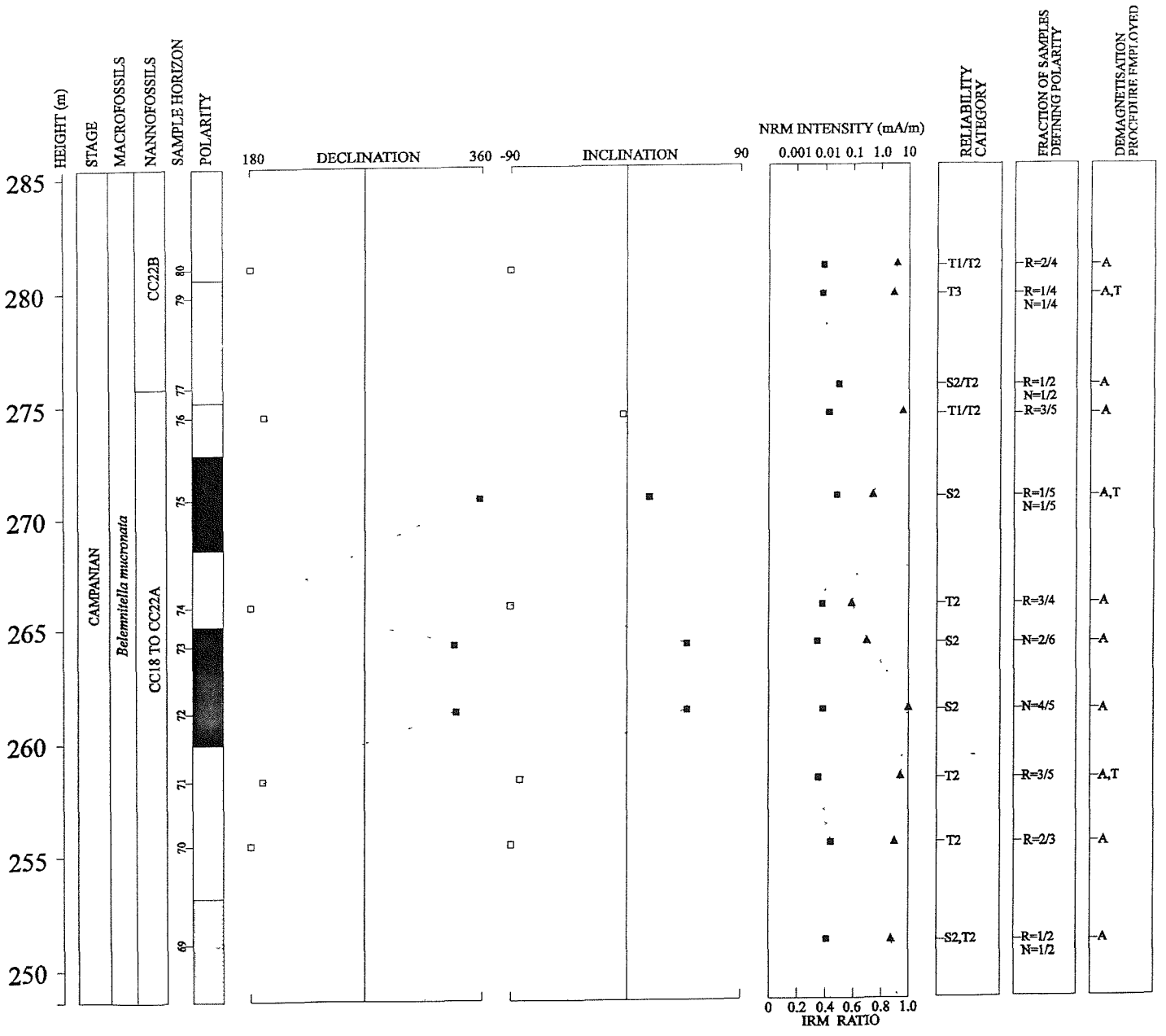
HEIGHT (m)
STAGE
MACROFOSSILS
NANNOFOSSILS
SAMPLE HORIZON
POLARITY
DECLINATION
INCLINATION
NRM INTENSITY (mA/m)
RELIABILITY CATEGORY
FRACTION OF SAMPLES DEFINING POLARITY
DEMAGNETISATION PROCEDURE EMPLOYED
CAMPANIAN
Belemnitella mucronata
CC22B
CC18 TO CC22A
IRM RATIO
T1/T2
T3
S2/T2
T1/T2
S2
T2
S2
S2
T2
T2
S2,T2
R=2/4
R=1/4 N=1/4
R=1/2 N=1/2
R=3/5
R=1/5 N=1/5
R=3/4
N=2/6
N=4/5
R=3/5
R=2/3
R=1/2 N=1/2
A
A,T
A
A
A,T
A
A
A
A,T
A
A

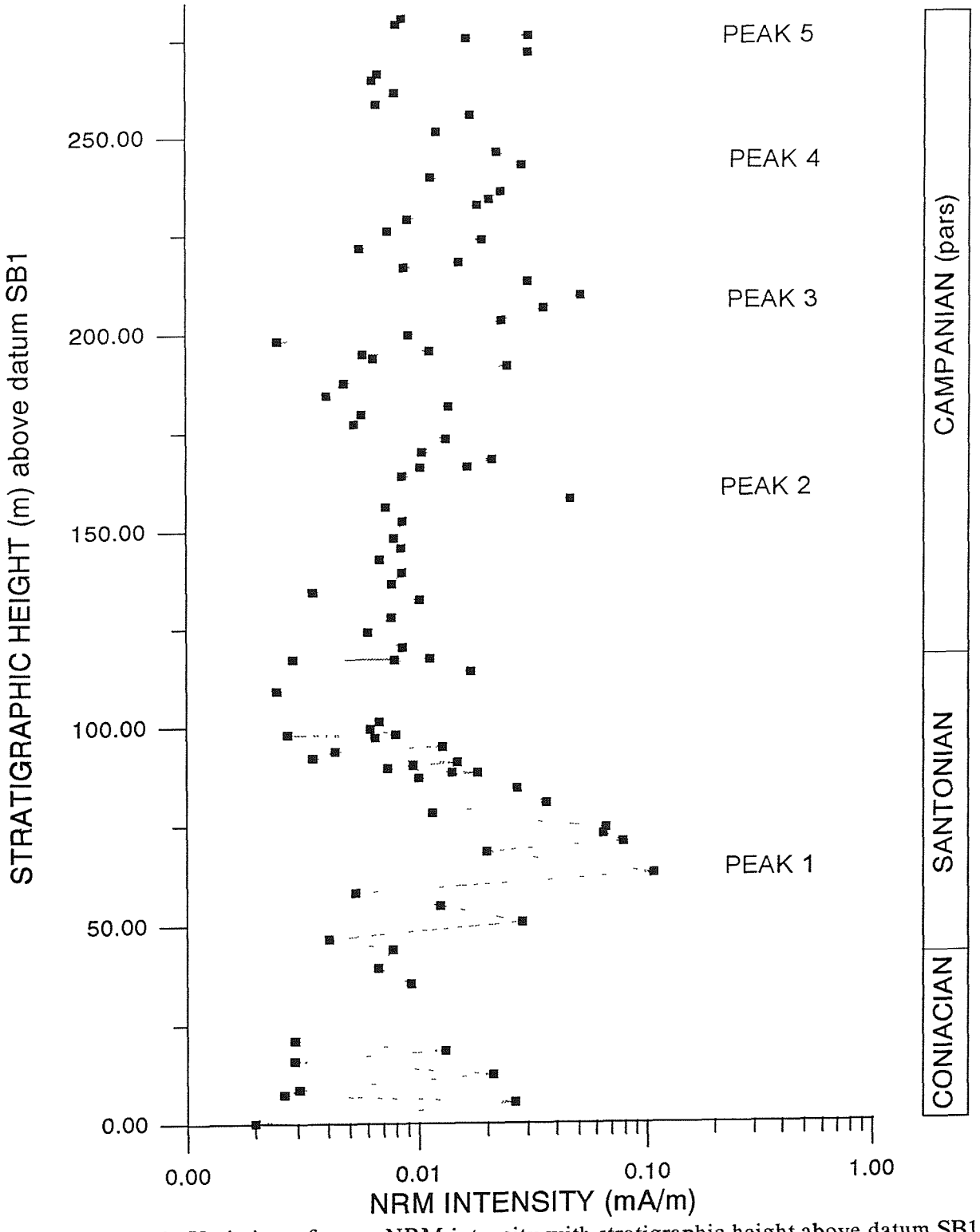

Figure 7.4. Variation of mean NRM intensity with stratigraphic height above datum SB1. The right-hand column indicates the Late Cretaceous Stages represented by the Chalk succession at Scratchell's Bay (Rawson et al., 1978).

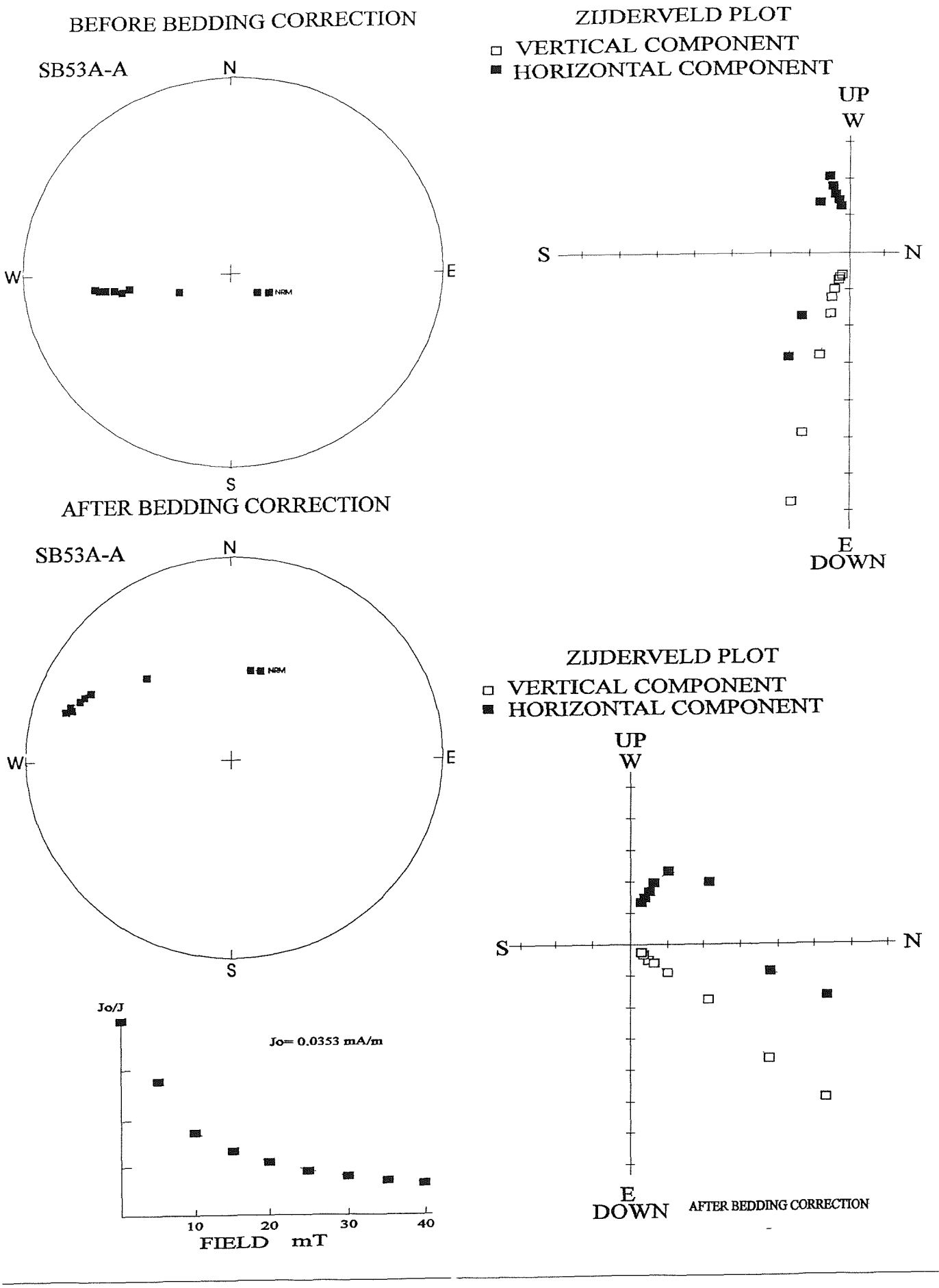

Figure 7.5. An example of the demagnetisation behaviour of a chalk palaeomagnetic sample from Scratchell's Bay when subjected to AF demagnetisation. The behaviour of sample SB53A-A, before and after application of a bedding correction of 260°/61°, is shown.

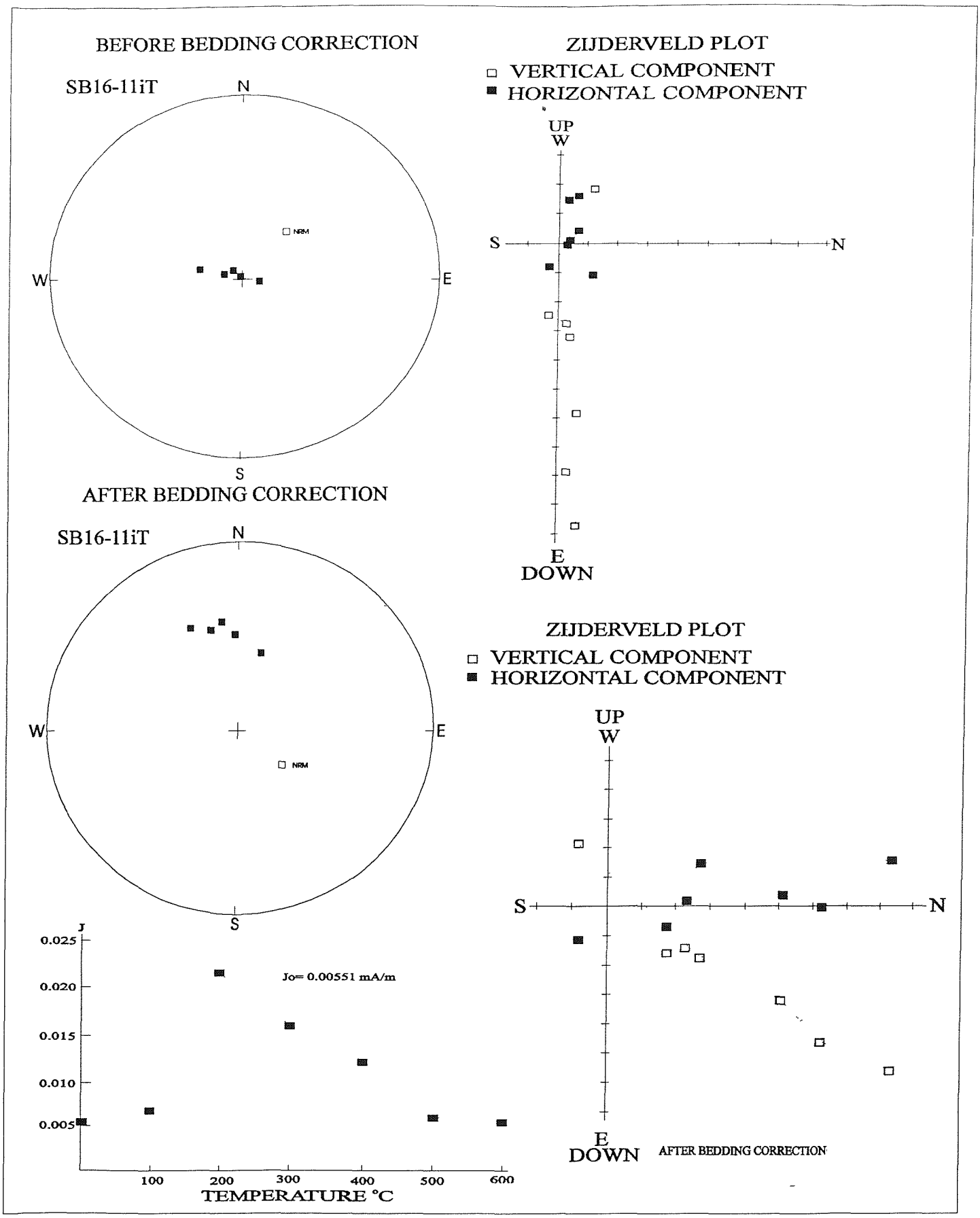

Figure 7.6. An example of the demagnetisation behaviour of a chalk palaeomagnetic sample from Scratchell's Bay when subjected to thermal demagnetisation. The behaviour of sample SB16-11iT, before and after application of a bedding correction of 270°/52°, is shown.

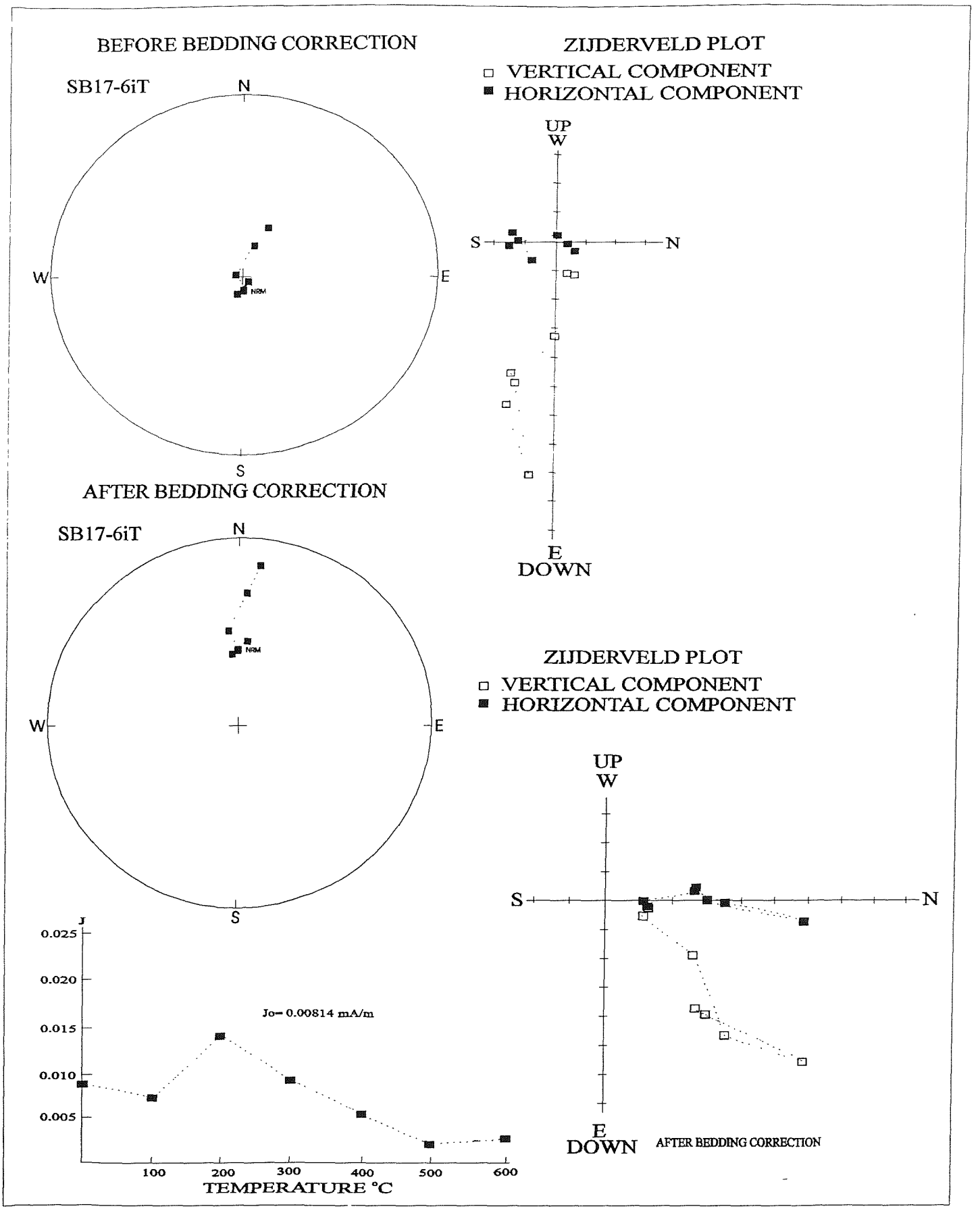

Figure 7.7. An example of the poor quality directional trends described during demagnetisation of chalk palaeomagnetic sample from Scratchell's Bay. The behaviour of sample SB17-6iT, before and after application of a bedding correction of 270°/52°, is shown.

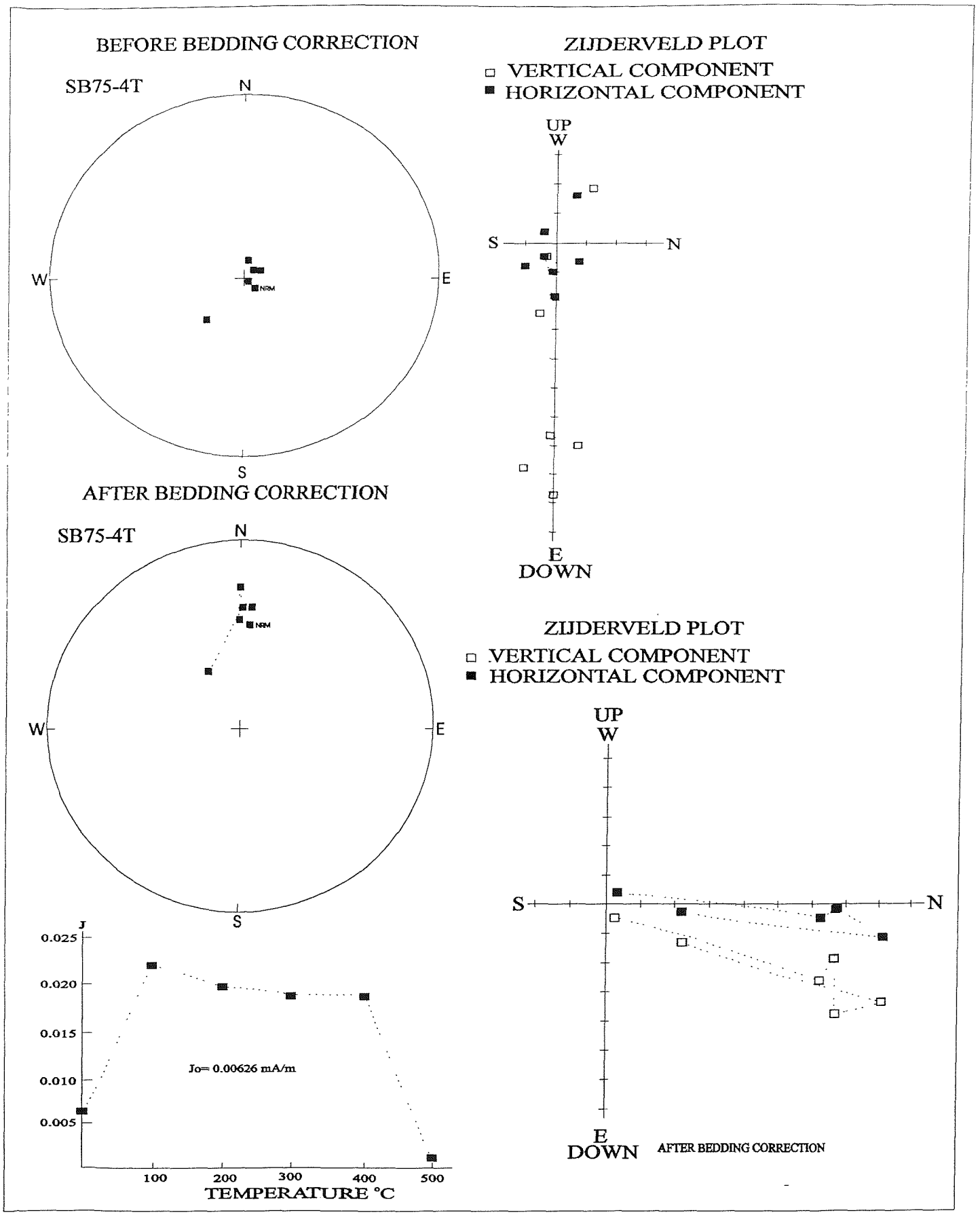

Figure 7.8. An example of the poor stable end points described during demagnetisation of chalk palaeomagnetic sample from Scratchell's Bay. The behaviour of sample SB75-4T, before and after application of a bedding correction of 265°/68°, is shown.

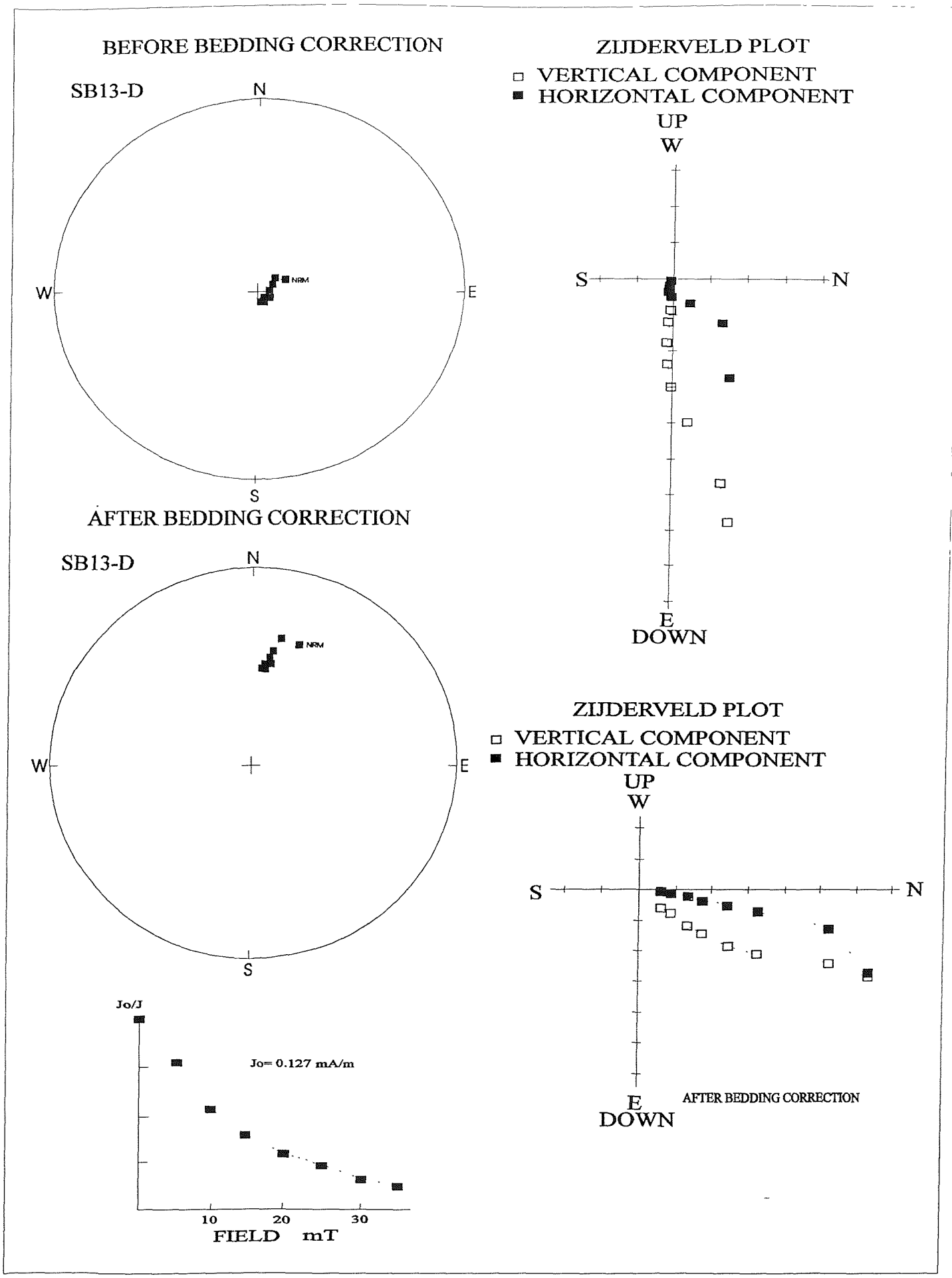

Figure 7.9a. An example of an 'S1 reliability category' A F demagnetised sample (SB13-1-D) before and after application of a bedding correction of 270°/52°.

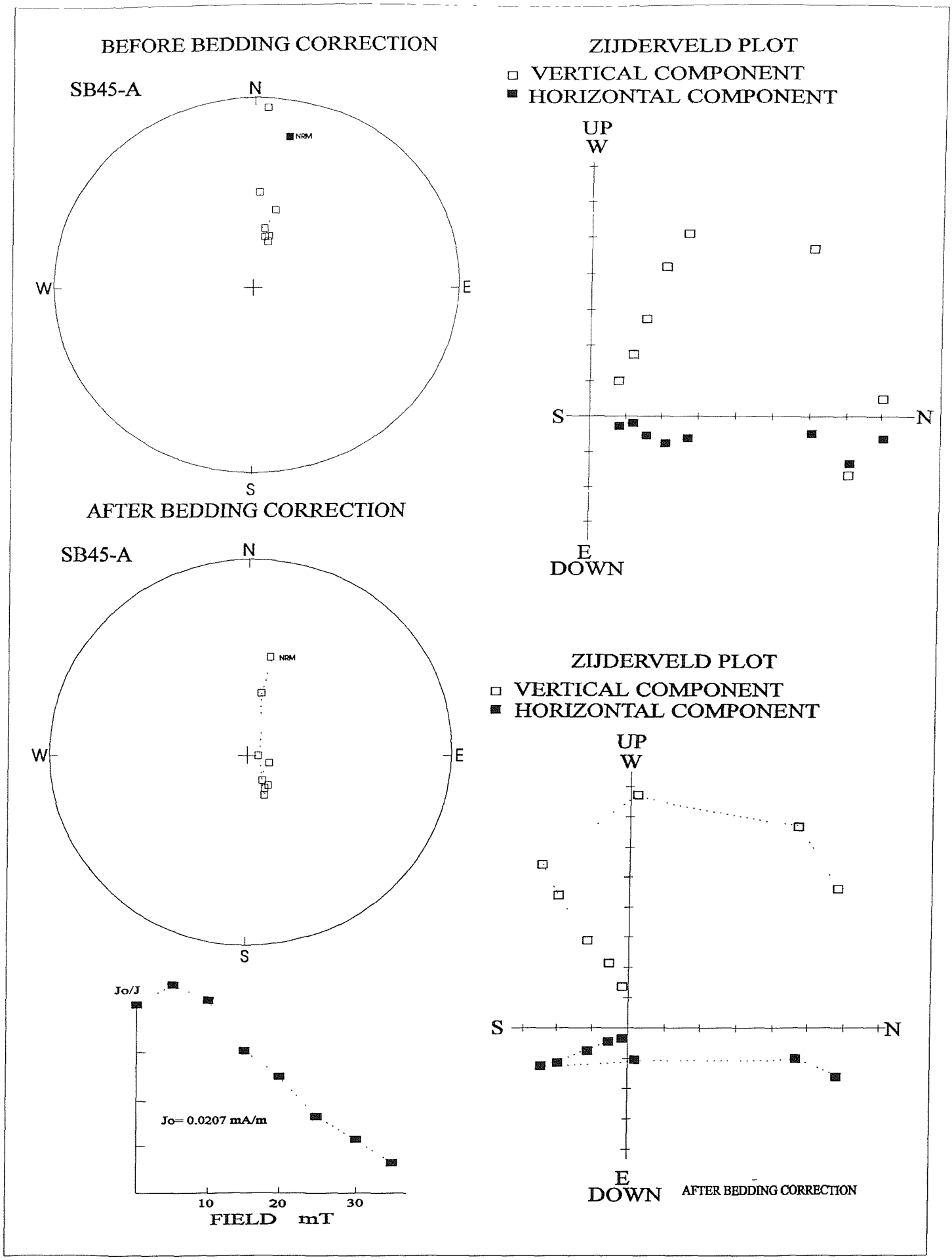

Figure 7.9b. An example of an 'S1 reliability category' A F demagnetised sample (SB45-A) before and after application of a bedding correction of 265°/52°.

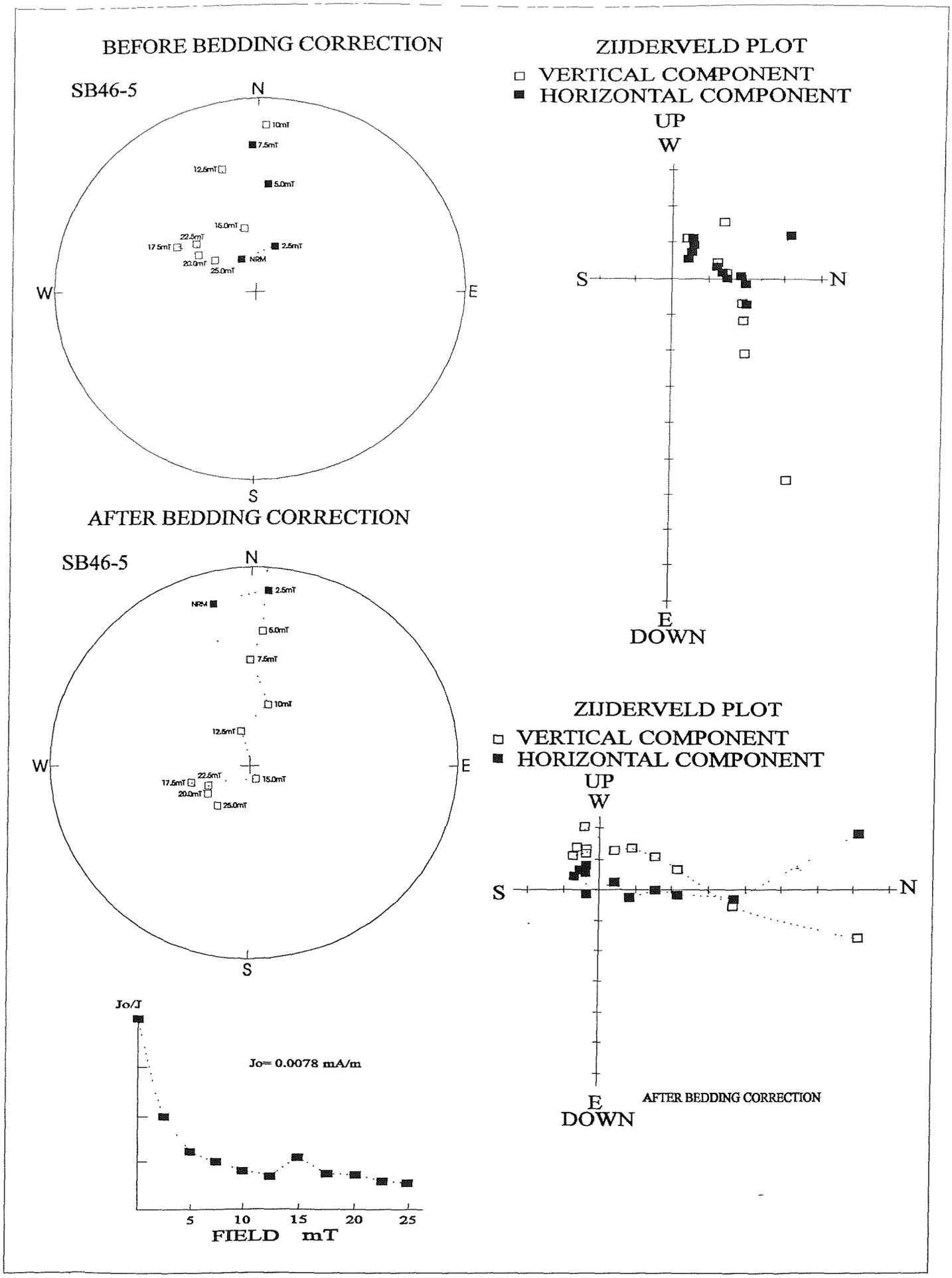

Figure 7.10a. An example of an 'S2 reliability category' A F demagnetised sample (SB46-5) before and after application of a bedding correction of 260°/52°.

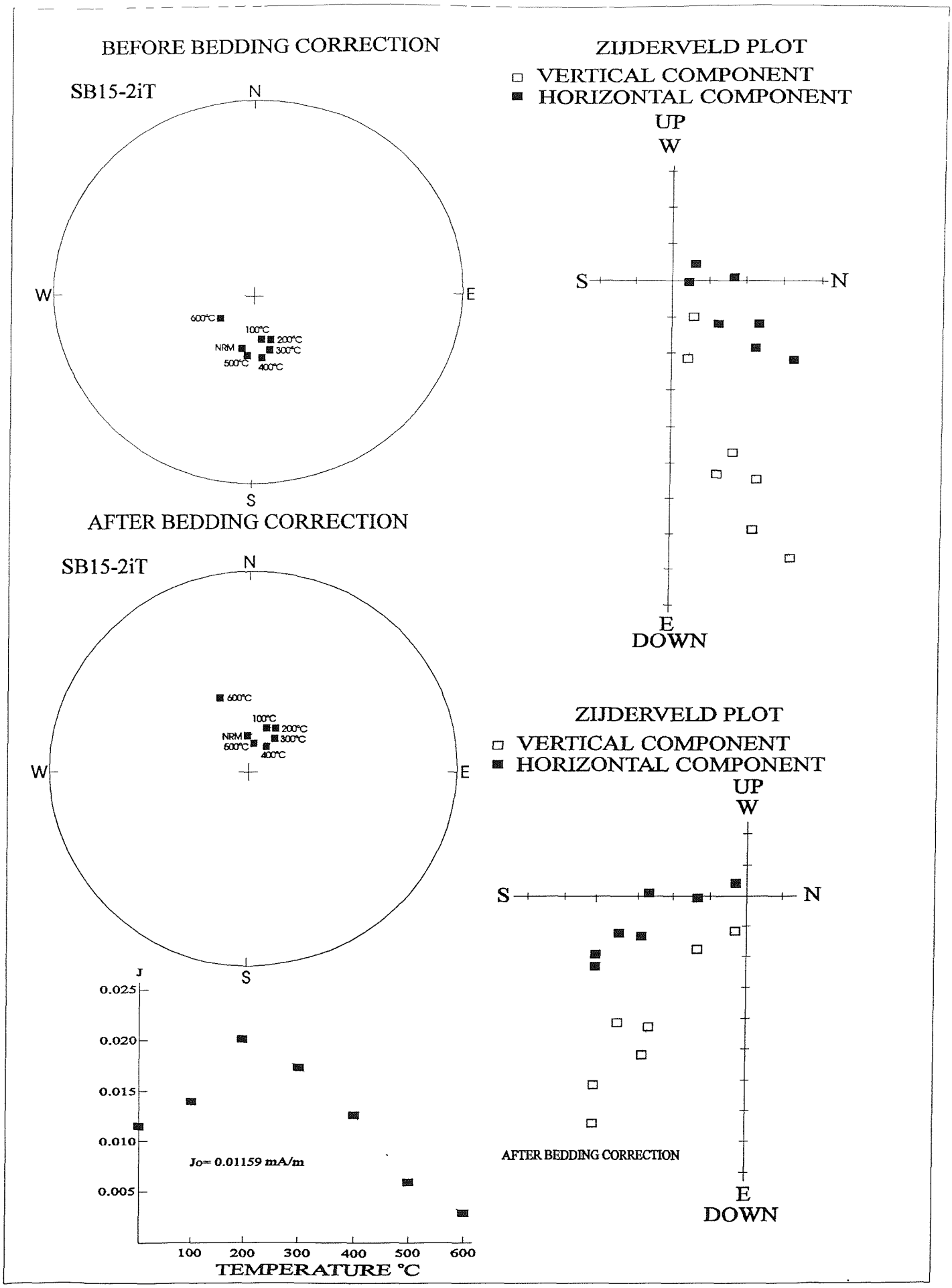

Figure 7.10b. An example of an 'S2 reliability category' thermally demagnetised sample (SB15-2iT) before and after application of a bedding correction of 270°/52°.

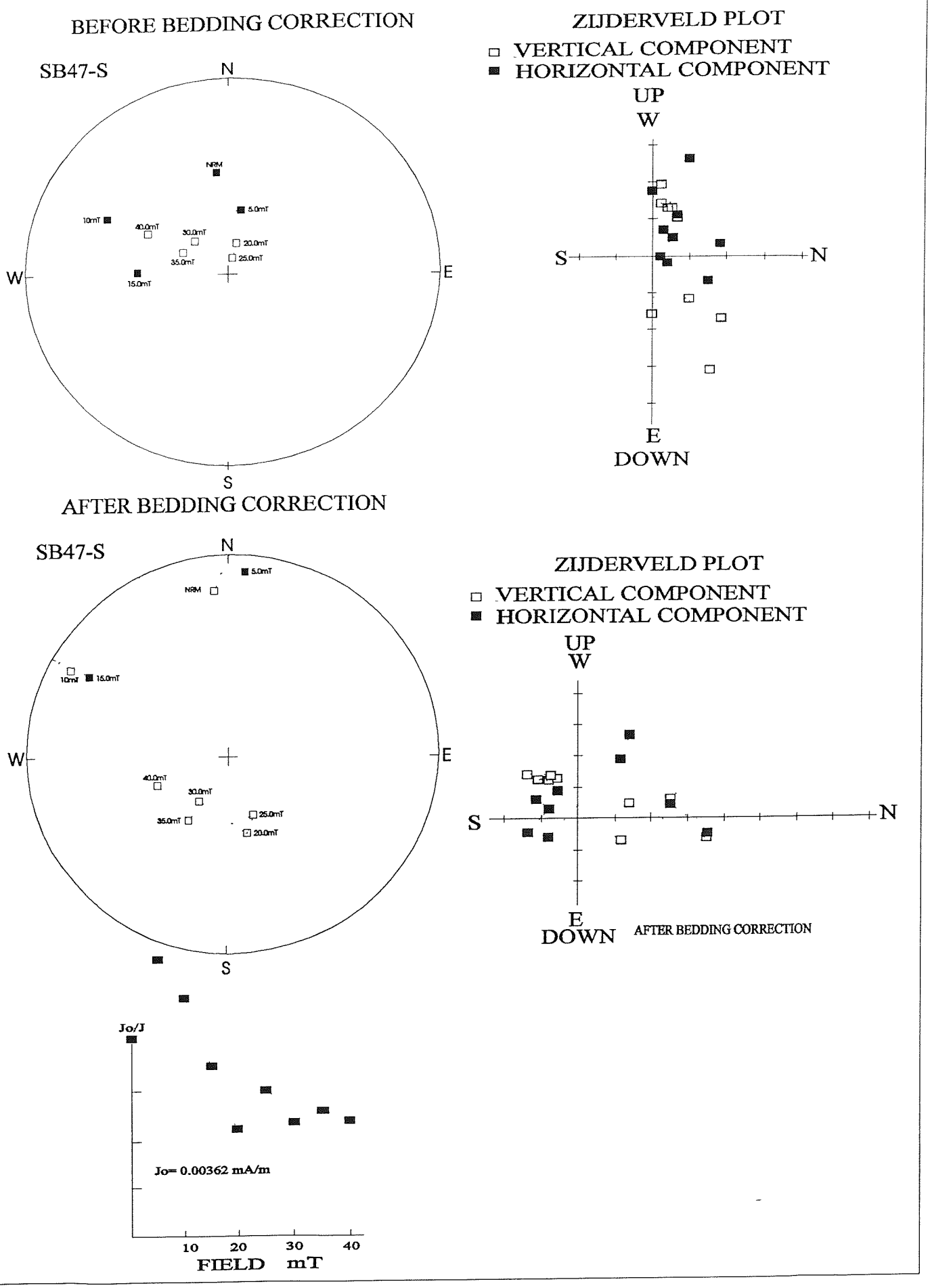

Figure 7.11a. An example of an 'S3 reliability category' A F demagnetised sample (SB47-S) before and after application of a bedding correction of 260°/52°.

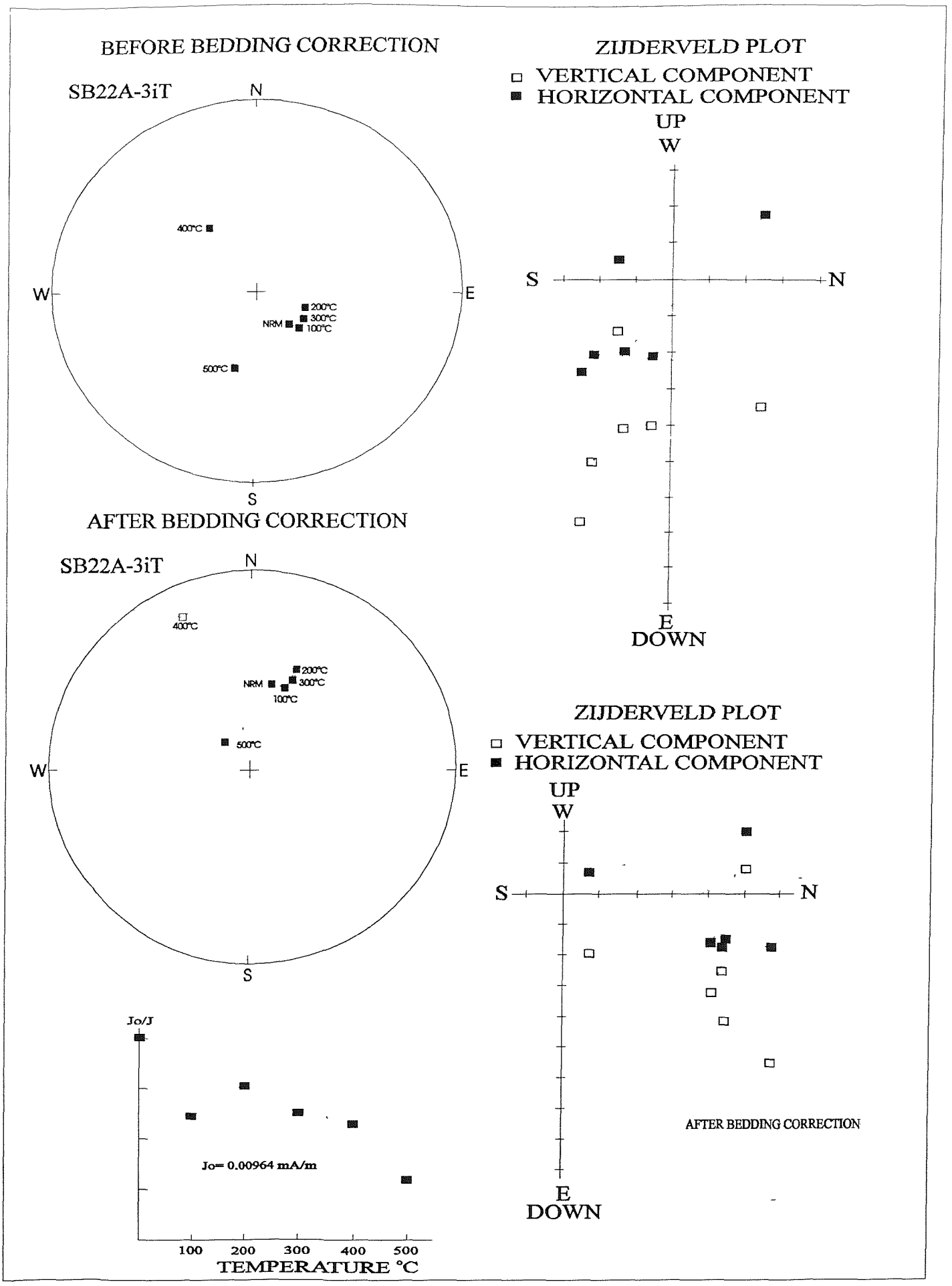

Figure 7.11b. An example of an 'S3 reliability category' thermally demagnetised sample (SB22A-3iT) before and after application of a bedding correction of 260°/52°.

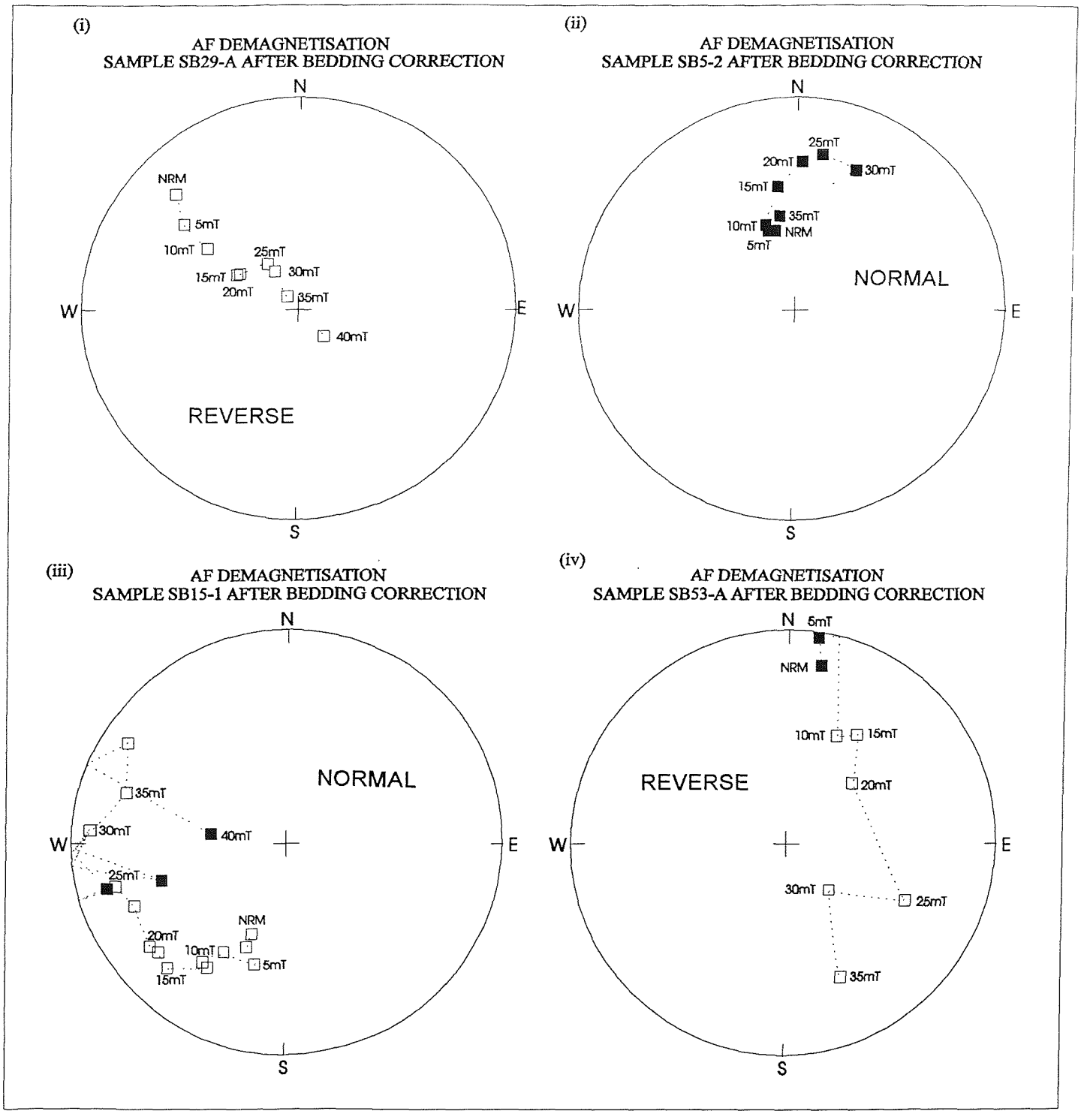

Figure 7.12. Examples of Chalk palaeomagnetic samples from Scratchell's Bay which, when subjected to AF (Figures i , ii, iii & iv) demagnetisation and application of a bedding correction, show 'T1 reliability category' trends to either normal or reverse polarity.

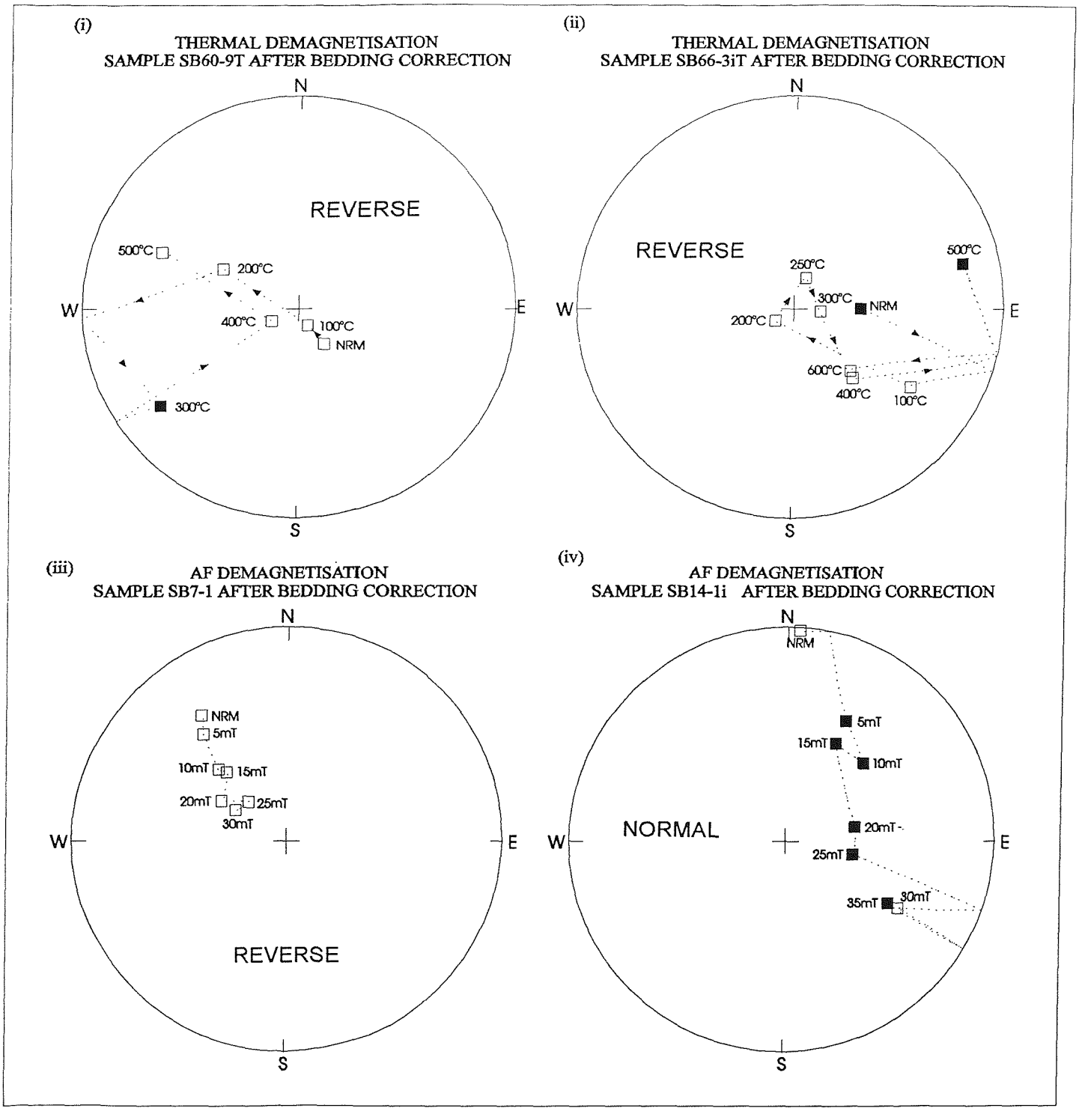

Figure 7.13. Examples of Chalk palaeomagnetic samples from Scratchell's Bay which, when subjected to thermal (Figures i & ii) or AF (Figures iii & iv) demagnetisation and application of a bedding correction, show 'T2 reliability category' trends to either normal or reverse polarity.

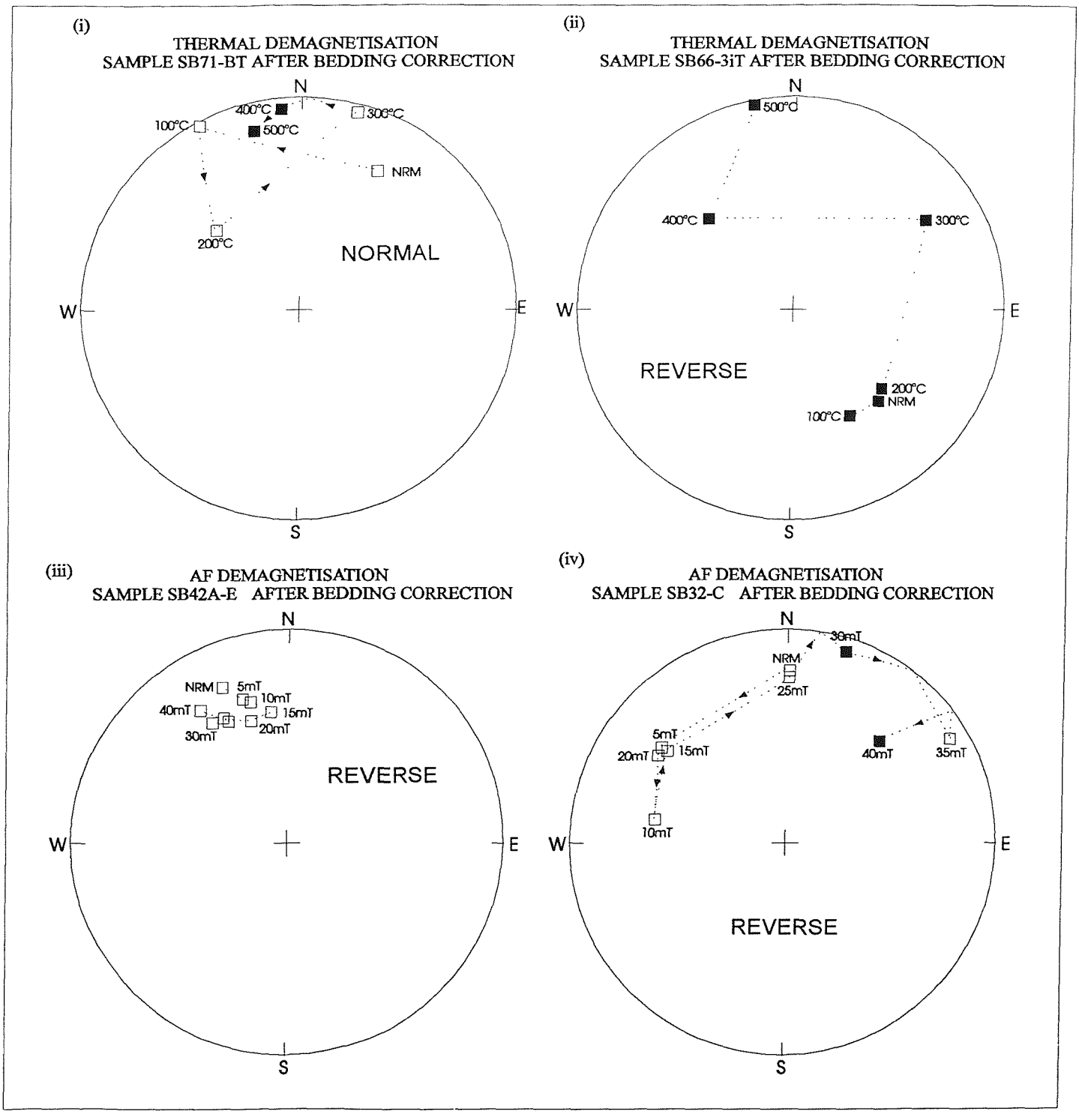

Figure 7.14. Examples of Chalk palaeomagnetic samples from Scratchell's Bay which, when subjected to AF (Figures i & ii) or thermal (Figures iii & iv) demagnetisation and application of a bedding correction, show 'T3 reliability category' trends to either normal or reverse polarity.

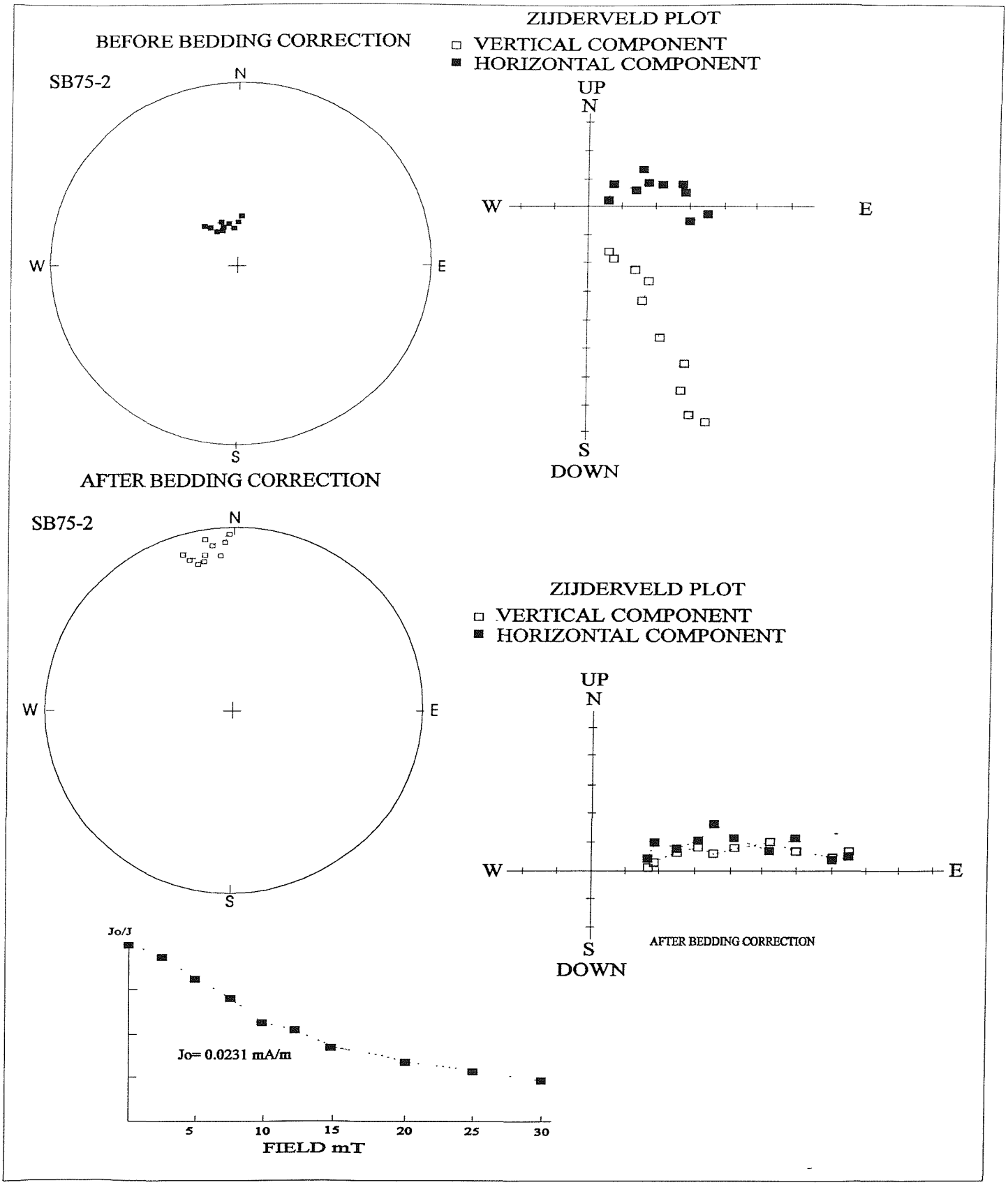

Figure 7.15a. An example of an 'Overprint reliability category' AF demagnetised sample (SB75-2) before and after application of a bedding correction of 265°/68°.

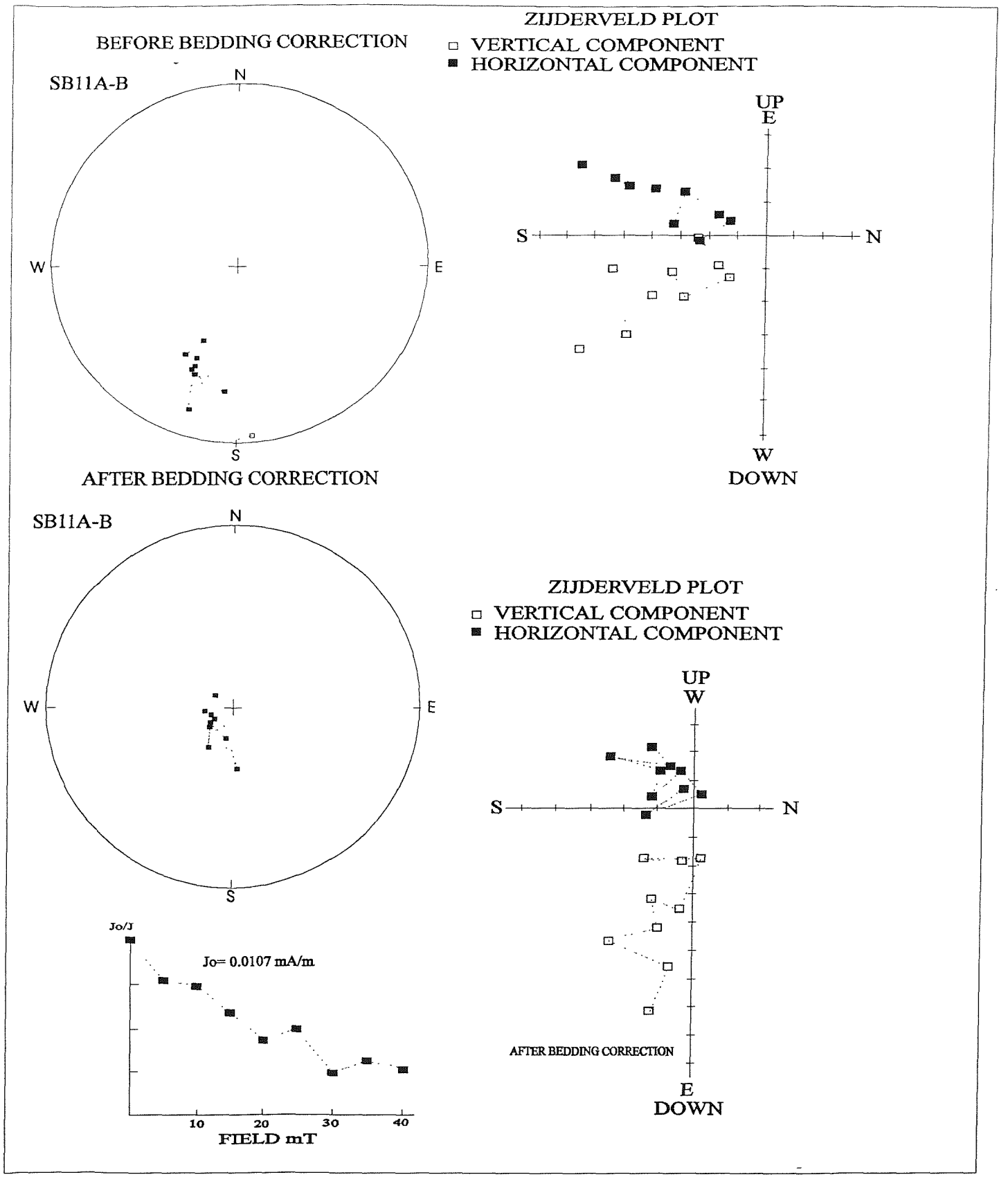

Figure 7.15b. An example of an 'Overprint reliability category' AF demagnetised sample (SB11A-B) before and after application of a bedding correction of 270°/52°.

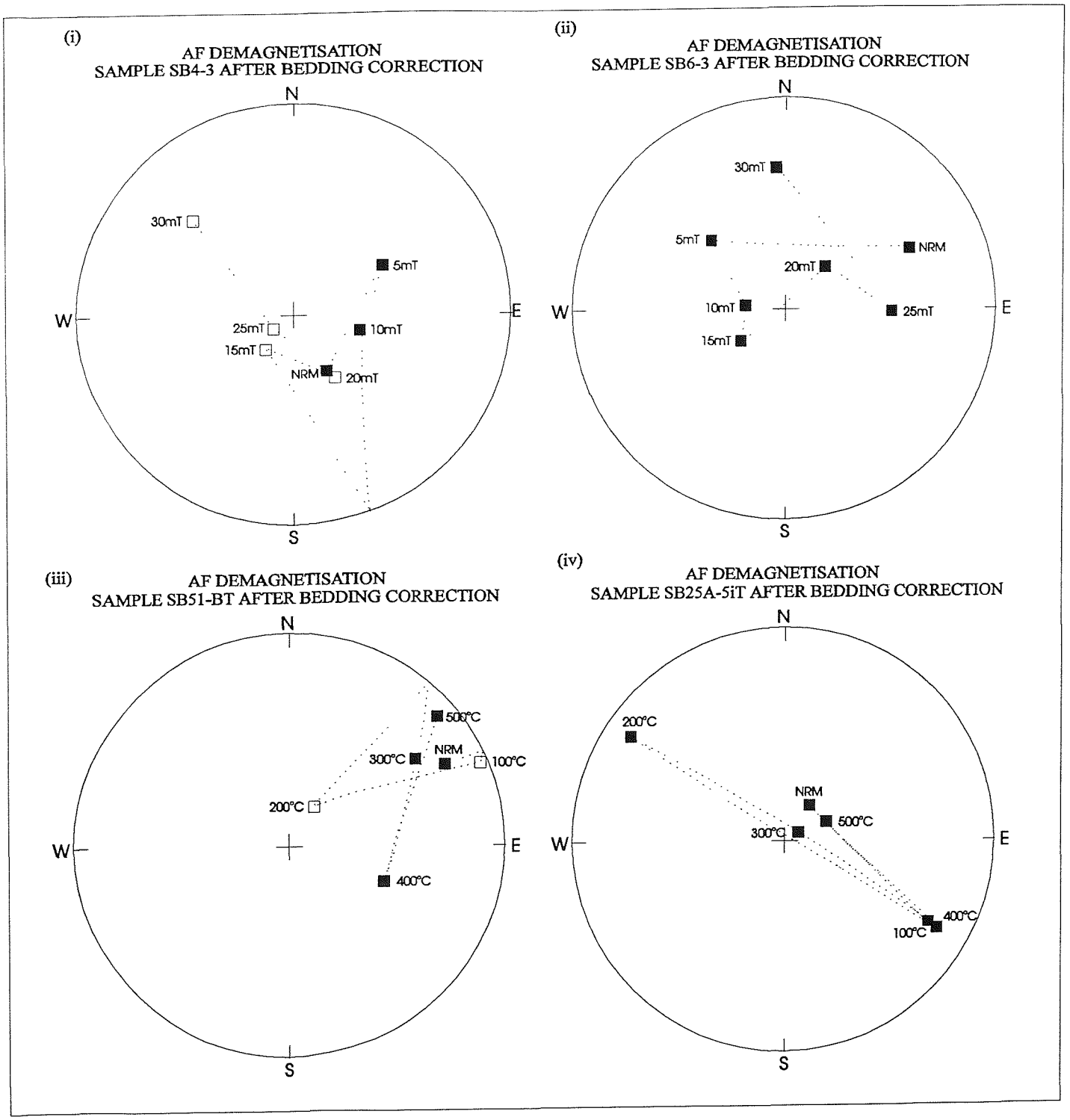

Figure 7.16. Examples of Chalk palaeomagnetic samples from Scratchell's Bay which, when subjected to AF (Figures i , ii) and thermal (iii & iv) demagnetisation and application of a bedding correction, show 'Erratic' behaviour. Polarity definition is impossible.

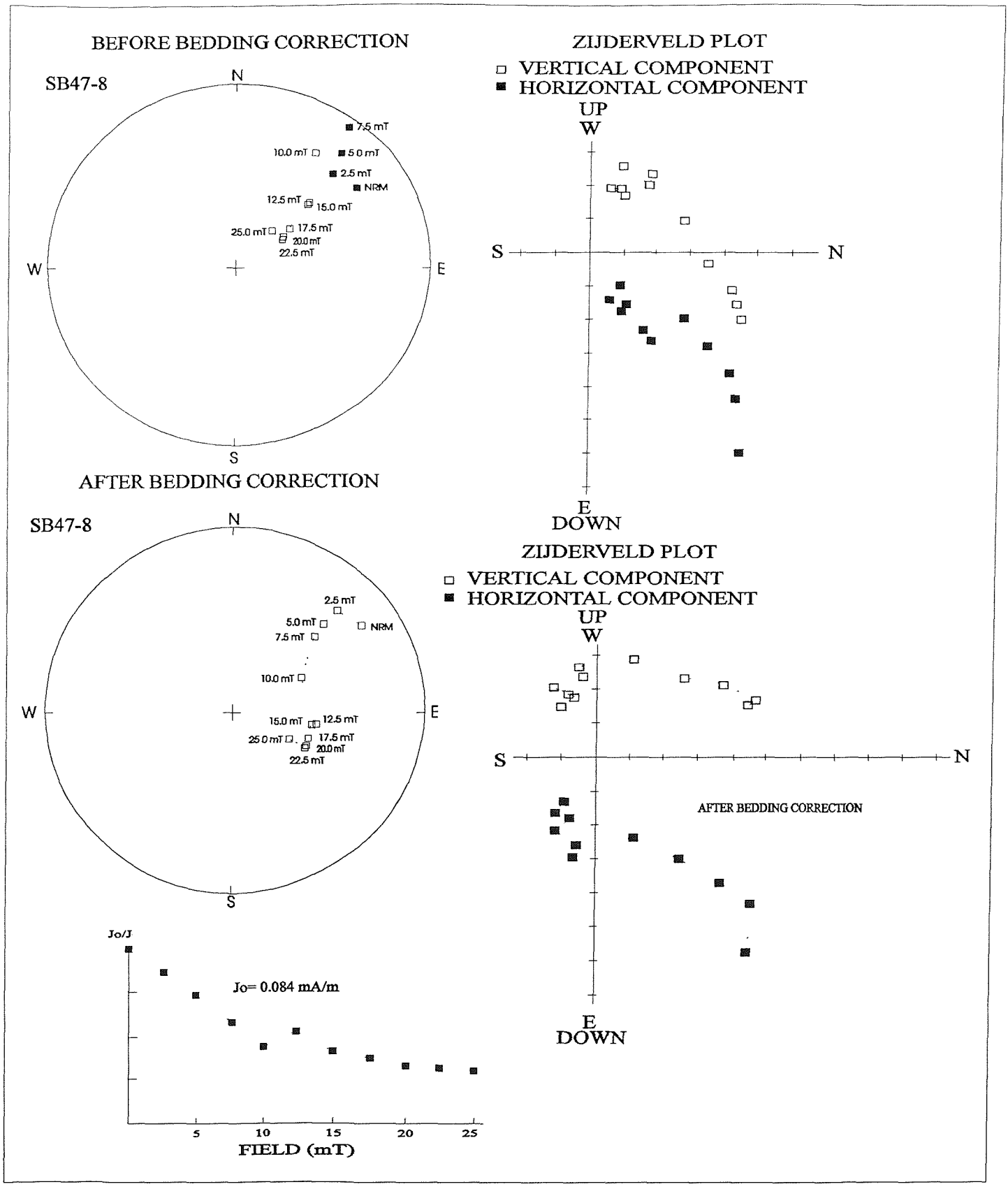

Figure 7.17a. Sample SB47-8 before and after a tectonic correction of 260°/52°. Prior to correction, sample SB47-8 displays a possible directional trend away from a overprint direction towards reverse polarity. After the tectonic correction is applied to the sample no doubt remains.

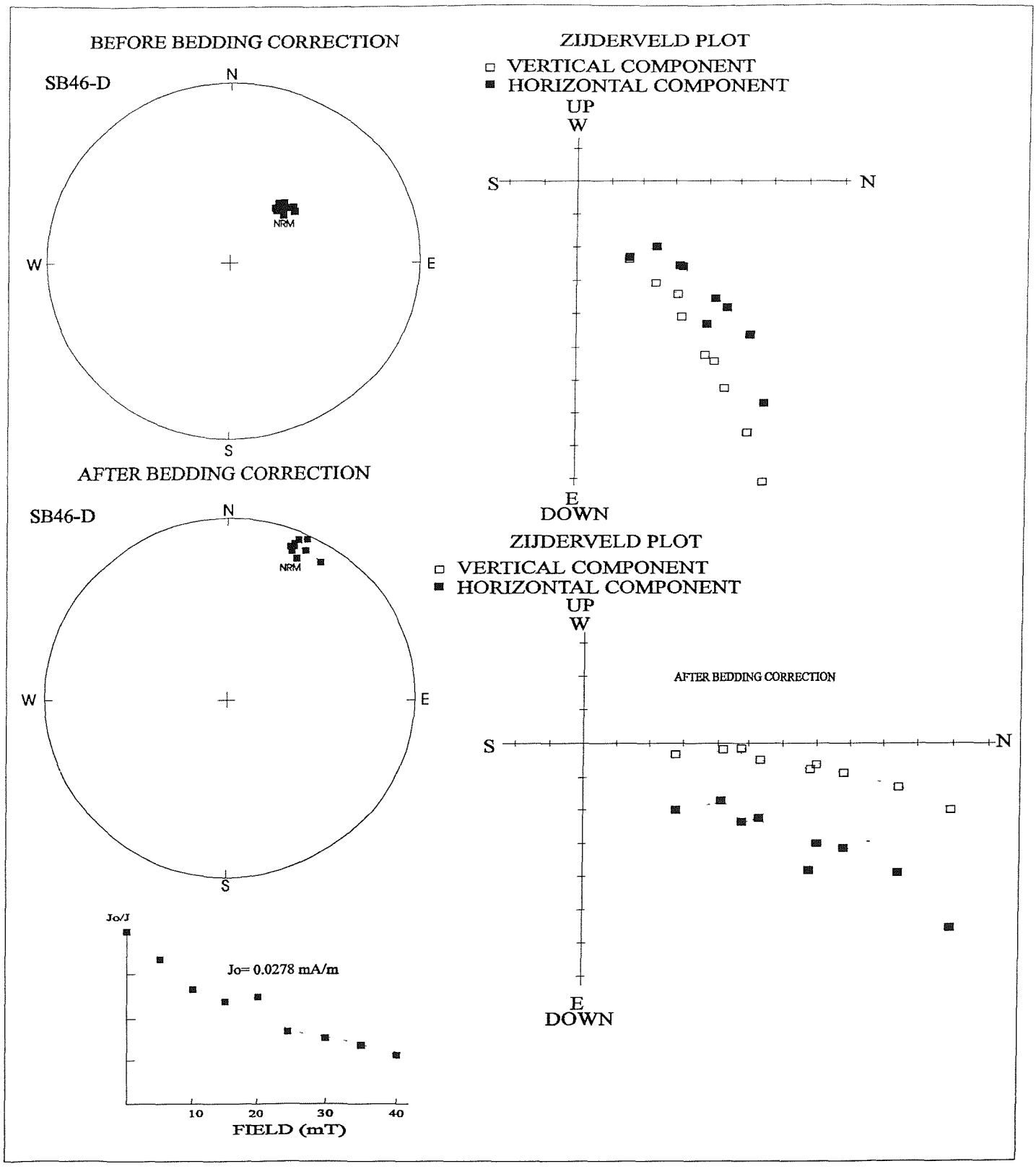

Figure 7.17b. A bedding correction of 260°/52° has been applied for sample SB46-D. The Stable Characteristic Magnetisation of the sample is rotated away from a normal polarity geomagnetic field direction to a direction with a shallow positive inclination (10°) and an approximately northerly declination.

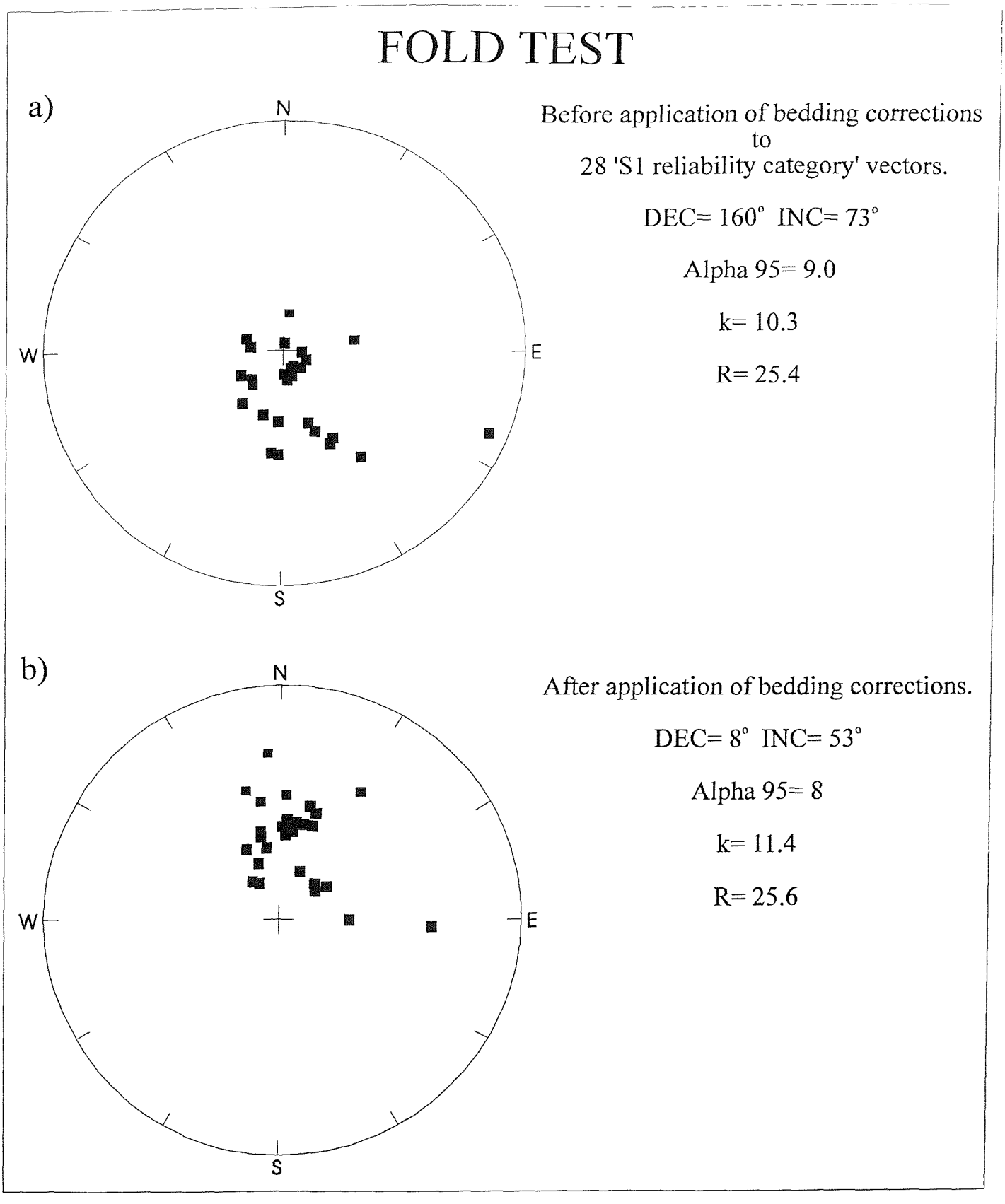

Figure 7.18. A stereographic equal area plot of the stable characteristic magnetisation for 28 'S1 reliability category' magnetic vectors from the complete Scratchell's Bay section, before (a) and after (b) bedding corrections have been applied to individual vectors. Bedding correction inclinations range between 52° and 68° while strikes range between 260° and 270°. Precision parameters 'k' and alpha 95 are reported before and after bedding correction.

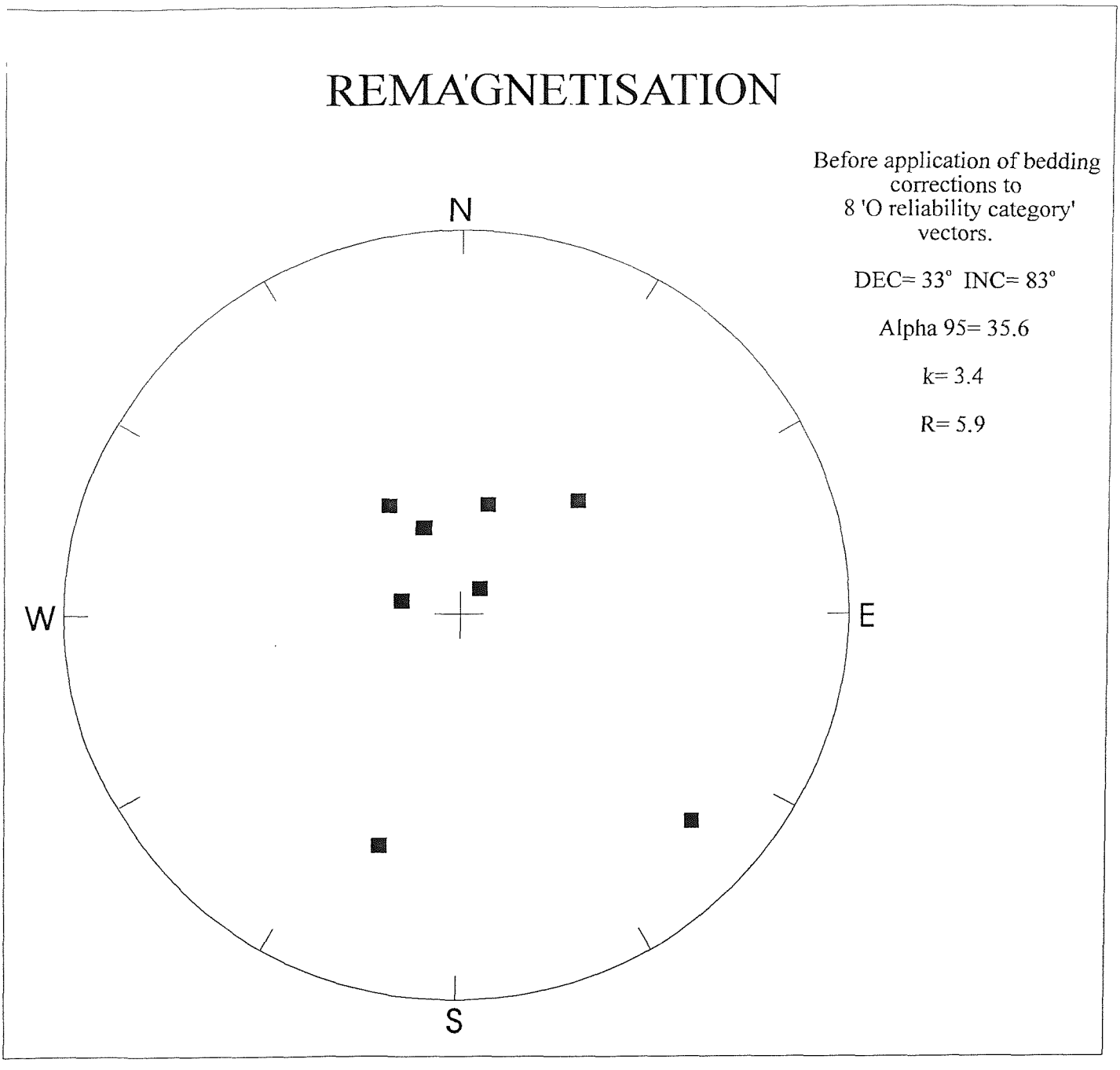

Figure 7.19. A stereographic equal area plot of overprint vectors for the Scratchell's Bay section. One and a half percent of the samples demagnetised possessed magnetic overprints which could not be removed using AF or thermal demagnetisation procedures. However, only 3 specimens from the 8 possessed stable end points which were well defined by a collection of closely spaced points on the stereographic projection and with the final linear segment (MAD≤5) on the vector plot directed through the origin. An overall mean overprint vector for all 8 specimens (declination=33°, inclination=83°) has a very poorly defined recent geomagnetic field direction and a very large alpha 95 value (>35°).

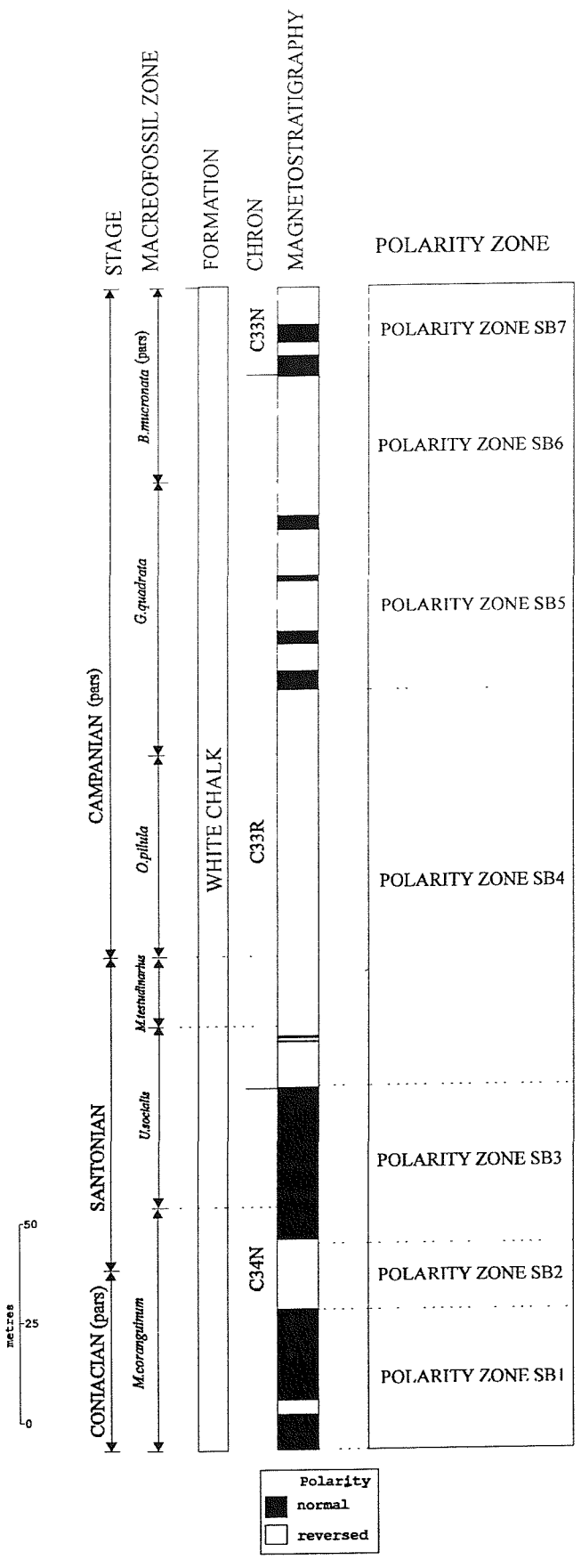

Figure 7.20. The Scratchell's Bay Chalk succession can be divided into seven polarity intervals. From left to right the diagram shows Late Cretaceous Stages, macrofossil zones (Rawson *et al.* 1978), Formation, geomagnetic polarity Chrons, the magnetostratigraphy of Scratchell's Bay and the associated polarity zones (SB).

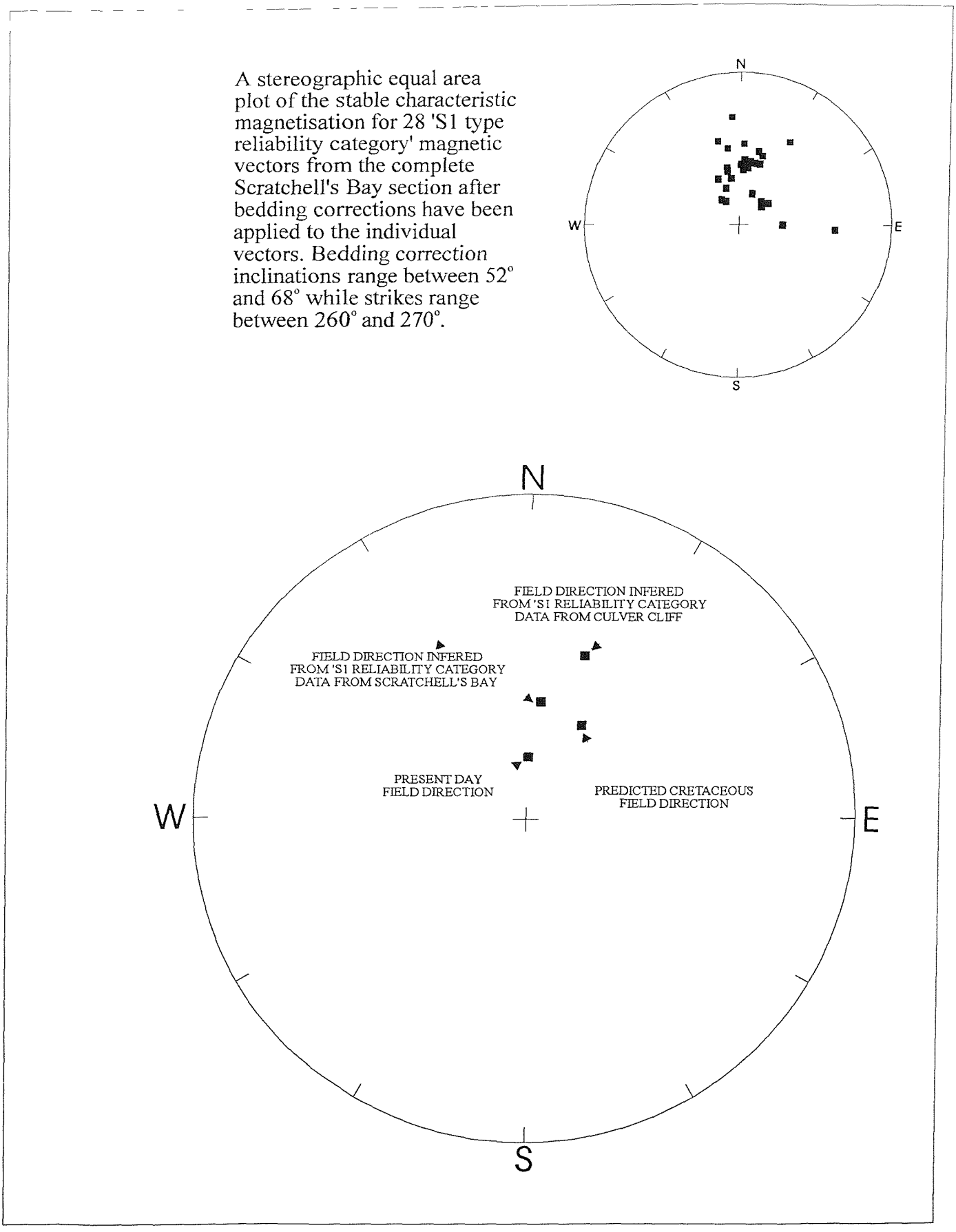

Figure 7.21. A stereographic projection showing the overall mean geomagnetic field direction for southern England (declination= 8°, inclination= 53°, k= 11.4 and alpha 95= 8.4) based on 'S1 reliability category' palaeomagnetic vectors derived from Late Cretaceous Chalk deposits, the predicted Late Cretaceous geomagnetic field direction for southern England based on the palaeocontinental reconstructions of Smith *et al.* (1981) and the present day geomagnetic field direction. Inset, a stereographic equal area plot of the stable characteristic magnetisation for 28 'S1 reliability category' magnetic vectors from the complete Scratchell's Bay section after bedding corrections have been applied to the individual vectors.

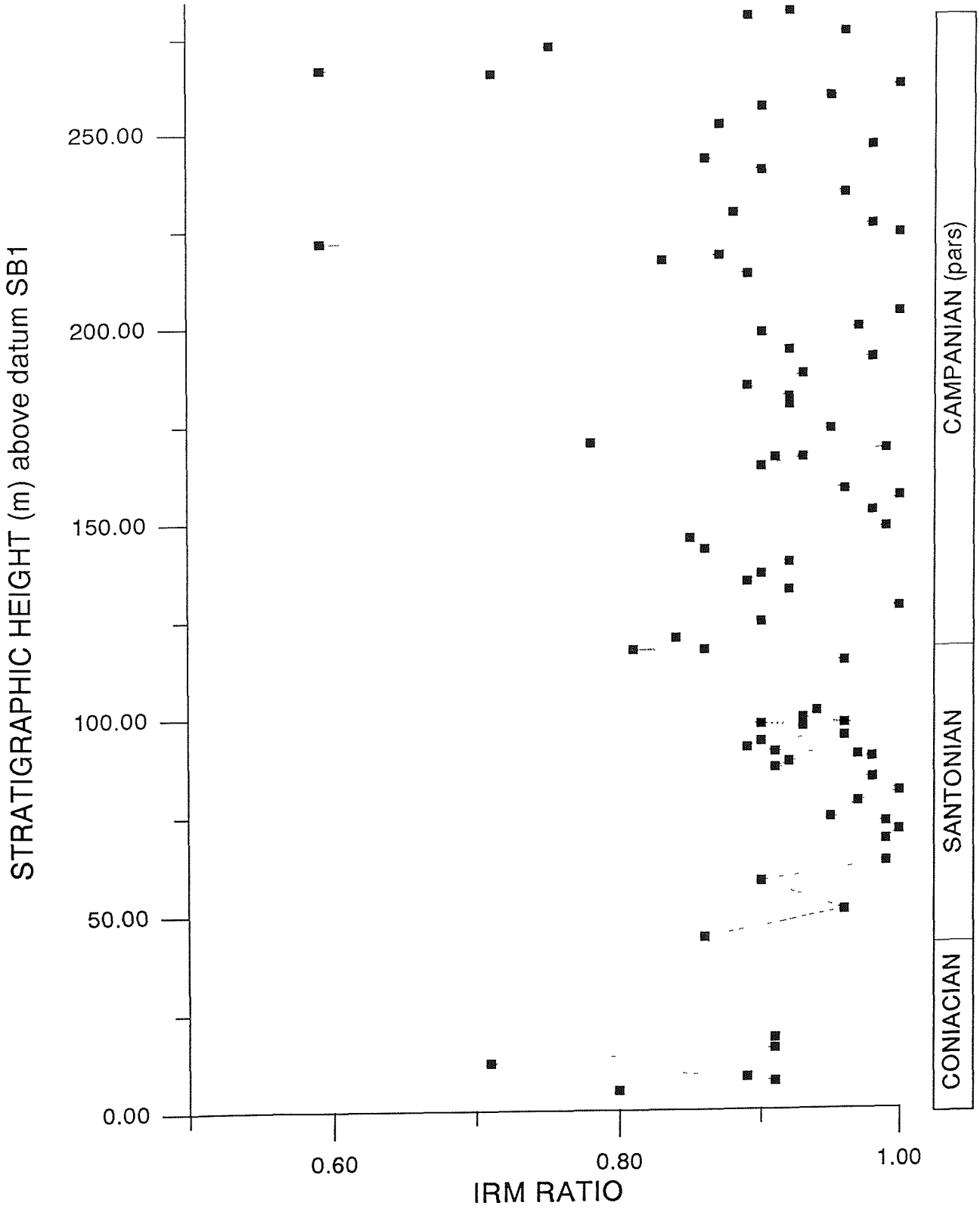

Figure 7.22. IRM ratio log of the chalk succession at Scratchell's Bay. The vast majority of samples exhibit IRM ratios above 0.9

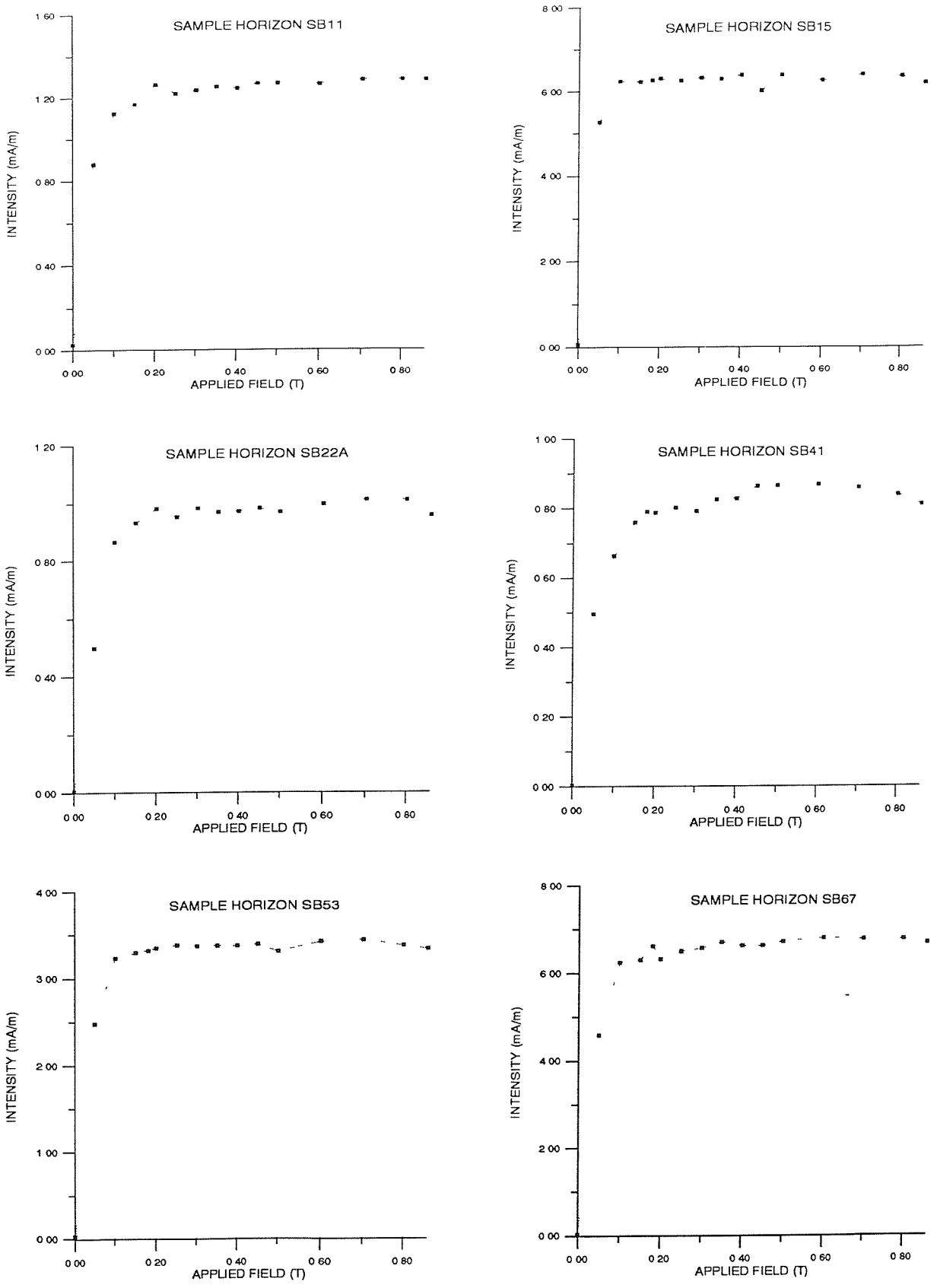

Figure 7.23. Examples of IRM acquisition curves whose shapes are diagnostic of titanomagnetite.

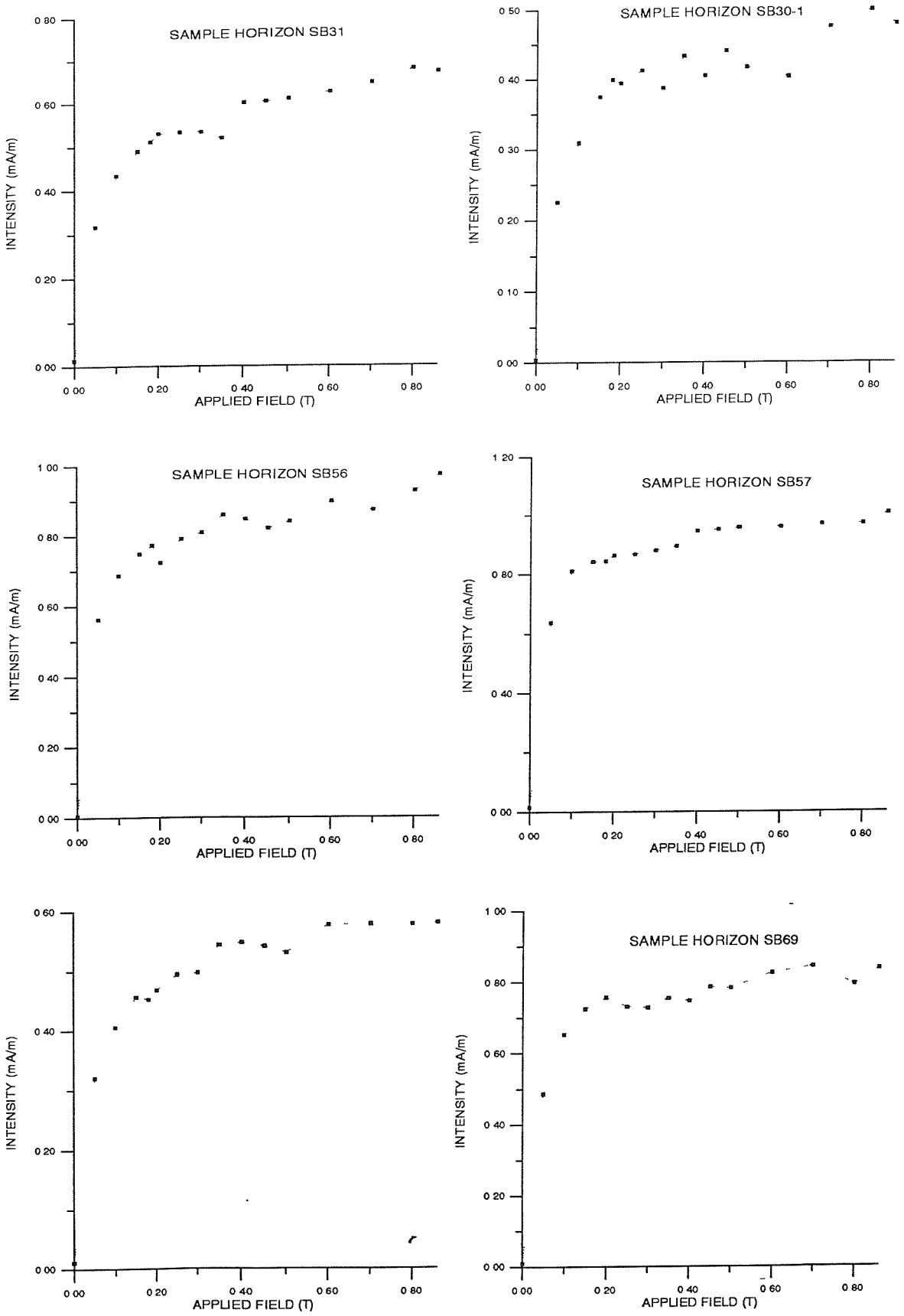

Figure 7.24. Examples of IRM acquisition curves whose shapes are diagnostic of a mixture of titanomagnetite and hematite.

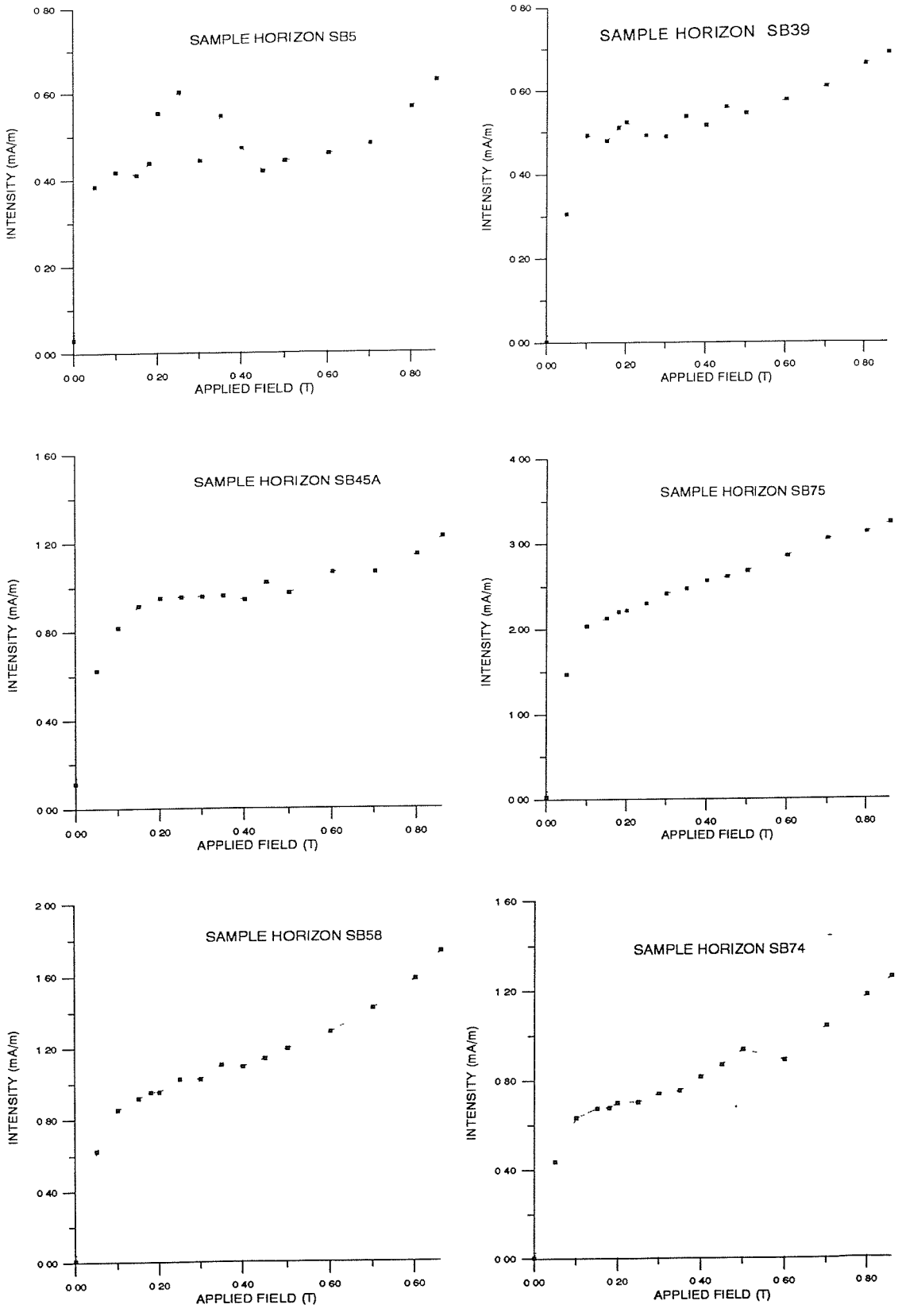

Figure 7.25. Examples of IRM acquisition curves whose shapes are diagnostic of hematite (with minor mixtures of titanomagnetite).

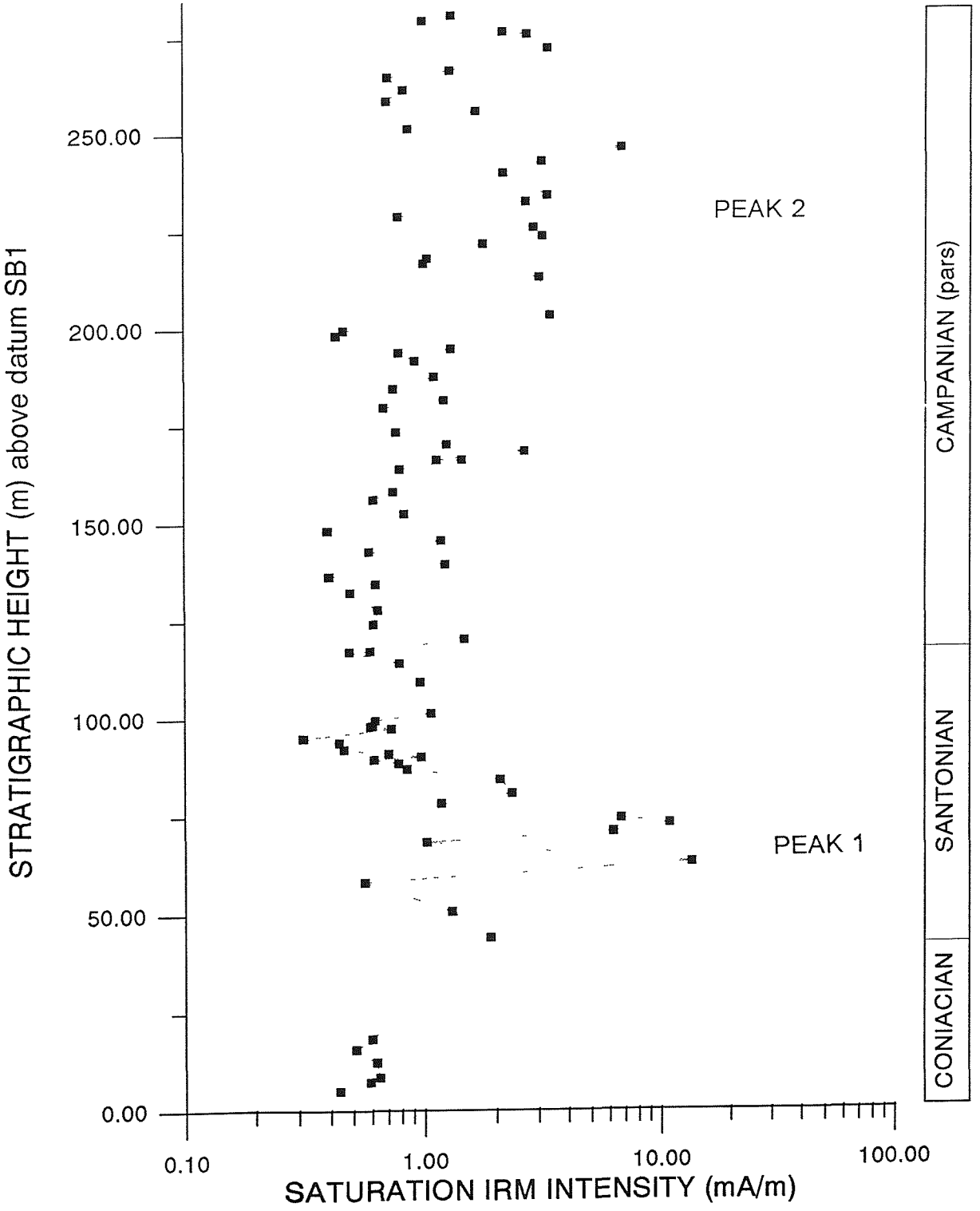

Figure 7.26. Variation of Saturation IRM with stratigraphic height above datum SB1. The right-hand column indicates the Late Cretaceous Stages represented by the Chalk succession at Culver Cliff (after Rawson et al. 1978).

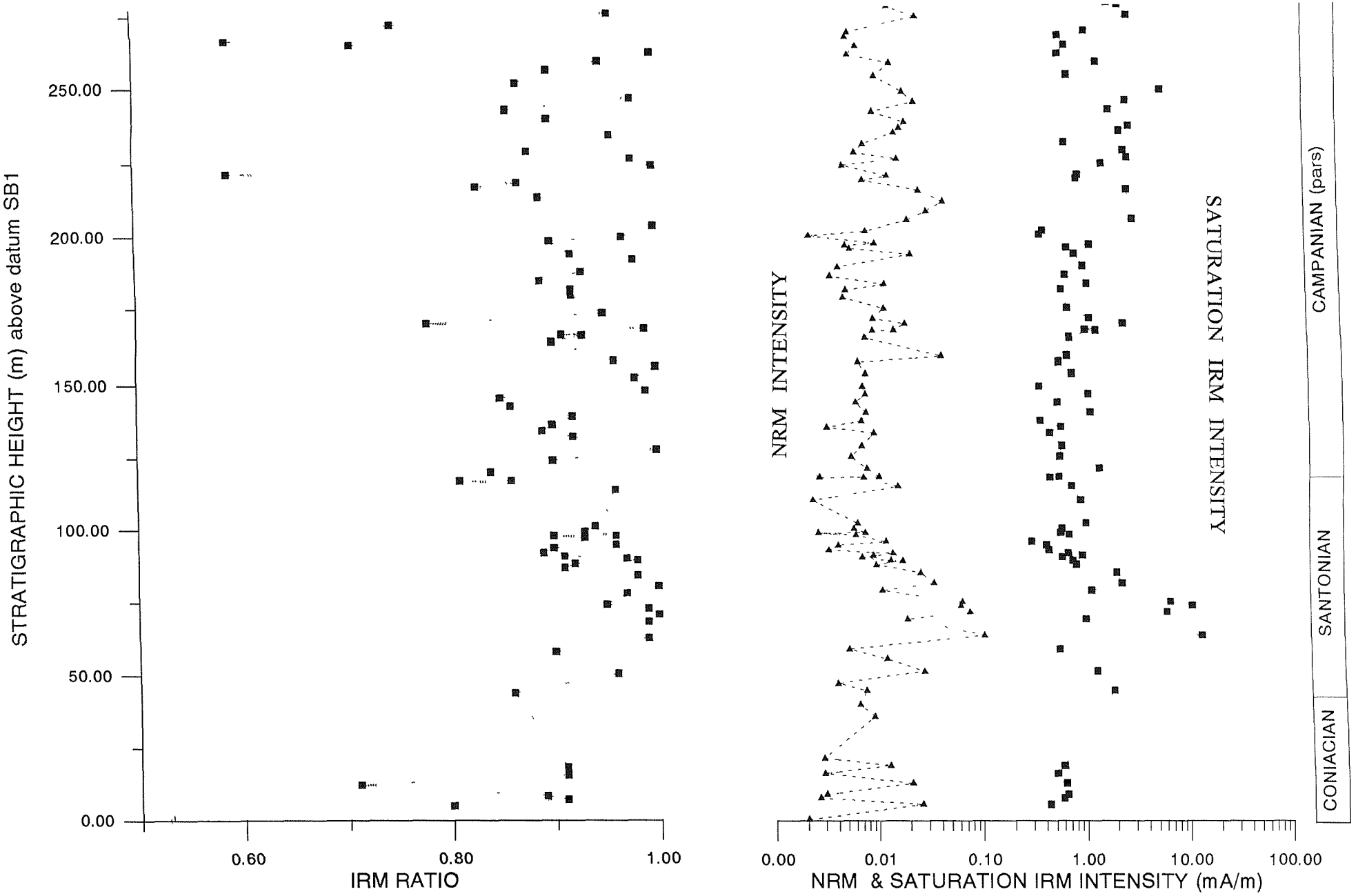

Figure 7.27. A plot of the IRM ratio log, NRM intensity and IRM_{sat} logs for Scratchell's Bay. A strong correlation can be seen between low IRM ratio values (hematite dominated sample horizons) and upper and lower limits of the successive peaks identified from the NRM and IRM_{sat} intensity logs.

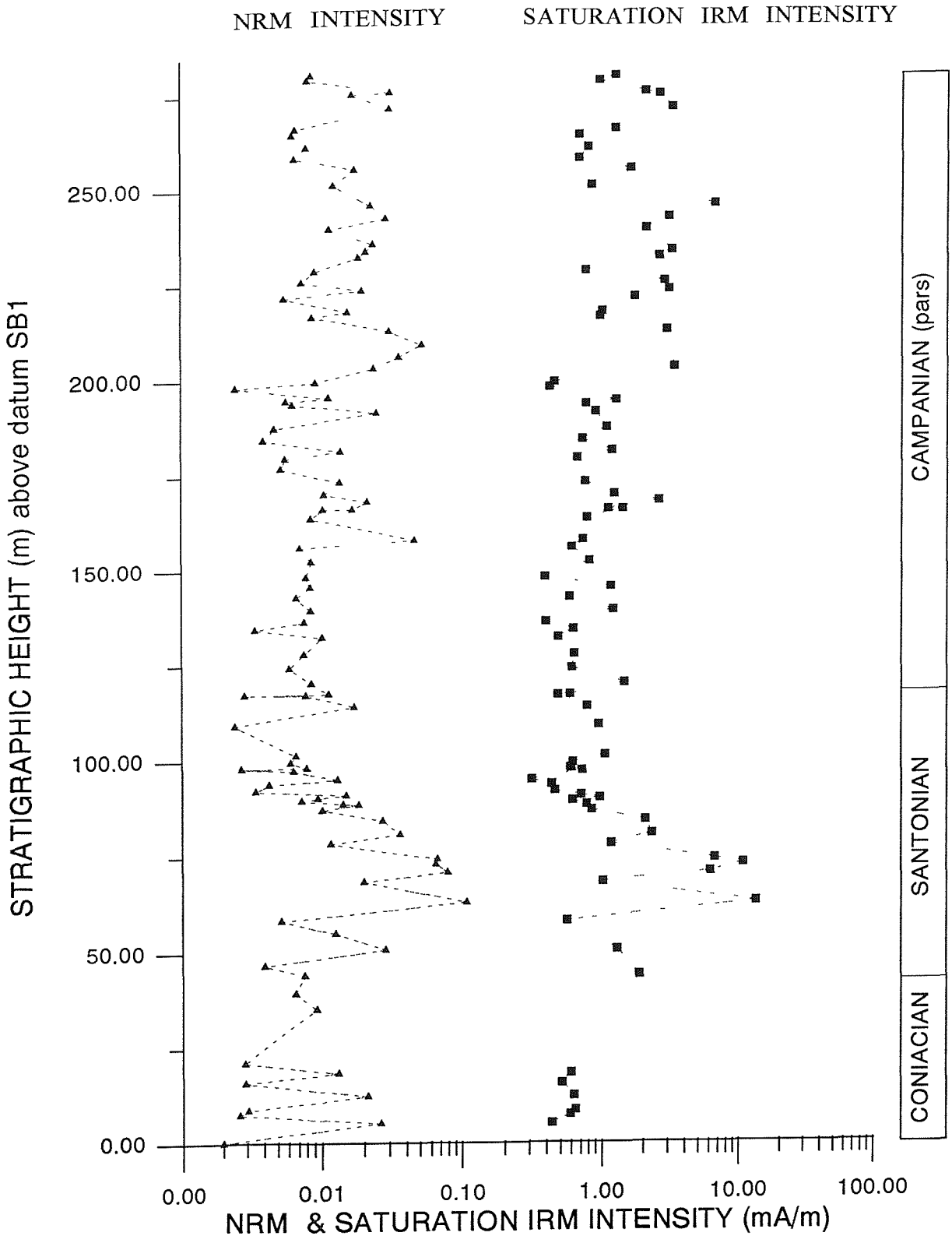

Figure 7.28. Variation of the mean NRM intensity and IRM_{sat} intensity with stratigraphic height above datum SB1. This datum occurs at the lowest sample horizon at Scratchell's Bay and lies approximately 20 metres above the Turonian-Coniacian boundary. The right-hand column indicates the Late Cretaceous Stages, based on Rawson *et al.* (1978) macrofossil zonation, represented by the Chalk succession at Scratchell's Bay.

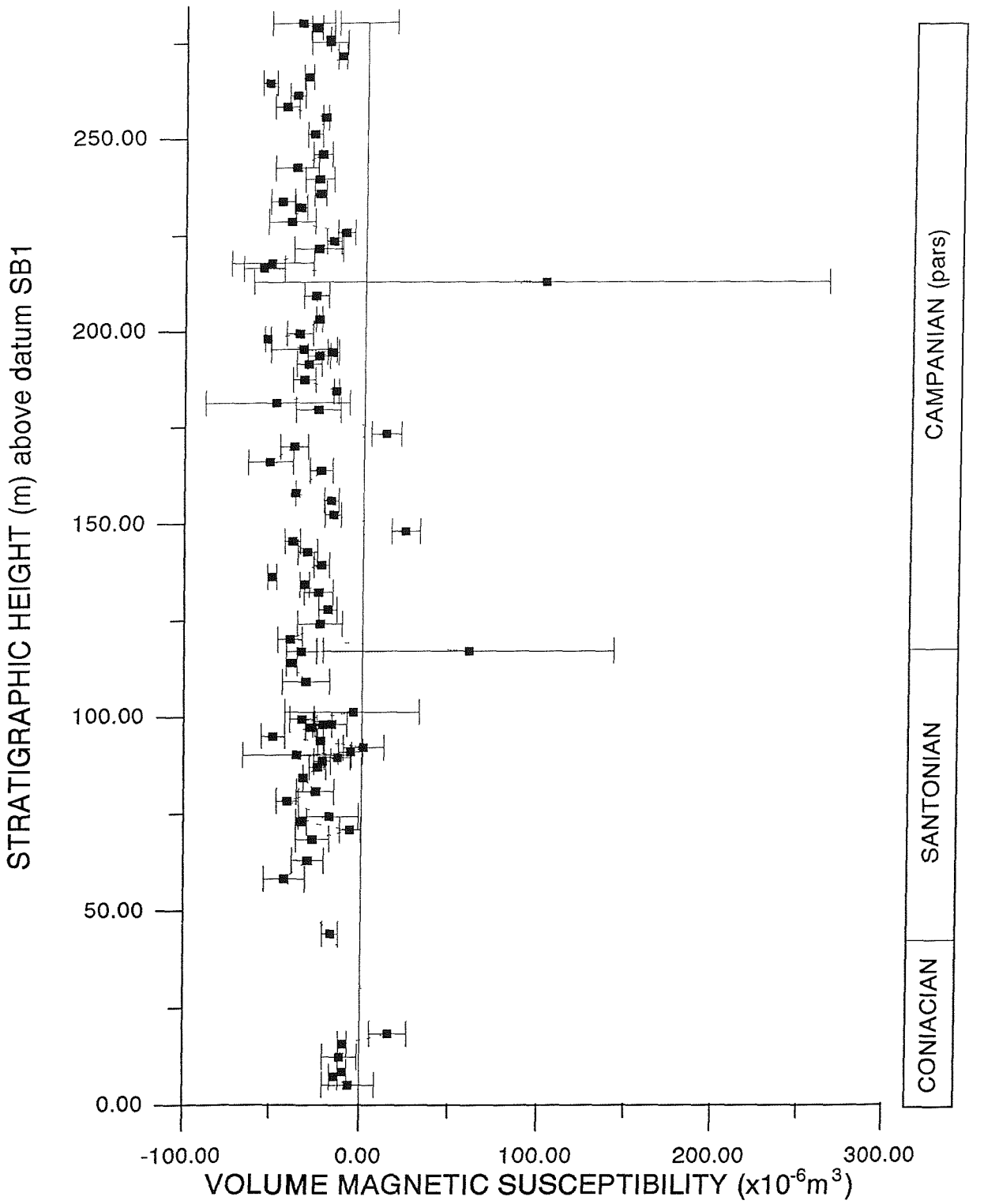

Figure 7.29. Variation of Volume Magnetic Susceptibility with stratigraphic height above datum SB1. The right-hand column indicates the Late Cretaceous Stages represented by the Chalk succession at Scratchell's Bay (Rawson *et al.*, 1978).

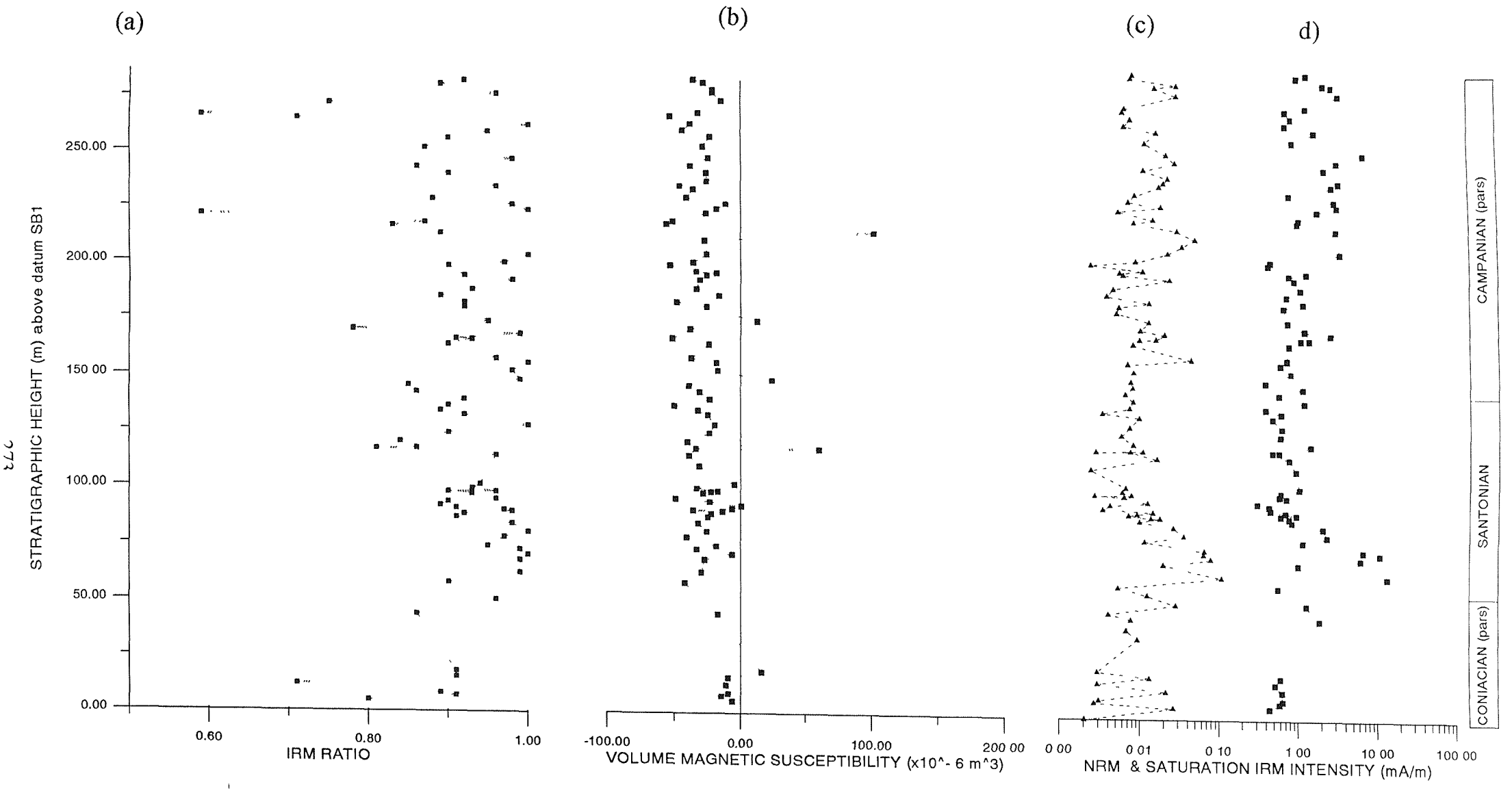

Figure 7.30. Diagram showing a) IRM ratio log; b) Volume Magnetic Susceptibility (VMS) log; c) NRM intensity log; and d) IRM_{sat} intensity log for Scratchell's Bay. Low IRM ratio values correspond with positive VMS readings, low NRM and low IRM_{sat} intensity values.

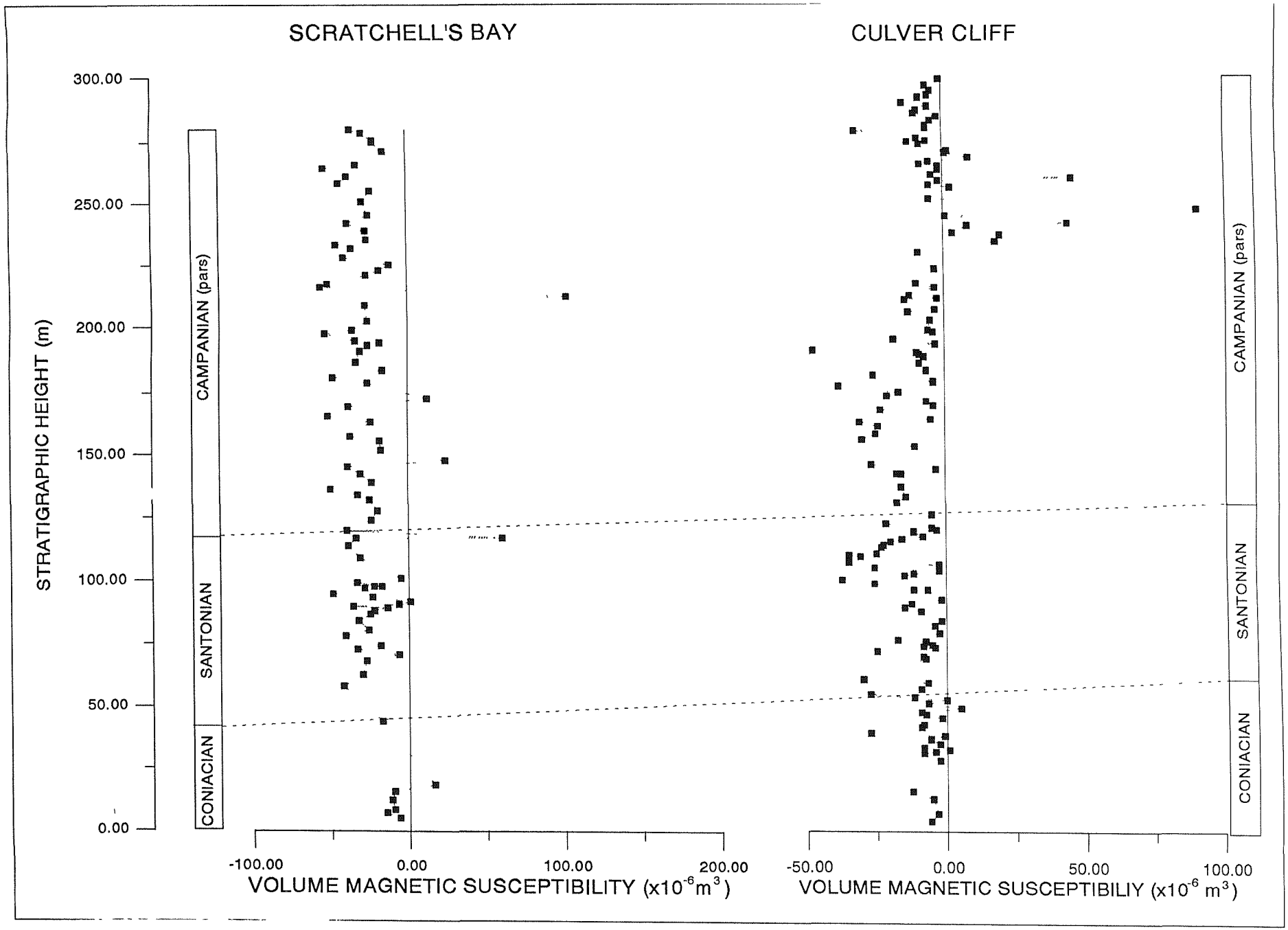

Figure 7.31. Correlation of volume magnetic susceptibility measurements from Scratchell's Bay and Culver Cliff. Such measurements proved unsuccessful in establishing worthwhile correlations between the two sections. No obvious correlations could be drawn.

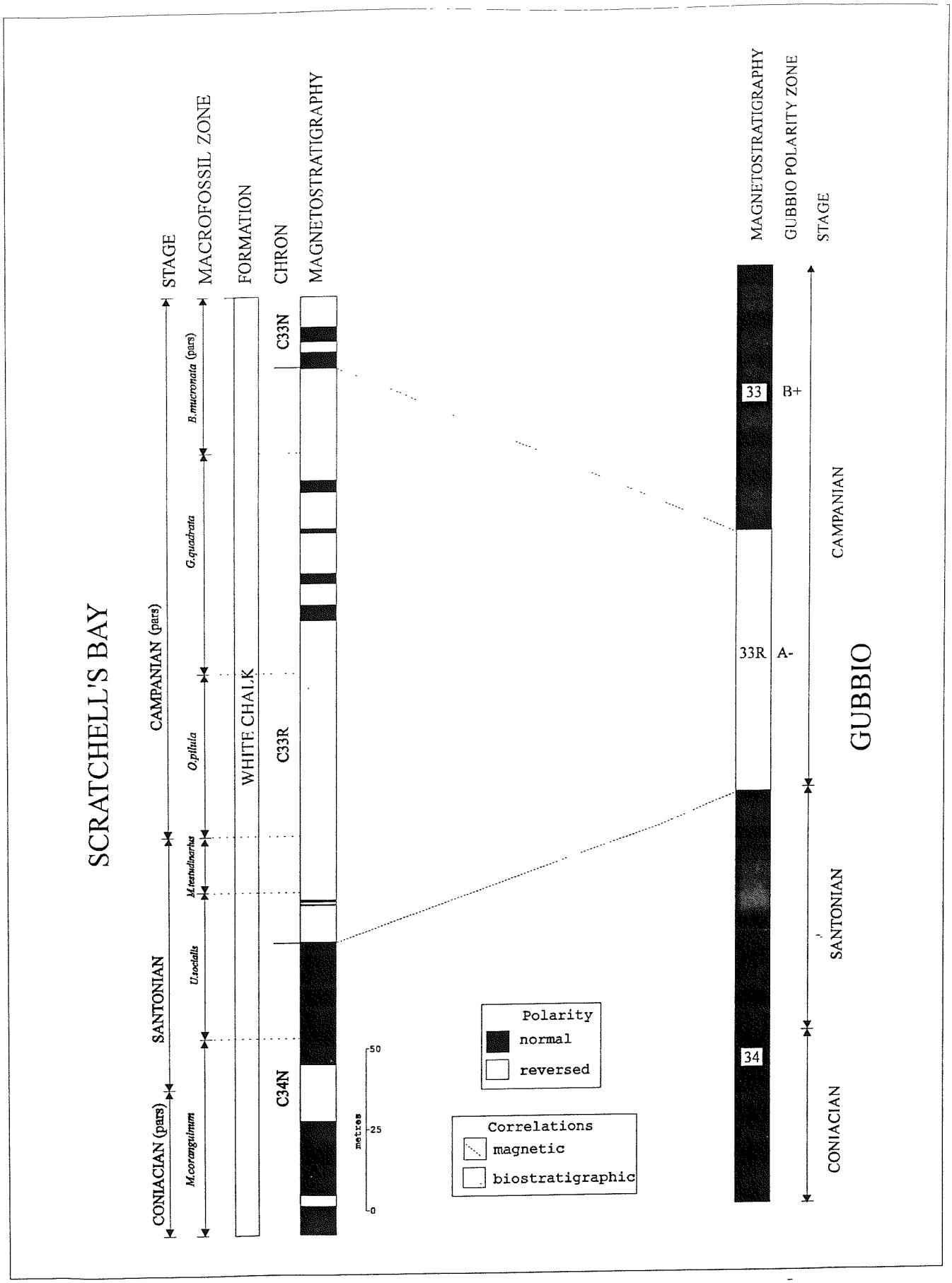

Figure 7.32. Correlation of magnetostratigraphic results from Scratchell's Bay, the Isle of Wight, with magnetostratigraphic results from Gubbio, northern Italy. The left hand side of the diagram shows Late Cretaceous Stage boundaries, macrofossil zones, geomagnetic polarity Chrons and the magnetostratigraphy determined for the study of Scratchell's Bay. The right hand side of the diagram shows the magnetostratigraphic results of Alvarez *et al.* (1977) study at Gubbio. Geomagnetic polarity Chrons are indicated, along with the polarity zones identified, and Late Cretaceous Stage boundaries.

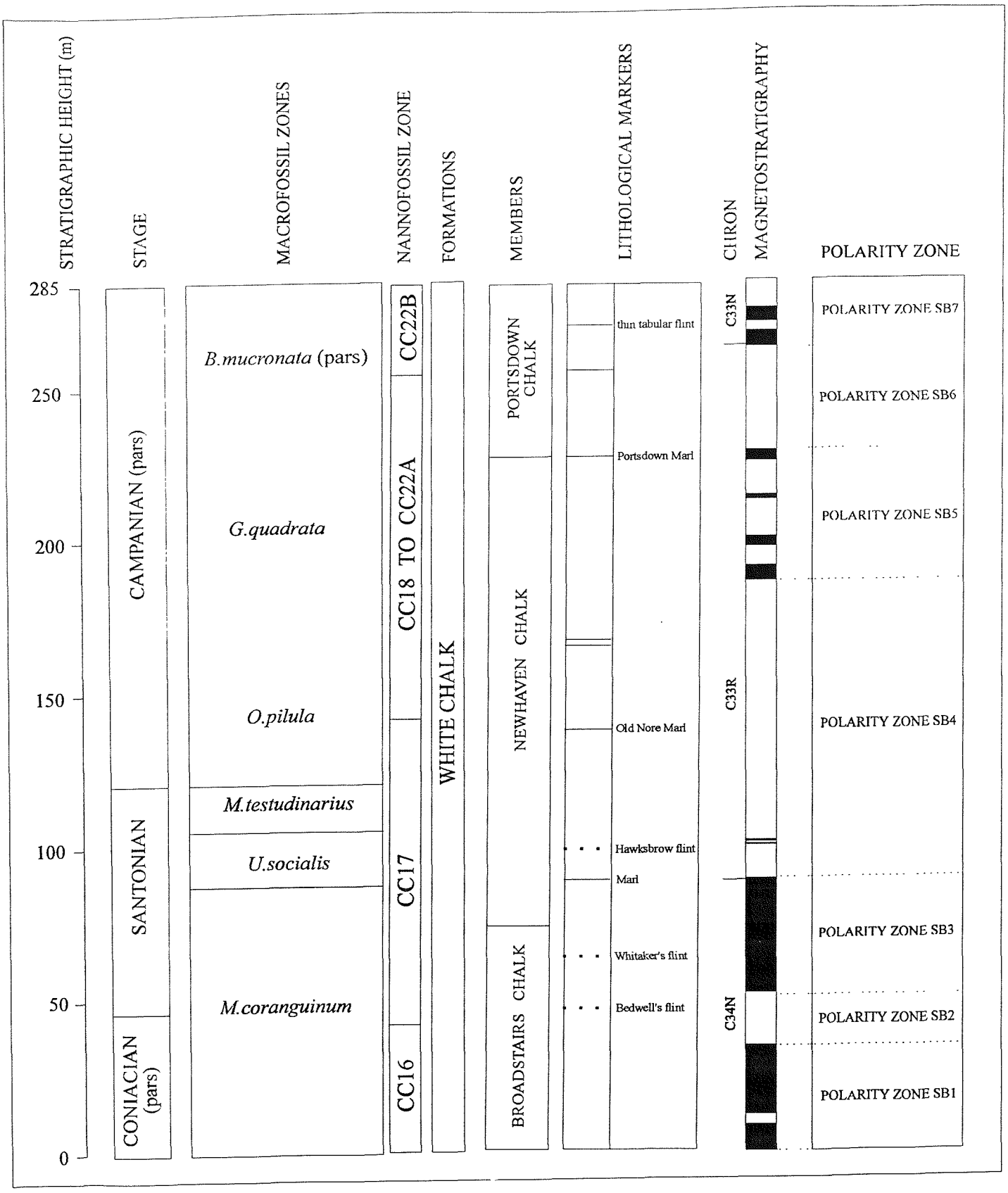

Figure 7.33. Summary diagram showing stratigraphical details of the Late Cretaceous Chalk sequence at Scratchell's Bay, the Isle of Wight. From left to right the diagram shows stratigraphic height above datum SB1 (approximately 20 metres above the Turonian-Coniacian boundary), Late Cretaceous Stages, macrofossil zones (Rawson *et al.*, 1978), nannofossil zones (Sissingh, 1978), formations, members, lithological markers, geomagnetic polarity Chrons, magnetostratigraphy and associated polarity zones.

	BEDDING CORRECTION	
HEIGHT (m)	STRIKE	DIP
0-82.0	270°	52°
82.0-92.5	264°	62°
92.5-167.5	265°	52°
167.5-194.0	260°	52°
194.0-227.0	260°	61°
227.0-257.0	264°	52°
257.0-272.5	265°	68°
272.5-285.0	264°	68°

Table 7.1. Bedding corrections for the Scratchell's Bay section, the Isle of Wight.

Chapter 8 Palaeomagnetic results from Coniacian-Late Campanian Chalk, Seaford Head, East Sussex, southern England

8.1 Introduction

The Late Cretaceous deposits exposed at Seaford Head (latitude=50.75°N, longitude=0.13°E), outcrop on the southern gently dipping limb of the Wealden anticline (Figure 8.1). The section ranges in age from early Coniacian to early Late Campanian and is represented by a condensed sequence of white chalks with black flints. This section offered a further opportunity to confirm the magnetostratigraphic results obtained from the Late Cretaceous deposits of the Isle of Wight. A preliminary magnetostratigraphic study was undertaken and the results from a 75 metre sequence of chalk deposits is presented.

8.2 Biostratigraphy

Both macrofossil (Rawson *et al.*, 1978) and nannofossil (Sissingh, 1978) zonations were determined, to provide a detailed stratigraphic framework within which to work. Dr. A. Gale provided the macrofossil biostratigraphy while Dr. J. Burnett developed a nannofossil biostratigraphy (Figure 8.2).

8.3 Stratigraphy

Lithological details of macrofossil zones proposed by Rawson *et al.* (1978) are presented in ascending stratigraphical order.

(a) Approximately 15 metres of the zone of *Micraster coranguinum* was sampled. The condition of exposed chalk surfaces was good. The chalk of this zone is smooth and massive with flint nodules occurring in numerous regular courses. Omission surfaces are visible within this zone.

(b) The *Uintacrinus socialis* Zone incorporates approximately 12 metres of chalk

containing regular courses of flint. The chalk of this zone is pure white in colour, compact and contains occasional marl seams. Flint bands are more widely spaced than in the *Micraster coranguinum* Zone.

(c) The zone of *Marsupites testudinarius* at Seaford Head consists of approximately 10 metres of chalk at Seaford Head. Lithologically, the chalk of this zone is similar to that of the preceding zone but contains only a few poorly developed flint bands. Marl seams are more common.

(d) The zone of *Offaster pilula* contains approximately 32 metres of chalk with numerous marl seams and courses of nodular flints.

(e) The chalk of the zone of *Gonioteuthis quadrata* is massive, white and traversed by tiny veins of marl. Larger scale marl seams and flint-courses are abundant; the flints being mostly black and solid, and large in size. At Seaford, only 20 metres of this zone is present due to erosion during the Tertiary. The chalk of this zone is discoloured by the weathering of the overlying Tertiary sediments. The uppermost limit of the zone is marked by an uncomfortable boundary with the Tertiary strata.

8.4 Structural history

The Chalk of Seaford Head lies on the southern limb of the Wealden anticline (Figure 8.3) and dips at approximately 16° with an approximately east-west strike (254°).

8.5 Palaeomagnetic results

Palaeomagnetic data from Seaford Head are summarised in Appendix C, Table 1 which includes details of every horizon sampled at this locality and lists details of all the specimens studied.

The magnetic polarity stratigraphy of Seaford Head is graphically summarised in the polarity log of Figure 8.4.

8.5.1 Natural Remanent Magnetisation

Figures 8.5 shows the variation of NRM intensities with stratigraphic height above a datum marked by Whitaker's 3-inch Flint band (Jenkyns *et al*, 1994). The top of the plot coincides with sample horizon SF1, the uppermost sampling horizon of the Seaford Head section, which lies 15 metres below the unconformable Cretaceous-Tertiary boundary.

Plotted NRM intensities are based on average values determined for each sample horizon. Values lie in the range 0.0017-0.0204 mA/m. The overall log mean NRM intensity for the section is 0.0079 mA/m. The highest NRM intensity measured for an individual specimen was 0.0433 mA/m from sample level SF12. The mean NRM value for this horizon was 0.0173 mA/m which is approximately an order of magnitude greater than the mean for the whole section.

No obvious cycle pattern can be inferred from the variation in the mean NRM intensity log. However, extreme fluctuations in magnetic intensity occur on a small scale which probably reflect variations in magnetic mineral content.

8.5.2 Stability of magnetisation

Specimens from each stratigraphic level were subjected to incremental demagnetisation analysis. To establish the optimum procedure, samples were subjected to both incremental alternating field (AF) demagnetisation and thermal demagnetisation.

8.5.2.1 AF demagnetisation

Virtually all of samples studied during the palaeomagnetic investigation of the Seaford Head section had extremely weak NRM intensities. Sixty percent of the samples possessed NRM intensities lower than 0.01 mA/m. For such weakly magnetised samples AF demagnetisation, at 2.5 mT or 5.0 mT steps, was employed. Sample SF7-C provides a typical example of chalk sample behaviour when subjected to this

treatment. After AF demagnetisation treatment and application of a bedding correction the sample shows a directional trend which can be extrapolated to a reversed polarity (southerly declination, negative inclination) end point (Figure 8.6). The remaining 40% of the samples had magnetic intensities of 0.05 mA/m or less. Due to difficulties in undertaking thermal demagnetisation of such weakly magnetised samples, AF treatment was used as the main form of demagnetisation treatment. However, thermal demagnetisation procedures were adopted for representative samples from 13 of the 21 sample horizons collected at Seaford.

8.5.2.2 Thermal demagnetisation

Thermal demagnetisation steps of NRM, 100, 150, 200, 250, 300°C, etc. were employed for this study (Figure 8.7). Seventy percent of the thermally demagnetised samples exhibited erratic behaviour (Figure 8.8) while 15% of the samples show low quality directional trend data (Figure 8.9). Poor quality stable end points were seen in the remaining 15% (Figure 8.10).

8.5.3 Reliability categories

The palaeomagnetic data obtained from the demagnetisation of samples from Seaford Head can be placed in reliability categories. These categories have been previously discussed and illustrated in Section 5.8.

Out of 102 specimens analyzed, demagnetisation stable end points were attained by 23% of the samples. However, only 7% belonged to the S1 category (Figure 8.11), 9% to category S2 (Figure 8.12), and 7% to category S3 (Figure 8.13). Directional trends were recognised in 60% (Figures 8.14; 8.15 & 8.16) of the samples demagnetised while less than 1%, possessed a recent geomagnetic field direction overprint (Figure 8.17a & b). 'T1-quality' trends accounted for 11%, 'T2-quality' trend data 32% and 'T3-quality' 17% of the analyzed samples. Erratic behaviour during demagnetisation was observed in 17% of the samples (Figure 8.18). The main reason for trend data providing the most significant contribution towards the palaeomagnetic

data set for chalk from Seaford Head is because of its extremely weak magnetic intensity. Long before a stable end point is reached during demagnetisation the sample's intensity drops below the background noise level of the magnetometer.

8.5.4 Age of remanence

8.5.4.1 Bedding Corrections

The deposits at Seaford Head outcrop on the southern limb of the Wealden Anticline and dip at approximately 16° and strike at approximately 254°. This average value is based on 30 separate measurements of bedding and has an alpha-95 value of 4.8° (Figure 8.19).

Where strata dip at high angles, application of a tectonic correction can assist in discriminating magnetic components acquired before tilting from those gained after tilting. However, it is less easy to discriminate between pre-tilt and post-tilt magnetic components in strata dipping at shallow angles.

Figures 8.20a & b. show the effect the bedding correction for Seaford Head has on the magnetization vectors of two chalk samples. In Figure 8.20a. the bedding correction of 254°/16° has been applied for sample SF5-D. The stable characteristic magnetization of the sample prior to application of the bedding correction represents a magnetic field direction of negative inclination and northerly declination. However, after correction the magnetic vector is rotated by only a very small amount. Prior to correction, this sample displays a possible directional trend towards reverse polarity. However, after correction the vector moves further away from the typical reverse polarity direction. Figure 8.20b. shows sample SF12-C before and after the same tectonic correction. Before bedding correction, the magnetic vector indicates a normal polarity, which is maintained after correction. The sample may display either a primary remanence representing the Late Cretaceous geomagnetic field direction or alternatively have acquired a secondary normal geomagnetic field overprint at some later instance in time. The bedding correction applied to the Seaford Head section is

thus unable to distinguish between pre-tilt and post-tilt magnetic components within the chalk. Thus, an important objective in the interpretation of palaeomagnetic data (i.e. to establish whether the components of remanent magnetisation identified in the rock represent primary magnetisation and to resolve the instances in the rock's past when other magnetic components were acquired) cannot be accomplished for most samples at this locality. However, the observed corrected declination/inclination of 5.4°/50.0° for sample SF12-C is closer to the expected declination/inclination of 359.8°/56.2° (based on the geomagnetic field direction predicted for southern England during the Late Cretaceous using the palaeomagnetic pole of Heller & Channell (1979)) than the uncorrected value of 16.8°/64.4°.

8.5.4.2 Fold test

No fold test can be applied to the palaeomagnetic data from Seaford Head due to the similarity of dip throughout the whole section.

8.5.4.3 Consistency

Identification of a corresponding direction of magnetisation in rock units of comparable age over a wide area implies that the magnetisation is stable, and dates from the time of formation of the rock or, at least, the time of a notable re-magnetisation event. Furthermore, where a specific sequence of magnetic polarity reversals can be recognised in several different sections of the same formation over a wide area, and these sequences display a sound correlation, it is highly likely that the magnetisation in primary (Hailwood, 1989).

Thus, the high level of consistency between the magnetostratigraphic results from Culver Cliff and Scratchell's Bay (Isle of Wight) with those from Seaford Head can be taken as evidence that the magnetisation in all these sections is primary.

8.5.5 Remagnetisation

Less than 1% of the samples from Seaford Head (actually 1 sample) analyzed during this study exhibited a magnetic overprint which could not be removed by using either A.F. or thermal demagnetisation procedures. However, due to the very limited size of the data-set no inferences can be drawn concerning the origin and time of acquisition of the magnetic overprint.

8.5.6 Magnetic polarity

The tilt-corrected SCM declination and inclination values described by incremental demagnetisation are plotted as a function of stratigraphic height above Whitaker's 3-inch flint band in Figure 8.4.

Polarity is based on a combination of demagnetisation stable end points and observation of directional trends during demagnetisation. The succession can be divided into three polarity intervals (Figure 8.21). These are, in ascending stratigraphic order:

a) **Polarity zone SF1.** A 10 metre thick reverse polarity interval (lower *M. coranguinum* Zone) representing part of Chron C34N.

b) **Polarity zone SF2.** A 12 metre normal polarity interval (upper *M. coranguinum* to lower *U. socialis* Zone) representing Chron C34N.

c) **Polarity zone SF3.** A 55 metre zone of reverse polarity (upper *U. socialis* to lower *G. quadrata* Zone) representing Chron C33R.

8.5.7 A Late Cretaceous palaeomagnetic pole for East Sussex, southern England

The directions of 10 'S1/S2 reliability' category vectors from Seaford Head are shown on an equal-area stereographic projection in Figure 8.22 (inset) together with the

overall mean 'S1/S2' category vector (declination=323°, inclination=49°, k=13.8, alpha-95=13.5°. From the mean magnetic vector a palaeomagnetic pole of 55.5°N 247.2°E, with quality factor, Q, equal to 4, was determined for the Coniacian-Late Campanian strata of Seaford Head. Only four of the seven criteria listed by van der Voo (1988) are fulfilled. A well-constrained biostratigraphic age, based on macrofossils, has been determined for the Chalk sequence at this locality. However, a large diecrepancy exists between the macrofossil and nannofossil age of these sediments. The palaeomagnetic-pole has been generated from 10 'S1/S2 reliability' category specimens and has a precision 'k' value greater than 10 with a 95% confidence angle of 13.5°. A fold test was not applied. However, the chalk succession at Seaford Head does show magnetostratigraphic consistency with the other sections studied in southern England. Tectonic coherence and good structural control have been documented by earlier workers for the Late Cretaceous of southern England (e.g. Chadwick, 1993). Four of the ten 'S1/S2' category specimens exhibit reverse polarity while the remaining samples are characterised by normal polarity. As a result, four antipodal reverse polarity magnetic vectors were used to insure a good time average of the geomagnetic field. However, this data set is defined exclusively from AF demagnetised samples. Three of the reliability criteria of van der Voo (1988) are thus failed.

From the mean ChRM inclination value of 49°, determined from the 'S1/S2 reliability category' data set, a palaeolatitude of 29.9±14°N is estimated for southern England during Coniacian-Late Campanian times. However, the predicted palaeolatitude places southern England at a palaeolatitude of 36.8±3°N during this time interval. A discrepancy of approximately 7° exists between the observed and expected palaeolatitudes. Within the experimental uncertainties (i.e. alpha 95=13.5°) the discrepancy must be regarded as insignificant.

As previously mentioned the Late Cretaceous system of northern Europe lacks reliable palaeomagnetic-pole data. However, the low quality palaeomagnetic-pole derived for Seaford Head should be treated with caution due to the low Q value obtained. The interpretation of this pole position is discussed further in Chapter 9.

8.6 Isothermal remanence

As at Culver Cliff and Scratchell's Bay, isothermal remanence experiments were carried out to gain an insight into the magnetic mineralogy of the remanence carrier in the chalk of Seaford Head.

8.6.1 IRM ratio

By determining the IRM ratio for all the sample horizons an IRM log of the Seaford Head section is presented (Figure 8.23). The majority of samples (52%) studied exhibit IRM ratios of 0.9 or above. A further 19% of the curves possessed IRM ratio values of 0.89. The remanent magnetism of the chalk at this locality can therefore be attributed either to the presence of titanomagnetite or maghemite.

8.6.2 IRM curves

IRM experiments carried out on AF demagnetised Chalk specimens suggest the presence not only of titanomagnetite but mixtures of hematite and magnetite. Magnetite-type IRM curves were observed in 52% of the samples studied (Figure 8.24), while curves indicative of magnetite and hematite mixtures represent 38% (Figure 8.25). Dominantly hematite-type IRM curves (with small admixtures of magnetite) were found in only 10% of the specimens studied (Figure 8.26).

8.6.3 Saturation IRM

Figure 8.27 shows a plot of IRM_{sat} versus stratigraphic height above Whitaker's 3-inch flint band. Two IRM_{sat} intensity peaks were identified at sample horizons SF11 and SF2A. These peaks probably represent mineralogy and magnetic mineral content. However, from Figure 8.28, no correlation can be seen between low IRM ratio values (hematite dominated sample horizon) and low NRM and IRM_{sat} intensity. Moreover, no obvious correlation can be drawn between the NRM intensity log and the IRM_{sat} intensity log (Figure 8.29). The curve representing IRM_{sat} intensity is approximately

2 orders of magnitude greater than the NRM intensity curve suggesting the presence of multi-domain titanomagnetite (NRM/IRM_{sat} ratio<0.1, Collinson, 1983).

8.7 Volume magnetic susceptibility measurements

Volume magnetic susceptibility measurements were carried out on large Chalk samples ($150cm^3$) to supply an additional possible means of correlating between Chalk sequences. Most of the chalk samples measured displayed diamagnetic behaviour. The extremely low content of strongly magnetizable ferromagnetic and moderately magnetizable paramagnetic minerals would generate only a very weak magnetic susceptibility signal. Chalk is composed almost entirely of biogenic calcium carbonate (98% in Late Cretaceous chalks, Hancock 1975) and as a result the few magnetisable minerals present would be swamped by the diamagnetic behaviour of the nannofossil micrites. Sample horizon SF2A displayed ferromagnetic or paramagnetic behaviour Figure 8.30 shows a log of volume magnetic susceptibility measurements against stratigraphic height. The curve exhibits some indication of cyclic fluctuation. This fluctuation may represent periodic changes in the ferromagnetic or paramagnetic mineral content of the chalk at Seaford Head, possibly as a result of changes in influence of terrigenous material. The positive VMS reading for sample SF2A (Figure 8.31d) corresponds with a IRM ratio value which signifies the presence of magnetite or a titanomagnetite (Figure 8.31a). A correlation of this horizon with high NRM and IRM_{sat} intensity values can also be observed (Figure 8.31b). The relationship between 'hematite-rich' horizons (Figure 8.31a), NRM intensity (Figure 8.31b) and saturation IRM intensity (Figure 8.31c) is less obvious. Nevertheless, an association does appear to exist; lower NRM intensity corresponds to higher concentrations of hematite. A similar correlation between the IRM_{sat} curve (Figure 8.31c) and the IRM ratio curve (Figure 8.31a) can be inferred.

No obvious correlations can be drawn between the Scratchell's Bay, Culver Cliff and Seaford sections using volume magnetic susceptibility measurements (Figure 8.32). Diamagnetic biogenic micrites form the major constituents of English chalk and as a result dominant VMS measurements. Volume Magnetic Susceptibility measurements

are therefore not recommended as a means of correlation between chalk sequences.

8.8 Conclusions

Results from Seaford Head suggest that a reverse polarity magnetozone is present within the chalk of this locality representing magnetochron C34N (Figure 8.33).

The boundary between magnetochron C34N and C33R is correlated with the interval between sampling levels SF16 and SF18 (Figure 8.3a, 20 metres above Whitaker's 3-inch flint and within the *U. socialis* Zone) with the overlying 55 metres of chalk defining a portion of Chron C33N (reverse polarity zone Gubbio A-). The chalk below sample horizon SF16 represents magnetochron C34N. Within this normal polarity magnetozone a reverse polarity interval was detected incorporating sample horizons SF18A and SF19.

From previous palaeomagnetic investigations of sedimentary sequences of equivalent age to the English Chalk (e.g. Alvarez *et al.*, 1977) and the examination of the Late Cretaceous marine magnetic anomaly record (e.g. Cande & Kent, 1992) Chron C34N was considered to be represented exclusively by normal polarity. However, the English chalk of Scratchell's Bay, Culver Cliff and Seaford Head have revealed the presence of reverse polarity intervals within this period of time. These are all located within the macrofossil zone *M. coranguinum*.

The same explanation, used to account for the magnetostratigraphic results from Culver Cliff and Scratchell's Bay, can be invoked to explain the occurrence of the previously undetected reverse polarity subzone within the Seaford Head section.

Though the 75 metres of sampled Chalk outcrop at Seaford represents a condensed sequence, when compared to Scratchell's Bay and Culver Cliff, it still represents a higher rate of sedimentation than equivalent aged strata at Gubbio. In excess of 75 metres of early Lower Campanian-late Upper Santonian Chalk outcrops at the Seaford Head section, compared with only 75 metres of limestone representing the whole of

the Campanian stage at Gubbio. A large portion of the Campanian stage is not present at Seaford Head, due to the widespread erosion prior to the deposition of the oldest Tertiary strata. Thus at Gubbio approximately 100 metres of sediment represents the Santonian to Campanian stages while at Seaford Head 75 metres of chalk represent just the Late Santonian to early-Late Campanian stages (Figure 8.34). This accounts for the improved magnetostratigraphic resolution at Seaford Head.

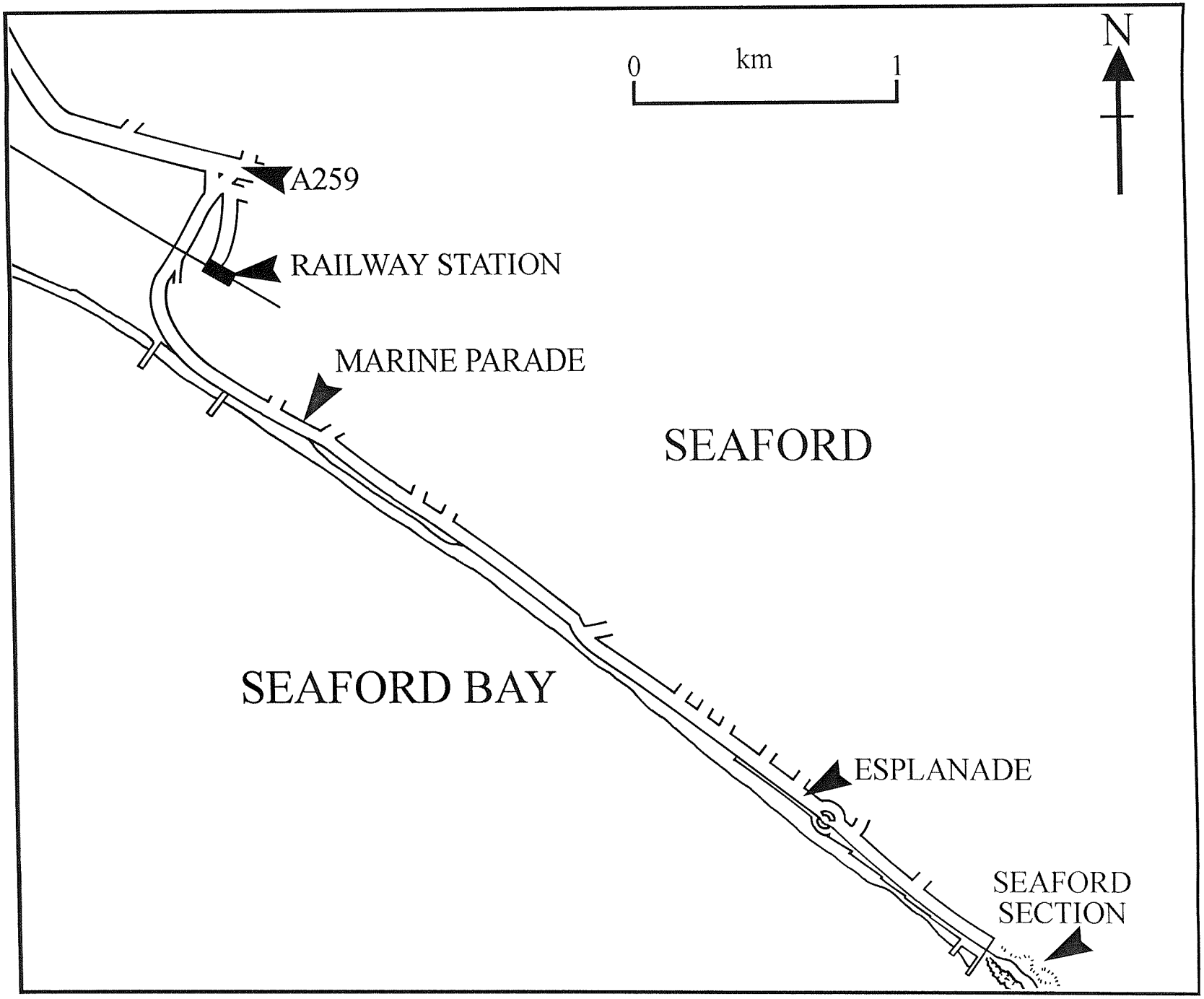

Figure 8.1. Location map of the Seaford Head section.

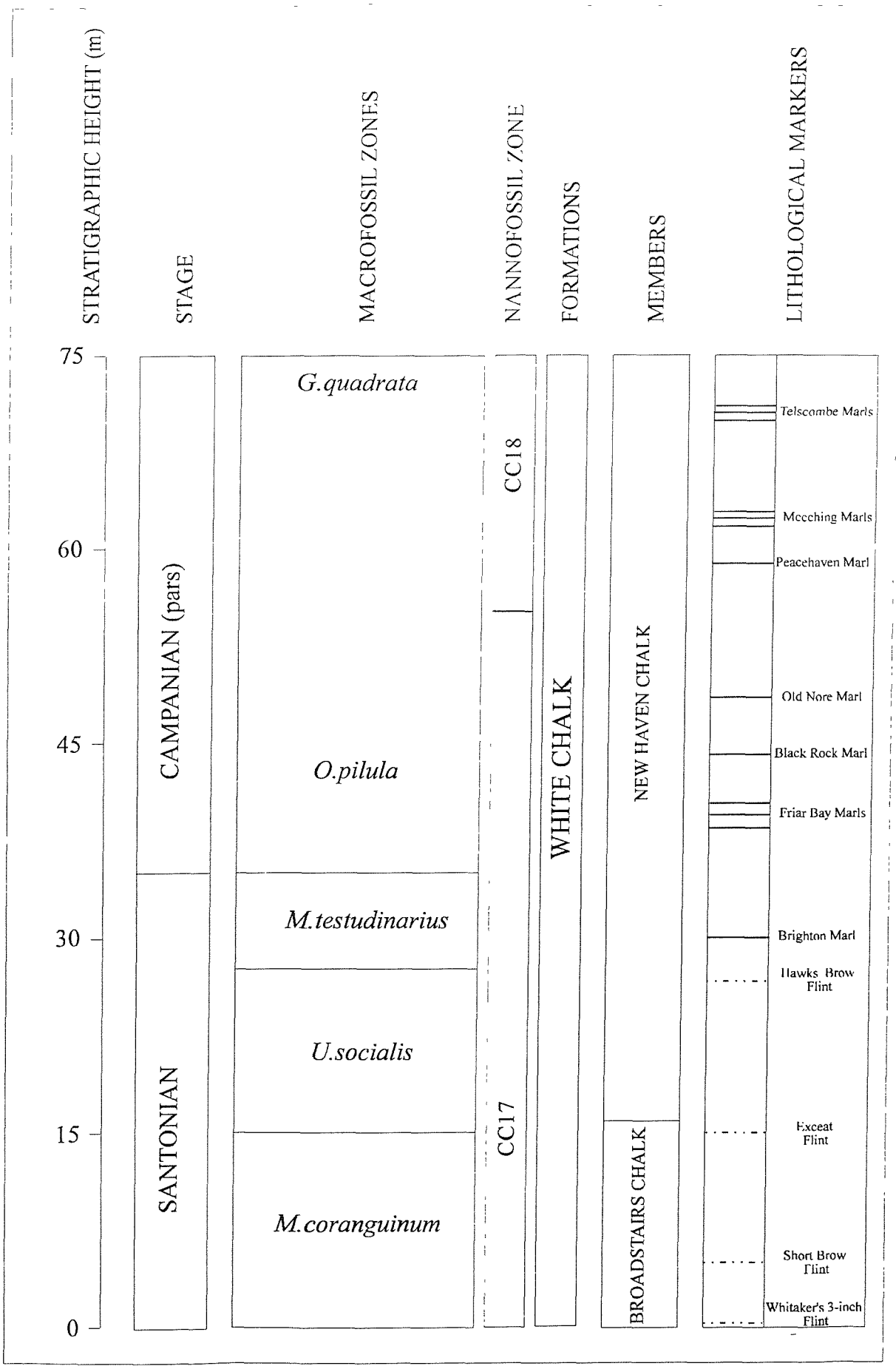

Figure 8.2. Summary diagram showing stratigraphical details of the Late Cretaceous Chalk sequence at Seaford Head, East Sussex. From left to right the diagram shows stratigraphic height above Whitaker's 3-inch Flint, Late Cretaceous Stages, macrofossil zones (Rawson *et al.*, 1978), nannofossil zones (Sissingh, 1978), formations, members and lithological markers.

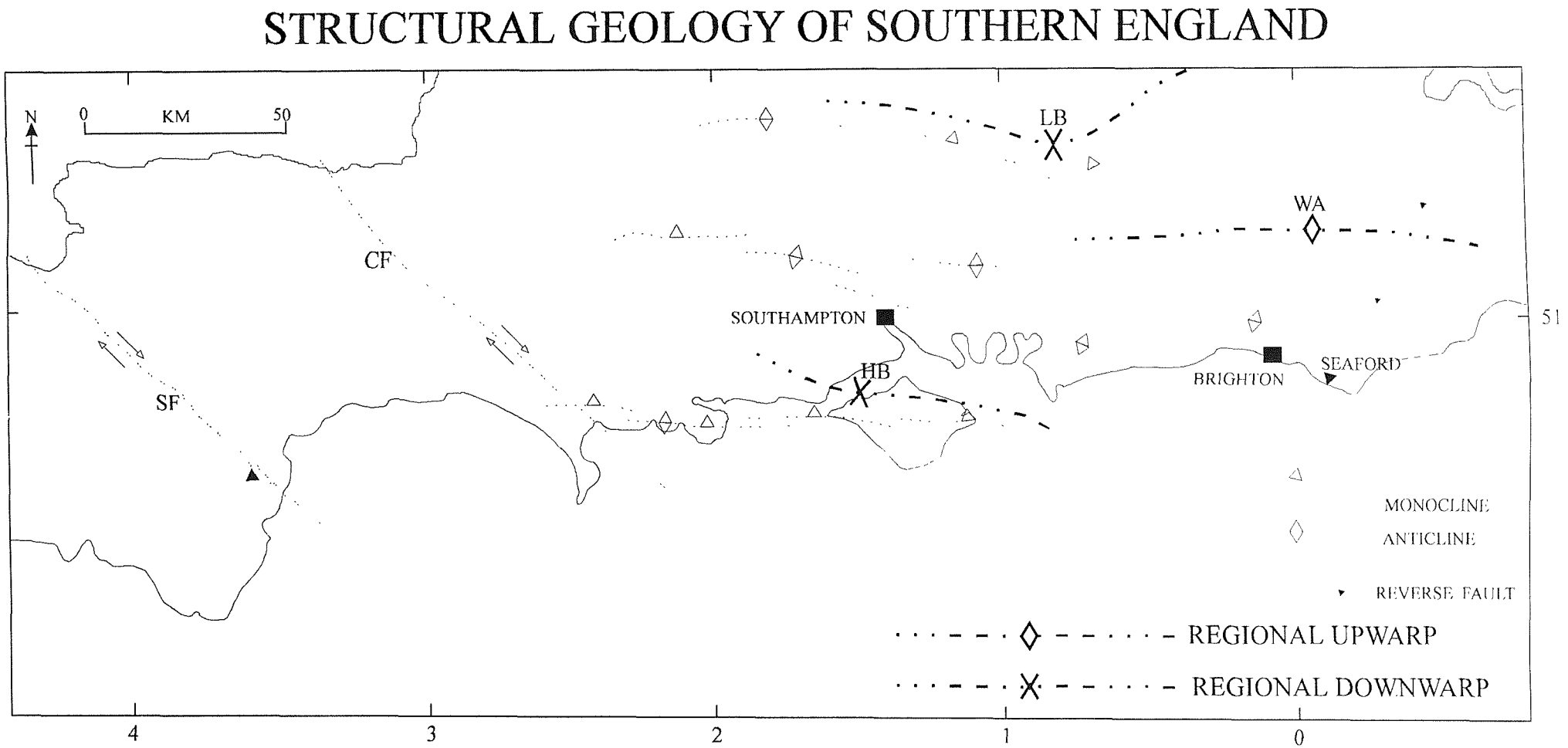

Figure 8.3. Principal inversion structures of the Wessex Basin. Abbreviations: LB, London Basin; WA, Weald Anticline; HB, Hampshire Basin; SF, Sticklepath-Lustleigh fault; and CF, Cothelstone-Hatch fault (from Chadwick, 1993).

Figure 8 4a & b The magnetic polarity stratigraphy of the Seaford Head section From left to right the diagram shows, i) stratigraphic height in metres, ii) Late Cretaceous Stages, iii) biostratigraphic macrofossil zones (Rawson *et al*, 1978), iv) biostratigraphic nannofossil zones (Sissingh, 1977); v) sampling levels, vi) geomagnetic polarity definition (black=normal, white=reverse, light shading=mixed and dark shading=intermediate); vii) the stratigraphic variation of the declination of characteristic remanent magnetisation (ChRM), viii) the stratigraphic variation of the mean natural remanent magnetisation intensity (solid square symbol), ix) the stratigraphic variation of IRM ratio (solid triangle symbol).

On the right hand side of the diagrams are three columns which, from left to right present, i) the reliability category of the SCM, ii) the fraction of the samples demagnetised which support the definition of polarity and; iii) the demagnetisation procedure employed to specify the polarity. Where polarity definition is based solely on directional trends, a ChRM vector is generated by great circle intersection. However, where directional trends do not produce intersection points a token declination/inclination vector (i e. reverse polarity=180°/-90°; normal polarity=360°/90°) is adopted.

a)

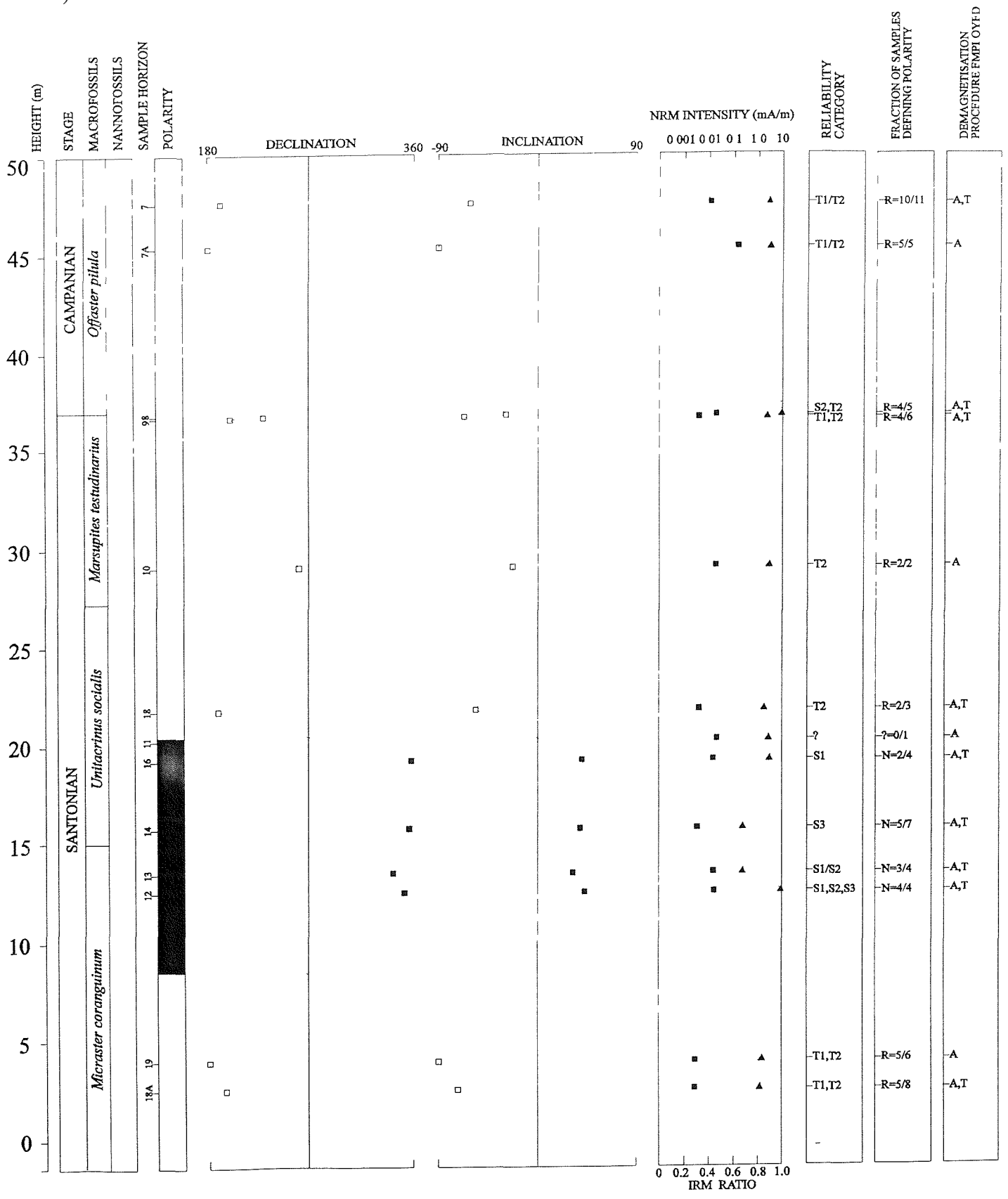
HEIGHT (m)
STAGE
MACROFOSSILS
NANNOFOSSILS
SAMPLE HORIZON
POLARITY
DECLINATION
INCLINATION
NRM INTENSITY (mA/m)
RELIABILITY CATEGORY
FRACTION OF SAMPLES DEFINING POLARITY
DEMAGNETISATION PROCEDURE FMPI OYHD
CAMPANIAN
SANTONIAN
Offaster pilula
Marsupites testudinarius
Uintacrinus socialis
Micraster coranguinum
IRM RATIO
T1/T2
T1/T2
S2,T2
T1,T2
T2
T2
?
S1
S3
S1/S2
S1,S2,S3
T1,T2
T1,T2
R=10/11
R=5/5
R=4/5
R=4/6
R=2/2
R=2/3
?=0/1
N=2/4
N=5/7
N=3/4
N=4/4
R=5/6
R=5/8
A,T
A
A,T
A,T
A
A,T
A
A,T
A,T
A,T
A,T
A
A,T

b)

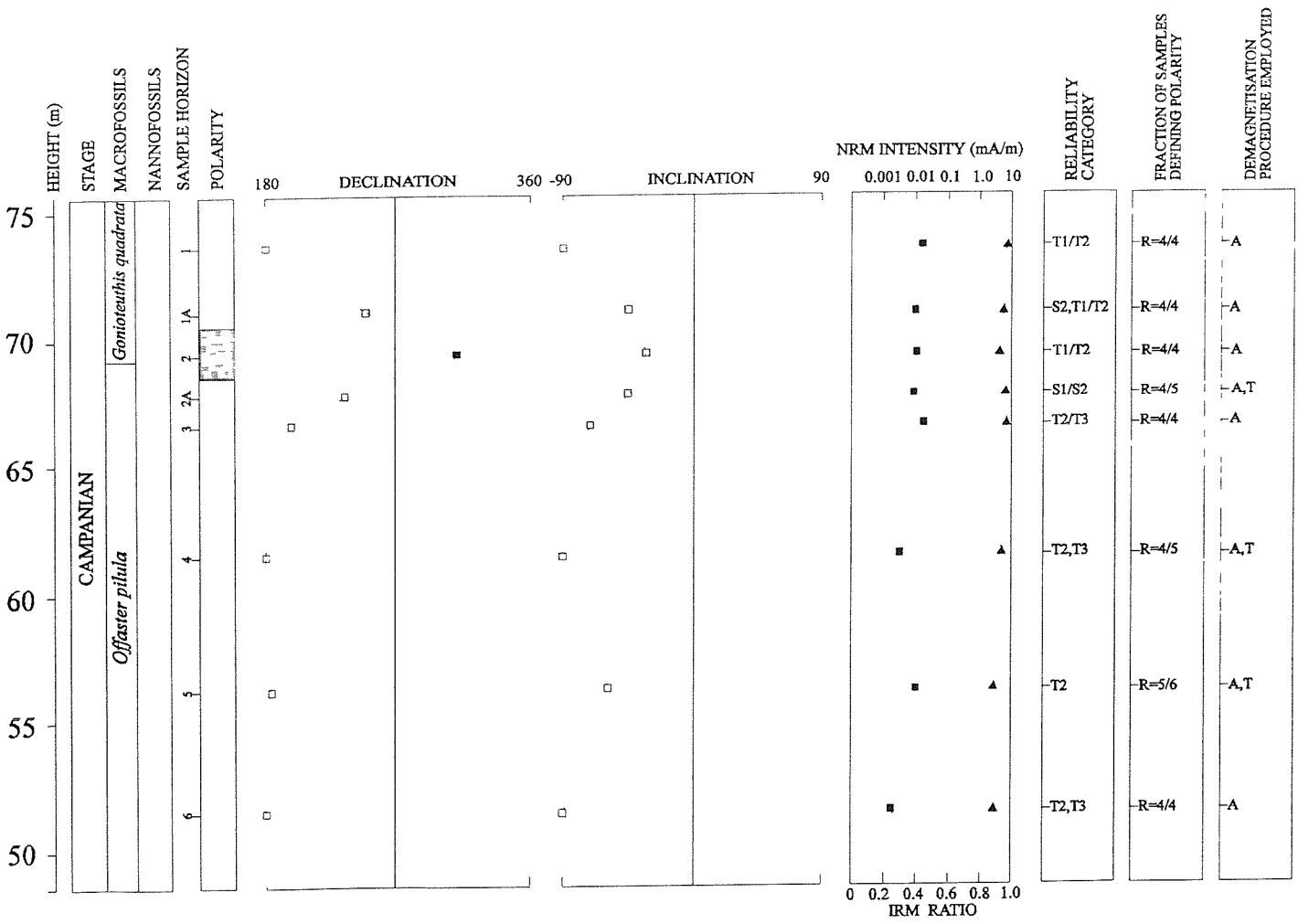
HEIGHT (m)
STAGE
MACROFOSSILS
NANNOFOSSILS
SAMPLE HORIZON
POLARITY
DECLINATION
INCLINATION
NRM INTENSITY (mA/m)
RELIABILITY CATEGORY
FRACTION OF SAMPLES DEFINING POLARITY
DEMAGNETISATION PROCEDURE EMPLOYED
CAMPANIAN
Gonioteuthis quadrata
Offaster pilula
180
360
-90
90
0.001 0.01 0.1 1.0 10
0 0.2 0.4 0.6 0.8 1.0
IRM RATIO
75
70
65
60
55
50
1
1A
2
2A
3
4
5
6
T1/T2
S2,T1/T2
T1/T2
S1/S2
T2/T3
T2,T3
T2
T2,T3
R=4/4
R=4/4
R=4/4
R=4/5
R=4/4
R=4/5
R=5/6
R=4/4
A
A
A
A,T
A
A,T
A,T
A

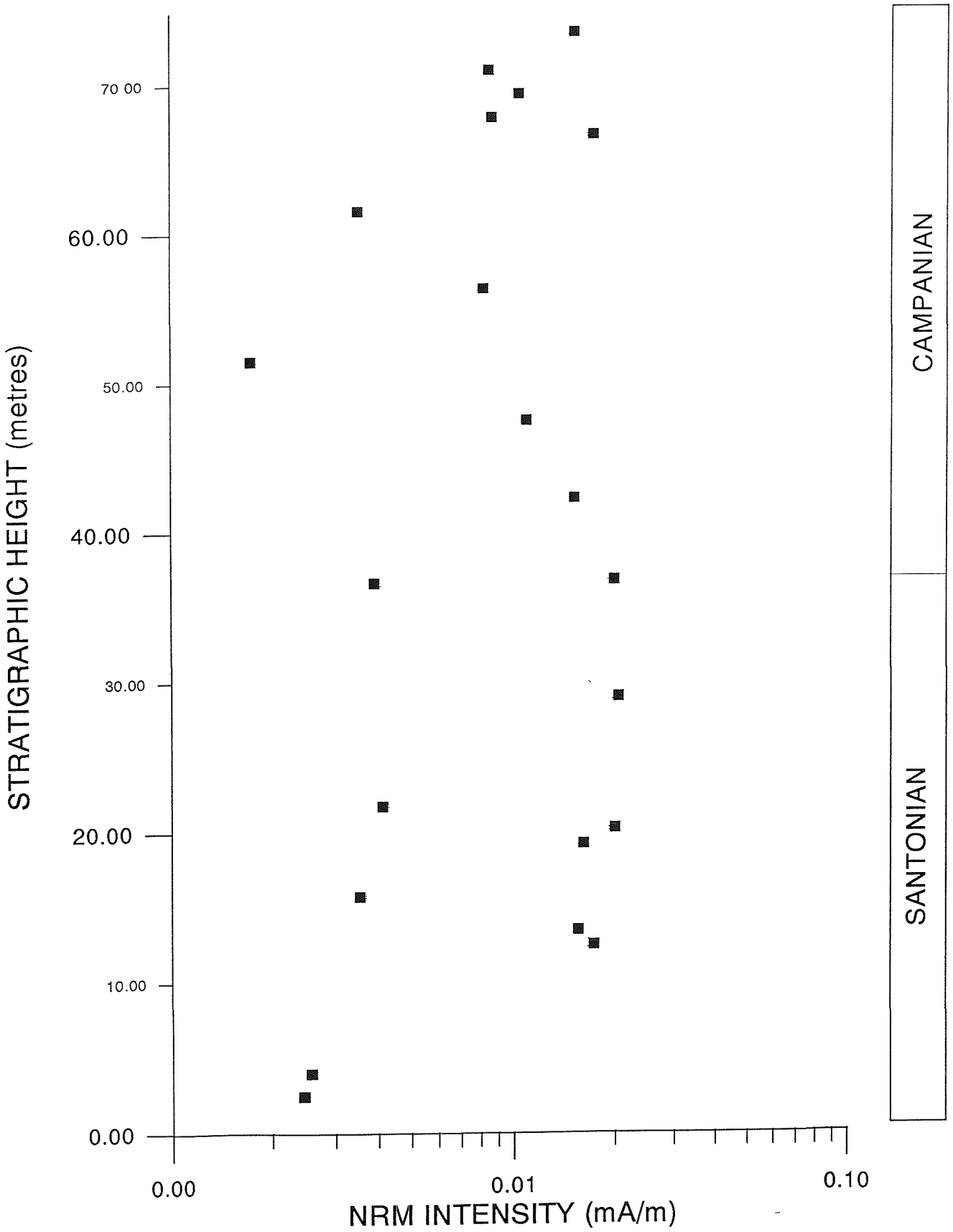

Figure 8.5. Variation of mean NRM intensity with stratigraphic height above Whitaker's 3-inch Flint band. The right-hand column indicates the Late Cretaceous Stages of the Chalk succession at Seaford Head (Rawson *et al.*, 1978).

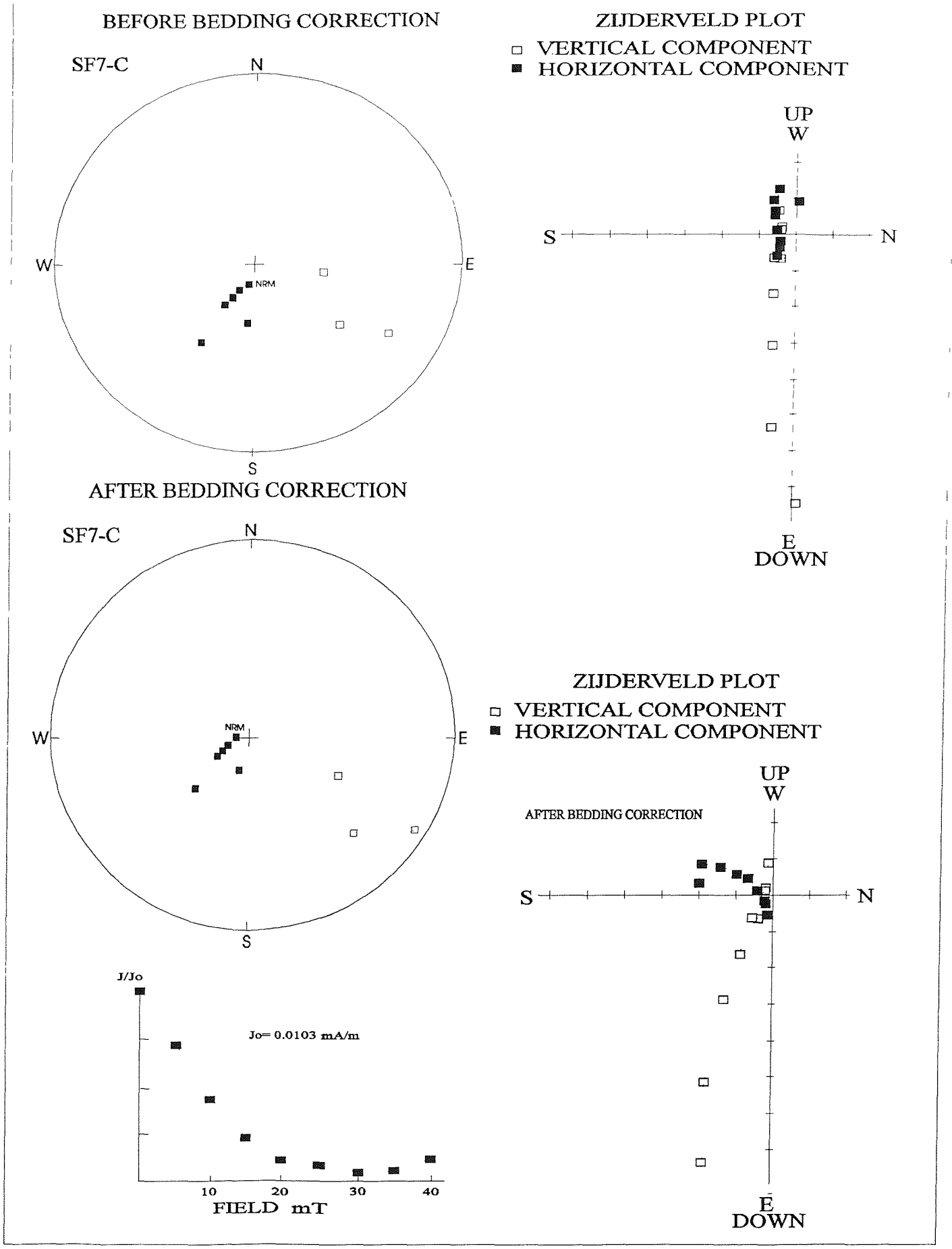

Figure 8.6. A typical example of the behaviour of a chalk sample from Seaford Head when subjected to A F demagnetisation. Sample SF7-C is shown before and after application of a bedding correction of 254°/16°.

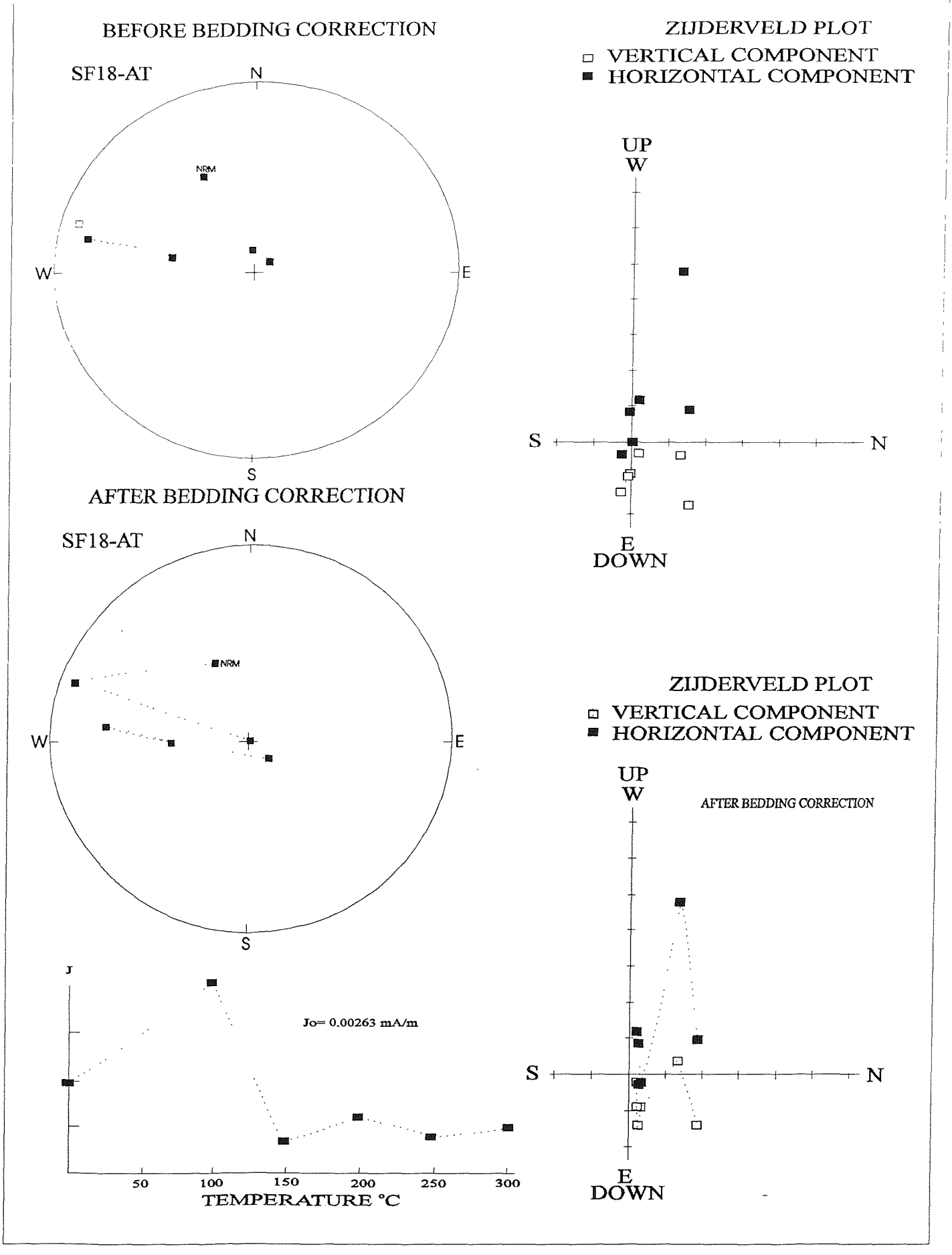

Figure 8.7. A typical example of the behaviour of a chalk sample from Seaford Head when subjected to thermal demagnetisation. Sample SF18-AT is shown before and after application of a bedding correction of 254°/16°.

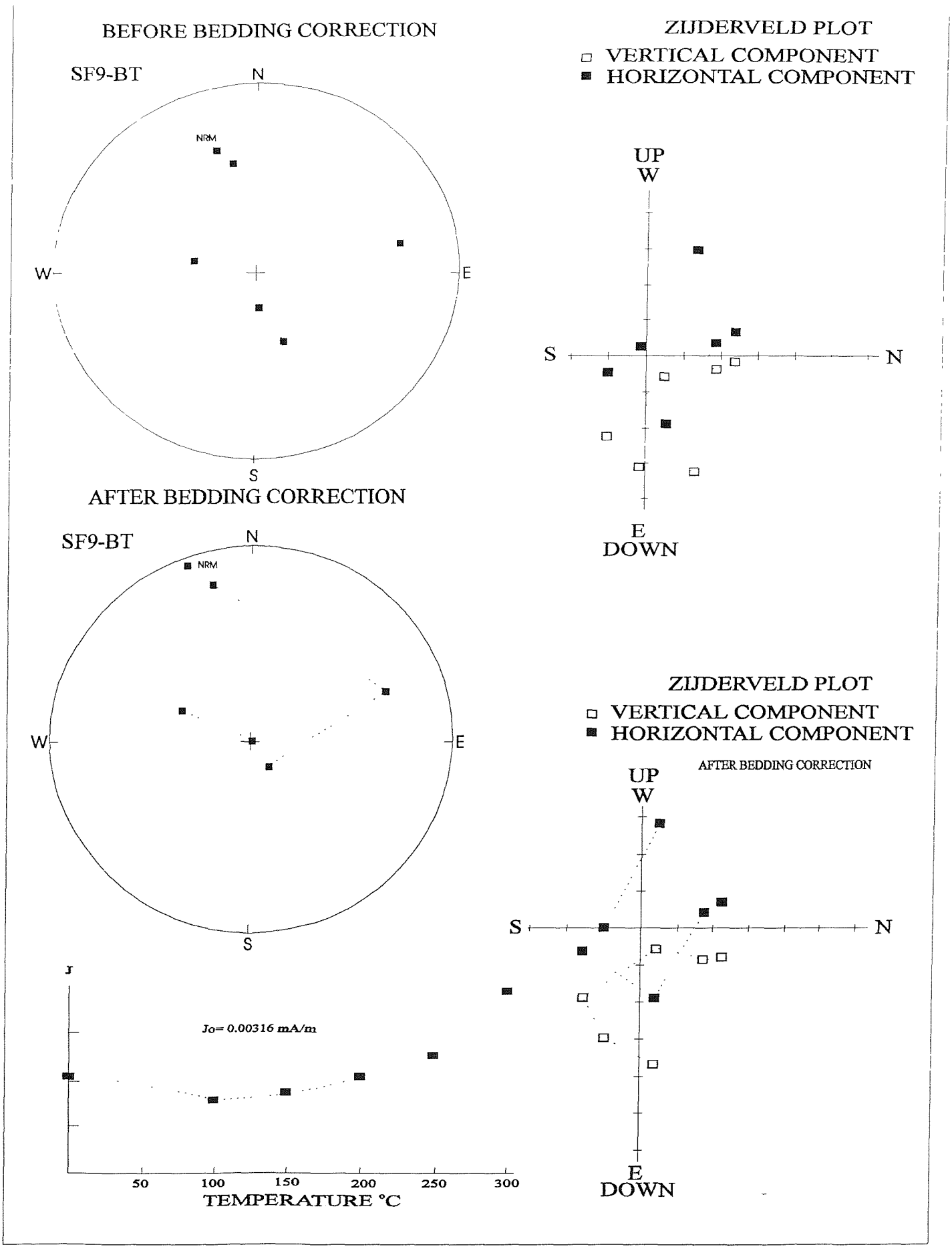

Figure 8.8. A typical example of erratic behaviour of a chalk sample from Seaford Head when subjected to thermal demagnetisation. Sample SF9-BT is shown before and after application of a bedding correction of 254°/16°.

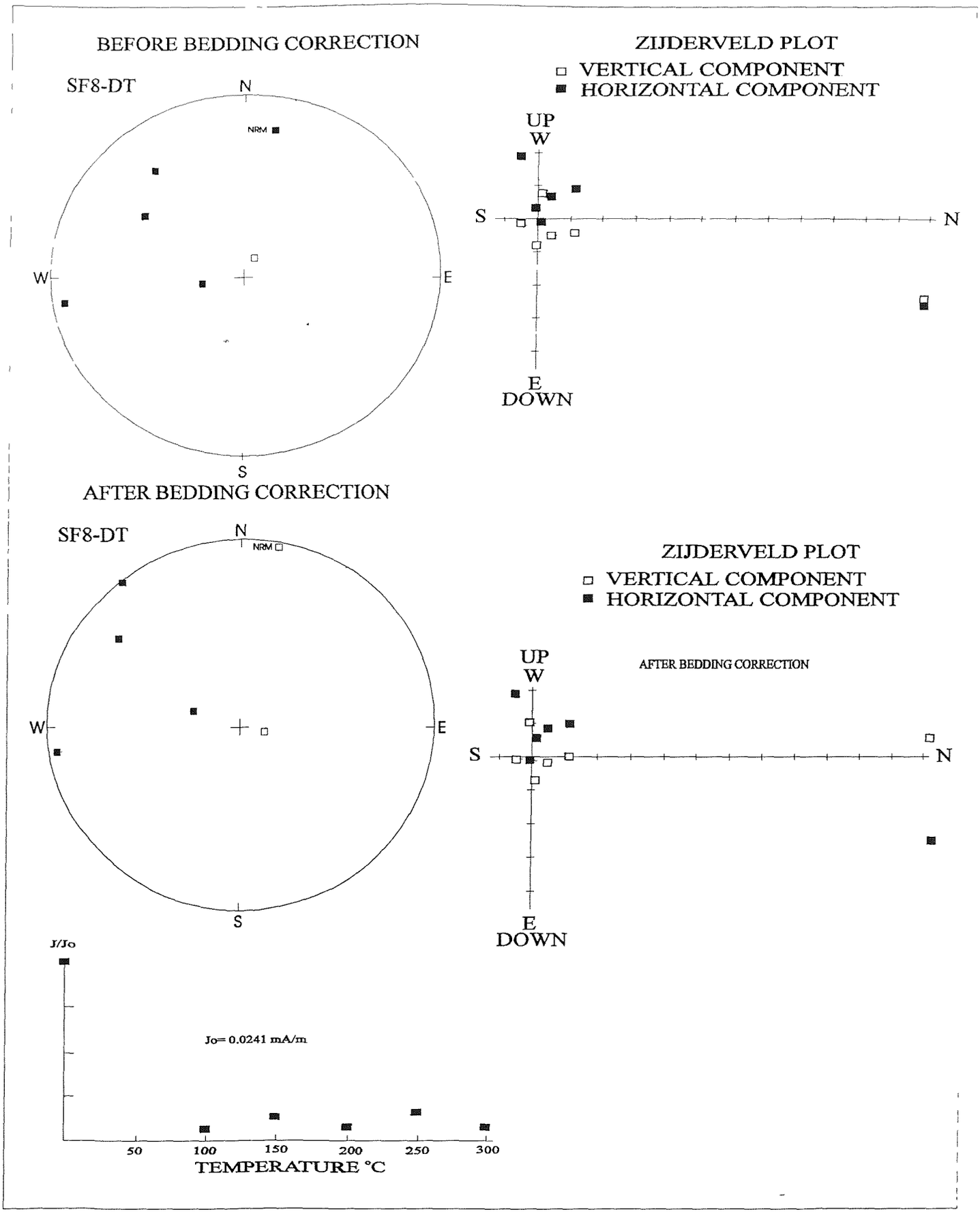

Figure 8.9. A typical example of a poor quality "trend" behaviour of a chalk sample from Seaford Head when subjected to thermal demagnetisation. Sample SF8-DT is shown before and after application of a bedding correction of 254°/16°. A trend to normal polarity is inferred.

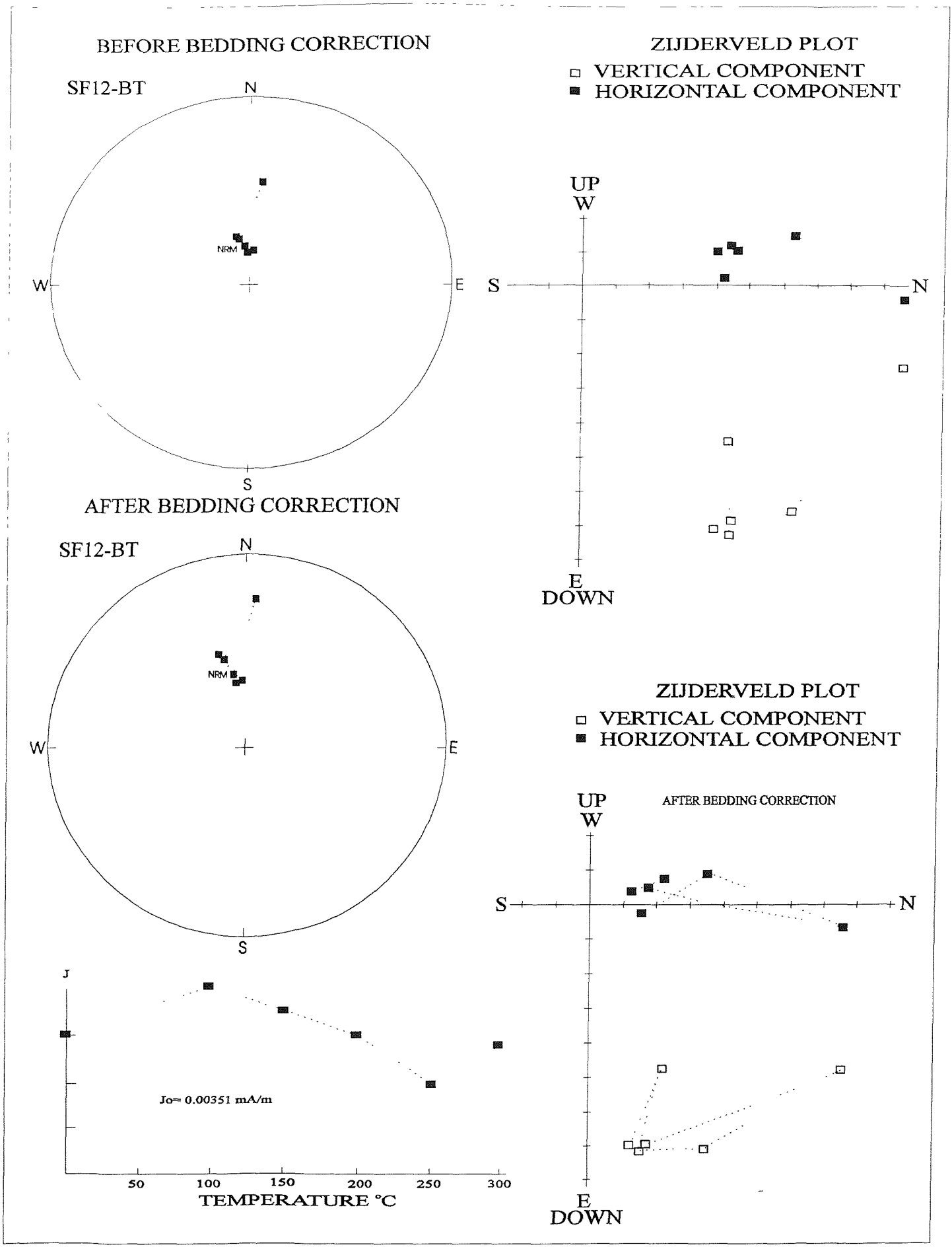

Figure 8.10. A typical example of the poor quality stable end point behaviour of a chalk sample from Seaford Head when subjected to thermal demagnetisation. Sample SF12-BT is shown before and after application of a bedding correction of 254°/16°.

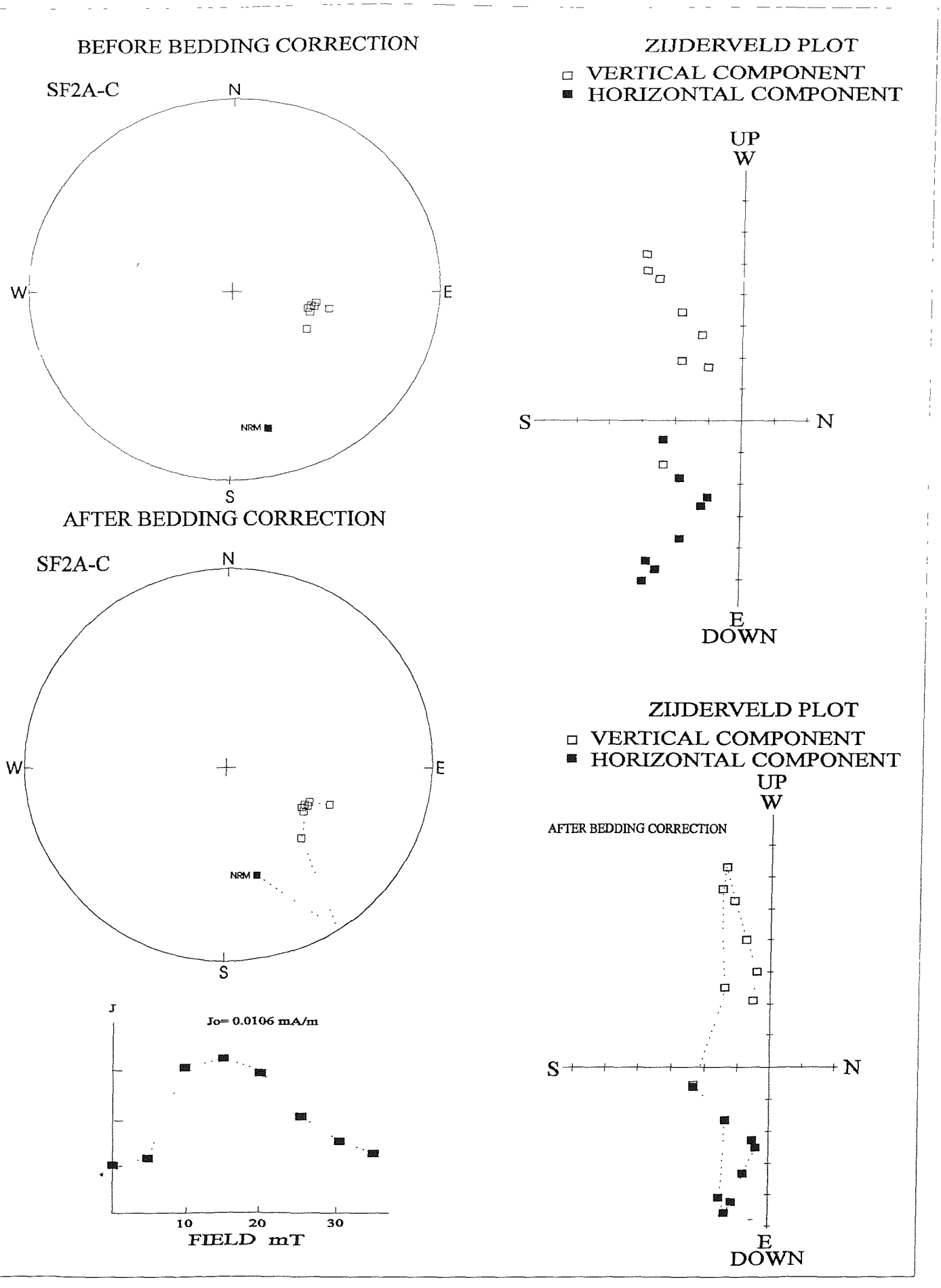

Figure 8.11a. An example of an 'S1 reliability' category chalk sample from Seaford Head after subjection to A F demagnetisation. Sample SF2A-C is shown before and after application of a bedding correction of 254°/16°.

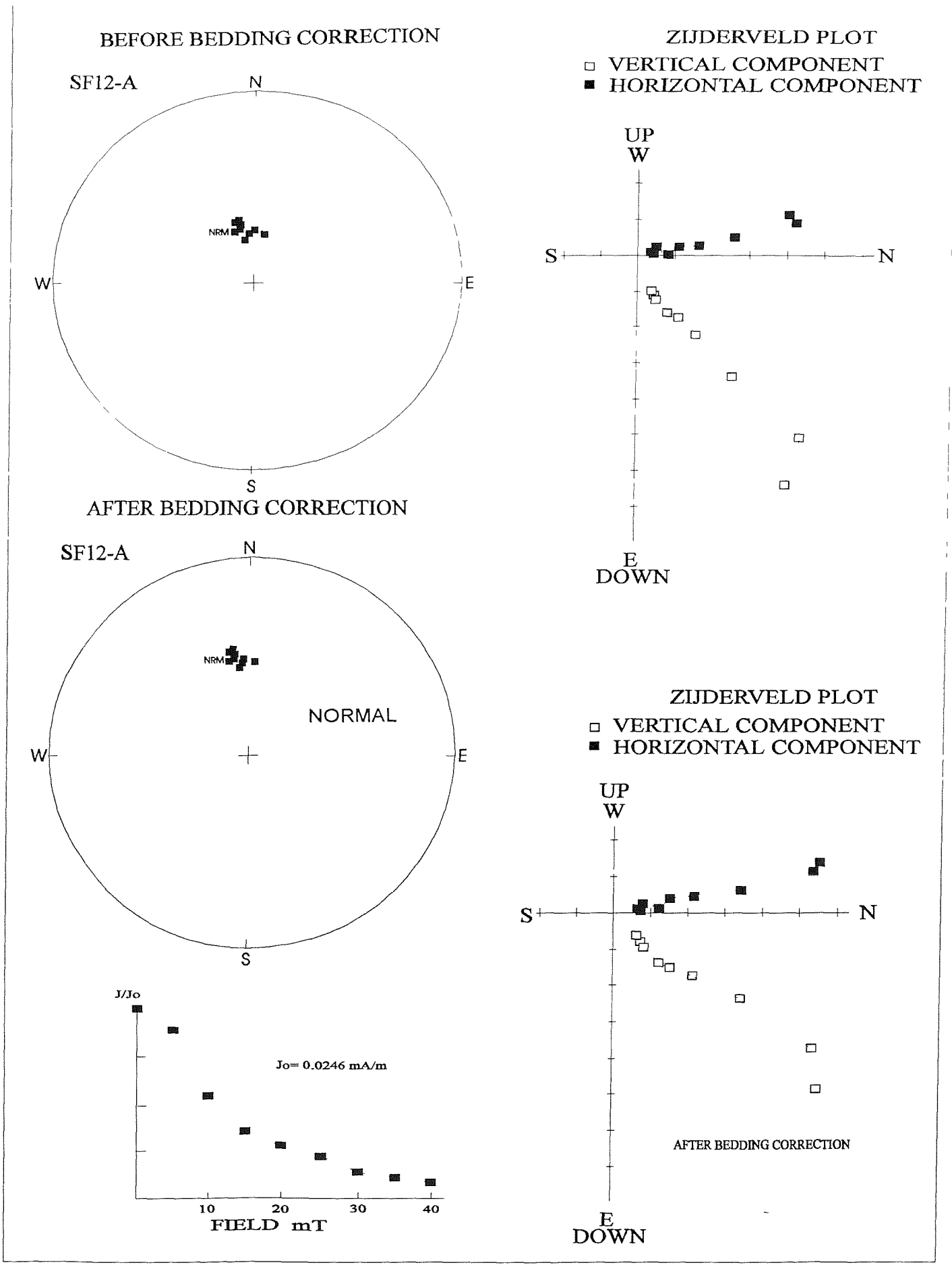

Figure 8.11b. An example of a 'S1 reliability' category chalk sample from Seaford Head after subjection to A F demagnetisation. Sample SF12-A is shown before and after application of a bedding correction of 254°/16°.

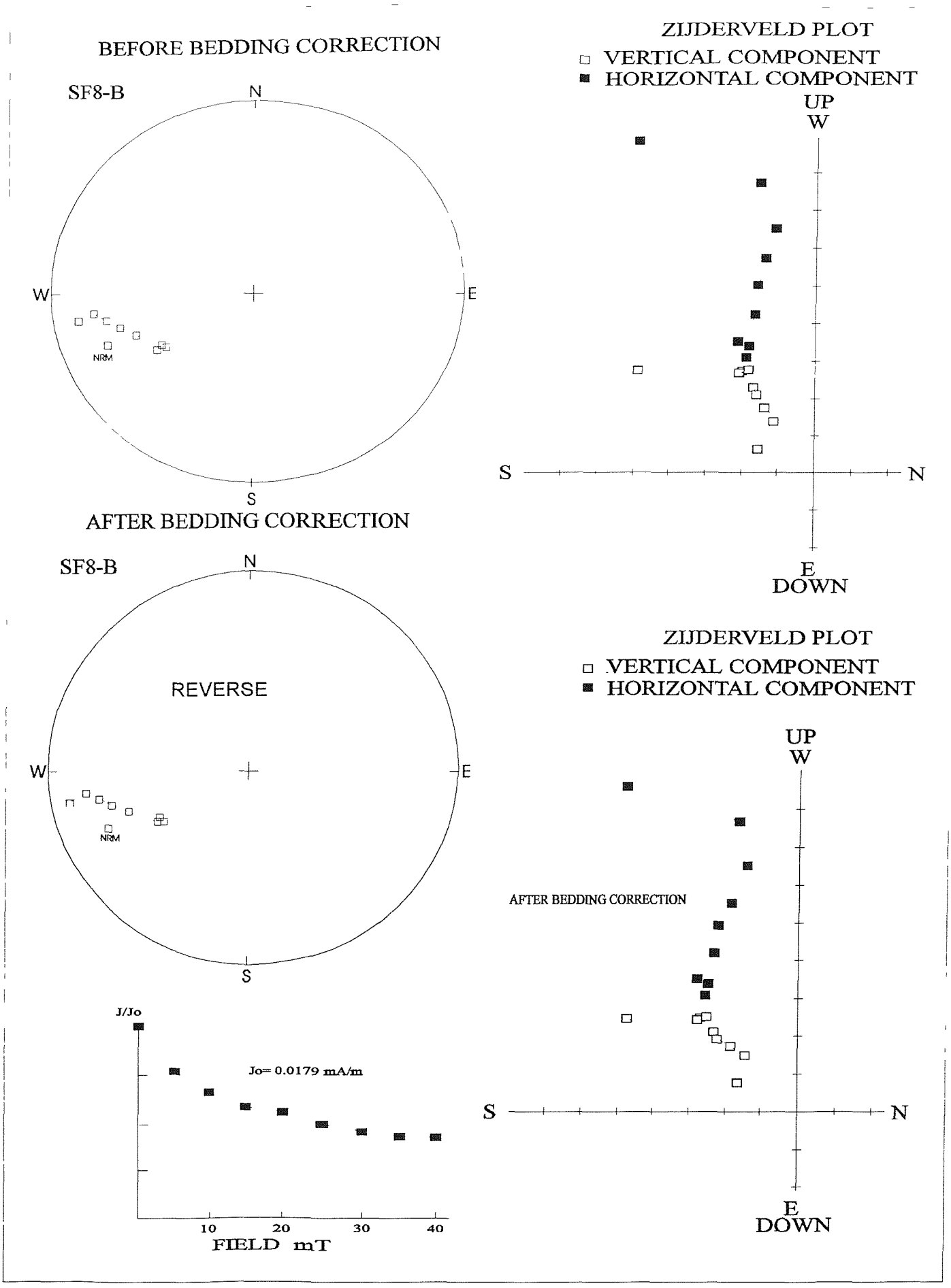

Figure 8.12a. An example of a 'S2 reliability' category chalk sample from Seaford Head after subjection to A F demagnetisation. Sample SF8-B is shown before and after application of a bedding correction of 254°/16°.

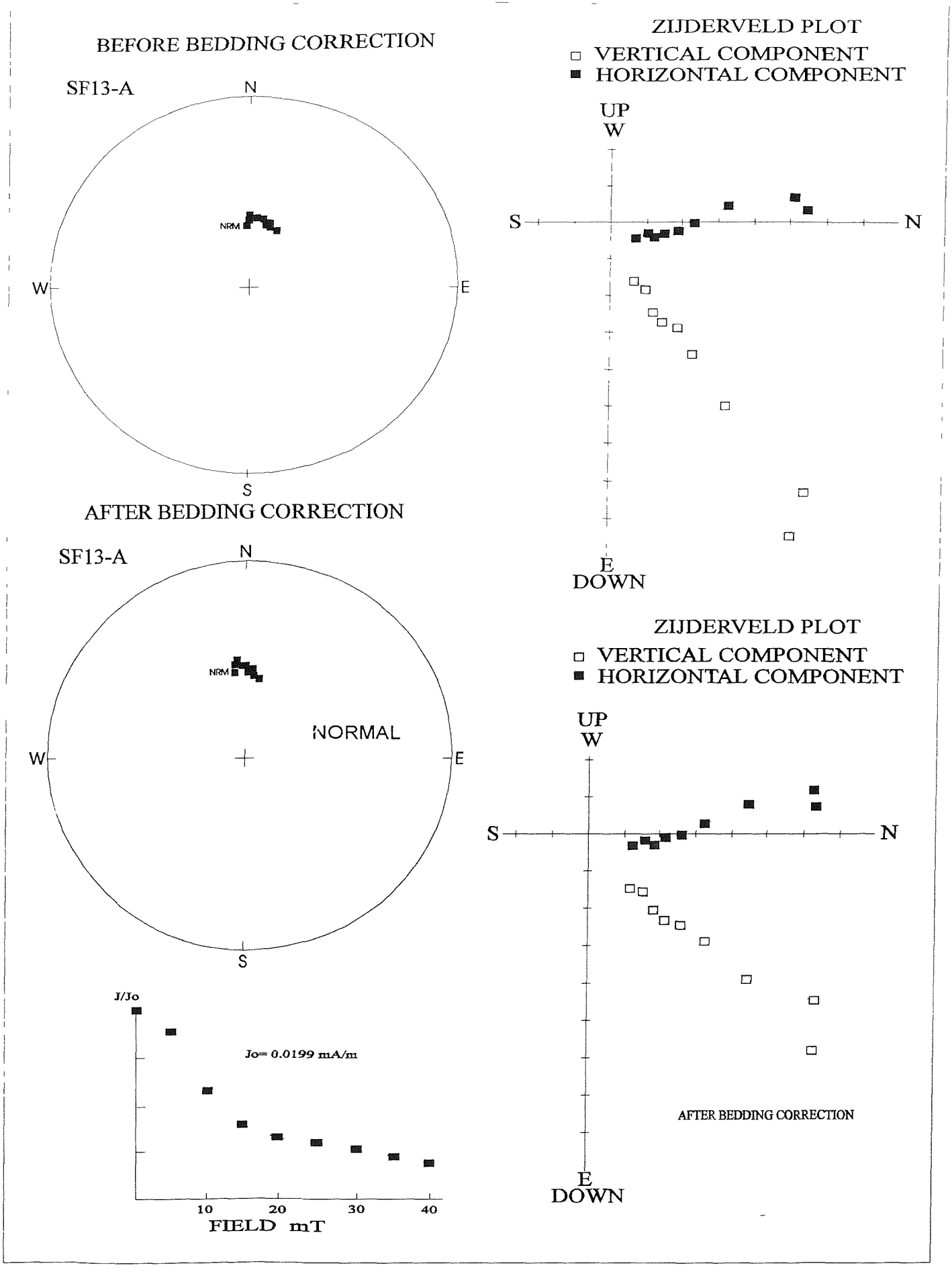

Figure 8.12b. An example of a 'S2 reliability' category chalk sample from Seaford Head after subjection to A F demagnetisation. Sample SF13-A is shown before and after application of a bedding correction of 254°/16°.

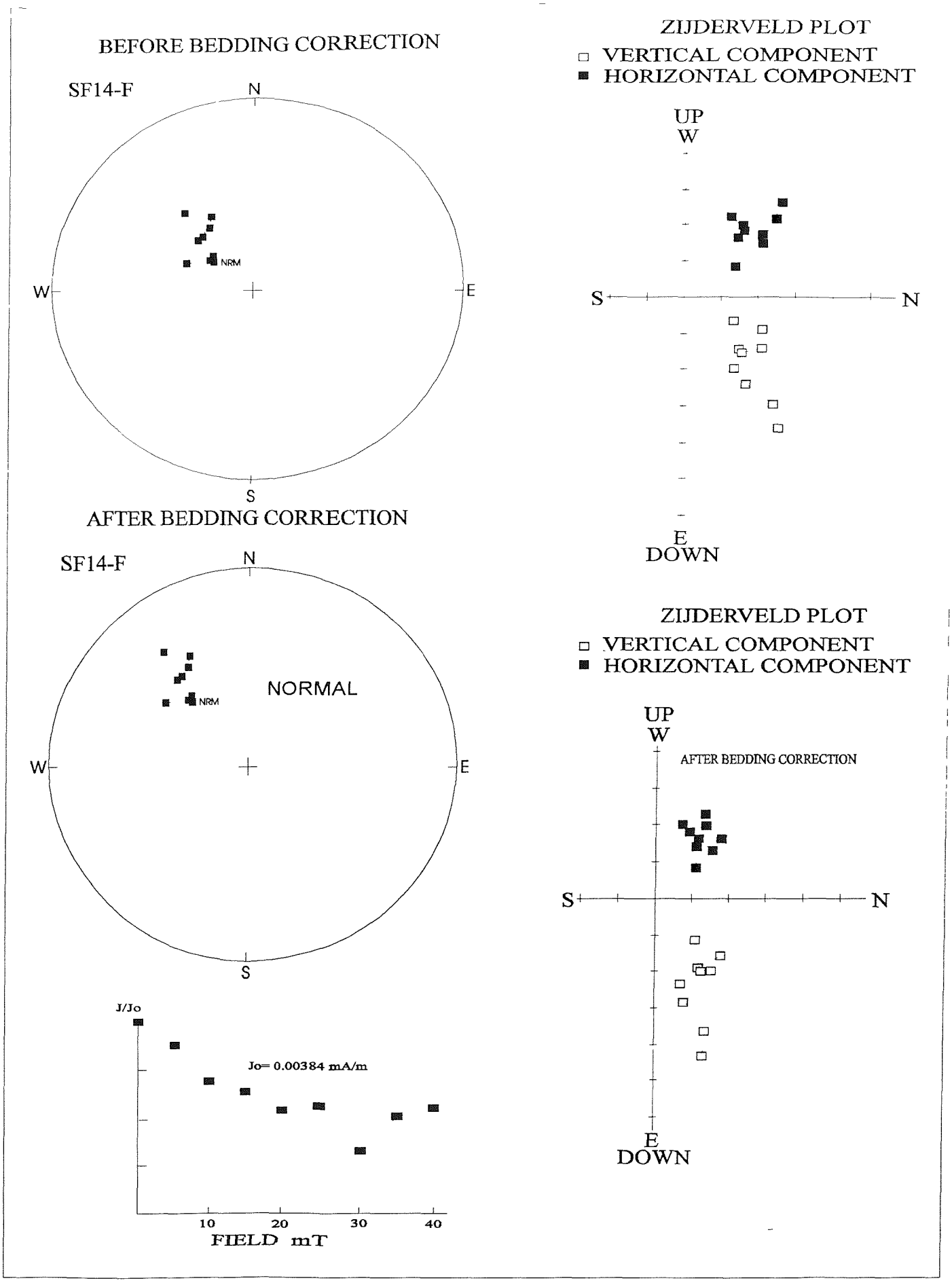

Figure 8.13a. An example of a 'S3 reliability' category chalk sample from Seaford Head after subjection to A F demagnetisation. Sample SF14-F is shown before and after application of a bedding correction of 254°/16°.

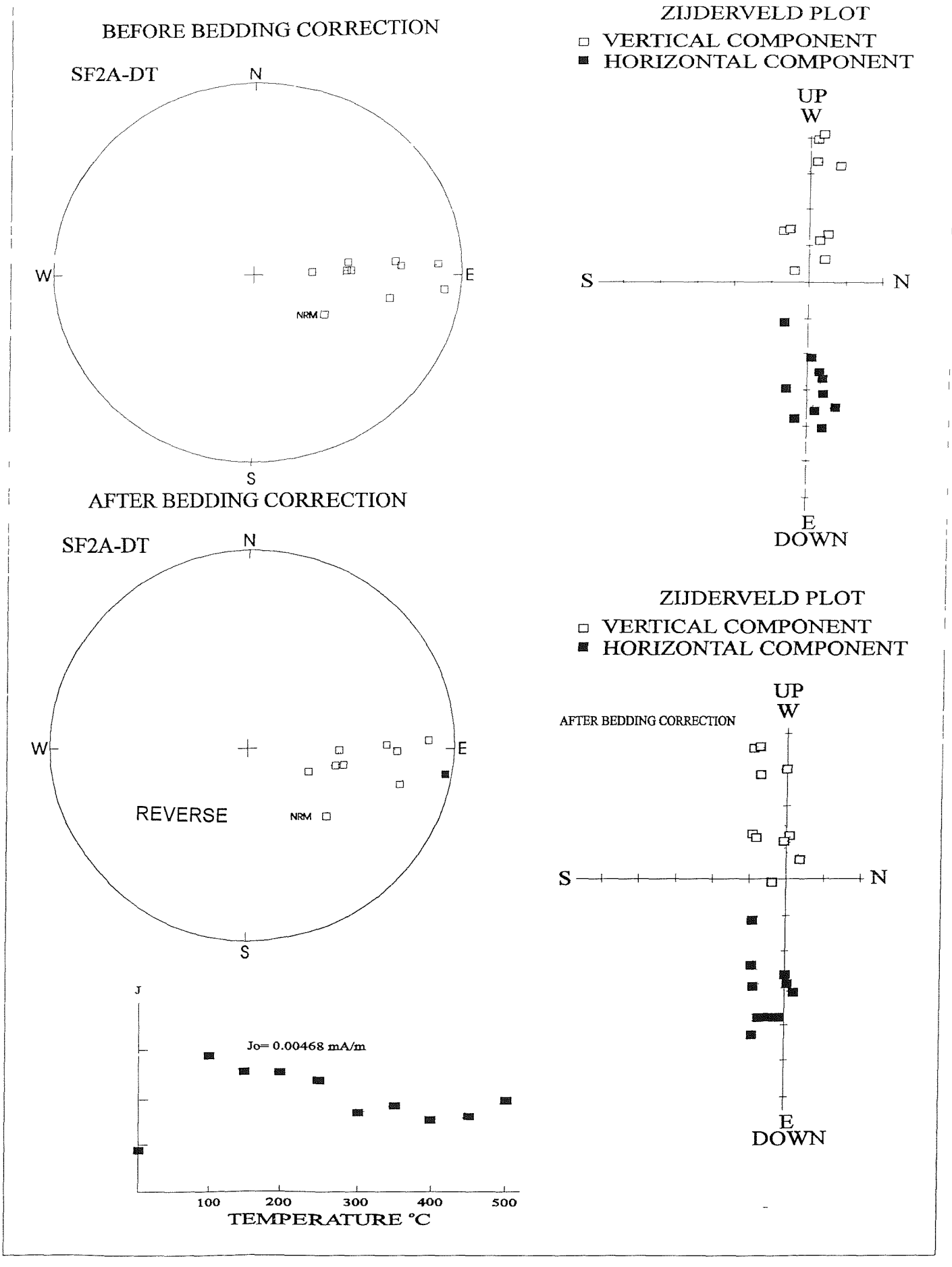

Figure 8.13b. An example of a 'S3 reliability' category chalk sample from Seaford Head after subjection to thermal demagnetisation. Sample SF2A-DT is shown before and after application of a bedding correction of 254°/16°.

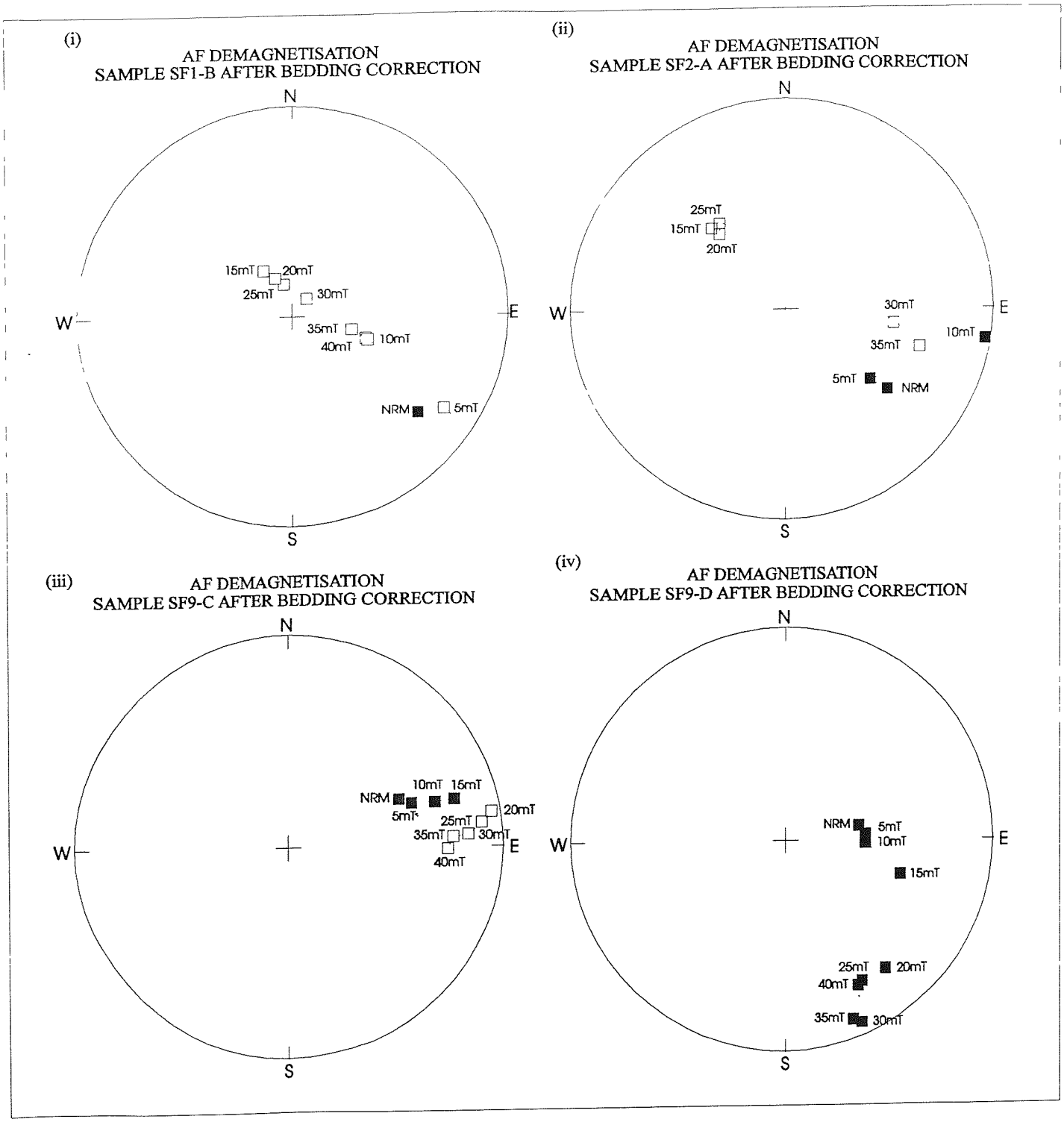

Figure 8.14. Examples of palaeomagnetic Chalk samples from Seaford Head which, when subjected to A.F demagnetisation and application of a bedding correction, show 'T1 reliability category' trends to reverse polarity.

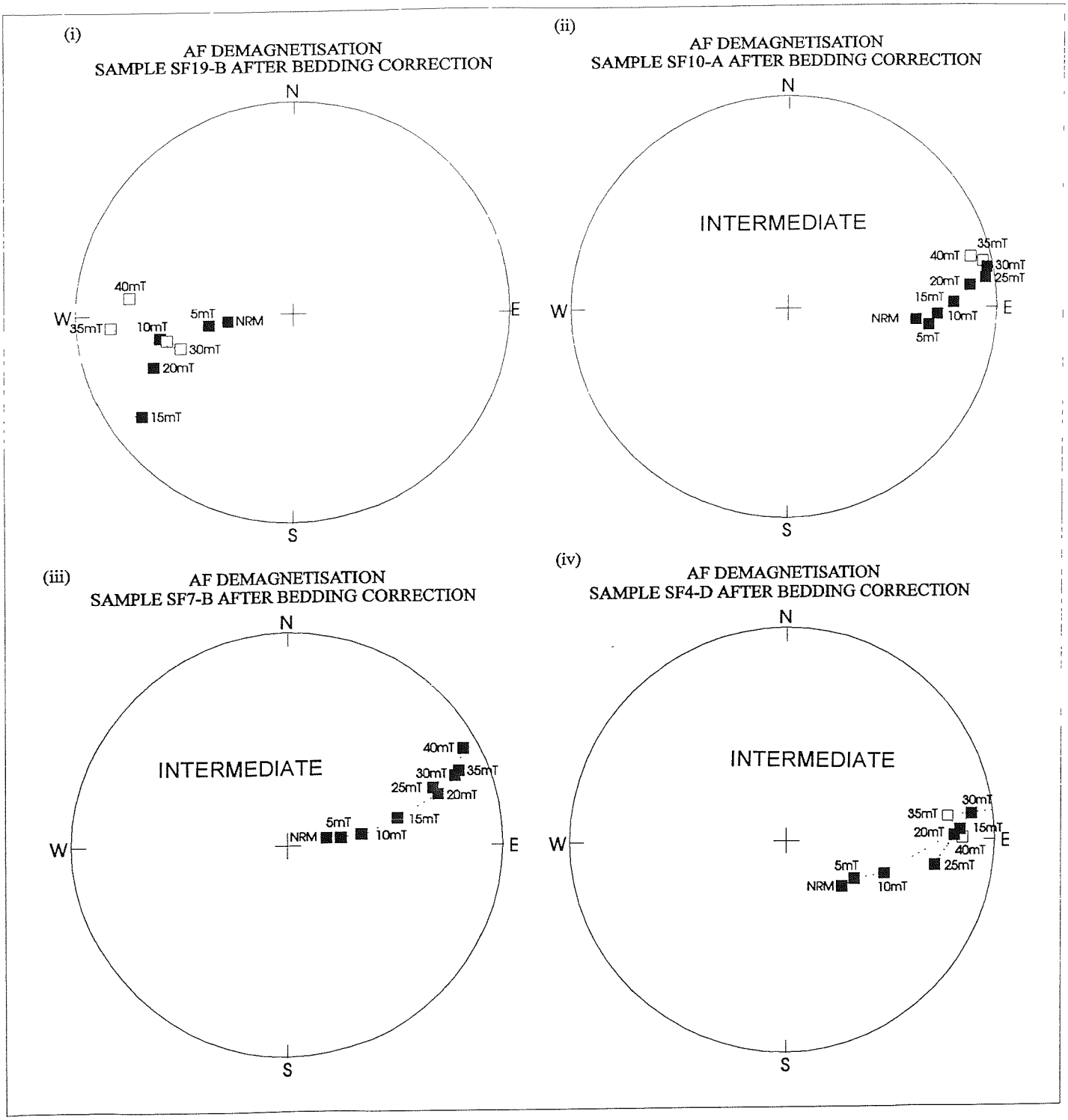

Figure 8.15. Examples of palaeomagnetic Chalk samples from Seaford Head which, when subjected to A F demagnetisation and application of a bedding correction, show 'T2 reliability category' trends to reverse polarity.

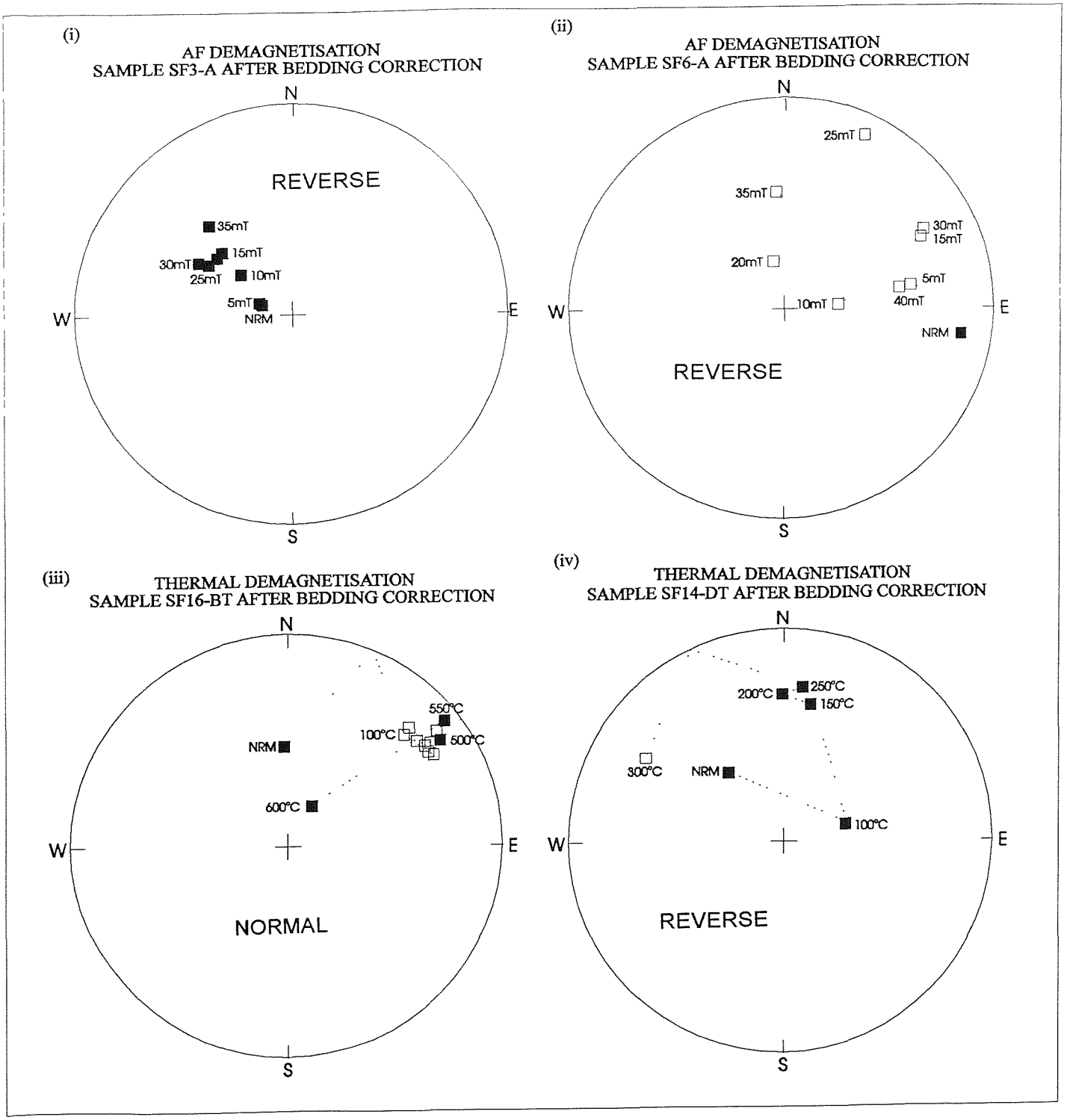

Figure 8.16. Examples of palaeomagnetic Chalk samples from Seaford Head which, when subjected to A.F. (i & ii) and thermal (iii & iv) demagnetisation and application of a bedding correction, show 'T3 reliability category' trends to either reverse or normal polarity.

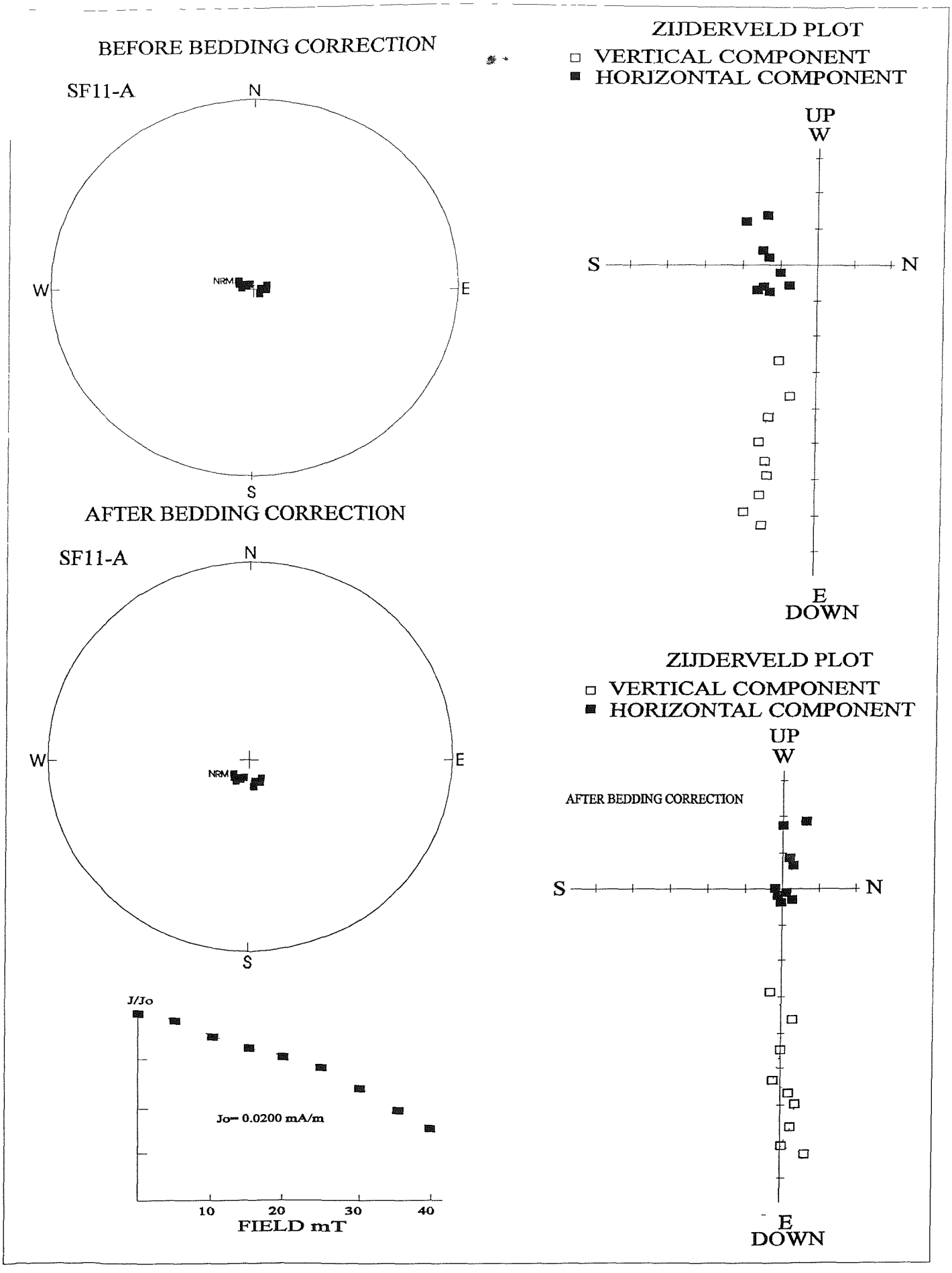

Figure 8.17. An example of a magnetic overprint acquired by a chalk sample from Seaford Head. Sample SF11-A is shown before and after application of a bedding correction of 254°/16°.

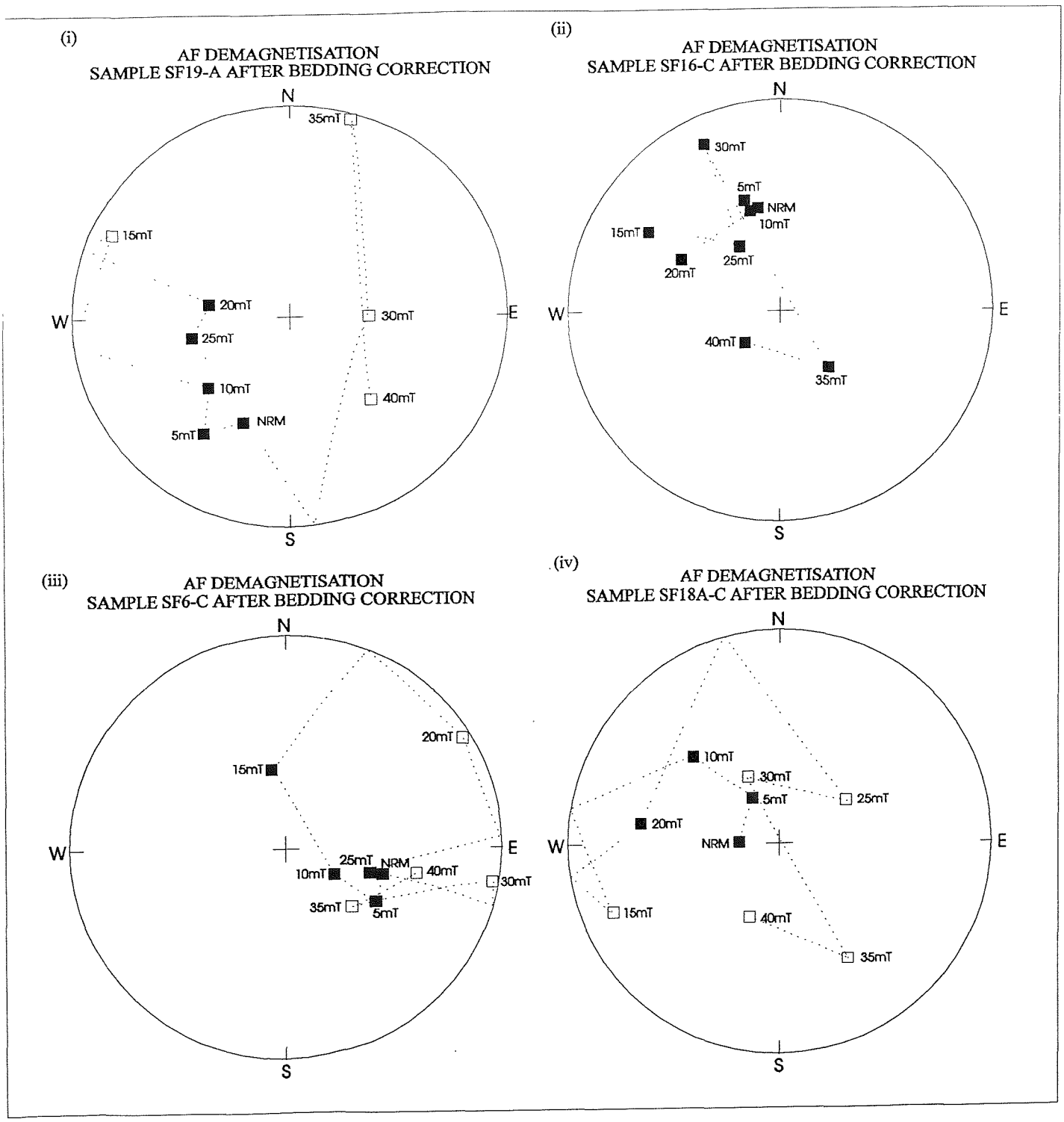

Figure 8.18. Examples of palaeomagnetic Chalk samples from Seaford Head which, when subjected to A F demagnetisation and application of a bedding correction, show 'Erratic' behaviour.

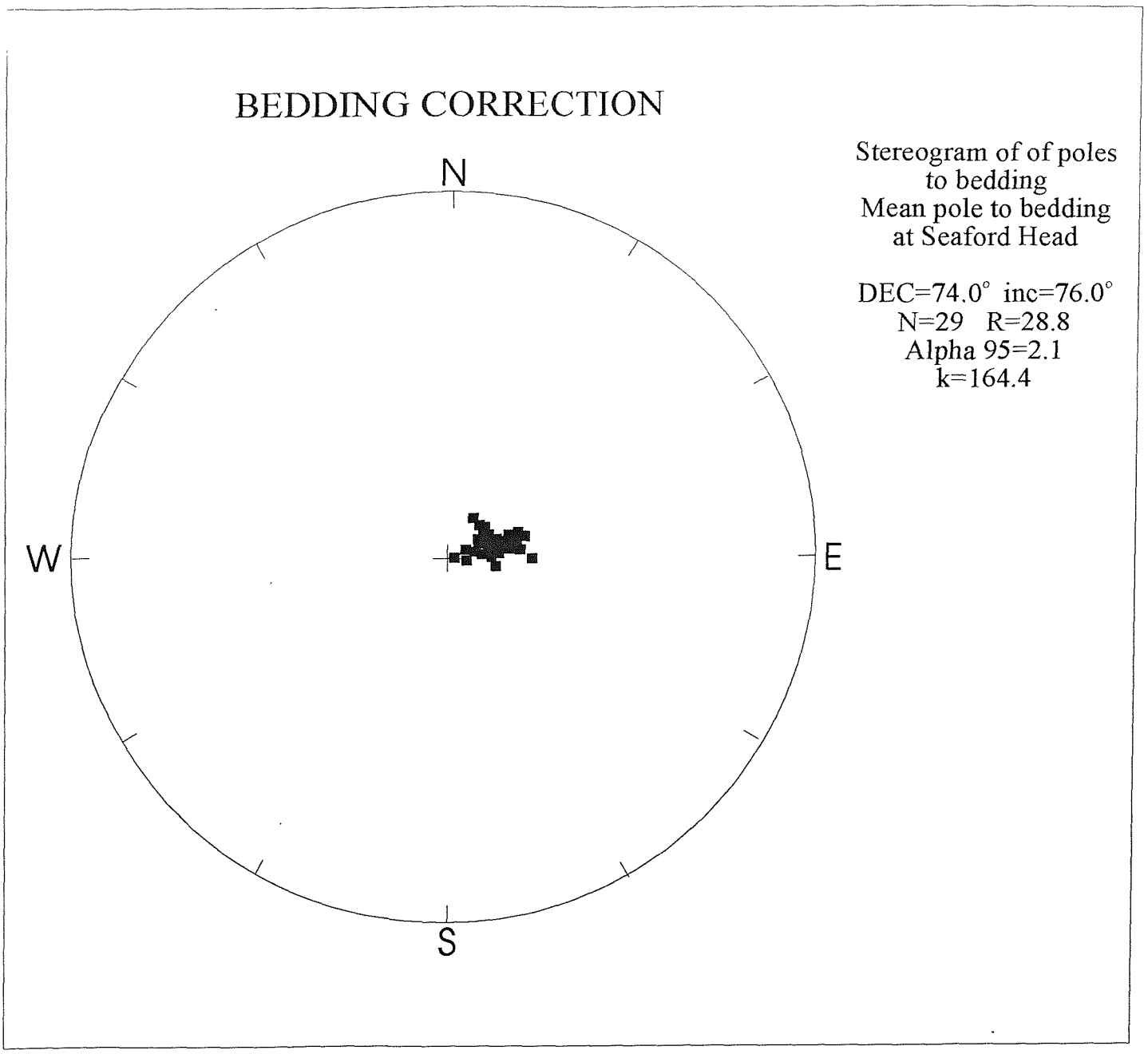

Figure 8.19. A stereographic equal area plot of poles to bedding at Seaford Head. Twenty- nine poles were plotted to produce a mean pole for the strata exposed at Seaford. A mean tilt correction value of 254°/16° was generated.

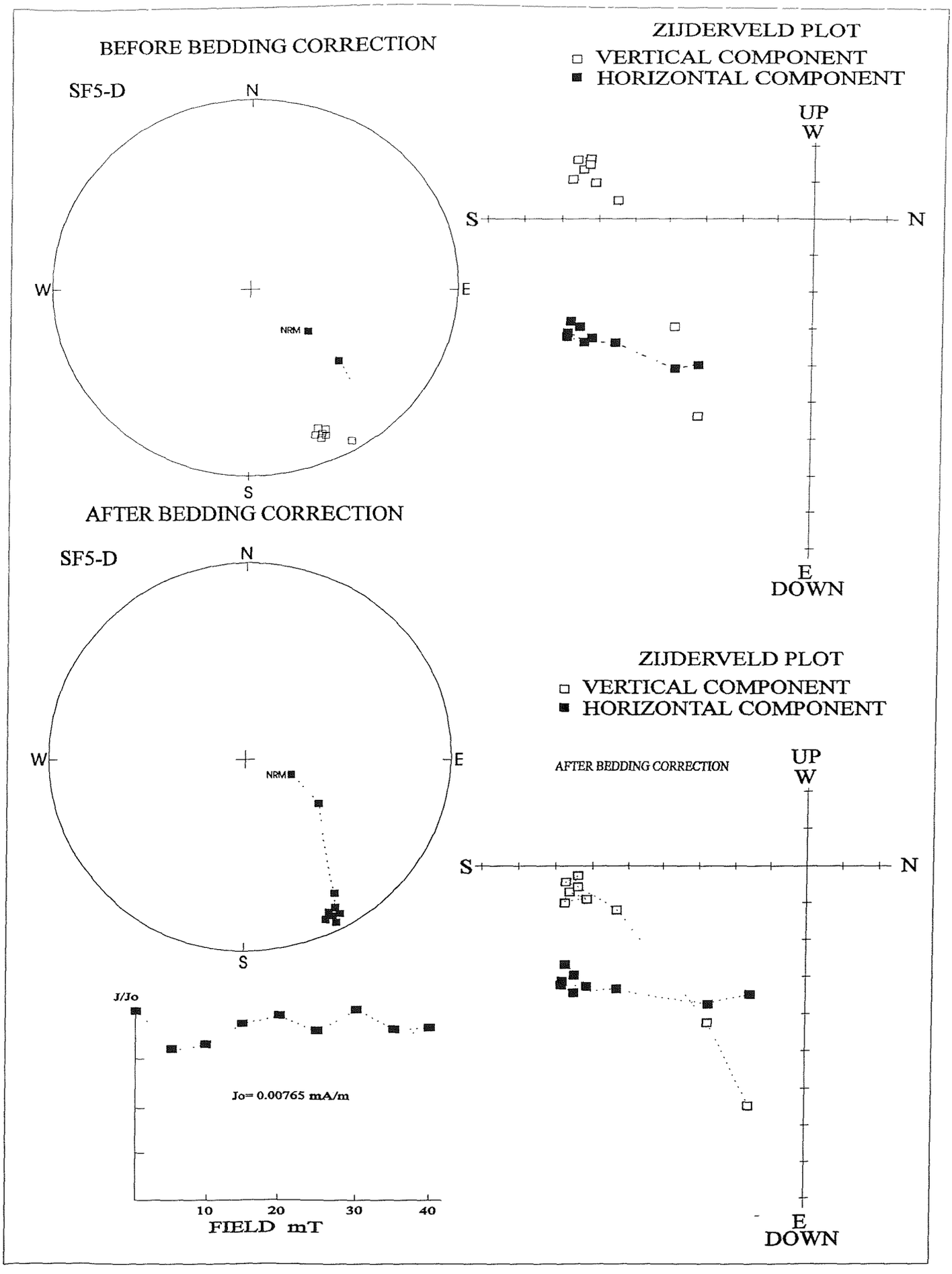

Figure 8.20a. Sample SF5-D is shown before and after application of a bedding correction of 254°/16°. Prior to the employment of the tectonic correction a trend to reverse polarity can be inferred. After correction the trend is less well developed.

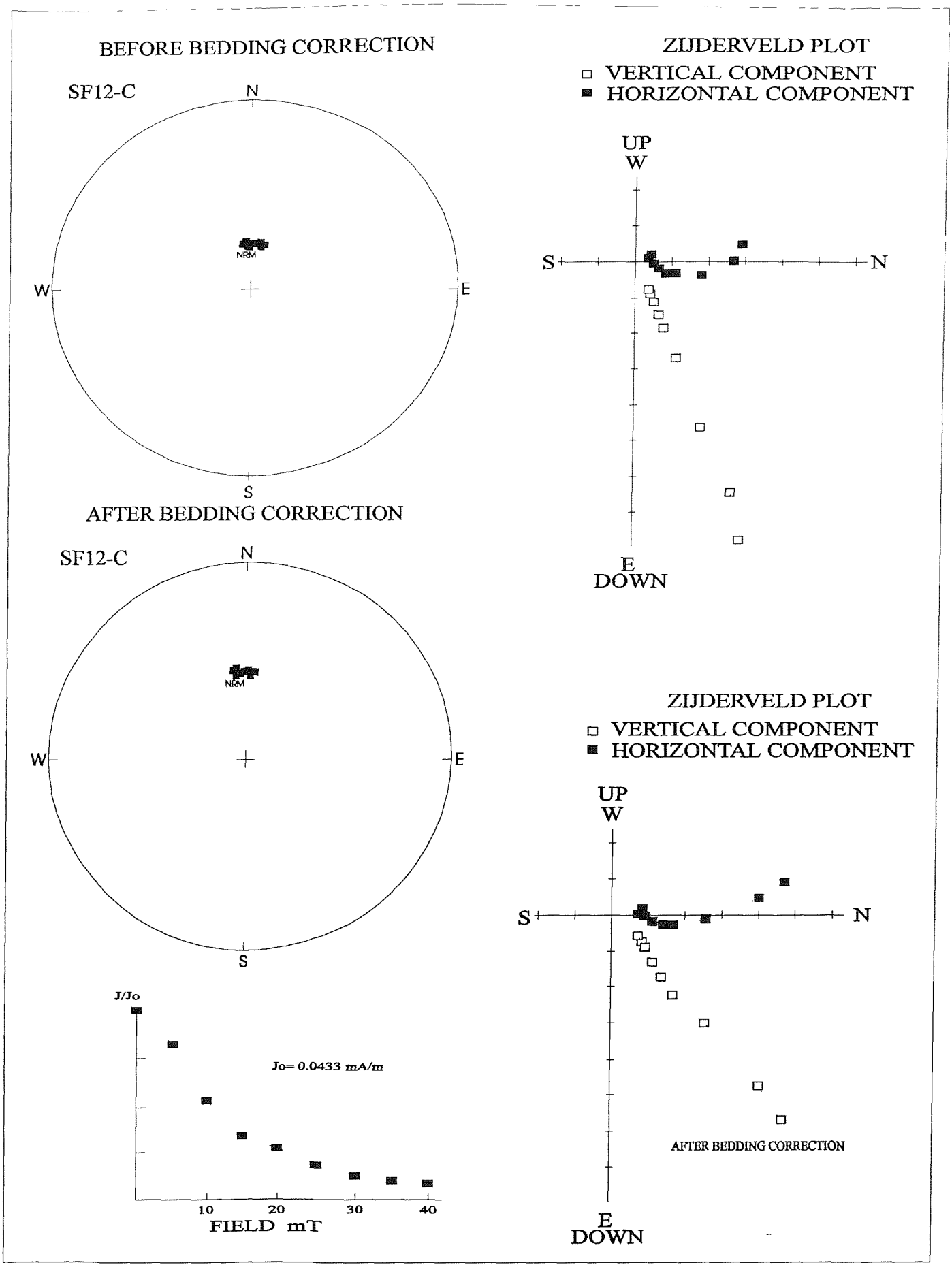

Figure 8.20b. Sample SF12-C is shown before and after application of a bedding correction of 254°/16°. Before correction the sample displays normal polarity. After correction the direction is maintained causing difficulties in identifying normal polarity from recent geomagnetic field overprints.

SEAFORD HEAD

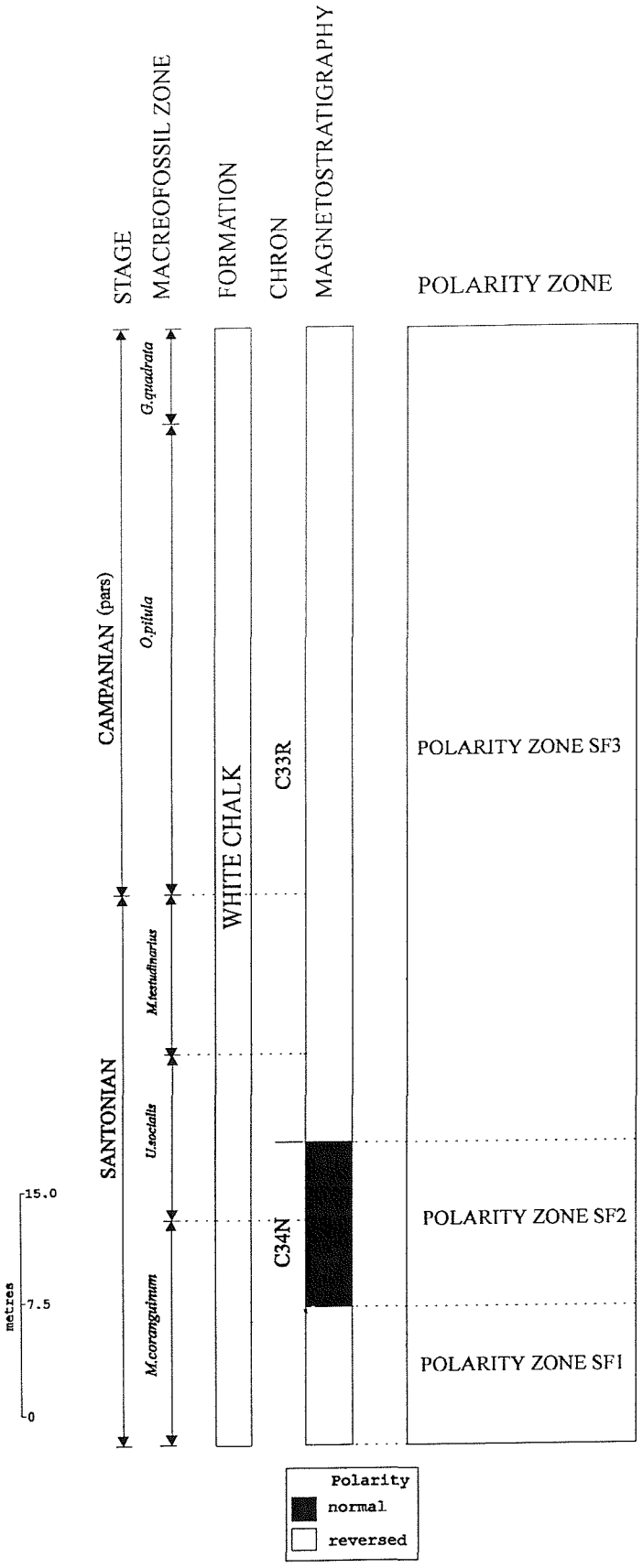

Figure 8.21. The Seaford Head Chalk succession can be divided into three polarity intervals. From left to right the diagram shows Late Cretaceous Stages, macrofossil zones (Rawson *et al.* 1978), Formation, geomagnetic polarity Chrons, the magnetostratigraphy of Seaford Head and the associated polarity zones (SF).

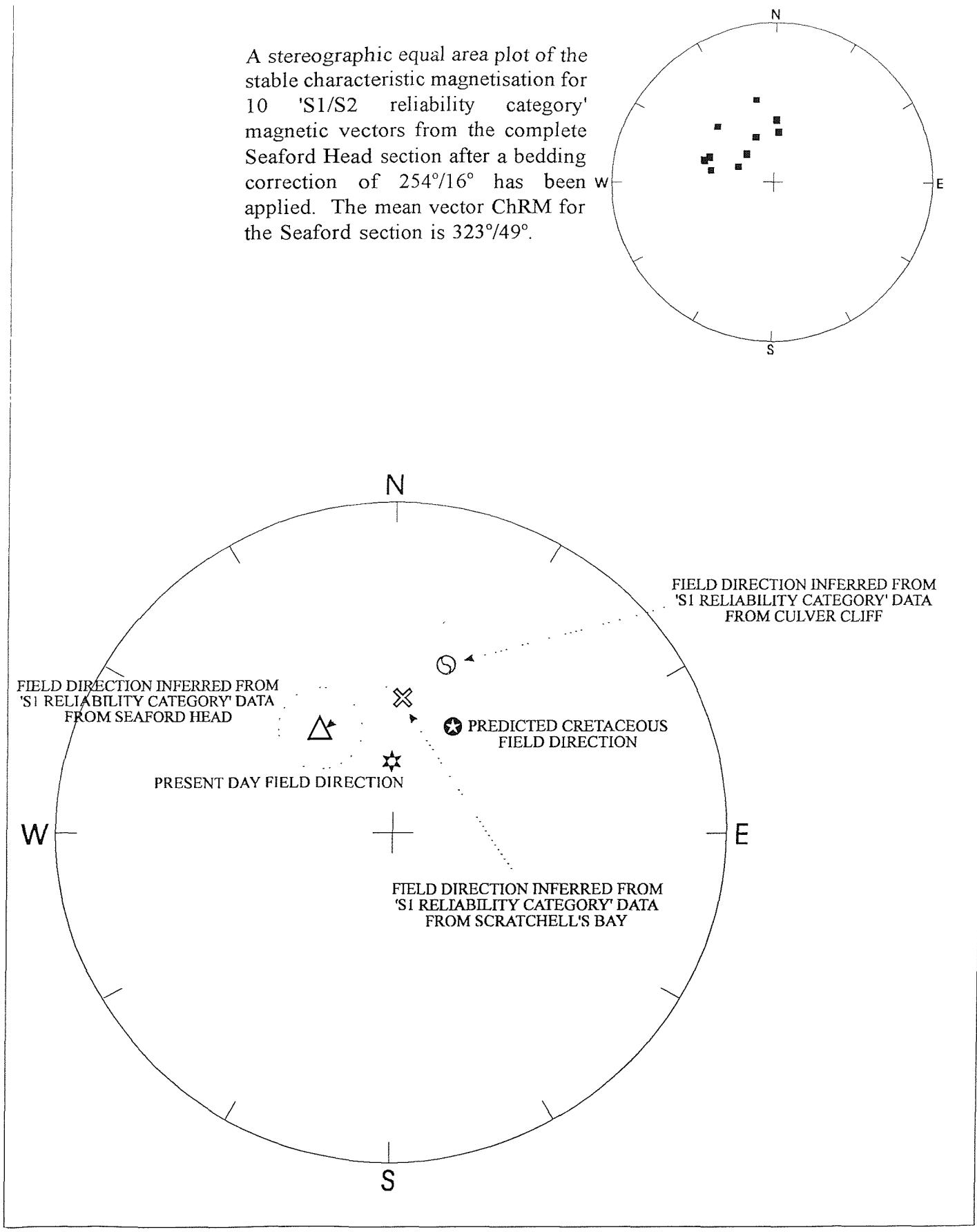

Figure 8.22. A stereographic projection of the mean geomagnetic field directions for southern England based on 'S1 reliability cateogory' magnetic vectors derived from Late Cretaceous deposits of Seaford Head, Culver Cliff and Scratchell's Bay; predicted Late Cretaceous geomagnetic field direction for southern England (Smith *et al.*, 1981); and the present day geomagnetic field direction. Inset, a stereographic projection of the stable ChRM for 'S1/S2 reliability category' magnetic vectors from Seaford Head (dec.=323°, inc.=49°, k=13.8 and alpha 95=13.5°) after correction.

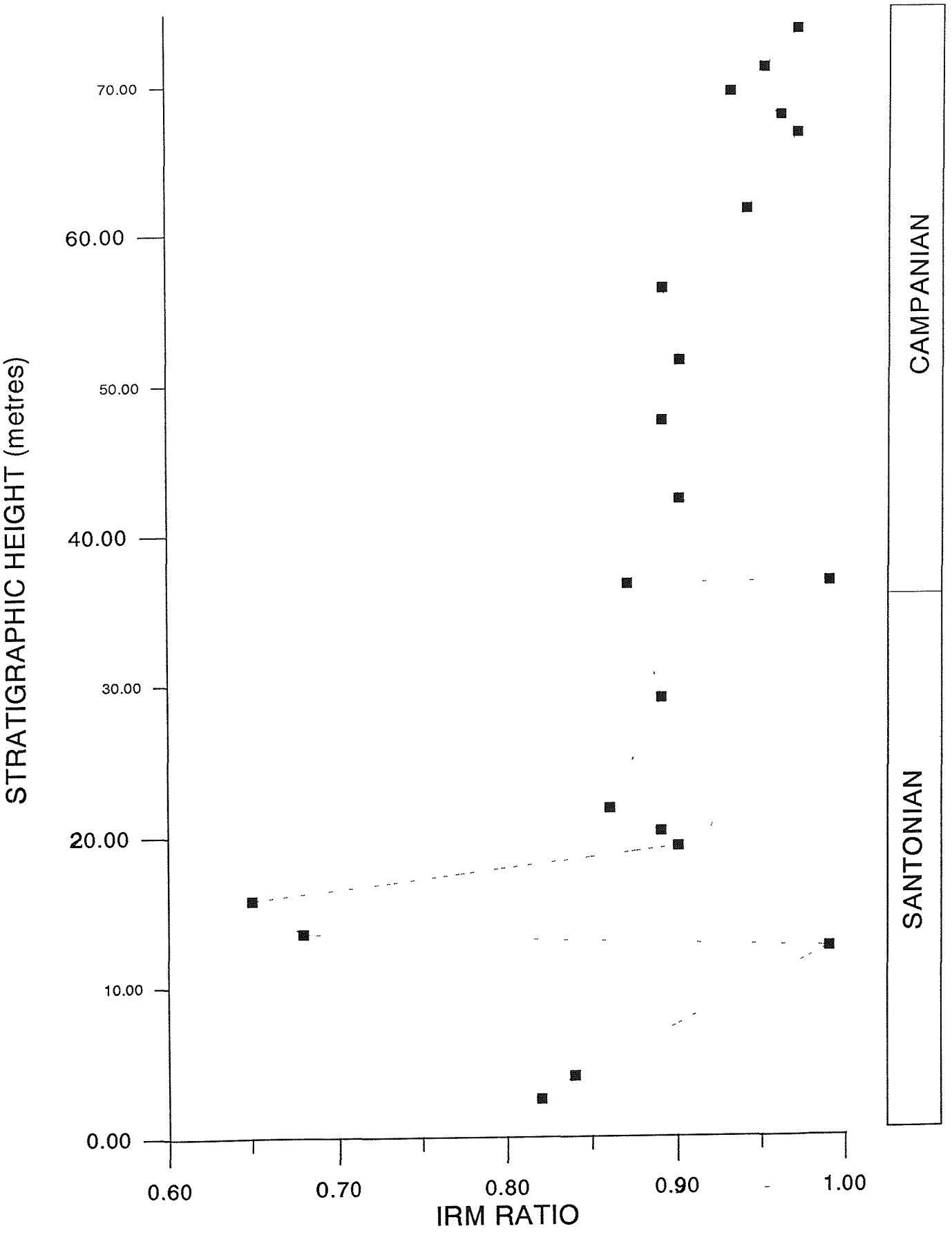

Figure 8.23. IRM ratio log of the chalk succession at Seaford Head. The vast majority of samples exhibit IRM ratios above 0.9

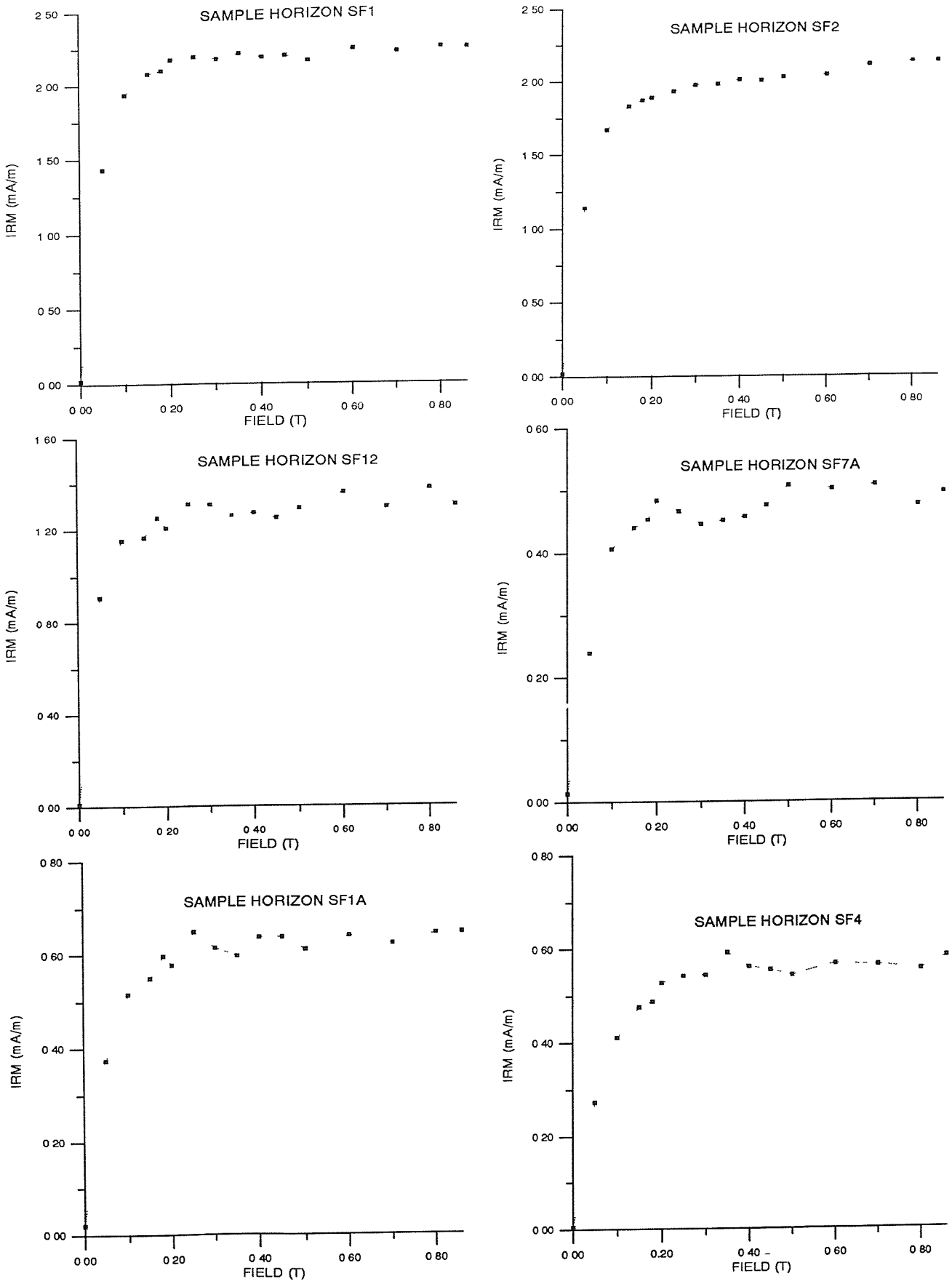

Figure 8.24. Examples of IRM acquisition curves whose shapes are diagnostic of titanomagnetite.

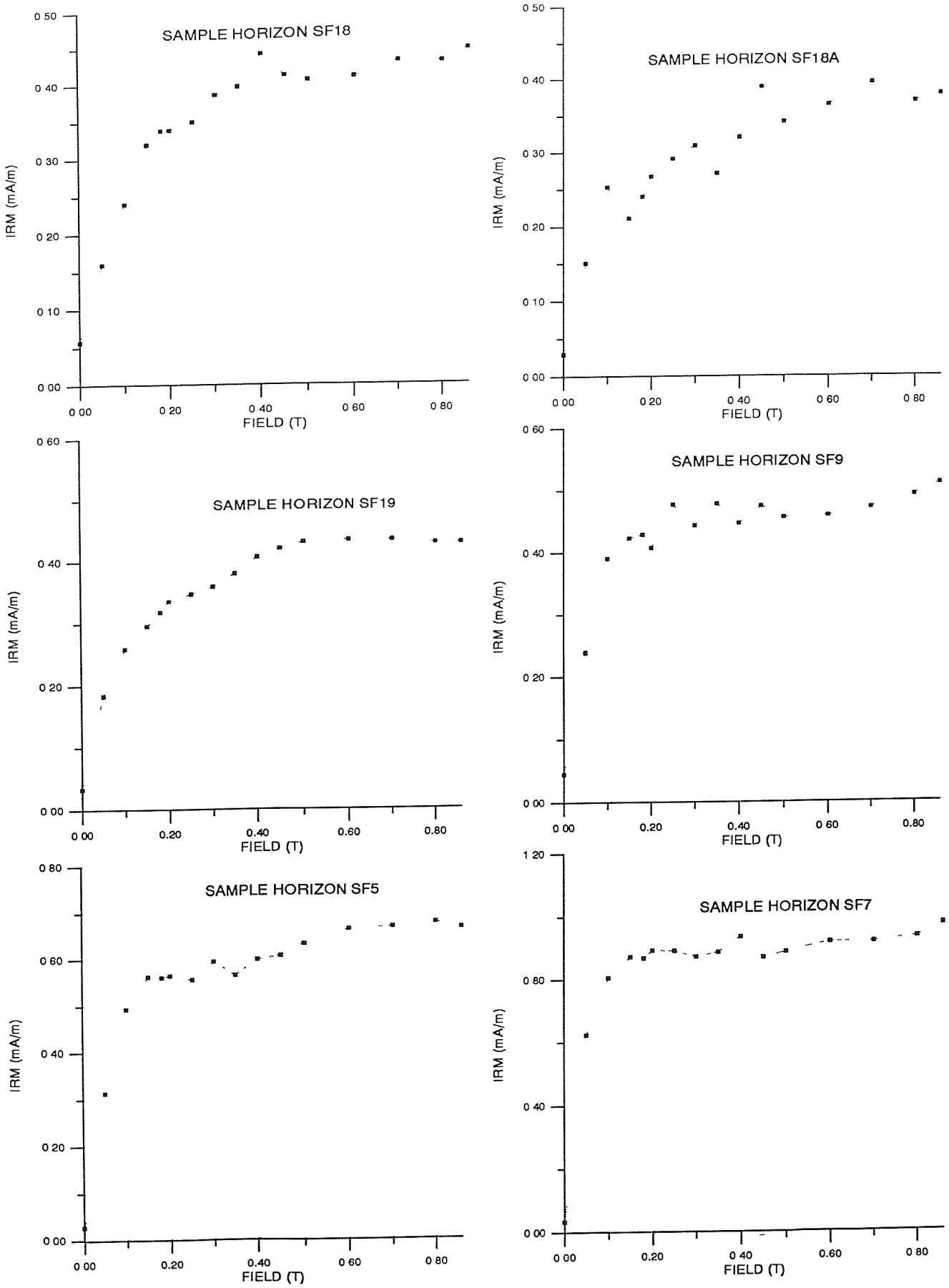

Figure 8.25. Examples of IRM acquisition curves whose shapes are diagnostic of a mixture of titanomagnetite and hematite.

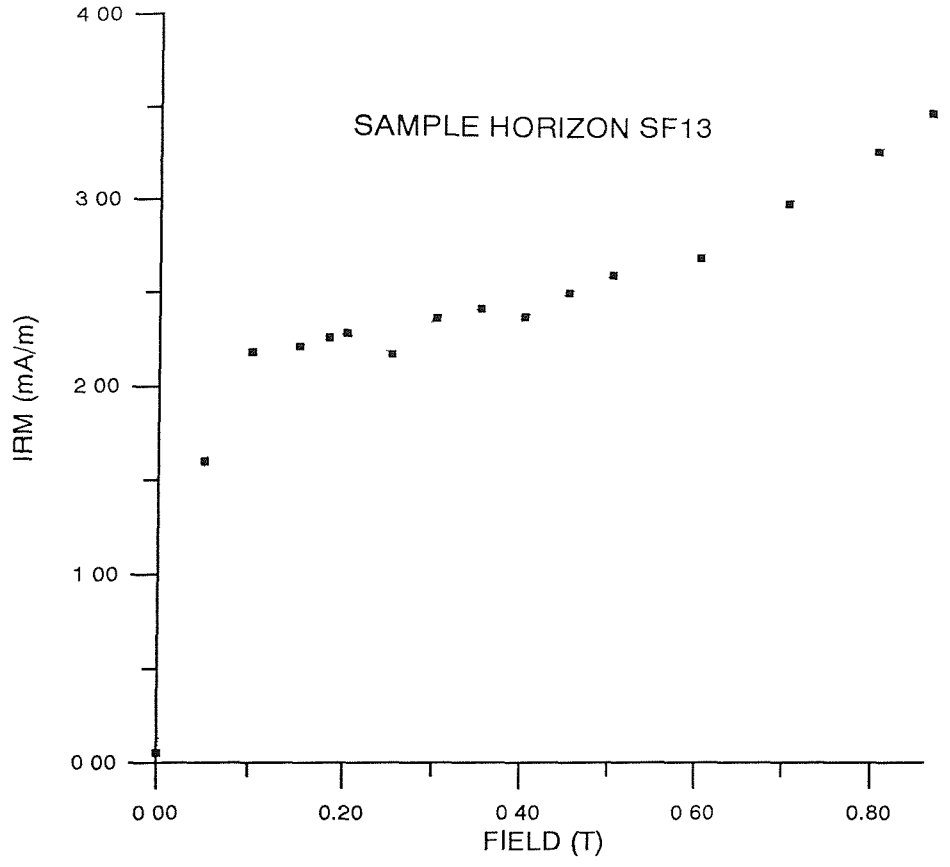

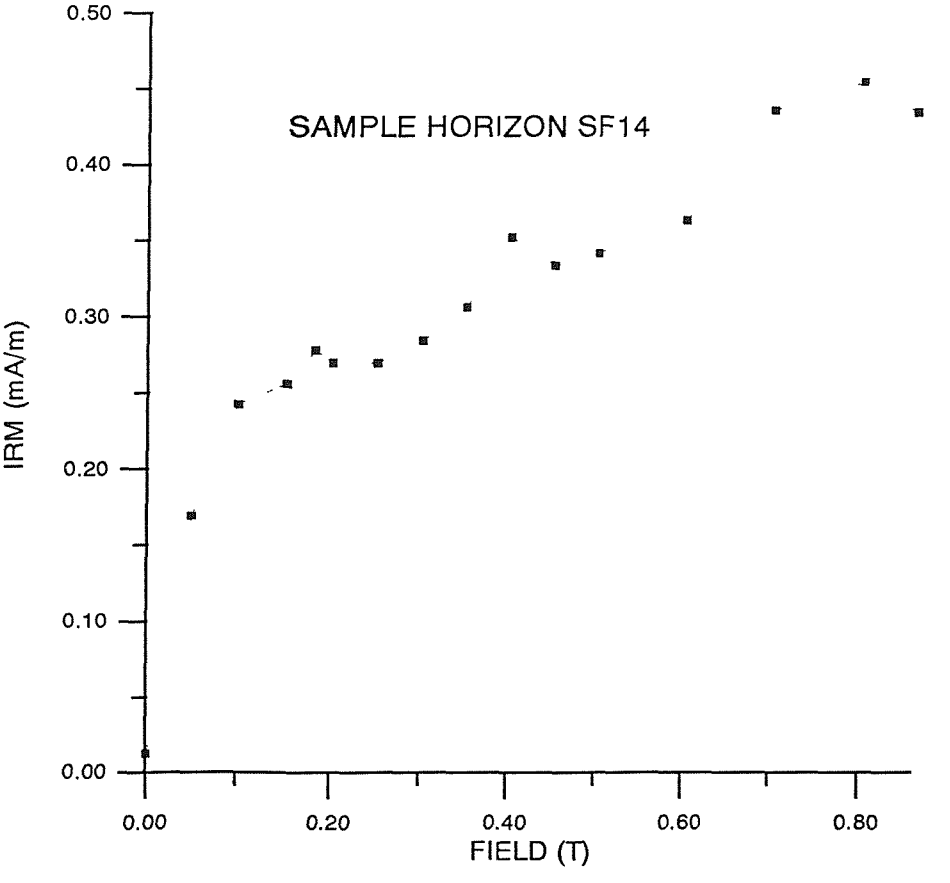

Figure 8.26. Examples of IRM acquisition curves whose shapes are diagnostic of hematite (with minor admixtures of magnetite).

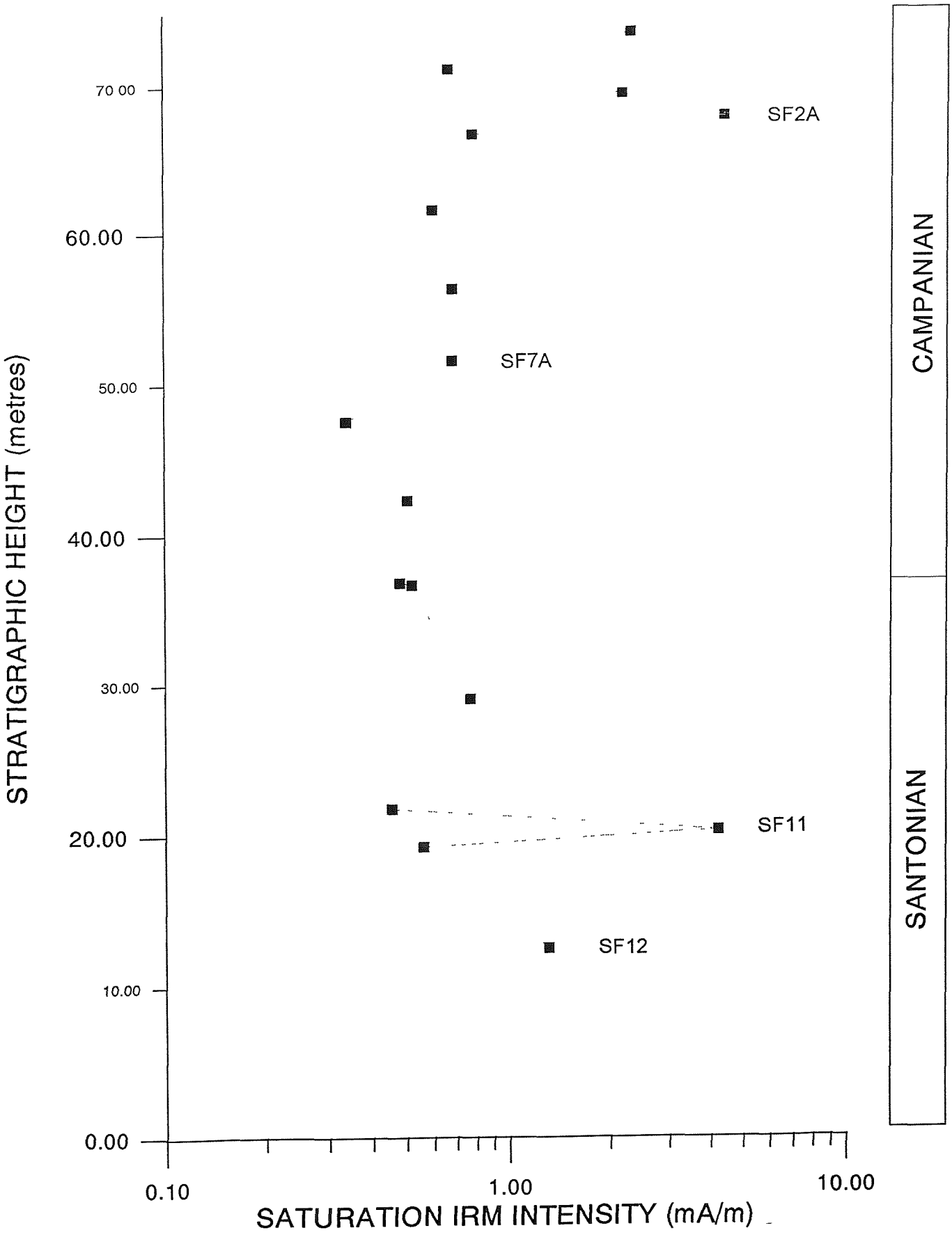

Figure 8.27. Variation of IRM_{sat} with stratigraphic height above Whitaker's 3-inch Flint band. The right-hand column indicates the Late Cretaceous Stages of the Chalk succession at Seaford Head (Rawson *et al.*, 1978).

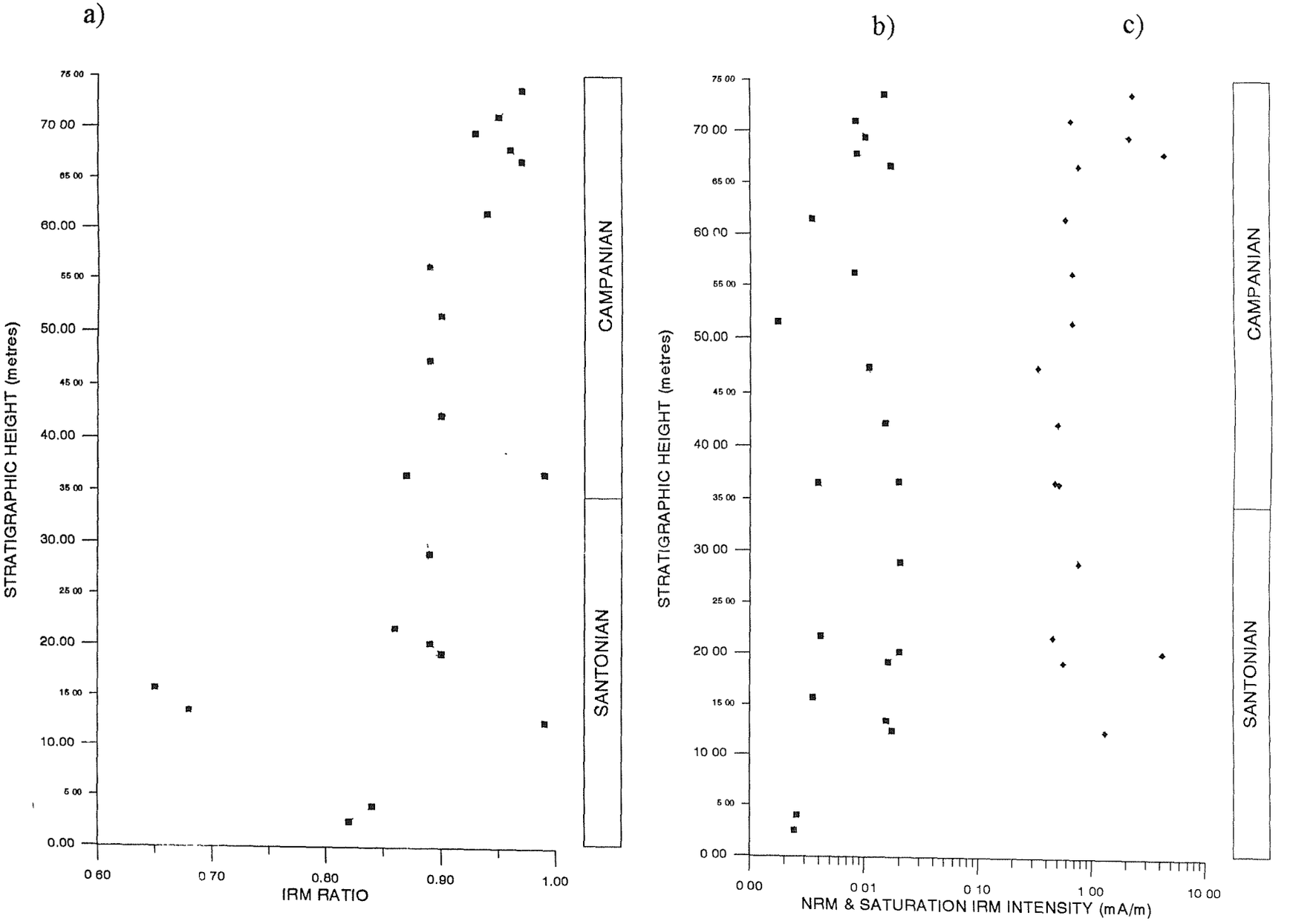

Figure 8.28. A plot of the variation of a) IRM ratio; b) NRM intensity; and c) IRM_{sat} intensity for the Seaford Head section. A correlation exists between low IRM ratio values (hematite dominated sample horizons) and relatively low NRM intensities. A correlation of IRM ratio and NRM intensity with IRM_{sat} intensity is not apparent.

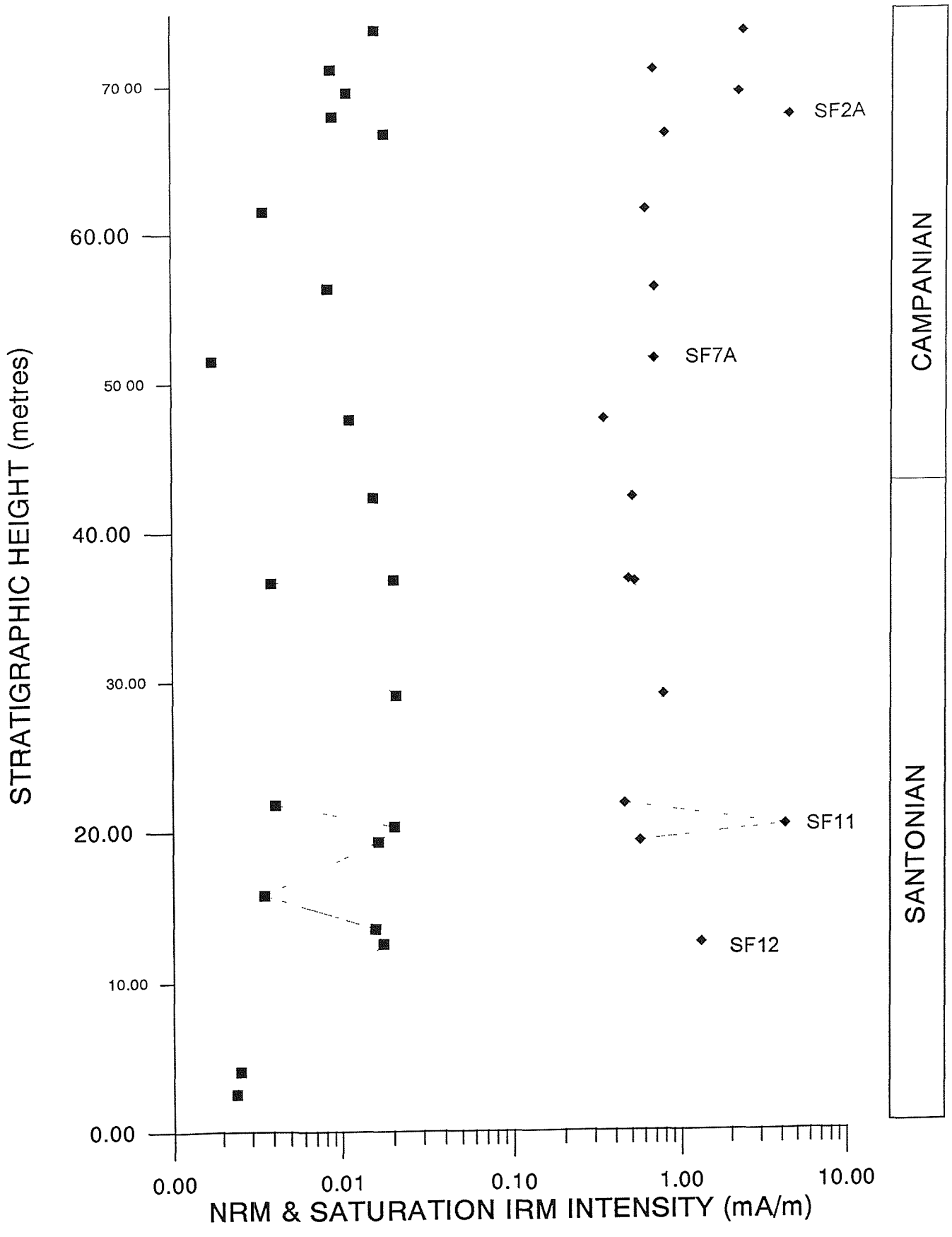

Figure 8.29. Variation of the mean NRM intensity and IRM_{sat} intensity with stratigraphic height above Whitaker's 3-inch Flint. The right-hand column indicates the Late Cretaceous Stages, based on the Rawson *et al.* (1978) macrofossil zonation, of the Chalk succession at Seaford Head.

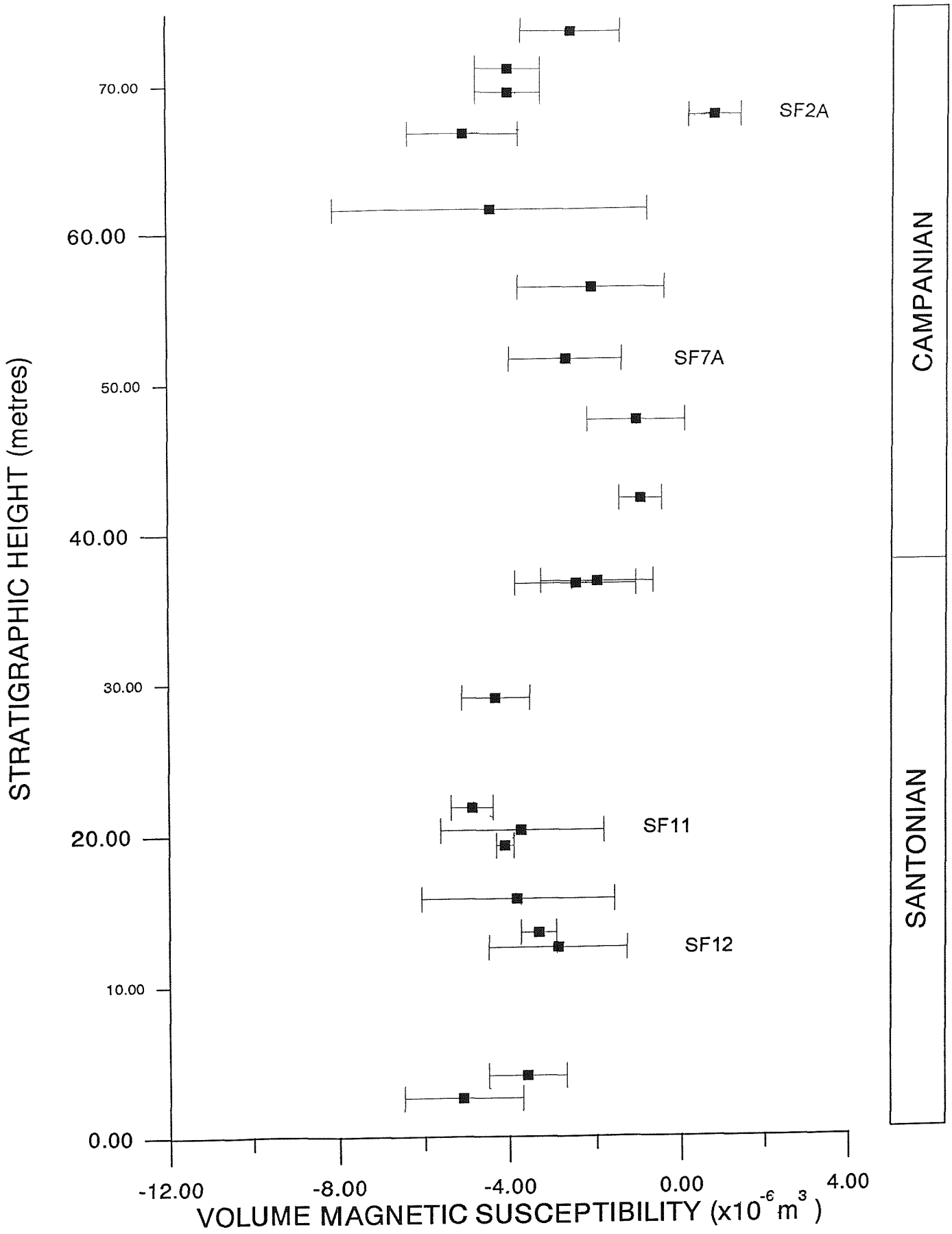

Figure 8.30. Variation of the Volume Magnetic Susceptibility with stratigraphic height above Whitaker's 3-inch Flint. The right-hand column indicates the Late Cretaceous Stages, based on the Rawson *et al.* (1978) macrofossil zonation, of the Chalk succession at Seaford Head.

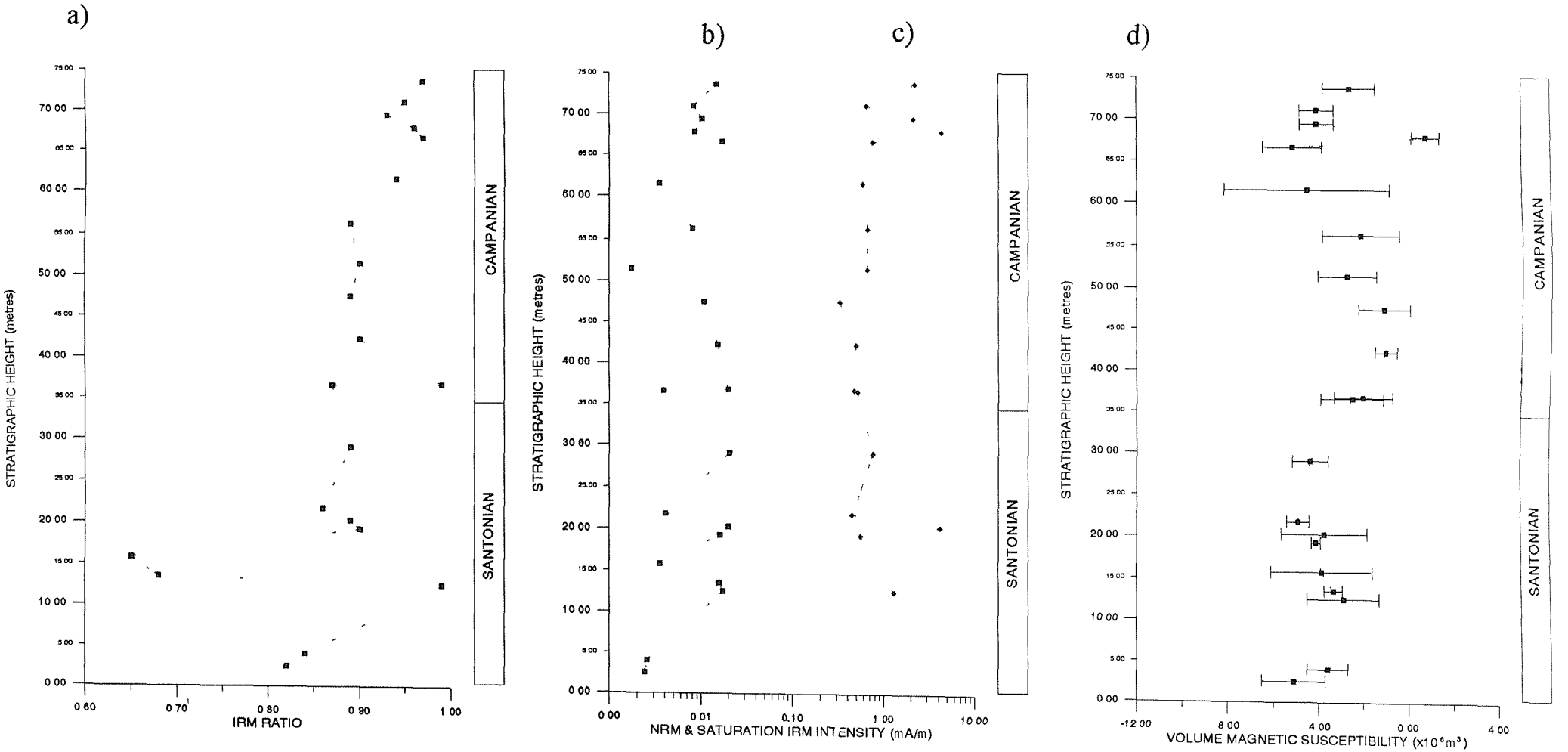

Figure 8.31. A plot of the variation of a) IRM ratio; b) NRM intensity; c) IRM_{sat} intensity; and d) VMS for the Seaford Head section Positive VMS readings correspond to relatively high IRM ratio and IRM_{sat} intensity values.

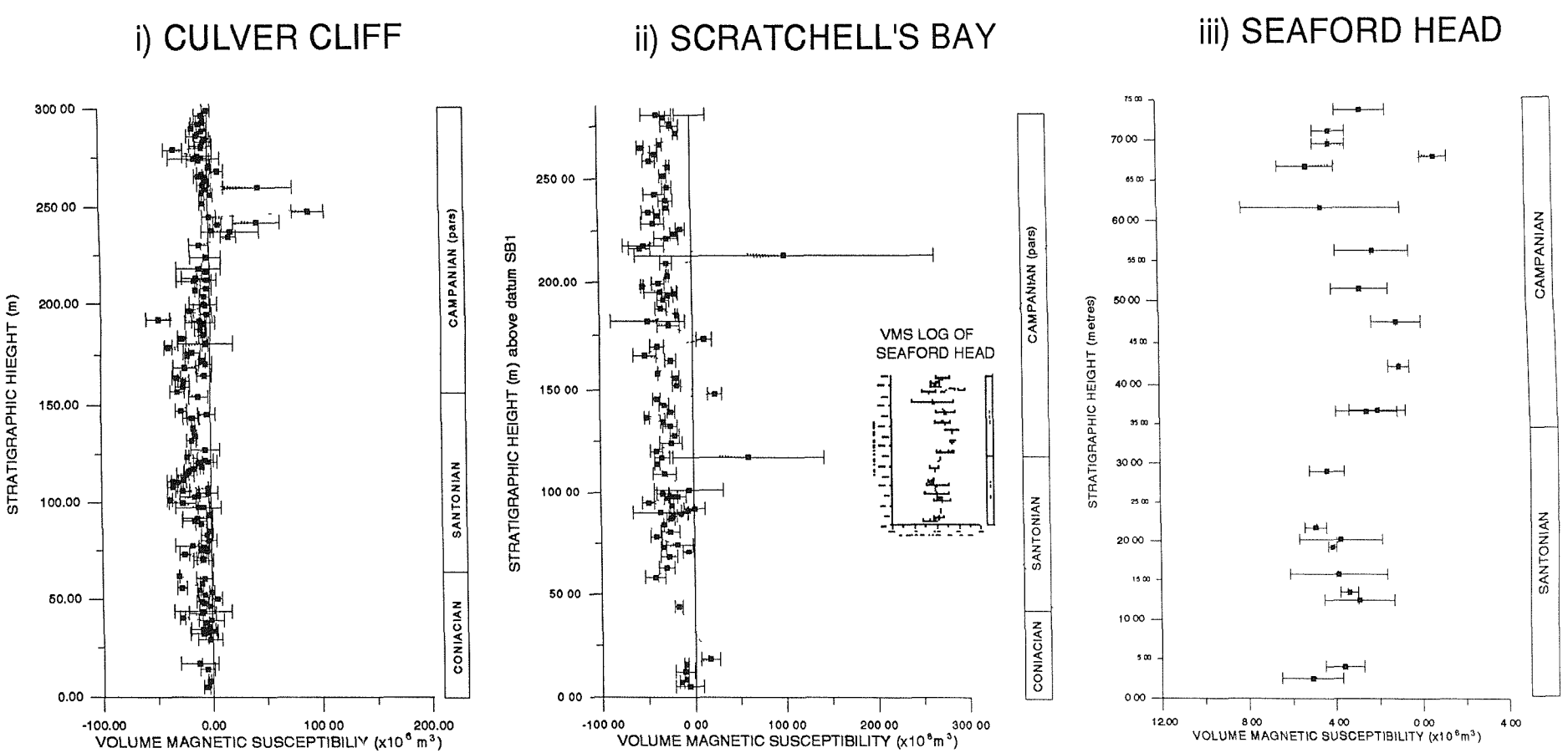

Figure 8.32. Plots of Volume Magnetic Susceptibility (VMS) for i) Culver Cliff; ii) Scratchell's Bay; and iii) Seaford Head. The plot of VMS for Scratchell's Bay contains an inset of the VMS log from Seaford Head drawn to an appropriate scale to match the stage boundaries. No obvious correlations can be drawn between the sections. Diamagnetic biogenic micrites form the major constituents of English Chalk and as a result dominate VMS measurements. However, fluctuations in the scale of negative magnetic susceptibility response would appear to reflect the very small variations in content of terrigenous material. Due to the very subtle nature of such changes, VMS measurements do not provide a useful means of correlation between chalk sequences. However, possible correlations can be drawn on a much smaller scale (10s of metres). An example of such a correlation can be observed between the Scratchell's Bay and Seaford Head VMS logs (ii & iii) across the Santonian-Campanian boundary.

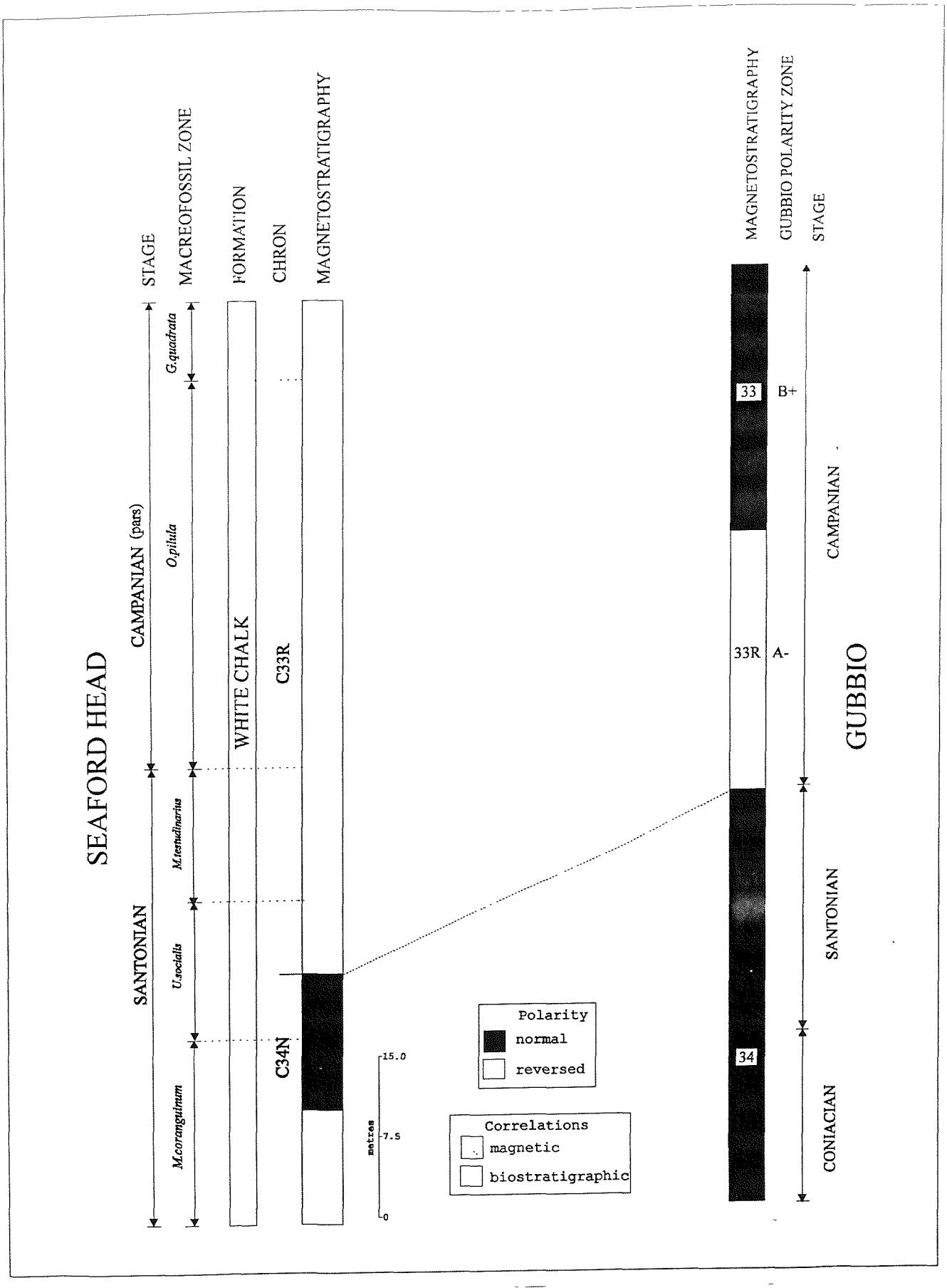

Figure 8.33. Correlation of magnetostratigraphic results from Seaford Head, East Sussex, with magnetostratigraphic results from Gubbio, northern Italy. The left hand side of the diagram shows Late Cretaceous Stage boundaries, macrofossil zones, geomagnetic polarity Chrons and the magnetostratigraphy determined for the study of Seaford head. The right-hand side of the diagram shows magnetostratigraphic results of the Alvarez *et al.* (1977) study at Gubbio. Geomagnetic polarity Chrons are indicated, along with the polarity zones identified, and the Late Cretaceous Stage boundaries.

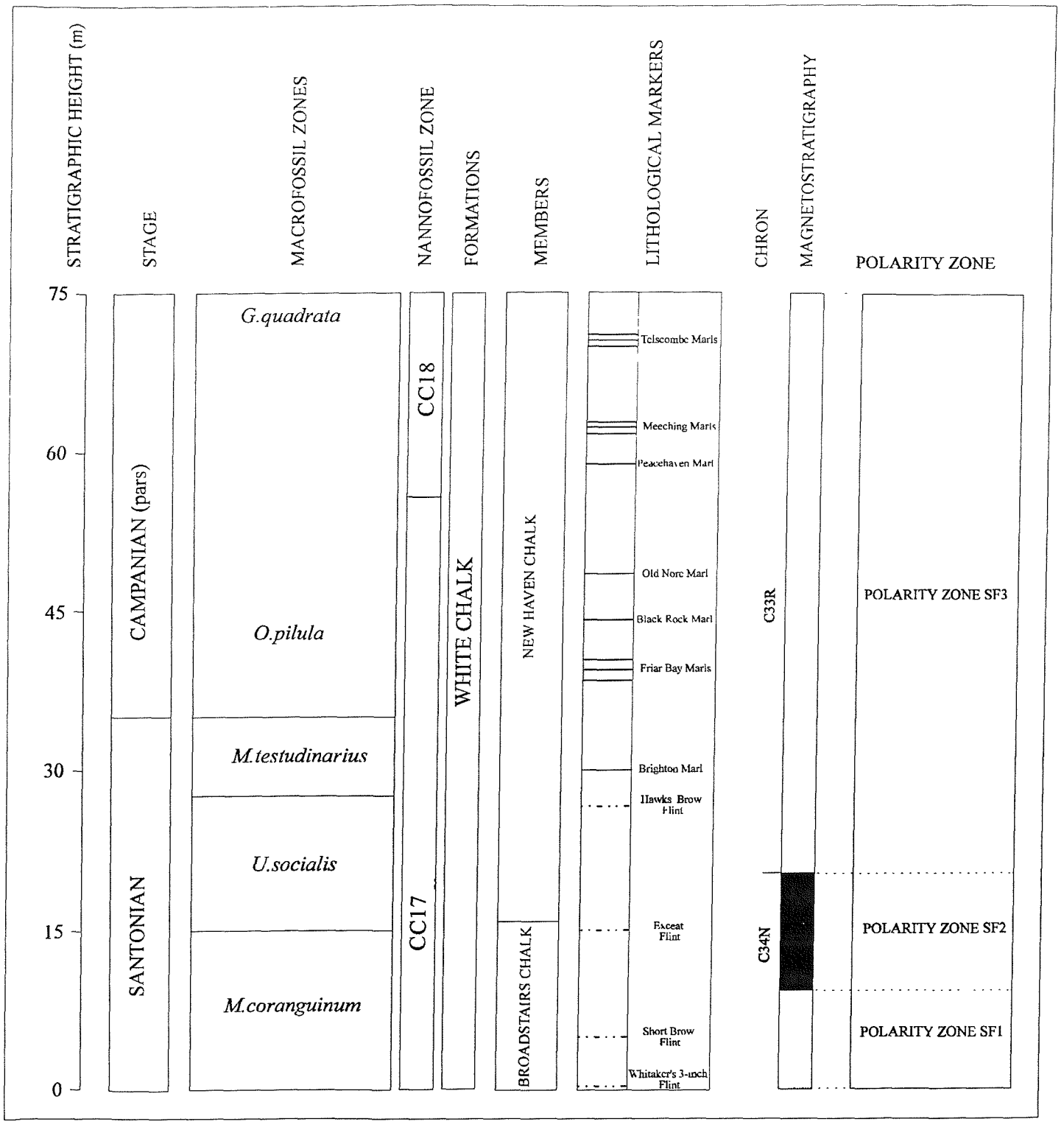

Figure 8.34. Summary diagram showing stratigraphical details of the Late Cretaceous Chalk sequence at Seaford Head, East Sussex. From left to right the diagram shows stratigraphic height above Whitaker's 3-inch Flint, Late Cretaceous Stages, macrofossil zones (Rawson *et al.*, 1978), nannofossil zones (Sissingh, 1978), formations, members, lithological markers, geomagnetic polarity Chrons, magnetostratigraphy and associated polarity zones.

Chapter 9 Conclusions

9.1 Summary of palaeomagnetic and magnetostratigraphical results

Results from detailed palaeomagnetic studies of the Late Cretaceous sequences of Culver Cliff and Scratchell's Bay (Isle of Wight) and Seaford Head, East Sussex have been presented. These are summarised in Figure 9.1. The sections range in age from latest Turonian to early Late Campanian and consist of white chalk with flints. Hand samples and large volume rock cores have been collected. Both thermal and AF demagnetization have been used to remove magnetic overprints. Measurements have been carried out using a CCL and a 2-G 'wholecore' cryogenic magnetometer. Averaged NRM intensities range between 0.0015 and 1.6008 mA/m. By carrying out repeat measurements on large volume samples, reliable determination of the remanence of such weakly magnetic rock has been possible. IRM acquisition experiments suggest the presence of single and multi-domain titanomagnetite. Hematite and mixtures of hematite and magnetite also occur. Polarity zones representing Chrons, C33N, C33R and C34N have been located and reliably tied to the macrofossil and nannofossil biostratigraphic zones in the sections studied.

Detailed magnetic mineral extraction experiments carried out by Dr M. Hounslow of the University of East Anglia have so far extracted silicate grains containing magnetic mineral inclusions and very small quantities of ultra-fine grained black magnetic particles from the chalk of Culver Cliff, Scratchell's Bay and Seaford Head (M. Hounslow, *pers. comm.*). The finest portion of the magnetic extract (≈10% of total extract) has revealed the presence of bacterial magnetite preserved as individual grains and chains. Sample horizons which contain the highest proportion of bacterial magnetite appear to have higher NRM intensities. No evidence has been detected from these studies to suggest that the growth of a secondary magnetic mineral has occurred. However, the major problem encountered during these studies is the extremely small quantity of non-carbonate material obtained from the samples after carbonate dissolution. Typical magnetic extracts from an 8000 gram sample weigh 1-2 mg. A 3500 cm^3 block of chalk was required to obtain a sufficient quantity of

non-carbonate material. An exact determination of the magnetic mineralogy, using XRD and microscopy (SEM and TEM), has yet to be carried out.

9.2 Biostratigraphy

A discrepancy exists between the macrofossil and the nannofossil biostratigraphies derived for the Late Cretaceous chalk successions of southern England.

According to the macrofossil zonation, based on the scheme proposed by Rawson *et al.* (1978), the Chalk successions range from Coniacian to early Late Campanian (Figure 9.1). However, the nannofossil zonation, based on the scheme of Sissingh (1977), places the sequence within the Late Santonian to early Late Campanian (Figure 9.1).

Current opinion (e.g. Haq *et al.*, 1988; Cande & Kent, 1992) places the geomagnetic polarity Chron C34N/33R boundary at or above the Santonian-Campanian Stage boundary. However, the exact relationship between these boundaries is a matter of some debate (Gale *et al.*, *in prep*). The magnetostratigraphic results from the present study place the C34N/33R boundary within the lower-middle portion of the *Uintacrinus socialis* macrofossil zone (early Late Santonian) and midway through the range of the nannofossil zone CC17 (Early Campanian).

McArthur *et al.* (1992) reported that the biostratigraphic examination of the British Geological Survey Trunch borehole has shown that the macrofossil and nannofossil schemes are in close agreement in northeast Norfolk. Though a distinct faunal divide can be inferred across Britain in Northern East Anglia the biostratigraphic scheme proposed by Rawson *et al.* (1978) was based on zones which could be recognised throughout the UK. Thus, from a stratigraphic viewpoint a basis existed to undertake correlations between the two subprovinces. The apparent diachroneity displayed by the biostratigraphic zonations for the Chalk successions of southern Britain therefore requires further examination.

The Late Cretaceous Tethyan nannofossil zonation proposed by Sissingh (1977) was based on the study of the section at El Kef, Tunisia. Numerous authors have since developed similar biostratigraphic schemes from many parts of the world, basing their studies on Sissingh's original work. Slightly different zonal schemes were proposed by Perch-Nielsen (1979) and Wise (1983) for the South Atlantic, by Roth (1978) and Doeven (1983) for the North Atlantic area, by Roth (1978) and Martini (1976) for the Pacific Ocean and by Verbeek (1976a, b, 1977a, b) for Tunisia and Europe. Therefore, the development of a magnetostratigraphy for the Tunisian Late Cretaceous successions would be of great benefit to Late Cretaceous stratigraphy as a whole. Such a study may help to establish whether the apparent diachroneity displayed by the biostratigraphic zonations of southern England is a localised problem or that this is a major problem which exists between the standard nannofossil zones and the local UK biostratigraphy (as proposed by Rawson *et al.*, 1978) developed by using benthonic fossils composed of calcite.

9.3 Correlation of Late Cretaceous chalk successions in southern England

Magnetozones within the chalk successions of southern England, corresponding to geomagnetic polarity Chrons C34N, C33R and C33N, can be identified and provide a pattern of magnetic polarity reversals which form the basis of the magnetostratigraphic correlation shown in Figure 9.2. The start of magnetochron C33R, represented by polarity zones CC2 (Culver Cliff, Figure 6.36), SB4 (Scratchell's Bay, Figure 7.33) and SF4 (Seaford Head, Figure 8.34) occurs within the middle of lower part of the *Uintacrinus socialis* Zone, while the start of magnetochron C33N, represented by polarity zones CC5 (Culver Cliff) and SB7 (Scratchell's Bay) is less well defined, falling in the *Belemnitella mucronata* Zone of the Late Campanian. Magnetochron C34N is represented by polarity zones CC1 (Culver Cliff), SB1 to SB3 (Scratchell's Bay), and SF1 to SF2 (Seaford Head).

The Chalk successions also preserve a record of numerous smaller scale geomagnetic polarity events which offer the potential for more detailed correlations. Differences in sampling frequency between the three sections has tended to distort the pattern of

reversals revealed and caution must be exercised when attempting to correlate the fine scale details. Moreover, the chalk at Culver Cliff has acquired a highly stable overprint in the recent geomagnetic field, which tends to obscure fine scale magnetic polarity reversals. This problem is further exascerbated by a reduction of approximately 20° in the bedding inclination for the lowest 125 metres of chalk at Culver Cliff. Thus, application of a bedding correction is less effective in distinguishing between primary and secondary magnetic components. However, thermal demagnetisation has indicated the presence of poorly defined reverse polarity events within this interval of chalk. Their position, in relation to the biostratigraphic zones, indicate that they might correspond to the reversed intervals defined at Scratchell's Bay (polarity zone SB1, SB2 and SB3, Figure 7.33) and Seaford Head (polarity zone SF1, Figure 8.34). Their approximate positions are indicated in Figure 9.2 by magnetic correlation lines terminated by a question mark (-?). For the exact position of these intervals please refer to Figure 6.7b & c. Further sampling and thermal demagnetisation should reveal the extent of these reverse polarity intervals within the chron C34N record at Culver Cliff.

A reverse polarity interval was found to straddle the Coniacian/Santonian boundary in the Scratchell's Bay section (polarity zone SB2). The detection of a potentially correlatable reverse polarity interval in what was previously regarded as an exclusively normal magnetic polarity interval (Chron C34N) is of great significance. Knowledge of the mid-Cretaceous geomagnetic polarity reversal pattern is based on the interpretation of marine magnetic anomalies (Larson & Pitman, 1972; Larson & Hilde, 1975) which have been confirmed by magnetostratigraphic study of uplifted Tethyan marine sequences (Lowrie *et al.*, 1980a, b: Lowrie & Alvarez, 1977). These studies have defined two reverse polarity zones, corresponding to chrons C33R and M0, bounding an approximately 34 million year interval of normal polarity, the Cretaceous Normal Polarity Superchron (K-N). However, other data sets indicate that the picture of mid-Cretaceous geomagnetic polarity may be incomplete (Tarduno *et al.*, 1992). Palaeomagnetic data from sediment cores retrieved on DSDP leg 26 in the Indian Ocean were construed by Green & Brecher (1974) and Jarrard (1974) as confirmation of some short intervals of reversed polarity in the Albian. Based on this interpretation,

van Hinte (1976) described a "site 263" mixed polarity interval in the mid-Cretaceous. Hailwood *et al.* (1980), interpreted palaeomagnetic data from the Bay of Biscay (DSDP leg 40) as representing several "short-period reversed events" in the Albian and correlated these with the "site 263" mixed polarity interval. Urrutia-Fucugachi (1988) has explained data from a preliminary magnetostratigraphic study of the Morelos Formation (southern Mexico) as recording a reverse polarity "event" in the Late Albian. Palaeomagnetic and palaeontologic data from the Valle delia Contessa (Umbrian Apennines, Italy) span a 14 million year gap in previously studied magnetostratigraphic sections and have revealed several intervals of reverse ChRM in limestones and marls of the Albian Marne a Fucoidi (Tarduno *et al.*, 1992). Moreover Hambach & Krumsiek (1989) describe a series of reversed polarity intervals of Albian and Cenomanian age from the study of drill cores in the Ruhr area (western Germany). The Cenomanian has been sampled in detail in several sections (e.g. Alvarez & Lowrie, 1978; Channell *et al.*, 1979a) and no intervals of reversed polarity had been previously identified in Cenomanian-age sediments. The only hitherto reported example of Cenomanian reversed polarity intervals were by Vandenburg & Wonders (1980) from the Quero-Schievenin section. However, it should be noted that the definition of the Santonian-Coniacian portion of the K-N is based, to a large extent, on the work of Lowrie & Alvarez (1977). This magnetostratigraphic study employed only AF demagnetisation to undertake polarity determinations. Tarduno *et al.* (1992) believe that the data from Gubbio and Moria may be biased by unremoved overprints. Furthermore, Gale *et al.* (*in prep.*) indicate that an unstudied interval of 24 metres was missed in the log of Arthur & Fisher (1977) which was used by Lowrie and Alvarez (1977) as the basis of their study.

Confirmation of the presence of the reverse polarity zone SB2 is required from other sections. By sampling at lower stratigraphic levels at Seaford Head it should be possible to detect the presence of this reverse magnetic polarity interval. At Culver Cliff re-sampling across the Coniacian-Santonian boundary, combined with the further application of thermal demagnetisation, may locate its position.

A geomagnetic polarity reversal of such magnitude (*c.* 400,000 year duration; Figure

9.4) should be preserved within the marine magnetic anomaly patterns of fast spreading ocean crusts. However, no evidence from marine magnetic anomaly or magnetostratigraphic studies has been reported to suggest the presence of a reverse magnetic polarity interval during this interval of time. A detailed re-examination of magnetic anomaly data within a fast spreading ocean basin is recommended (e.g. South Atlantic).

The reverse polarity magnetozone SF1 located at the base of the Seaford Head section has been correlated with a mixed but dominantly reverse polarity interval magnetozone SB3 within the Scratchell's Bay section. Good control for this correlation is provided by Whitaker's 3-inch flint band which underlies this polarity zone and can be recognised in all three sections. This reverse polarity interval has not yet been identified at Culver Cliff due to the extremely low magnetic intensity of the chalk in this part of the section. However, by re-sampling and using thermal demagnetisation, location of its position should be possible. It must be noted that a fluctuating transition between normal and reverse magnetic polarity at the Chron C34N/C33R boundary has not been reported by any former study, nor from the examination of the marine magnetic anomaly record.

A further magnetostratigraphic correlation can be made between polarity zones CC3 at Culver Cliff and SB5 at Scratchell's Bay. These zones represent an interval of time in which a rapid fluctuation between reverse and normal polarity occurred. Though more normal polarity events can be recognised within polarity zone CC3 than in SB5 this might be explained by the higher sampling frequency (sample interval of 1.45 metres) within this part of the section at Culver Cliff compared with that used at Scratchell's Bay (sample interval of 2.40 metre). However, the possibility exists that during the intervening time between deposition of the Chalk and the Miocene folding event (a period of time which saw the uplift of the British Isles, gentle folding of the Chalk and subsequent erosion of Maastrichtian-latest Campanian strata) a secondary magnetic remanence has been acquired. Additional thermal demagnetisation of samples collected within polarity zone CC3 may resolve this discrepancy. It should be noted that both Hambach & Krumsiek (1991) and Lerbekmo (*pers. comm*) report

the presence of normal polarity intervals midway through Chron C33R.

This distinctive magnetic polarity interval is not preserved at Seaford Head. The possibility remains that 15 metres of unsampled chalk at the top of the Seaford Head section may preserve a record of the lower limits of these geomagnetic polarity reversal events. Through the chalk at this level is poorly preserved magnetostratigraphic examination of this part of the section would be possible.

9.4 A composite magnetostratigraphy for the Late Cretaceous chalk successions of southern England

The completeness of marine sedimentary successions on continental shelves is controlled by such factors as variation in sediment supply, fluctuating subsidence rates, and eustatic sea level changes, which are interrelated in a complex fashion (e.g. Haq *et al.*, 1988). Few, if any, shelf successions have a reasonably even representation of time over intervals of more than a million or so years (Gale, 1990). Thus, the traditional practice of biostratigraphy has been to construct a composite faunal succession by the intercalation of data from the most complete sections available (e.g. Hazel & Kauffman, 1975). The same approach can be adopted to construct a composite magnetostratigraphy.

Results from these detailed palaeomagnetic studies of the Late Cretaceous sequences of Culver Cliff, Scratchell's Bay and Seaford Head have been presented in Figure 9.2 with polarity zones, representing Chrons C33N, C33N and C34N, have been located and reliably tied to the biostratigraphic zones in the sections studied. By constructing a composite magnetic stratigraphy from the most complete successions representing geomagnetic polarity Chrons C34N, C33R and C33N a standard magnetic polarity stratigraphy for Late Cretaceous deposits in southern England is proposed (Figure 9.3).

Chron C33N is based on results obtained at Culver Cliff while the rest of the composite is based mainly on the magnetostratigraphic results obtained from Scratchell's Bay. The lowest part of the magnetic polarity composite is based on data

from Culver Cliff. Magnetostratigraphic details from Seaford Head confirmed the position of the reversal at the top of Chron C34N.

9.5 Calibration of the Late Cretaceous magnetostratigraphic timescale for southern England.

In recent years numerous geomagnetic polarity time scales have been published (e.g. Heirtzler *et al.* (1968); LaBreque *et al.* (1977); Lowrie & Alvarez (1981); Berggren *et al.* (1985b); Kent & Gradstein (1985); Harland *et al.* (1990); and Cande & Kent 1992). Of these, the time scale of Kent & Gradstein (1985), Harland *et al.* (1990) and Cande & Kent (1992) have received popular acceptance. However, each time scale varies according to the age calibration points used.

The Kent & Gradstein (1985) time scale draws on the geochronology and chronostratigraphy proposed by Berggren *et al.* (1985a) and is based on an assessment of Late Cretaceous plankton datums directly correlated with magnetostratigraphy in deep-sea sediment cores and land sections. Magnetochronological estimates are derived from an age-calibration model for the ridge-crest marine magnetic anomalies published by Berggren *et al.* (1985b). A derived age of 56.14 Ma for the older end of anomaly 24 and a tie-point age of 84 Ma for anomaly 34 or the older end of the Cretaceous Long Normal (Campanian/Santonian boundary; Obradovich & Cobban 1975; Lowrie & Alvarez, 1977) serve to calibrate the portion of the geomagnetic reversal sequence that extends into the Cretaceous. Numerical ages for the Santonian to Aptian stage boundaries are taken directly from the geochronometric estimates of Harland *et al.* (1982) which are largely based on assessment of isotopic ages from the list of Armstrong (1978) since no well-documented magnetozones or anomalies can be correlated and used for interpolation.

The time scale of Harland *et al.* (1990) uses dates based on the evaluation of all the accessible diagnostic radio-isotopic age data derived in the form of chronograms for geologic stage boundaries. A chronogram represents a gauge of the general inconsistency in a set of constraining radioisotopic age data as a function of trial ages

for a particular boundary. The best chronogram approximation of a boundary age is that which minimizes the measure of inconsistency among the dates weighted according to their particular analytical errors. Therefore, in principle, a chronogram estimate represents the influence of all the available radioisotopic data and as a result should provide a date which is particularly robust. The Late Cretaceous portion of the Harland *et al.* (1990) time scale (about 50 to 85 Ma) is poorly constrained by four chronograms. As a result, Harland *et al.* (1990) used values of 65 Ma for the Danian/Maastrichtian boundary and 83 Ma for the Campanian/Santonian boundary relying on values previously employed by the Harland *et al.* (1982) time scale.

The two age calibration points by Cande & Kent (1992) for the Late Cretaceous portion of time scale were based on K-Ar dates and are described in detail in section 4.4.

Palaeomagnetic studies of the chalk successions in southern England have thus provided two magnetostratigraphic age calibration points; the geomagnetic polarity Chron boundaries C34N/33R and C33R/33N. Each time scale provides a different duration for this interval of time. Harland *et al.* (1990) allot ages of 79.09 Ma and 83.00 Ma to the younger and older limits of Chron C33R, inferring a duration of 3.91 million years, while Kent & Gradstein (1985) assign ages of 79.75 Ma and 84.00 Ma inferring a duration of 3.75 million years. Cande & Kent (1992) specify ages of 83.00 and 78.78 Ma for the geomagnetic polarity Chron boundaries C34N/33R and C33R/33N inferring that this Chron spanned 4.22 million years.

By assuming that the deposition of the Chalk was relatively constant, an assumption based on the regular repetition of flint bands at 0.5-2.0 metre intervals throughout the Chalk, three magnetostratigraphic time scales for southern England are presented (Figure. 9.4).

Figure 9.4 provides a comparison of the ages generated for the Late cretaceous chalk succession of southern England using the magnetostratigraphic age calibration points of the C34N/33R and C33R/33N boundaries and the dates assigned to them by Cande

& Kent (1992), Harland *et al.* (1990) and Kent & Gradstein (1985). The separate time-scales indicate durations for Chron C33R which are in close accord. However, the good agreement between authors does not mean that their dates are accurate, only that they are precise (McArthur *et al.*, 1992).

When comparing the time scale produced by the different calibration points of Cande & Kent (1992), Kent & Gradstein (1985) and Harland *et al.* (1990) the differences are relatively minor (Figure 9.4). Table 9.1 shows dates and durations of UK stages and macrofossils zones for these time scales.

9.6 A Late Cretaceous magnetostratigraphic time scale for southern England

Since the time scale of Cande & Kent (1992) employed the most recently available radioisotopic age data for the calibration points the dates they suggest for the older and younger limits of Chron C33R have been adopted for this study.

The magnetostratigraphic studies of the chalk successions in Southern England have thus provided magnetostratigraphic age calibration points of 83.000 and 78.781 Ma (the C34N/33R and C33R/33N boundaries of Cande & Kent, 1992). By assuming that the deposition of the Chalk was relatively constant a magnetostratigraphic time scale for southern England is proposed (Figure 9.5).

The proposed magnetostratigraphic time scale for southern England relies on the positional accuracy of the age calibration points used by Cande & Kent (1992) to construct their time scale. It should be noted that uncertainty exists in assigning numerical ages to stage and biostratigraphic zone boundaries due to problems of boundary definition and recognition.

This time scale has made it possible to assign dates to the stage and macrofossil zone boundaries located within the English chalk, calculate their durations and date rhythmic fluctuations in sedimentation.

9.7 Magnetostratigraphic calibration of the McArthur *et al.* (1992) Strontium isotope stratigraphy for the Late Cretaceous

In recent years, as knowledge of the Sr-isotope evolution of oceans has become more refined, there have been significant developments in strontium isotope stratigraphy and its application to correlating and dating ancient marine carbonate sequences. Numerous papers recently in print or in press have added tremendously to the detail and definition of the Strontium isotopic curve available for the last 200 million years (McArthur *et al.*, 1993). For this technique to reach its full potential, the period for which the isotope curve has been generated must be accurately calibrated against well documented biostratigraphy and magnetostratigraphy (e.g. Miller *et al.*, 1988). Until recently, neither condition applied to the Late Cretaceous.

McArthur *et al.* (1992) have recently published a 'standard' marine $^{87}Sr/^{86}Sr$ isotope curve for the Late Cretaceous (Figure 9.6) based on the study of macrofossils and nannofossil chalk through a section of the English Chalk, at Trunch in Norfolk. The study closely integrated the strontium isotope stratigraphy with macrofossil (Rawson *et al.*, 1978) and nannofossil biostratigraphic zonations (Sissingh, 1978). English Chalk, and its macrofossils have been shown to be good preservers of Late Cretaceous marine $^{87}Sr/^{86}Sr$ variations (McArthur *et al.*, 1992). However the curve has not yet been calibrated against a magnetostratigraphy, due to difficulties in measuring the extremely weak remanent magnetism of the Chalk.

As has been shown, developments in measurement procedures using CCL and 2G cryogenic magnetometers, with large sample volumes and employing multiple measurement procedures during progressive demagnetisation, have resulted in successful magnetostratigraphic investigations of such weakly magnetised deposits. Results of these studies indicate that deposition of the English Chalk spanned geomagnetic Chrons C34N, C33R and C33N, thus providing two potential magnetostratigraphic calibration points for the marine $^{87}Sr/^{86}Sr$ isotope curve (the C34N/33R and C33R/33N boundaries). An age uncertainty of ±0.5 million years and a positional uncertainty of ±5 metres for the chron C34N/33R and C33R/33N

boundary calibration points has been assumed. By plotting the age of the upper and lower limits of Chron C33R against stratigraphic height of the composite magnetostratigraphy for southern England it is possible to date both stage and macrofossil zone boundaries (Figure 9.7). These ages (with associated errors) can be transferred to the biostratigraphic macrofossil and stage boundaries identified in the Trunch Borehole (Figure 9.8).

The approximately linear increase in $^{87}Sr/^{86}Sr$ that occurs from Coniacian to the early Maastrichtian was interpreted by McArthur *et al.* (1992) to suggest that neither the temporal evolution of marine $^{87}Sr/^{86}Sr$, nor the sedimentation rate of the Chalk, varied greatly during this period. Moreover, McArthur *et al.* (1992) report that due to near-perfect linearity in $^{87}Sr/^{86}Sr$ with thickness of section being shown by other Late Cretaceous sections numerical ages may be assigned to biostratigraphic boundaries by interpolation assuming a linear change in $^{87}Sr/^{86}Sr$ per million years. This assumption appears to be supported by the plot depth within the Trunch Borehole versus age of Coniacian-Campanian macrofossil and stage boundaries (Figure 9.9). The straight line indicated fits the data extremely well.

By plotting the $^{87}Sr/^{86}Sr$ data reported by McArthur *et al.* (1992) for the Coniacian to the early Late Campanian stages versus age (using Figure 9.8 to determine the age of each $^{87}Sr/^{86}Sr$ sample horizon) and by assuming that the $^{87}Sr/^{86}Sr$ ratio increased in an approximately linear fashion an age-calibration graph can be generated (Figure 9.10) from which any $^{87}Sr/^{86}Sr$ curve for Conician-Campanian times can be dated. Figure 9.11 shows the $^{87}Sr/^{86}Sr$ curve of McArthur *et al.* (1992), the time scale generated from the magnetostratigraphic correlation points determined from the Chalk of southern England and the macrofossil zonation of Rawson *et al.* (1978). Due to the major discrepancy between the macrofossil and nannofossil biostratigraphy determined for the Late Cretaceous only the macrofossil zonation was used to position the magnetostratigraphic calibration points against the $^{87}Sr/^{86}Sr$ curve. Table 9.2 lists ages of the macrofossil biostratigraphic zones according to the magnetostratigraphic time-scale developed in section 9.6 along with the $^{87}Sr/^{86}Sr$ values which mark these boundaries.

9.8 Orbitally induced chalk-flint cycles in Late Cretaceous deposits of southern England

Milankovitch (1941) proposed that the orientation of the earth's axis of rotation and the shape of its orbit affect the distribution of the sun's insolation on the earth's surface. Strong support for this theory has been obtained from the study of the deep-sea sediment record (Kennett, 1982). Power-spectrum analysis of records for the last 500,000 years have revealed that the climatic curve was dominated by fluctuations with period-lengths close to 100,000 years, 40,000 years and 20,000 years (Hays *et al.*, 1976).

Rhythmic alternations in carbonate content and other characters of pelagic sediments are found in many stratigraphic successions (e.g. De Boer & Wonders, 1984). Suggested mechanisms for the formation of such sequences include variations in the supply of the sediment components, dissolution and diagenic processes (De Boer & Wonders, 1984). Mean periodicities of near 20, 40, 100 and 400 kyr have been recognised with some confidence for Mesozoic sediments (e.g. Herbert & Fisher, 1986). Frequently, reference is made by authors to astronomical influences as possible causes of such rhythmicity. Moreover, the above periodicities are found also in parameters which define the orbital elements; precession, obliquity and eccentricity respectively (Fisher & Schwarzacher, 1984).

Precession is the change in the orientation of the earth's axis during its orbital motion around the Sun, and determines at what point on the earth's elliptical orbit winter and summer occur at the Earth's surface. When the earth is closer to the sun warmer winters occur. The quasi-periodic precession index has a periodicity of 23,000 years. *Obliquity* is the tilt of the Earth's axis away from the plane of the Earth's orbit and varies between 22.1° and 24.5°. It takes 41,000 years to complete one cycle. *Eccentricity* describes variations in ellipticity of the Earth's orbit and occurs on a 100,000 year cycle. The eccentricity cycle causes at most a 0.1% change in insolation at the earth's surface (Kennett, 1982).

The characteristic rhythmic bedding of the Upper Cretaceous pelagic carbonate sequences of the UK, as represented by flint bands and marl seams (Plate 9.1), have been interpreted as a result of such orbital variations (Hart, 1987). Though investigation of the chalk-flint cycles within the English Chalk have been previously attempted, difficulties in locating and dating Late Cretaceous stage boundaries has proved a major hindrance in such studies (e.g. Hart, 1987). The recent development of a magnetostratigraphic time-scale for the Late Cretaceous of southern England has alleviated these problems.

9.8.1 Chalk facies and flint formation

The Cretaceous Chalk of western Europe consists predominantly of pelagic micrites. The bulk of this pelagic material is the debris from carbonate coccolithophorid planktonic algae. Coccolithophores are predominately autotrophic nannoplankton (i.e. between 5-60 μm in size) utilising the energy fron sunlight to photosynthesise organic materials from inorganic ones (Brasier, 1980). Living cells are therefore largely restricted to the photic zone of the water column (0-200 metres depth). They thrive either in zones of oceanic upwelling or pronounced vertical mixing where vital minerals are most readily available. Tiny calcareous scales called coccoliths (3-15 μm in diameter) form around these cells a protective armour (Brasier, 1980). After death, coccolithophores sink through the water column, dissolving or disaggregating into finely dispersed carbonate matter at depth. Their minute skeletons amass between the limits of wave effectiveness and the calcium carbonate compensation depth (approximately 3 km, Anderton *et al.*, 1979).

Little evidence exists to suggest strong scouring and current action on the floor of the Chalk sea, and accumulation in 'deepish' water is suggested (Hancock, 1975). However, chalk ooze was not merely deposited in flat spreads, but was sometimes piled into heaps and banks. British examples of such features seem to represent current sweepings or differential erosion shortly after original deposition (Hancock, 1975).

Contradictory evidence from separate fossil groups for the depth of the Chalk sea exists (Anderton *et al.*, 1979). Particular foraminifers indicate shallow water (a few metres), whereas the occurrence of hexactinellid sponges imply depths of 80-100 metres (Reid, 1968). Well-developed coccoliths in outcropping chalk suggest that little etching has occurred and that deposition between 100 metres and 600 metres seems probable (Hancock, 1975).

Thin marl seems are a common feature of the Chalk successions. The chalk-marl rhythms portray primary sedimentary features and therefore depict true bedding. Most marl seams rest on erosional surfaces (Jefferies, 1963) which mark a break in calcite deposition accompanied by a supply of clay. However, most chalk sequences contain frequent small breaks in sedimentation, without interventions of marl, which Bromley *et al.* (1975) describes as "omission surfaces".

The flints in the Upper Cretaceous or western Europe are a product of early diagenetic silica precipitation. An understanding of the processes responsible for flint formation is of great importance when attempting to investigate the apparent rhythmicity in their formation. The mechanism of flint formation (Figure 2.5) was first described in detail by Clayton (1984). Aerobic bacterial degradation of organic matter in the upper layers of the chalk sediment progressively depletes the pore waters of dissolved oxygen, creating at depth (several metres), oxygen concentration too low to sustain aerobic bacteria. Oxidation of organic matter continues below this depth using sulphate (SO_4^{-2}) as the ultimate electron acceptor, thus causing the sediment to become sulphate reducing.

Under such conditions, large amounts of dissolved sulphide, in the form of H_2S, are released into the pore water and migrate towards more oxic levels. At the redox boundary, sulphide-oxidising bacteria re-oxidise the H_2S to SO_4^{-2}, liberating hydrogen ions as a by-product. The hydrogen ions released lead to intensive but local calcite dissolution, and the carbonate ions initiate seeding of silica from a saturated solution.

The morphology of the flint appears to have been determined by the geometry of the

H_2S-O_2 mixing zone. In homogeneous, well-bedded sediments, where burrows were either absent of poorly defined, mixing occurred in an even, regular layer, resulting in the formation of a tabular flint. However, where burrows were clearly defined, and the sediment contained within them was substantially more permeable than the surrounding chalk, mixing was confined largely to within burrow systems, creating nodular or burrow-form flints.

The depth of the 'redox-boundary' within the chalk was probably quite variable. However, dilution of clay minerals within flint imply that a sediment porosity of 75-80% existed when the silica structures became resistant to compaction. It can thus be deduced that flint formation occurred within the top 10 metres of sediment. Moreover, the minimum depth of flint formation can be inferred from the height of the tallest paramoudra; paramoudra are large columnar, barrel or pear shaped flints which are unusual in that they clearly formed around a central pyritised, glauconitised, and frequently phosphatised central burrow within a cemented chalk core (see Bromley *et al.*, 1975; Clayton, 1984) and form within generally oxidising conditions above the redox boundary. In general, therefore, a depth of between 5 and 10 metres below the sediment surface is implied for flint formation, though in some cases silicification may have started at a shallower depth (Clayton, 1986).

The regular repetition of flint bands appears to reflect the underlying rhythmicity of Chalk sedimentation (Plate 9.2). Each hiatus in sedimentation provided a prolonged period whereby a stationary redox boundary, several metres below the sediment surface, gave rise to a flint band. On re-commencement of sedimentation, the comparatively rapid accumulation of sediment restricted the development of a stable redox stratification, and thus prevented flint band formation until the next hiatus. Thus it can be concluded that well-developed, laterally continuous flint bands may represent breaks in sedimentation, while small impersistent flints may form below local washout or sheltered environments. Every gradation from omission-surfaces to well-marked diagenetic hard-grounds have been reported in Chalk sequences (Kennedy & Garrison, 1975).

Most chalk sequences record small breaks in sedimentation about 0.5-2.0 metres apart. Many of these lithological features within the U.K. succession can be traced over substantial areas, suggesting basin-wide control of the sedimentary environment. Thus, it has been concluded that an external control rather than a local set of conditions is responsible for flint band formation (Robinson, 1986).

The lack of re-worked flints is associated with the complex growth history of the flint, following nucleation (Clayton, 1982, 1986). Replacement of the calcite begins with fine scale displacement of skeletal calcite, and then proceeds in the principal stage of growth by intense precipitation of disordered cristobalite (opal-CT) lepispheres (spherical aggregates of bladed crystals). Re-working of flints at this stage of growth would tend to disaggregate the lepispheres. Although the lepisphere skeletal fragment framework was self-supporting, it did not become firmly cemented until some time later, upon precipitation of interstitial opal-CT chalcedony phase. Only during later 'burial' diagenesis did the opal-CT proto-flint recrystallised to its current α-quartz mineralogy.

Flint bands are therefore the result of chemical segregation of silica which was originally dissolved in pore waters of the sediment, probably derived ultimately from the dissolution of biogenic silica, particularly sponges (Clayton, 1986). Though they are not primary depositional features their formation is a direct response to variations in the sedimentation rate. Flint bands thus represent a binary signal driven by pauses in sedimentation.

Hiatuses in the sedimentation of chalk thus represent a drastic decrease in the production of coccolithophore remains, either as a result of decreased insolation or as a product of a reduction in the availability of essential minerals.

9.8.2 Lithostratigraphical analysis

Attempts to identify orbital parameters from rhythmically bedded marine Mesozoic succession have utilised several approaches which include i) time-series analysis of

bed thickness, calcimetry and densitometry (Fisher & Schwarzacher, 1984; Weedon, 1985; Herbert & Fisher, 1986); ii) division of counted numbers of rhythms into radiometrically dated periods of time or assumed mean durations of ammonite zones (House, 1985; Hart, 1987) and iii) sedimentary characteristics of rhythms produced by different orbital parameters (Fisher *et al.*, 1985; Fisher, 1986). Of these approaches only approach ii) has proved applicable to the examination of chalk-flint cycles.

The magnetostratigraphic time scale proposed in the previous section has made possible the dating of the Chalk successions in southern England. By adopting a similar approach to that used by Hart (1987) examination of the chalk-flint cycles exposed in southern England was attempted.

Using the mean cycle frequency from a sequence of strata it is possible to arrive at an 'idealised' number of cycles for a dated sequence of rock. This was estimated using the mean cycle frequency and the total known thickness of strata in a particular interval of time. Mean cycle duration can then be calculated by dividing the number of 'idealised' cycles into the period of time represented by the sequence of strata. By measuring successions in detail it is possible to plot histograms of the various cycle thickness. The histogram peak indicates the mean cycle frequency present within the sequence.

By determining the mean frequency of the chalk-flints, inaccuracies in section and cycle measurement can be reduced, and an 'idealised' number of cycles for the chalk representing C33N calculated. A histogram of the chalk-flint cycle thickness for the strata enclosed within the 170 metre thick, reverse polarity magnetozone representing Chron C33R at Scratchell's Bay (Isle of Wight) reveals a mean cycle frequency of 0.7 metres (Figure. 9.12). The duration of Chron C33R is approximately 4.219 million years (Cande & Kent, 1992). Around 243 chalk-flint cycles, with a mean duration of 17,362 years, were counted within this time interval at Scratchell's Bay. Similarly, a mean cycle frequency of 0.7 metres was confined by a histogram of 418 flint band cycles from the complete Scratchell's Bay section (Figure 9.13). A mean cycle length of 17,270 years was inferred. Of the orbital parameters described by Milankovitch

(1941) the precession cycle (18 and 23 kyr) have mean periodicities which correspond most closely with the cyclicity deduced from the chalk-flint alternations.

By applying the magnetostratigraphic time scale to other Late Cretaceous sections in southern England, using biostratigraphic correlation, it is possible to examine the cyclicity of chalk-flint cycles elsewhere. Figure 9.14 shows histograms of chalk-flint cycle widths measured for the complete sections at Culver Cliff (i) and Seaford Head (ii). These both reveal single histogram peaks with mean cycle frequencies of 0.7 and 0.5 metres respectively. The complete chalk-flint sequence at Culver Cliff is roughly 300 metres thick and spans a time interval of about 7.68 million years. By dividing the mean flint band cycle frequency into the overall sequence thickness an average value for the number of cycles present within the Coniacian to early Late Campanian chalk of Culver Cliff can be determined. Around 429 cycles, with mean durations of 17,902 years, were calculated for this sequence. Once again, this suggests an astronomical influence exerted by the precession cycle. Similarly, the chalk-flint cycle histogram for Seaford Head indicates an average cycle length of 18,981 years. From these estimates an overall mean duration of 18.7 (±0.56) kyr is obtained. This strongly suggests that the precession orbital parameter (18-23 kyr) was responsible for modulating flint band formation within the Late Cretaceous chalk of southern England.

Evidence to suggest that the longer-duration orbital parameters of obliquity and eccentricity have an effect on chalk sedimentation has not been detected. The reason for this can be easily explained. In a depositional environment where sedimentation rate is uniformly high and where no major erosional events occur, a complete record of the effects of precession, obliquity and eccentricity should be preserved. By undertaking a simple experiment which assumes that all three orbital parameters controlled sedimentation within the Chalk sea it is possible to examine the interference pattern generated by these different wavelength phenomena. Figure 9.15 shows the hypothetical pattern of flint bands generated by the sole operation of i) precession; ii) obliquity; and iii) eccentricity, together with the combined pattern (iv) for 1.2 million years of chalk sedimentation at a rate of 1 metre per 1000 years. From the histogram (Figure 9.16) of the simulated cycle widths it is apparent that, even though

all three orbital parameters may have influenced formation of the flint band sequence, only the shortest frequency event (precession) is detected. Thus, cycle-width histograms tend only to highlight the presence of the shortest wavelength cycles recorded, because of the interference of the longer wavelength cycles.

Fourier analysis has been used in other circumstances (e.g. magnetic susceptibility measurements) to extract the different signals of precession, obliquity and eccentricity from ancient and modern sedimentary sequences. However, flint bands represent a binary signal and therefore this analytical technique cannot be simply applied. The shape of the cycle-width histograms for Scratchell's Bay, Culver Cliff and Seaford Head all show skewed distributions incorporating cycle-widths as great as 2.3 metres. Such shapes indicate that sedimentation rates varied quite considerably during deposition. Moreover, the tails of these plots suggest the possible involvement of other longer-wavelength cycles in flint formation.

9.8.3 Summary

The way in which changes in the earth's orbit or axis of rotations may have had a pronounced influence on Mesozoic climate, ocean circulation and sedimentation in the absence of major ice caps is not well understood (Arthur *et al.*, 1984). However, according to Arthur *et al.* (1984) the influence of insolation variations on local and regional patterns of evaporation and precipitation is the most likely cause of rhythmic patterns observed in Cretaceous sedimentation. Periodic salinity variations in surface and deep waters, and possible changes in surface wind stress, probably influenced nutrient availability, rates of primary productivity, rates of deep-water generation, rates of carbonate dissolution, deep water oxygen content, and other parameters of deep-water chemistry.

Flint bands formed as a result of stable 'redox boundaries' being established within the chalk sediment during pauses in sedimentation. The stability of these boundaries relied on a drastic reduction in chalk sedimentation which was maintained for a significant period of time thus allowing flint formation. The flint bands at the three

sections examined display a mean cyclicity of 18.7 (±0.56) kyr which probably represents the astronomical influence exerted by the precession cycle. Hence, it can be concluded that chalk sedimentation was modulated by the precession cycle. The influence of the other orbital parameters may also have been recorded, but this is not discernable, for reasons discussed above. Chalk sediment was produced by the death and accumulation of coccolithophorid planktonic algae tests and therefore a decrease in sedimentation reflects a decrease in coccolithophorid production or increase in dissolution. Coccolith productivity depends on two essential ingredients; sunlight and the availability of mineral nutrients supplied by upwelling ocean currents. A reduction in either would be responsible for a decline in chalk sedimentation. The orbital precession parameter governs the points on the Earth's elliptical orbit where winter and summer occur; as the earth draws nearer the sun, winters become gradually warmer. Accordingly, coccolith productivity will rise due to an increase in available sunlight. A direct link between coccolith productivity and the influence of an astronomical parameter can therefore be inferred.

The exact cause, or combination of causes, responsible for periodic declines in coccolithophorid productivity within the Chalk seas is presumably far more complex and probably impossible to ascertain. Nevertheless, a link between coccolithophorid productivity and the quasi-periodic precession index has been established.

9.9 A palaeomagnetic pole for the Late Cretaceous of southern England.

The magnetic vectors recorded by rocks of a specific age can be utilised to calculate the location of their corresponding palaeomagnetic pole on the geocentric dipole model for the average geomagnetic field (Tarling, 1983). Any rocks magnetised at a similar time should have the same palaeomagnetic pole position. However, separate areas of the earth's surface, in the form of tectonic plates, are moving relative to each other and so, although the earth's axis of rotation remains fixed in space, the pole position appears to change relative to the tectonic block (Tarling, 1983). Thus successive determination of a pole relative to any one stable block defines a polar wandering path. Every tectonic block will have a unique polar wandering path which

depicts its motion relative to the earth's axis of rotation (Tarling, 1983).

9.9.1 Eurasian Late Cretaceous palaeopoles

Polar wander paths are of vital importance not only in dating but also structural analysis. They are a prerequisite to meaningful palaeogeographic reconstructions. The lack of reliable data of Cretaceous age for Eurasia is a well known problem. Besse & Courtillot (1991) reviewed palaeomagnetic data available for Eurasian, African, North American and Indian plates over the last 200 million years with a view to construct polar wander paths for the aforementioned tectonic blocks. Selection criteria was as follows:

a) At least six sites per pole and six samples per site.

b) A 95% confidence interval less than 15°.

c) Evidence for successful A.F. and/or thermal demagnetisation.

d) A maximum dating uncertainty of 15 million years.

e) Application of a fold test to assess remagnetisation and tectonic structure.

Only two poles for the Upper Cretaceous satisfy the criteria demanded by Besse & Courtillot (1991). These were a palaeomagnetic pole of Long.=181°E and Lat.=76°N derived by Heller & Channell (1979) from the Münster basin (West Germany) and a palaeomagnetic pole of Long.=173°E and Lat.=76°N obtained by Kent *et al.* (1986) from near Nanjing (China).

9.9.2 Calculation of a Late Cretaceous palaeopole for southern England

By using the reliability criteria defined in section 5.8 it has been possible to distinguish between high quality and low quality palaeomagnetic data. By determining

the mean ChRM of each section using only 'S1 reliability' category palaeomagnetic data a series of poles were presented (Section 6.5.8, 7.5.8, and 8.5.8) which represent the Culver Cliff, Scratchell's Bay and Seaford Head sections respectively. The large number of magnetic vectors used to determine each ChRM direction resulted in a seemingly high level of precision. However, such accuracy merely reflects the large number of vectors employed to produce the mean ChRM. By using mean ChRM directions for individual, or groups of closely spaced sample horizons, a palaeopole for southern England can be estimated which avoids such problems and provides a truer reflection of the precision of the palaeopole generated. The inclusion of mean ChRM vectors depends on exhibition of a low alpha 95 values ($\leq 15°$). Twenty-six mean ChRM vectors (Table 9.3) from all three Chalk sections (Figure 9.17) were used to derive a pole to represent southern England during the Late Cretaceous (Figure 9.18).

The directions of 26 'S1 category' vectors before and after bedding correction are displayed on an equal-area stereographic projection in Figure 9.18. The overall mean magnetic direction for southern England has a declination=12°, inclination=36°, k=24.7 and α_{95}=5.6°). From the mean magnetic vector a palaeomagnetic pole of Long.=157.3°E and Lat.=58.2°N was generated.

The criteria proposed by Van der Voo (1988) to classify published palaeopole data was used to assess the reliability and quality of this pole. Six of the seven criteria suggested by Van der Voo (1988) are satisfied. A well constrained biostratigraphic/magnetic age has been determined for the Chalk sequences of southern England. The palaeopole has been generated from 26 'S1 reliability' category specimens and has a precision 'k' value greater than 10 and a low 95% confidence level. Both thermal and AF demagnetisation techniques have been employed to define the data set. A fold test, with respect to the McElhinny (1964) (see section 6.5.5.2), was failed.

As previously mentioned, McFadden & Jones (1980) have shown that the statistical test proposed by McElhinny (1964) is inappropriate. However, analysis using the

more suitable alternative test proposed by McFadden & Jones (1980) was not possible since the palaeomagnetic samples obtained from southern England were not disposed on different limbs of a single fold. As a result only the McElhinny fold test has been applied.

Tectonic coherence and good structural control has been established by previous workers for the Late Cretaceous sequences in southern England (Chadwick, 1993). Apart from one specimen, displaying reverse polarity, all other S1 category specimens are characterised by normal polarity. As a result, only one antipodal reverse was used to assure a good time average of the geomagnetic field. However, the magnetostratigraphic information indicates that these vectors span a time interval of several million years and thus a good time average for the geomagnetic field can be assumed.

Thus, of the seven criteria proposed by Van der Voo (1988), only one is failed. A 'Quality factor' (Q) equal to 6 has therefore been assigned to this palaeopole

On comparing this pole with the Eurasian APW path of Besse & Courtillot (1991) for the last 200 million years (Figure 9.19) it is apparent that a large incompatibility exists between the APW path and the palaeomagnetic pole derived for southern England. Besse & Courtillot (1991) used the pole of Heller & Channell (1979) for the Late Cretaceous portion of their APW path.

Heller & Channell (1979) investigated the palaeomagnetism of Upper Cretaceous Limestones from the Münster Basin, Germany. Marine dominantly horizontal sediments of Late Cretaceous age are exposed throughout an extensive area of the basin. During Cenomanian, Turonian and Campanian times fine-grained, grey, marly to pure limestones were deposited. The Campanian limestones display magnetization components of unidentified age owing to the presence of goethite and hematite. However, in the Cenomanian and Turonian rocks the natural remanent magnetisation is due to detrital magnetite and can be identified with the time of deposition. Fold tests affirm a Late Cretaceous age of magnetisation in the magnetite bearing

limestones, since the NRM pre-dates latest Cretaceous deformation along the northern edge of the basin. Thus, according to Heller & Channell (1979) the Münster Basin Limestone provides a reliable Cretaceous pole positions (Lat.=76°N, Long.=181°E) from stable Europe.

Following the assumption that the palaeopole proposed by Heller & Channell (1979) is accurate, a magnetic field direction of 360°/56° can be predicted for southern England during Cenomanian-Turonian times.

However, on comparison with the observed magnetic field direction (13°/36°) recorded by Chalk of southern England during the Coniacian to Campanian times, a significant divergence between predicted and observed geomagnetic field direction is evident.

Deep-sea sediments, such as chalk, appear to faithfully record the magnetic field direction without inclination error (see section 1.6.6). Moreover, inclination errors caused by sediment compaction require compaction values of greater than 50% before they become significant (see section 6.5.8). It is thus concluded that the apparent error in inclination and declination cannot be attributed to compaction or sedimentation processes during deposition.

The difference is predicted, and observed magnetic directions could be explained by the acquisition of a magnetic overprint during sampling. IRM studies (section 6.6 indicate that the magnetic mineralogy of Chalk consists of hematite, and MD and SD titanomagnetite. Moreover, the SD titanomagnetite appeared strongly resistant to AF demagnetisation. At AF demagnetisation levels of 40 mT the NRM intensity was reduced by less than 50%. Furthermore, cutting discs used during sampling were non-magnetic and it seems unlikely that an AF field would be generated capable of remagnetising such stable magnetic grains.

Figure 9.20 shows six mean ChRM directions (after tectonic correction), based on all available SEP data from each section studied, for the Coniacian, Santonian and Campanian Stages. Apart from the data from Culver Cliff the ChRM directions plot

reasonably close to the geomagnetic direction (360°/56°) predicted for southern England using the palaeopole of Heller & Channell (1979).

The most likely explanation for the difference in the palaeopole positions is that 'S1 reliability' category data used to determine the palaeopole for southern England is dominated by data from the Santonian and Coniacian stages at Culver Cliff. The presence of a pre-Miocene post-Late Cretaceous magnetic component appears to have caused the primary Late Cretaceous magnetic vectors inclination to shallow. By using the mean ChRM inclination value of 36°, determined from 'S1 reliability category' data, a palaeolatitude of 20°N is inferred for southern England during Coniacian-Late Campanian times. From the palaeopole of Heller & Channell (1979) the latitude of southern England can be shown to be approximately 37°N (α_{95}=3.0°) during this interval of time. A discrepancy of 17° exists between the two palaeolatitudes.

Why only the chalk from the Culver Cliff section has been effected by this remagnetisation is not known. Nevertheless, as this chalk appears to carry a secondary magnetic component a palaeomagnetic pole has been generated by using site mean directions from Santonian/Campanian chalk at Scratchell's Bay and Seaford Head. This chalk appears to carry a well defined low coercivity magnetisation component and does not appear to be affected by any secondary magnetic components. The site mean directions (Figure 9.21) after bedding correction, cluster loosely (α_{95}=19.4°) around a mean direction of declination=355.0° and inclination=50.0°. This provides a well dated, but poorly grouped Upper Cretaceous Pole for stable Europe (Long.=193.3°E, Lat.=69.5°N). However, on considering the experimental uncertainties in measuring the extremely weakly magnetised chalk a reasonable similarity exists when comparing with the palaeomagnetic pole of Heller & Channell (1979). Alternatively, by combining all the 'S1 reliability' magnetic direction data from Seaford Head and Scratchell's Bay a less rigorous mean magnetic direction for southern England can be derived. Figure 9.22 shows magnetic directions from Seaford Head and Scratchell's Bay (α_{95}=6.9°), after bedding correction, around a mean direction of declination=359.0° and inclination=53.0°. A palaeomagnetic pole of Long.=184.0°E and Lat.=73.0°N corresponds to this magnetic direction (Q=5). A close similarity

between Heller & Channell's (1979) palaeomagnetic pole position and this pole for southern England is demonstrated in Figure 9.23. Thus during the Coniacian-Late Campanian times southern England lay at a palaeolatitude of 34±6.9°N.

The deficiency of reliable palaeopole data of Cretaceous age for Europe is a well chronicled dilemma and, as few alternative poles exist, these data provide a potential alternative palaeopole for northern Europe during the Late Cretaceous (Figure 9.24).

9.10 Further Study

This magnetostratigraphic study has revealed that a far more complex pattern of geomagnetic polarity reversals occurred during the Late Cretaceous than has previously been reported for this period of time. As a result, it is of great importance to establish whether these geomagnetic polarity inversions are correlatable over wide areas and are not the product of remagnetisation. Subsequent magnetostratigraphic studies in the UK and further abroad are therefore required to confirm these results.

9.10.1 Further magnetostratigraphic investigations of UK Chalk

With regard to the sections studied in this investigation supplementary thermal demagnetisation should be undertaken (especially Culver Cliff). The detection of a reverse polarity interval with Chron C34N, at Scratchell's Bay, is of great significance and requires further examination. Re-examination of the Chalk succession at the Coniacian-Santonian boundary at Culver Cliff, using thermal demagnetisation should reveal this magnetozones presence. However, other chalk sections in southern England may preserve a record of this geomagnetic polarity inversion. Ideal candidates for further investigation are cliff sections on the east Kent coast and Sussex coast (Seaford Head), which provide extensive exposures of gently dipping Cenomanian to Lower Campanian Chalk. At Seaford Head, the preliminary investigation reported within this thesis, should be extended to incorporate Lower Santonian and Coniacian strata, as well as approximately 15 metres of unsampled Campanian strata at the top of the section.

The location of the Chron C33R/C33N boundary within the English Chalk successions is based on the magnetostratigraphic results obtained from Culver Cliff and Scratchell's Bay. Confirmation of the position of this boundary should be obtained within the 70 metres of Late Campanian (*B. mucronata* Zone) chalk at Alum Bay, the Isle of Wight.

9.10.2 Combination of stratigraphic techniques

Jenkyns *et al.* (1994) have recently published a detailed carbon- and oxygen-isotope stratigraphy generated from Upper Cretaceous coastal Chalk sections in southern England (East Kent; Culver Cliff, Isle of Wight; Eastbourne and Seaford Head, Sussex; Norfolk Coast) and the British Geological Survey (BGS) Trunch Borehole, Norfolk. This was presented alongside data from a section through the Scaglia facies exposed near Gubbio, Italian Apennines.

Both the Chalk and Scaglia carbon-isotopic curves show good correlation between minor and major positive and negative excursions. The remarkable similarity in the carbon-isotope curves from England and Italy enables cross-referencing of macrofossil and microfossil zones and pinpoints considerable discrepancy in the relative positions of the Turonian, Coniacian and Santonian stages (Jenkyns *et al.*, 1994). The oxygen-isotope values of the various Chalk sections also showed a consistent trend.

McArthur *et al.* (Palaeoceanography *in press*; Palaeogeography, Palaeoclimatology and Palaeoecology, *in press*) have provided a very detailed $^{87}Sr/^{86}Sr$ curve for the Late Cretaceous, based on sections through the Chalk, and the western interior of the USA.

Wherever possible magnetostratigraphic investigations of Late Cretaceous Chalk successions should be combined not only with macrofossil, microfossil and nannofossil biostratigraphic control, but also isotope stratigraphical techniques (Sr-, O-, and C-isotope stratigraphies). Due to the difficulty in obtaining high quality geomagnetic polarity determinations from chalk, additional control, provided by other stratigraphical techniques, would equip Cretaceous stratigraphers with an extremely powerful correlation and dating tool.

Miller *et al.* (1988) showed how well the method works when magnetostratigraphy, biostratigraphy and strontium isotope stratigraphy are determined simultaneously within the same section. By undertaking such a study in a section which contains macrofossils, nannofossils and planktic forams, many problems which beset global correlations could be resolved. This may best be tackled in the Late Cretaceous deposits of Texas. By undertaking a combined magnetostratigraphic/strontium isotopic investigation of the Late Cretaceous Texas chalk, with good biostratigraphic control, it would be possible to provide a quantitative isotopic/magnetostratigraphic template with which to correlate Late Cretaceous strata of the U.S. interior with strata in Europe and worldwide, and against which to match and integrate diverse stratigraphic schemes via magnetostratigraphic/isotopic signatures.

In contrast to western Europe, the chalks of North America contain few hardgrounds and a greater proportion of siliciclastics. The Upper Cretaceous deposits of Texas (Eagle Ford, Austin, Taylor and Navarro outcrops) span the Turonian to Maastrichtian stages (Pessagno, 1969); Young, 1977; Young & Woodruff, 1985), and thus should include 12 potential magnetostratigraphic calibration points (according to the polarity time-scale of Cande & Kent, 1992). Laterally continuous bentonites, which vary in thickness from less than a centimetre to as much as 0.4 metres, are found throughout the Atco Chalk Member (Austin Chalk, Coniacian-Santonian stages) and provide important correlation points (Larson *et al.*, 1991). The potential thus exists to directly assign K-Ar or $^{39}Ar/^{40}Ar$ dates to various parts of the Chalk sequences.

Thus, a magnetostratigraphically calibrated Strontium isotope curve for the Late Cretaceous could be used to resolve many stratigraphic problems which other procedures might not do so well; dating and correlating reef-carbonate sequences, defining rates of transgressions and regressions, examining biostratigraphic boundaries for diachroneity, integrating diverse biostratigraphic schemes, and correlating sediment dates directly to the Geomagnetic Polarity Time Scale without having to do this via second order and third order biostratigraphic (potentially diachronous) correlations (McArthur, 1993). The calibrated $^{87}Sr/^{86}Sr$ curve thus provides a new way to date and correlate marine sedimentary sequences.

9.10.3 Possible overseas locations for magnetostratigraphic/isotopic investigations

Several stratigraphically important Late Cretaceous Chalk successions which should be studied in this way are as follows; the Austin Chalk of Texas, USA; the Gingin Chalk (Perth Basin) and the Toolonga Calcilutite (Carnarvon Basin) in Western Australia; northern Aquitaine area, France; and Lagerdorf Quarry, Schweisteg-Holstein, NW Germany. However, the major problem with many of these successions is that they do not incorporate all of the Late Cretaceous and only provide an opportunity to study Santonian to Campanian aged strata. However, the Late Cretaceous sequences of Tunisia may provide a more complete succession of Late Cretaceous strata. These sections (e.g. El Kef and the Tseldje Gorge) expose Maastrichtian age sediments which incorporate the K/T boundary. Moreover, it was from the study of the El Kef section that Sissingh (1977) devised the Late Cretaceous nannofossil (CC) zones which form the basis of the many subsequent and widely applied nannofossil zonations.

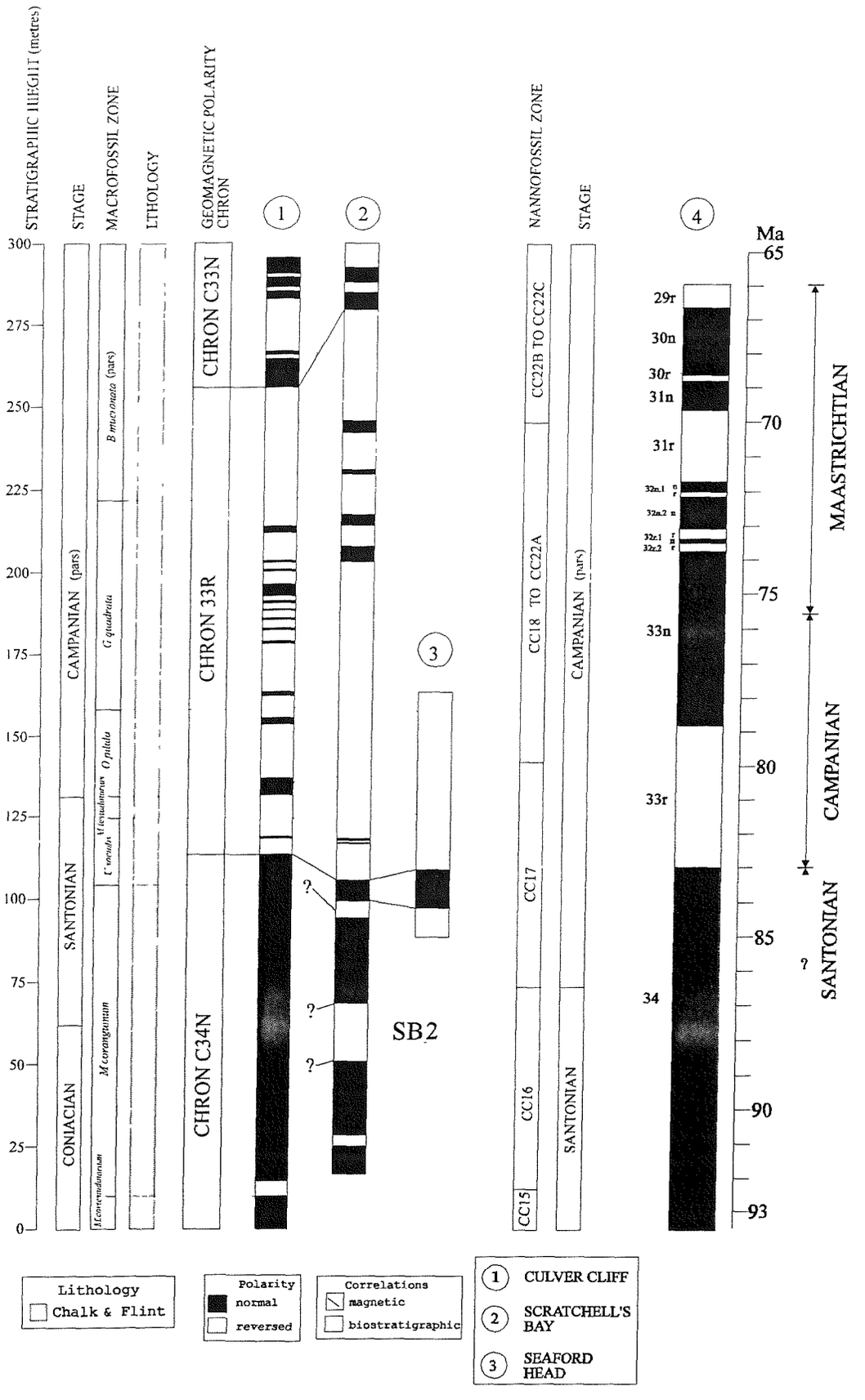

Figure 9.1. Late Cretaceous magnetostratigraphy of Chalk sections in southern England compared with sea-floor magnetic anomalies. Left hand columns: stratigraphic height above Turonian-Coniacian boundary, Cretaceous stages, macrofossil zonation (Rawson *et al.*, 1977), lithology and geomagnetic polarity chron. Columns 1 to 3 show detailed magnetostratigraphic sections from southern England. Column 1 indicates the magnetostratigraphic results from the Culver Cliff section, Isle of Wight; column 2 those from Scratchell's Bay, the Isle of Wight; and column 3 those from Seaford Head section, East Sussex. The nannofossil zonation, based on Sissingh's (1977) zones, is shown at the right-hand side of column 3. The Cande & Kent (1992) geomagnetic polarity time-scale for the Late Cretaceous, based on marine magnetic anomalies, is indicated in column 4.

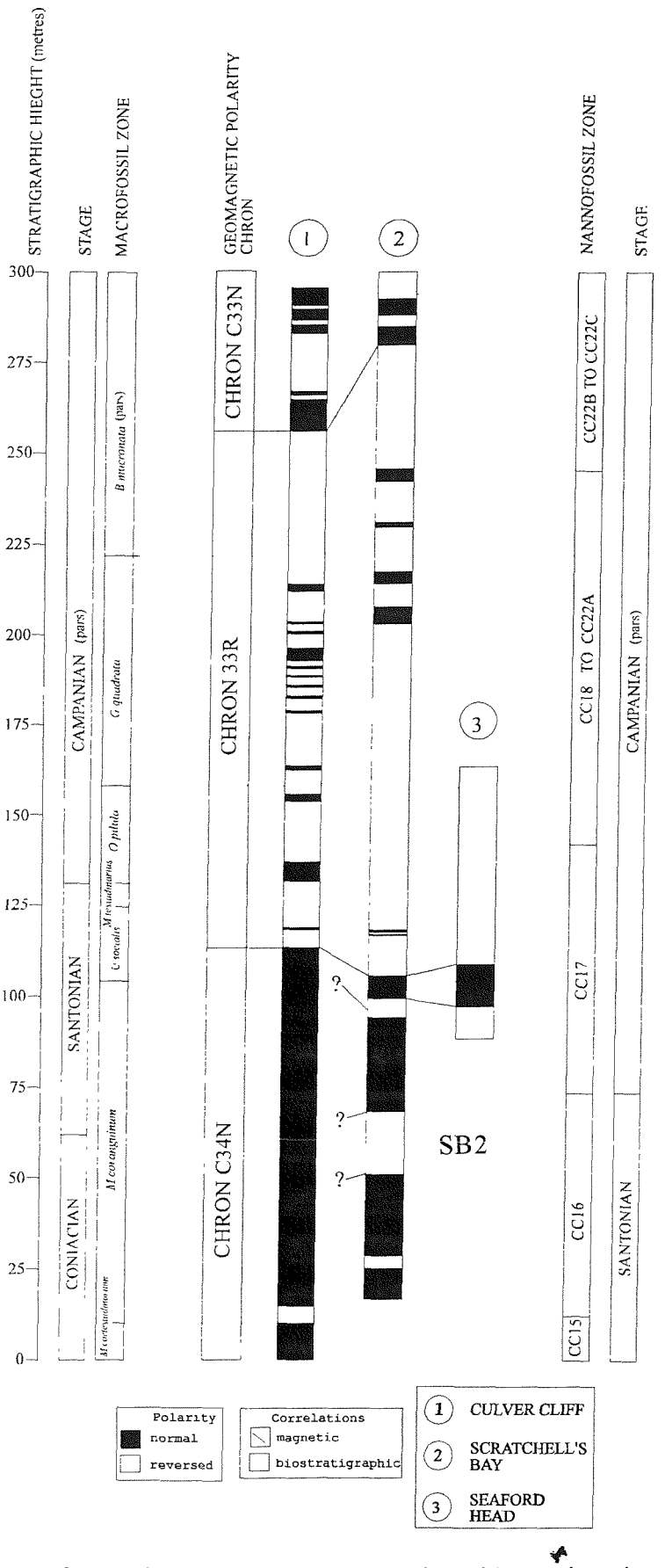

Figure 9.2. Correlation of Late Cretaceous magnetostratigraphic sections in southern England. Left hand columns: stratigraphic height above Turonian-Coniacian boundary, Cretaceous stages, macrofossil zonation (Rawson *et al.*, 1977), lithology and geomagnetic polarity chron. Columns 1 to 3 show detailed magnetostratigraphic sections from southern England. Column 1 indicates the magnetostratigraphic results from the Culver Cliff section, Isle of Wight; column 2 those from Scratchell's Bay, the Isle of Wight; and column 3 those from Seaford Head section, East Sussex. The nannofossil zonation, based on Sissingh's (1977) zones, is shown at the right-hand side of column 3.

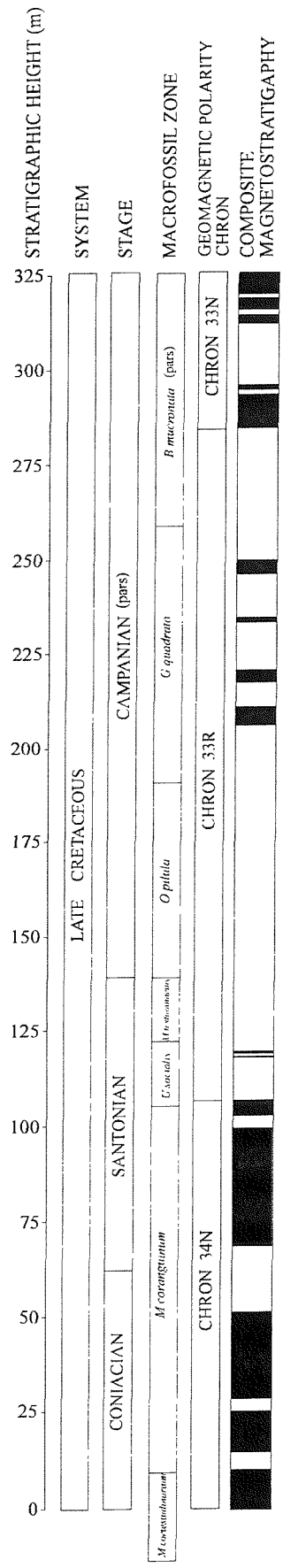

Figure 9.3. A composite magnetic polarity stratigraphy of southern England. The lowest portion of Chron C34N and all of Chron C33N are based on results obtained at Culver Cliff. However the rest of the composite is based on the magnetic polarity results obtained at Scratchell's Bay. This is due to the chalk at Culver Cliff possessing a high coercivity magnetic component which made polarity assignment difficult. The diagram shows from left to right: stratigraphic height above the Turonian-Coniacian boundary; System, Stages, macrofossil zones, geomagnetic polarity chrons and composite magnetostratigraphy.

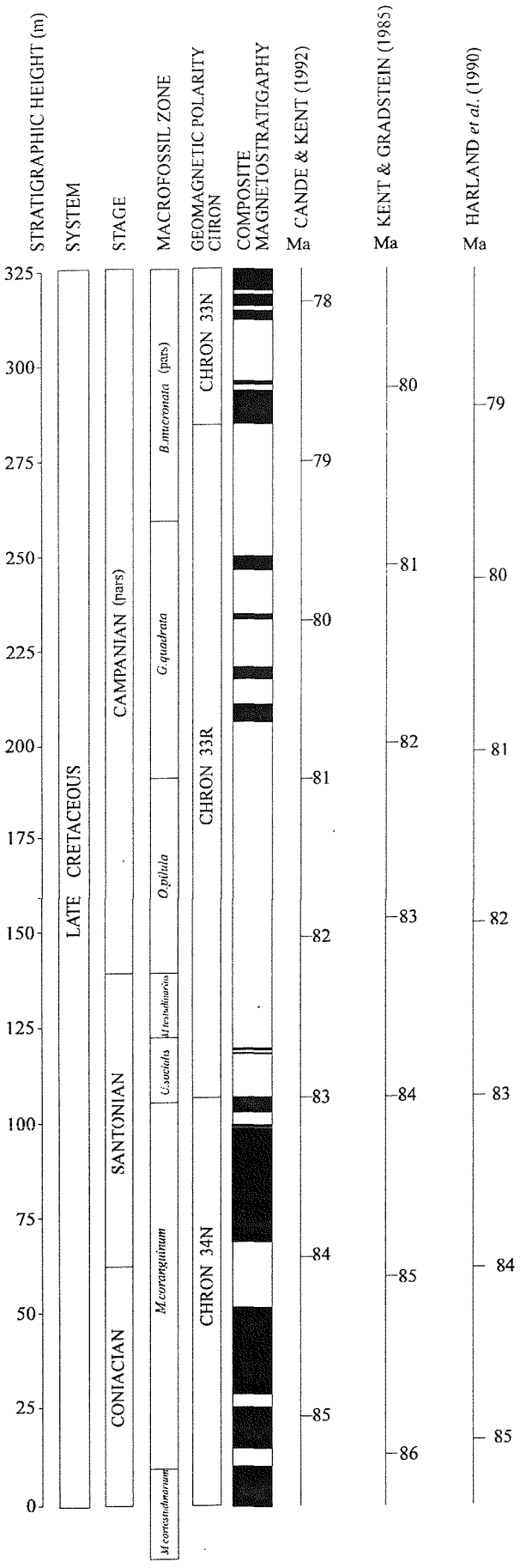

Figure 9.4. Magnetostratigraphic time scales for the Late Cretaceous of southern England, based on Cande & Kent (1992), Kent & Gradstein (1985) and Harland *et al.* (1990), respectively.

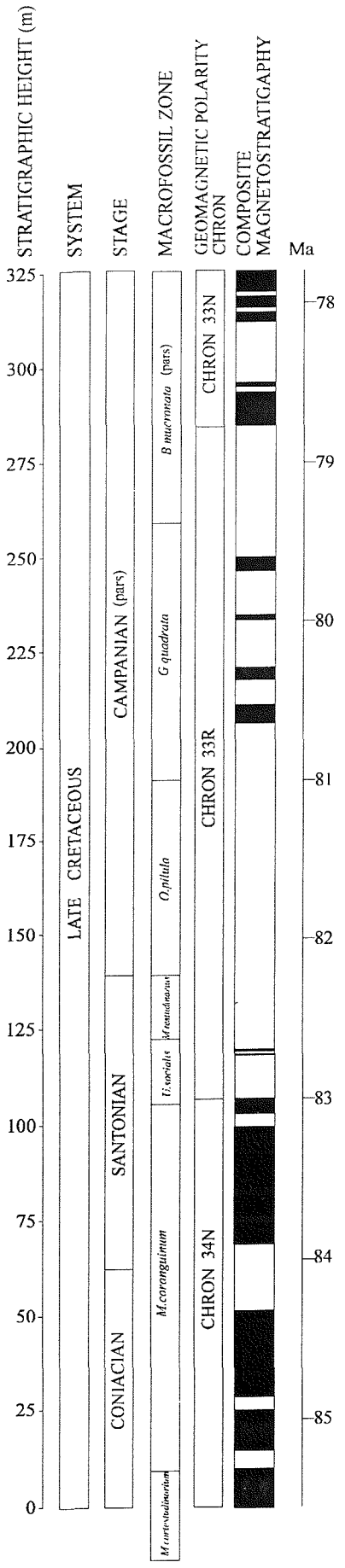

Figure 9.5. A magnetostratigraphic time scale for the Late Cretaceous of southern England.

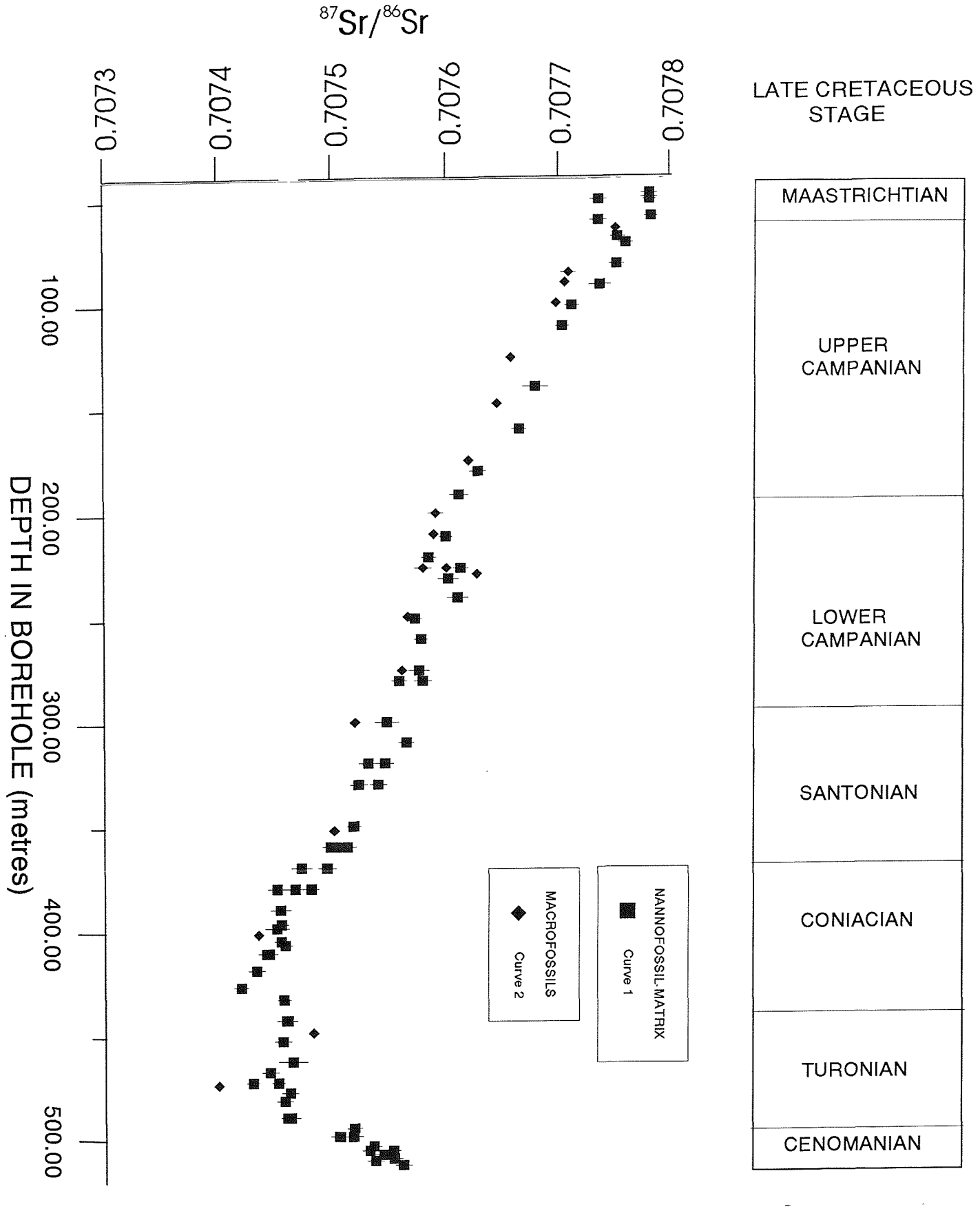

Figure 9.6. $^{87}Sr/^{86}Sr$ with depth for the Trunch Borehole, Norfolk, UK (from McArthur *et al.*, 1992).

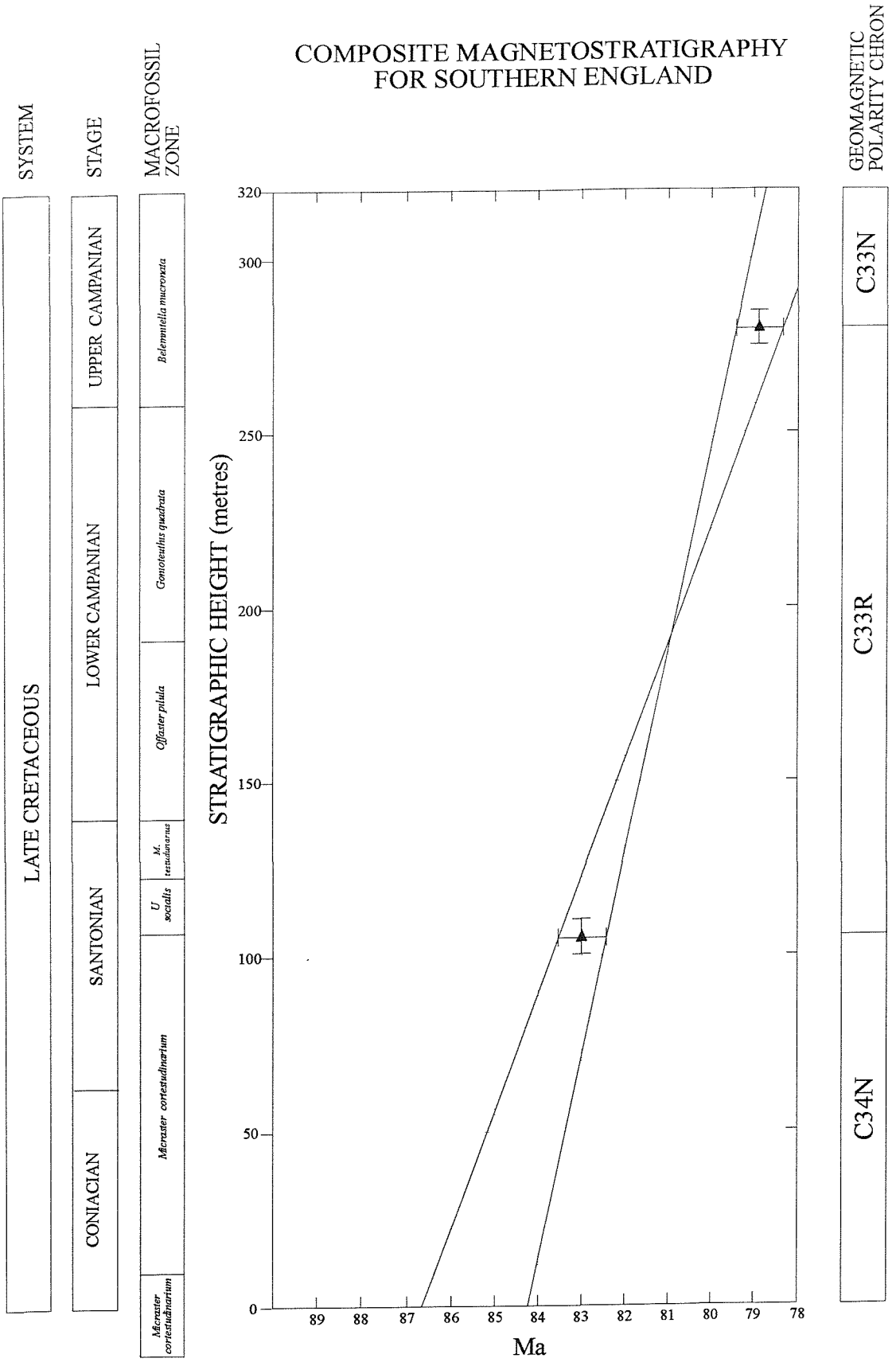

Figure 9.7. Plot of the composite magnetostratigraphic section height versus numeric age of magnetostratigraphic calibration points (i.e. the Chron C34N/C33R and C33R/C33N boundaries defined during the present study). Left hand columns: system, Cretaceous stages and macrofossil zonation (Rawson *et al.*, 1977). Stratigraphic height is measured from Turonian-Coniacian boundary. Horizontal error bars indicate an uncertainty of ±0.5 m.y. for numeric dates of the magnetostratigraphic calibration points. Vertical error bars indicate the an uncertainty of ±5 metres in placing the chron boundaries within the section. A measure of the uncertainty in age assignment to macrofossil zone and stage boundaries can be gained by constructing an envelope around the error bars associated with the magnetostratigraphic calibration points.

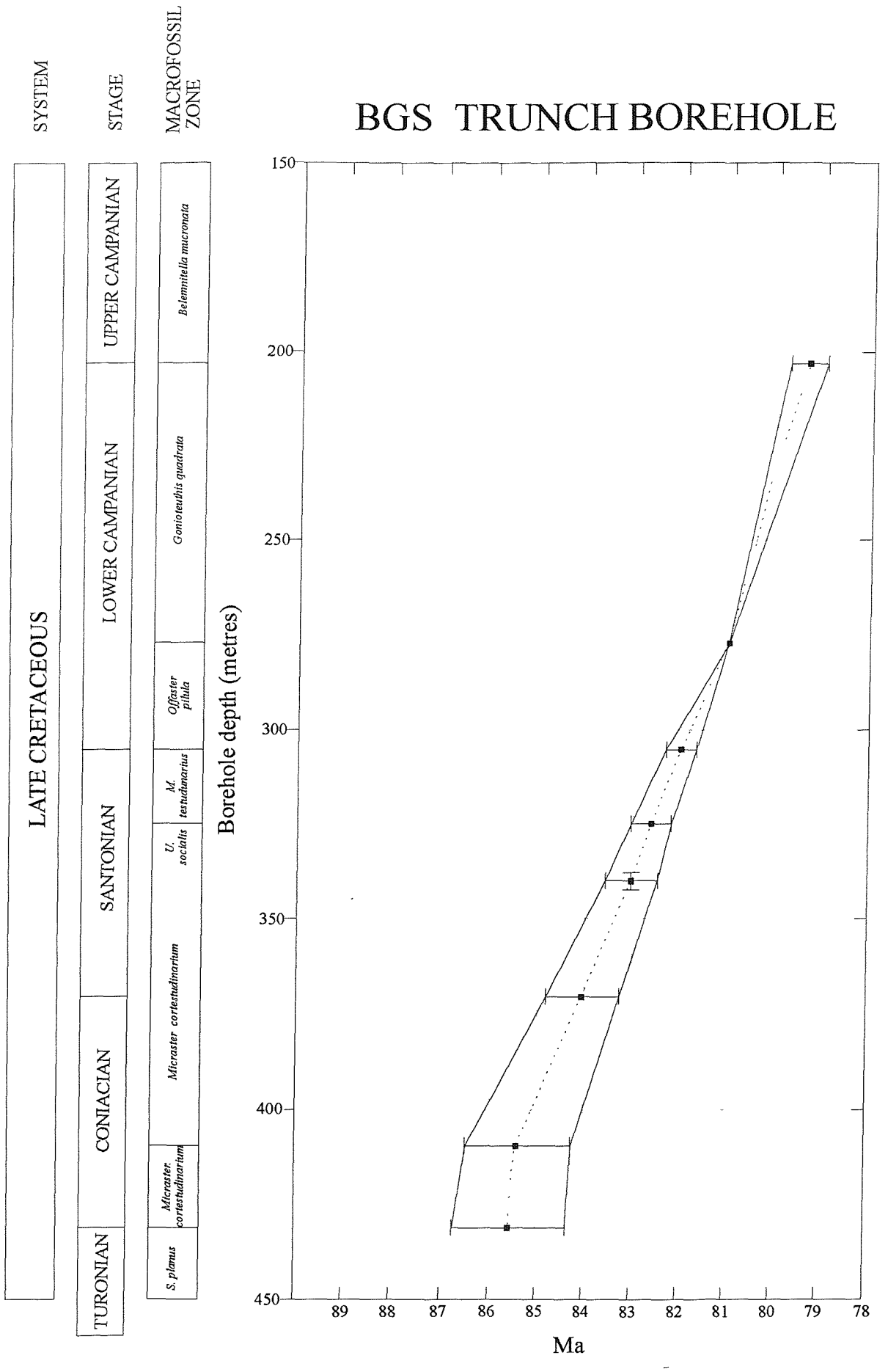

Figure 9.8. Plot of borehole depth at Trunch, Norfolk, versus numeric age of macrofossil zone and stage boundaries (defined by the present study). Left hand columns: system, Cretaceous stages and macrofossil zonation (McArthur *et al.*, 1992). Horizontal error bars indicate the uncertainty of numeric dates derived from Figure 9.7. Vertical error bars indicate an uncertainty of <±3 metres in placing macrofossil boundaries within the core as suggested by McArthur *et al.* (1992).

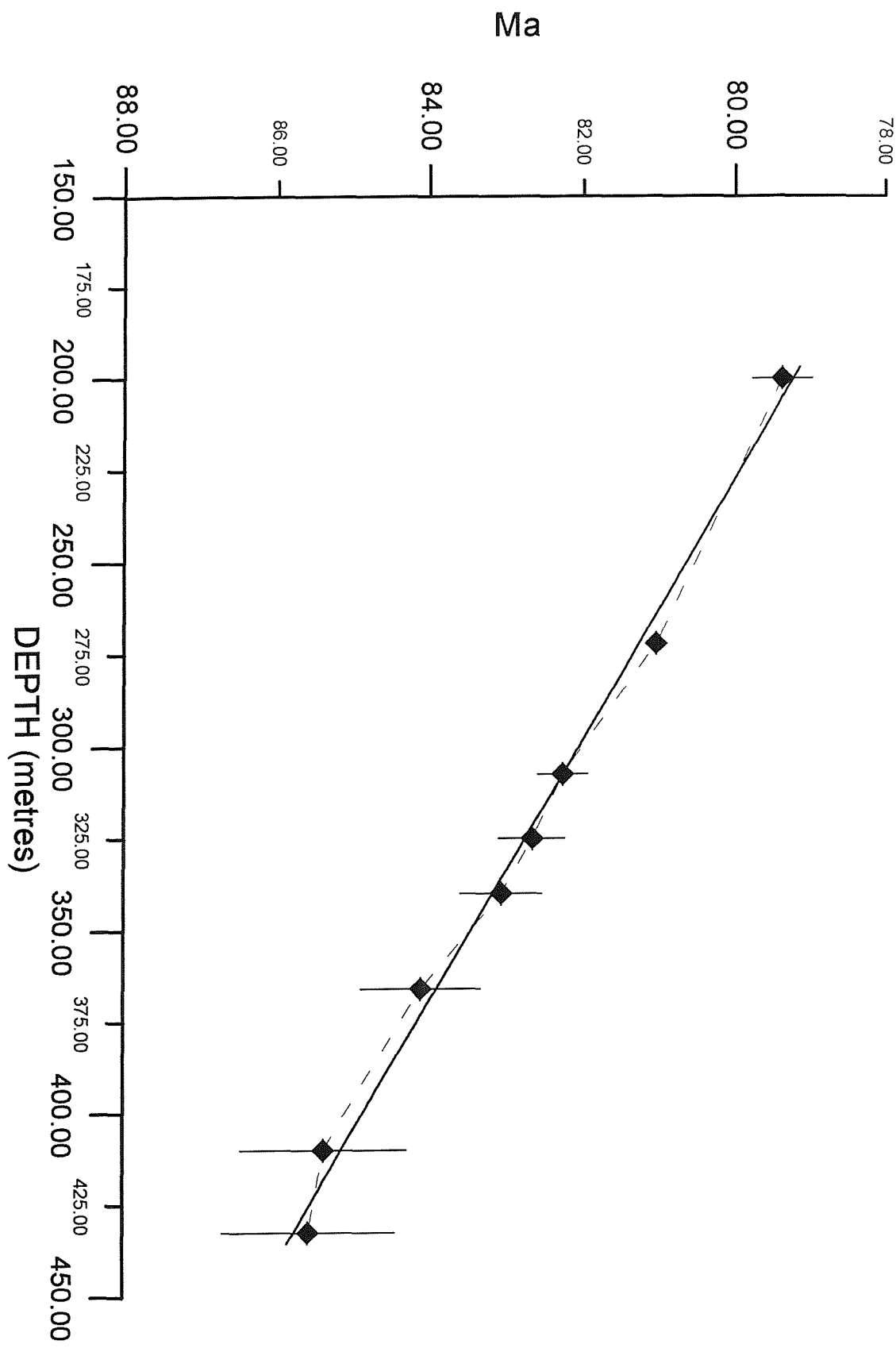

Figure 9.9. Plot of borehole depth at Trunch, Norfolk, versus numeric age of macrofossil zone and stage boundaries (defined by the present study). Best straight-line fit is indicated. Horizontal error bars indicate the uncertainty of numeric dates derived from Figure 9.7. Vertical error bars indicate an uncertainty of <±3 metres in placing macrofossil boundaries within the core as suggested by McArthur *et al.* (1992).

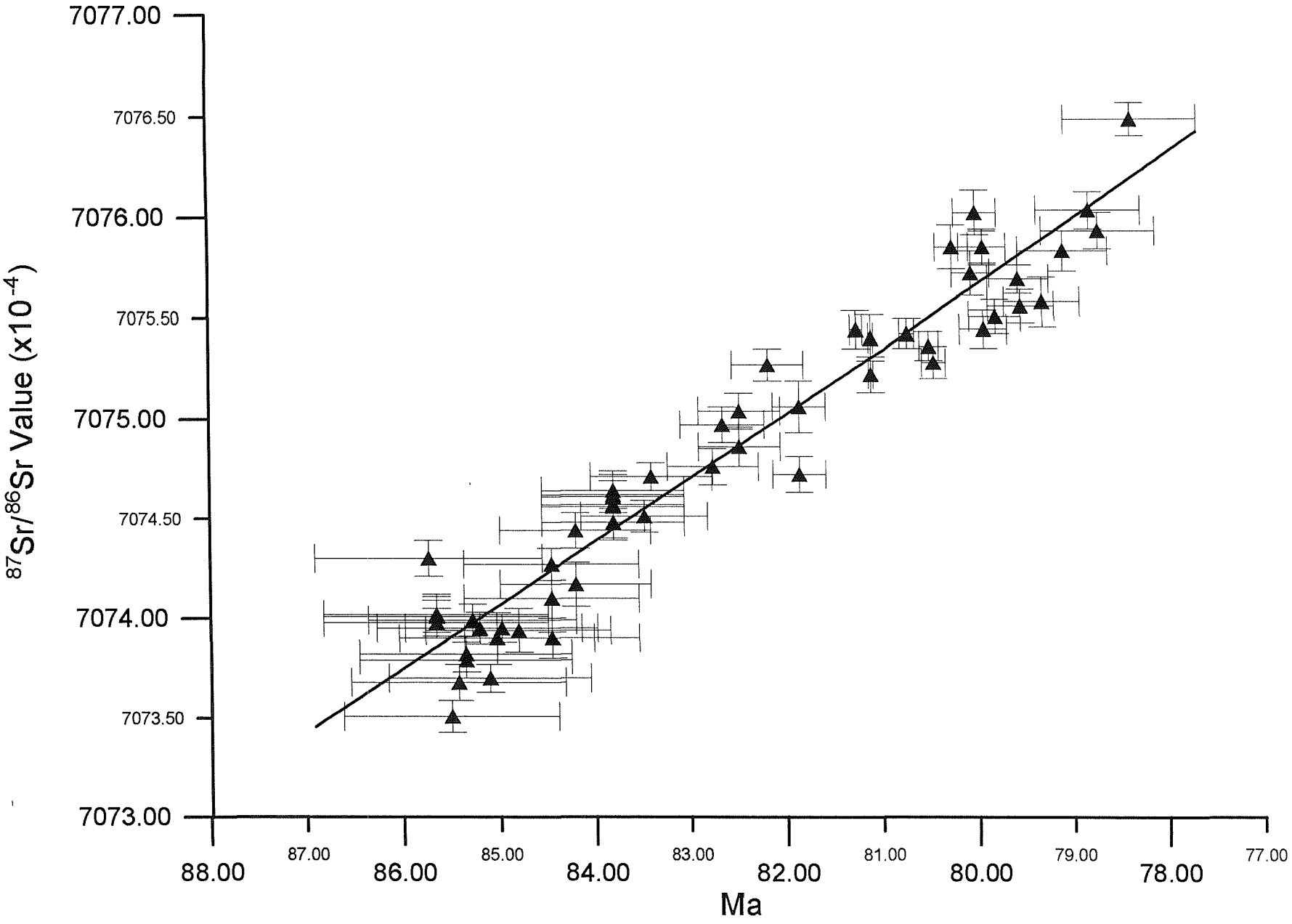

Figure 9.10. Age-calibration graph for $^{87}Sr/^{86}Sr$ values based on the assumption that neither the temporal evolution of marine $^{87}Sr/^{86}Sr$, nor sedimentation rate of Chalk varied greatly during Coniacian-Campanian times.

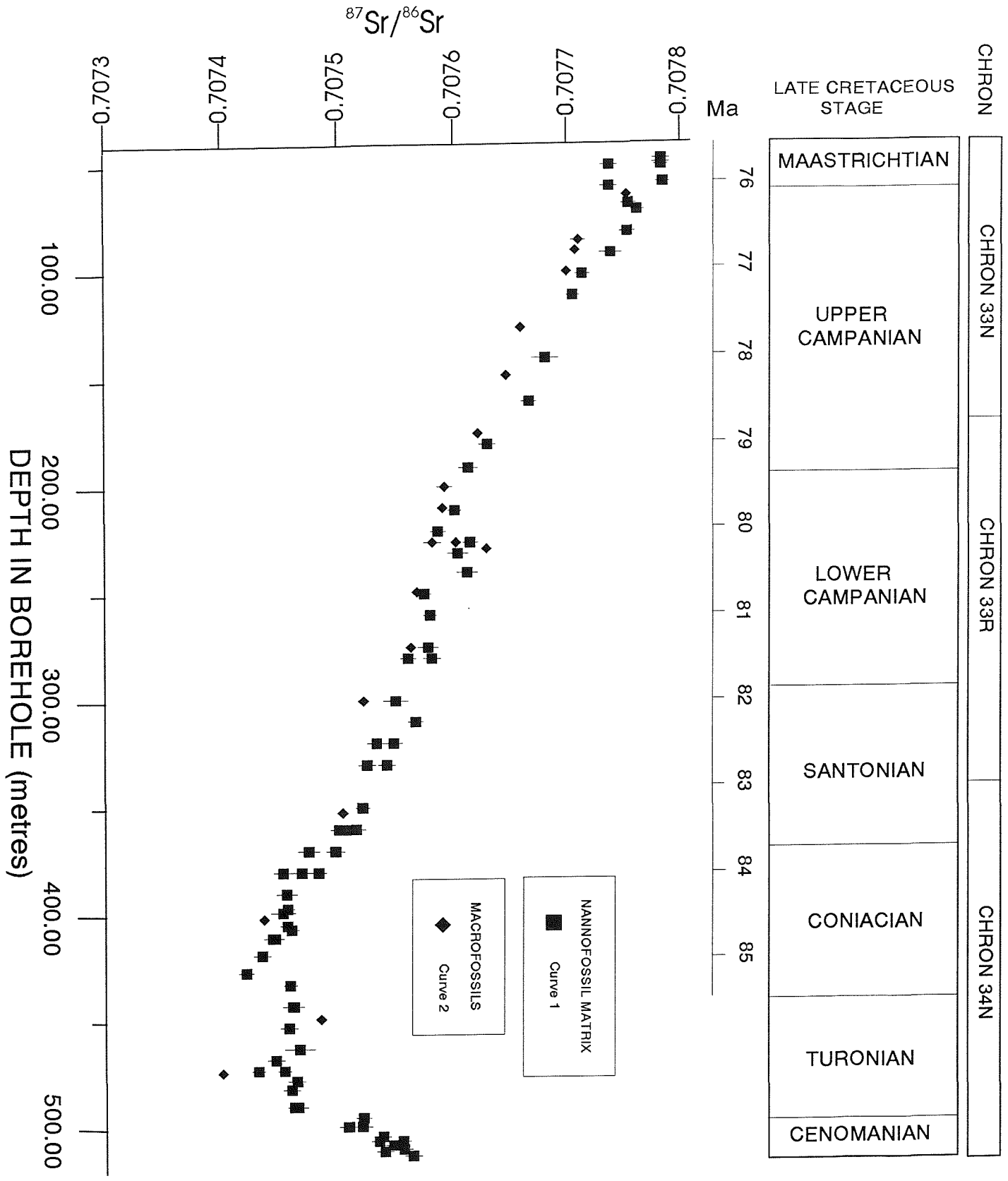

Figure 9.11. $^{87}Sr/^{86}Sr$ variation with depth for the Trunch Borehole, Norfolk, UK (from McArthur *et al.*, 1992). From right to left, the diagram shows geomagnetic polarity Chron, Late Cretaceous stage and age (according to the magnetostratigraphic time-scale derived for the Chalk of southern England).

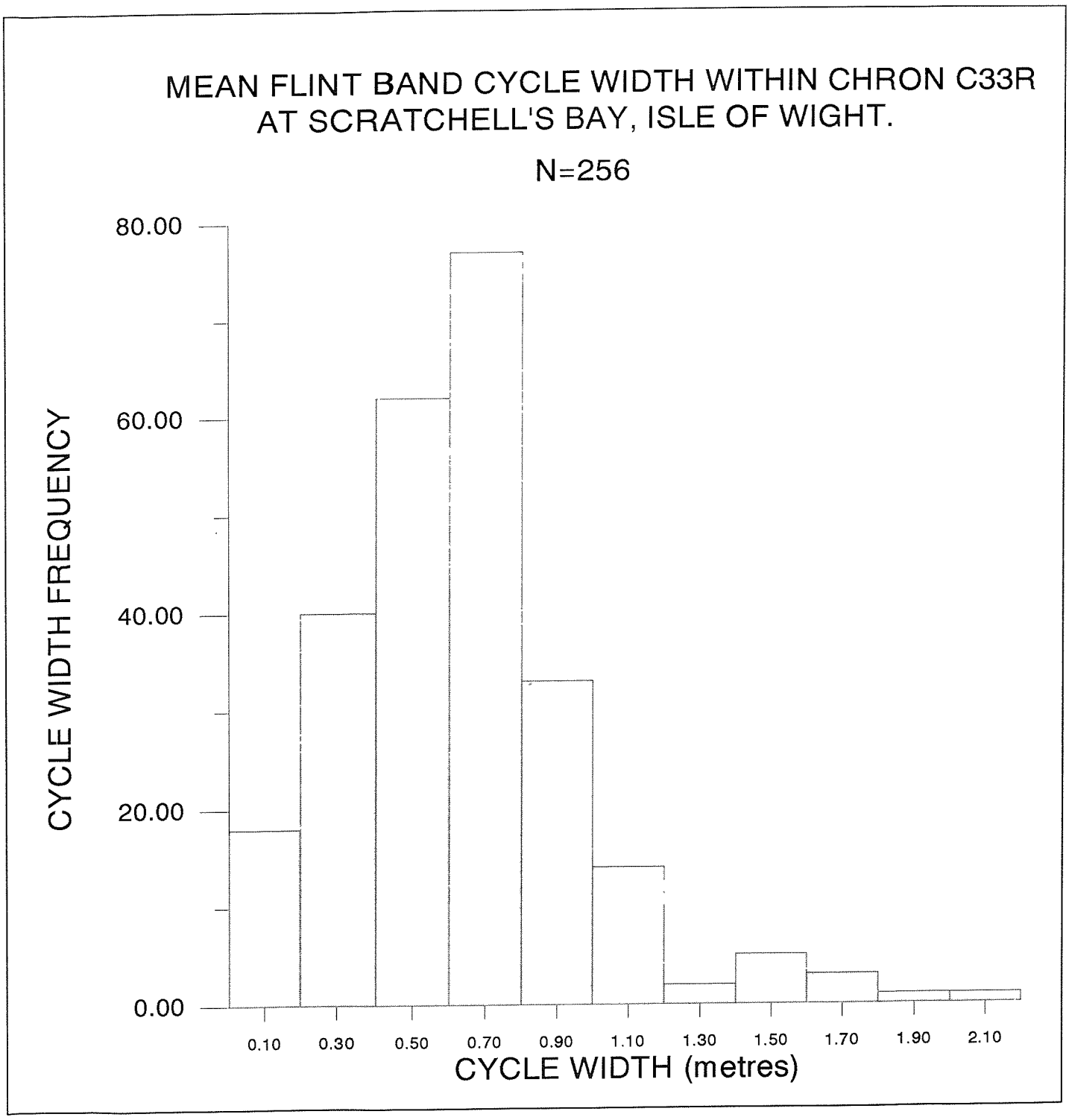

Figure 9.12. Histogram of mean flint band cycle widths within Chron C33R at Scratchell's Bay, the Isle of Wight.

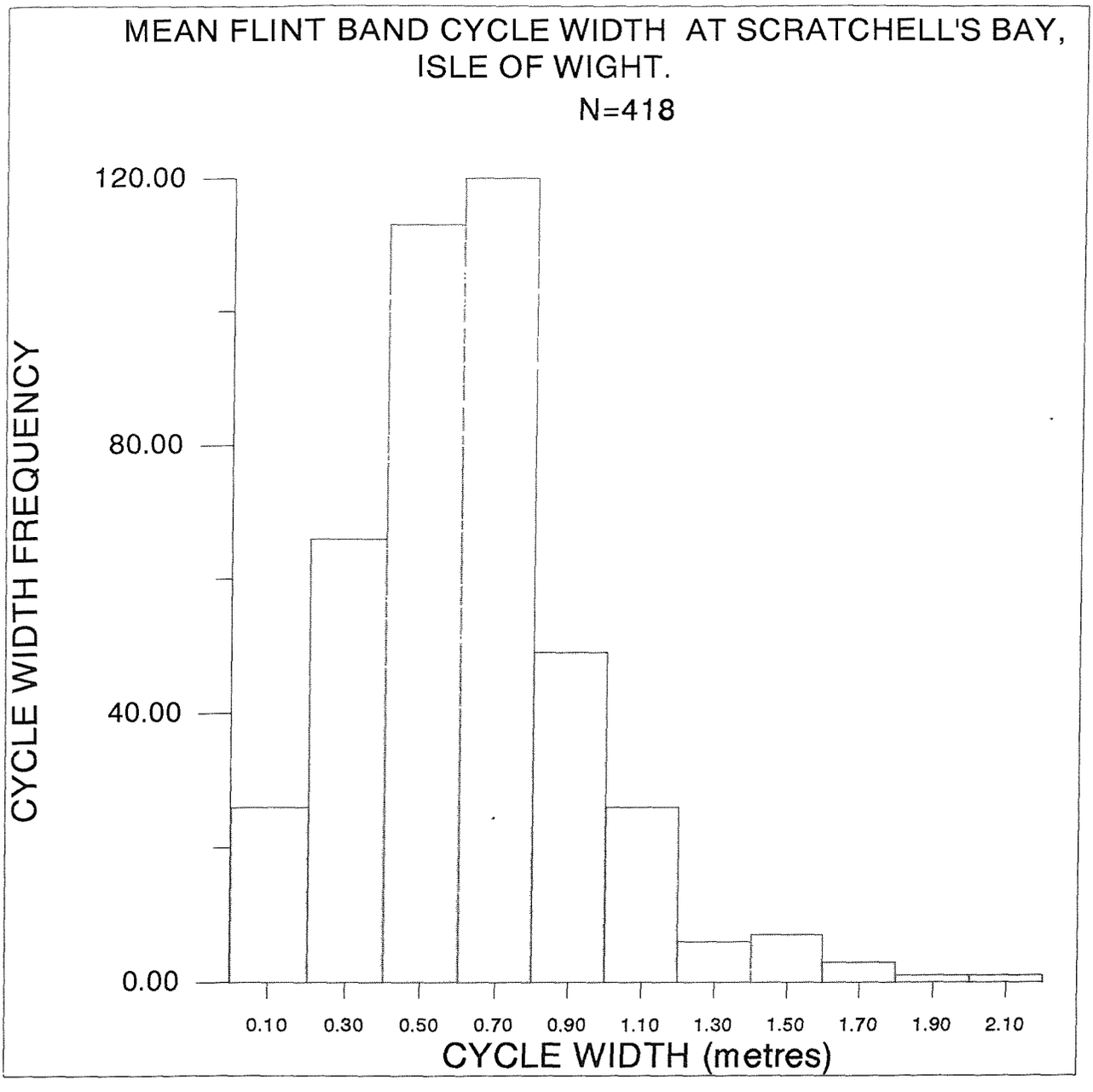

Figure 9.13. Histogram of mean flint band cycle widths at Scratchell's Bay, the Isle of Wight.

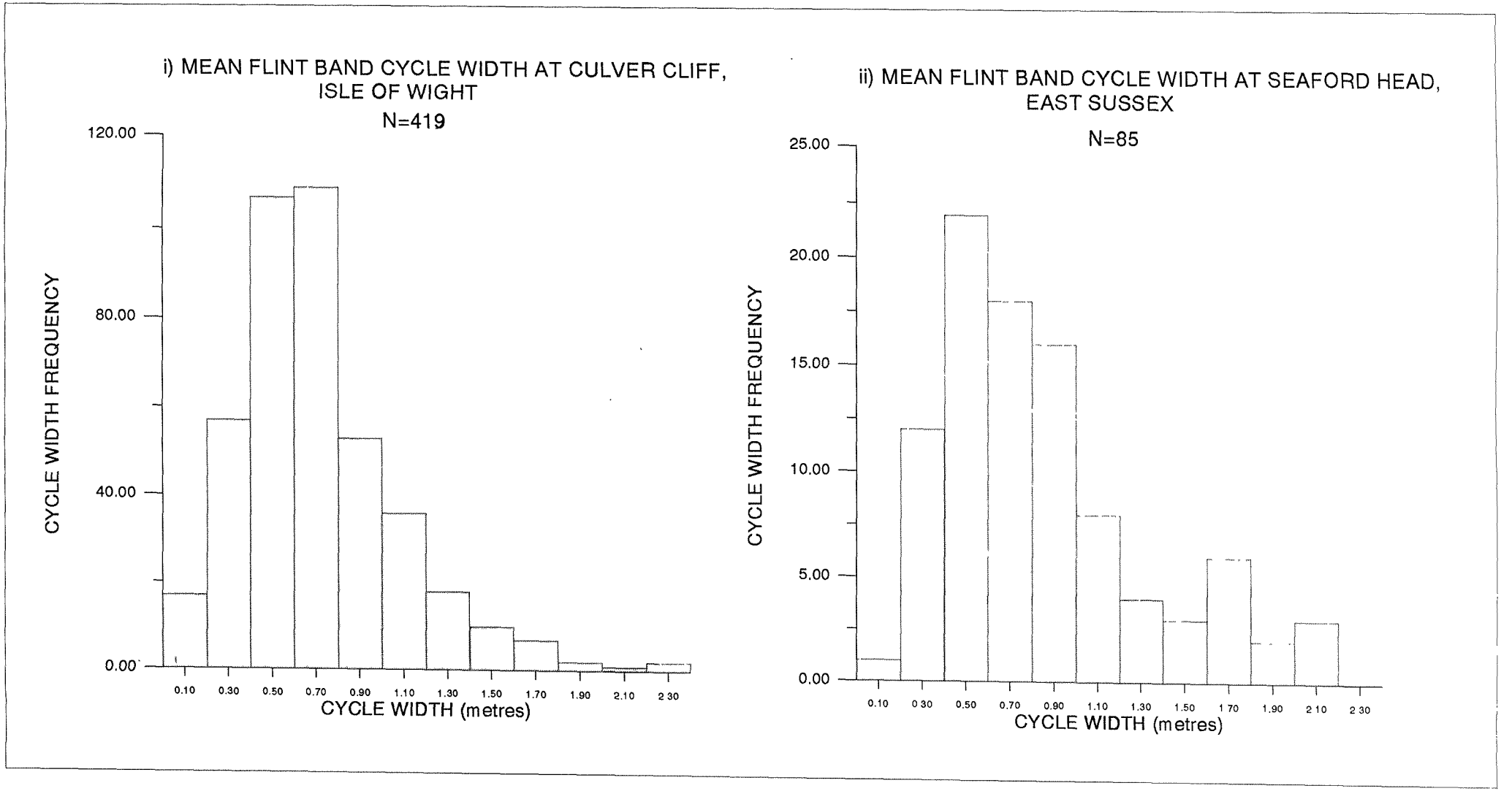

Figure 9.14. Histograms of mean flint band chalk cycle widths at i) Culver Cliff, the Isle of Wight and ii) Seaford Head, East Sussex.

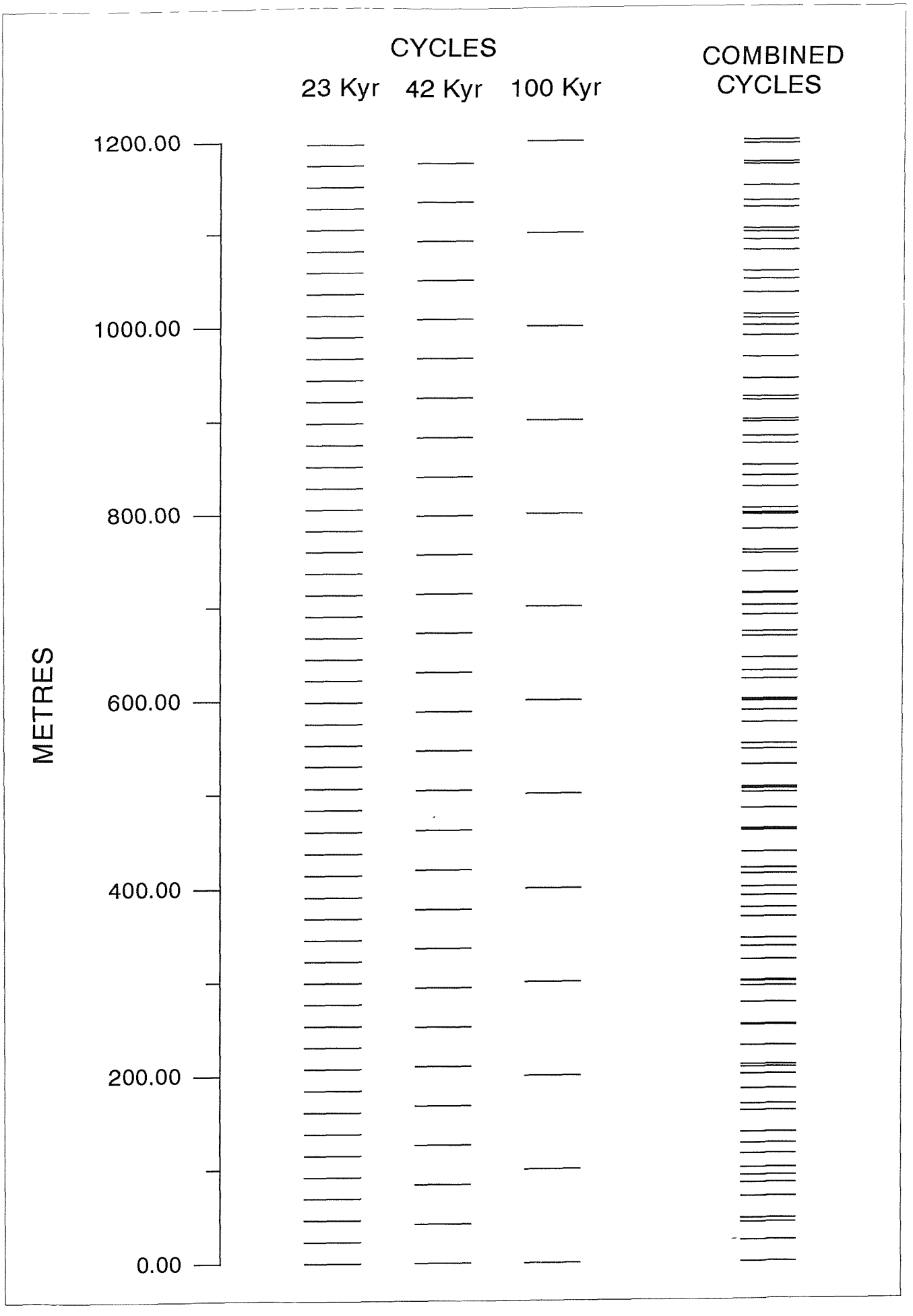

Figure 9.15 Hypothetical pattern of flint bands generated by the sole operation of i) presession; ii) obliquity; and iii) eccentricity, together with the combined pattern iv) for 1.2 million years of chalk sedimentation at a rate of 1 metre per 1000 years.

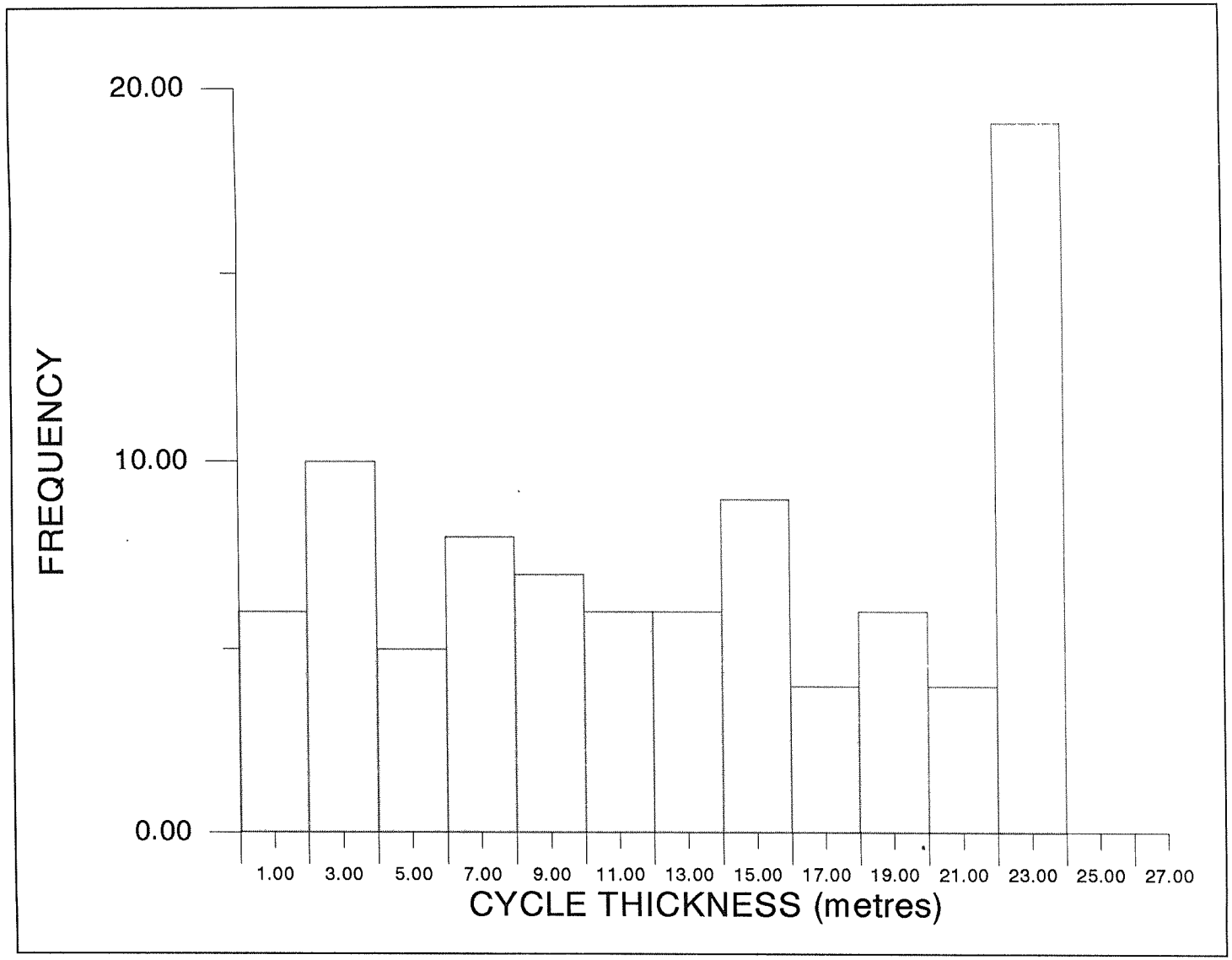

Figure 9.16. Histogram of simulated flint band-chalk cycle widths.

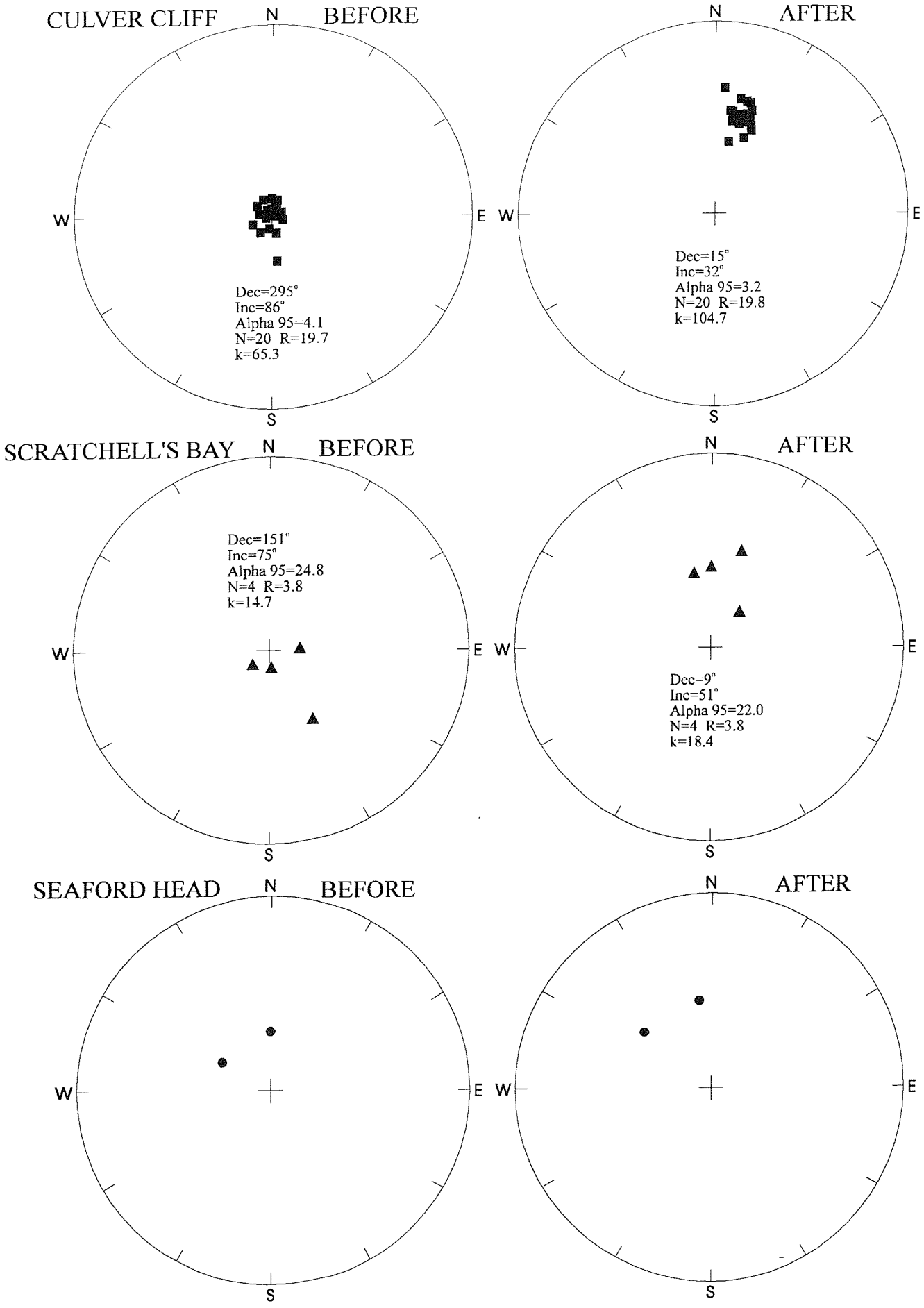

Figure 9.17. Twenty-six 'S1 category' site mean magnetic directions, before and after bedding correction, for i) Culver Cliff; ii) Scratchell's Bay; and iii) Seaford Head.

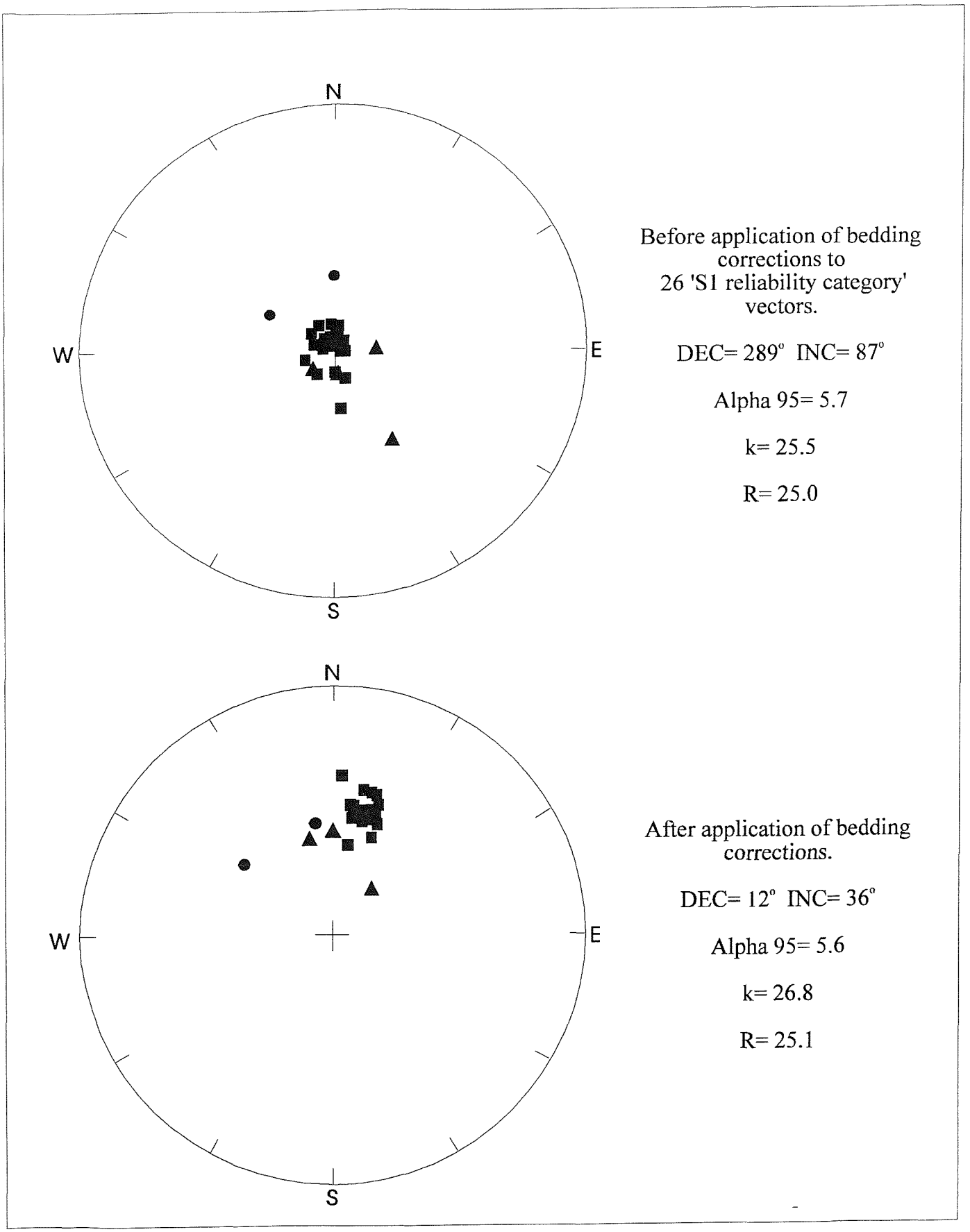

Figure 9.18. Stereographic equal area plot of 26 'S1 category' magnetic vectors, before and after bedding correction, from Coniacian-Campanian Chalk, southern England.

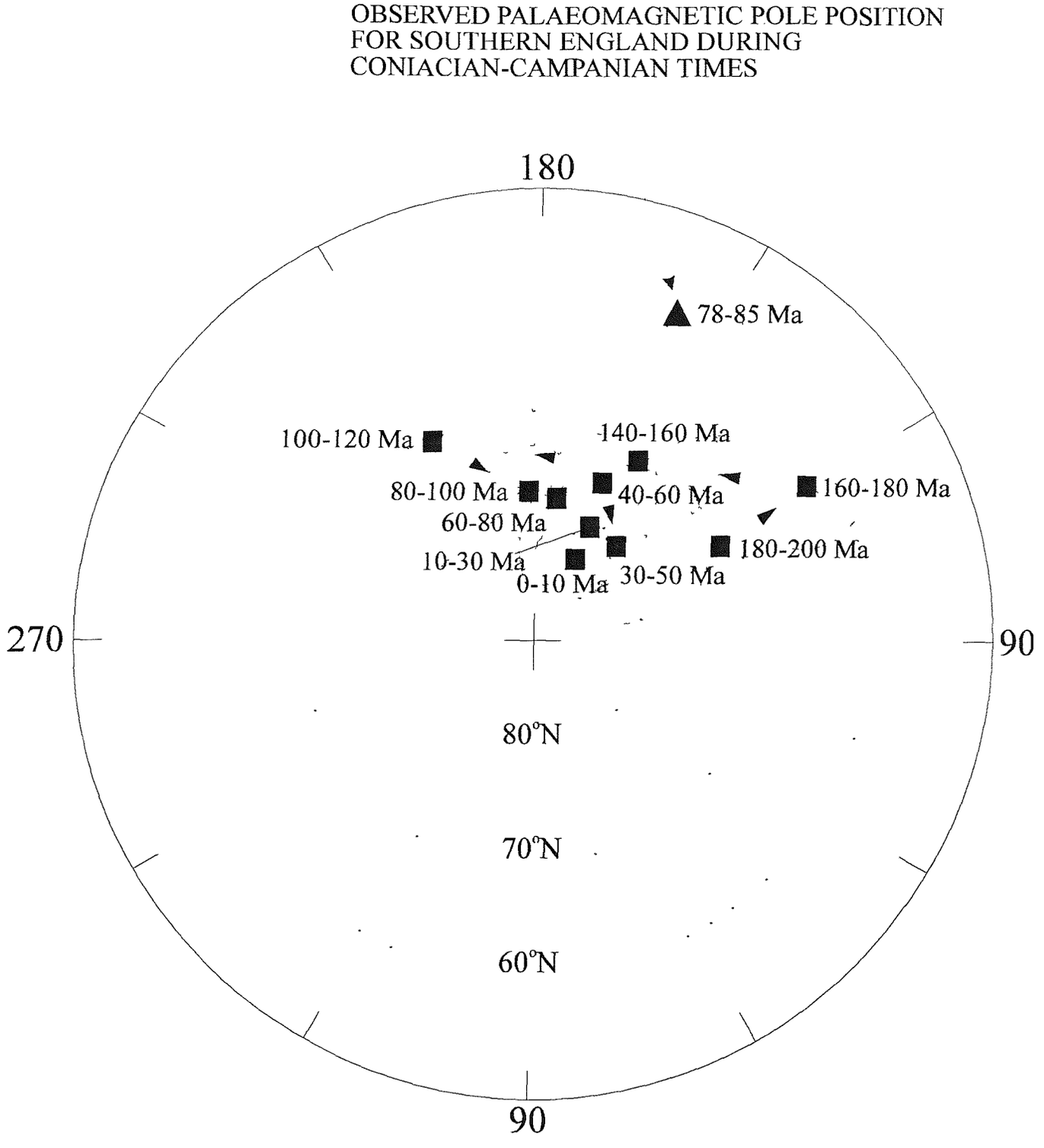

Figure 9.19 Apparent polar wander path for Eurasian plate, from present back to 200 Ma. Connected squares are mean poles for Eurasian palaeomagnetic data only (Besse & Courtillot, 1991). Alpha 95 values are shown as broken line circles. The solid triangle symbol indicates the palaeomagnetic pole position derived from palaeomagnetic data from the English Chalk (Culver Cliff, Scratchell's Bay and Seaford Head) during the Coniacian-Campanian stages.

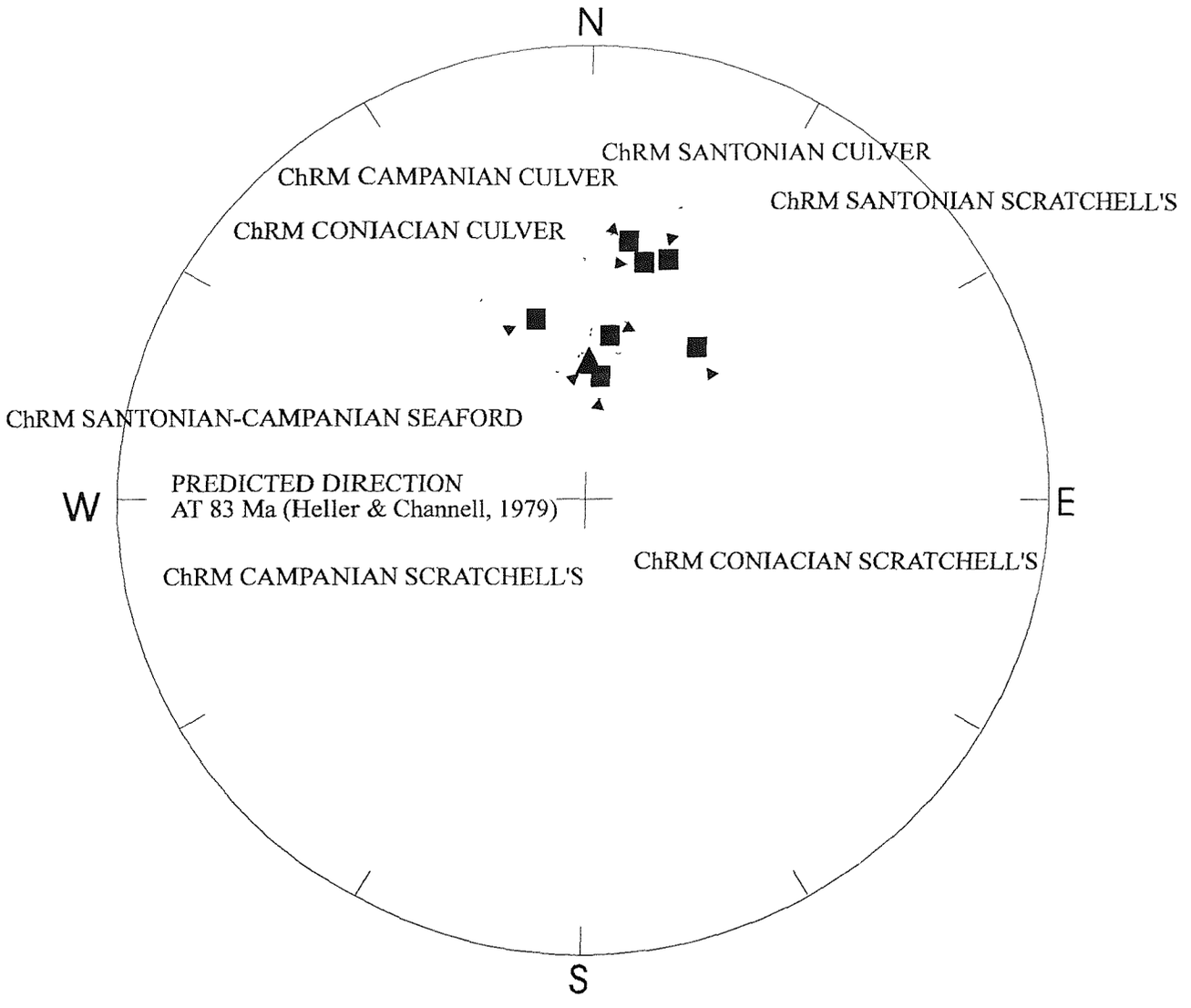

STAGE	ChRM CULVER CLIFF	ChRM SCRATCHELL'S BAY	ChRM SEAFORD HEAD
CAMPANIAN	Dec=8° Inc=31° N=200 R=189.5 Alpha 95=2.4 k=18.9	Dec=38° Inc=46° N=5 R=4.4 Alpha 95=30.5 k=7.3	Dec=337° Inc=47° N=23 R=19.8 Alpha 95=12.4 k=6.9
SANTONIAN	Dec=18° Inc=35° N=200 R=185.5 Alpha 95=2.8 k=13.7	Dec=7° Inc=49° N=82 R=74.4 Alpha 95=5.0 k=10.7	
CONIACIAN	Dec=13° Inc=37° N=120 R=114.6 Alpha 95=2.8 k=21.9	Dec=5° Inc=59° N=65 R=74.4 Alpha 95=7.4 k=6.0	

Figure 9.20. Stereographic projection and table showing the ChRM directions, after bedding correction, based on all available SEP data from Scratchell's Bay, Culver Cliff and Seaford Head (solid squares) for the Campanian, Santonian and Coniacian stages. The predicted magnetic direction for southern England (Dec=0°, Inc=56°), according to the palaeomagnetic pole of Heller & Channell (1979), is shown (solid triangle).

Figure 9.21. Stereographic projection showing the mean site magnetic directions, before and after bedding correction, based on available 'SI reliability' category data from Scratchell's Bay and Seaford Head (solid squares). The mean magnetic direction for southern England is shown (cross) along with the associated alpha 95 value (dotted circle).

Figure 9.22. Stereographic projection showing the magnetic directions, before and after bedding correction, based on all available 'SI reliability' category data from Scratchell's Bay and Seaford Head (solid squares). The mean magnetic direction for southern England is shown (cross) along with the associated alpha 95 value (dotted circle).

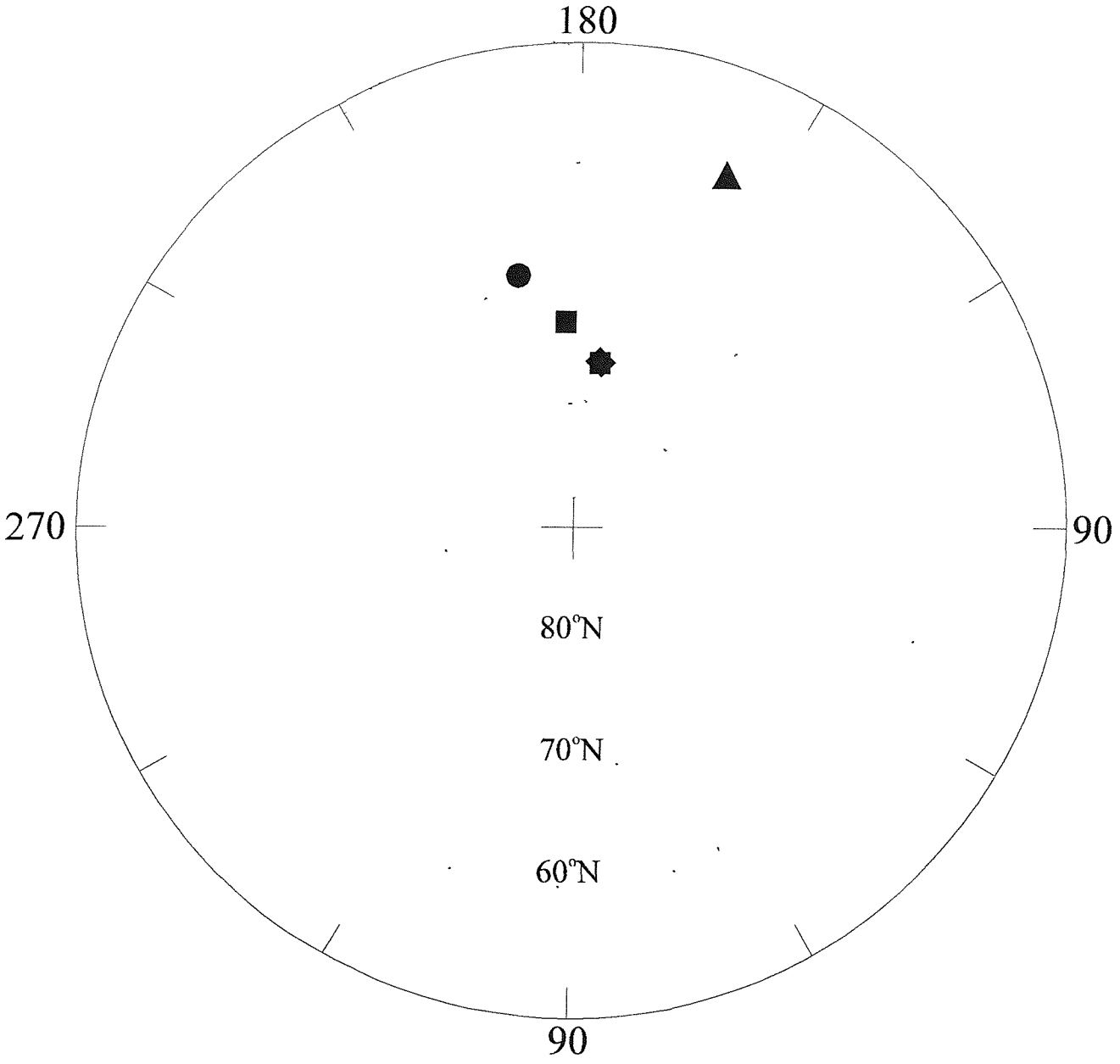

Figure 9.23. Palaeomagnetic pole positions for stable Europe during the Late Cretaceous. The solid square represents the palaeopole based on all 'S1 reliability' category palaeomagnetic data from Scratchell's Bay and Seaford Head. The solid triangle indicates the palaeomagnetic pole position derived from 'S1 reliability' category site mean data (alpha 95<15°) from the English Chalk (Culver Cliff, Scratchell's Bay and Seaford Head) during the Coniacian-Campanian stages. The solid star represents the palaeomagnetic pole position of Heller & Channell (1979) for the Münster Basin during Late Cretaceous times Alpha 95 values are shown by broken-line circles.

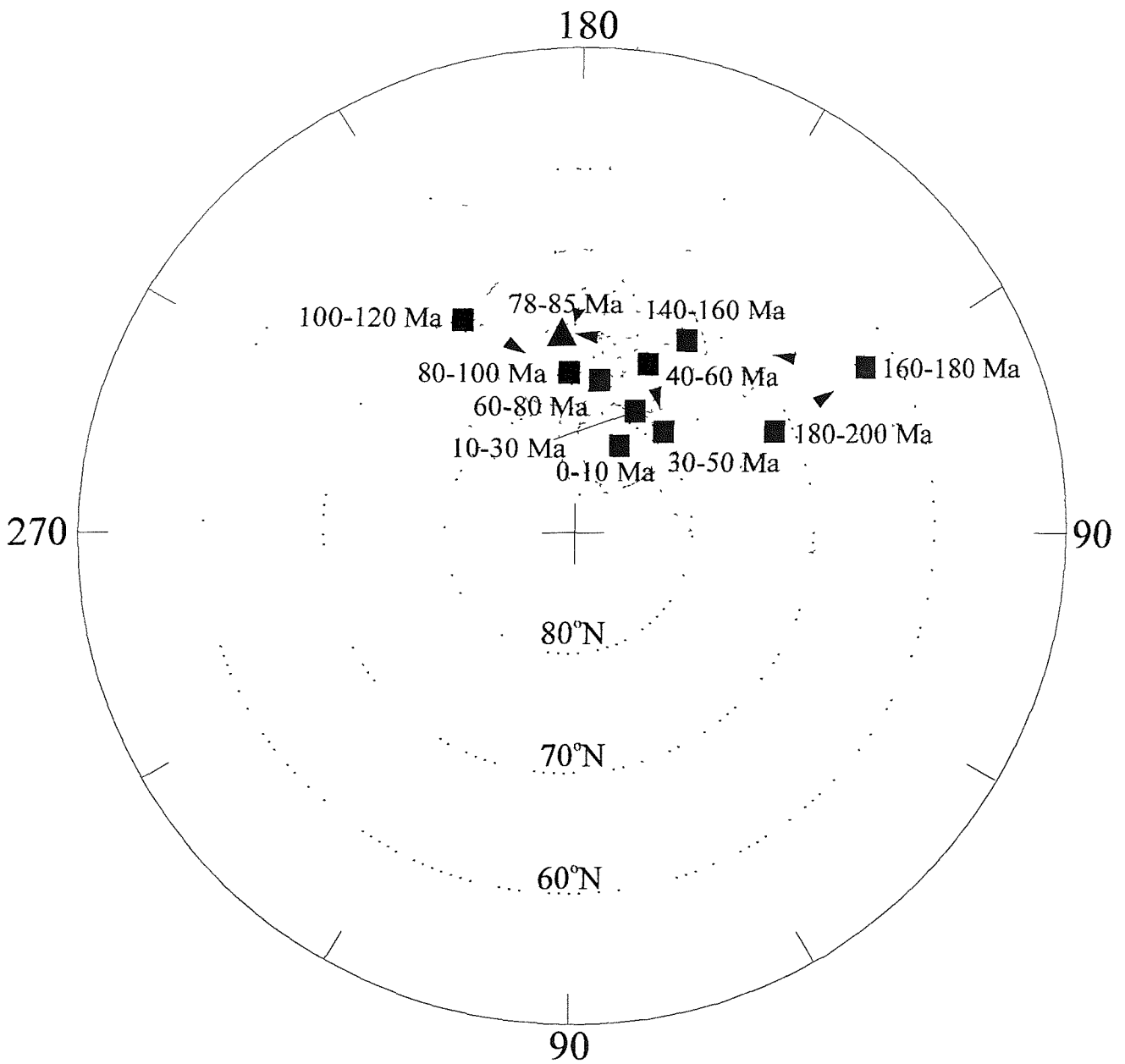

Figure 9.24. Apparent polar wander path for the Eurasian plate, from present back to 200 Ma. Connected squares are mean poles for the Eurasian palaeomagnetic data only (after Besse & Courtillot, 1991). Alpha 95 values are shown as broken-line circles. The solid triangle indicates the palaeomagnetic pole position derived from 'S1 reliability' category palaeomagnetic data from the English Chalk (Scratchell's Bay and Seaford Head) during the Coniacian-Campanian stages (78-85 Ma).

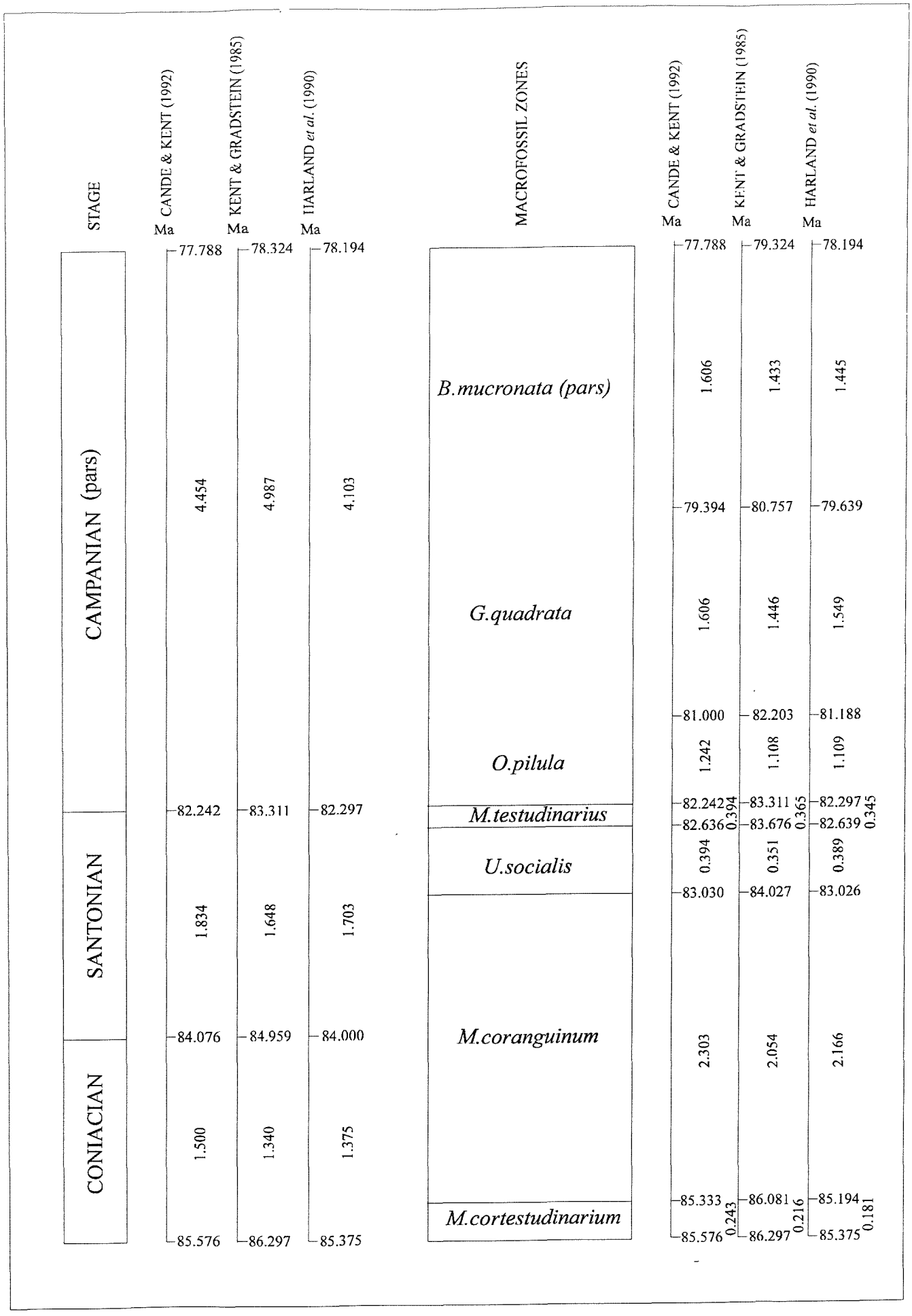

Table 9.1 Ages and durations of Late Cretaceous stages and macrofossil zones in southern England according to magnetostratigraphic time scales based on calibration points derived from the time scales of Cande & Kent (1992), Kent & Gradstein (1985) and Harland *et al.* (1990) respectively

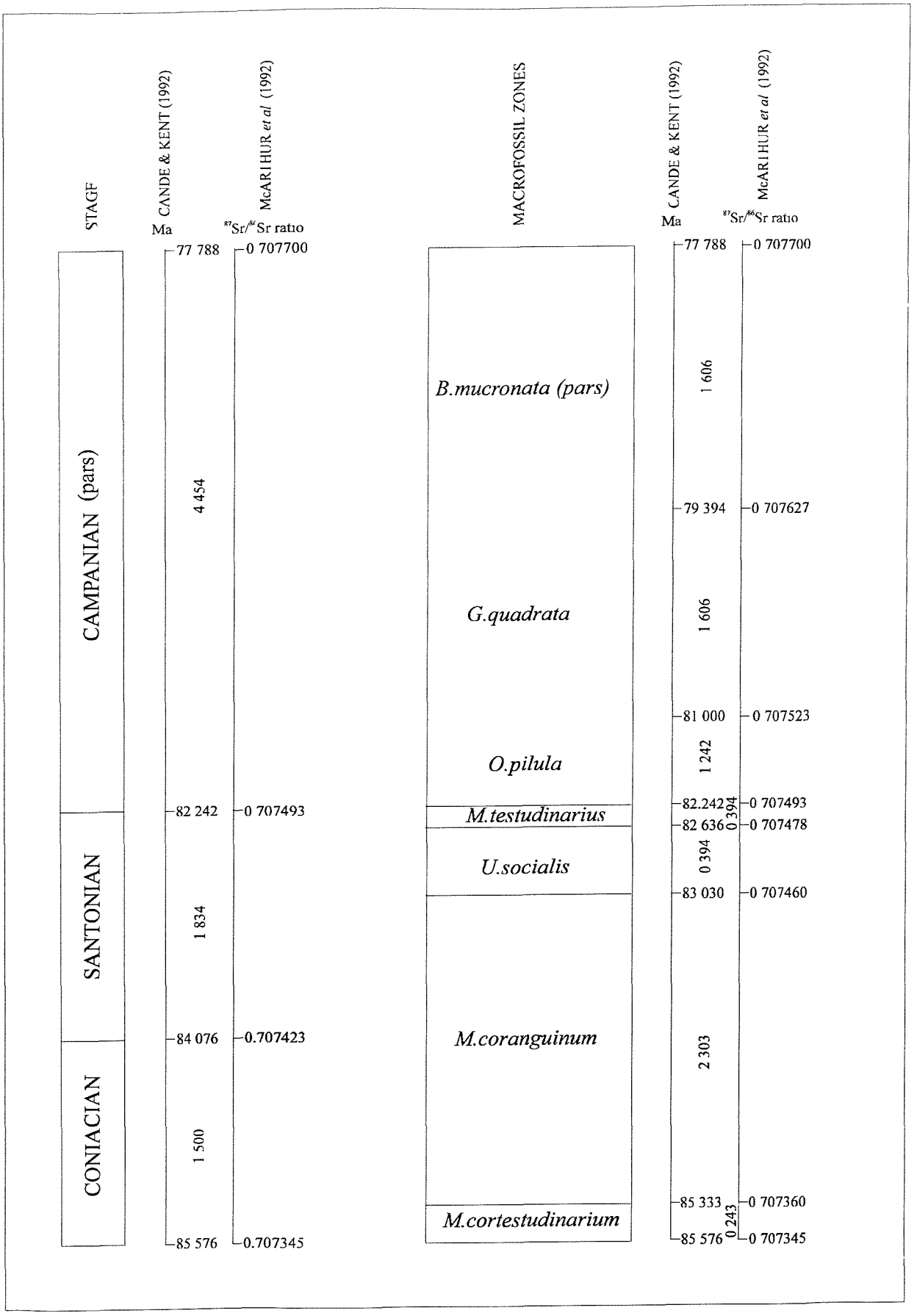

Table 9.2. Ages, durations and $^{87}Sr/^{86}Sr$ ratio values of Late Cretaceous stages and macrofossil zones in southern England according to a magnetostratigraphic time scale for southern England, based on calibration points derived from the time scale of Cande & Kent (1992) and the $^{87}Sr/^{86}Sr$ isotope curve of McArthur *et al.* (1990) respectively. Strontium isotope signatures marking stage and macrofossil zone boundaries are derived by biostratigraphic correlations and extrapolation using a best fit straight line for the Coniacian-Campanian stages

SAMPLE HORIZON	BEFORE		AFTER		N	R	ALPHA 95	K	MACROFOSSIL ZONE	STAGE	TREATMENT	POLARITY
	DEC	INC	DEC	INC								
CC3	244	78	4	22	3	2.981	11.9	107.7	*B.mucronata*	CAMPANIAN	A	N
CC9	175	66	24	38	3	2.978	12.9	92.9	*B.mucronata*	CAMPANIAN	A/T	N
CC81	76	87	17	26	6	5.943	7.2	87.086	*G.quadrata*	CAMPANIAN	A/T	N
CC82	175	80	18	36	3	2.994	6.6	345.551	*G.quadrata*	CAMPANIAN	A	N
CC89	12	85	21	30	3	2.983	11.5	116.319	*M.coranguinum*	SANTONIAN	A/T	N
CC96-98	273	84	15	37	8	7.501	15.3	14.028	*M.coranguinum*	SANTONIAN	A/T	N
CC100-101	327	88	20	34	5	4.9	11.5	45.6	*M.coranguinum*	SANTONIAN	A/T	N
CC104	357	83	19	29	3	2.99	8.7	200.2	*M.coranguinum*	SANTONIAN	A/T	N
CC105	354	78	16	25	6	5.931	7.9	72.559	*M.coranguinum*	SANTONIAN	A	N
CC106	359	79	17	25	13	12.954	2.6	260.462	*M.coranguinum*	SANTONIAN	A/T	N
CC107	2	81	18	26	13	12.926	3.3	162.067	*M.coranguinum*	SANTONIAN	A/T	N
CC108-111	303	78	9	32	6	5.839	12.2	31.079	*M.coranguinum*	SANTONIAN	A/T	N
CC112-113	203	82	22	43	12	10.705	15.8	8.496	*M.coranguinum*	SANTONIAN	A/T	N
CC115	331	77	11	26	5	4.99	3.9	386.4	*M.coranguinum*	SANTONIAN	A	N
CC119	329	85	17	32	7	6.844	9.9	38.339	*M.coranguinum*	SANTONIAN	A	N
CC120-121	297	84	15	34	7	6.746	12.7	23.649	*M.coranguinum*	CONIACIAN	A	N
CC122-125	293	83	13	34	7	6.803	11.1	30.494	*M.coranguinum*	CONIACIAN	A	N
CC126-129	280	80	10	36	8	7.65	12.7	19.982	*M.coranguinum*	CONIACIAN	A	N
CC140	209	77	12	49	11	10.917	4.2	120.306	*M.coranguinum*	CONIACIAN	A	N
CC145-146	358	79	12	26	9	8.968	3.2	252.38	*M.cortestudinarium*	CONIACIAN	A	N
SB13	90	77	16	37	4	3.939	13.3	49.031	*M.coranguinum*	SANTONIAN	A	N
SB15	146	46	47	67	3	2.987	10	152.96	*M.coranguinum*	SANTONIAN	A	N
SB16	173	83	1	45	8	7.88	7.3	58.349	*M.coranguinum*	SANTONIAN	A	N
SB17	217	77	348	48	6	5.873	10.8	39.483	*M.coranguinum*	SANTONIAN	A	N
SF2A	114	-54	127	-42	4	7.981	7.4	154.068	*O.piliula*	CAMPANIAN	A	R
SF12	357	58	354	42	3	2.963	17	53.696	*U.socialis*	SANTONIAN	A	N

Table 9.3. Site mean magnetic directions for Late Cretaceous strata exposed at Culver Cliff, Scratchell's Bay and Seaford Head. The table presents, from left to right; sample horizon code; the mean declination and inclination of the palaeomagnetic field (before and after bedding correction) at each defined site; the number of 'S1 reliability' observations at each site used to derive the mean magnetic direction (N); the length of the resultant vector (R) of the observations; alpha 95 of the observations; precision (k) of the observations; the macrofossil zone the sample site lies in; the stage the sample site lies in; the demagnetisation treatment used (either A.F. (A) or thermal (T)) and; the defined polarity of the sample site.

Plate 9.2 Flint band and marl seams in *G. quadrata* Zone chalk at Culver Cliff, Isle of Wight.

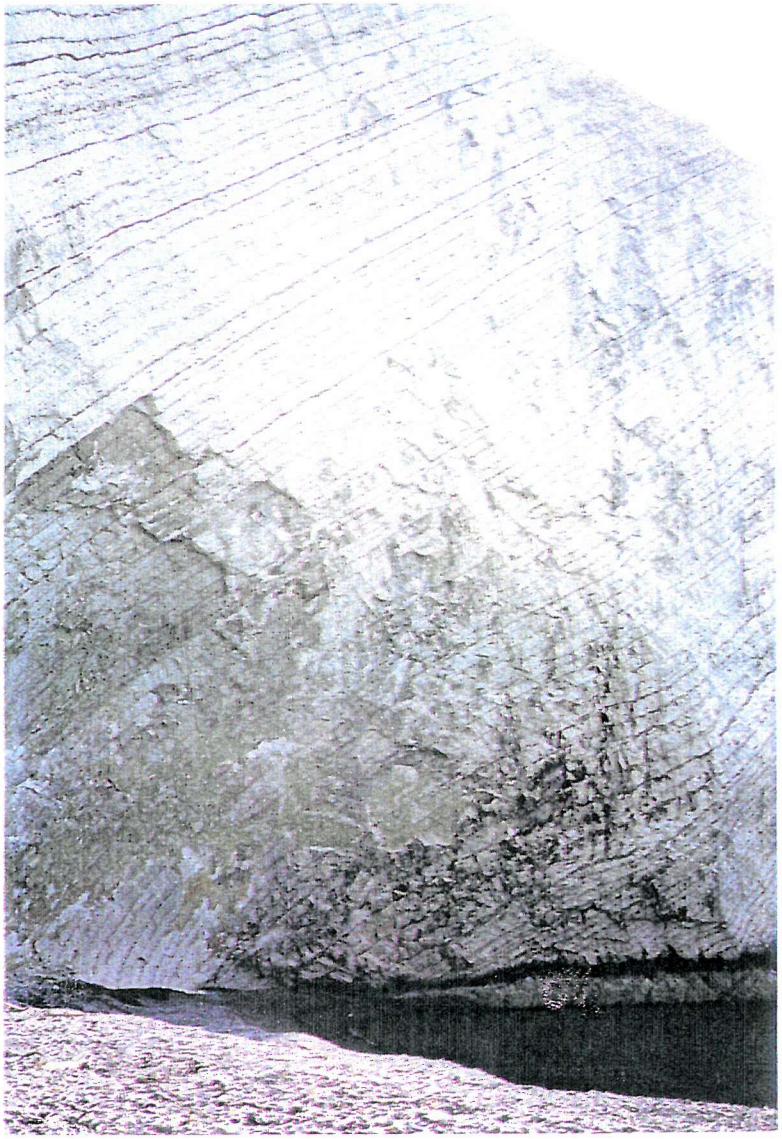

Plate 9.1 Flint bands exposed in the 'Grand Arch' Scratchell's Bay (*M. coranguinum* Zone), Isle of Wight.

REFERENCES

ADAMS, P.R. & W.E. FRERICHS 1973. Foraminifera from the type area of the Hilliard Formation, in the Greater Green River Basin Symposium Guidebook. Casper, Wyo., Wyoming Geol. Assoc., 193-199.

ALI, J.R. 1989. Magnetostratigraphy of Early Palaeogene sediments fron NW Europe. Unpublished Ph.D. thesis, University of Southampton.

ALVAREZ, W., ARTHUR, M.A., FISHER, A.G., LOWRIE, W., NAPOLEONE, G., PREMOLI SILVA, I. & W.M. ROGGENTHEN 1977. Upper Cretaceous-Paleocene magnetic stratigraphy at Gubbio, Italy V. Type section for the Late Cretaceous-Paleocene geomagnetic reversal time-scale. *Geol. Soc. Am. Bull.*, **88**, 383-389.

ALVAREZ, W. & W. LOWRIE 1978. Upper Cretaceous palaeomagnetic stratigraphy at Moria (Umbrian Apennines, Italy): verification of the Gubbio section. *Geophys. J. R. astr. Soc.*, **55**, 1-17.

AMERIGIAN, C. 1974. Sea-floor dynamic processes as the possible cause of correlations between paleoclimatic and paleomagnetic indices in deep-sea sedimentary cores. *Earth Planet. Sci. Lett.*, **21**, 321-326.

ANDERTON, R., BRIDGES, P.H., LEEDER, M.R. & B.W. SELLWOOD 1979. *A dynamic stratigraphy of the British Isles*. George Allen and Unwin Ltd.

ANSON, G.L. & K.P. KODAMA 1987. Compaction-induced shallowing of post-depositional remanent magnetization in a synthetic sediment. *Geophys. J. R. astr. Soc.*, **88**, 673-692.

ARASON, P. & S. LEVI 1990. Models of Inclination Shallowing During Sediment Compaction. *J. Geophys. Res.*, **95**, 4481-4499.

ARKEL, W.J., FURNISH, W.M., KUMMEL, B., MILLER, A.K., MOORE, R.C., SCHINDEWOLF, O.H., SYLVESTER-BRADLEY, P.C. & C.W. WRIGHT 1957. *Treatise on Invertebrate Paleontology. L. Mollusca 4.* Geol. Soc. Am. & Univ. Kansas Press, 490+xxii pp.

ARMSTRONG, R.L. 1978. Pre-Cenozoic Phanerozoic time scale-Computer file of critical dates and consequences of new and in-progress decay-constant revisions. *In*: Cohee, G., Glaessener, M. and H. Hedberg (eds.), *Contributions*

to the geologic time scale. Tulsa, Oklahoma, AAPG, 73-91.

ARTHUR, M.A. & A.G. FISHER 1977. Upper Cretaceous-Paleocene magnetic stratigraphy at Gubbio, Italy I. Lithostratigraphy and sedimentology. *Bull. Geol. Soc. Am.*, **88**, 383-389.

ARTHUR, M.A., DEAN, W.E. BOTTJER, D. & P.A. SCHOLLE 1984. Rhythmic bedding in Mesozoic-Cenozoic pelagic carbonate sequences; the primary and diagenetic origin of Milankovitch-like cycles. *In*: A.L. Berger *et al.* (eds.), *Milankovitch and Climate*, Part 1, 191-222. Reidel, Dordrecht.

BAILEY, H.W, GALE, A.S., MORTIMORE, R.N., SWIECICKI, A. & C.J. WOOD 1983. Criteria for defining the Coniacian to Maastrichtian Stage boundaries in England. *In*: Birkelund, T., Bromley, R., Christensen, W.K., Håkansson, E. & F. Surlyk (eds.), *Symposium on Cretaceous Stage Boundaries*, Abstracts, Copenhagen 1983, 9-12.

BAILEY, H.W. & M.B. HART 1979. The correlation of the Early Senonian in Western Europe using foraminiferida. *Aspekte der Kreide Europas*, IUGS ser. 1, no. **6**, 159-169.

BARR, F.T. 1962. Upper Cretaceous planktonic foraminifera from the Isle of Wight, England. *Palaeontology*, **4**, 552-580.

BARROIS, C. 1876. Recherches sur le Terain Cretace Superior de l'Angleterre et de l'Irlande. Lille, 232 pp.

BARTON, C.E., McELHINNY, M.W. & D.J. EDWARDS 1980. Laboratory studies of depositional DRM. *Geophys. J. R. astr. Soc.*, **61**, 355-377.

BERGGREN, W.A., KENT, D.V. & J.J. FLYN 1985a. Palaeogene geochronology and chronostratigraphy. *In*: Snelling, N.J. (ed.). Geochronology of the geological record. *Mem. Geol. Soc. London*, No. **10**, 141-195.

BERGGREN, W.A., KENT, D.V., FLYN, J.J. & J.A. VAN COUVERING 1985b. Cenozoic geochronology. *Geol. Soc. Am. Bull.*, **96**, 1407-1418.

BERGSTRESSER, T.J. & W.E. FRERICHS 1982. Planktonic Foraminifera from the Upper Cretaceous Pierre Shale at Red Bird, Wyoming. *J. Foram. Res.*, **12**, 1088-1097.

BERNER, R.A. 1969. Goethite stability and the origin of red beds. *Geochim. Cosmochim. Acta*, **33**, 267-273.

BESSE, J. & V. COURTILLOT 1991. Revised and synthetic apparent polar wander paths of African, Eurasian, North American and Indian Plates, and True Polar Wander since 200 Ma. *J. Geophys. Res.*, **96**, 4029-4050.

BLAKEMORE, R.P. 1982. Magnetotactia bacteria. *Ann. Rev. Microbiol.*, **36**, 217-238.

BLOW, R.A. & N. HAMILTON 1978. Effect of compaction on the acquisition of a detrital remanent magnetisation in fine-grained sediments. *Geophys. J. R. astr. Soc.*, **52**, 13-23.

BOLLI, H.M. 1966. Zonation of Cretaceous to Pliocene marine sediments based on planktonic foraminifera. *Boletin Informatvo Associacion Venezolana de Geologia, Mineria y Petroleo*, **9**, 3-32.

BLAKELY, R.J. 1974. Geomagnetic reversals and crustal spreading rates during the Miocene. *J. Geophys. Res.*, **79**, 2979-2985.

BRASIER, M.D. *Microfossils*. George Allen and Unwin, London.

BROCK, A. 1971. An experimental study of palaeosecular variation. *Geophys. J. R. astr. Soc.*, **24**, 303-317.

BROMLEY, R.G., SCHULZ, M.G. & N.B. PEAKE 1975. Paramoudras:giant flints, long burrows and early diagenesis of chalks. *K. dansk. Vidensk. Selsk. Geol. Skr.*, **20**, pt. 10, 3-31.

BURNETT, J.A. 1990. A new nannofossil zonation scheme for the Boreal Campanian. *INA Newsletter*, **12/3**, 67-70.

BURNS, R.G. & V.M. BURNS 1981. Authigenic oxides. *In*: Emilliani, C (ed.) *The Oceanic Lithosphere* (*The Sea, Vol. 7*). John Wiley and Sons, New York, 875-914.

CANDE, S.C. & D.V. KENT 1992. A New Geomagnetic Polarity Time Scale for the Late Cretaceous and Cenozoic. *J. Geophys. Res.*, **97**, 13917-13951.

CANDE, S.C. & J.L. LaBREQUE 1974. Behaviour of the Earth's paleomagnetic field from small scale marine magnetic anomalies. *Nature*, **247**, 26-28.

CARON, M. 1985. Cretaceous planktic foraminifera. *In*: H.M. Bolli, J.B. Saunders and K. Perch-Nielsen (eds.), *Plankton stratigraphy, vol. 1, Planktic foraminifera, calcareous nannofossils and calpionellids*. Cambridge University Press.

CELAYA, M.A. & B.M. CLEMENT 1988. Inclination shallowing in deep sea sediments from the north Atlantic. *Geophys. Res. Lett.*, **15**, 52-55.

CHADWICK, R.A. 1993. Aspects of basin inversion in southern England. *J. Geol. Soc.*, **150**, 311-322.

CHANNELL, J.E.T., FREEMAN, R., HELLER, F. & W. LOWRIE 1982. Timing of diagenetic growth in red pelagic limestones. *Earth Plant. Sci Lett.*, **58**, 189-201.

CHANNELL, J.E.T, LOWRIE, W. & F. MEDIZZI 1979. Middle and Early Cretaceous magnetic evidence stratigraphy from the Cismon section, northern Italy. *Earth Planet. Sci. Lett.*, **85**, 153-166.

CHAVE, A.D. 1980. Upper Cretaceous-Paleocene magnetic stratigraphy. DSDP Leg 74 (abs.). *EOS* (A.G.U. Trans.), **61**, 944.

CLARKE, R.F.A. & J.P. VERDIER, 1967. An investigation of microplankton assemblages from the Chalk of the Isle of Wight, England. *Verh. K. Ned. Akad. Wet.*, **24**, 1-96.

CLAYTON, C.J. 1982. Growth history and microstructure of flints. *IAS 3rd EUR. MTG.*, Copenhagen, Abstr., pp 105-7.

CLAYTON, C.J. 1984. Geochemistry of chert formation in Upper Cretaceous Chalks. Unpubl. PhD Thesis, Univ. of London.

CLAYTON, C.J. 1986. The Chemical Environment of Flint Formation in Upper Cretaceous Chalks. *In*: Sieveking, G. & M.B. Hart (eds) *The Scientific Study of Flint and Chert*, 43-54, Cambridge University Press.

COBBAN, W.A. & J.B. REESIDE, Jr., 1952. Correlation of the Cretaceous formations of the western interior of the United States. *Geol. Soc. America Bull.*, **63**, 1011-1044.

COLLINSON, D.W. 1983. *Methods in Palaeomagnetism and Rock Magnetism*. Chapman and Hall, London, p.500.

COX, A. 1970. Latitude dependance on the angular dispersion of the geomagnetic field. *Geophys. J. R. astr. Soc.*, **20**, 253-269.

COX, A.V. 1982. Magnetostratigraphic time scale. *In*: HARLAND, W.B., COX, A.V., LLEWELLYN, P.G., PICKTON, A.G., SMITH, A.G., & R. WALTERS 1982. *A Geologic Time Scale*. Cambridge University Press, Cambridge, UK.

COX, A., DOELL, R.R. & G.B. DALRYMPLE 1965. Quaternary palaeomagnetic stratigraphy. *In*: The Quaternary of the United States, a second volume. Princeton University Press, Princeton, NJ, USA.

CREER, K.M. 1957. Palaeomagnetic investigations in Great Britain-IV. The natural remanence magnetization for certain stable rocks from Great Britain. *Phil. Trans. R. Soc., London.*, **A250**, 111-129.

DEAMER, G.A. & K.P. KODAMA 1990. Compaction-induced inclination shallowing in synthetic and natural clay rich sediments. *J. Geophys. Res.*, **95**, 4511-4529.

de BOER, P.L. & A.A.H. WONDERS 1984. Astronomically induced rhythmic sedimentation in Cretaceous pelagic sediments near Moria. *In*: A.L. Berger *et al.* (eds.), *Milankovitch and Climate*, Part 1, 177-190. Reidel, Dordrecht.

DIETZ, R.S. 1961. Continent and ocean basin evolution by spreading of the sea floor. *Nature*, **190**, 854-857.

DOUGLAS, R. & W.V. SILTER 1966. Regional distribution of some Cretaceous Rotaliporidae and Globotruncanidae (Foraminiferida) within North America. *Tulane Stud. Geol.*, **4**, 89-130.

DOEVEN, P.H. 1983. Cretaceous nannofossil stratigraphy and paleoecology of the Canadian Atlantic Margin. *Bull. geol. Surv. Can.*, **356**, 1-70.

DUNLOP, D.J. Magnetic mineralogy of unheated and heated red sediments by coercivity spectrum analysis. *Geophys. J. R. astr. Soc.*, **27**, 37-55.

DUNLOP, D.J. & J.M. STIRLING 1977. 'Hard' viscous remanent magnetization (VRM) in fine-grained hematite. *Geophys. Res. Letters.*, **21**, 288-294.

EATON, J.G. 1987. The Campanian-Maastrichtian boundary in the Western Interior of the North America. *Newsletters on Stratigraphy*, **18**, 31-39.

FELDER, P.H. 1981. Onderzoek van de meso-fosielen in de Krijtafzettingen van Limberg. *Natuurhist. Maanndblad*, **70**, 69-76.

FISHER, R.A. 1953. Dispersion on a sphere. *Proc. R. Soc.*, **A217**, 295-305.

FISHER, A.G. & W. SCHWARZACHER 1984. Cretaceous bedding rhythms under orbital control? *In*: A.L. Berger *et al.* (eds.), *Milankovitch and Climate*, Part 1, 163-175. Reidel, Dordrecht.

FITTON, W.H. 1847. A stratigraphical account of the section from Atherfield to

Rocken End, on the south-west coast of the Isle of Wight. *Q. Jl. geol. Soc. Lond.*, **3**, 289-327.

FRANKEL, R.B., BLAKEMORE, R.P. & R.S. WOLFE 1979. Magnetite in freshwater magnetotactic bacteria. *Science*, **203**, 369-372.

FRERICHS, W.E. & P.R. ADAMS 1973. Correlation of theHilliard Formation with the Niobrara Formation. *In*: Greater Green River Basin Symposium Guidebook. Casper,Wyo., Wyoming Geol. Assoc., 187-192.

FRY, G., BOTTJER, D.J. & P.S. LUND 1985. Magnetostratigraphy of displaced Upper Cretaceous strata in southern California. *Geology*, **13**, 648-651.

GALE, A.S. 1990. A Milankovitch scale for Cenomanian time. *Terra Nova*, **1**, 420-425.

GALE, A.S., MONTGOMERY, P., HANCOCK, J.M., KENNEDY, W.J. McARTHUR, J. & J.A. BURNET, in prep. Global correlation and definition of the Santonian-Campanian boundary.

GASTER, C.T.A. 1941. The Chalk Zones of Offaster pilula and Actinocamax quadratus. *Proc. Geol. Ass.*, **52**, 210- 215.

GEE, J., KLOOTWIJK, C.T. & G.M. SMITH 1991. Magnetostratigraphy of Paleocene and Upper Cretaceous sediments from Broken Ridge, Eastern Indian Ocean. *In*: Weissel, J., Peirce, J., Taylor, E., Alt, J., *et al. Proc. Ocean Drill. Prog., Scientific Results*, **121**; 359-375.

GOREE, W.S. & M.D. FULLER 1976. Magnetometers using R.f.-driven squids and their application in rock magnetism and paleomagnetism. *Revs. Geophys. Space Phys.*, **14**, 591-608.

GRAY, D.A. 1965. The stratigraphical significance of electrical resistivity marker bands in the Cretaceous strata of the Leatherhead (Fetcham Mill) borehole, Surrey. *Bull. Geol. Surv. Gt Br.*, **23**, 65-115.

GREEN, K.A. & A. BRECHER 1974. Preliminary palaeomagnetic results from sediments from site 263, leg 27. *Initial Rep. Deep Sea Drill. Proj.*, **27**, 405-413.

GRIFFITH, C. & R.M. BRYDONE 1911. The Zones of the Chalk in Hants. London Dulau & Co., Ltd., 35pp.

GRIFFITHS, D.H., KING, R.F., REES, A.I. & A.E. WRIGHT 1960. Remanent

magnetism of some recent varved sediments. *Proc. R. Soc. London, Ser. A*, **256**, 359-383.

HAILWOOD, E.A., HAMILTON, N. & G.E. MORGAN 1980. Magnetic polarity dating of tectonic events at passive continental margins. *Philos. Trans. R. Soc. London*, **294**, 189-208.

HAILWOOD, E.A. 1989. *Magnetostratigraphy*. Geol. Soc. London, Special Report No. **19**, 84pp.

HAILWOOD, E.A., GROTHIER, C., TING, F. & P.J. RIDDY 1992. Magnetostratigraphic resolution using the 2G whole-core magnetometer: an experimental study. Annales Geophysicae. Atmosphere, Hydrospheres and Space Sciences. Part 1, Solid Earth Geophysics and Natural Hazards. Supplement 1 to 10, C23. European Geophysical Society, Springer International.

HÅKANSSON, E., BROMLEY, R.G. & K. PERCH-NIELSEN 1974. Maastrichtian chalk of north-west Europe-a pelagic shelf sediment. *In:* Hsü, K.J. & H.C. Jenkyns (eds.), Pelagic Sediments on land and under the sea. *Spec. Publ. int. Ass. Sediment.*, **1**, 211-233.

HALLAM, A. & B.W. SELLWOOD 1968. Origin of Fuller's earth in the Mesozoic of southern England. *Nature*, **220**, 1193-1195.

d'HALLOY, O. 1822. Observations sur un essai de carte géologique de la France, des Valanginien und Hauterivien. *Bull. Verein. schweiz. Petrol. Geol. u.-Ing.*, **31**, 41-75.

HAMBACH, U. & K. KRUMSIEK 1989. A magnetostratigraphic subdivision of the Upper Albian and Lower Cenomanian on the basis of drill cores from wells in the Ruhr area. *Geol. Jb.*, **A113**, 401-425.

HAMBACH, U. & K. KRUMSIEK 1991. Magnetostratigraphie im Santon und Campen des Munsterlander Kriedebeckens. *Facies*, **24**, 113-124. Erlagen.

HANCOCK, J.M. 1975. The petrology of the Chalk. *Proc. Geol. Ass.*, **86**, 499-536.

HANCOCK, J.M. & P.F. RAWSON 1992. Cretaceous. *In*: Cope, J.C.W., Ingham, J.K. and Rawson, P.F. (eds.), *Atlas of Palaeogeography and Lithofacies*. Geological Society, London, Memoir 13, 131-139.

HAQ, B.U. HARDENBOL, J. & P.R. VAIL 1987. The chronology of fluctuating sea

level since the Triassic. *Science*, **235**, 1156-1167.

HARGRAVES, R.B. 1959. Magnetic anisotropy and remanent magnetism in hemo-ilmenite from ore deposits at Allard Lake, Quebec. *J. Geophys. Res.*, **64**, 1565-1578.

HARLAND, W.B., COX, A.V., LLEWELLYN, P.G., PICKTON, A.G., SMITH, A.G., & R. WALTERS 1982. *A Geologic Time Scale*. Cambridge University Press, Cambridge, UK.

HARLAND, W.B., ARMSTRONG, R.L., COX,A.V., CRAIG, L.E., SMITH, A.G. & D.G. SMITH 1990. *A geologic time scale*. Cambridge University Press. London.

HART, M.B., WEAVER, P.P.E., CLEMENTS, R.G., BURNETT, J.A., TOCHER, B.A., BATTEN, D.J., LISTER, J.K. & A.M. MacLENNAN 1987. Cretaceous. *In*: Mesozoic and Cenozoic Stratigraphical Micropalaeontology of Dorset and the Isle of Wight, Southern England. Field Guide for the XXth. European Micropalaeontological Colloquium. Lord, A.R. & P.R.Bown (eds.), British Micropalaeontological Society Guide Book 1.

HART, M.B. 1987. Orbitally induced cycles in the chalk facies of the United Kingdom. *Cret. Res.*, **8**, 335-348.

HAYS, J.D., IMBRIE, J. & N.J. SHACKLETON 1976. Variations in the Earth's orbit-pacemaker of the ice ages. *Science*, **194**, 1121-1132.

HAZEL, J.E. & E.G. KAUFFMAN 1975. *Concepts and Methods in Biostratigraphy*. Dowden, Hutchinson and Ross, Stroudsberg, 658 pp.

HEBERT, E. 1863. Note sur la craie blanche et la craie marneuse dans le bassin de Paris, et sur la division de ce dernier etage en quatre assises. *Bull. Soc. geol. Or.* (2) **20**, 605-31.

HEDBERG, H.D., (ed.), 1976. International stratigraphic guide. New York, John Wiley & Sons, Inc., 200p.

HEIRTZLER, J.R., DICKSON, G.O., HERRON, E.M., PITMAN, W.C., III, & X. Le PICHON 1968. Marine magnetic anomalies, geomagnetic field reversals and motions of the ocean floor and continents. *J. Geophys. Res.*, **73**, 2119-2136.

HELLER, F. & J.E.T. CHANNELL 1979. Paleomagnetism of Upper Cretaceous limestone from South Germany. *J. Geophys.*, **42**, 475-488.

Pages 397-401
missing

of the Western Interior of North America. *In*: W.G.E. Caldwell (ed.), *Cretaceous System in the Western Interior of North America. Geol. Ass. Canada Spec. Pap.*, **13**, 31-54.

OBRADOVICH, J.D., SUTTER, J.F. & M.J. KUNK 1986. Magnetic polarity chron tie points for the Cretaceous and early Tertiary. *Terra Cognita*, **6**, 140.

OPDYKE, N.D. 1972. Paleomagnetism of deep-sea cores. *Rev. Geophys.*, **10**, 213-249.

OPDYKE, N.D. & K.W. HENRY 1969. A test for the dipole hypothesis. *Earth Planet. Sci. Lett.*, **6**, 138-151.

ONSTOTT, T.C. 1980. Application of the Bingham distribution function in paleomagnetic studies. *J. Geophys. Res.*, **85**, 1500-1510.

OSBOURNE WHITE, H.J. 1921. *A short account of the Geology of the Isle of Wight.* Memoirs of the Geological Survey of Great Britain. London, HMSO.

PACKARD, M. & R. VARIAN. 1954. Free nuclear induction in the earth's magnetic field. *Phys. Rev.* Series 2, **93**, 941.

PEAKE, N.B & J.M. HANCOCK 1961. The Upper Cretaceous of Norfolk. *Trans. Norfolk & Norwich Nat. Soc.*, **19**, 293-339.

PECHERSKY, D.M., NAIDIN, D.P. & E.A. MOLOTOVSKY 1983. The Santonian-Campanian reversed polarity magnetozone and the Cretaceous magnetostratigraphical timescale. *Cret. Res.*, **4**, 251-257.

PESSAGNO, E.A. 1969. Upper Cretaceous stratigraphy of the western Gulf coast of Mexico, Texas, and Arkansas. *Geol. Soc. of America Mem.*, **111**, 139pp.

PETLEY, B.W. 1980. The ubiquitous SQUID. *Contemp. Phys.*, **21**, 407-630.

PHILLIPS, F.C. 1971. *The Use of the Stereographic Projection in Structural Geology* (3rd Edn). E.Arnold, London, p.90.

PITMAN. W.C., III, HERRON, E.M & J.R. HEIRTZLER 1968. Magnetic anomalies in the Pacific and seafloor spreading. *J. R. Geophys.*, **73**, 2069-2085.

PITMAN. W.C., III, LARSON, R.L. & E.M. HERRON 1974. Magnetic lineations of the oceans. *Geol. Soc. America Map and Chart Ser. MC-6.*

PITMAN, W.C. & M. TALWANI 1972. Sea-floor spreading in the North Atlantic. *Bull. Geol. Soc. Am.*, **83**, 619-46.

PERCH-NIELSEN, K. 1977. Albian to Pliestocene calcareous nannofossils from the

Western South Atlantic, DSDP Leg 39. *Initial Rep. Deep Sea drill. Proj.*, **39**, 699-825.

PERCH-NIELSEN, K. 1979. Calcareous nannofossils from the Cretaceous between the North Sea and the Mediterranean. *IUGS Series A*, **6**, 223-272.

PERCH-NIELSEN, K. 1985. Mesozoic calcareous nannofossils. *In*: H.M. Bolli, J.B. Saunders and K. Perch-Nielsen (eds.), *Plankton stratigraphy, vol. 1, Planktic foraminifera, calcareous nannofossils and calpionellids*. Cambridge University Press.

PERRIN, R.M.S. 1957. The clay mineralogy of some tills in the Cambridge district. *Clay Miner. Bull.*, **3**, 193- 205.

PERRIN, R.M.S. 1971. *The Clay Mineralogy of British Sediments*. Mineralogy Society, London, 247 + v pp.

PREMOLI SILVA, I. 1977. Upper Cretaceous-Paleocene magnetic stratigraphy at Gubbio, Italy II. Biostratigraphy. *Geol. Soc. America Bull.*, **88**. 371-374.

PREMOLI SILVA, I., NAPOLEONE, G. & A.G. FISHER 1974. Risultati preliminari sulla stratigrafia paleomagnetica della Scaglia cretaceo-paleocenica della sezione di Gubbio (Appennino centrale). *Società Geologica Italiana Memorie*, **15**, 647-659.

RAFF, A.D., 1966. Boundaries of an area of very long magnetic anomalies in the northeast Pacific. *J. Geophys. Res.*, **71**, p.2631-2636.

RAWSON, P.F., D.CURRY, F.C.DILLEY, J.M. HANCOCK, W.J.KENNEDY, J.W. NEALE, C.J.WOOD & B.C. WORSAM 1978. A correlation of Cretaceous rocks in the British Isles. *Geol. Soc. Lond. Spec. Rep.*, No. **9**.

RESCHER, K. 1991. Biostratigraphische Gliederung der höheren Oberkreide mit benthonischen Foramainiferen im nordwestlichen Münsterland (Bohrung Metelen 1001). *Facies*, **24**, 99-108, Taf. 17, 3 Abb., 1 Tab, Erlangen.

REES, A.I. 1966. The effect of depositional slopes on the anisotropy of magnetic susceptibility of laboratory deposited sands. *J. Geol.*, **74**, 856-876.

REID, R.E.H. 1968. Bathymetric distributions of Calcarea and Hexactinellida in the present and the past. *Geol. Mag.*, **105**, 546-59.

REID, R.E.H. 1973. The Chalk Sea. *Ir. nat. J.*, **17**, 357-375, Belfast.

REID, R.E.H. 1976. Late Cretaceous climatic trends, faunas and hydrography in

Britain and Ireland. *Geol. Mag.*, **113**, 115-28.

ROBASZYNSKI, F. & M. CARON (coordinators). 1979. Atlas de Foraminiféres planctonoques du Crétacé moyen. Parts 1-2. *Cah. Micropaleontol.*, **1** and **2**, 1-185 amd 1-181.

ROBINSON, S.G. 1992. Lithostratigraphic applications for magnetic susceptibility logging of deep-sea sediment cores: examples from ODP Leg 115. *In*: Hailwood, E.A. & R.B. Kidd (eds), *High Resolution Stratigraphy*. Geological Society Special Publication, No. **70**, 65-98.

ROGGENTHEN, W.M. & G. NAPOLEONE 1977. Upper Cretaceous-Paleocene magnetic at Gubbio, Italy: IV. Upper Maastrichtian-Paleocene magnetic stratigraphy. *Bull. Geol. Soc. Am.*, **88**, 378-382.

ROTH, P.H. 1973. Calcareous nannofossils - Leg 17, DSDP. *Initial Rep. Deep Sea drill. Proj.*, **17**, 695-793.

ROTH, P.H. 1978. Cretaceous nannoplankton biostratigraphy and oceanography of the Northwestern Atlantic Ocean. *Initial Rep. Deep Sea drill. Proj.*, **44**, 731-759.

ROTH, P.H. 1983. Jurassic and Lower Cretaceous calcareous nannofossils in the western North Atlantic (Site 534): Biostratigraphy, preservation, and some observations on biogeography and paleoceanography. *Initial Rep. Deep Sea drill. Proj.*, **76**, 587-621.

ROWE, A.W. 1908. The Zones of the White Chalk of the English Coast. *Proc. Geol. Ass.*, **20**, 209-352.

SCHWERTMANN, U. & H. THALMANN 1976. The influence of (FE II), (Si) and pH on the formation of lepidocrocite and ferrihydrite during oxidation of aqueous FeCl solutions. *Clay Miner.*, **11**, 189-200.

SCLATER, J.G. & R.L. FISHER 1974. Evolution of the east-central Indian Ocean, with emphasis on the tectonic setting of the Ninetyeast Ridge. *Geol. Soc. America Bull.*, **85**, 683-702.

SHIVE, P.N. & W.E. FRERICHS 1974. Palaeomagnetism of the Niobrara Formation in Wyoming, Colorado, and Kansas. *J. Geophys. Res.*, **79**, 3001-3008.

SHMELEVA, A.N. 1963. Paleomagnetic investigation of some sections of the Upper Cretaceous sediments at western foothills of Fergana Ridge. *Trudy*

Vsesoyusnogo Neftyanogo nauchno-issledovatel'skogo instituta, vypusk **204**, 212-219.

SIGAL, J. 1977. Essai de zonation du Crétacé méditerranéen à l'aide des foraminiféres planctonoques. *Geologie Mediterraneenne*, **4**, 99-108.

SISSINGH, W. 1977. Biostratigraphy of Cretaceous calcareous nannoplankton. *Geol. Mijnbouw.*, **56** (1), 37-65.

SISSINGH, W. 1978. Microfossil biostratigraphy and stage-stratotypes of the Cretaceous. *Geol. Mijnbouw*, **57** (3), 433-440.

SMART, J.G.O. & C.J. WOOD 1976. (Field meeting to) South Humberside. *Proc. Yorks. geol. Soc.*, **40**, 586-93.

SMITH, A.G., HURLEY, A.M. & J.C. BRIDEN 1981. *Phanerozoic palaeocontinental world maps*. Cambridge University Press.

SMITH, P.P.K. 1979. The identification of single-domain titanomagnetite particles by means of transmission electron microscopy. *Can. J. Earth Sci.*, **16**, 375-379.

STOLZ, J.F., CHANG, S.R. & J.L. KIRSCHVINK 1986. Magnetotactic bacteria and single domain magnetite in hemipelagic sediments. *Nature*, **321**, 849-851.

SUBCOMMISSION ON MAGNETOSTRATIGRAPHIC NOMENCLATURE, 1973. Magnetic polarity time scale. *Geotimes*, **18**, 21-22.

TARDUNO, J.A. 1990. Brief reversed polarity intervals with the Cretaceous Normal Polarity Superchron. *Geology*, **18**, 683-686.

TARDUNO, J.A, LOWRIE, W., SLITER, W.V., BRALOWER, T.J. & F. HELLER 1992. Reversed Polarity Characteristic Magnetizations in the Albian Contessa Section, Umbrian Apennines, Italy: Implications for the Existence of a Mid-Cretaceous Mixed Polarity Interval. *J. Geophys. Res.*, **97**, 241-271.

TARLING, D.H. 1983. *Palaeomagnetism: principles and applications in geology, geophysics, and archaeology*. Chapman and Hall Ltd.

TAUXE, L. & D.V. KENT 1984. Properties of detrital remanence carried by haematite from the study of modern river deposits and laboratory redeposition experiment. *Geophys. J. R. astr. Soc.*, **77**, 543-561.

TAUXE, L., LaBREQUE, J.L., HSÜ, K., & OTHERS 1980. Paleogene magnetostratigraphy from DSDP Leg 73. *Geol. Soc. America Abstracts with Programs*, **12**, 533.

TAUXE, L., TUCKER, P., PETERSEN, N.P. & J.L. La BREQUE 1984. Magnetostratigraphy of leg 73 sediments. *Initial Rep. Deep Sea Drill. Proj.*, **73**, 609-621.

TAYLOR, R.M. & U. SCHWERTMANN 1974. Maghemite in soils and its origin, II, Maghemite synthesis at ambient temperature and pH 7. *Clay Miner.*, **10**, 289-298.

TING, F. 1991. Magnetostratigraphy of Lower Cretaceous and Oligocene Formations in the UK and Northwest Belgium. Unpublished Ph.D thesis, University of Southampton, England.

TORRES DE ARAUJO, F.F., PIRES, M.A., FRANKEL, R.B. & C.E.M. BICUDO 1986. Magnetite and magnetoaxis in algae. *Biophys. J.*, **50**, 375-378.

TOWE, K.M. & T.T. MOENCH 1981. Electron-optical characterization of bacterial magnetite. *Earth Planet. Sci. Lett.*, **52**, 213-220.

THOMPSON, R. & F. OLDFIELD 1986. *Environmental Magnetism*. Allen and Unwin, London.

TURNER, P. 1975. Depositional magnetization of Carboniferous limestones from Craven basin of northern England. *Sedimentology*, **22**, 563-581.

URRUTIA-FUCUGAUCHI, J. 1988. Palaeomagnetic study of the Cretaceous Morelos Formation, Guerrero State, southern Mexico. *Tectonphysics*, **147**, 121-125.

VALETON, I. 1960. Vulkanische Tuffiteinlagerung in der nordwestdeutschen Oberkreide. *Mitt. geol. StInst. Hamb.*, **29**, 26-41.

VANDENBERG, J., KLOOTWIJK, C.T. & A.A.H. WONDERS 1978. The Late Mesozoic and Cenozoic movements of the Umbrian Peninsula: Further palaeomagnetic data from the Umbrian Peninsula. *Geol. Soc. Am. Bull.*, **89**, 133-150.

VANDENBERG, J. & A.A.H. WONDERS 1980. Palaeomagnetism of Late Mesozoic pelagic limestones from the southern Alps. *J. Geophy. Res.*, **85**, 3623-3627.

VAN DER VOO, R. & W. LOWRIE 1979. A preliminary magnetic study of Jurassic limestone from the Swiss Jura Mountains and adjacent areas (abstract). *Eos Trans. AGU.*, **60**, 569.

VAN DER VOO, R. 1988. Paleomagnetism of North America: The Craton, its

margins and the Appalachians. *In*: Pakier, L.C. & W.D. Mooney (eds.), *Geophysical framework of the continental United States.* Geol. Soc. America Memoir.

van HINTE, J.E. 1972. The Cretaceous time scale and planktonic foraminiferal zones. *Proc. K. Ned. Akad.Wet.*, **B 75**, 61-68. Amsterdam.

van HINTE, J.E. 1976. A Cretaceous time scale. *AAPG Bull.*, **60**, 498-516.

VERBEEK, J.W. 1976a. Upper Cretaceous calcareous nannoplankton from Ballon and Théligny, in the type area of the Cenomanian stage. *Proc. Kon. Ned. Akad. Wetensch.*, **B 79**, 69-82.

VERBEEK, J.W. 1976b. Upper Cretaceous nannoplankton zonation in a composite section near El Kef, Tunisia. *Proc. Kon. Ned. Akad. Wetensch.*, **B 79**, 129-148.

VERBEEK, J.W. 1977a. Late Cenomanian to Early Turonian calcareous nannofossils from a section SE of Javernant (Dépt. Aube, France). *Proc. Kon. Ned. Akad. Wetensch.*, **B 80**, 20-22.

VERBEEK, J.W. 1977b. Calcareous nannoplankton biostratigraphy of Middle and Upper Cretaceous deposits in Tunisia, Southern Spain and France. *Utrecht Micropaleotol. Bull.*, **16**, 1-157.

VINE, F.J. & D.H. MATHEWS 1963. Magnetic anomalies over ocean ridges. *Nature*, **199**, 947-949.

VOIGT, E. 1963. Über Randtröge Bedeutung der Hartgründe ('Hardgrounds') in der pberen Kreide. *Paläont. Z.*, **33**, 129-147.

WEEDON, G.P. 1985. Hemipelagic shelf sedimentation and climatic cycles: the basal Jurassic (Blue Lias) of southern Britain. *Earth Planet. Sci. Lett.*, **76**, 321-335.

WEEKS, R., LAJ, C., ENDIGNOUX, L., FULLER, M., ROBERTS, A., MANGANNE, R., BLANCHARD, E. & W. GOREE, in press. Improvements in long core measurement techniques: applications in paleomagnetism and paleoceanography. *Geophys. J. Int.*

WEIR, A.H. & J.A. CATT, 1965. The mineralogy of some Upper Chalk samples from the Arundel area, Sussex. *Clay Miner.*, **6**, 97-110.

WHITE, R. & D. McKENZIE 1989. Magmatism at Rift Zones: The Generation of Volcanic Continental Margins and Flood Basalts. *J. Geophys. Res.*, **94**, No. B6,

7685-7729.

WISE, S.W. Jr 1983. Mesozoic and Cenozoic calcareous nannofossils recovered by Deep Sea Drilling Project Leg 71 in the Falkland Plateau Region, Southwest Atlantic Ocean. *Initial. Rep. Deep Sea drill. Proj.*, **71**, 481-550.

WOLFE, M.J. 1968. Lithification of a carbonate mud: Senonian chalk in Northern Ireland. *Sedim. Geol.*, **2**, 263-290.

WRIGHT, C.W. & E.V. WRIGHT 1942. The Chalk of the Yorkshire Wolds. *Proc. Geol. Ass.*, **53**, 112-27.

YOUNG, K. 1977. *Guidebook to the geology of Travis County.* Student Geological Society, University of Texas, 171pp.

YOUNG, K. & C.M. WOODRUFF. 1985. *Austin Chalk in its type area- stratigraphy and structure*. Austin Geological Society Guidebook 7, 88pp.

APPENDIX A

TABLE 1

Table 1 lists every horizon sampled at Culver Cliff and includes palaeomagnetic details of all the specimens studied. Sample code (CC), NRM intensity, maximum demagnetization level (mT or °C), reliability category (see section 5.8), magnetic polarity (N=normal, R=reverse, I=intermediate and ?=unknown), low coercivity component, high coercivity component (B.B.C.=before bedding correction, A.B.C.=after bedding correction), IRM ratio, saturation IRM intensity (S.IRM) and volume magnetic susceptibility are tabulated from left to right. Details of the demagnetisation range (either °C or mT) at which the magnetic polarity is best defined are also included. Where demagnetisation stable end points are identified, the direction of the ChRM before and after bedding correction is listed, together with the MAD or 95% confidence angle, which provides a measure of reliability. Where directional trends were observed, poles to the 'best fit' great circles were recorded, along with the MAD and number of demagnetisation vectors defining it. Great circle poles are indicated by an asterisk and can be found in both the low and high coercivity component columns.

This table should be read in conjunction with Figure 6.7 which displays graphically the magnetic polarity stratigraphy of the Culver Cliff section. The five columns on the right hand side of the table summarises the sample horizon's mean magnetic, the number of samples defining that direction (N), the general reliability category of the mean direction, the associated alpha 95 value or MAD and the mean NRM intensity (mA/m).

CODE	NRM mA/m	MAX TEMP AF LEVEL	RELIABILITY CATEGORY	POLARITY	LOW COERCIVITY COMPONENT OR TREND(*)	RANGE	MAD/ ALP 95	HIGH COERCIVITY COMPONENT B B C	HIGH COERCIVITY COMPONENT A B C	RANGE	MAD/ ALP 95	IRM RATIO	S IRM mA/m	VOLUME M S (S I UNITS) x10^-6	MEAN MAGNETIC DIRECTION	N	GENERAL RELIABILITY CATEGORY	MAD/ ALP 95	MEAN NRM mA/m
CC1-1AV1	0 0674	40	O	?	6 4/73 0 (N=9)	5-O	8 6												
CC1-1AV2	0 0274	40	S2	N				283 7/87 8	11 7/15 0 (N=7)		@4 1								
CC1-1AV3	0 0647	40	O	?	12 7/74 0 (N=6)	20-O	10 8												
CC1-1T1	0 067	40	T2	R	*132 7/53 1 (N=9)		27 3												
CC1-2T1	0 039	40	T2	N	*146 7/52 3 (N=9)		42 1												
CC1-1T2	0 034	35	S1	N				210 6/70 9	7 6/33 2 (N=8)	15-O	4								
CC1-2AV1	0 0244	40	S2	N				234 8/66 4	356 0/32 0 (N=8)		@8 0								
CC1-2AV3	0 053	40	T2	R	*129 2/41 1 (N=5)		25 8												
CC1-2T2	0 18	560	T2	N	*282 7/3 0 (N=6)		33 7												
CC1-3AV1	0 0199	40	E	?								0 97	2 124	-5 0(5 0)	7 6/32 2	1	S1		0 0522
CC1-3AV2	0 0177	40	T2	R	*133 2/53 0 (N=8)		23 9												
CC1-3T2	0 025	35	S2	N	45 0/72 3 (N=3)	0-10	16 7	223 4/76 8	6 8/26 4 (N=8)	10-O	6 2								
CC1-4AV1	0 0349	40	T2	N	*275 5/12 8 (N=7)		23												
CC1-4AV2	0 0356	40	S2	N	327 2/36 8 (N=4)	0-15	10	220 1/76 5	7 4/27 0 (N=7)	15-O	14 6								
CC1-4AV3	0 0535	40	T3	N	*282 5/27 5 (N=9)		38 5												
CC1-5AV1	0 0357	40	S2	N				127 4/81 8	21 9/81 8 (N=9)	5-O	18 1								
CC1-5AV2	0 071	40	T2	N	*302 8/1 0 (N=9)		17 9												
CC1-5AV3	0 106	40	O	?	135 7/63 2 (N=9)	0-40	15 9												
CC1-6AV1	0 00229	40	S2	N				104 4/87 1	17 0/15 0 (N=8)		@3 2								
CC1-6AV2	0 0423	40	S2	N				257 7/75 4	0 0/21 0 (N=6)		@8 1								
CC2-1AV1	0 0764	40	S2	N				233 0/78 6	6 2/23 7 (N=9)	5-O	11 1								
CC2-1AV2	0 0716	40	S2	N				250 8/67 5	353 1/26 2 (N=7)	10-40	16 2								
CC2-1AV3	0 0901	40	O	?	332 8/67 9 (N=9)	5-O	7 1												
CC2-1AV4	0 0191	40	O	?	306 0/57 0 (N=9)		@7 4												
CC2-1T2	0 073	35	O	?				274 9/76 4	0 0/16 7 (N=10)	0-O	3 8								
CC2-1T3	0 09	35	S1	N				234 9/62 4	352 4/34 6 (N=8)	10-O	5 4								
CC2-2T1	0 11	40	T3	N	321 5/68 4 (N=8)	5-40	8 9		*91 9/12 2 (N=6)		15 6	0 94	3 67	-0 85 (3 8)	352 4/34 6	1	S1		0 0574
CC2-2AV2	0 0652	40	S2	N				161 7/86 4	16 0/18 0 (N=7)		@7 8								
CC2-2AV3	0 0495	40	S2	N				219 4/75 5	7 0/28 0 (N=7)		@6 6								
CC2-3AV2	0 0664	40	S2	N				241 3/72 9	0 1/26 1 (N=8)	10-O	8 1								
CC2-3AV3	0 0951	40	S2	N				270 2/81 3	5 2/16 9 (N=10)	0-O	6 5								
CC2-4AV2	0 033	40	S2	N				183 1/71 1	18 2/33 5 (N=8)	10-O	7 3								
CC2-4AV3	0 0299	40	S2	N				194 0/68 0	14 0/37 0 (N=9)		@8 2								
CC2-5AV3	0 0297	40	T2	N	*99 4/38 0 (N=6)		21 5												
CC3-1AV1	0 0748	40	S2	N				239 9/84 3	9 7/18 9 (N=7)	15-O	9 6								
CC3-1AV2	0 0652	40	S2	N				195 1/80 6	13 8/24 4 (N=9)	5-O	8 3								
CC3-1AV3	0 0602	40	O/S2	N?				71 4/85 6	17 8/12 6 (N=6)	5-O	14								
CC3-1T1	0 134	35	O/S1	N?				281 4/82 9	6 7/15 2 (N=8)	10-O	2 8								
CC3-1T2	0 072	35	S1	N				220 4/78 0	8 1/25 7 (N=8)	10-O	2 3								
CC3-2AV1	0 0525	40	S1	N				244 9/71 7	358 3/25 9 (N=10)	0-O	5 1								
CC3-2AV2	0 0879	40	S2	N				191 0/76	15 0/29 0 (N=8)		@6 5								
CC3-2AV3	0 0517	40	S3	N				219 4/71 1	4 6/31 8 (N=7)	15-O	18 3								
CC3-2AV4	0 0506	40	S2	N				266 4/82 3	6 3/17 2 (N=8)	10-O	14 2								
CC3-3AV1	0 037	40	T2	R	*102 1/14 8 (N=5)		22 7												
CC3-3AV2	0 0877	40	S2	N				187 5/82 7	14 9/22 3 (N=9)	5-O	7 8								
CC3-3AV3	0 0703	40	S2	N				157 5/80 9	19 8/22 2 (N=9)	5-O	9 8	0 93	8 553	-5 85 (5 75)	4 0/22 0	3	S1	@11 9	0 0569
CC3-3AV4	0 0506	40	O	?	34 9/72 3 (N=3)	0-10	14 4	106 8/67 3	37 5/14 9 (N=8)	10-O	11 2								
CC3-4AV1	0 0199	40	S2	N				267 0/57 0	340 0/22 0 (N=7)		@11 3								
CC3-4AV2	0 0571	40	S2	N				178 3/56 5	26 6/46 8 (N=6)	15-40	11 3								
CC3-4AV3	0 0498	40	S2	N				189 0/81 1	14 7/23 9 (N=10)	0-O	10								
CC3-5AV2	0 0552	40	S2	N				233 4/67 0	357 0/32 0 (N=9)		@8 6								
CC3-5AV3	0 0519	40	O	?	322 1/65 0 (N=9)	5-O	13 7												
CC3-5AV4	0 1138	40	S2	N				197 1/72 6	12 9/32 4 (N=8)	10-O	12 1								
CC3-6AV2	0 0448	40	S2	N				250 3/82 6	7 5/19 0 (N=9)	5-O	9 9								
CC3-6AV3	0 0433	40	O	N?				300 7/80 8	5 0/12 2 (N=7)	5-O	12 3								
CC3-6AV4	0 0283	40	S2	N				254 9/79 2	4 0/22 0 (N=7)		@8 2								
CC3-4BV3	0 0689	40	S2	N				233 0/69 0	359 0/30 0 (N=8)		@4 7								
CC3-1BV2	0 0654	40	S2	N				214 0/79 0	10 0/26 0 (N=8)		@2								
CC3-3BV4	0 0426	40	S2	N				233 0/80 0	7 0/23 0 (N=5)		@7 7								
CC4-1AV2	0 0353	40	S2/O	N?				286 8/79 2	2 9/14 2 (N=9)	5-O	12 9								

CC4-1T3	0 115	35	O	?	10 4/75 0 (N=10)	2 5-O	6 3											
CC4-2AV3	0 0402	40	S2/O	N?				282 0/75 5	359 0/15 0 (N=8)		@5 4							
CC2AV4	0 038	40	S2	N				232 5/76	4 4/25 7 (N=10)	0-O	14 3							
CC4-3AV1	0 0195	40	S2	N				194 0/67 0	14 0/38 0 (N=7)		@13 0							
CC4-3AV2	0 0263	40	S2	N				176 7/83 7	16 0/21 0 (N=5)		@6 9							
CC4-3AV3	0 0317	40	S2	N				265 8/71 2	355 0/20 0 (N=9)		@5 1							
CC4-1T1	0 091	40	O	?	303 6/68 2 (N=8)	10-O	4 1											
CC4-ST3	0 046	40	O	?	328 9/87 1 (N=7)	15-O	6 3					0 97	2 941	-4 15 (1 45)	9 9/26 4	11	S2	@8 1	0 0385
CC4-2T2	0 045	40	S2	N				185 0/76 0	17 0/29 0 (N=8)		@6 3							
CC4-1T2	0 03	40	O	?	84 0/48 0 (N=8)		@7 6											
CC4-2T1	0 075	40	O	?	289 0/45 0 (N=8)		@7 0											
CC4-2T3	0 063	40	S2	N				178 0/64 0	23 0/39 0 (N=9)		@7 5							
CC4-3T2	0 035	35	S2	N				235 4/74 3	2 5/26 4 (N=8)	10-O	11 6							
CC4-4AV2	0 0353	40	O	?	315 4/70 3 (N=9)	5-O	18 1											
CC4-4AV3	0 0247	40	S2	N				127 0/67 0	36 0/22 0 (N=9)		@5 3							
CC4-5AV2	0 0177	40	T2	R	*109 0/43 8 (N=8)		15 2											
CC4-1AV4	0 0235	40	S2	N				223 4/67 7	1 0/34 0 (N=9)		@12 1							
CC5-1AV2	0 034	40	T3	R														
CC5-1T1	0 212	460	T2	R	*110 0/9 1 (N=5)		9 4											
CC5-1T2	0 068	35	S2	N?				106 6/49 2	56 1/13 0 (N=7)	15-O	7 7							
CC5-2AV1	0 0437	40	O	?	322 8/60 6 (N=7)	15-O	8 6					0 94	1 207	-8 35 (6 3)	198 0/-5 0	1	T2/T3		0 062
CC5-2AV2	0 0448	40	T3	R														
CC5-3AV1	0 0661	40	T3	R	*282 1/52 4 (N=7)		37 9											
CC5-1AV1	0 0555	40	O/T3	R?	*338 1/45 4 (N=7)	15-O	7 5		*301 1/61 8 (N=4)		34							
CC6-1AV1	0 0712	40	O	?	17 1/82 7 (N=9)		7 7											
CC6-1AV2	0 0475	40	S2	N				209 6/51 6	358 5'51 3 (N=6)	20-O	10							
CC6-1AV3	0 0242	40	S2	N				228 1/75 9	5 2/26 5 (N=9)	5-O	16 9							
CC6-1AV4	0 0205	40	S3	N				251 4/67 5	353 0/26 0 (N=6)		@12 7							
CC6-1T1	0 031	35	S2	N				190 5/45 4	18 9/59 5 (N=5)	15-O	7 9							
CC6-1T1A	0 011	7	T3	R	*94 0/54 9 (N=3)		0 1											
CC6-2AV1	0 0273	40	T2	R	*111 2/46 4 (N=7)		32											
CC6-2AV2	0 0294	40	S2/T3	N/R?				275 8/75 1	358 6/16 6 (N=9)	5-O	10 3	0 95	2 626	-14 15 (1 45)	9 0/34 0	9	S2	@12 6	0 0307
CC6-2AV3	0 0205	40	E	?														
CC6-2AV4	0 0231	40	S3	N				123 6/73 0	31 0/20 0 (N=9)		12 7							
CC6-2T2	0 035	35	S2	N				191 1/65 3	15 6/39 7 (N=8)	10-O	6 7							
CC6-3AV1	0 0523	40	O	?	6 0/76 0 (N=9)		@11 1											
CC6-3AV2	0 0278	40	T3	R	*145 2/46 4 (N=4)		15 4											
CC6-3AV3	0 0527	40	S2	N				211 1/57 3	0 8/45 8 (N=6)	20-O	13 6							
CC6-2BV3	0 0345	40	S2	N				88 0/87 0	17 0/14 0 (N=9)		@5 1							
CC7-1AV1	0 0131	40	E	?														
CC7-1T3	0 018	35	O	?	6 3/82 5 (N=4)	25-O	10 5											
CC7-2AV3	0 0342	40	S2	N				192 6/74 5	14 4/74 5 (N=9)	5-O	9 8							
CC7-2T2	0 016	35	O	?	57 2/76 4 (N=8)	7 5-O	10 3											
CC7-3AV1	0 0213	40	S2	N				113 6/74 5	30 0/17 0 (N=8)		@5 9							
CC7-3AV2	0 0362	40	O/S2	N?				8 4/87 0	13 7/12 9 (N=9)	5-O	13 3							
CC7-3AV3	0 2175	40	S1	N				243 8/85 1	10 1/18 1 (N=9)	5-O	2 6							
CC7-4AV1	0 0175	40	S2	N				244 4/68 1	355 0/28 0 (N=8)		11 9	0 94	0 939	-5 0 (4 35)	10 1/18 1	1	S1		0 0283
CC7-4AV3	0 1036	40	O/S2	N?				44 1/85 5	16 3/11 1 (N=7)	15-O	4 4							
CC7-5AV3	0 0185	40	T3	R?	*99 7/59 4 (N=7)		23 9											
CC7-2T1	0 06	40	O	?	357 1/45 1 (N=6)	20-O	9 7											
CC7-2T3	0 007	15	E	?														
CC7-3T2	0 029	40	S2	N				170 0/44 0	44 0/54 0 (N=6)		@6 6							
CC7-1T1	0 126	40	O	?	17 0/52 0 (N=9)		@2 4											
CC7-6AV1	0 0095	40	T2	R	*134 0/49 8 (N=7)		26 3											
CC7-6AV2	0 016	40	T3	R														
CC8-1V3T	0 0331	490	O	?	319 0/72 0 (N=5)	15-O	@10 1											
CC8-2V1	0 199	40	T2	N/R?	320 8/76 4 (N=5)		4 8		*105 8/65 3 (N=6)		2 8							
CC8-1V2	0 128	40	T2	R	*263 3/58 7 (N=8)		15 4											
CC8-1V3	0 111	40	T2	R	*101 5/23 1 (N=7)		32 4							-9 15 (3 8)	188 0/-6 0	6	T2/T3	@3 6	0 1207
CC8-1V1	0 116	40	O	?	25 6/80 8 (N=4)	20-O	2 5											
CC8-3V2	0 167	40	O	?	347 4/80 2 (N=4)	20-O	2 2											
CC8-2V3	0 206	40	T3	R	356 3/76 9 (N=4)	20-O	3		*278 3/9 1 (N=7)		28 1							
CC9-1T1	3 409	35	O	?	345 2/68 8 (N=11)	0-O	4 8											
CC9-2V1	0 654	40	S1	N				169 6/64 5	27 0/37 7 (N=10)	0-O	2 2							
CC9-1T1T	2 219	525	T3	N	*85 3/51 8 (N=4)		2 4											

CC9-1T2	1 08	530	T3	N	*98 5/32 5 (N=5)		0 8					0 99	21 82	-10 0 (9 0)	24 0/38 0	3	S1	@12 9	1 3008
CC9-1V1	0 739	500	S1	N				161 0/62 8	32 1/36 9 (N=9)	200-O	5								
CC9-3V1	1 227	500	S1	N				198 6/66 8	11 7/38 1 (N=8)	400-O	2								
CC9B-3V1	0 1958	40	O	?	333 7/69 8 (N=10)	0-O	6 1												
CC9B-3V4	0 1473	40	O	?	0 0/70 0 (N=6)	20-O	3								180 0/-90 0	T	T3		0 1326
CC9B-4V4	0 1486	40	O	?	328 8/68 8 (N=10)	0-O	7 7												
CC9B-4AV4T	0 0722	470	T3	R	*11 8/72 1 (N=7)	0-O	2 2		*294 0/74 7 (N=6)		33 1								
CC10-2T2	0 203	560	T3	N	*95 9/15 8 (N=10)		23												
CC10-2V1	0 108	40	O	?	346 3/64 7 (N=9)	5-O	7 5												
CC10-1T1	0 024	40	T2	R	*134 9/30 7 (N=7)		32 8												
CC10-3V2	0 231	40	S2	N				189 0/78 0	15 0/27 0 (N=5)		@7 2								
CC10-5V3	0 118	40	O	?	348 0/67 0 (N=7)		@1 8					0 93	0 7	-1 65 (3 8)	15 0/27 0	1	S2		0 0617
CC10-4V2	0 022	40	S2	N				193 0/70 0	193 0/35 0 (N=7)		@10 0								
CC10-1T2	0 059	40	O	?	10 0/79 0 (N=6)		@4 6												
CC10-1V1	0 063	40	O	?	344 0/77 0 (N=8)		@3 7												
CC10-2T3	0 011	25	T2	N?	*280 5/19 2 (N=8)		15 3												
CC11-2AV3	0 0103	35	S2	N				188 0/66 8	17 0/38 0 (N=9)		@4 4								
CC11-4AV1	0 021	35	T1	R	*275 6/28 8 (N=8)		41 5												
CC11-4AV3	0 027	35	T1	R	*271 9/26 4 (N=7)		37 1					0 88	0 676	-4 15 (7 65)	193 0/-34 0	1	T1/T2		0 0169
CC11-2T1	0 02	40	O	?	359 0/80 0 (N=9)		@7 4												
CC11-1T1	0 022	35	T2	R	*113 7/14 3		16 9												
CC11-1T2	0 009	25	S2/O	N?				281 8/73 6	357 0/15 0 (N=7)		@6 9								
CC12-A	0 0344	40	T3	R	*311 5/8 7 (N=9)		18 3												
CC12-B	0 00897	40	S2	N				224 5/40 6	333 9/53 2 (N=7)	15-O	10 4								
CC12-C	0 00431	40	T2	R	*263 0/25 3 (N=9)		38 3												
CC12-D	0 00635	40	S3	N				195 8/30 4	8 2/74 5 (N=10)	0-O	17 3								
CC12-1T1	0 028	35	T3	R	*92 3/26 9 (N=9)		15 3												
CC12-1T2	0 016	15	T2	R	*106 5/57 0 (N=5)		22 9					0 92	1 449	-5 85 (10 1)	165 0/-70 0	1	S2		0 0142
CC12-2T3	0 02	40	S2	N				162 0/79 0	20 0/24 0 (N=9)		@11 8								
CC12-2T1	0 025	40	O	?	280 0/80 0 (N=8)		@6 9												
CC12-2T2	0 014	24	S2	R	*102 2/15 4 (N=11)		23	30 0/-37 0	165 0/-70 0 (N=6)		@10 3								
CC12-3T1	0 018	35	T3	R	*270 6/11 7 (N=7)		30 7												
CC12-3T2	0 021	30	T2	R	*102 2/52 1 (N=13)		22												
CC12-1T3	0 007	10	T3	R															
CC13-1T1	0 031	26	T3	R	*79 3/18 5 (N=3)		0												
CC13-1T1X	0 118	540	T2	R	*283 0/26 2 (N=5)		3 8												
CC13-2T1	0 057	40	O	?	349 7/64 7 (N=5)	5-O	8												
CC13-1T2	0 122	35	O	?	31 8/35 8 (N=5)	5-25	11												
CC13-4T2	0 024	40	S2	?	111 0/42 0 (N=9)	5-O						0 97	4 264	-9 15 (13 75)	243 3/-62 1	1	S2		0 0528
CC13-1T1	0 167	40	O	?	327 6/68 6 (N=4)	30-O	2 7												
CC13-2T2	0 052	35	T2	R	*272 0/24 7 (N=8)		18 5												
CC13-3T2	0 026	22 5	S2	R				351 8/-37 3	243 3/-62 1 (N=6)	12 5-O	10 1								
CC13-4T1	0 023	35	T2	R	*98 2/28 0 (N=7)		28												
CC14-1T1	0 35	500	O	?	357 5/70 8 (N=8)	100-O	7 8												
CC14-1T2	0 111	35	O	?	316 9/52 3 (N=7)	10-O	8												
CC14-1T3	0 079	35	T3	R															
CC14-1V3	0 108	40	O	?	26 7/67 8 (N=8)	10-O	5 1												
CC14-1V1	1 45	510	T1	R	*251 1/21 3 (N=7)		26 9												
CC14-2V1	0 927	510	T1	R	*116 6/13 0 (N=8)		29 1												
CC14-1V2	0 086	40	O	?	323 4/84 8 (N=9)		@7 5												
CC14-1V2T	0 053	520	T3	R								0 97	11 7	-12 5 (23 85)	190 0/-52 0	1	T1		0 194
CC14-2V2	0 303	40	O	?	359 6/70 8 (N=10)	0-O	3 4												
CC14-2V2T	0 193	540	T2	R	*281 3/11 7 (N=13)		29 1												
CC14-3V3	0 092	40	O	?	33 0/74 8 (N=9)	5-O	9 6												
CC14-3V3T	0 064	510	T2	R	*290 0/70 0 (N=9)		22 9												
CC14-3V2	0 1	40	O	?	336 2/62 9 (N=8)		@11 4												
CC14-3V2	0 071	510	T2	R	*90 7/26 4 (N=9)		11 6												
CC14-2V2X	0 617	510	T2	R	*78 8/26 2 (N=4)		34 2												
CC14-3V1	0 466	500	T2	R	*278 3/19 8 (N=4)		32 8												
CC14-1T1A	0 248	35	O	?	335 9/68 2 (N=4)	200-O	6 1												
CC15-1T1T	0 218	525	O	?	358 7/65 3 (N=11)	0-O	5 6												
CC15-1T2	0 156	35	O	?	350 2/64 5 (N=9)	0-O	2 7												
CC15-1V2	0 201	500	T2	R	*94 3/48 3 (N=4)		24 3												
CC15-1V3	0 222	500	T3	R	*93 2/39 8 (N=7)		11 4												
CC15-2V2	0 111	500	T2	R	*96 5/28 3 (N=7)		40 3												

CC15-2V1	0 04	40	O	?	326 7/70 1 (N=6)	20-O	6 4					0 98	8 056	+0 85 (1 45)	180 0/-90 0	T	T1/T2/T3		0 1067
CC15-3V2	0 035	40	O	?	22 0/84 0 (N=9)		2 5												
CC15-1V1	0 061	40	O	?	333 5/72 5 (N=10)	0-O	5 3												
CC15-2V3	0 096	500	T1	R	*96 6/30 8 (N=5)		25 5												
CC15-3V1	0 043	35	T3	R	*283 1/53 6 (N=7)		39 7												
CC15-1T1	0 344	35	O	?	0 0/65 2 (N=9)	0-O	2 6												
CC16-11V1	0 0185	35	S2	N				226 5/38 8	348 6/67 2 (N=4)	25-O	12 1								
CC16-1T1	0 074	35	T3	R?	48 3/70 8 (N=9)	0-O	8		*278 0/33 7 (N=8)		34 6								
CC16-1T2	0 03	35	T3	N	*247 8/57 5 (N=8)														
CC16-7V3	0 063	65	T3	R	*239 7/16 9 (N=4)		32 1												
CC16-9V2	0 024	65	E	?															
CC16-12V	0 042	65	T2	R	*88 4/1 2 (N=10)		35 1												
CC16-1AV	0 0146	35	T2	R	*75 2/51 4 (N=5)		6 4												
CC16-2AV	0 017	35	O	?								0 93	1 832	-15 85 (2 9)	178 0/-58 0	1	T2		0 0368
CC16-5V2	0 035	65	T2	R	*310 8/62 1 (N=5)		23 2												
CC16-10V3	0 036	40	T2	N	*82 3/8 1 (N=9)		30 3												
CC16-6V3	0 052	65	T2	R	*166 6/31 1 (N=10)		33 8												
CC16-8V2	0 1	65	T2	R	*324 4/30 1 (N=12)		14 9												
CC16-1AV2	0 0146	40	T2	R	*125 4/50 6 (N=8)		36 7												
CC16-1AV1	0 0256	40	T2	R	*259 4/73 8 (N=7)		16 5												
CC16-1AV4	0 0152	40	E	?															
CC16-2AV3	0 0478	40	O	?	317 9/81 4 (N=8)	5-O	13												
CC16A-2V2	0 0098	25	T2	R	*255 6/40 8 (N=4)		16 1												
CC16A-4AV2	0 0062	25	T2	R	*264 4/50 3 (N=6)		29 7							-8 35 (1 45)	257 0/-46 0	5	T2	14 4	0 0069
CC16A-2V	0 0054	20	T3	R	*283 5/41 3 (N=6)		24 5												
CC16A-1V	0 0074	15	T3	R	*71 1/15 05 (N=5)		14 8												
CC16A-4V3	0 0063	20	T3	R	*292 3/39 9 (N=6)		21 6												
CC16B-1V1	0 0077	20	S2	I?				34 1/50 5	9 5/-21 5 (N=9)	2 5-O	9								
CC16B-2V	0 0068	20	T3	R	*268 6/60 8 (N=5)		5 2							-11 65 (3 8)	7 2/-23 6	1	S2	8	0 0081
CC16B-3V	0 0063	15	T3	N	*301 5/31 6 (N=6)		21 7												
CC16B-4V	0 0068	15	S2	I?				31 0/48 3	7 2/-23 6 (N=5)	5-O	8								
CC16B-1V1	0 016	20	T3	N	*98 6/11 9 (N=7)		25 8												
CC17-1AV	0 0323	40	T3	N	*184 9/72 1 (N=5)		32 2												
CC17-1T1	0 015	49 5	O	?	353 4/68 4 (N=9)	0-O	10 8												
CC17-1T2	0 027	65	T3	R															
CC17-1T2X	0 016	30	T2	R	*94 2/24 4 (N=3)		0												
CC17-1T2A	0 016	30	S2	R	336 6/15 9 (N=4)	0-15	7	251 1/40 2	324 4/52 4 (N=4)	15-30	10 8	0 95	0 939	-5 0 (7 5)	180 0/-90 0	T	T2/T3		0 0205
CC17-2T1	0 022	35	T3	R	*83 3/41 9 (N=8)		28 2												
CC17-3T1	0 013	65	T3	R															
CC17-1T1	0 033	35	T2	R	*275 7/40 3 (N=11)		37 5												
CC18-15V3	0 071	510	T2	R	*98 0/13 9 (N=10)		21 6												
CC18-11V	0 03	65	T3	R															
CC18-12V	0 083	65	T3	R	*114 2/61 1 (N=5)		16 9												
CC18-1T1	0 059	30	O	?	337 5/27 9 (N=5)	0-O	8 4												
CC18-1T2	0 072	35	T3	R	*93 3/27 9 (N=5)		26 5												
CC18-14V3	0 144	40	O	?	14 5/66 9 (N=10)		@7 8					0 95	2 056	-5 0 913 25)	181 0/-15 0	5	T3	10 1	0 0664
CC18-10V1	0 077	40	O	?															
CC18-1T2	0 031	40	T2	R	*126 0/8 1 (N=8)		19 8												
CC18-13V2	0 073	40	O	?	358 0/65 9 (N=7)	10-O	11 4												
CC18-2AV1	0 0616	40	S2	S2				266 7/36 0	318 3/27 7 (N=6)	20-O	8 9								
CC18-2AV3	0 0687	40	O	?	36 3/55 0 (N=10)	0-O	9 4												
CC18-2AV2	0 0926	40	T3	R	*102 0/30 3 (N=7)		34 7												
CC19-A	0 00535	40	T3	R	*216 0/15 6 (N=7)		18 6												
CC19-1T1	0 086	49 5	S2	N				322 8/73 7	359 2/16 8 (N=7)	15-O	14 4								
CC19-1T2	0 008	10	T3	N	*106 8/39 2 (N=3)		0												
CC19-1V2	0 0096	10	E	?															
CC19-1V3	0 0074	12 5	T3	N/R								0 9	0 971	-14 15 (1 45)	359 2/16 8	1	S2		0 0061
CC19-2V1	0 0092	35	T3	N	*146 3/57 5 (N=5)		8 5												
CC19-2V2	0 004	10	S3	N	*119 1/56 3 (N=8)		16 3												
CC19-1V1	0 002	0	E	?				105 5/61 5	44 0/26 0 (N=3)		@22 9								
CC19-1V2	0 002	0	E	?															
CC19-3V1	0 002	0	E	?															
CC20-1T1	0 01	22 5	S2	N				74 7/81 8	20 0/24 0 (N=7)	15-O	14 4								
CC20-1T2	0 006	5	E	?															
CC20-1V1	0 081	40	T2	R	*96 3/25 4 (N=7)		17 2												

CC20-1V2	0 009	40	T2	R	*59 0/65 2 (N=7)		22 4					0 91	1 072	-3 35 (8 05)	180 0/-90 0	T	T2		0 0119
CC20-1V3	0 007	25	T2	R	*276 7/19 5 (N=5)		12 7												
CC20-3V1	0 007	35	T2	R	*95 9/15 9 (N=5)		13 7												
CC20-2V1	0 022	40	S2	N				262 0/82 0	4 0/30 0 (N=8)		@9 1								
CC20-3V3	0 015	40	T3	R															
CC20-4V3	0 007	35	T2	R	*90 1/17 0 (N=10)		33 6												
CC21-A	0 0168	40	S2	N				161 9/72 8	23 6/43 4 (N=10)	0-O	9 3	0 95	3 94	-30 0 (6 6)	9 9/42 1	1	S1		0 0238
CC21-B	0 0278	40	S1	N				198 3/75 8	9 9/42 1 (N=10)	0-O	2 5								
CC21-1T1	0 048	35	O	?	24 6/56 7 (N=5)	20-O	3 8												
CC21-2T2	0 029	35	O	?	21 2/51 0 (N=8)		10 9												
CC21-2T3	0 018	40	S2	N				123 0/56 0	52 0/34 0 (N=8)		@8 8								
CC21-2T2X	0 034	40	S2	N				89 3/68 6	34 5/21 5 (N=9)		@10 3								
CC21-1T3	0 061	40	O	?	64 5/41 7 (N=10)		@10 2												
CC21-8	0 032	40	S2	N				249 0/74 0	355 0/36 0 (N=9)		@7 9								
CC21-2	0 04	40	S2	N				137 9/71 3	31 1/37 6 (N=9)	5-O	9 6								
CC21-1	0 037	40	S2	N				220 4/82 1	7 4/34 9 (N=10)	0-O	15 3								
CC21-10	0 024	40	S2	N				147 0/82 0	19 0/34 0 (N=10)		@3 3								
CC21-4	0 028	40	S2	N				234 0/70 0	354 0/42 0 (N=9)		@5 1								
CC21-6	0 028	40	S2	N				130 0/57 0	50 0/38 0 (N=8)		@3								
CC21-7	0 024	40	S2	N				335 0/84 0	8 0/23 0 (N=8)		@8 5								
CC21-5	0 028	40	S2	N				228 0/81 0	5 0/35 0 (N=8)		@4 2								
CC21-3	0 042	40	S2	N				145 0/81 0	20 0/34 0 (N=8)		@4 2								
CC21-9	0 03	40	S2	N				203 0/73 0	7 0/45 0 (N=8)		@9								
CC21-1T2	0 004	0	E	?															
CC21-2T3	0 002	0	E	?															
CC22-1T1	0 048	35	E	R?															
CC22-3T2	0 017	40	S2	N				259 0/71 0	351 0/34 0 (N=8)		@12 2								
CC22-1T2	0 013	35	O	?	328 1/64 6 (N=8)	5-O	13 3					0 96	2 139	-5 0 (6 6)	354 0/34 0	1	S2		0 0289
CC22-2T1	0 072	35	O	?	344 9/70 4 (N=4)	25-O	3 1												
CC22-2T2	0 01	35	O	?	342 9/69 1 (N=7)	5-35	8 7												
CC22-1T12	0 077	49 5	E	R															
CC23-4AV3	0 0145	40	E	?															
CC23-2T1	0 004	10	T3	R	*79 2/28 0 (N=3)		0					0 87	0 568	-6 65 (2 90	180 0/-90 0	T	T3		0 007
CC23-3T2	0 006	7 5	T3	?	*169 5/22 5 (N=4)		19 8												
CC24-A	0 0143	40	O	?	332 7/66 7 (N=8)	0-O	7												
CC24-B	0 00483	40	T3	R	*296 3/42 4 (N=5)		12 4												
CC24-1T3	0 038	35	T3	N?	*115 8/48 4 (N=7)		11 5												
CC24-2T1	0 024	35	T3	R	*279 2/34 9 (N=7)		13 3					0 95	1 527	-25 85 (3 8)	193 0/-6 0	1	T3		0 0141
CC24-1AV2	0 0168	470	E	?															
CC24-2T2	0 008	7 5	T3	R	*107 1/31 3 (N=11)		0 1												
CC24-3T3	0 013	35	S2/O	N				346 0/76 0	5 0/15 0 (N=11)		@5 3								
CC25-1AV1	0 0471	40	S2	N				304 8/68 4	351 1/18 1 (N=10)	0-O	10 2								
CC25-1AV2	0 0789	40	O	?	45 3/71 4 (N=9)	5-O	9 5												
CC25-2AV1	0 0859	40	S2	N				181 6/44 4	36 2/71 6 (N=10)	0-O	6 1								
CC25-2AV2	0 0723	40	S2	N				19 0/78 9	13 4/17 0 (N=10)	0-O	6								
CC25-2AV1B	0 0931	40	O	?	36 2/71 6 (N=10)	0-O	6 1												
CC25-2AV3	0 0526	40	O	?	4 8/72 4 (N=10)	0-O	13 1												
CC25-3AV2	0 089	40	S1	N				196 2/79 2	11 0/38 8 (N=6)	20-O	2 9								
CC25-3AV3	0 084	40	S2	N				242 4/68 5	350 4/40 3 (N=10)	0-O	6 7								
CC25-3AV4	0 0633	40	S2	N				44 9/78 4	18 6/18 1 (N=10)	0-O	6 8								
CC25-4AV1	0 0491	40	S2	N				264 8/75 6	355 9/31 3 (N=5)	25-O	9 7								
CC25-4AV2	0 1769	40	O	?	38 5/71 5 (N=10)	0-O	3 4					0 98	6 02	-10 0 (6 0)	11 0/38 8	1	S1		0 0826
CC25-4AV3	0 0734	40	S2	N				340 0/84 6	8 9/23 4 (N=10)	0-O	8 2								
CC25-4AV3T	0 0507	470	S2	N				318 3/78 9	2 5/21 1 (N=4)	400-O	7 5								
CC25-4AV4	0 0979	40	S2	N				203 4/67 2	5 1/50 2 (N=7)	15-O	6 1								
CC25-5AV1	0 0292	40	E	?															
CC25-5AV4	0 0804	40	O	?	14 3/52 4 (N=6)	20-O	6 5												
CC25-6AV2	0 0596	40	O	?	69 9/66 8 (N=9)	5-O	7 7												
CC25-1T1	0 078	35	O	?	38 2/61 0 (N=9)	0-O	9 9												
CC25-1T2	0 161	480	S1	N	349 2/73 2 (N=8)	100-490	11 4	256 5/85 4	7 2/29 9 (N=5)	460-O	2 7								
CC25-2T2	0 212	500	O	?	352 5/66 9 (N=11)	0-O	2 8												
CC25-T2A	0 29	35	O	?	352 5/66 8 (N=10)	0-O	2 7												
CC26-B	0 193	40	O	?	339 7/64 7 (N=10)	0-O	3												
CC26-1T1A	0 049	35	O	?	351 3/62 5 (N=10)	2 5-O	4 8												
CC26-3T2	0 019	40	O	?	71 0/54 0 (N=9)		@8 3												

CC26-1T2	0 022	40	S2	N				328 0/80 0	5 0/21 0 (N=9)		@5 6							
CC26-1T1	0 315	525	T3	N/R	*103 8/45 1 (N=9)		29 4							-4 15 (5 3)	5 0/21 0	1	S2		0 0807
CC26-2T2	0 352	520	O	?														
CC26-3T1	0 215	500	T2	N	274 0/17 9 (N=10)		17 9											
CC26-4T1	0 171	470	O	?	9 0/70 3 (N=6)	200-O	0 7											
CC26-4T2	0 009	30	E	?														
CC27-1T1	0 459	520	O	?	347 0/66 3 (N=12)	100-O	8 9											
CC27-1V1	0 165	480	T3	N	*107 6/14 9 (N=4)		31 4											
CC27-9	0 077	40	S2	N				304 0/71 2	355 2/19 2 (N=10)	0-O	6 9							
CC27-2	0 062	40	S2	N				315 0/77 7	2 8/20 2 (N=10)	0-O	6 6							
CC27-8	0 151	40	O	?	322 5/68 8 (N=10)	0-O	3											
CC27-1V2	0 331	490	T2	N	*107 6/20 5 (N=6)		5 8							-13 0 (0 0)	2 8/20 2	1	S2		0 2158
CC27-2T1	0 575	35	O	?	8 7/67 8 (N=9)	0-O	2 3											
CC27-2T1T	0 286	520	T3	N	*101 6/23 6 (N=5)		7 7											
CC27-2V1	0 179	480	O	?	49 5/67 5 (N=8)	200-O	13 3											
CC27-2V2	0 412	500	T2	N/R	*99 3/3 2 (N=5)		29 3											
CC28-1T1	0 096	35	O	?	337 3/66 0 (N=9)	0-O	2 3											
CC28-1T2	0 04	40	S2	N				163 6/75 5	23 4/39 2 (N=6)	20-O	8 8							
CC28-5	0 02	40	O	?	19 0/62 0 (N=9)		@6 2											
CC28-10	0 038	40	S2	N				290 4/71 9	353 3/23 6 (N=9)	5-O	13							
CC28-3	0 084	40	T3	R	30 8/73 7 (N=6)	0-25	11 1											
CC28-4	0 028	40	T3	R	167 7/62 2 (N=6)	10-35	14		*113 1/16 3 (N=4)		24 7							
CC28-11	0 028	40	T3	R	*113 5/43 8 (N=4)		24 6											
CC28-6	0 083	40	T3	R	298 4/69 5 (N=6)	0-25	12		*94 4/43 0 (N=4)		9 8							
CC28-9	0 046	40	S2	N				231 0/76 0	4 0/38 0 (N=8)		@9 5	0 98	6 02	-3 35 (3 8)	8 0/37 0	4	S2	@16 6	0 0596
CC28-2	0 027	40	T3	N/R	*117 5/19 9 (N=9)		38 6											
CC28-7	0 126	40	O	?	310 0/68 0 (N=10)	0-O	7 7											
CC28-8	0 056	40	S2	N				188 0/70 8	16 8/46 1 (N=10)	0-O	12 8							
CC28-7T	0 071	500	T2	R	*82 7/14 3 (N=8)		9											
CC28-1T3	0 206	35	O	?	329 8/61 1 (N=9)	0-O	4 3											
CC28-1T3T	0 124	500	T3	N/R	*102 0/10 2 (N=6)		16											
CC28-2T1	0 131	460	T3	N	*289 0/6 0 (N=5)		8 2											
CC28-2T2	0 045	35	O	?	343 1/63 9 (N=6)	15-O	2 3											
CC29-1T1	0 416	510	T3	R	*102 8/17 7 (N=4)		6 5											
CC29-1T2	0 415	520	T3	N	*98 8/19 8 (N=4)		10 6											
CC29-1T3	0 3	35	S1	R				94 2/-72 3	174 1/-28 6 (N=9)	5-O	3 2							
CC29-2T1	0 589	500	T3	N?								0 93	14 061	-3 35/ (14 2)	174 1/-28 6	1	S1		0 2192
CC29-2T2	0 142	530	T3	T3	*282 3/33 2 (N=5)		20 2											
CC29-2T3	0 106	35	T2	R	*289 9/66 0 (N=10)		43 4											
CC29-2T3T	0 053	500	T2	N/R	251 6/47 4 (N=8)		16 1											
CC30-1A2	0 566	35	O	?	350 9/66 2 (N=9)	0-O	5 7											
CC30-1T2	0 356	525	T3	N?	*99 9/24 0 (N=7)		15 8											
CC30-1V2	0 263	480	T2	N	*90 2/31 1 (N=6)		7 8											
CC30-1V4	0 347	40	O	?	348 1/66 6 (N=10)	0-O	2 5											
CC30-2V4	0 111	40	S1	N				23 4/89 6	14 1/26 6 (N=10)	0-O	4 6							
CC30-1V3	0 203	40	O	?	13 3/70 5 (N=10)	0-O	3 6											
CC30-1V1	0 129	40	O	?	330 4/76 5 (N=10)	0-O	4 2											
CC30-2V1X	0 057	510	T2	R	*269 1/21 0 (N=4)		19 9											
CC30-1V1Z	0 071	490	T3	R	*245 3/53 0 (N=6)		10 1											
CC30-1V1A	0 129	40	O	?	330 1/76 5 (N=10)	0-O	4 2					0 93	8 059	-9 15 (8 8)	176 0/-28 0	3	T2/T3	@31 6	0 1663
CC30-1V3	0 123	500	T3	N	*279 9/1 7 (N=5)		25 8											
CC30-1V3A	0 203	40	O	?	13 3/70 5 (N=10)	0-O	3 6											
CC30-1V4	0 175	500	T3	R	*130 4/79 0 (N=4)		10 6											
CC30-1V4A	0 347	40	O	?	348 1/66 6 (N=10)	0-O	2 5											
CC30-2V4	0 057	510	T3	R	*143 0/40 1 (N=3)		0											
CC30-2T2	0 302	480	T3	R														
CC30-2V1	0 123	480	T2	N	*100 6/24 0 (N=6)		26											
CC30-2V2	0 228	500	T3	R?	*94 9/39 9 (N=7)		37 4											
CC30-2V3	0 115	480	T2	N	*104 6/31 3 (N=5)		9 4											
CC31-1T1	0 111	35	S1	N				281 6/44 7	324 8/20 2 (N=6)	15-O	5 6							
CC31-2V1	0 036	40	T3	R?	'*121 0/26 5 (N=6)		15 5											
CC31-1V3	0 061	40	T3	R?	23 0/75 0 (N=5)		@3 2		*107 5/31 6 (N=4)		36 4							
CC31-1V2	0 039	40	S3	N				15 0/57 0	14 0/24 0 (N=4)		@11 8							
CC31-1T2	0 041	35	T2	N?								0 97	4 5	+3 3 (1 45)	187 0/-33 0	3	T1/T2/T3	@16 1	0 0936
CC31-1V1	0 172	500	T2	R	*206 7/42 5													

CC31-2T1	0 143	520	O	?	29 0/67 5 (N=8)	400-500	3											
CC31-2V2	0 282	500	T1	R	*275 5/4 1 (N=9)													
CC31-2V3	0 203	480	T1	R	*284 9/45 5 (N=5)													
CC32-1T1	0 181	490	O	?	355 0/66 0 (N=5)	200-460	1 6											
CC32-2T1	0 205	520	O	?	339 9/66 9 (N=10)	200-O	8 4											
CC32-2T2	0 063	35	O	?	322 9/67 0 (N=8)	5-O	2 4											
CC32-2V2	0 277	470	O	?	357 5/69 6 (N=5)	20-O	6 2											
CC32-2V3	0 079	480	S2/O	N?				22 6/76 9	16 0/14 0 (N=5)		@12 6							
CC32-3A2	0 097	35	O	?	324 2/67 9 (N=9)	2 5-35												
CC32-3T2	0 051	500	T3	N	*104 6/49 2 (N=6)		1 2											
CC32-1V2A	0 063	40	O/S2	N?				304 8/80 3	4 1/23 2 (N=7)	15-O	13 1							
CC32-1V2	0 041	510	T2	R	*273 9/28 3 (N=8)		30 4											
CC32-3V3A	0 325	40	O	?	17 2/63 1 (N=10)	0-O	3 2					0 99	50 1	+8 5 (3 8)	180 0/-90 0	T	T2/T3	0 1212
CC32-1V1	0 151	40	O	?	23 5/75 1 (N=10)	0-O	6 5											
CC32-1V3	0 141	40	O	?	0 2/72 8 (N=10)	0-O	6 4											
CC32-2V1	0 097	40	O/S2	N?				316 6/80 7	5 6/21 7 (N=9)	5-O	4 9							
CC32-3V3	0 169	510	T2	R	*273 1/59 0 (N=5)		17 7											
CC32-1T3BA	0 158	40	O	?	339 9/65 3 (N=10)	0-O	4 5											
CC32-1T3BAT	0 079	490	T3	R	*110 1/48 5 (N=5)		12 5											
CC32-1T3A	0 1	40	O	?	345 4/74 3 (N=9)	5-O	7 2											
CC32-1T3	0 061	500	T2	R	*272 6/10 7 (N=5)		14 4											
CC32-3V1	0 306	490	T3	N	*265 5/44 7 (N=4)		10 6		*269 0/20 2 (N=10)		19 6							
CC32-3V2	0 27	490	O	?														
CC33-1A2	0 207	35	O	?	346 9/63 7 (N=7)	10-O	3 4											
CC33-1T1	0 108	35	T2	R	346 2/62 4 (N=7)	10-O	2 8											
CC33-1T2	0 122	420	T3	R														
CC33-1V1	0 015	35	T2	R	*63 3/31 5 (N=4)		13 2											
CC33-2V1	0 071	480	T3	R								0 99	3 381	-5 0 (2 5)	218 0/-60 0	1	T2	0 0523
CC33-3V1	0 084	490	T3	R	*282 5/34 3 (N=6)		6 6											
CC33-2V2	0 035	40	S2	N				200 0/61 0	6 0/53 0 (N=9)		@3 3							
CC33-1V3	0 016	40	S2	N				238 0/64 0	348 0/41 0 (N=9)		@7 1							
CC33-1T1A	0 053	40	O	?	331 0/69 0 (N=9)		@1 7											
CC33-3V2	0 021	35	T2	R	*288 1/11 6 (N=4)		4 1											
CC34-1T1	0 032	35	S2	R				15 1/-53 6	188 2/-61 3 (N=6)	15-O	9							
CC34-1T2	0 042	35	S2	R				17 4/-42 3	178 9/-72 1 (N=6)	15-O	8 9							
CC34-2V1	0 032	35	T2	R	*113 2/37 7 (N=4)		22 9											
CC34-1V1	0 023	40	T2	R	*168 8/61 3 (N=5)		29 6											
CC34-3AV2	0 027	40	T1	R	*108 1/27 0 (N=5)		21 6											
CC34-3AV2T	0 006	450	E	?								0 91	0 6291	-5 0 (2 5)	182 0/-25 0	3	T1/T2	@10 1	0 0218
CC34-2AV2	0 029	40	T3	R	*128 4/57 6 (N=6)		32 9											
CC34-2AV2T	0 0098	460	E	?														
CC34-1AV2	0 031	40	T3	R	*111 5/44 4 (N=3)		0											
CC34-2V3	0 017	15	T3	R	*268 6/9 7 (N=4)		4 5											
CC35-1A2	0 62	35	O	?	352 4/72 4 (N=9)	0-O	2 9											
CC35-1T2	0 42	520	T3	N	356 3/66 1 (N=8)	100-460	4 9		*100 7/21 4 (N=6)		5 1							
CC35-1V2	0 266	480	T2	N	*107 7/47 2 (N=4)		2 2											
CC35-1V3	0 141	500	T3	R	5 0/65 4 (N=6)	200-480	3 1											
CC35-2V3	0 357	490	O	?	6 5/66 0 (N=8)	200-490	2 2											
CC35-3V1	0 139	40	O	?	16 1/68 1 (N=10)		@6 0					0 96	12 76	-4 15 (5 2)	11 7/22 3	1	S2	0 2426
CC35-1T1	0 389	40	O	?	5 0/63 9 (N=10)	0-O	6 7											
CC35-2V2	0 235	40	S2	N				5 5/87 3	11 7/22 3 (N=10)	0-O	4 2							
CC35-1V1	0 256	40	O	?	11 3/68 1 (N=10)		@2 1											
CC35-2V1	0 09	40	S2	N				352 7/86 4	10 7/21 6 (N=10)	0-O	7 7							
CC35-3V3	0 139	40	O	?	6 7/71 5 (N=5)	25-O	1 9											
CC35-3V2	0 293	480	T3	N	*100 9/28 7 (N=6)		13 5											
CC36-1A2	0 396	35	O	?	353 5/68 3 (N=9)	0-O	1 5											
CC36-1BT2	0 92	560	T2	N?	359 5/69 3 (N=11)	100-520	5 4		*96 0/23 6 (N=3)		0							
CC36-1T2	0 276	500	T3	N?	11 7/70 3 (N=8)	100-O	6 2		*100 3/45 3 (N=5)		8 1							
CC36-1T3	0 084	35	O	?	344 8/27 2 (N=5)	0-20	5 1											
CC36-1V1	0 144	480	T3	N?	2 9/70 4 (N=6)	0-460	2		*107 9/31 3 (N=4)		6 3							
CC36-1V2	0 043	35	O	?	58 2/73 7 (N=7)	5-35	8 6											
CC36-1V3	0 464	480	T3	N?	*92 8/24 2 (N=8)		18 5											
CC36-2V4	0 185	480	T2	N?	338 6/58 9 (N=5)	200-460	7		*84 3/30 3 (N=6)		7 1							
CC36-3V1	0 048	40	S2	N				2 7/87 6	11 2/22 6 (N=10)	0-O	12 7	0 98	10 56	-5 0 (4 35)	352 0/23 0	1	S2	0 1037
CC36-2V1T	0 074	510	T3	R	*85 1/6 1 (N=9)		21 1											

CC36-2V1	0 117	40	O	?	326 2/71 6 (N=10)	0-O	4 5												
CC36-2V3T	0 038	490	T3	R	*254 8/25 2 (N=4)		21 7												
CC36-2V3	0 046	40	O/S2	N?				309 1/74 5	357 6/17 3 (N=9)		@7 3								
CC36-1T3A	0 048	40	O/S2	N?				327 0/77 0	2 0/15 0 (N=9)		@1 7								
CC36-1T3T	0 044	490	T2	R	*99 3/4 2 (N=5)		16												
CC36-3V3	0 031	40	S2	N				284 0/71 0	352 0/23 0 (N=9)		@2 9								
CC36-2V2	0 044	40	O	?	312 0/71 0 (N=9)		@2 8												
CC36-3V2	0 221	500	T2	N?	343 1/62 5 (N=8)	0-480	5 1		*92 6/37 3 (N=7)		15 5								
CC41-1BT1	0 028	35	T3	R	322 3/71 2 (N=7)	0-30	8 4		*101 1/40 8 (N=4)		13 6	0 92	1 449		180 0/-90 0	T	T3		0 0562
CC41-1T1	0 113	560	T3	N?	12 8/77 1 (N=11)	0-500	11 6		*109 7/18 9 (N=5)		29 6								
CC42-1T1	0 284	560	O	?	4 5/66 0 (N=14)	0-O	7												
CC42-1T2	0 217	500	T3	R	335 9/72 0 (N=8)	0-490	3 4		*88 1/35 9 (N=4)		18 4								
CC42-1V1	0 134	500	T2	R	338 7/73 6 (N=6)	200-480	3 1		*96 9/39 0 (N=6)		11 6								
CC42-2T1	0 299	500	O	?	341 3/68 4 (N=7)	200-490	6 5												
CC42-2T2	0 07	35	O	?	344 0/72 2 (N=5)	20-O	6 7					0 98	5 641	-5 8 (5 2)	180 0/-90 0	T	T2/T3		0 138
CC42-5V1	0 107	500	T2	R	357 8/73 2 (N=7)	200-490	3 6		*97 8/52 4 (N=7)		16 9								
CC42-2V1	0 08	500	T3	R	355 8/75 7 (N=7)	0-480	2 6		*278 1/27 0 (N=7)		25 1								
CC42-3V1	0 139	500	T3	R	351 6/76 1 (N=8)	0-490	4 9		*91 8/38 6 (N=6)		38 6								
CC42-4V1	0 088	35	O	?	329 7/70 0 (N=5)	20-O	4 3												
CC43-2T1	0 213	40	O	?	350 7/69 4 (N=9)	5-O	2 4												
CC43-1A2	0 136	35	O	?	337 8/73 3 (N=9)	0-O	2 1												
CC43-1T1	0 527	560	O	?	2 6/69 9 (N=15)	0-O	4 7												
CC43-1T2	0 096	500	T3	N/R	34 2/66 8 (N=7)	100-460	10 4		*94 6/31 3 (N=6)		16 1								
CC43-1V1	0 45	500	T2	R	348 1/65 1 (N=8)	0-490	1 7		*88 2/34 0 (N=8)		18 7								
CC43-2T2	0 089	35	O	?	345 1/64 5 (N=9)	0-O	4 9					0 99	5 215	-31 65 (8 8)	180 0/-90 0	T	T1/T2		0 1924
CC43-2V1	0 636	500	T2	R	352 1/65 7 (N=7)	0-480	2 6		*74 0/70 1 (N=8)		3 9								
CC43-3V1	0 132	500	T2	R	331 8/67 1 (N=6)	200-480	3 9		*86 3/49 5 (N=7)		9 9								
CC43-4V1	0 202	500	T2	R					*84 9/56 8 (N=7)		19 4								
CC43-5V2	0 113	500	T2	R	346 6/69 5 (N=3)	0-400	1 3		*84 8/53 8 (N=7)		7								
CC43-6V1	0 119	490	T1	R	331 1/65 7 (N=9)	0-400	1		*93 0/37 6 (N=6)		9 7								
CC44-1T1	0 376	500	O	?	6 4/56 7 (N=4)	0-425	4 9												
CC44-1T2	0 13	500	O	?	310 4/66 9 (N=3)	0-200	10 2												
CC44-1V2	0 068	40	T2	N					*281 2/44 0 (N=6)		12 5								
CC44-2V1	0 075	35	T3	R	22 7/72 6 (N=3)	0-10	1 1		*307 6/55 9 (N=8)		24 1								
CC44-2V2	0 131	500	T1	R	0 0/53 7 (N=5)	200-470	8 6		*99 1/11 7 (N=6)		7 8	0 94	12 795	-5 85 (5 15)	128 0/-63 5	1	S2		0 1312
CC44-2V3	0 158	500	S2	R	347 9/59 4 (N=6)	0-470	2 7	44 9/-27 2	128 2/-63 5 (N=4)		11 5								
CC44-3V1	0 046	35	T2	R					*278 7/3 5 (N=13)		13 7								
CC44-3V2	0 246	500	T1	R	343 8/62 3 (N=5)	0-450	2		*89 4/40 9 (N=9)		28 5								
CC44-3V3	0 197	500	T1	R	354 0/64 7 (N=5)	200-470	2 2		*94 7/35 1 (N=8)		8 3								
CC45-1T1	0 696	560	O	?	12 7/66 2 (N=12)	100-540	5 9												
CC45-1T2	0 225	500	T2	R	14 9/61 5 (N=5)	100-420	8		*101 3/47 8 (N=7)		23 3								
CC45-1V1	0 278	470	T3	R	8 1/70 8 (N=5)	0-450	1 7												
CC45-1V2	0 284	500	T1	R	357 2/68 7 (N=5)	0-450	1 7		*100 0/47 8 (N=8)		25 9								
CC45-1V3	0 305	500	T1	R	355 3/69 4 (N=5)	0-450	0 9		*102 0/42 4 (N=7)		9 8	0 91	22 39	-8 35 (10 4)	180 0/-90 0	T	T1/T2/T3		0 3501
CC45-2V1	0 368	500	T1	R	8 4/66 3 (N=5)	0-450	1		*102 0/11 3 (N=8)		13								
CC45-2V1B	0 351	500	T1	R	8 8/69 3 (N=5)	0-450	3 6		*100 5/31 4 (N=7)		22								
CC45-2V3	0 463	490	T1	R	2 7/68 7 (N=5)	0-450	2 1		*105 2/27 5 (N=6)		12								
CC46-1T2T	0 07	510	T3	R															
CC46-1T2	0 104	40	S2	N?				278 0/81 7	8 2/21 1 (N=8)	5-40	11 2								
CC46-1V2T	0 095	470	T3	R					*275 7/19 1 (N=5)		19 9								
CC46-1V2	0 232	40	O	?	345 4/69 4 (N=10)	0-O	3												
CC46-1V3T	0 177	500	T3	R					*286 9/53 7 (N=7)		10 4								
CC46-1V3	0 382	40	O	?	343 1/70 8 (N=8)	10-O	3					0 98	6 918	+1 65 (1 45)	351 3/36 3	1	S2		0 1752
CC46-1T1	1 094	560	T3	R	359 4/70 4 (N=13)	0-540	6 6												
CC46-1V1	0 404	510	T3	N	26 3/70 0 (N=9)	0-490	4 2		*276 0/33 2 (N=8)		29 5								
CC46-2V1	0 123	480	S2	N	343 1/68 2 (N=6)	0-460	15 1	245 6/60 2	351 3/36 3 (N=3)	460-0	11 7								
CC46-2V2	0 107	510	T2	N	358 4/68 5 (N=10)	0-500	5 9		*106 0/37 0 (N=9)		17 9								
CC46-2V3	0 113	480	T2	N	343 5/63 7 (N=6)	200-470	7 6		*92 1/18 2 (N=6)		27 5								
CC46-3T2	0 117	540	T2	N	12 8/67 4 (N=4)	100-380	8		*102 6/36 5 (N=8)		28 7								
CC47-1V2	0 068	510	E	?															
CC47-1V1	0 119	500	T2	N	10 2/63 6 (N=5)	200-460	4 9		*102 5/22 4 (N=8)		23								
CC47-1V2	0 137	40	S2/O	N				297 4/76 0	2 6/16 9 (N=10)	0-O	3 7	0 98	8 793	+9 15 (5 2)	2 6/16 9	1	S2		0 1066
CC47-2V1	0 099	480	T3	N	354 3/68 4 (N=5)	200-460	4		*95 5/40 4 (N=6)		18 3								
CC47-2V2	0 141	500	T2	N	343 0/68 4 (N=7)	200-480	6 6		*98 7/51 8 (N=8)		10 7								
CC47-2V3	0 095	510	T2	N	359 0/69 0 (N=8)	200-490	5 8		*98 7/51 8 (N=10)		20 4								

CC47B-1T1	0 145	500	T3	N	21 2/58 4 (N=8)	100-480	5 6		*98 8/22 3 (N=7)		12 3				360 0/90 0	T	T3		0 145
CC48-1T1	0 197	540	T3	N	348 2/71 9 (N=12)	0-520	6 5		*107 8/27 3 (N=8)		15								
CC48-1V2	0 017	35	T3	R					*91 7/55 7 (N=8)		27 1								
CC48-2T2	0 013	17 5	T3	R?					*93 2/9 1 (N=5)		20 8								
CC48-2V1	0 482	5	T3	R?															
CC48-2V2	0 23	480	T2	N?					*97 0/16 8 (N=6)		10 3								
CC48-2V3	0 212	490	T2	N?	12 4/67 8 (N=5)	0-450	5 2		*107 2/65 8 (N=8)		11 5	1	1 274	-8 35 (3 8)	10 6/25 6	1	S2		0 0443
CC48-3V3	0 006	0	E	?															
CC48-3V2	0 007	0	E	?															
CC48-2T	0 056	40	O	?	358 4/77 8 (N=9)	5-O	11 8												
CC48-1V1	0 149	40	S2	N				255 0/88 6	10 6/25 6 (N=6)	5-O	7 9								
CC48-1T2	0 11	30	T1	N					*107 8/27 3 (N=8)		15								
CC49-2V2T	0 092	490	T3	R					*112 4/1 7 (N=7)		23 4								
CC49-2V2	0 149	40	S2	N?				316 0/76 6	0 4/17 1 (N=10)	0-O	4								
CC49-3V2T	0 058	500	T2	R	*265 5/24 0 (N=9)		21 5												
CC49-3V2	0 085	40	O	?	350 7/62 2 (N=9)	5-O	1 9												
CC49-SVST	0 136	490	T3	R					*274 8/24 0 (N=9)		3								
CC49-3V3	0 233	40	O	?	38 8/70 6 (N=10)	0-O	4 1					0 96	8 958	-1 65 (1 45)	0 4/17 1	1	T1/T2		0 1564
CC49-1T1	0 275	540	T2	N	21 3/62 1 (N=8)	100-480	5 3		*104 8/29 4 (N=11)		19 9								
CC49-1V1	0 188	480	T2	N	21 0/63 4 (N=6)	200-470	2 9		*104 8/29 4 (N=7)		12 5								
CC49-1V2	0 239	480	T1	N	21 3/64 0 (N=5)	200-460	2 3		*105 8/18 4 (N=6)		4 8								
CC49-2V1	0 166	490	T2	N	14 1/62 0 (N=5)	200-460	3		*101 6/35 9 (N=5)		28 2								
CC49-2V3	0 312	480	T2	N	21 2/62 0 (N=5)	200-460	1 7		*104 5/36 1 (N=6)		14 3								
CC50-1T1	0 493	540	S2	N	1 5/66 3 (N=7)	100-440	4 9	274 6/74 6	355 0/26 0 (N=3)		@12 7								
CC50-1T2	0 335	560	T2	N	357 6/66 7 (N=11)	0-500	3 2		*96 9/14 5 (N=13)		30 5								
CC50-1V2	0 179	500	T3	N?	0 9/73 5 (N=6)	0-460	18 1		*275 4/48 0 (N=4)		9 6								
CC50-2V2	0 205	470	T2	N?	8 5/72 8 (N=4)	200-450	11 2		*101 9/25 7 (N=7)		25			-1 65 (3 8)	355 0/26 0	1	S2		0 2888
CC50-3V2	0 189	480	O/T3	R?	342 2/66 9 (N=5)	0-450	1 3												
CC50-4V2	0 518	500	T3	N	357 9/67 1 (N=6)	0-460	1 8		*250 1/70 3 (N=4)		33 6								
CC50-5V2	0 155	480	O	?	2 4/68 6 (N=7)	0-470	2 6												
CC50-6V2	0 526	480	O/T3	R?	357 9/67 4 (N=5)	0-450	2												
CC51-1T1	0 553	560	T2	N	0 3/62 8 (N=12)	0-520	8 7		*102 2/44 2 (N=6)		9 8								
CC51-1T2	0 388	540	T2	N	19 0/60 1 (N=7)	100-480	5 7		*100 0/49 1 (N=10)		17 9								
CC51-2T1	0 615	530	O	?	2 8/61 1 (N=12)	0-520	4 4												
CC51-2T2	0 66	530	T2	N	2 9/62 0 (N=8)	0-480	2		*93 9/35 4 (N=9)		8 9								
CC51-4V2	0 422	490	T1	R	348 4/57 3 (N=5)	0-450	3 3		*94 8/7 1 (N=4)		15 9								
CC51-1V2	0 094	510	T2	R					*276 3/14 6 (N=7)		10 7								
CC51-3V2	0 062	510	T2	R					*93 6/5 9 (N=7)		17 1	0 97	10 54	+45 85 (31 25)	182 0/-14 0	1	T1/T2		0 1947
CC51-1V2A	0 138	40	O?	?	358 4/77 1 (N=9)	5-O	4 8												
CC51-5V2A	0 062	40	O	?	3 0/66 9 (N=8)	10-O	9												
CC51-2V2A	0 056	40	S2	N				121 0/69 6	34 3/29 9 (N=6)	25-O	6 3								
CC51-3V2A	0 076	40	O	?	344 7/68 7 (N=9)	5-O	6 9												
CC51-6V2	0 381	490	O	?	346 4/64 4 (N=7)	0-470	2 2												
CC52-1T1	0 41	500	O	?	31 6/69 4 (N=7)	200-500	7												
CC52-1V1	0 026	35	T1	R	25 3/50 7 (N=6)	0-16	9		*110 2/2 6 (N=4)		19 6								
CC52-1V2	0 694	530	O	?	26 5/65 9 (N=11)	0-510	1 8							-1 65 (5 2)	180 0'-90 0	T	T1/T2/T3		0 303
CC52-2T1	0 513	580	T3	R	21 3/71 2 (N=11)	0-520	10 1		*271 2/81 7 (N=4)		13 3								
CC52-2V1	0 673	500	T2	R	26 1/65 8 (N=5)	200-460	2 4		*111 1/12 8 (N=5)		21 4								
CC53-2V2	0 599	500	T2	R	354 4/65 8 (N=9)	0-490	3 5		*278 2/1 5 (N=5)		23 9								
CC53-2V3	0 591	500	S2	R	64 8/60 8 (N=4)	200-450	11 1	42 4/-55 5	164 1/-52 3 (N=5)	470-O	17 5								
CC53-1V2	0 364	500	S2	R	354 5/66 6 (N=4)	0-425	5 6	31 2/-54 3	171 1/-57 4 (N=5)	470-O	16 9								
CC53-2V1	0 222	500	T1	R	357 7/62 2 (N=5)	0-450	4 6		*95 1/50 2 (N=10)		27 9								
CC53-1T3	0 152	540	T3	R															
CC53-1T2	0 405	520	S2	R	26 2/51 6 (N=7)	100-480	7 7	40 5/-67 1	176 9/-44 4 (N=3)	510-O	8 7								
CC53-1V1	0 192	40	O	?	9 7/67 2 (N=10)	0-O	4 6												
CC53-1V1T	0 113	520	T2	R	*98 6/31 8 (N=10)		38 6					0 97	17 88	+2 5 (2 5)	171 0/-51 0	3	S2		0 1949
CC53-1V3	0 17	40	O	?	318 8/67 2 (N=8)	10-O	5 6												
CC53-1V3T	0 102	520	T2	R	*94 8/23 8 (N=10)		33 4												
CC53-3V3	0 182	40	O	?	17 3/62 1 (N=9)	5-O	4 4												
CC53-3V3T	0 083	510	T2	R	354 4/65 8 (N=9)	0-490	3 5		*278 2/1 5 (N=5)		23 9								
CC53-3V2	0 147	40	O	?	26 2/80 1 (N=8)	10-O	6 2												
CC53-2T2	0 245	40	O	?	332 5/65 9 (N=9)	5-O	3 6												
CC53-2T3	0 071	40	O	?	66 6/82 8 (N=4)	30-O	10 6												
CC53-6V2	0 169	40	O	?	313 5/74 3 (N=10)	0-O	6 1												
CC54-5V2	0 427	500	T2	R	343 4/68 9 (N=5)	0-470	2 3		*87 8/5 4 (N=7)		20								

CC54-3V2	1 51	530	T2	R	355 2/65 8 (N=6)	0-470	0 8		*96 0/30 3 (N=11)		13 5								
CC54-4V2	1 33	500	T2	R	349 2/67 2 (N=6)	0-460	0 9		*94 1/5 1 (N=5)		8 4								
CC54-2T1	1 684	530	T2	R	1 1/58 1 (N=11)	0-520	2 7		*95 4/27 4 (N=4)		11 6	0 95	57 53	+90 85 (14 2)	180 0/-90 0	T	T2/T3		0 7312
CC54-3T1	0 696	540	T3	R	21 2/57 1 (N=9)	100-500	4 5												
CC54-2V2	0 628	40	O	?	329 8/56 4 (N=10)	0-O	6												
CC54-1V2	0 177	40	O	?	88 9/66 3 (N=10)	0-O	3 4												
CC54B-1T1	0 005	7 5	T3	R															
CC54B-1T2	0 006	7 5	T3	R	*122 2/76 5 (N=3)		0 1					0 95	1 197		180 0/-90 0	T	T3		0 0053
CC54B-2T2	0 005	7 5	T3	R															
CC55-1T1	0 533	500	O	?	31 4/65 2 (N=8)	100-480	5 9												
CC55-1T2	0 358	560	T3	N	1 0/75 1 (N=10)	100-500	5 4		*95 7/7 8 (N=5)		20 5								
CC55-2V3B	0 153	490	T3	R	14 0/62 5 (N=5)	0-425	14 1		*186 5/37 7 (N=4)		16								
CC55-1V2	0 15	490	T3	R	42 2/69 2 (N=5)	0-450	16 9		*291 2/27 6 (N=7)		7 9	0 96	17 81	+0 85 (6 3)	MIXED		S2/T2/T3		0 2412
CC55-1V3	0 093	490	S2	N				183 6/78 9	14 0/36 0 (N=7)		@12 3								
CC55-2T1	0 404	520	T2	N	2 1/66 8 (N=7)	200-480	3 5		*280 4/20 4 (N=11)		18 5								
CC55-2V2	0 261	470	T2	R	36 4/69 5 (N=5)	0-450	6		*114 9/45 3 (N=4)		10 8								
CC55-2V3	0 267	500	T3	R	358 2/71 4 (N=7)	0-450	19 7												
CC56-1T2	0 072	35	O	?	327 4/78 7 (N=6)	10-35	4 8												
CC56-1V1	0 48	490	O	?	355 9/71 6 (N=6)	200-470	3 6												
CC56-2T1	0 098	35	O	?	336 4/69 2 (N=7)	5-35	4 9												
CC56-2T2	0 077	35	O	?	329 7/64 2 (N=8)	0-35	3 5												
CC56-1T1	0 32	580	T2	R	9 3/66 2 (N=9)	100-540	15 2		*89 1/27 7 (N=4)		2 5	1	4 706	+44 15 (21 25)	180 0/-90 0	T	T2		0 1899
CC56-3V1	0 164	500	O	?	350 3/68 9 (N=6)	0-460	4 3												
CC56-2V1	0 25	460	E	?															
CC56-1V2	0 495	470	O	?	349 7/67 6 (N=6)	0-460	8 1												
CC57A-1V1	0 478	500	E	?															
CC57A-1V2	0 734	490	T2	R	333 8/77 2 (N=6)	200-470	5 9		*104 0/48 5 (N=5)		11 6								
CC57A-2V1	0 533	500	O	?	341 4/61 9 (N=7)	200-470	5							+20 0 (26 35)	180 0/-90 0	T	T2		0 6052
CC57-AV3	0 777	490	O	?	347 8/61 9 (N=6)	200-480	2 6												
CC57A-2V2	0 626	490	T2	R	339 1/69 0 (N=5)	200-460	6 8		*268 5/16 9 (N=8)		19								
CC57A-1T2	0 54	540	O	?	4 5/62 1 (N=8)	100-480	8 8												
CC57-3T1	0 387	500	T3	R	353 6/63 9 (N=8)	0-480	2 3		*103 7/81 1 (N=7)		19 4								
CC57-1T1	0 226	500	T2	R	29 0/60 6 (N=5)	100-420	8 8		*109 8/19 0 (N=4)		12 8	0 97	9 051	+18 35 (7 2)	180 0/-90 0	T	T2/T3		0 2837
CC57-2T1	0 261	560	O	?	10 6/62 0 (N=13)	0-540	4 7												
CC58-1T2	0 127	470	T3	R	2 0/64 5 (N=5)	200-460	2 7		*276 9/29 0 (N=5)		29 4								
CC58-2T1	0 305	530	T3	N	0 8/64 5 (N=10)	200-510	15 9		*278 1/6 4 (N=5)		32 4								
CC58-3T1	0 663	490	O	?	21 0/67 2 (N=6)	0-460	1 6												
CC58-1T1	0 353	530	T3	R	3 5/63 7 (N=10)	0-500	4		*278 5/67 9 (N=8)		25 1								
CC58-2T2	0 039	35	T3	R	318 3/60 7 (N=5)	0-10	5 4												
CC58-4T2	0 03	35	T3	N	355 2/41 7 (N=3)	5-15	21 3		*278 1/28 8 (N=5)		6 6								
CC58-3T2	0 021	30	T3	N	336 6/58 3 (N=7)	0-30	6 8		*261 1/39 6 (N=5)		30 1	0 98	1 86	-10 0 (20 45)	MIXED		S2/T3		0 1112
CC58-2V2	0 194	40	O	?	352 2/68 8 (N=10)	0-O	3 3												
CC58-1V2	0 111	40	O	?	329 2/78 3 (N=10)	0-O	4 4												
CC58-1V3	0 119	40	O	?	0 8/79 4 (N=10)	0-O	4 7												
CC58-1V1	0 161	40	O	?	347 3/73 4 (N=10)	0-O	2 8												
CC58-2V3	0 177	40	O	?	347 1/73 4 (N=10)	0-O	4 6												
CC58-2T2X	0 029	40	S2	N				183 0/56 1	26 2/59 8 (N=5)	25-O	10 4								
CC58-2V4	0 094	40	O	?	3 5/70 9 (N=9)	0-O	9 6												
CC60-6V3A	0 0488	40	S2	N				247 2/72 7	340 1/25 2 (N=6)	20-O	13 8								
CC60-3V4A	0 3852	40	T3	R	*28 7/66 8 (N=9)		23 4												
CC60-2V2A	0 2024	40	O	?	302 0/80 6 (N=6)	20-O	2												
CC60-1V1	0 067	65	S2	N				142 3/83 8	2 0/25 0 (N=7)		@5 8								
CC60-3V3	0 488	65	T3	R	318 0/60 5 (N=9)	30-O	8 4												
CC60-4V2	0 138	65	T3	R	*259 3/28 2 (N=8)		19					0 92	2 892	-11 65 (3 8)	349 0/24 0	3	S2	@16 7	0 109
CC60-2V3	0 122	65	O	?	2 3/75 9 (N=12)	0-65	7 8												
CC60-4V4A	0 1898	40	S3	N				313 1/85 8	354 9/17 0 (N=8)	5-40	21 8								
CC60-2V4A	0 0838	40	O	?	59 6/69 9 (N=5)	5-25	22 6												
CC60-3V1A	0 0414	40	S2	N				261 2/76 9	344 0/21 0 (N=9)		@5 3								
CC60-2AV2	0 0188	40	E	?															
CC60A-1V3	0 1591	40	S2	I				15 8/49 9	10 0/-18 3 (N=9)	5-O	9 3								
CC60A-3V2	0 1619	40	S2	I				23 3/36 3	21 1/-28 9 (N=9)	5-O	6 7	1	5 6	-3 36 (9 45)	16 0/-21 0	3	S2	@14 2	0 1216
CC60A-1V2	0 1401	40	S2	I				30 0/50 1	18 5/-14 4 (N=9)	5-O	5 8								
CC60A-2V2	0 0606	40	T2	R	*274 5/16 0 (N=4)		33 8												
CC61-X	0 00585	40	S2	N				130 6/58 6	27 4/38 6 (N=5)	25-O	8 2								
CC61-D	0 00444	40	T3	N	*304 5/9 4 (N=6)		25 1												

CC61-1AV2	0 012	40	T3	R															
CC61-4AV3	0 0161	40	S2	N				153 5/85 6	0 0/24 0 (N=7)		@9 2	0 99	1 696	-21 65 (1 45)	MIXED		S2/T2/T3		0 0252
CC61-3AV2	0 0399	40	T3	R	*274 6/42 0 (N=8)		20 3												
CC61-2AV3	0 0349	40	S2	N				70 1/81 0	7 0/17 0 (N=7)		@6 4								
CC61-1V1	0 045	65	T3	R	*118 2/74 2 (N=11)		26 7												
CC61-3V1	0 084	65	T2	R	*269 8/26 0 (N=13)		22 4												
CC61-2V2	0 051	65	E	?															
CC61-4V1	0 076	65	T2	R	*95 3/63 0 (N=14)		9												
CC62-A	0 00957	40	T3	R	*249 2/56 2 (N=9)		21 5												
CC62-B	0 00443	40	T3	R	*254 1/38 4 (N=4)		25												
CC62-D	0 00961	40	T2	R	*75 9/28 6 (N=9)		27 6												
CC62-E	0 0129	40	T3	R	*253 3/25 4 (N=9)		35 1												
CC62-2V1	0 036	65	T3	R															
CC62-1V1	0 044	65	T3	R	*90 2/62 5 (N=12)		14					1	1 537	-17 5 (4 35)	180 0/-90 0	T	T2/T3		0 0163
CC62-2V3	0 012	35	T3	R	354 0 (N60 0 (N=6)	15-O	6 6		*85 7/1 5 (N=7)		19 2								
CC62-3V2	0 026	35	O	?	356 2/66 1 (N=7)	5-35	9 5												
CC62-2V1	0 032	65	T3	R			17												
CC62-2V2	0 053	65	T3	R	*257 2/47 9 (N=5)														
CC62-2V2X	0 005	40	E	?															
CC63-A	0 0217	40	S1	?				157 3/36 4	96 4/54 0 (N=4)	30-O	4								
CC63-B	0 0109	40	S2	N				191 8/43 3	12 6/74 7 (N=8)	10-O	6 6								
CC63-3V1	0 024	65	E	r?															
CC63-2V1	0 017	40	S2	N				179 0/59 0	24 0/57 0 (N=8)		@7 2			-15 85 (1 45)	12 6/74 7	1	S2		0 0253
CC63-1V2	0 027	40	O	?	357 0/69 0 (N=9)		@6 4												
CC63-2V3	0 056	40	T2	R?	*182 4/32 1 (N=9)		13 3												
CC63-1V3	0 041	65	T3/E	R?	*72 0/73 0 (N=4)		7 4												
CC63-1V1	0 028	65	E	?															
CC64-1V2	0 103	65	T2	R	*108 5/42 2 (N=14)		14 9												
CC64-1V4	0 059	65	T2	N?	*131 0/65 8 (N=14)		16 9												
CC64-2V2	0 198	40	T3	R?	331 1/73 9 (N=6)	20-O	12 1		*116 5/56 3 (N=9)		12 1								
CC64-1V3	0 146	40	T3	R?	*263 8/48 2 (N=9)		27 6					1	2 927		180 0/-90 0	T	T3/T2		0 1434
CC64-1V3B	0 176	40	T3	R?	*100 7/13 0 (N=9)		39 2												
CC64-1V1	0 265	40	E	?															
CC64-2V4	0 152	40	T3	R?	*209 7/61 2 (N=9)		20 2												
CC65-A	0 00243	40	E	?															
CC65-B	0 0235	40	T3	R	*133 0/44 0 (N=4)		23												
CC65-2V2	0 014	60	T3	R															
CC65-2V1	0 008	25	T1	R	*111 8/15 2 (N=8)		22 9					0 87	1 297	-15 85 (5 2)	'178 0/-32 0		T1/T2/T3		0 0076
CC65-1V2	0 006	22 5	T2	R	*277 0/3 5 (N=7)		22 5												
CC65-1V3	0 005	35	T2	R	*97 2/34 3 (N=5)		14 6												
CC66-1V0	0 008	35	T1	R	*278 5/29 4 (N=8)		31 8												
CC66-A	0 0111	40	T3	R	*91 5/8 3 (N=9)		26 2												
CC66-B	0 02	40	T3	R	*335 8/14 0 (N=8)		28 3					0 74		-17 5 (7 5)	108 0/-72 0	1	T1		0 0128
CC66-1V1	0 013	30	T1	R	*100 4/18 9 (N=9)		14 7												
CC66-2V2	0 006	35	T1	R	*86 5/16 9 (N=8)		19 7												
CC66-1V2	0 031	40	T3	R	*157 8/62 2 (N=8)		30												
CC67-A	0 00967	40	T3	R	*231 5/64 1 (N=8)		17 7												
CC67-AX	0 00756	40	T2	R	*275 7/17 3 (N=9)		37 8												
CC67-1V3	0 036	35	O	?	350 0/64 7 (N=7)	30-O	12 3												
CC67-2V1	0 025	60	T2	R	*115 072 9 (N=7)		16 4					0 97	2 174	-26 65 (5 2)	190 0/-14 0	1	T2		0 0251
CC67-2V2	0 098	60	O	?	350 0/64 7 (N=7)	30-60	8 7												
CC67-1V2	0 034	60	T3	R	*131 7/41 7 (N=6)		34 4												
CC67-1V3	0 066	60	O	?	339 9/63 4 (N=8)		12 3												
CC67-2V3	0 011	35	T2	R	*105 2/14 0 (N=8)		24 5												
CC68-A	0 0105	40	T3	R	*120 6/16 7 (N=9)														
CC68-AX	0 00818	40	T3	R	19 1/70 6 (N=5)	25-O	9 6		*281 6/4 3 (N=6)		19								
CC68-B	0 0168	40	T3	R	*276 2/17 0 (N=9)		28 6												
CC68-2V2	0 04	40	T3	R?	*92 4/30 1 (N=9)		34 4												
CC68-2V3	0 023	40	S2	N				266 5/77 8	338 4/26 4 (N=7)	0-O	12	0 94	3 651	-10 85 (8 8)	164 0/-37 0	1	T2		0 0199
CC68-3V2	0 018	35	T2	R	*83 4/31 3 (N=9)		21												
CC68-1V2	0 019	35	T2	R	*268 8/8 3 (N=6)		23 4												
CC68-3V1	0 017	35	T2	R	*86 6/23 6 (N=6)		16 2												
CC68-1V1	0 03	40	O	?	51 0/61 0 (N=9)		@4 2												
CC68-2V1	0 042	40	T2	R	*144 1/51 2 (N=4)		0 3												
CC69-A	0 00859	40	T3	R	*283 8/25 0 (N=5)		5 1												

CC69-B	0 00546	40	T3	N/R?	*290 7/9 2 (N=9)		39 9					0 99	0 8788	-25 0 (6 6)	180 0/-90 0	T	T1/T2		0 0102
CC69-1V1	0 006	35	T1	R	*288 5/22 6 (N=7)		25												
CC69-1V2	0 008	35	T1	R	*284 2/7 3 (N=10)		27 8	98 0/75 0	28 0/26 0 (N=9)		@3 5								
CC69-2	0 026	40	S2	N				4 0/83 0	11 0/21 0 (N=9)		@4 8								
CC69-2V2	0 019	40	S2	N															
CC70-A	0 00818	40	T3	R	*261 8/0 9 (N=9)		25 2												
CC70-B	0 012	40	T3	N/R?	*49 5/49 3 (N=9)		16 5												
CC70-2V3	0 016	40	T3	R	*238 6/57 5 (N=4)		37 9												
CC70-1V1	0 008	35	T1	R	*143 0/51 0 (N=8)		27 1							-24 15 (5 2)	196 0/-30 0		T1/T2		0 0193
CC70-2V2	0 026	35	T1	R	*143 3/34 0 (N=8)		8 8												
CC70-3V3	0 054	35	T1	R	*149 7/58 8 (N=8)		28 9												
CC70-2V3B	0 016	40	S2	N				240 0/69 0	352 0/41 0 (N=8)		@9 1								
CC70-2V1	0 069	40	T2	R	*102 7/19 4 (N=9)		22 6												
CC71-A	0 0147	40	S2	N				343 4/85 8	9 8/24 3 (N=9)	5-O	6 5								
CC71-B	0 0175	40	S2	N				260 3/75 5	356 1/32 4 (N=8)	10-O	7								
CC71-C	0 0124	40	S2	N				166 9/76 1	19 7/40 4 (N=6)	20-O	5 4			-30 85 (3 8)	113 0/-38 0		T1/T2/T3		0 0127
CC71-1V4	0 008	35	T2	R	*91 2/49 7 (N=7)		17												
CC71-1V3	0 008	35	T1	R	*161 0/40 3 (N=4)		4 8												
CC71-2V3	0 021	35	T3	R	*111 4/50 6 (N=6)		25 1												
CC72-2V3	0 0114	25	T1	R	*292 3/24 5 (N=6)		16 2												
CC72-1V2	0 0084	20	T1	R	*299 0/11 3 (N=5)		11 3												
CC72-3V3	0 0094	35	T1	R	*95 8/45 7 (N=8)		20 7					0 97	3 223		213 0/-22 0		T1/T2		0 0109
CC72-2V2	0 0137	30	T2	R	*303 7/56 7 (N=3)		0												
CC72-1V3	0 0126	35	T1	R	*112 7/30 5 (N=8)		7												
CC73-A	0 0961	40	T3	R	21 8/62 1 (N=6)	15-O	5 6		*107 4/15 7 (N=9)		12 4								
CC73-B	0 015	40	S2	N				156 2/70 1	27 2/43 0 (N=7)	15-O	6								
CC73-1V1	0 005	15	O	?	20 5/64 3 (N=4)	10-O	4 8												
CC73-1V2	0 026	25	T3	R	*112 8/10 8 (N=8)		20 4												
CC73-2V3	0 009	25	T3	R	58 7/75 6 (N=8)	0-35	3 8		*278 8/42 4 (N=7)		32 6								
CC73-3V3	0 015	25	S2	I				49 3/39 3	41 0/-14 3 (N=10)	2 5-O	4 4								
CC73-5	0 038	40	O	?	64 1/49 8 (N=7)		@9 9												
CC73-1	0 023	40	E	?															
CC73-3	0 025	40	S2	N				234 0/73 0	357 0/40 0 (N=9)		@4 8								
CC73-7	0 069	40	T3	R	51 1/67 4 (N=6)	0-25	9 6		*240 5/73 6 (N=3)		0 9	0 99	3 095	-23 35 (10 4)	MIXED		S2/T3		0 0499
CC73-2	0 103	40	O	?	22 2/75 4 (N=10)	0-O	2 2												
CC73-6	0 08	40	O	?	30 1/59 7 (N=10)	0-O	6 4												
CC73-4	0 056	40	T3	R	*92 4/53 2 (N=6)		7 5												
CC73-8	0 326	40	T3	R?	55 0/38 8 (N=10)	0-O	5 5		*124 2/40 8 (N=9)		10 9								
CC73-9	0 271	40	T3	R	39 0/50 2 (N=10)	0-O	6 4		*96 0/69 8 (N=9)		20								
CC73-1V1	0 125	40	T3	R?	20 6/79 7 (N=9)	0-40	6 7												
CC73-2V1	0 045	40	S2	N				267 3/82 0	3 1/29 7 (N=10)	0-O	7								
CC73-2V2	0 113	40	O	?	350 0/51 7 (N=10)	0-O	3 9												
CC73-1V3	0 025	40	S2	N				203 0/72 0	7 0/45 0 (N=9)		@5 2								
CC74-3V2	0 085	35	T3	R	*107 6/67 7 (N=7)		23 9												
CC74-2V2	0 03	35	T3	R?															
CC74-1V3	0 008	35	T3	R?	*133 3/45 7 (N=4)		20 9												
CC74-1V2	0 01	30	O	?	338 6/73 5 (N=7)	0-O	17 9												
CC74-2V3	0 01	35	T3	R	*125 9/46 2 (N=9)		21 3												
CC74-3V1	0 062	40	T3	N?	43 9/64 6 (N=4)	30-O	7 7		*121 4/52 4 (N=7)		21 2								
CC74-3V3	0 048	40	T2	N	*126 5/11 2 (N=7)		15 2							-4 15 (6 3)	MIXED				0 0364
CC74-10	0 017	40	S2	N				238 0/70 0	353 0/40 0 (N=9)		@3 3								
CC74-9	0 063	40	T3	R?	*102 9/5 2 (N=5)		22 4												
CC74-1	0 023	40	T3	R	*141 2/39 7 (N=4)		39 2												
CC74-12	0 072	40	O	?	337 6/72 2 (N=9)	5-O	6 7												
CC74-6	0 123	40	O	?	7 6/76 3 (N=10)	0-O	5 6												
CC74-5	0 177	40	O	?	11 1/62 5 (N=10)	0-O	2 6												
CC74-7	0 031	40	O	?	359 3/63 5 (N=10)	0-O	18												
CC75-A	0 00753	40	S2	N				225 2/35 6	305 5/60 9 (N=5)	25-O	5 7								
CC75-9	0 052	40	T3	N	318 9/69 8 (N=9)	5-O	6 3		*255 5/33 5 (N=9)		32 8								
CC75-2	0 017	40	T2	R	*156 3/52 2 (N=9)		40 6												
CC75-1	0 0097	40	T3	R	*293 6/33 3 (N=6)		46 3												
CC75-3V3	0 055	40	S2	N				206 4/72 9	6 1/44 4 (N=10)	0-O	9 5								
CC75-1V1	0 007	35	T3	R?	*268 0/47 6 (N=4)		24 5												
CC75-1V2	0 009	35	T3	R?	*263 9/52 3 (N=4)		40 9							-20 85 (1 45)	226 0/-13 0		T2		0 0129
CC75-3V1	0 0147	35	T2	R	*239 9/78 8 (N=4)		11												

CC75-1V3	0 009	30	T3	R?	*196 0/66 4 (N=5)		25											
CC75-1V3T	0 0112	400	E	?														
CC75-2V1	0 007	20	T3	R?	*152 3/50 5 (N=6)		15 7											
CC75-2V2	0 017	35	T3	R?	*125 0/13 3 (N=5)		28 7											
CC75-2V3	0 0072	30	T2	R	*135 8/7 8 (N=4)		3											
CC75B-3V2	0 0795	40	O	?	341 4/68 0 (N=10)	0-O	8 1											
CC75B-X	0 1282	40	O	?	346 9/64 5 (N=6)	20-O	3 6											
CC75B-2V2	0 1182	40	O	?	344 7/64 8 (N=10)	0-O	5 6											
CC75B-2V2T	0 0225	480	E	?														
CC75B-1V2	0 058	40	T3	N?	337 8/66 7 (N=9)	0-40	17 4		*264 1/34 4 (N=9)		34 8	0 96	4 397	-16 65 (7 65)	181 0/-9 0	1	T2		0 0672
CC75B-1V2T	0 0138	470	T2	N	*108 8/31 5 (N=9)		8 8											
CC75B1V3	0 1377	40	O	?	354 1/66 7 (N=6)	20-O	3 9											
CC75B-1V1	0 1009	40	O	?	356 2/68 4 (N=10)	0-O	5 2											
CC75B-3V3	0 1587	40	T2	R	*116 0/68 5 (N=9)		20 5											
CC75B-3V3T	0 039	480	T2	R	*100 5/43 8 (N=4)		0 4											
CC76-A	0 00544	40	T3	N/R?	302 6/1 4 (N=7)		31 1											
CC76-AX	0 00632	40	T2	R	*27 9/4 1 (N=7)		18 4											
CC76-4	0 014	40	T3	R?	*110 6/18 8 (N=4)		9 4							-38 35 (3 8)	65 0/-80 0		T2/T3		0 0101
CC76-1V2	0 0069	40	E	?														
CC76-2V2	0 032	40	T3	R	*326 7/2 3 (N=3)		0 1											
CC76A-5V2	0 5324	40	T1	R	*354 6/19 7 (N=9)		10 1											
CC76A-5V3	0 072	40	T1	R	*358 1/38 1 (N=9)		13 4											
CC76A-3V1	0 0376	40	T2	R	*117 7/30 7 (N=8)		23 1											
CC76A-4V2	0 0108	40	T2	R	*259 1/9 5 (N=5)		26 9							-4 15 (2 9)	58 1/-53 8	1	S1		0 0545
CC76A-3V3	0 0799	40	S2	R				71 3/-0 2	86 6/-26 9 (N=10)		9 4							
CC76A-2V1	0 0195	40	E	?														
CC76A-2V3	0 0343	40	S2	R				18 0/12 0	21 0/-51 0 (N=9)		@5 2							
CC76A-3V4	0 0937	40	S1	R				37 2/-1 0	58 1/-53 8 (N=10)	0-O	5 6							
CC76B-2V3	0 043	40	O	?	16 2/52 3 (N=3)	15-30	4 5											
CC76B-1V4	0 0584	40	T3	R	0 7/76 1 (N=5)	25-O	7 5		*264 1/42 8 (N=8)		27 7							
CC76B-3V3	0 0632	40	S2	N				332 0/75 0	0 0/18 0 (N=9)		@2 8							
CC76B-1V1	0 0165	40	S2	N				319 0/76 0	0 0/19 0 (N=9)		@8 8							
CC76B-3V2	0 0317	40	O	?	306 0/60 0 (N=9)		@2 8					1	2 764	-4 15 (25 05)	359 0/18 0	3	S2	@2 9	0 0338
CC76B-2V2	0 0233	40	O	?	329 0/61 0 (N=9)		@7 3											
CC76B-1V2	0 0339	40	O	?	62 0/72 0 (N=9)		@2 3											
CC76B-1V2T	0 0243	490	E	?														
CC76B-1V3	0 0364	40	S2	N				317 0/73 0	357 0/17 0 (N=9)		@8 4							
CC77-1AV3	0 077	40	S2	N				342 5/78 8	6 2/18 1 (N=8)	10-O	9 5							
CC77-1V3	0 055	40	T2	N	*111 1/42 7 (N=9)		30 8											
CC77-2AV3	0 0864	40	O	?	49 2/58 7 (N=10)	0-O	5 8											
CC77-2AV3X	0 0558	40	S2	N				294 4/74 7	355 6/23 8 (N=9)	5-O	9 9	1	6 896		4 0/19 0	3	S1/S2	@12 4	0 0541
CC77-2V3	0 028	25	T3	R?	28 8/62 9 (N=9)	0-O	5											
CC77-1V1	0 244	40	S1/O	N?				1 9/77 3	9 7/15 5	5-O	3 8							
CC77-1V3X	0 024	15	E	?														
CC77-1V3	0 022	30	O	?	16 8/65 7 (N=8)	0-O	4 4											
CC78-3V1	0 024	35	O	?	321 7/59 0 (N=9)		6 2											
CC78-1V3	0 01	35	T2	N?	*99 4/9 1 (N=5)		25 5					0 93	1 804	-7 5 (2 5)	MIXED		S1?/T2		0 015
CC78-2V3	0 007	35	T2	R	*96 7/9 0 (N=10)		24											
CC78-1V1	0 03	35	S1	N	38 2/61 2 (N=5)	0-20	16 2	23 1/80 8	13 9/19 0 (N=4)	25-O	4 6							
CC79-A	0 102	40	T2	R	*287 8/21 3 (N=9)		9 2											
CC79-B	0 028	40	T3	R	*107 2/38 2 (N=9)		23 4											
CC79-1V1	0 03168	50	T1	R	*94 3/52 5 (N=10)		36 7							-47 5 (10 9)	190 0/-11 0	1	T2/T3		0 049
CC79-2V1	0 02285	50	T2	R	*274 9/30 5 (N=9)		24											
CC79-1V3	0 06069	50	O	?	322 6/59 6 (N=8)	20-O	9 5											
CC79-3V3	0 11	40	T3	R	319 3/51 5 (N=7)	15-O	8		*74 0/26 4 (N=5)		4 3							
CC80-B	0 0169	40	S1	N				350 3/82 1	8 9/20 6 (N=6)	20-O	4							
CC80-BX	0 023	40	S2	N				303 3/75 7	357 4/22 5 (N=7)	15-O	15 1							
CC80-1V1	0 033	40	S2	N				213 7/58 9	352 2/55 7 (N=6)	30-O	8 8			-18 35 (3 8)	8 9/20 6	1	S1		0 0223
CC80-2V1	0 008	25	S2	N				205 7/60 7	0 0/56 0 (N=7)		@9 3							
CC80-1V1	0 05606	50	S2	N				209 4/58 9	355 6/56 8 (N=5)		9 4							
CC80-1V1A	0 02141	50	S2	N				250 9/56 6	334 0/40 0 (N=12)		@6 2							
CC81-6	0 223	40	S2	N				213 0/63 0	356 0/52 0 (N=9)		@4 5							
CC81-4	0 259	40	S1	N				84 4/72 9	29 5/21 7 (N=10)	0-O	2 1							
CC81-1V1A	0 4577	50	O	?	6 0/60 7 (N=13)	0-O	1 8											
CC81-1V1	0 205	40	O	?	16 0/75 8 (N=5)	10-40	9 3											

CC81-1V1T	0 193	470	O	?	359 1/67 0 (N=6)	200-O	4 8											
CC81-1V2	0 342	40	O	?	2 1/68 4 (N=7)	5-O	2 5											
CC81-2V3	0 041	40	S3	N				218 5/59 1	352 9/53 7 (N=8)	0-O	17 9							
CC81-1	0 263	40	S1	N				285 2/87 1	10 7/26 9 (N=7)	15-O	1 3							
CC81-1V1X	0 193	40	S2	N				90 7/62 7	42 0/18 0 (N=9)		@1 7	0 99	14 16	-5 0 (4 35)	17 0/27 0	5	S1	@9 0	0 2165
CC81-2	0 27	40	O	?	323 2/69 8 (N=9)	5-O	2 3											
CC81-2V1	0 236	40	O	?	2 6/74 1 (N=10)	0-O	3 5											
CC81-2V2	0 299	40	O	?														
CC81-2V2T	0 1993	470	O	?	350 6/69 8 (N=7)	0-O	5 2											
CC81-3	0 231	40	O	?	10 6/75 5 (N=6)	20-O	2 9											
CC81-3	0 224	40	S1/O	N?				43 9/84 0	17 2/21 8 (N=7)	15-O	1 2							
CC81-5	0 1292	470	S1	N				344 8/83 7	11 7/22 7 (N=6)	200-O	4 5							
CC81-5T	0 229	40	S1	N				22 7/86 4	14 6/23 4 (N=7)	15-O	4 7							
CC81-7	0 165	40	S1	N				172 4/78 7	19 2/37 4 (N=8)	10-O	2							
CC81-8	0 33	40	S1/O?	N?				5 0/78 9	12 2/16 0 (N=6)	20-O	1 2							
CC81-9	0 087	50	T3	N?	326 8/64 9 (N=8)	5-O	22		*96 1/37 3 (N=6)		25 1							
CC82-2V2	0 1	50	S2	N				273 3/76 4	358 7/28 7 (N=10)		@3 2							
CC82-2V1	0 365	40	O	?	344 5/65 9 (N=10)	0-O	1 8											
CC82-8X	0 125	40	S2	N				185 7/88 2	14 3/28 8 (N=7)	15-O	9 2							
CC82-4	0 319	40	O	?	341 6/68 7 (N=8)	10-O	3 3											
CC82-3A	0 132	40	O	N				259 5/78 9	2 2/31 1 (N=10)	0-O	8 1							
CC82-4B	0 372	40	S1	?	326 2/75 2 (N=5)	25-O	1 4											
CC82-7	0 541	40	T3	?	340 9/71 1 (N=8)	10-O	1 4											
CC82-1V3	0 141	40	O/S1	N				192 6/77 4	14 4/39 6 (N=6)	20-O	4	1	3 894	-3 35 (5 2)	MIXED		S2/T2/T3		0 2113
CC82-2V3B	0 0475	480	T2	R	*230 3/63 1 (N=5)		15 1											
CC82-2V3BT	0 312	40	O	N?				337 0/78 2	6 6/17 4 (N=6)	20-O	1 1							
CC82-1V1	0 1815	500	T2	N	*97 0/0 8 (N=6)		16 9											
CC82-1V2	0 536	40	O	?	346 1/74 7 (N=8)	10-O	0 9											
CC82-1V2T	0 2734	500	T2	R	313 6/76 9 (N=8)	200-O	2 6		*112 4/43 4 (N=8)		16							
CC82-2V3	0 148	40	S1	N				150 1/82 3	20 3/32 4 (N=7)	5-O	4 7							
CC82-6	0 467	40	O	?	340 4/64 8 (N=8)	10-O	1 5											
CC82-3	0 131	40	S1	N				173 0/79 6	18 6/36 6 (N=6)	20-O	3 9							
CC82-5	0 418	40	O	?	350 0/67 4 (N=8)	10-O	1 2											
CC83-1V2	0 193	40	O/S1	N?				350 6/77 8	9 0/15 7 (N=7)	15-O	2 3							
CC83-1V1	0 133	40	O/S1	N?				348 6/79 2	9 2/17 2 (N=4)	30-O	2 3							
CC83-1V1T	0 0582	500	O	?	22 1/70 1 (N=6)	200-O	11 5											
CC83-2	0 091	40	O	?	23 6/72 8 (N=9)	5-O	7 5											
CC83-3	0 077	40	S2	N				322 0/79 0	5 0/20 0 (N=9)		@8 1							
CC83-3X	0 0198	470	T3	R	*239 5/65 7 (N=4)		33					0 99	25 27		180 0/-9 0	T	T3	0 1031	
CC83-4	0 315	40	O	?	332 5/70 1 (N=7)	15-O	1 5											
CC83-5	0 215	40	O	?	20 2/75 1 (N=9)	5-O	1 4											
CC83-5T	0 0703	470	T3	R	8 6/73 1 (N=4)	400-O	5 2		*278 1/29 2 (N=9)		11 4							
CC83-6	0 2	40	O/S1	N?				356 7/77 6	10 2/15 1 (N=9)	5-O	2 4							
CC83-1	0 071	40	S2	N				139 9/88 8	15 1/27 7 (N=9)	5-O	13 6							
CC85-A	0 0119	40	S2	?				114 0/16 5	99 5/11 0 (N=6)	20-O	7 1							
CC85-3V2	0 024	40	S2	N				224 4/56 1	353 0/64 0 (N=8)		@11 6							
CC85-2V4	0 189	40	S3	N				211 2/58 2	10 0/66 0 (N=7)		@14							
CC85-2V1X	0 037	50	T2	R	*111 3/4 3 (N=7)		28 6											
CC85-1V1	0 008	35	S2	R				329 0/-29 0	283 0/-45 0 (N=12)		@5 7							
CC85-1V1X	0 008	35	T2	R	*16 3/2 6 (N=12)		14 1					0 98	1 111	-22 5 (2 5)	MIXED		S2/T2/T3	0 0237	
CC85-2V1/2	0 077	30	T3	R	*215 6/39 0 (N=5)		28 3											
CC85-3V2X	0 046	15	T2	N	*109 6/18 9 (N=3)		1 1											
CC85-3V3	0 005	15	T2	N	*16 9/46 2 (N=4)		12											
CC85-1V2	0 021	50	E	?														
CC85-1V4	0 025	50	S2	N				143 8/71 2	44 0/43 0 (N=11)		@10 3							
CC85-2V2	0 026	40	T3	R	*331 5/48 1 (N=5)		21 3											
CC85A-1V1	0 007	5	T3	R	*252 8/14 9 (N=3)		0 1							-20 0 (2 5)	180 0/-90 0	T	T3	0 0079	
CC85A-2V2	0 009	35	T3	R														
CC86-A	0 0133	40	T3	R/N?	*307 6/36 2 (N=9)		29 3											
CC86-AX	0 00692	40	S2	N				152 8/44 9	81 7/24 2 (N=9)	5-O	11 4			-23 35 (8 05)	9 5/40 7	1	S2	0 0112	
CC86-B	0 00725	40	S2	N				258 1/78 6	9 5/40 7 (N=10)	0-O	11 2							
CC86-1V3	0 024	40	S3	N				190 1/52 8	43 7/70 3 (N=9)	5-O	24 2							
CC87-A	0 00947	40	T2	N	*211 9/16 5 (N=8)		10 2											
CC87-AX	0 0146	40	S2	N				117 5/37 8	81 7/24 2 (N=10)	0-O	5 7							
CC87-B	0 0125	40	S2	N				145 6/37 5	91 5/45 1 (N=6)	20-O	8 3							

CC87-3V2	0 036	45	S3	N				260 9/70 5	359 0/43 0 (N=10)		@13 6							
CC87-3V4	0 025	45	S2	N				188 1/70 2	30 0/54 0 (N=8)		@8 8							
CC87-4V2	0 022	45	S2	N				335 5/76 2	11 0/25 0 (N=9)		@5 5	0 95	1 588	-25 0 (2 5)	11 0/25 0	4	S2	0 0178	
CC87-4V5	0 011	40	E	?															
CC87-2V3	0 0079	40	S3	N				273 0/78 4	8 0/38 0 (N=7)		@16 1							
CC87-2V1	0 029	45	S3	N				249 7/61 4	349 0/50 0 (N=4)		@11 5							
CC87-4V4	0 037	45	T3	N														
CC87-5V5	0 018	40	E	?														
CC88-A	0 00752	40	T2	R	*80 8/5 9 (N=9)		40 3											
CC88-B	0 00928	40	S2	N				246 9/75 0	7 0/44 7 (N=6)	20-O	7 6							
CC88-1V2	0 089	40	S1	N				340 1/82 1	16 0/29 0 (N=5)	25-O	5 3	0 99	13 7	-30 85 (5 2)	MIXED		S1/S2/T2/T3	0 0263	
CC88-1V3	0 024	40	T3	R	*157 4/58 4 (N=6)		19 6											
CC88-2V2	0 017	40	S2	N				191 0/85 9	23 0/39 0 (N=7)		@10 6							
CC88-1V4	0 13	40	S2	N				183 3/70 6	32 2/53 0 (N=9)	5-O	11 4							
CC89-2V2	0 055	40	S2	N				192 2/68 5	284 0/56 0 (N=9)		@4 9							
CC89-A	0 0455	40	S1	N				297 2/53 6	341 4/24 7 (N=5)	25-O	3							
CC89-B	0 1326	40	T3	R	*218 8/53 1 (N=9)		24 2											
CC89-1V3	0 158	40	O	?	357 7/29 9 (N=10)	0-O	4 9											
CC89-3V2	0 192	40	S1	N				188 8/87 2	22 8/37 7 (N=6)	10-O	5 3							
CC89-4V1	0 024	40	S2	N				287 1/76 1	5 0/35 0 (N=6)		@7 5							
CC89-3V3	0 105	40	O	?	351 9/51 6 (N=9)	5-O	3 5					0 99	13 7	-35 0 (5 2)	11 0/30 0	4	S1	@21 6	0 0764
CC89-1V1	0 083	40	S2	N				254 6/72 9	3 0/44 0 (N=9)		@10 4							
CC89-3V1	0 065	40	S3	N				351 8/68 6	11 0/16 0 (N=9)		@10 4							
CC89-2V3	0 048	40	O	?	18 1/63 8 (N=9)	5-O	8 4											
CC89	0 0173	25	S2	N				341 1/75 5	11 7/23 6 (N=5)	5-O	8 2							
CC89-1V2	0 198	40	S1	N				10 6/77 8	19 4/23 0 (N=8)	10-O	2 5							
CC89-1V2T	0 1334	490	S1	N				12 9/84 2	21 0/29 3 (N=6)	0-O	3 2							
CC90-A	0 00687	40	S1	N				135 7/69 5	48 2/43 5 (N=10)	0-O	4 7							
CC90-B	0 0734	40	S1	N				135 7/58 1	62 2/41 4 (N=10)	0-O	2 5							
CC90-2V3	0 056	40	S2	N				337 8/79 4	13 7/27 1 (N=7)	5-O	10 8							
CC90-2V1T	0 0397	470	T3	R	*267 5/55 5 (N=3)		0											
CC90-1V2	0 083	40	S1	N				25 4/82 4	22 5/27 4 (N=7)	15-O	4 2							
CC90-2V2	0 056	40	S2	N				316 7/70 1	2 0/25 0 (N=9)		@6 5							
CC90-1V3	0 15	40	S1	N				59 7/70 2	34 6/18 7 (N=4)	20-O	2							
CC90-1V4	0 091	40	S2	N				269 6/80 6	10 9/38 1 (N=9)	5-O	8 8							
CC90-1V1	0 108	40	O	?	22 8/60 7 (N=7)	10-O	9 5					0 99	3 588	-35 0 (4 35)	20 0/39 0	7	S1	@20 8	0 0577
CC90-2V4	0 046	40	S1	N				244 9/51 5	333 9/55 3 (N=4)	20-O	5 6							
CC90-4	0 096	40	S3	N				254 0/60 1	345 6/48 5 (N=8)	5-40	17 1							
CC90-5	0 027	40	S2	N				141 2/75 4	39 0/41 0 (N=9)		@4 4							
CC90-2	0 121	40	S1	N				298 2/65 2	353 5/28 9 (N=8)	10-O	3 2							
CC90-7	0 065	40	S1	N				288 7/17 1	358 9/33 9 (N=10)	0-O	5 8							
CC90-3	0 055	40	S3	N				333 0/75 9	10 3/25 2 (N=9)	5-O	17 4							
CC90-1	0 049	40	S3	N				274 6/66 5	352 9/38 6 (N=9)	5-O	15 5							
CC90-9	0 078	40	T2	N	*134 1/35 6 (N=9)		29 1											
CC90-8	0 033	40	S3	N				223 2/76 9	15 1/47 0 (N=9)	5-O	19 3							
CC91-1V1	0 346	40	S1/O	N?				304 3/46 9	337 6/17 4 (N=7)	5-O	1			-2 5 (0)	337 6/17 4	1	S1?		0 1794
CC91-1V3	0 093	40	O	?	2 8/69 4 (N=4)	20-O	5 7												
CC92-1V1	0 132	40	S1	N				182 3/47 0	67 6/71 0 (N=7)	5-O	3 4							
CC92-1V3	0 147	40	S1	N				336 3/72 2	8 4/21 8 (N=7)	5-O	4 2							
CC92-1V1X	0 482	40	S1	N				63 9/69	36 6/18 5 (N=6)	10-O	3 1	0 99	18 87	-25 85 (6 3)	36 6/18 5	1	S1		0 1812
CC92-1V4	0 042	40	T3	N	*290 7/41 7 (N=7)		35 9												
CC92-1V4T	0 2895	510	T3	N	*243 1/19 6 (N=3)		0												
CC92-2V3	0 311	40	O	?	47 7/60 7 (N=8)	0-O	3 6												
CC93-1V1	0 036	40	O	?	36 2/62 3 (N=8)	0-O	12 5												
CC93-1V1T	0 24	490	O	?	56 4/58 6 (N=6)	450-O	2 5					1	23 83	-2 5 (9 0)	OVERPRINT				0 1303
CC93-1V2	0 256	40	O	?	29 7/66 7 (N=4)	200-O	5 3												
CC94-3V2	0 09	40	S2	N				339 5/74 1	10 4/22 7 (N=7)	5-O	8 5	1	8 979	-11 65 (1 45)	353 9/39 8	1	S2		0 0972
CC94-1V1	0 105	40	S2	N				271 5/67 3	353 9/39 8 (N=8)	0-O	7 2							
CC95-1V1T	0 0799	490	S2	N				334 0/70 3	6 5/20 8 (N=6)	0-O	7							
CC95-3V3	0 172	40	S1/O	N				354 3/72 8	13 6/19 5 (N=6)	10-O	2 6	1	6 288	-15 0 (13 25)	8 3/30 3	1	S2		0 1543
CC95-2V3	0 185	40	S2	N				317 6/74 0	8 3/30 3 (N=7)	0-40	3 3							
CC95-2V2	0 223	40	T3	R	23 1/67 1 (N=7)	5-O	4		*285 1/28 7 (N=7)		22 3							
CC96-2V2	0 103	40	S1	N				263 4/63 4	349 2/43 5 (N=7)	5-O	5							
CC96-1V3	0 56	40	S2	N				74 1/59 5	46 4/13 8 (N=7)	20-O	6							
CC96-1V1	0 371	40	S2	N				187 6/69 3	30 8/54 8 (N=7)	5-O	12 7							

CC96-1V1T	0 1987	490	T2	N/R?	*186 1/74 8 (N=5)		20 8					1	6 288	-37 5 (2 5)	34 3/59 4	1	S1		0 2815
CC96-1V2	0 171	40	S1	N				25 3/75 1	23 1/20 1 (N=7)	5-O	4								
CC96-2V1A	0 306	40	O	?	48 7/61 2 (N=7)	5-O	2 6												
CC96-2V1	0 63	40	S1	N				187 5/64 3	34 3/59 4 (N=7)	5-O	1 9								
CC97-1V1	0 352	40	S2	N				19 6/64 3	21 5/23 8 (N=7)	5-O	12 3								
CC97-2V2T	0 0963	490	S1	N				288 7/75 6	4 4/34 6 (N=6)	0-O	3 9	0 98	9 35	-25 85 (12 35)	4 4/34 6	1	S1		0 2079
CC97-1V3	0 265	40	S1	N				261 6/74 7	4 3/41 5 (N=4)	5-O	5								
CC98-1V4	0 145	40	S2	N				37 1/72 9	26 6/18 4 (N=6)	10-O	6								
CC98-1V1	0 41	40	S1	N				322 9/65 8	359 9/20 5 (N=4)	20-O	2 6								
CC98-2V2	0 187	40	S1	N				38 3/70 4	27 6/16 1 (N=5)	15-O	2 8								
CC98-1V2	0 194	40	S1	N				150 6/66 4	49 2/46 9 (N=7)	5-O	3 5	1	7 853	-11 65 (20 8)	359 9/20 5	1	S1		0 2143
CC98-2V4	0 461	40	O	?	0 0/69 4 (N=8)	0-O	2 8												
CC98-3V2	0 272	40	S2	N				289 7/59 8	346 2/30 8 (N=5)	10-O	8 7								
CC98-3V2T	0 0487	470	S2	N				113 6/79 4	34 9/34 6 (N=5)	0-O	6 4								
CC98-1V3	0 338	40	O	?	17 7/70 1 (N=8)	0-O	2 6												
CC99-1V2	0 15	40	O	?	54 5/54 8 (N=4)	20-O	3 5												
CC99-4	0 117	40	S2	N				23 5/75 6	22 4/20 6 (N=9)	5-O	6 4								
CC99-4T	0 0561	480	S1	N				51 1/74 1	30 2/20 8 (N=6)	200-O	4 8								
CC99-2	0 345	40	S1	N				73 9/55 2	49 2/10 5 (N=7)	15-O	1 5								
CC99-2T	0 1792	500	S2	N				73 8/57 4	47 1/12 1 (N=8)	200-O	7 4								
CC99-5	0 057	40	S2	N				251 5/68 7	358 2/46 7 (N=8)	10-O	6 8			-6 65 (5 2)	22 0/27 0	11	S1/S2	@16 2	0 0984
CC99-6	0 084	40	S2	N				73 1/73 7	35 8/24 0 (N=9)	5-O	5 9								
CC99-1	0 178	40	S1	N				55 0/72 4	32 1/19 8 (N=8)	10-O	4 6								
CC99-3	0 104	40	S2	N				65 9/81 6	28 6/28 8 (N=9)	5-O	6 6								
CC99-3T	0 058	470	S3	N				88 0/77 0	33 0/14 5 (N=5)		@14 5								
CC99-1V1	0 104	40	S2	N				23 2/72 2	22 4/17 2 (N=7)	5-O	6 8								
CC99-X	0 032	40	S2	N				246 4/46 0	324 0/55 0 (N=7)		@7								
CC100-1V3	0 277	40	S1	N				350 0/78 9	15 5/25 4 (N=7)	5-O	2 9								
CC100-1V4	0 0726	490	S1	N				303 4/84 1	15 0/33 6 (N=5)	0-O	4 2			-1 65 (2 9)	13 0/28 0	3	S1/S2	@8 8	0 1868
CC100-1V2	0 324	40	S2	N				330 1/75 4	9 3/25 3 (N=7)	5-O	7 3								
CC101-1V2	0 265	40	S1	N				309 2/78 2	8 9/30 8 (N=4)	20-O	3 5								
CC101-1V2T	0 1734	490	S1	N				123 3/73 2	42 7/36 5 (N=5)	400-O	2 6	0 97	2 171	-12 5 (13 25)	23 0/36 0	3	S1	@22 9	0 2413
CC101-1V3	0 576	40	S1	N				236 0/85 0	18 4/39 1 (N=7)	5-O	2 4								
CC101-1V4	0 128	40	O	?	*27 0/57 5 (N=4)	20-O	5 2												
CC102-1V3	0 144	40	S1	N				83 0/68 9	42 0/23 1 (N=6)	10-O	4 3								
CC102-1V4	0 252	40	S1	N				256 7/61 4	347 1/46 9 (N=5)	15-O	5 2								
CC102-2V1	0 247	40	S1	N				284 6/74 2	2 6/35 5 (N=7)	5-O	4 3			-15 0 (11 45)	11 0/37 0	5	S1	@15 5	0 2494
CC102-2V3	0 325	40	S1	N				248 4/77 0	9 1/43 3 (N=4)	20-O	1 2								
CC102-1V1	0 331	40	S1	N				310 7/74 8	5 5/29 0 (N=5)	15-O	1 5								
CC103-1V3	0 107	40	S1	N				132 7/67 7	49 5/39 6 (N=4)	20-O	2								
CC103-2V2	0 221	40	S1	N				83 0/61 7	47 9/18 5 (N=4)	20-O	1 8								
CC103-2V2T	0 07	490	T2	R	*133 9/8 3 (N=4)		4 2					1	4 61	-9 15 (5 2)	MIXED		S1/T2/T1		0 2236
CC103-2V3	0 551	40	T1	N/R?	*96 8/16 9 (N=6)		11 1												
CC103-3V2	0 613	40	S1	N				278 6/51 4	334 6/34 5 (N=4)	20-O	3 3								
CC104-1V3	0 599	40	S1	N				32 2/80 9	23 8/26 0 (N=8)	0-O	3 5								
CC104-2V3	0 141	40	S1	N				348 4/80 5	16 1/26 9 (N=7)	5-O	3 2	1	8 875		19 0/29 0	3	S1	@8 7	0 2487
CC104-2V3T	0 1821	510	S1	N				305 0/85 3	16 5/33 8 (N=7)	0-O	4 5								
CC105-1V2	0 608	40	S1	N				331 3/77 2	11 0/26 4 (N=7)	5-O	2								
CC105-2V1	0 799	40	S1	N				306 5/67 6	357 6/26 9 (N=5)	15-O	2 8								
CC105-2V1T	0 4601	510	S2	N				20 8/79 6	21 8/24 6 (N=7)	0-O	6 4								
CC105-2V2	0 308	40	S1	N				7 9/78 3	18 9/23 6 (N=7)	5-O	3	0 99	15 04	-1 65 (2 9)	16 0/25 0	5	S1	@7 9	0 6123
CC105-3V2	0 962	40	S1	N				26 5/74 3	23 3/19 3 (N=4)	20-O	2 4								
CC105-2V3	0 608	40	S1	N				19 6/81 4	21 6/26 4 (N=5)	15-O	0 9								
CC105-2V1A	0 801	40	S1	N				26 2/78 7	22 9/23 7 (N=5)	15-O	1 8								
CC106-4	0 267	40	S1	N				354 5/74 7	14 5/21 2 (N=6)	20-O	1 7								
CC106-1	0 311	40	S1	N				341 9/79 6	14 5/26 8 (N=4)	25-O	3 8								
CC106-7A	0 53	40	S1	N				339 6/82 1	15 9/29 0 (N=8)	10-O	1 4								
CC106-8	0 686	40	S1	N				356 1/81 0	17 6/26 8 (N=6)	20-O	1								
CC106-8T	0 2249	510	S1	N				357 9/78 3	16 8/24 2 (N=10)	0-O	3 4								
CC106-9	0 351	40	S1	N				27 4/80 3	23 0/26 3 (N=5)	25-O	3 6								
CC106-5	0 225	40	S1	N				337 6/81 2	15 0/28 5 (N=6)	20-O	2 5								
CC106-2	0 45	40	S1	N				17 2/80 3	21 1/25 3 (N=9)	5-O	1 9	0 99	26 36	-4 15 (5 2)	17 0/26 0	13	S1	@2 5	0 3204
CC106-2T	0 182	510	S1	N				3 8/79 9	18 5/25 3 (N=8)	0-O	3 3								
CC106-6	0 641	40	S1	N				350 4/74 6	13 4/25 2 (N=6)	20-O	0 8								
CC106-7	0 491	40	S1	N				8 6/76 3	18 6/21 6 (N=8)	10-O	1 5								

CC106-7T	0 2437	510	S1	N				311 5/80 5	11 5/31 4 (N=9)	200-O	4 9							
CC106-3	0 344	40	S1	N				35 4/74 3	25 8/19 7 (N=7)	15-O	1 6							
CC106-1V2	0 663	40	S1/O	N				16 8/70 3	20 2/15 4 (N=6)	0-O	1 5							
CC106-1V1	0 05	40	S2	N				136 2/68 2	48 7/41 1 (N=5)	15-O	6 8							
CC107-7	0 355	40	S 1	N				20 3/77 3	21 6/22 3 (N=6)	15-O	1 2							
CC107-9	0 385	40	S1	N				355 3/79 7	16 9/25 7 (N=6)	20-O	0 7							
CC107-4	0 412	40	S1	N				344 3/77 0	13 3/24 4 (N=8)	10-O	1 1							
CC107-3	0 421	40	S1	N				0 5/76 8	16 8/22 6 (N=8)	10-O	0 7							
CC107-1	0 429	40	S1	N				355 3/80 4	17 2/26 3 (N=8)	10-O	3 6							
CC107-10	0 275	40	S1	N				9 4/76 2	18 8/21 5 (N=9)	5-O	2 5							
CC107-10T	0 2369	510	S1	N				348 6/80 6	16 2/27 0 (N=8)	200-O	3							
CC107-8	0 188	40	S1	N				0 3/82 8	19 0/28 3 (N=6)	20-O	2 2	0 98	9 568		19 0/26 0	13	S1	@3 6	0 0731
CC107-6	0 413	40	S1	N				10 4/78 6	19 5/23 8 (N=7)	15-O	1 4							
CC107-10A	0 422	40	S1	N				357 0/80 0	17 3/25 8 (N=8)	10-O	1 4							
CC107-2	0 109	40	S1	N				217 9/82 9	19 4/41 8 (N=7)	15-O	3 5							
CC107-2T	0 0531	470	S3	N				203 0/48 0	22 0/47 0 (N=5)		@12 1							
CC107-5	0 467	40	S1	N				10 4/73 2	18 5/18 5 (N=7)	15-O	1 1							
CC107-5T	0 2714	500	T2	N	9 4/72 4 (N=8)	200-O	3 8		*116 7/25 7 (N=6)		37 5							
CC107-1V2	0 617	40	S1	N				71 9/85 5	26 1/32 0 (N=7)	5-O	3 5							
CC108-1V3	0 157	40	S2	N				78 3/77 5	33 7/27 5 (N=6)	5-O	6 9							
CC108-4V2	0 028	40	S3	N				28 7/78 9	23 4/24 0 (N=7)	5-O	13 8							
CC108-1V2	0 069	40	S1	N				45 8/78 9	26 9/24 7 (N=5)	15-O	4 2							
CC108-1V1	0 157	40	S2	N				264 8/79 8	10 3/39 1 (N=6)	10-O	6 7			-2 5 (7 5)	24 0/36 0	4	S1/S2	@12 7	0 0731
CC108-3V2	0 078	40	S2	N				131 2/83 9	29 2/36 8 (N=7)	5-O	7 4							
CC108-4V1	0 05	40	S1	N				238 7/81 1	14 9/41 9 (N=4)	20-O	4 2							
CC108-3V1	0 06	40	T3	R	*293 3/34 5 (N=6)		13											
CC109-1V3	0 131	40	S1	N				286 9/80 6	10 5/35 3 (N=7)	15-O	3 7							
CC109-2V2T	0 0518	510	S3	N				232 0/71 0	7 0/50 0 (N=4)		@11 4	0 99	6 773		10 5/35 3	1	S1		0 1202
CC109-1V1	0 256	40	S1	N				306 4/55 6	346 1/21 0 (N=9)	5-O	3 8							
CC110-1V3	0 082	40	S2	N				81 5/82 2	29 8/30 8 (N=9)	5-O	7 4							
CC110-1V4	0 073	40	S1	N				266 2/81 0	11 6/38 5 (N=8)	0-O	5 4			-17 5 (15 6)	18 0/39 0	3	S1/S2	@17 7	0 836
CC110-3V3	0 141	40	O	?	0 6/67 9 (N=7)	5-O	2 7												
CC110-2V1	0 058	40	S2	N				234 8/76 0	11 1/46 3 (N=4)	25-40	3							
CC111-2V2	0 143	40	S1	N				314 9/72 2	4 6/27 2 (N=7)	5-O	4 4							
CC111-2V2T	0 0592	510	S3	N				278 8/60 9	345 9/36 3 (N=6)	400-O	14 2	0 99	3 674	-7 5 (4 35)	4 6/27 2	1	S1		0 0864
CC111-1V2	0 106	40	S2	N				321 9/66 2	0 0/21 1 (N=7)	5-O	7 4							
CC111-1V3	0 062	40	S3	N				283 1/66 4	353 0/35 2 (N=9)	5-O	14 3							
CC112-1V1	0 127	40	S1	N				286 0/64 6	351 1/33 7 (N=7)	5-O	4 6							
CC112-1V2	0 249	40	S1	N				142 7/62 4	56 0/44 6 (N=8)	0-O	2 1							
CC112-1V2T	0 158	490	S1	N				133 7/56 6	64 1/40 2 (N=8)	0-O	4 2							
CC112-1V4	0 096	40	S1	N				98 8/61 9	52 3/24 7 (N=5)	15-O	2 6							
CC112-2V2B	0 148	40	S1	N				203 6/74 0	21 3/51 0 (N=5)	15-O	5 1	0 98	1 542	-5 0 (5 0)	34 0/45 0	9	S1	@16 6	0 1513
CC112-1V2X	0 249	40	S1	N				142 7/62 4	56 0/44 6 (N=8)	0-O	2 1							
CC112-1V4	0 096	40	S1	N				97 3/63 9	50 0/25 0 (N=8)	0-O	4 9							
CC112-3V3	0 188	40	S1	N				212 2/71 6	16 7/53 0 (N=3)	30-O	5 7							
CC112-2V2	0 13	40	S1	N				252 9/54 9	338 0/50 0 (N=5)	15-O	4 1							
CC113-3V2	0 051	40	S2	N				37 0/76 2	25 8/44 6 (N=7)	5-O	9 9							
CC113-1V4	0 1	40	S1	N				294 2/43 0	330 2/21 6 (N=8)	0-O	4 3							
CC113-1V3	0 063	40	S1	N				302 3/78 9	9 0/32 3 (N=8)	0-O	5 2	1	3 638	-8 35 (3 8)	9 0/37 0	4	S1/S2	@20 8	0 0805
CC113-2V2	0 11	40	S1	N				289 1/68 6	356 1/33 3 (N=8)	0-O	5 4							
CC113-1V1T	0 0954	470	T2	N	*93 5/25 2 (N=5)		10 6											
CC114-X	0 228	40	S1	N				260 7/53 1	334 8/45 6 (N=8)	0-O	3							
CC114-3V1	0 394	40	S2	N				219 6/46 5	335 4/73 0 (N=6)	5-40	6 1							
CC114-2V2	0 331	40	S1	N?				94 5/49 1	62 5/15 8 (N=7)	5-O	3 1	1	6 359	-4 15 (3 8)	334 8/45 6	1	S1		0 3065
CC114-1V2	0 231	40	S1	N				286 9/49 5	334 4/28 9 (N=7)	5-O	3 1							
CC114-2V1	0 394	40	S1	N?				98 1/45 5	67 0/15 7 (N=8)	0-O	3							
CC115-A	0 22	40	S1	N				355 4/81 5	17 7/27 4 (N=10)	0-O	2 2							
CC115-B	0 329	40	S1	N				334 5/74 4	9 5/23 8 (N=9)	5-O	4 5							
CC115-C	0 243	40	S1	N				327 5/78 9	11 8/28 1 (N=6)	0-O	2	0 99	14 78	-25 0 (4 35)	11 0/25 0	5	S1	@3 4	0 1911
CC115-2V2	0 154	40	S1	N				323 6/74 2	7 1/25 8 (N=6)	10-O	4 3							
CC115-2V4	0 32	40	S1	N				325 4/75 1	8 2/26 0 (N=8)	0-O	1 8							
CC115-2V1	0 0562	510	S3	N				342 8/73 4	10 8/21 6 (N=6)	400-O	11 8							
CC116-1V2/3	0 29	40	S1	N				87 8/64 3	47 2/21 8 (N=7)	5-O	4 3							
CC116-1V1	0 728	40	S1	N				342 6/72 1	10 0/20 6 (N=4)	20-O	1	0 96	8 879	-8 35 (5 2)	MIXED				0 3282
CC116-1V1T	0 327	510	T3	R	*283 2/1 9 (N=11)		25 9												

CC116-1V1/2	0 168	40	S1	N				139 2/76 7	37 5/40 1 (N=8)	0-O	3 1							
CC117-1V2	0 204	40	S1	N				358 4/73 6	15 1/19 8 (N=5)	15-O	1							
CC117-1V3	0 343	40	O	?				239 0/63 7	355 4/53 5 (N=8)	0-O	1 7	0 97	3 032	-7 5 (9 0)	15 1/19 8	1	S1	0 1677
CC117-1V3T	0 0813	490	S2	N				246 2/48 7	325 0/56 6 (N=8)	400-O	7 3							
CC117-1V4	0 139	40	S1	N				89 7/52 3	27 9/15 3 (N=7)	5-O	3 2							
CC118-1V2	0 777	40	S1/O	N?				4 1/68 8	15 4/14 6 (N=6)	10-O	1 2							
CC118-3V4	0 152	40	S1	N				317 8/69 2	1 5/24 2 (N=7)	5-O	4 2							
CC118-3V4T	0 0575	490	S3	N				238 2/71 2	5 1/49 1 (N=9)	200-O	12 7							
CC118-2V3	0 058	40	S2	N				232 0/85 3	19 0/39 0 (N=9)		@6 8							
CC118-1V4	0 064	40	S2	N				324 8/75 8	8 7/26 6 (N=9)	5-O	7 8	1	3 082	-30 0 (0)	13 0/40 0	8	S1/S2	@13 6	0 129
CC118-1V3	0 058	40	S2	N				29 2/82 9	23 0/28 0 (N=9)		@7 5							
CC118-1V1	0 465	40	S1	N				292 1/76 6	5 8/33 9 (N=4)	30-O	5 5							
CC118-2V5	0 066	40	S1	N				196 4/47 6	38 5/76 7 (N=4)	20-O	4 1							
CC118-4V5	0 093	40	S1	N				203 8/76 5	20 9/55 5 (N=6)	10-O	4 3							
CC118-4V4	0 305	40	S2	N				300 8/76 5	6 2/31 9 (N=5)	10-O	6 5							
CC119-3V3	0 296	40	S1	N				324 5/75 3	8 2/26 3 (N=5)	15-O	1 8							
CC119-2V2	0 892	40	S1	N				330 4/82 7	15 4/30 3 (N=5)	10-O	3 3							
CC119-2V2T	0 1434	470	T2	N	*150 0/48 6 (N=6)		22 8											
CC119-2V4	0 672	40	S1	N				0 3/81 6	18 5/ 27 1 (N=4)	20-O	2 6							
CC119-2V4	0 1285	400	S2	N				30 8/76 1	24 3/21 3 (N=6)	400-O	9 7							
CC119-4V3	0 828	40	S1/O	N?				57 8/65 9	36 3/14 6 (N=5)	10-O	3 4							
CC119-2V3	1 003	40	S1	N				44 8/83 2	25 0/28 7 (N=7)	5-O	5 5	0 97	2 04	-6 65 (7 65)	19 0/28 0	7	S1	@7 0	0 309
CC119-1V1X	0 0794	40	S1	N				239 2/81 6	14 2/41 5 (N=5)	20-O	4 3							
CC119-1V3	1 195	40	S1	N				23 1/81 0	22 2/26 0 (N=5)	15-O	2 6							
CC119-1V2X	0 088	40	S2	N				225 2/70 1	9 2/52 7 (N=5)	15-O	7 3							
CC119-1V1	0 699	40	S1	N				43 4/72 1	28 8/18 1 (N=8)	0-O	2 4							
CC119-2V1T	0 1033	470	T1	N	*139 6/36 3 (N=5)		17 6											
CC119-3V2	0 143	40	S1/O	N?				354 1/70 8	12 7/17 7 (N=4)	20-O	1 9							
CC120-1V4	0 031	40	S2	N				278 1/78 2	7 6/37 0 (N=3)	30-O	9 1							
CC120-2V3T	0 19	470	S1	N				246 5/72 1	3 8/46 5 (N=7)	200-O	3	0 99	5 067	-9 15 (1 45)	8 0/44 0	3	S1/S2	@10 4	0 0944
CC120-2V4	0 143	40	S1	N				226 0/75 7	13 4/47 8 (N=6)	10-O	3 1							
CC121-A	0 254	40	S1	N				264 9/66 9	353 8/42 4 (N=10)	0-O	3 5							
CC121-2V1	0 166	40	S1	N				107 4/81 0	32 8/33 8 (N=6)	10-O	5							
CC121-3V1	0 234	40	S1	N				28 7/79 8	23 3/24 9 (N=7)	5-O	2 4			-27 5 (4 35)	16 0/33 0	5	S1	@1 5	0 1673
CC121-4V1	0 024	40	S2	N				233 0/70 0	6 0/51 0 (N=7)		@5 7							
CC121-3V3	0 181	40	S1	N				34 1/73 1	25 7/18 4 (N=5)	15-O	3							
CC121-1V1	0 511	40	S1	N				332 1/70 4	6 0/21 3 (N=7)	5-O	3 1							
CC122-2V3	0 356	40	S1	N				255 8/60 5	346 0/47 5 (N=7)	5-O	5 9							
CC122-2V3T	0 0614	470	O	?	14 7/66 3 (N=7)	200-O	6 3											
CC122-4V1	0 117	40	S1/O	N?				25 0/71 3	23 0/16 3 (N=5)	15-O	4 9	0 97	1 406	-11 65 (1 45)				
CC122-1V4	0 324	40	S1	N				347 2/75 9	13 3/23 1 (N=8)	0-O	3							
CC122-3V3	0 0385	40	S3	N				211 5/64 3	13 8/23 1 (N=7)	5-O	13 2							
CC122-3V1	0 281	40	S1	N				8 6/78 9	19 4/24 2 (N=7)	5-O	2 9							
CC123-2V1	0 096	40	S3	N				334 5/81 4	14 8/29 0 (N=7)	5-O	11 6							
CC123-2V3	0 126	40	T2	N	*65 4/24 0 (N=5)		22 4					0 94	1 426	0 0 (2 5)	20 8/38 6	1	S1		0 1059
CC123-1V1	0 16	40	S1	N				216 6/86 3	20 8/38 6 (N=5)	15-O	3 9							
CC123-3V4	0 065	30	S2	N				310 5/85 6	17 0/33 5 (N=8)	0-O	9 4							
CC124-4V1	0 0091	40	T2	R	*224 8/17 3 (N=3)		O											
CC124-1V3	0 0112	40	T3	R	*198 9/31 6 (N=4)		19 2											
CC124-4V2	0 054	40	S2	N				252 7/46 2	324 4/50 5 (N=7)	5-O	8 7							
CC124-2V1	0 07	40	S3/T2	R	*155 0/12 8 (N=9)		23 3	69 0/-2 1	85 7/-35 4 (N=7)	10-40	14 2							
CC124-1V1	0 086	40	T1	R	*105 7/29 8 (N=8)		23 1											
CC124-1V2	0 034	40	S3	N				206 9/69 7	19 0/55 2 (N=7)	5-O	21 6	0 98	6 686	-6 65 (6 3)	MIXED				0 0329
CC124-2V2	0 024	40	S3	N				189 0/52 0	47 0/71 0 (N=6)		@12							
CC124-3V3	0 117	40	S1	N				277 1/75 1	3 7/37 5 (N=6)	10-O	5 3							
CC124-3V2	0 114	40	E	?														
CC124-4V3	0 014	40	T3	R	*302 1/54 7 (N=7)		30 7											
CC124-4V3T	0 00969	400	E	?														
CC125-3V3	0 769	40	S1	N				209 4/82 0	20 6/42 9 (N=7)	10-O	1 8							
CC125-1V1	0 278	40	S1	N				27 8/77 1	23 4/22 0 (N=7)	10-O	1 9							
CC125-1V1T	0 0848	470	S2	N				18 2/76 9	21 1/21 9 (N=6)	0-O	5 7							
CC125-4V1	0 551	40	T3	R	*165 5/63 4 (N=7)		31 5					0 99	20 46	-5 0 (4 35)	25 0/26 0	5	S1/S2	@14 7	0 3094
CC125-1V3	0 539	40	S2/O	N?				45 8/70 5	30 1/16 9 (N=7)	10-O	9 2							
CC125-1V3T	0 1416	470	S2	N				346 8/76 1	13 3/23 3 (N=6)	0-O	7 1							
CC125-1V2T	0 3559	480	S2	N				80 6/61 9	47 0/17 7 (N=6)	400-O	6 5							

CC126-4V1	0 556	40	S1	N				301 8/52 2	341 5/21 6 (N=5)	20-O	5 2							
CC126-5V2	0 618	40	S1	N				193 0/83 7	23 3/41 2 (N=7)	10-O	3							
CC126-5V2T	0 1433	480	S1	N				233 2/84 3	18 2/39 8 (N=8)	0-O	4 8							
CC126-2V1	0 143	40	O	?	34 0/66 8 (N=8)													
CC126-6V1	0 253	40	S1	N				300 9/56 7	345 5/24 2 (N=7)	5-O	5 6	0 96	18 77	-9 15 (5 2)	6 0/32 0	5	S1/S2	@20 2	0 1181
CC126-3V1	0 099	40	S3	N				345 3/74 2	11 9/21 9 (N=8)	10-O	13 6								
CC126-1V2	0 102	40	S3	N				129 3/75 1	40 2/38 1 (N=8)	10-O	14								
CC126-1V2T	0 01289	470	S3	N				55 0/79 0	28 0/26 0 (N=5)		@11								
CC126-3V2	0 068	40	S3	N				317 1/80 8	12 3/30 7 (N=8)	10-O	15 4								
CC126-2V2T	0 0336	470	S2	N				39 0/79 0	25 0/25 0 (N=5)	450-O	9 3								
CC127-3V1	1 04	40	S1	N				223 8/74 4	13 2/49 2 (N=6)	10-O	3 3								
CC127-1V2	0 415	40	S1	N				39 9/77 7	26 1/23 2 (N=7)	5-O	2	1	16 46	-7 5 (4 35)	13 2/49 0	1	S1,		0 5019
CC127-2V3	0 293	40	O	?	77 2/57 3 (N=7)	5-O	2 7												
CC128-1V1	0 18	40	O	?	1 2/68 2 (N=5)	15-O	2 4												
CC128-1V3	0 393	40	S1	N				182 6/82 0	25 6/42 5 (N=7)	5-O	3 8			-1 65 (3 8)	25 6/42 5	1	S1		0 0966
CC128-1V3T	0 0352	470	E	?															
CC128-3V3	0 035	40	S2	N				319 3/64 7	358 0/21 0 (N=6)	10-O	8 7								
CC129-1V1	0 082	40	S3	N				348 2/76 7	12 2/26 4 (N=9)	5-O	15 6								
CC129-1V1T	0 0296	480	S2	N				40 4/86 3	21 6/34 0 (N=9)	200-O	10 8								
CC129-2V2	0 115	40	O	?	1 7/67 3 (N=9)	5-O	6 4					1	19 55	-8 35 (26 25)	7 4/42 2	1	S1		0 0927
CC129-2V2T	0 0568	480	S2	N				321 0/74 6	4 9/29 1 (N=5)	400-O	10 1								
CC129-2V3	0 01	40	S2	N				132 7/70 6	44 9/43 0 (N=9)	5-O	9 5								
CC129-2V3T	0 0809	480	S3	N				138 2/67 7	48 3/45 3 (N=7)	200-O	12 2								
CC129-1V4	0 459	40	S1	N				262 5/79 5	7 4/42 2 (N=7)	5-O	5								
CC130-3V2	0 039	40	S3	N				342 5/83 9	15 6/33 1 (N=9)	5-O	27 6								
CC130-3V3	0 065	40	S3	N				273 6/80 7	342 6/40 3 (N=8)	10-O	13 2	0 98	3 312	-9 15 (12 6)	342 6/40 3	1	S3		0 024
CC130-1V3	0 032	40	S3	N				252 6/80 7	9 9/43 2 (N=7)	5-O	20 1								
CC130-1V3T	0 00407	400	E	?															
CC131-A	0 0265	40	S1	N				152 9/66 0	48 4/51 3 (N=10)	0-O	3 7								
CC131-B	0 0114	40	T2	N	*134 0/25 8 (N=9)		21												
CC131-2V1X	0 062	40	S2	N				330 7/80 8	13 5/31 9 (N=8)	10-O	9 8								
CC131-4V2	0 056	40	S2	N				331 9/73 7	6 5/26 3 (N=9)	5-O	10 4								
CC131-1V1	0 064	40	S2	N				327 4/85 4	15 1/35 1 (N=9)	5-O	6 6	0 95	2 861	-27 5 (2 5)	48 4/51 3	1	S1		0 0354
CC131-5V2	0 064	40	S2	N				180 7/73 8	28 8/53 0 (N=9)	5-O	11 9								
CC131-5V2T	0 01065	470	E	?															
CC131-2V1	0 054	40	S2	N				337 0/81 9	13 5/31 9 (N=8)	10-O	9 8								
CC132-2V1	0 0287	470	S2	N				297 4/67 2	353 0/31 9 (N=5)	200-O	6 7			-0 85 (11 55)	353 0/31 9	1	S2		0 0287
CC133-3V4	0 023	40	S3	N?				32 4/81 9	22 0/30 1 (N=6)	5-O	21 7								
CC133-2V3	0 024	40	S3	N				327 2/63 8	358 0/20 0 (N=5)		@11 7	0 94	1 918	-5 85 (2 9)	358 0/20 0	1	S3		0 018
CC133-2V3T	0 00799	450	E	?															
CC133-1V5	0 024	40	T3	R?	*244 0/47 2 (N=9)		34 4												
CC134-1V4	0 05	40	S3	N				184 4/71 0	29 0/56 0 (N=7)		@14 1	0 92	1 207	-2 5 (2 5)	29 0/59 0	1	S3		0 0332
CC134-3V4	0 022	40	E	N?															
CC135-1V1	0 034	40	S3	N				276 4/72 8	358 0/40 0 (N=9)		@13								
CC135-2V1	0 058	40	S2	N				349 1/69 6	9 0/20 0 (N=6)		@4 4	0 95	1 871	-8 35 (11 25)	17 1/57 1	1	S2		0 0399
CC135-2V1T	0 0313	470	S2	N				204 8/70 8	17 1/57 1 (N=5)	0-O	5 7								
CC135-2V2	0 041	40	S3	N				225 7/86 3	17 7/41 3 (N=8)	5-O	13 4								
CC136-1V2	0 132	40	S1	N				97 2/69 7	43 3/31 1 (N=7)	5-O	4								
CC136-1V5	0 054	40	S3	N				176 7/74 3	30 0/52 0 (N=7)		@15 6	0 98	0 993	+0 85 (3 8)	43 3/31 1	1	S1		0 0351
CC136-1V5	0 0031	460	E	?															
CC136-1V1	0 069	40	T3	N															
CC137-1V2	0 017	40	E	?															
CC137-1V1	0 015	40	E	?								1	0 879		20 0/60 0	1	S3		0 12
CC137-2V3	0 012	40	S3	N				200 0/68 0	20 0/60 0 (N=9)		@13 4								
CC138-1V3	0 016	40	E	?															
CC138-2V1	0 082	40	E	?								0 89	0 931	-4 15 (2 9)	348 0/29 0	1	S2		0 0307
CC138-6V4	0 022	40	S2	N				299 1/62 0	348 0/29 0 (N=9)		@10 2								
CC139-3V2	0 09	40	S1	N				221 5/71 7	3 0/52 9 (N=5)	20-O	2 9								
CC139-1V2	0 078	40	S2	N				192 7/87 3	16 2/39 7 (N=9)	5-O	7 6								
CC139-1V2T	0 0138	480	S2	N				193 0/69 0	18 0/58 0 (N=5)		@11 5								
CC139-5V3	0 038	40	S3	N				221 8/65 3	356 0/57 9 (N=10)	0-O	14 5								
CC139-2V2	0 096	40	S3	N				213 6/87 0	14 8/39 9 (N=8)	5-O	13 3								
CC139-2V3	0 062	40	S2	N				318 6/76 5	3 0/29 0 (N=8)		@8 3	0 92	3 565	-8 35 (12 35)	3 0/52 9	1	S1		0 0353
CC139-1V3	0 032	40	S3	N				335 8/81 7	9 8/30 5 (N=9)	5-O	14								
CC139-4V3	0 056	40	S2	N				228 7/73 6	2 3/50 1 (N=9)	5-O	13 4								

CC139-4V3T	0 00484	470	E	?														
CC139-3V4	0 054	40	S3	N				194 9/79 7	16 3/47 3	5-O	14 5							
CC139-3V4T	0 0129	470	E	?														
CC139-2V4	0 028	40	S3	N				69 7/69 3	34 1/23 3 (N=8)	5-O	19 9							
CC140-2V2	0 234	40	S1	N				211 0/77 3	11 0/49 2 (N=7)	15-O	2 7							
CC140-1V3	0 364	40	S2	N				182 7/82 0	18 6/44 8 (N=8)	5-O	6							
CC140-2V3	0 232	40	S1	N				207 5/81 8	13 7/45 0 (N=7)	10-O	2 8							
CC140-3V3	0 314	40	S1	N				197 9/79 8	15 5/47 2 (N=8)	5-O	3 8							
CC140-4V3	0 225	40	S1	N				202 0/70 5	12 4/57 2 (N=6)	15-O	2 6							
CC140-1V1	0 078	40	S2	N				185 1/85 6	17 1/41 3 (N=8)	5-O	6 4							
CC140-6V3	0 165	40	S1	N				201 6/69 7	12 4/57 2 (N=6)	15-O	4 7							
CC140-3V4	0 185	40	S2	N				201 6/83 3	15 1/43 7 (N=8)	10-O	8							
CC140-2V2	0 192	40	S1	N				212 3/79 9	11 9/46 6 (N=8)	5-O	4 3	0 97	8 212	-2 5 (11 45)	12 0/49 0	11	S1	0 1815
CC140-5V4	0 174	40	S1	N				175 8/79 4	21 3/46 8 (N=7)	15-O	3 7							
CC140-5V4	0 045	510	S2	N				200 0/64 0	12 0/63 0 (N=8)		@7 4							
CC140-4V2	0 194	40	S1	N				306 3/87 0	12 5/35 9 (N=8)	5-O	4							
CC140-3V2	0 265	40	S1	N				218 0/70 7	3 7/54 4 (N=6)	15-O	3 3							
CC140-1V5	0 087	40	S2	N				313 9/86 3	12 0/35 2 (N=8)	5-O	6 7							
CC140-2V4	0 182	40	S1	N				196 1/78 1	15 9/48 9 (N=7)	15-O	4 9							
CC140-3V5	0 301	40	S2	N				167 4/70 3	31 7/53 4 (N=7)	10-O	8 3							
CC140-4V5	0 224	40	S1	N				229 7/68 5	356 0/53 5 (N=7)	10-O	5 7							
CC140-1V4	0 166	40	S2	N				278 5/67 7	348 0/36 6 (N=7)	15-O	8 5							
CC141-4V3	0 021	40	E/T3	R?														
CC141-1V1X	0 021	40	S1	N				17 9/76 0	16 5/23 0 (N=7)	5-O	2 8	0 94	1 712		16 5/23 0	1	S1	0 0349
CC141-1V1	0 021	40	S3	N?				278 2/62 5	341 7/35 7 (N=7)	5-O	22							
CC141-3V1	0 161	40	T3	R	*102 2/10 1 (N=7)		15 5											
CC142-1V1	0 0304	40	S3	N				225 0/55 7	339 0/63 0 (N=4)		@12 6							
CC142-1V1T	0 00623	470	E	?								0 89	1 397		26 2/52 1	1	S2	0 0191
CC142-2V1	0 0366	40	S2	N				173 8/73 3	26 2/52 1 (N=6)	15-O	9 9							
CC143-2V5	0 075	40	O	?	3 9/65 9 (N=7)	5-O	4 8											
CC143-1V2	0 156	40	S1	N				344 4/72 4	6 2/21 6 (N=7)	5-O	1 8							
CC143-1V4	0 16	40	S1/O	N				0 1/68 5	10 0/16 2 (N=7)	5-O	1	0 99	2 182	-12 5 (17 3)	6 2/21 6	1	S1	0 1059
CC143-1V3	0 073	40	S2	N				343 1/74 4	6 8/27 1 (N=7)	5-O	8 1							
CC143-1V5	0 073	40	S2	N				350 4/75 3	9 1/23 5 (N=8)	0-O	8 5							
CC143-1V1	0 141	40	S1	N				16 1/75 4	16 0/22 4 (N=5)	15-O	2 1							
CC144-1V3	0 028	40	T3	R	*327 1/65 9 (N=7)		0 4											
CC144-1V3T	0 00882	470	E	R?														
CC144-2V4	0 1	40	T3	R	*108 3/14 0 (N=7)		14 8											
CC144-3V4	0 065	40	T3	R	*111 4/21 3 (N=6)		7 5							-5 0 (6 6)	180 0/-9 0	T	T1/T3	0 0307
CC144-3V4T	0 011	470	E	R?														
CC144-2V1	0 08	40	S2	N				351 9/73 2	8 7/21 4 (N=7)	5-O	11							
CC144-2V1T	0 0184	470	T1	R	*279 3/36 7 (N=4)		12 9											
CC145-4V3B	0 106	40	S1	N				353 6/80 4	11 9/28 1 (N=6)	10-O	5 3							
CC145-1V4	0 149	35	S2	N				0 6/83 2	13 9/30 4 (N=8)	5-O	8 3							
CC145-1V4T	0 0939	510	S1	N				331 9/82 4	9 8/31 3 (N=7)	0-O	5 5							
CC145-2V3	0 221	35	S1	N				358 5/76 9	11 7/24 4 (N=9)	0-O	4 8							
CC145-1V3	0 126	35	S1	N				1 1/77 5	12 5/24 9 (N=8)	5-O	4 3	1	3 877	-3 35 (1 45)	13 0/27 0	8	S1	@3 3	0 1079
CC145-1AV3	0 163	35	S1	N				350 2/80 0	11 1/27 9 (N=8)	5-O	3 8							
CC145-1V2	0 084	35	S1	N				20 0/85 1	16 4/32 1 (N=6)	15-O	3 5							
CC145-3V2	0 074	35	S1	N				16 0/71 5	16 0/18 5 (N=8)	5-O	4 7							
CC145-X	0 048	35	S2	N				277 6/79 3	2 6/37 8 (N=8)	5-O	6							
CC145-4V3	0 106	40	S1	N				353 6/80 5	11 9/28 1 (N=6)	10-O	5 4							
CC146-1V1	0 514	40	T3	R	*227 3/64 1 (N=7)		19 8											
CC146-3V2	0 144	40	S2	N				350 8/79 1	10 8/27 0 (N=9)	5-O	5 9							
CC146-3V2T	0 055	480	S2	N				315 3/75 5	1 5/29 0 (N=7)	200-O	10 5							
CC146-4V2	0 143	40	S1	N				352 4/72 5	8 6/20 7 (N=9)	5-O	5 4	0 97	6 152	-5 85 (2 9)	MIXED			0 1136
CC146-4V2T	0 0527	480	S2	N				337 1/68 3	1 8/19 2 (N=6)	400-O	10 8							
CC146-2V2	0 153	40	T3	R	*205 0/58 5 (N=6)		11 6											
CC146-2V2T	0 052	480	T2	R	*203 6/66 4 (N=7)		19											
CC160-3V3	0 0423	40	T3	R?	*309 0/44 9 (N=7)		24 8											
CC160-1V6	0 069	40	T3	R	31 0/62 1 (N=7)	0-O	14 6		*121 0/66 1 (N=4)		9 3							
CC160-2V3	0 0342	40	S3	N?				285 7/56 5	335 8/21 1 (N=8)	5-40	26 8							
CC160-2V3T	0 00455	470	E	?														
CC160-2V4	0 0364	40	S3	N				271 2/81 1	2 0/29 3 (N=9)	5-O	15 6	0 96	3 332	-6 65 (3 8)	180 0/-90 0	T	T3	0 0275
CC160-2V5	0 0367	40	T3	R	*140 1/51 2 (N=6)		19											

CC160-2V5T	0 0192	470	T3	R															
CC160-5V3	0 0368	40	S2	N				282 3/75 8	356 0/27 0 (N=7)		@5 6								
CC160-3V4	0 0423	40	T3	R?															
CC160-3V4T	0 01343	480	E	?															
CC161-5V3	0 0718	40	T3	R	*125 2/69 9 (N=6)		17 9												
CC161-3V4	0 0533	40	S3	N				339 8/78 9	5 8/18 5 (N=7)	10-O	15 1								
CC161-3V1	0 0683	40	S2	N				329 8/80 5	5 2/20 8 (N=7)	10-O	11 2								
CC161-3V1	0 0299	470	T2	R	*266 8/25 8 (N=4)		23 5					0 98	3 332	-9 15 (5 2)	180 0/-9 0	T	T2		0 0537
CC161-4V4	0 0219	40	S2	N				147 1/68 8	32 0/41 6 (N=7)	10-O	12 2								
CC161-2V3	0 1193	40	S3	N				247 8/87 1	349 4/38 2 (N=7)	10-O	12 7								
CC161-5V2	0 0631	40	T3	R?	328 2/70 2 (N=7)	5-O	5 9		*114 8/55 6 (N=9)		19 4								
CC162-A	0 0182	40	S2	N				27 3/79 2	15 0/17 4 (N=10)	0-O	9 7				10 2/30 4	1	S1		0 0195
CC162-B	0 0208	40	S1	N				224 2/87 1	10 2/30 4 (N=5)	25-O	4								
CC163-1V3	0 8598	40	O	?	48 7/58 2 (N=7)	10-O	1 4												
CC163-3V2	0 1571	40	O	?	10 2/68 3 (N=8)	0-O	5 7												
CC163-3V2A	0 2147	40	O	?	10 2/71 5 (N=8)	0-O	4 6												
CC163-5V1	0 2537	40	S1	N				315 8/80 1	3 1/2 2 (N=7)	10-O	4 3								
CC163-3V2	0 2709	40	O	?	53 3/58 1 (N=8)	10-O	3 7												
CC163-2V1	0 1202	40	S2	N				349 5/82 7	9 0/21 2 (N=5)	25-O	2 4								
CC163-3V1	0 1167	40	S2	N				241 4/68 4	350 5/40 4 (N=6)	20-O	8								
CC163-1V4	0 9644	40	O	?	43 6/59 8 (N=7)	15-O	1 4												
CC163-1V4T	0 4509	510	T2	R	*302 1/0 4 (N=8)		13 1					0 98	2 92	-9 15 (13 75)	189 0/-56 0		T1/T2/T3		0 1878
CC163-4V1	0 18227	40	S1	N				229 5/78 3	3 1/37 0 (N=8)	10-O	5 3								
CC163-2V1T	0 0676	500	T1	R	*268 1/1 7 (N=8)		11 3												
CC163-3V4	0 3764	40	O	N	14 5/74 4 (N=9)	5-O	2 8												
CC163-1V2	0 125	40	O	?	51 0/55 0 (N=9)	0-O	17 1												
CC163-2V4	0 0791	40	T2	R	*149 2/43 2 (N=8)		15 1												
CC163-1V1	0 0968	40	S2	N				336 7/77 0	4 2/17 2 (N=5)	25-O	6								
CC163-4V3	0 252	40	O	?	21 8/67 0 (N=10)	0-O	3 2												
CC163-4V3T	0 1432	480	T3	R	*251 6/7 0 (N=6)		40 3												
CC163-2V2	0 0818	40	S1	N				307 4/85 6	7 6/26 0 (N=5)	25-O	4 2								
CC163-2V3	0 0993	40	S2	N				330 5/86 2	9 2/25 1 (N=7)	15-O	5 7								
CC164-A	0 0111	40	S2	N?				166 5/42 5	59 9/65 0 (N=6)	20-O	13 5	0 89	1 894		59 9/65 0		S2		0 0111
CC165-1V1	0 1963	40	E	?															
CC165-4V2	0 0443	40	T2	R	*138 7/75 3 (N=11)		13 6												
CC165-4V2T	0 0282	510	T1	R	*60 6/24 5 (N=6)		34 8												
CC165-6V3	0 1493	40	O	?	23 8/64 8 (N=7)	15-O	3 4												
CC165-1V4	0 0623	40	S3	N				170 0/61 7	14 0/32 3 (N=10)	5-O	15 1								
CC165-1V4T	0 0187	470	T3	R	*206 7/61 6 (N=4)		30 7												
CC165-3V4	0 0749	40	O	?	18 7/54 1 (N=12)	0-O	13 7					0 99	12 66	-3 35 (5 2)	145 0/-15 0	1	T1/T2		0 086
CC165-2V4	0 044	40	S3	N				220 7/46 2	350 7/41 3 (N=8)	10-O	23 4								
CC165-4V4	0 0973	40	O	?	43 3/76 4 (N=7)	15-O	5 1												
CC165-5V3	0 0731	40	S1	N				266 1/46 2	321 5/30 4 (N=3)	35-O	2 6								
CC165-3V3	0 0386	40	T3	R	*113 7/15 4 (N=11)		32 7												
CC165-3V3	0 0224	480	E	?															
CC166-2V4	0 0326	40	S3	N				93 4/85 3	17 2/27 2 (N=8)	10-O	20 1								
CC166-1V4	0 0651	40	T2	R	*111 0/37 0 (N=10)		14 9					0 98	6 997	-5 85 (12 85)	180 0/-90 0	T	T2		0 0651
CC166-2V1	0 1067	40	O	?	12 8/76 5 (N=11)	2 5-O	16 4												
CC166-2V1T	0 0543	470	O	?	354 3/73 9 (N=6)	200-O	1 5												
CC167-P	0 0059	40	T2	R	*112 4/7 9 (N=5)		22 9								180 0/-90 0	T	T3		0 0059
CC168-K	0 0115	40	T3	R	*267 6/51 4 (N=9)		39 5					0 97	1 336		180 0/-90 0	T	T3		0 0115
CC169-A	0 0068	40	S2	N				301 2/73 1	356 7/21 0 (N=10)	0-O	14 2	0 86	1 856		356 7/21 0	1	S2		0 0068
CC171-3V4	0 0729	40	T3	R	25 7/64 0 (N=10)	0-O	7 4		*288 8/54 0 (N=3)		0								
CC171-3V1	0 0472	40	S2	N				237 7/33 8	305 3/52 0 (N=8)	10-O	10 2	0 98	1 838	-14 15 (15 9)	MIXED		S2/T3		0 0417
CC171-3V4	0 021	40	O	?	60 0/65 0 (N=8)		@10 8												
CC172-1V4	0 0315	40	S3	N				106 2/48 2	59 6/21 2 (N=9)	0-O	16 1								
CC172-1V4T	0 0199	470	E	?								0 84	2 682	-2 5 (9 0)	333 0/30 0	1	S2		0 0208
CC172-3V4	0 0143	40	S2	N				269 3/54 0	333 0/30 0 (N=4)		@10 2								
CC173-3V4T	0 0046	470	E	?															
CC173-4V2	0 0252	40	T3	R	*101 6/28 4 (N=5)		23 5												
CC173-4V2	0 00519	450	T3	R															0 0135
CC173-1V2	0 0283	40	S3	N				206 8/57 0	0 6/58 7 (N=8)	10-O	15 7	0 93	3 443	-12 5 (13 0)	180 0/-90 0	T	T3		
CC173-4V3	0 0239	40	S3	N				187 6/62 7	19 0/54 0 (N=5)	15-O	14 4								
CC173-3V3T	0 00938	450	T3	R	*258 2/13 5 (N=3)		0												
CC173-1V1	0 0209	40	T3	R	*222 3/26 4 (N=5)		17 7												

APPENDIX B

TABLE 1

Table 1 lists every horizon sampled at Scratchell's Bay and includes palaeomagnetic details of all the specimens studied. Sample code (SB), NRM intensity, maximum demagnetization level (mT or °C), reliability category (see section 5.8), magnetic polarity (N=normal, R=reverse, I=intermediate and ?=unknown), low coercivity component, high coercivity component (B.B.C.=before bedding correction, A.B.C.=after bedding correction), IRM ratio, saturation IRM intensity (S.IRM) and volume magnetic susceptibility are tabulated from left to right. Details of the demagnetisation range (either °C or mT) at which the magnetic polarity is best defined are also included. Where demagnetisation stable end points are identified, the direction of the ChRM before and after bedding correction is listed, together with the MAD or 95% confidence angle, which provides a measure of reliability. Where directional trends were observed, poles to the 'best fit' great circles were recorded, along with the MAD and number of demagnetisation vectors defining it. Great circle poles are indicated by an asterisk and can be found in both the low and high coercivity component columns.

This table should be read in conjunction with Figure 7.3 which displays graphically the magnetic polarity stratigraphy of the Scratchell's Bay section. The five columns on the right hand side of the table summarises the sample horizon's mean magnetic direction, the number of samples defining that direction, the general reliability category of the mean direction, the associated alpha 95 value or MAD and the mean NRM intensity (mA/m).

CODE	NRM mA/m	MAX TEMP AF LEVEL	RELIABILITY CATEGORY	POLARITY	LOW COERCIVITY COMPONENT OR TREND(*)	RANGE	MAD/ ALP 95	HIGH COERCIVITY COMPONENT B B C	HIGH COERCIVITY COMPONENT A B C	RANGE	MAD/ ALP 95	IRM RATIO	S IRM mA/m	VOLUME M S (S I UNITS) x10^-6	MEAN MAGNETIC DIRECTION	N	GENERAL RELIABILITY CATEGORY	MAD/ ALP 95	MEAN NRM mA/m
SB1-A	0 002	35	E	?															
SB1-B	0 002	5	E	?											?		E		0 002
SB1-C	0 002	5	E	?															
SB1-D	0 002	5	E	?															
SB2-2A	0 0262	25	T2	N	*54 8/34 6 (N=9)		35 8					0 8		-6 5 (15 0)	360 0/90 0	T	T2		0 0262
SB3-5	0 00377	30	E	?															
SB3-6	0 00192	30	T3	N								0 91	0 6411	-15 0 (2 5)	360 0/90 0	T	T2/T3		0 00264
SB3-4	0 00153	30	T2	N	*231 3/31 9 (N=6)		22 1												
SB3-2	0 0044	30	T3	N	*236 9/49 9 (N=5)		38 6												
SB4-A	0 00364	40	S2	R				339 9/-69 2	193 0/-57 0 (N=5)		@9 9								
SB4-B	0 00362	40	T2	R	*247 5/5 2 (N=7)		31 5												
SB4-C	0 00155	40	T3	R															
SB4-4	0 00484	30	T2	N	*93 7/13 4 (N=6)		25 8					0 89	0 6536	-10 0 (2 5)	193 0/-57	1	S2		0 00304
SB4-3	0 00129	30	E	?															
SB4-6	0 00335	30	T3	N	*262 7/27 4 (N=6)		13 7												
SB4-5	0 00239	30	T3	N	*231 3/20 9 (N=7)		28 8												
SB4-D	0 00718	40	T2	R	*47 4/25 9 (N=7)		12 3												
SB5-6A	0 0301	35	T3	R?	*167 0/7 5 N=7)		42 9												
SB5-1	0 0117	35	S2	N				111 3/38 2	67 0/37 3 (N=11)	5-O	10 4	0 071		-11 5 (10 0)	67 0/37 3	1	S2		0 021
SB5-2	0 0263	35	T1	N	*98 4/22 3 (N=8)		33 8												
SB6-A	0 00267	40	T2	N	*325 6/43 5 (N=8)		13 8		*261 5/23 9 (N=5)		14 7								
SB6-B	0 00271	40	T2	R	*298 0/48 5 (N=9)		35 8												
SB6-C	0 00338	40	T2	N	*29 1/12 9 (N=9)		34 7					0 91	0 4706	-10 0 (2 5)	360 0/90 0	T	T1/T2/T3		0 00291
SB6-1	0 00196	30	T3	N															
SB6-3	0 00214	30	E	?															
SB6-X	0 00591	40	T1	N	*70 6/30 8 (N=9)		30 3												
SB7-1A	0 0146	25	S2	N				80 9/46 2	47 0/21 0 (N=4)		@7 7								
SB7-4A	0 0176	25	S2	N				65 5/52 0	46 4/32 1 (N=4)	17 5-O	3 8								
SB7-1	0 0143	30	T2	R	*241 5/10 8 (N=7)		25 4					0 91	0 5993	16 0 (10 5)	46 4/32 1	1	S2		0 01297
SB7-5	0 01	25	T3	R?	*307 6/30 8 (N=9)		37 9												
SB7-2	0 01	25	S2	R??				15 4/6 2	21 4/-43 5 (N=10)	5-O	13 1								
SB8-A	0 00225	40	T2	N	*70 6/30 8 (N=9)		30 3												
SB8-C	0 00317	40	S2	N				209 7/56 5	323 0/63 0 (N=4)		@5 8				323 0/63 0	1	S2		0 00291
SB8-B	0 00257	40	T2	N	*231 3/18 1 (N=4)		0												
SB8-D	0 00392	40	T2	N	*39 2/7 5 (N=5)		13 5												
SB8A-A	0 00565	40	T2	N	*185 1/7 2 (N=5)		18 8								282 0/50 0	1	T2		0 00921
SB8A-B	0 015	40	T2	N	*57 5/31 8 (N=9)		24 5												
SB8B-A	0 0073	40	T2	R	*221 2/25 7 (N=9)		5 6												
SB8B-B	0 00887	40	T2	R	*222 1/19 9 (N=9)		5 7								180 0/-90 0	T	T2		0 00663
SB8B-C	0 00185	40	T2	R	*216 6/17 4 (N=6)		16 1												
SB8B-D	0 01612	40	T3	R	*215 0/8 1 (N=9)		19 4												
SB9-2A	0 0459	22 5	T1	R?	*70 3/26 3 (N=10)		23 5												
SB9-A	0 00512	40	T2	R	*215 0/21 8 (N=9)		5					0 86	1 877	-17 5 (4 5)	138 0/-46 0	1	T1/T2		0 00766
SB9-B	0 00191	40	T1	R	*212 3/21 7 (N=9)		3 5												
SB10-A	0 00366	40	T2	R	*211 5/12 3 (N=8)		13												
SB10-B	0 0326	40	S2	?											180 0/-90 0	T	T2		0 00403
SB10-C	0 00502	40	T2	R	*308 0/35 4 (N=5)		17 8												
SB10-D	0 00442	40	T3	R?															
SB11-5A	0 0282	22 5	T2	R	*102 6/41 6 (N=9)		24 5					0 96	1 288		180 0/-90 0	T	T2		0 0282
SB11A-A	0 0142	40	S2	N	2 5/70 5 (N=4)		3 1	306 1/86 3	356 3/35 8 (N=7)	15-O	15 3				356 3/25 8	1	S2		0 01233
SB11A-B	0 0107	40	O	?				200 4/25 1	239 4/68 5 (N=10)	0-O	18 8								
SB12-1	0 00396	20	S2	N				183 3/64 3	356 7/63 6 (N=5)	5-O	9 4								
SB12-2	0 00742	40	S3	N?								0 9	0 5566	-42 5 (11 0)	356 7/63 6	1	S2		0 00527
SB12-3	0 00497	40	S3	N?															
SB13-1-B	0 119	40	S1	N	20 9/52 3 (N=3)		2 3	72 7/61 7	30 1/25 5 (N=7)	15-O	5 7								
SB13-1-C	0 0891	40	S1	N	41 0/59 0 (N=5)		9 2	100 0/78 6	14 5/39 1 (N=6)	20-O	2 4	0 99	13 5	-30 0 (8 5)	16 0/37 0	4	S1	@13 3	0 1066
SB13-1-D	0 127	40	S1	N	53 0/54 4 (N=4)		9 7	90 5/80 8	11 7/37 5 (N=6)	15-O	2 4								
SB13-1	0 0959	40	S1	N	37 0/58 7 (N=4)		8 4	146 2/82 2	6 0/44 3 (N=7)	15-O	2 3								
SB14-15	0 0124	12 5	T3	N															
SB14-3	0 034	40	S2	N				90 7/78 7	14 7/37 2 (N=13)	2 5-O	23								

SB14-4	0 027	40	S2	N				38 1/74 5	10 5/25 3 (N=11)	5-O	17 2							
SB14-6	0 0454	40	S2	N				27 0/72 0	9 0/22 0 (N=14)		@3							
SB14-7	0 033	40	S2	N				340 8/70 8	353 4/19 7 (N=13)	0-O	16 3	0 99	0 9923	-27 5 (9 0)	7 0/28 0	7	S2	@10 1	0 01964
SB14-S1	0 0108	40	T2/T3	R?	*256 2/2 2 (N=3)		0 5											
SB14-S2	0 0142	40	S2	N	271 2/58 9 (N=3)	0-10	0 4	270 9/84 0	352 4/37 7 (N=8)	10-O	20 6							
SB14-1X	0 0117	40	S2	N	19 5/72 3 (N=3)	0-10	1 9	11 8/71 6	4 0/19 9 (N=8)	10-O	12 2							
SB14-1i	0 0137	40	T2	N	*272 8/42 4 (N=6)		13 8											
SB14-2i	0 0204	40	S2	N	12 3/65 8 (N=3)	0-10	4 3	26 6/66 3	28 6/33 0 (N=8)	10-O	15 2							
SB15-1	0 073	40	T1	N	*65 8/56 0 (N=10)		37 6											
SB15-10	0 0881	40	T2	N	*25 9/58 8 (N=13)		11 5											
SB15-1i	0 1554	40	T3	N	*149 7/52 8 (N=12)		26 4											
SB15-17	0 173	40	S2	N	334 1/73 5 (N=4)	5-12 5	5 7	144 9/67 5	22 4/54 6 (N=12)	12 5-O	11 7							
SB15-4	0 132	40	S2	N	309 8/62 7 (N=6)	0-12 5	9 7	150 8/67 3	19 9/56 4 (N=13)	12 5-O	14 4							
SB15-7	0 167	40	S2	N	325 6/47 5 (N=5)	0-10	9 9	141 7/64 1	28 6/55 5 (N=13)	12 5-O	11 7	1	6 176	-6 5 (6 0)	48 0/67 0	3	S1	@9 9	0 07814
SB15-8	0 0932	40	T2	N	*191 1/53 1 (N=12)		31											
SB15-S	0 152	40	S1	N	87 0/73 4 (N=5)	0-20	9 6	146 7/46 0	61 3/64 2 (N=6)	20-O	4 1							
SB15-2i	0 1117	40	T2	R?	*205 4/43 0 (N=8)		19 6											
SB15-2iT	0 01159	600	S2	N	303 8/-51 7 (N=3)	0-200	9 6	149 7/54 5	41 5/63 8 (N=6)	200-O	8							
SB15-1X	0 00742	40	S1	N	328 5/66 5 (N=4)	0-15	9 9	158 2/56 4	31 1/66 6 (N=7)	15-O	5 6							
SB15-2ii	0 0999	40	S1	N	310 0/71 6 (N=5)	0-20	10 1	156 4/50 3	49 7/68 1 (N=7)	20-O	5 2							
SB16-S2	0 127	40	S1	N	59 0/69 8 (N=4)	0-15	5 2	170 5/74 5	4 2/53 2 (N=7)	15-O	4 4							
SB16A-A	0 00791	40	E	?														
SB16A-B	0 0064	40	E	?														
SB16A-C	0 0265	40	S2	N	218 9/37 8 (N=4)	0-15	33 2	266 9/35 9	298 0/23 7 (N=5)	15-O	12 5							
SB16A-D	0 0199	40	S2	I?	120 0/14 9 (N=3)	0-15	17 7	134 1/-17 9	134 6/20 1 (N=6)	20-O	11 2							
SB16A-E	0 00492	40	E	?														
SB16-10i	0 174	40	S1	N	25 2/62 6 (N=3)	0-10	14 6	278 8/80 9	348 9/36 1 (N=8)	10-O	4 1							
SB16-11i	0 1188	40	S1	N	0 7/58 0 (N=4)	0-15	4 6	298 8/76 3	346 0/30 5 (N=7)	15-O	5 2							
SB16-1i	0 00551	600	S2	N	79 9/-78 0 (N=3)	0-200	8	309 1/83 3	353 8/33 6 (N=6)	200-O	11	0 99	10 86	-33 5 (3 0)	1 0/45 0	8	S1	@7 3	0 06395
SB16-2i	0 2408	40	S1	N	12 0/66 2 (N=4)	0-15	2 6	169 0/77 0	3 9/50 7 (N=7)	15-O	2 8							
SB16-8i	0 2385	40	S1	N	44 1/58 8 (N=4)	0-15	9 4	160 3/78 8	5 7/48 4 (N=7)	15-O	3							
SB16-9i	0 2808	40	S1	N	39 1/58 0 (N=4)	0-15	8 4	172 3/79 0	2 2/48 9 (N=7)	15-O	2 7							
SB16-12	0 2702	40	S1	N	39 9/58 8 (N=4)	0-15	5 1	127 0/77 7	13 8/44 6 (N=7)	15-O	2 5							
SB16-4	0 157	40	S2	N	35 8/69 9 (N=7)	2 5-17 5	9	176 5/66 4	2 9/61 5 (N=11)	17 5-O	17							
SB16-9	0 188	40	S2	N	48 7/64 0 (N=5)	0-12 5	8 4	178 2/78 7	0 5/49 3 (N=13)	12 5-O	11 5							
SB16-A	0 14	40	S3	N	23 3/67 7 (N=4)	5-12 5	7 9	184 4/72 5	357 7/55 4 (N=13)	12 5-O	19 3							
SB17-S	0 1462	20	S1	N	43 1/64 3 (N=6)	0-12 5	5 4	129 7/79 6	11 2/44 2 (N=4)	12 5-O	5 9							
SB17-S2	0 11	40	S1	N	329 6/50 0 (N=3)	0-10	11 9	28 6/85 0	2 9/33 6 (N=8)	10-O	4 4							
SB17-SX	0 0517	40	S2	N	331 5/44 8 (N=5)	0-20	14 1	331 9/80 9	1 6/26 4 (N=7)	15-O	9 4							
SB17-1i	0 0075	40	E/T3	N														
SB17-2i	0 1705	40	S1	N	304 0/59 5 (N=3)	0-10	6 2	218 0/73 1	343 8/50 6 (N=7)	15-O	5 6							
SB17-3i	0 1025	40	S1	N	3 0/71 6 (N=4)	0-15	4 4	214 3/71 2	342 7/52 4 (N=7)	15-O	3							
SB17-4i	0 0737	40	S1	N	313 5/65 8 (N=6)	0-25	7 1	220 9/62 2	327 6/55 3 (N=5)	25-O	5 6							
SB17-6i	0 0884	40	S1	N	322 4/63 4 (N=4)	0-15	9	234 5/69 8	6 4/44 3 (N=7)	15-O	3 4	0 95	6 689	-18 5 (16 5)	353 0/48 0	6	S1	@10 8	0 0657
SB17-6iT	0 1148	40	S1	N	42 0/68 9 (N=4)	0-15	10 3	144 4/82 1	4 0/44 1 (N=7)	15-O	5 5							
SB17-1	0 00814	600	T3	R	237 4/-72 9 (N=3)	0-200	3 3	163 7/78 3	5 0/49 1 (N=6)	200-O	10 1							
SB17-4	0 0848	40	S3	N	344 7/70 9 (N=6)	2 5-15	4 9	206 1/74 0	348 7/51 8 (N=12)	15-O	21 6							
SB17-12	0 109	40	S3	N	163 9/84 0 (N=7)	0-15	12 3	327 9/76 7	352 1/26 4 (N=14)	10-O	27 6							
SB17-6	0 06	40	S2	N				248 0/85 0	354 0/40 0 (N=17)		@6 1							
SB17-8	0 1	40	S2	N				217 3/81 0	352 3/45 0 (N=14)	7 5-O	9 8							
SB18-1i	0 111	40	S2	N	343 3/56 9 (N=4)	0-7 5	5 1	175 5/75 9	1 8/52 1 (N=13)	12 5-O	9 3							
SB18-2i	0 0242	40	S2	N	47 8/77 0 (N=3)	5-15	1 2	200 5/60 6	336 9/64 0 (N=7)	15-O	12 3							
SB18-3i	0 0131	40	S3	N	38 0/60 1 (N=3)	5-15	2 1	239 5/53 2	310 6/47 1 (N=6)	20-O	23 3							
SB18-A	0 01034	40	E	?														
SB18-B	0 0038	40	T3	N	*332 8/42 6 (N=7)		11 8					0 97	1 072	-41 0 (6 0)	MIXED		S2/T1/T2		0 01144
SB18-B	0 00198	40	T3	N														
SB18-A2	0 0155	40	T2	N	*216 7/46 3 (N=5)		8 2											
SB18-C	0 0331	40	T1	R	*256 5/16 9 (N=10)		13											
SB18-D	0 0232	40	S2	R	325 7/-56 5 (N=4)	2 5-10	5 8	121 0/-65 8	157 5/-23 3 (N=5)	20-O	16 3							
SB19-A	0 037	40	T2	R	*321 2/42 4 (N=6)		8 8											
SB19-B	0 037	40	T2	R	*270 1/11 0 (N=9)		5 7					1	2 313	-26 0 (10 0)	MIXED				0 03576
SB19-C	0 0334	40	S2	N				115 0/86 3	4 4/39 5 (N=8)	10-O	8 1							
SB20-A	0 0198	40	S2	N	235 8/84 4 (N=3)	0-10	6 8	89 0/81 0	4 2/28 4 (N=8)	10-O	9 1	0 98	2 103	-32 5 (0 0)	4 2/28 4	1	S2		0 02674
SB20-B	0 00361	40	T3	R	*73 6/25 0 (N=5)		24 2											
SB21-2-A	0 0272	40	S2	R	344 3/-24 2 (N=4)	0-15	11 8	358 1/-38 7	157 5/-78 8 (N=7)	15-O	12 7							

SB21-2-B	0 0051	40	S1	R	292 7/1 8 (N=4)	0-15	3 5	292 4/-5 8	272 7/-27 8 (N=7)	15-O	4 4	0 91	0 8495	-25 0 (4 5)	MIXED				0 00997
SB21-2-S	0 00938	40	S2	N	279 4/25 7 (N=3)	0-10	32 3	193 7/64 3	340 4/51 6 (N=6)	10-O	7 6								
SB21-2-8	0 0076	40	S3	N				136 5/48 8	37 7/54 5 (N=4)	5-O	8 4								
SBB22-1	0 01086	40	T3	R?	*190 3/56 2 (N=9)		14 8												
SB22-3i	0 0272	40	T2	R	*221 8/3 0 (N=7)		14 6												
SB22-12	0 0514	40	S2	N	320 0/-20 5 (N=11)	0-25	11 5	178 4/85 9	353 6/32 1 (N=8)	25-O	11 5				32 7/62 6	1	S2		0 01802
SB22-15	0 0272	40	S2	N				57 4/79 5	4 2/22 9 (N=4)	35-O	10 7								
SB22-1-3	0 0272	40	T2	R	*220 8/8 0 (N=7)		23												
SB22-1-4	0 0178	40	S2	N	78 5/3 5 (N=3)	2 5-10	3 5	149 0/47 2	32 7/62 6 (N=6)	10-O	7 2	0 92	0 7722	-22 5 (4 5)					
SB22-2B2	0 0203	40	S2	N				135 2/68 0	13 0/43 9 (N=9)	5-O	15 6								
SB22-2B	0 0354	40	S2	N				134 9/65 9	15 4/45 1 (N=6)	5-O	10 1								
SB22-2-C	0 0193	40	T2	R	*209 9/47 8 (N=8)		32 4								346 3/58 5	1	S1		0 01386
SB22-2	0 0267	40	S2	N	210 2/38 9 (N=3)	0-10	12 6	162 5/33 6	51 6/78 6 (N=8)	10-O	9 5								
SB22-M	0 0188	40	S1	N				181 8/59 0	346 3/58 5 (N=9)	5-O	5 6								
SB22-S	0 0102	40	S2	N	109 0/-4 0 (N=3)	0-10	1 8	178 6/60 1	349 7/57 7 (N=6)	20-O	9 1								
SB22A-1B	0 0059	12 5	T3	R															
SB22A-7B	0 0053	12 5	T3	R															
SB22A-EX	0 00244	17 5	S2	N	206 1/56 0 (N=3)	0-5	8 7	204 1/71 0	340 9/43 8 (N=6)	2 5-O	9 1								
SB22A-A	0 0146	40	T3	N	*76 3/52 3 (N=8)		17 2												
SB22A-B	0 00392	40	E	?															
SB22A-C	0 00411	40	T2	R	*275 1/29 7 (N=4)		11 5												
SB22A-D	0 0145	40	T2	R	*206 9/10 3 (N=9)		33 8					0 97	1 012	-36 0 (30 0)	MIXED		S2/T2		0 00937
SB22A-1i	0 025	40	S2	N				130 8/50 4	37 3/50 5 (N=9)	5-O	11 1								
SB22A-2i	0 0123	40	T2	N	*316 2/38 6 (N=5)		11 3												
SB22A-3i	0 0156	40	S2	N				118 0/39 6	54 6/42 8 (N=9)	15-O	9 1								
SB22A-3iT	0 00964	500	S3	N				123 0/61 0	25 0/43 0 (N=4)		@8 1								
SB22A-4i	0 0233	40	S2	N				122 3/59 2	27 5/43 1 (N=10)	0-O	11 2								
SB22A-5i	0 0153	40	T3	R?	*148 4/11 0 (N=5)		11												
SB22B-1	0 0202	40	E	?															
SB22B-2	0 0161	40	S2	R	16 7/-27 1 (N=6)	0-30	20 1	68 4/-22 4	97 9/-23 6 (N=4)	30-O	5 7								
SB22B-3	0 0203	40	E	?								0 91	0 7364	-6 5 (7 0)	98 0/-24 0	1	S2		0 01464
SB22B-4	0 0208	40	T2	R	*300 5/18 9 (N=6)		40 7												
SB22B-5	0 0049	40	E	?															
SB22i-15	0 0047	15	T2	R	*236 2/18 7 (N=5)		8												
SB22i-20	0 0109	15	T3/E	R?															
SB22i-EX	0 00122	15	E	?															
SB22i-B	0 0193	40	S2	N	81 4/-5 7 (N=4)	0-15	8 8	300 3/38 5	300 3/69 7 (N=6)		11 1	0 98	0 6089	-14 0 (7 5)	148 0/-9 0	1	S2		0 00727
SB22i-A	0 00978	40	E	?															
SB22i-4	0 0178	40	S2	R				117 0/-59 0	148 0/-9 0 (N=4)		@4 4								
SB22i	0 0051	15	E	?															
SB23-S	0 00149	40	E/T3	R															
SB23-M	0 00248	40	E	?															
SB23-1i	0 00516	40	E/T3	R															
SB23-1iB	0 00222	40	E	?															
SB23-2i	0 01028	40	E/T3	R															
SB23-2x	0 0041	40	T2	R	*37 2/8 9 (N=5)		22 2					0 89	0 4862	+0 85 (11 5)	249 0/-31 0	1	S2		0 00345
SB23-A2	0 00373	40	T2	R?	*194 0/28 5 (N=8)		25 9												
SB23-B2	0 00244	40	S2	R				287 0/-26 0	249 0/-31 0 (N=5)		@5 1								
SB23-C2	0 00418	40	T2	N/R?	*200 5/31 9 (N=9)		22 9												
SB23-D2	0 006	40	T2	R	*209 6/51 3 (N=9)		5 3												
SB23-3i	0 00389	40	T3	R	*188 1/61 3 (N=9)		33 5												
SB23-A	0 00181	20	T2	N	*231 8/18 2 (N=5)		22 1												
SB23A-S	0 00342	40	E	?															
SB23A-1i	0 00471	40	T2	R	*184 5/31 3 (N=8)		9 3					0 9	0 4334	-23 5 (1 5)	179 0/-60 0	1	T2/T3		0 00429
SB23A-1X	0 00285	40	T3	R	*202 4/28 7 (N=7)		23 5												
SB23A-2i	0 00736	40	T2	R	*211 5/26 2 (N=5)		6												
SB24-M	0 00781	40	T3	R															
SB24-1i	0 00589	40	S2/T3	N/R?	*149 6/16 5 (N=5)		39 9	112 5/52 1	38 0/39 0 (N=8)		@6 0								
SB24-A	0 00469	40	S2	N				107 1/25 0	70 1/30 8 (N=9)		11 4								
SB24-B	0 00489	40	T2	N/R?	*198 2/32 3 (N=8)		18 5					0 96	0 3118	-49 0 (6 5)	MIXED		S1/S2/T2/T3		0 01259
SB24-C	0 00901	40	S1	N				132 4/40 5	52 7/53 8 (N=5)		3 4								
SB24-D	0 00756	40	T2	N	*194 5/28 0 (N=5)		9 3												
SB24-2i	0 00337	40	T2	R	*160 3/13 3 (N=6)		25 1												
SB24A-S	0 00274	40	E	?															
SB24A-1i	0 00844	40	S3	N				120 7/66 2	19 0/40 0 (N=4)		@12								

SB24A-2i	0 00662	40	T2	R	*58 1/6 8 (N=5)		4 4					0 93	0 7181	-28 5 (3 0)	180 0/-90 0	T	T2		0 006413
SB24A-3i	0 00881	40	T2	R	*273 1/2 9 (N=5)		18 1												
SB24A-4i	0 00804	40	T2	R	*60 3/2 4 (N=5)		12 8												
SB25-1-E	0 0029	40	S3	N					354 0/36 0 (N=4)		@13 9	0 9	0 5884	-22 5 (5 0)	326 0/66 0	1	S2		0 00274
SB25-1i	0 00259	40	S2	N				192 0/48 0	326 0/66 0 (N=3)		@8 8								
SB25-2i	0 0086	40	T3	R	*182 5/29 8 (N=9)		22 2												
SB25-2-A	0 00118	40	E	?															
SB25-2-B	0 00451	40	T3	R?	*266 9/23 5 (N=6)		39 4					0 96	0 6365	-17 5 (9 0)	216 0/-56 0	1	T3/T3		0 0079
SB25-2-C	0 0206	40	T3	R?	*344 6/24 6 (N=6)		18												
SB25-2-D	0 00326	40	T2	R	*210 1/34 2 (N=6)		14 1												
SB25A-1	0 0068	40	T2	N	*14 7/2 8 (N=7)		24												
SB25A-CU	0 00512	40	E/T3	R?															
SB25A-2i	0 00342	40	E	?								0 93	0 6174	-33 5 (6 5)	86 9/62 9	1	S1		0 00611
SB25A-5i	0 0053	40	E	?															
SB25A-5iT	0 0094	500	E	?															
SB25A-6i	0 00874	40	S1	N/I?	128 0/58 9 (N=3)		21	142 4/32 4	86 9/62 9 (N=4)	25-O	5 7								
SB26-X	0 0102	40	S2	N				126 9/85 8	359 1/40 7 (N=6)	5-O	10 9								
SB26-XA	0 002	40	S2	R				312 0/-42 0	245 0/-57 0 (N=7)		@7 3	0 94	1 134	-5 0 (37 5)	245 0/-57 0	1	S2		0 00667
SB26-D	0 00752	40	T2	R	*224 3/19 6 (N=3)		0 6												
SB26-B	0 0129	40	T3	R?	*238 9/64 5 (N=11)		16 6												
SB28-A	0 00344	40	T3	R?	*237 1/10 9 (N=8)		26 1												
SB28-B	0 0035	40	T2	R	*68 7/30 5 (N=3)		0							-31 5 (12 5)	149 0/-14 0	1	T2/T3		0 00246
SB28-C	0 00123	40	E	?															
SB29-A	0 0147	40	T1	R	*222 2/1 9 (N=9)		15 7												
SB29-C	0 0177	40	T3	N/R?	*247 1/4 3 (N=3)		0												
SB29-B	0 0137	40	T2	R	*149 0/79 1 (N=6)		33 8					0 96	0 8148	-39 0 (12 5)	139 0/-24 0	5	T1/T2/T3	@26 5	0 01676
SB29-D	0 0273	40	T3	R	*199 4/31 9 (N=9)		7 9												
SB29-E	0 0136	40	E	?															
SB30-1-3	0 0043	12 5	E	?															
SB30-1-7	0 003	12 5	E	?								0 81		-34 0 (8 0)	180 0/-90 0	T	T2		0 00776
SB30-10	0 0102	35	T2	R	*265 9/22 1 (N=7)		21 6												
SB30-1-1	0 0276	35	E	?															
SB30-2-A	0 00105	40	E	?															
SB30-2-D	0 00113	40	T3	R?								0 86	0 5849	+60 0 (82 5)	180 0/-90 0	T	T2/T3		0 00287
SB30-2-B	0 00777	40	T2	R	*301 5/34 0 (N=9)		27 2												
SB30-2-C	0 00738	40	T2	R	*283 8/34 3 (N=6)		17 7												
SB30-M	0 00276	40	T2	R/I?	*0 6/53 1 (N=9)		38 5								180 0/-90 0	T	T2		0 01108
SB30-2i	0 00445	40	E	?															
SB31-D	0 014	40	T3	R?	*226 9/54 0 (N=5)		9 6												
SB31-F	0 0106	40	T2	R	*242 7/44 7 (N=6)		22 4												
SB31-A	0 00807	40	S2	N				263 1/58 0	316 1/32 4 (N=6)	0-25	5 3	0 94		-40 0 (6 5)	213 0/-41 0	1	T1/T2		0 00841
SB31-B	0 0049	40	T1	R	*139 3/18 7 (N=7)		31												
SB31-C	0 00718	40	T3	R?															
SB32-A	0 00328	40	T2	R	*265 9/70 6 (N=6)		29 4												
SB32-B	0 0026	20	T1	R	*132 8/10 6 (N=5)		17												
SB32-C	0 0107	40	T3	R								0 9	0 6031	-24 0 (12 0)	195 0/-65 0	1	T1		0 00596
SB32-D	0 0053	40	S2	R	185 1/52 6 (N=4)	0-15	11 9	290 2/7 3	286 8/-14 5 (N=5)	25-O	15 5								
SB32-E	0 0147	40	S2	R				297 9/-11 5	276 8/-32 9 (N=9)	5-O	7 3								
SB32-F	0 00629	40	T1	R	*256 4/11 2 (N=8)		34 9												
SB33-C	0 011	40	T3	R?	*176 4/51 8 (N=4)		14												
SB33-D	0 00247	40	T3	R															
SB33-A	0 0159	40	T1	R	*331 2/39 1 (N=9)		21 8												
SB33-B	0 0035	40	T2	R	*322 6/47 3 (N=8)		17 4					1	0 4902	-20 0 (5 0)	264 0/-26 0	1	T1/T2		0 00756
SBB33-C2	0 00393	40	T1	R	*252 6/6 1 (N=8)		25 3												
SB33-B2	0 0207	40	S2	N				8 3/73 6	359 0/22 0 (N=5)		@8 7								
SB33-A2	0 0114	40	T2	R	*335 4/26 5 (N=6)		19 5												
SB34-B	0 0021	40	E	?															
SB34-A	0 00607	40	T2	R	*118 8/39 1 (N=9)		24 4												
SB34-C	0 00421	40	T3	R	*305 5/44 3 (N=5)		32					0 92	0 5778	-25 0 (7 5)	196 0/-16 0	1	T2		0 00998
SB34-1	0 00415	40	T3	N/R?	*183 5/75 2 (N=10)		31												
SB34-F	0 0261	40	T2	R	*279 3/22 0 (N=7)		18 1												
SB34-D	0 027	40	T2	N/R	*148 3/47 1 (N=9)		12 4												
SB34-G2	0 0148	40	T3	R	*286 0/46 8 (N=4)		37 3												
SB34-G	0 0424	40	S2	N	124 7/25 0 (N=3)	0-10	17 3	97 8/24 9	71 7/24 7 (N=8)	10-O	7 6								
SB35-1i	0 00604	40	T1	R	*288 8/21 7 (N=7)		38 9												

SB35-2i	0 00359	40	T1	R	*110 9/38 4 (N=7)		25 5												
SB35-S	0 00218	40	E	?								0 89	0 6189	-32 5 (2 5)	206 0/-17 0	1	T1/T2		0 00344
SB35-A	0 00254	20	T3	R	*231 0/37 0 (N=7)		10 4												
SB35-B	0 004	20	T2	R	*119 8/10 2 (N=6)		19 1												
SB36-B	0 00406	40	E	?															
SB36-D	0 0127	40	T3	N/R	*168 7/36 0 (N=9)		32 1					0 9	0 4083	-50 0 (2 5)	MIXED				0 00758
SB36-A	0 0116	35	S2	N	349 7/6 6 (N=3)	5-15	10 3	356 3/78 1	355 3/26 1 (N=6)	15-O	7 5								
SB36-C	0 00552	40	S2	R	337 0/14 2 (N=4)	15-30	8 3	329 7/-41 4	247 1/-70 3 (N=4)	30-O	8 8								
SB37-A	0 00836	40	T2	R	*192 6/51 8 (N=7)		19 7					9 2	1 209	-23 5 (4 0)	196 0/-39 0	1	T2		0 00839
SB37-B	0 00843	40	T2	R	*275 2/12 8 (N=8)		30 7												
SB38-3	0 0113	40	T3	R	*193 3/23 7 (N=5)		23 4												
SB38-M	0 00576	40	T2	R	*38 0/40 7 (N=5)		33 1												
SB38-1i	0 01	40	T2	R	*56 1/13 8 (N=8)		16 5												
SB38-2i	0 00483	40	E	?								0 86	0 5794	-31 0 (5 0)	180 0/-90 0	T	T1/T2		0 00669
SB38-2iT	0 00608	500	T3	N/R	*258 8/38 5 (N=5)		14 6												
SB38-4i	0 00592	40	T2	R	*240 4/19 9 (N=9)		34 6												
SB38-5i	0 0053	40	T2	R	*243 9/31 0 (N=6)		18 5												
SB39-D	0 0137	40	T2	R	*84 7/72 8 (N=5)		27 6												
SB39-E	0 0122	40	T3	R															
SB39-A	0 00959	40	T3	R								0 85		-39 0 (4 0)	180 0/-90 0	T	T1/T2		0 00828
SB39-C	0 00538	40	T3	R															
SB39-D2	0 00404	35	T3	R	*265 7/70 7 (N=3)		0												
SB39-F	0 00928	35	T1	R	*282 0/62 0 (N=8)		19 3												
SB40-1	0 00679	30	T2	R	*236 3/34 3 (N=6)		14 2												
SB40-5	0 0145	30	S3	N															
SB40-2	0 00487	30	T1	R	*105 8/3 3 (N=9)		17 6												
SB40-3	0 0264	30	T3	R?	*157 7/24 7 (N=9)		14 1												
SB40-4	0 00645	30	T2	R	*257 3/37 5 (N=8)		18 5					0 99	0 387	+24 0 (8 0)	177 0/-32 0	1	T1/T2		0 00775
SB40-6	0 00605	30	T1	R	*100 1/49 9 (N=7)		37 4												
SB40-8A	0 00578	30	T2	R	*241 4/30 5 (N=7)		34 2												
SB40-7	0 00785	30	T2	R	*100 2/40 1 (N=7)		24 7												
SB40-8	0 00452	30	T2	R	*244 7/28 9 (N=7)		32 1												
SB41-1	0 0056	35	T1	R	*267 0/32 5 (N=7)		35 5												
SB41-5	0 00661	30	T2	N/R	*317 4/79 7 (N=7)		20 4					0 98	0 8689	-17 5 (4 5)	180 0/-90 0	T	T1/T2		0 00841
SB41-6	0 0185	30	E	?															
SB41-7	0 0073	35	T2	R	*283 9/66 4 (N=6)		28 9												
SB42-1	0 006	15	T1	R	*167 7/37 0 (N=7)		12												
SB42-7	0 0053	10	T3	R?	*79 3/6 8 (N=4)		20 3												
SB42-9	0 0054	20	T2	R	*264 5/44 1 (N=5)		13 2												
SB42-1A	0 0133	40	T3	R?	*126 7/52 6 (N=4)		5 7												
SB42-1C	0 00341	40	T3	R?	*45 0/12 3 (N=4)		5 4					1	0 603	-18 5 (4 0)	164 0/-52 0	1	T1		0 0071
SB42-B	0 0113	40	T1	R	*135 6/57 8 (N=6)		4												
SB42-C	0 00763	40	T1	R	*135 1/34 6 (N=5)		26 1												
SB42-1B	0 00916	40	T2	R	*142 7/64 5 (N=8)		18 5												
SB42-1E	0 0175	40	T2	R	*330 9/62 5 (N=5)		21 3												
SB42-SZ	0 00304	40	E	?															
SB42A-D	0 00685	40	T2	R	*178 9/74 0 (N=6)		25 5												
SB42A-A	0 0191	40	T2	R	*301 7/9 2 (N=8)		34 8												
SB42A-B	0 0271	40	O	?				131 8/11 7	107 6/43 5 (N=11)	0-O	14 9								
SB42A-C	0 0196	40	T1	R	*110 4/38 7 (N=9)		19 1					0 96	0 7291	-37 5 (0 0)	186 0/-16 0	1	T1/T2		0 01535
SB42A-E	0 0235	40	T3	R	*52 5/47 4 (N=5)		2 5												
SB42A-F	0 00802	40	T3	N/R?															
SB43-1	0 00687	40	T3	R	*254 6/63 4 (N=5)		25					0 9	0 7767	-24 0 (6 0)	201 0/-17 0	1	T1/T3		0 00837
SB43-2	0 0102	40	T1	R	*281 1/29 8 (N=7)		23 2												
SB44-B	0 0227	40	T2	R	*269 6/-11 8 (N=6)		7 4												
SB44-C	0 00481	40	S2	R				39 0/-41 0	108 0/-57 0 (N=4)		@8 7	0 93	1 413	-51 5 (12 5)	108 0/-57 0	1	S2		0 01007
SB44-D	0 0934	40	T2	R	*78 5/41 8 (N=7)		25 4												
SB44A-A	0 0189	40	T2	R	*115 2/7 1 (N=4)		3 9												
SB44A-B	0 0219	40	T3	R?	*297 2/8 3 (N=4)		12 8					0 91	1 108		180 0/-90 0	T	T1/T2		0 01616
SB44A-X	0 0102	40	T1	R	*304 4/20 7 (N=4)		2 7												
SB45-A	0 0207	40	S1	R				15 9/-62 3	153 9/-62 5 (N=6)	15-O	4 8	0 99	2 653						
SB45A-A	0 0112	40	T1	R	*95 9/40 4 (N=5)		17 2					0 78		-38 5 (7 5)	153 9/-62 5	1	S1		0 0207
SB45A-B	0 0093	40	T1	R	*262 4/22 7 (N=7)		31 1												
SB46-1B	0 00642	40	T2	R	*89 2/17 0 (N=7)		19 7												
SB46-D	0 0269	40	O	?	45 6/47 3 (N=10)	0-O	7 7												

SB46-D1	0 0278	40	T3	N/R	*288 6/81 5 (N=8)		24 7											
SB46-1C	0 0361	40	T1	R	*274 9/77 7 (N=9)		3 3											
SB46-SX	0 00545	40	T2	N/R	*101 5/0 6 (N=4)		12 9					0 95	0 7896	+12 5 (8 5)	242 3/-59 2	1	S2	0 01304
SB46-1	0 0142	40	T2	R	*105 3/19 9 (N=10)		26 8											
SB46-5	0 0078	40	S2	R	46 6/70 6 (N=7)	2 5-17 5	14 4	310 1/-40 6	242 3/-59 2 (N=4)	17 5-O	10 4							
SB46-7	0 008	40	T2	R	*128 6/73 1 (N=9)		34 3											
SB46A-A	0 00599	40	T2	N	*278 3/0 4 (N=6)		21 9											
SB46A-B	0 00627	40	S2	N				143 9/44 6	53 0/69 4 (N=9)	5-O	6 4				MIXED		S2/T2/T3	0 00518
SB46A-C	0 00355	40	T3	R														
SB46A-D	0 00541	40	T2	R	*176 1/2 0 (N=7)		10 4											
SB47-1i	0 00462	40	T1	R	*272 8/17 5 (N=4)		8 8											
SB47-2i	0 00939	40	T2	R	*141 1/18 5 (N=5)		6 9											
SB47-3i	0 00388	40	S2	R				327 0/-82 0	174 0/-45 0 (N=3)		@7 8							
SB47-5i	0 00163	40	E	?								0 92	0 6648	-26 0 (12 0)	174 0/-45 0	1	S2	0 00557
SB47-S	0 00362	40	S3	R				328 4/-73 5	180 0/-53 0 (N=4)		@18 5							
SB47-2	0 0172	20	T3	R														
SB47-6	0 0065	12 5	T1	R	*256 0/32 8 (N=5)		11 9											
SB47-8	0 0084	25	S2	R	46 5/43 0 (N=4)		4 3	59 2/-49 9	117 6/-40 6 (N=5)	17 5-O	10 8							
SB48-A	0 0076	35	E	?														
SB48-B	0 00936	35	T2	N	*282 0/12 4 (N=4)		30 3		*247 8/39 2 (N=4)		7 7							
SB48-A2	0 0139	40	S2	N				143 9/44 6	53 0/69 4 (N=9)	5--O	6 4							
SB48-B2	0 00867	40	S2/T2	N	*273 7/11 8 (N=5)		17 2					0 92	1 183	-48 5 (4 0)	MIXED		S2/T1/T2	0 01336
SB48-C2	0 00788	40	E	?														
SB48-D2	0 19	40	E	?														
SB48-1i	0 00594	40	T1	R	*197 6/44 8 (N=8)		21 3											
SB48A-1	0 00488	25	T3	R?	*354 6/5 3 (N=6)		38 8											
SB48A-2	0 0053	30	T3	R?								0 89	0 7246	-16 5 (1 5)	162 0/-38 0	1	S2	0 00393
SB48A-3	0 00497	30	T3	R	*264 6/40 0 (N=7)		22 4											
SB48A-4	0 00186	40	S2	R				82 0/-84 0	162 0/-38 0 (N=9)		@7 3							
SB49-13	0 0088	20	T2	R	*25 2/2 5 (N=6)		32 5											
SB49-7	0 0039	25	T2	R	*110 6/33 0 (N=9)		36 8											
SB49-1X	0 00582	40	T2	R														
SB49-1i	0 00188	40	T2	R	*78 3/4 5 (N=5)		21 8											
SB49-S1X	0 00272	40	E/T3	R								0 93	1 084	-33 5 (6 0)	167 0/-38 0	13	T2	@16 9 0 0047
SB49-S2	0 00367	40	E/T3	R														
SB49-S3	0 00358	40	T2	R	*227 3/14 9 (N=5)		24 6											
SB49-10	0 0088	10	T2	R	*285 9/51 0 (N=5)		23 1											
SB49-12	0 00616	12 5	T2	R	*101 5/20 5 (N=4)		3 7											
SB49-5	0 00721	12 5	T2	R	*114 1/51 7 (N=4)		25 2											
SB50-1	0 0209	40	S1	N				9 0/70 9	356 5/19 7 (N=9)	5-O	2 7							
SB50-3	0 067	40	O	?				339 7/64 4	345 5/12 8 (N=10)	0-O	2 7	0 98	1 048	-31 0 (6 5)	356 5/19 7	1	S1	0 02406
SB50-4	0 0105	40	S2	N				15 0/78 0	356 0/27 0 (N=9)		@8 0							
SB50-2	0 0228	40	T2	R?	*203 6/37 8 (N=5)		11 2											
SB50A-1i	0 0103	40	T2	R	*210 8/19 7 (N=5)		0 6											
SB50A-15	0 0062	12 5	T1	N/R	*205 3/23 0 (N=4)		7 4											
SB50A-S1	0 00449	40	E	?														
SB50A-S2	0 00434	40	E	?								0 92	0 7135	-26 0 (6 0)	157 0/-58 0	1	T1/T2	0 00623
SB50A-S3	0 00485	40	S3	N				155 2/49 6	27 8/74 3 (N=8)	10-O	20 3							
SB50A-5	0 0074	10	E	?														
SB50A-7	0 008	15	T1	R	*198 6/26 2 (N=5)		6 8											
SB51-A	0 00844	35	T2	R?	*254 6/20 8 (N=4)		19 5											
SB51-B	0 00244	35	S2	R				274 0/-33 0	235 0/-26 0 (N=8)		@7 6							
SB51-BT	0 00626	500	E	?										-18 5 (3 0)	167 0/-6 0	1	T2	0 00503
SB51-C	0 008	30	T2	R	*262 5/35 6 (N=6)		12											
SB51-A2	0 00548	40	T2	R	*86 3/53 8 (N=8)		17 3											
SB51A-A	0 0129	40	T2	R	*90 4/10 2 (N=7)		33 9											
SB51A-B	0 0103	40	T2	R	*90 2/57 7 (N=7)		17 8							-34 0 (17 5)	180 0/-9 0	T	T1/T2	0 01098
SB51A-C	0 00995	40	T1	R	*288 9/23 0 (N=8)		14 3											
SB52-1i	0 00169	40	T2	R	*7 7/4 7 (N=5)		22 2											
SB52-2i	0 00193	40	E	?														
SB52-1iA	0 00651	40	T2	R	*202 4/5 0 (N=4)		15 4					0 9	0 4187	-53 5 (1 5)	180 0/-90 0	T	T2	0 00247
SB52-2X	0 00159	40	E	?														
SB52-A	0 00344	22 5	S3	N														
SB52-S	0 00195	40	E	?														
SB52A-S	0 0507	40	T2	N?	*51 1/5 6 (N=9)		25 8											

SB52A-A	0 00256	22 5	S2	N	307 4/13 5 (N=4)	0-7 5	13 5	161 0/47 9	7 7/69 9 (N=6)		@14 2							
SB52A-1i	0 00841	40	T2	R	*172 6/30 7 (N=7)		20 2					0 97	0 4484	-36 0 (7 0)	325 0/71 0	1	S1		0 00893
SB52A-1	0 00634	25	S2	N				166 1/66 3	352 6/52 7 (N=7)	0-O	8							
SB52A-3	0 03	40	S2	?				264 9/21 1	280 8/6 1 (N=9)	5-O	10 5							
SB52A-3B	0 0245	40	S1	N	167 5/41 4 (N=3)	0-15	0 6	181 4/45 7	325 0/71 0 (N=4)	20-O	2 8							
SB53-C	0 0202	40	S2	R	34 0/17 7 (N=4)	0-15	12 4	39 4/-38 0	105 9/-48 3 (N=7)	15-O	11 4							
SB53-A	0 00972	40	T1	R	*106 2/46 7 (N=6)		18 5											
SB53-B	0 021	40	S2	R	28 9/45 9 (N=4)	0-15	6 1	322 5/-28 7	254 0/-66 0 (N=5)	15-O	6 1							
SB53-BA	0 0178	35	T2	R/N	*186 0/71 0 (N=8)		20 2											
SB53-C	0 0352	35	T2	R?	*182 3/59 5 (N=6)		20 9											
SB53-D	0 0408	30	T2	R	*160 1/62 0 (N=6)		17 4					1	3 333	-26 0 (1 5)	254 0/-66 0	1	S2		0 02276
SB53-X	0 0341	40	T1	R	*170 7/30 5 (N=7)		10 8											
SB53-E	0 02	30	T2	R	*171 5/60 0 (N=6)		24 7											
SB53A-A	0 0353	40	T2	R	*183 4/47 6 (N=9)		1 2											
SB53A-B	0 0297	40	T2	R	*188 1/41 9 (N=8)		2 3								163 0/-46 0	4	T2	@16 1)	0 03475
SB53A-C	0 045	40	T2	N/R	*175 6/42 3 (N=8)		6 3											
SB53A-D	0 0309	40	T2	N R	*164 7/45 9 (N=8)		6 1											
SB54-B	0 0593	40	S2	R				331 6/-28 0	254 0/-73 8 (N=7)	15-O	7 5							
SB54-C	0 0342	35	S2	R	21 9/61 9 (N=4)	5-20	7 3	354 1/-33 6	133 5/-84 3 (N=5)	20-O	13 5			-27 5 (6 5)	254 0/-73 8	1	S2		0 0507
SB54-D	0 0572	35	T2	R	*83 3/13 6 (N=4)		14											
SB54-A	0 091	40	T2	R	*186 0/19 8 (N=5)		12 8											
SB55-1	0 04	40	S2	R	265 7/87 1 (N=4)	0-15	5 4	330 2/-25 0	220 7/-78 7 (N=5)	15-40	4 4							
SB55-1i	0 0187	40	T1	R	*228 9/7 9 (N=5)		30 4											
SB55-2	0 0423	30	S2	R	304 9/85 8 (N=4)	0-15	5 8	344 0/-34 0	214 5/-82 9 (N=5)	15-O	6 7							
SB55-4	0 0247	30	S1	R	23 0/77 5 (N=4)	0-15	5 7	6 3/-46 6	138 5/-68 3 (N=5)	15-O	2 7	0 89	2 983	+101 5 (163 0)	138 5/-68 3	1	S1		0 02969
SB55-6	0 0401	40	S2	R				1 6/-37 5	124 4/-77 1 (N=5)	15-O	6 4							
SB55-3	0 00277	40	T1	R	*225 2/24 1 (N=5)		11 9											
SB55-5	0 0234	40	T1	R	*282 7/26 2 (N=8)		18 2											
SB56-1i	0 0058	40	T2	N	*121 6/36 8 (N=5)		4 7											
SB56-2X	0 00816	40	T1	N	*156 9/39 5 (N=9)		35 7											
SB56-2i	0 00462	40	T1	N	*244 3/7 8 (N=8)		38											
SB56-3i	0 00897	35	S2	R				328 0/-77 0	176 0/-41 0 (N=5)		@6 3							
SB56-1	0 0026	12 5	T3	N														
SB56-10	0 0046	12 5	T1	N	*136 0/24 8 (N=4)		1 8											
SB56-2	0 00479	12 5	T1	N	*111 4/4 1 (N=4)		3 2					0 83		-56 0 (11 5)	335 1/60 9	1	S2		0 00851
SB56-3	0 01222	12 5	T2	N	*5 0/3 4 (N=4)		17 8											
SB56-A	0 00894	40	S2	N				179 3/56 2	339 0/62 0 (N=4)		@10 3							
SB56-B	0 0145	40	T2	N/R	*221 7/20 2 (N=8)		11											
SB56-C	0 0185	40	S2	N				183 1/56 6	335 1/60 9 (N=5)	25-O	7 2							
SB56-X	0 0127	40	T2	N	*202 4/11 9 (N=9)		24											
SB56-4	0 00364	12 5	E/T2	R														
SB56-9	0 069	15	E/T2	R														
SB57-1	0 0153	40	T1	R	*260 9/10 2 (N=6)		10 8											
SB57-A	0 00959	35	T1	R	*252 3/5 8 (N=6)		28 8					0 87	1 007	-51 5 (22 5)	179 0/-45 0	3	T1	@24 3	0 01483
SB57-B	0 0178	30	T1	R	*258 6/17 4 (N=8)		28 1											
SB57-C	0 0185	30	T1	R	*93 4/5 4 (N=8)		27 9											
SB58-S	0 0105	40	T2	R	*340 2/59 4 (N=7)		35 1											
SB58-1i	0 00696	40	T2	R	*138 4/45 7 (N=7)		36 4					0 59		-26 5 (13 0)	221 0/-6 0	1	T2		0 00545
SB58-2i	0 00221	35	T2	R	*134 0/24 1 (N=6)		19 2											
SB59-S	0 083	40	T3	N/R														
SB59-1i	0 0213	40	T1	R	*65 7/10 9 (N=8)		6 6											
SB59-2i	0 0159	40	S2	R	9 4/48 8 (N=4)	0-15	6	347 8/-44 1	176 1/-74 8 (N=4)	20-O	9 6							
SB59-1	0 0253	40	E/T3	R														
SB59-12	0 0146	15	T1	R	*265 7/5 8 (N=5)		9 3					1	3 079	-18 5 (4 0)	176 1/-74 8	1	S2		0 01876
SB59-3	0 0151	12 5	T3	N/R														
SB59-5	0 0185	12 5	T2	R	*272 8/56 4 (N=4)		12 1											
SB59-6	0 0122	12 5	T3	R?	*262 7/46 6 (N=3)		0											
SB59-7	0 0208	35	T1	R	*120 5/62 9 (N=15)		27 7											
SB60-9	0 0173	40	T2	R	*241 4/66 8 (N=9)		8 3											
SB60-9T	0 0155	500	T2	R	*213 6/9 2 (N=6)		12 6											
SB60-2	0 00318	40	T3	R?	*200 3/19 9 (N=9)		24 1											
SB60-3	0 027	40	T3	R?								0 98	2 835	-11 5 (5 0)	171 0/-72 0	4	S2	@20 2	0 00723
SB60-4	0 0025	40	S2	R				359 0/-65 0	164 0/-53 0 (N=9)		@1 8							
SB60-5	0 0025	30	S2	R	165 9/61 2 (N=5)	2 5-12 5	6 7	351 6/-43 4	165 3/-75 5	25-O	10 9							
SB60-6	0 0216	30	S2	R	147 0/51 7 (N=5)	2 5-12 5	8 8	332 5/-30 4	250 5/-74 7 (N=5)	15-O	10 7							

SB60-7	0 0239	30	S2	R	164 5/56 6 (N=5)	2 5-12 5	8 1	2 6/-46 3	143 8/-70 1 (N=4)	15-O	6 6								
SB61-1	0 0125	40	E/T3	N?															
SB61-A	0 00972	30	S2	N				222 0/82 0	348 0/43 0 (N=7)		@7 2	0 88	0 7586	-41 0 (12 5)	348 0/43 0	1	S2		0 00881
SB61-B	0 00563	40	T2	N	*197 0/27 4 (N=8)		18												
SB62-A	0 00653	40	T1	R	*168 9/35 9 (N=5)		20 6												
SB62-B	0 0316	40	S2	N				196 2/50 8	310 3/69 8 (N=5)	5-O	10								
SB62-C	0 028	40	S2	R				333 6/-52 4	212 0/-69 8 (N=7)	15-O	9 2			-36 0 (3 0)	222 0/-66 0	3	S2	@15 5	0 01777
SB62-D	0 0198	40	S2	R	358 0/56 5 (N=4)	5-20	10	334 8/-49 6	217 8/-72 0 (N=6)	20-O	9 6								
SB62-X	0 0155	40	S2	R	86 5/70 4 (N=5)	0-20	8 3	307 3/-48 8	230 8/-55 0 (N=7)	20-O	8 9								
SB63-1i	0 00584	40	T2	R	*24 7/25 8 (N=8)		2												
SB63-1	0 026	40	T2	R	*61 6/52 9 (N=5)		30 6												
SB63-10	0 0296	40	T2	R	*83 4/1 5 (N=16)		29 2												
SB63-11	0 0263	40	T2	R	*277 5/11 0 (N=8)		24 8												
SB63-13	0 0391	40	T2	R	*102 7/4 7 (N=8)		31 7												
SB63-15	0 0278	40	T2	R	*80 6/5 9 (N=7)		28 5					0 96	3 233	-46 0 (6 5)	163 0/-58 0	35	T1/T2	@10 8	0 02004
SB63-2	0 0156	17 5	T1	R	*130 2/15 9 (N=5)		21 6												
SB63-3	0 022	15	S2	N	118 7/30 0 (N=3)	5-O	5 7	148 2/53 1	35 4/66 7 (N=4)	7 5-O	8 6								
SB63-4	0 0151	15	T2	R	*212 9/16 4 (N=4)		4 1												
SB63-5	0 0163	15	T2	R?	*204 9/20 0 (N=4)		0												
SB63-6	0 0185	15	T2	R	*200 9/28 1 (N=4)		2 2												
SB63-9	0 0309	40	T2	R	*280 0/27 0 (N=6)		16 5												
SB64-B	0 0468	40	T2	N/R	*232 1/56 6 (N=7)		30												
SB64-C	0 0109	40	T2	R	*215 0/18 0 (N=9)		9							-26 0 (3 0)	144 0/-67 0	1	S2		0 02265
SB64-A	0 0215	40	T2	R	*144 0/-67 0 (N=3)		13 9												
SB64-D	0 024	40	T2	R	*40 8/20 3 (N=9)		4 4												
SB65-16	0 0107	15	T1	R	*143 2/19 3 (N=4)		11 1												
SB65-17	0 0079	15	T3	R															
SB65-21	0 0109	30	T3	N/R?															
SB65-A	0 00389	40	T1	R	*192 3/21 2 (N=8)		7 8					0 9	2 106	-26 5 (7 5)	272 5/-28 4	1	S2		0 0111
SB65-C	0 0122	40	T2	R	*197 2/24 8 (N=8)		2 5												
SB65-1M	0 0133	40	S2	R	141 7/56 4 (N=3)	10-20	3 5	291 7/-11 0	272 5/-28 4 (N=5)	25-O	10 9								
SB65-2M	0 0163	40	T2	R	*190 2/29 1 (N=5)		2 3												
SB65-B	0 0243	40	T3	N/R?	*193 8/25 9 (N=9)		2 8												
SB66-1i	0 0135	40	S1	N				149 2/44 2	57 8/70 4 (N=9)	5-O	2 3								
SB66-2i	0 035	40	T2	R	*223 3/23 9 (N=6)		4 4												
SB66-3i	0 0239	40	S2	R	154 0/44 5 (N=3)		4 3	343 1/-38 4	257 6/-81 4 (N=5)	20-O	15 8								
SB66-3iT	0 00669	600	T2	R	*197 1/7 6 (N=7)		18 3												
SB66-4i	0 0156	40	T2	N/R?	*220 2/17 4 (N=6)		2 3	334 6/-34 9	269 4/-74 1 (N=6)	15-O	17 6								
SB66-1	0 1	25	O	?	13 0/59 0 (N=18)		7 9												
SB66-10	0 0278	40	T2	R	*108 8/42 3 (N=9)		29 5					0 86	3 059	-38 5 (11 5)	257 6/-81 4	1	S2		0 02797
SB66-12	0 042	40	T2	R	*107 4/3 1 (N=11)		22 4												
SB66-13	0 044	40	T2	R	*81 2/51 6 (N=10)		33 2												
SB66-14	0 0266	40	T2	R	*279 6/2 1 (N=9)		15 9												
SB66-15	0 0217	40	E	R?															
SB66-2	0 0356	40	T2	R	*101 5/12 1 (N=7)		29 8												
SB66-5	0 0439	40	T1	R	*96 7/34 1 (N=8)		32												
SBB66-7	0 0329	40	T1	R	*89 9/23 6 (N=8)		31 7												
SB67-1	0 0393	40	S2	R	177 1/58 4 (N=5)		9	354 0/-52 4	125 0/-52 5 (N=6)	12 5-O	16 8								
SB67-3	0 0253	40	T1	R	*209 4/22 4 (N=9)		8 8												
SB67-4	0 00206	40	E	R?															
SB67-6	0 0469	40	T1	R	*198 9/19 3 (N=9)		9					0 98	6 766	-25 0 (5 0)	174 0/-75 6	1	S2		0 02162
SB67-2	0 0234	40	T2	R	*209 4/18 1 (N=7)		1 3												
SB67-8	0 0321	40	S2	R				354 0/-52 4	174 0/-75 6 (N=6)	12 5-O	6 5								
SB67-62	0 0306	40	T1	R	*207 6/14 9 (N=9)		3 4												
SB69-1i	0 0094	40	T2	R	*97 4/13 3 (N=9)		22					0 87	0 8429	-29 0 (4 0)	MIXED		S2/T2		0 01175
SB69-3	0 0147	40	S2	N				280 1/76 8	338 8/33 4 (N=9)	5-O	14 4								
SB70-A	0 0217	40	E	?															
SB70-B	0 00711	40	T2	R	*126 8/30 6 (N=4)		1 9					0 9	1 613	-23 5 (1 5)	180 0/-90 0	T	T2		0 0165
SB70-C	0 0291	40	T2	R	*65 1/51 9 (N=5)		17 1												
SB71-A	0 00402	40	T2	R	*185 2/67 1 (N=8)		26 4												
SB71-B	0 00709	40	T2	N/R?	*303 9/50 5 (N=4)		10 9												
SB71-BT	0 0063	500	T3	N								0 95	0 6793	-44 0 (6 5)	172 0/-19 0	1	T2		0 00642
SB71-C	0 0066	40	T2	R	*98 4/47 6 (N=8)		15 6												
SB71-D	0 00923	40	T2	R	*261 8/20 7 (N=9)		12 2												
SB72-2	0 00649	40	S2	N				147 8/49 6	26 2/55 1 (N=8)	10-O	5 5								

SB72-3	0 0107	40	E	?														
SB72-1	0 00451	40	S2	N				143 0/64 0	14 0/43 0 (N=9)		@7 9	1	0 8011	-38 5 (4 0)	21 0/48 0	1	S2	0 00774
SB72-5	0 0136	40	T2	N	*146 7/56 5 (N=9)		8 5											
SB72-6	0 00652	40	S2	N	244 1/67 4 (N=5)	0-20	13 1	138 5/55 6	24 4/46 9 (N=5)	25-O	8 8							
SB73-1i	0 00338	40	T3	R?														
SB73-1	0 01098	40	S2	N	97 0/-22 1 (N=4)	2 5-10	1 6	140 0/56 0	23 0/47 0		@12 1	0 71		-53 5 (4 0)	23 0/47 0	1	S2	0 00617
SB73-2	0 00334	40	T2	R	*58 7/23 7 (N=8)		19 3											
SB73-3	0 01169	40	S2	N	208 8/3 5 (N=5)	0-10	12 2	191 4/76 3	350 3/35 3 (N=7)	10-40	16 9							
SB73-4	0 0029	40	T2	N/R	*236 8/52 4 (N=7)		21 7											
SB74-A	0 0108	40	T2	R	*75 4/5 1 (N=6)		34 9											
SB74-B	0 0055	40	T2	R	*59 6/60 8 (N=8)		26					0 59		-32 5 (2 5)	180 0/-90 0	T	T2	0 00653
SB74-C	0 00402	40	E	?														
SB74-D	0 00326	40	T2	R	*290 9/58 2 (N=7)		31 1											
SB75-1	0 032	40	T2	R	*203 6/23 0 (N=7)		23 8											
SB75-4T	0 00626	500	S2	N				59 2/80 6	3 8/17 7 (N=4)	300-O	6 4							
SB75-4	0 1218	35	O	?	3 2/62 3 (N=5)	0-10	15 4	33 3/80 9	356 5/15 2 (N=6)	15-O	1 5	0 75		-15 0 (2 5)	3 8/17 7	1	S2	0 02966
SB75-3	0 0407	40	S1	N/O?				289 9/73 5	336 9/15 2 (N=4)	20-O	3 4							
SB75-2	0 0231	40	O	?	329 2/55 0 (N=6)	12 5-O	11 5											
SB76-A	0 0212	30	T1	R	*101 4/14 1 (N=7)		37 2											
SB76-B	0 0189	40	T2	R	*279 7/17 7 (N=6)		26 8					0 96	2 647	-21 5 (9 5)	190 0/-2 0	1	T1/T2	0 01594
SB76-C	0 0101	40	T3	R?														
SB77-1	0 0341	40	S2	N					353 0/21 0 (N=3)		@2 7			-21 5 (0 0)	MIXED		S2/T2	0 02983
SB77-2	0 0261	40	T2	R	*66 4/23 5 (N=11)		18 4											
SB79-C	0 0022	40	E	?														
SB79-CT	0 01021	500	T2	R	*311 5/16 5 (N=6)		15 5					0 89	0 9578	-28 5 (3 0)	360 0/90 0	T	T3	0 00782
SB79-A	0 022	40	T2	R	*291 8/40 7 (N=9)		36 3											
SB79-B	0 00755	40	E	?														
SB80-A	0 0118	40	T3	N														
SB80-B	0 00188	40	E	?														
SB80-C	0 0175	40	T2	R	*81 3/72 4 (N=9)		26 3					0 92	1 263	-36 0 (16 5)	180 0/-90 0	T	T1/T2	0 00827
SB80-D	0 0118	40	T1	R	*265 3/4 0 (N=8)		28 7											

APPENDIX C

TABLE 1

Table 1 lists every horizon sampled at Seaford Head and includes palaeomagnetic details of all the specimens studied. Sample code (SF), NRM intensity, maximum demagnetization level (mT or °C), reliability category (see section 5.8), magnetic polarity (N=normal, R=reverse, I=intermediate and ?=unknown), low coercivity component, high coercivity component (B.B.C.=before bedding correction, A.B.C.=after bedding correction), IRM ratio, saturation IRM intensity (S.IRM) and volume magnetic susceptibility are tabulated from left to right. Details of the demagnetisation range (either °C or mT) at which the magnetic polarity is best defined are also included. Where demagnetisation stable end points are identified, the direction of the ChRM before and after bedding correction is listed, together with the MAD or 95% confidence angle, which provides a measure of reliability. Where directional trends were observed, poles to the 'best fit' great circles were recorded, along with the MAD and number of demagnetisation vectors defining it. Great circle poles are indicated by an asterisk and can be found in both the low and high coercivity component columns.

This table should be read in conjunction with Figure 8.4 which displays graphically the magnetic polarity stratigraphy of the Seaford Head section. The five columns on the right hand side of the table summarises the sample horizon's mean magnetic direction, the number of samples defining that direction, the general reliability category of the mean direction, the associated alpha 95 value or MAD and the mean NRM intensity (mA/m).

CODE	NRM mA/m	MAX TEMP AF LEVEL	RELIABILITY CATEGORY	POLARITY	LOW COERCIVITY COMPONENT OR TREND(*)	RANGE	MAD/ ALP 95	HIGH COERCIVITY COMPONENT B B C	HIGH COERCIVITY COMPONENT A B C	RANGE	MAD/ ALP 95	IRM RATIO	S IRM mA/m	VOLUME M S (S I UNITS) x10^-6	MEAN MAGNETIC DIRECTION	N	GENERAL RELIABILITY CATEGORY	MAD/ ALP 95	MEAN NRM mA/m
SF1-A	0 0117	40	T2	R	*36 3/9 1 (N=7)		2 9					0 97	2 249	-2 65 (1 15)	180 0/-90 0	T	T1/T2		0 01495
SF1-B	0 0414	40	T1	R	*33 3/12 4 (N=9)		1 9												
SF1-C	0 0141	40	T2	R	*41 1/3 9 (N=8)		1 4												
SF1-D	0 0215	40	T2	R	*34 4/11 3 (N=9)		1												
SF1A-A	0 00706	40	S2	R	137 9/26 5 (N=5)	0-20	14 5	73 6/-60 4	99 7/-56 8 (N=6)	20-O	15 3	0 95	0 6452	-4 10 (0 75)	106 8/-46 4	1	S2		0 00832
SF1A-B	0 00983	40	T1	R	*31 0/14 5 (N=9)		1 4												
SF1A-B	0 00783	40	T2	R	*220 9/0 1 (N=9)		9												
SF1A-D	0 0088	40	S2	R	136 8/23 6 (N=7)	0-35	9	89 4/-53 0	106 8/-46 4 (N=3)	35-O	2 7								
SF2-A	0 0126	40	T1	R	*22 1/27 5 (N=8)		10					0 93	2 123	-4 10 (0 75)	310 0/-33 0	1	T1/T2		0 01026
SF2-B	0 00721	40	T3	R?	*30 9/15 7 (N=7)		2 3												
SF2-C	0 0108	40	T3	R?	*29 3/17 1 (N=8)		11												
SF2-D	0 0113	40	T2	R	*33 3/11 2 (N=8)		7 6												
SF2A-A	0 00639	40	S2	R	274 0/55 8 (N=4)	0-15	11 6	106 8/-55 4	114 0/-40 9 (N=6)	15-40	6 6	0 96	4 303	+0 75 (0 65)	122 0/-44 0	3	S1		0 00852
SF2A-B	0 0107	40	S1	R	303 6/54 8 (N=4)	0-15	2 9	124 1/-49 7	134 5/-34 3 (N=6)	15-40	5 4								
SF2A-C	0 0106	40	S1	R	258 1/58 5 (N=4)	0-15	6 5	105 8/-52 8	119 0/-42 4 (N=6)	15-O	5 2								
SF2A-D	0 0132	40	S1	R	301 3/76 7 (N=4)	0-15	8 7	94 3/-66 8	120 2/-57 8 (N=6)	15-O	3 7								
SF2A-DT	0 00468	600	S3	R				89 0/-33 0	98 0/-28 0 (N=10)		@12 4								
SF3-A	0 0157	40	T3	R	*221 8/3 6 (N=8)		25 8					0 97	0 7597	-5 15 (1 3)	198 0/-72 0	1	T2/T3		0 0171
SF3-B	0 0204	40	T2	R	*313 7/19 5 (N=5)		17 7												
SF3-C	0 0171	40	T3	R?	*111 1/0 2 (N=8)		31 6												
SF3-D	0 0156	40	T3	R?	*250 8/11 2 (N=8)		24 7												
SF4-A	0 00653	40	T2/T3	R?	*243 9/1 1 (N=9)		36 3					0 94	0 582	-4 5 (3 65)	180 0/-90 0	T	T2/T3		0 00346
SF4-B	0 0037	40	T2/T3	R?	*312 1/56 6 (N=4)		26 6												
SF4-C	0 00279	40	T3	R?	*17 1/17 8 (N=6)		20 1												
SF4-CT	0 00145	300	E	?															
SF4-D	0 00511	40	T2	R	*358 4/25 3 (N=7)		30 1												
SF5-A	0 0074	40	T2	R	*254 4/9 5 (N=9)		27 3					0 89	0 6653	-2 15 (1 7)	176 0/-60 0	9	T2	@16 0	0 00806
SF5-AT	0 00526	300	E	?															
SF5-B	0 0102	40	T2	R	*236 5/9 9 (N=9)		34 8												
SF5-C	0 00958	40	T2	R	*208 1/16 3 (N=4)		14 2												
SF5-D	0 00765	40	T2	R	*244 3/24 7 (N=9)		23 3												
SF5-E	0 00941	40	T2	R	*105 0/35 9 (N=4)		3 7												
SF6-A	0 00081	40	T2	R								0 9	0 6653	-2 75 (1 3)	180 0/-90 0	T	T2/T3		0 00173
SF6-B	0 00331	40	T3	R??															
SF6-C	0 00114	40	E	R?															
SF6-D	0 00293	40	T3	R??															
SF7-A	0 0106	40	T2/T3	R	*343 1/54 0 (N=5)		38					0 89	0 3306	-1 1 (1 15)	192 0/-61 0	1	T1/T2		0 01083
SF7-B	0 009	40	T2	R	*335 4/7 0 (N=9)		17 5												
SF7-C	0 0103	40	T2	R	*133 1/5 4 (N=4)		1 1												
SF7-D	0 01157	40	T2	R	*61 3/15 7 (N=8)		36 9												
SF7-E	0 01216	40	T2	R	*151 0/2 2 (N=9)		26 3												
SF7-F	0 01446	40	T1	R	*214 1/28 4 (N=9)		33 3												
SF7-G	0 02076	40	T3	R?	*337 2/7 4 (N=8)		25 1												
SF7-H	0 00692	40	T3	R??															
SF7-HT	0 00131	300	E	?															
SF7-I	0 0366	40	T3	R?	*131 7/13 1 (N=9)		17 2												
SF7-J	0 0175	40	T1	R	*87 5/12 5 (N=8)		33 9												
SF7A-A	0 00959	40	T1	R	*45 6/4 1 (N=9)		6 7					0 9	0 4956	-1 0 (0 5)	180 0/-90 0	T	T1/T2		0 01507
SF7A-B	0 00643	40	T1	R	*43 8/7 2 (N=8)		3 4												
SF7A-C	0 0388	40	T2	R	*228 5/1 2 (N=9)		14 2												
SF7A-D	0 0275	40	T3	R?	*45 5/3 2 (N=9)		11 1												
SF7A-E	0 0118	40	T2	R	*46 7/0 1 (N=9)		11 9												
SF8-A	0 0171	40	T2	R	*193 8/29 0 (N=9)		24 6					0 99	0 4712	-2 0 (1 3)	231 1/-28 6	1	S2		0 01987
SF8-B	0 0179	40	S2	R	288 7/23 4 (N=5)	0-30	4 2	240 4/-33 7	231 1/--28 6 (N=4)	30-O	16 8								
SF8-C	0 0311	40	S2	R				161 0/-30 0	161 0/-14 0 (N=7)		@1 3								
SF8-D	0 0135	40	T2	R	*285 4/40 1 (N=9)		38 4												
SF8-DT	0 0241	300	E	?															
SF9-A	0 00358	40	T2	R	*209 3/21 3 (N=5)		28 8					0 87	0 5102	-2 5 (1 4)	200 0/-66 0	3	T1/T2	@19 3	0 00388
SF9-AT	0 0016	300	E	?															
SF9-B	0 00508	40	T2	R	*257 2/19 7 (N=6)		33 9												

SF9-BT	0 00316	300	E	?															
SF9-C	0 00845	40	T1	R	*170 9/24 7 (N=7)		20 8												
SF9-D	0 00438	40	T1	R	*257 2/57 5 (N=5)		11 6												
SF10-A	0 0129	40	T2	R	*348 6/36 8 (N=8)		25					0 89	0 7592	-4 35 (0/8)	97 0/-22 0	1	T2		0 02041
SF10-B	0 0323	40	T2	R	*25 2/37 6 (N=6)		13 7												
SF11-A	0 02	40	O	?	74 0/87 6 (N=6)	20-O	5 8					0 89	4 178	-3 75 (1 9)	OVERPRINT				0 02
SF12-A	0 0246	40	S1	N				348 5/48 7	347 5/32 7 (N=9)	5-O	4								
SF12-B	0 0241	40	S2	N	324 0/61 2 (N=4)	0-15	5 9	353 2/57 8	350 5/42 0 (N=7)	15-O	8 9	0 99	1 301	-2 9 (1 6)	353 0/44 0	4	S1/S2/S3	@11 3	0 01733
SF12-BT	0 00351	300	S3	N				352 0/65 0	349 0/49 0 (N=5)		@8 2								
SF12-C	0 0433	40	S1	N	330 1/65 5 (N=3)	0-10	2 9	16 8/64 4	5 4/50 0 (N=8)	10-O	5								
SF13-A	0 0199	40	S2	N				351 3/55 0	342 0/34 9 (N=7)	10-O	9 2								
SF13-AT	0 0037	40	E	?								0 68		-3 35 (0 4)	342 0/34 9	1	S2 [1]		0 01557
SF13-B	0 0242	40	S2	N	338 9/59 0 (N=6)	0-25	3 7	29 2/63 5	14 0/50 6 (N=5)	25-O	11 1								
SF13-C	0 033	40	S2	N				351 2/67 0	348 4/51 1 (N=7)	10-40	6 3								
SF14-A	0 00465	40	E	?															
SF14-B	0 00286	40	S3	N				76 0/46 0	60 0/44 0 (N=3)		@4 1								
SF14-C	0 00459	40	S3	N				347 0/35 0	346 0/19 0 (N=5)		@9 2	0 65		-3 85 (2 25)	356 0/41 0	5	S3	@42 8	0 00353
SF14-D	0 00403	40	S3	N				294 0/52 0	306 0/40 0 (N=7)		@8 9								
SF14-DT	0 00206	300	T3	?															
SF14-E	0 0036	40	S3	N				47 0/34 0	*39 0/26 0 (N=4)		@11 3								
SF14-F	0 00384	40	S3	N				309 0/48 0	*316 0/35 0 (N=7)		@8 0								
SF16-A	0 0125	40	S1	N				301 4/71 6	*320 2/58 0 (N=6)	20-O	5 6								
SF16-B	0 0396	40	S1	N				9 3/58 1	2 0/43 2 (N=6)	20-O	2 7	0 9	0 554	-4 125 (0 2)	2 0/43 2	1	S1		0 0161
SF16-BT	0 0227	600	T3	N	*142 5/2 0 (N=4)		23 9												
SF16-C	0 00598	40	E	?															
SF18-A	0 00504	40	T2	R	*230 3/21 4 (N=8)		22												
SF18-AT	0 00263	300	E	?								0 86	0 4484	-4 9 (0 5)	172 0/-56 0	1	T2		0 00411
SF18-B	0 00523	40	T2	R	*141 0/29 6 (N=8)		36 1												
SF18A-A	0 00269	40	E	?															
SF18A-B	0 00265	40	T2	R	*57 0/17 2 (N=6)		15 9												
SF18A-C	0 00252	40	E	?															
SF18A-CT	0 00077	300	E	R??								0 82		-5 1 (1 4)	164 0/-72 0	5	T1/T2	@22 3	0 00243
SF18A-D	0 0039	40	T1	R	*303 9/13 8 (N=7)		28 6												
SF18A-E	0 00304	40	E	?															
SF18A-F	0 00219	40	T2	R	*107 2/1 8 (N=5)		11 4												
SF18A-G	0 00341	40	T1	R	*85 2/19 3 (N=9)		18 5												
SF19-A	0 00218	40	E	R??															
SF19-B	0 00187	40	T2	R	*166 3/4 9 (N=6)		30 3												
SF19-C	0 00311	40	T2	R	*67 7/3 1 (N=7)		36 1												
SF19-D	0 0029	40	T2	R	*55 5/17 9 (N=5)		19 3					0 84		-3 6 (0 9)	180 0/-90 0	T	T1/T2		0 00255
SF19-E	0 0041	40	T1	R	*202 8/15 6 (N=9)		36 4												
SF19-F	0 00184	40	T2	R	*235 2/22 8 (N=6)		33 3												